Deciphering changes in cellular identity during development, reprogramming and oncogenesis

Giacomo Furlan

N°d'ordre NNT: 2019LYSE1309

THESE de DOCTORAT DE L'UNIVERSITE DE LYON
opérée au sein de
l'Université Claude Bernard Lyon 1

Ecole Doctorale N°340
(BMIC Biologie Moléculaire Intégrative et Cellulaire)

Spécialité de doctorat : Biologie cellulaire
Discipline : Biologie cellulaire

Soutenue publiquement le 06/12/2019, par :
Giacomo FURLAN

Deciphering changes in cellular identity during development, reprogramming and oncogenesis

Devant le jury composé de :

Nom, prénom	grade/qualité	établissement/entreprise	**Président.e (à préciser)**
LI Han		CR, CNRS, Institut Pasteur, Paris	**Rapporteure**
DAVID Laurent		Maitre de conférences, CRTi, Nantes	**Rapporteur**
BERNET Agnès		Professeure, CRCL, Lyon	**Examinatrice**
CHAZAUD Claire		DR, INSERM, GReD, Clermont-Ferrand	**Examinatrice**
SAVATIER Pierre		DR, INSERM, SBRI, Lyon	**Examinateur**
LAVIAL Fabrice		CR, INSERM, CRCL, Lyon	**Directeur de thèse**

Summary

ABBREVIATIONS LIST

Atoh8: Atonal homolog 8
BAM: Brn2, Ascl1, and Mytl1 combination
bHLH: basic Helix-loop-helix
bHLHZ: basic Helix-loop-helix leucine zipper
CSC: cancer stem cell
DCC: deleted in colorectal carcinoma
Dox: doxycyline
DKO: double knock-out
DN: double negative
DP: double positive
E.N: embryonic day.N
Epi: epiblast
EpiSC: epiblast stem cell
EC: embryonic carcinoma
EMT: epithelial to mesenchymal transition
ESC: embryonic stem
ICM: inner cell mass
iN: induced neurons
iPSCs: induced pluripotent stem cells
KO: knock-out
MEF: mouse embryonic fibroblast
MET: mesenchymal to epithelial transition
MR: malignant reprogramming
NR: non-reprogramming
Neo-1: neogenin-1
OSK: Oct4, Sox2 and Klf4 combination
OSKM: Oct4, Sox2, Klf4 and c-Myc combination
OSN: Oct4, Sox2 and Nanog combination
PaniN: pancreatic intraepithelial neoplasia
P-Erk: Phospho-Erk
PE : primitive endoderm
PR: pluripotent reprogramming
TE: trophoectoderm
TF: transcription factor
Unc: uncoordinated

INTRODUCTION

1. PROCESSES INVOLVED IN CHANGES IN CELLULAR IDENTITY

During my PhD studies, I studied the mechanisms that safeguard cellular identity or, on the contrary, allow cells to lose their initial identity and convert to a new cell type.

In the classical view of development, changes of cellular identity mainly take place during differentiation. In this process, the pluripotent stem cell, capable of forming the whole organism, stops to self-renew and, through stepwise cell divisions, differentiates into terminally specified somatic cells. This differentiation is always accompanied by (i) the loss of cellular plasticity, which is the ability to give rise to multiple cell types, and (ii) the acquisition of specific cellular features (Patel and Hobert, 2017).

This concept was well described in 1957 by Conrad Hal Waddington, a developmental biologist who connected for the first time the embryology and the genetic fields. He displayed the development of an organism as the synchronized descent of a hillside towards different valleys (**Fig.1**). In the model, a single stem cell descends the hillside during differentiation. When it enters a valley, it cannot climb back the mountain side and enter a second valley. In the same way, a cell that has completely differentiated into a specific cell type, cannot lose its somatic identity, reacquire plasticity and convert into a new different cell type. This limitation is due to the plasticity restriction associated with differentiation. Thus, embryonic stem cells descend different valleys to give rise to the several cell types composing the whole organism. Moreover, the eminent scientist hypothesized that the mechanisms allowing cells to choose between the several valleys have an epigenetic origin. For these reasons, he developed the idea of the epigenetic landscape of development. (Hochedlinger and Plath, 2009).

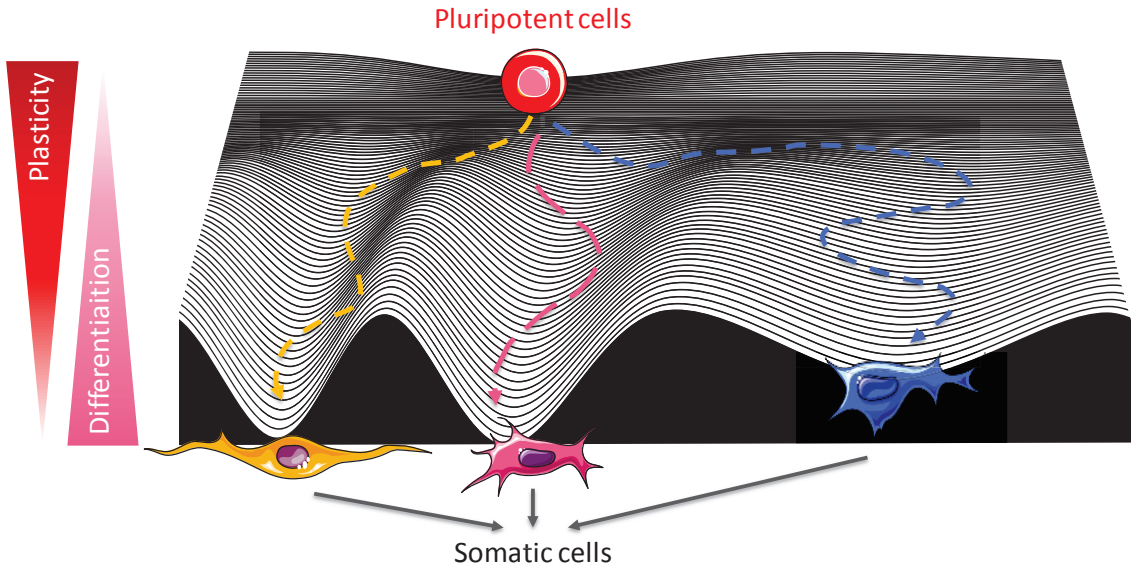

Figure 1: (Adapted from Puisieux et al., 2018). The epigenetic landscape of development, proposed by Waddington. A pluripotent cell differentiates into a specific cell type, a process accompanied by acquisition of specific features and loss of cellular plasticity.

Even if Waddington described remarkably the role of epigenetic in developmental fate choices, new advances in developmental biology proved him partially wrong. It has been well documented that cells advanced in a given developmental state can revert to a less differentiated condition.

As a first example, in the pluripotent compartment of the embryo we can identify multiple stem cell populations harbouring different features. *In vitro* models showed that cells more committed can go back to more naïve states. Notably, these processes are interconvertible, highlighting the plasticity of the differentiation process (Bao et al., 2009; Ying et al., 2008).

Secondly, in the last twenty years, it has been shown that a differentiated cell can lose its somatic identity and go through profound molecular and epigenetic changes, resulting in a completely different somatic cell, in a process known as trans-differentiation (Davis et al., 1987; Vierbuchen et al., 2010).

Thirdly, a somatic cell can revert to the pluripotent state, which leads to the formation of induced pluripotent stem cells (iPSCs). This process is called pluripotent reprogramming (PR) (Takahashi and Yamanaka, 2006).

According to these changes in cellular identity, development is a more plastic process compared to what postulated by the British scientist (**Fig.2**)

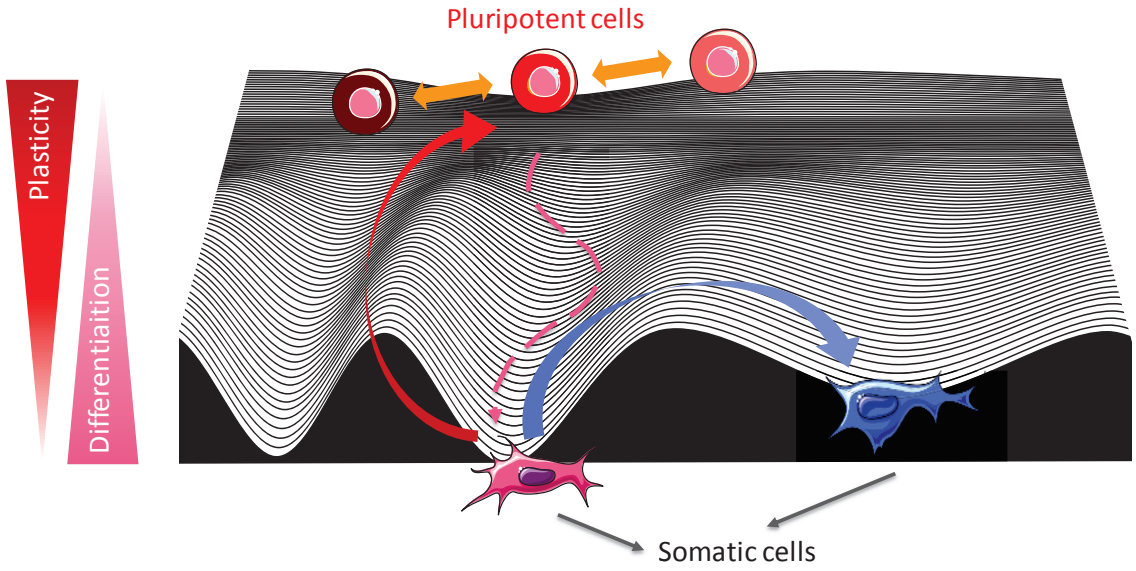

Figure 2: (Adapted from Puisieux et al., 2018). Revisiting Waddington landscape. Pluripotent cells consist in a heterogeneous population harbouring multiple pluripotent configurations, interconvertible one with each other. Differentiated cells can convert into other somatic cells or revert to pluripotency through trans-differentiation and pluripotent reprogramming.

During my PhD, I studied the processes that mediate loss of cellular identity, plasticity acquisition and conversion into new cellular types. In particular, I investigated the role of Netrin-1 in the promotion of naïve pluripotency both *in vitro* and *in vivo*.

In the second part of my PhD, I examined the loss of somatic identity and reacquisition of cellular plasticity in two processes sharing interesting similarities: the iPSCs generation and the malignant transformation.

1.1. Plasticity in the embryonic pluripotent compartment

In the pluripotent compartment of the embryo, stem cells can exist in two configurations: naïve and primed, respectively associated to a less and a more committed state. Interestingly, *in vitro* these two states are inconvertible, and primed cells can revert to more naïve states (Bao et al., 2009). Moreover, heterogeneous naïve cells can be stabilized in a pure naïve configuration, known as ground state (Ying et al., 2008). The two processes are interconvertible, suggesting a certain cellular plasticity in the embryonic development. In this first part of the introduction, we will read about the embryonic development until the early post-implantation and the *in vitro* culture developed to capture different embryonic stages. I will describe the signalling pathways controlling embryonic development and analyse the cellular conversions happening at this developmental stage.

1.1.1. Embryonic development from the zygote to the post-implantation embryo.

Organism development is orchestrated by two opposite tendencies, which need to be precisely tuned in time and space: restriction of cellular plasticity and increase in the number of specialized cells and tissue types (Bedzhov et al., 2014).

Diploid organism's development starts with the fusion of the mother oocyte with the father sperm cell, forming the zygote, the first cell of the organism. The zygote is totipotent, thus it has the ability to form not only the embryonic compartment, that will develop into the adult organism, but also the extraembryonic tissues, precursors of important structures, such as placenta, that sustain embryonic development (Sheng and Foley, 2012). During early development until post-implantation stages, the embryo enters two cellular plasticity restrictions and tissue specifications, fundamental to establish the different compartments generating the extraembryonic and embryonic tissues (**Fig.3**).

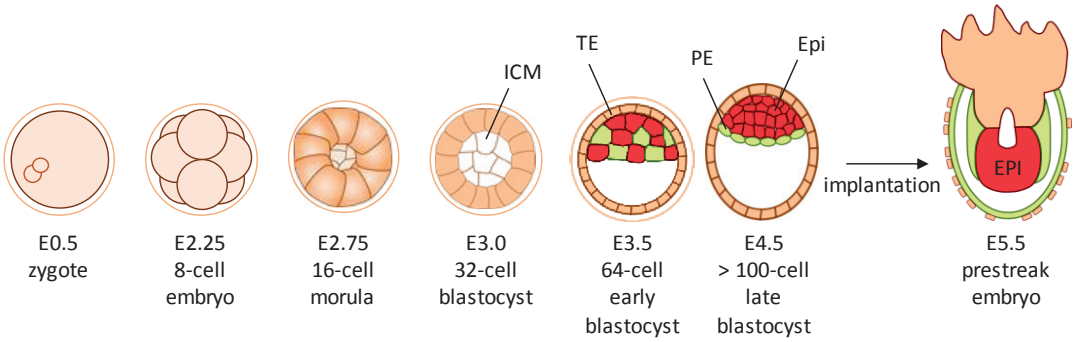

Figure 3: (Adapted from Posfai et al., 2014). Embryonic development from zygote to early post-implantation, representing the first and second segregations, generating TE (orange), Epi (red) and PE (green).

1.1.1.1. First phase of lineage restriction: The ICM/TE segregation

After three cell divisions, the embryo enters the first plasticity restriction, which form the trophectoderm (TE) and the inner cell mass (ICM) (**Fig.4**). While trophectoderm generates extraembryonic tissues, the ICM is composed by pluripotent stem cells, capable of ensuring the whole embryo development (Stephenson et al., 2012). Their ability to proliferate and form the entire organism is the effect of the characteristics associated to the pluripotent state: pluripotent cells can self-renew, a process which combines maintenance of the proliferation potential with inhibition of apoptosis and blockage of differentiation, and, at the same time, they can differentiate into the three germ layers, ectoderm, mesoderm and endoderm, precursor of all the cell types forming the organism (Nichols and Smith, 2012).

In mice, the first plasticity restriction takes places after few divisions of the zygote, at the 16-cells stage, at embryonic day (E) 2.75 (E2.75).

At this phase of development, the eight cells, also called blastomeres, start to form adherent junctions (AJs) through E-Cadherin expression, and they develop an apico-basal polarization, characterized by the accumulation on the apical/exterior border of F-actin, myosin and clathrin (Ducibella et al., 1977; Shirayoshi et al., 1983). These newly polarized cells go through another cellular division, giving rise to the 16-cell embryo. There, we can identify two different populations: the internal apolar cells, enclosed in high cell-cell contacts, and the external polar cells, with the apical domain facing the outer environment. This cellular diversification shapes the first plasticity restriction and specification towards the inner cell mass (ICM) and the trophoectoderm (TE). In this phase, the TE forms an external layer surrounding the ICM and an internal cavity known as blastocoel. The resulting structure is called blastocyst (Stephenson et al., 2012).

In this first specification, the Hippo pathway plays a crucial role in modulating the expression of two opposite transcription factors (TFs), which are expressed in a fluctuating way before specification: the pluripotency marker Oct4 and the TE transcription factor Cdx2 (Dietrich and Hiiragi, 2007). During the specification, their expression is determined by the state of the transcriptional regulator YAP, which is expressed in both cellular types, but with different cellular compartmentalization. In external cells, Hippo pathway is not active, thus YAP translocates to the nucleus and interacts with Tead4. The formed complex upregulates the fluctuating expression of Cdx2, which in turn inhibits Oct4 transcription. (Yagi et al., 2007; Yu and Guan, 2013). On the other hand, in internal cells which will give rise to ICM, Hippo pathway is active, and YAP is phosphorylated and degraded in the cytoplasm by the Hippo effectors Lats1/2. In this way, the lack of Cdx2 upregulation leads to Oct4 de-repression and the enhanced Oct4 levels avoid ectopic Cdx2 expression in ICM (Niwa et al., 2005; Strumpf, 2005). The link between the cellular polarity and the first specification seems to be provided from E-Cadherin-mediated adherent junctions. These structures sequestrate angiomotin (Amot) proteins, which act as a scaffold for Hippo signals. In the outer cells, Amot proteins are sequestrated to the adherent junctions and cannot activate Hippo pathway by Lats1/2 phosphorylation. YAP can translocate to the nucleus and activate Cdx2, inducing TE specification. On the contrary, TE cannot be induced in inner cells, where Amots are free to phosphorylate Lats1/2, which in turn inhibits YAP-dependent Cdx2 activation (Hirate et al., 2013).

Following this mechanism, the Hippo pathway regulates the formation of both ICM and TE. After another cell division, the 64-cell ICM represents the *in vivo* tissue used to derive *in vitro* embryonic stem cells (ESCs), at (Evans and Kaufman, 1981; Martin, 1981).

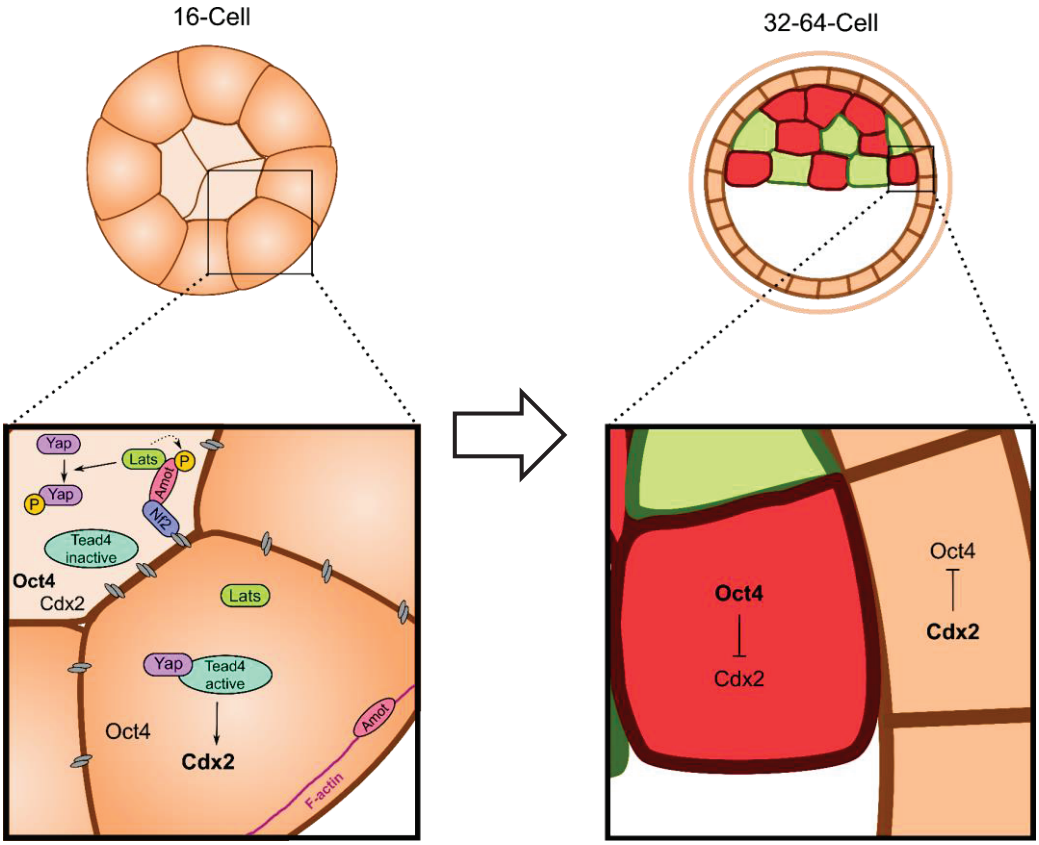

Figure 4: (Adapted from Posfai et al., 2014). First lineage segregation generating TE (orange) and ICM (red+green). In outer cells, the complex composed by Yap and Tead4 activates the TE-master gene Cdx2, leading to TE formation. In inner cells, Hippo signalling inhibits the complex formation, resulting in de-repression of Oct4 expression and ICM development

1.1.1.2. Second phase of lineage restriction: The Epi/PE segregation

During second lineage restriction, around E4.5, the ICM generates two different cell populations, the epiblast (Epi) and the primitive endoderm (PE) (**Fig.5**). The former constitutes a cellular mass that, after implantation, will generate the three germ layers. The latter forms a tiny layer between the epiblast and the blastocoel and its derivates are the principal elements of the yolk sac (Hermitte and Chazaud, 2014).

The Fgf pathway plays a fundamental role in this lineage restriction, as embryos mutants for Fgf4, the principal ligand expressed in blastocyst, fail to generate PE and quickly die after implantation (Feldman et al., 1995). In pre-implantation embryos, Fgf4 and Fgfr2 represent the principal ligand-receptor couple, with Fgfr1 emerging only during the maturation of PE (Molotkov et al., 2017). Until the 16-cell stage, their expression fluctuates in the cells of the ICM, but, at the following cellular division, they become asymmetrically expressed, with Fgf4 specifically expressed in the Epi and Fgfr2 in the PE (Guo et al., 2010).

Two transcriptional factors are correlated with the Fgf pathway and their combined action is the key determinant for the second segregation: Nanog and Gata6, markers of the Epi and the PE, respectively. The expression of these TFs fluctuates in the ICM until 32-cell stage, the same time of the onset of Fgf4/Fgfr2 compartmentalization (Guo et al., 2010). This could suggest a role of the Fgf signalling in the Nanog and Gata6 regionalization. Indeed, small molecules inhibiting Fgf signalling leads to a homogenized Nanog-expressing ICM, while embryos treated with Fgf4 express Gata6 uniformly (J. Nichols et al., 2009; Yamanaka et al., 2010).

Gata6 and Nanog are not simply markers of the Epi and PE, but rather master-genes: the homeodomain TF Nanog acts as a major regulator of naïve pluripotency and its deletion leads to failure in epiblast formation (Mitsui et al., 2003). On the other hand, the zinc finger TF Gata6 ensures PE development, as far as its absence results in PE developmental defects and peri-implantation lethality (Koutsourakis et al., 1999). Notably, the two TFs orchestrate a reciprocal regulation, Nanog being necessary for non-autologous organisation and development of PE (Frankenberg et al., 2011). Interestingly, even if the maintenance and restriction of Gata6 to PE require Fgf signalling (Kang et al., 2013), the onset of Gata6 transcription does not depend on Fgf (Frankenberg et al., 2011). The exact molecular mechanisms linking Fgf signalling to Epi/PE segregation still need to be elucidated, as well as the onset of Gata6 expression (and thus PE program induction).

The pluripotency marker Oct4 seems to play a role in the Epi/PE segregation, where it could potentially represent a second level of regulation. Indeed, while Oct4 is dispensable for initiating Epi program, the TF is required both cell-autonomously and non-autonomously for PE specification (Frum et al., 2013). In the Epi, it regulates Fgf transcription, with consequent non-autonomous effects on PE, while its presence in PE drives the expression of PE markers Pdgfra, Sox17 and Gata4. Moreover, once the segregation is complete, Gata6 expression in PE is Oct4-dependent (Frum et al 2013). It has been shown in ESCs that Oct4 can interact both with the pluripotency factor Sox2 and the PE marker Sox17, and the choice between the two Sox partners identify Oct4 as a pluripotent or endodermal determinant (Aksoy et al., 2013). Indeed, Sox17 competes with Nanog by displacing it from its binding sites (Niakan et al., 2010). It is thus possible that Oct4 different circuits constitute a further level in the regulation and maintenance of the Epi/PE segregation.

Soon after the second restriction, the embryo implants in the mother uterus and the epiblast starts the lineage specification towards the three germ layers

Exit from pluripotency starts between E4.75 and E5.75 and lasts until gastrulation, at E6.5 dpc (Sheng, 2015). During implantation, the epiblast goes through deep molecular, epigenetic and cellular changes, and, even if it maintains the same pluripotent features (self-renewal and differentiation potential), it is profoundly different from the pre-implantation Epi. Thus, to distinguish between the pluripotent compartment before and after implantation (ICM/pre-implantation epiblast versus post-implantation epiblast), the two different developmental stages are labelled as naïve and primed pluripotency (Weinberger et al., 2016).

From the post-implantation epiblast it has been possible to derive *in vitro* epiblast stem cells (EpiSCs), which recapitulate the characteristics of the *in vivo* primed pluripotent compartment (Brons et al., 2007; Tesar et al., 2007).

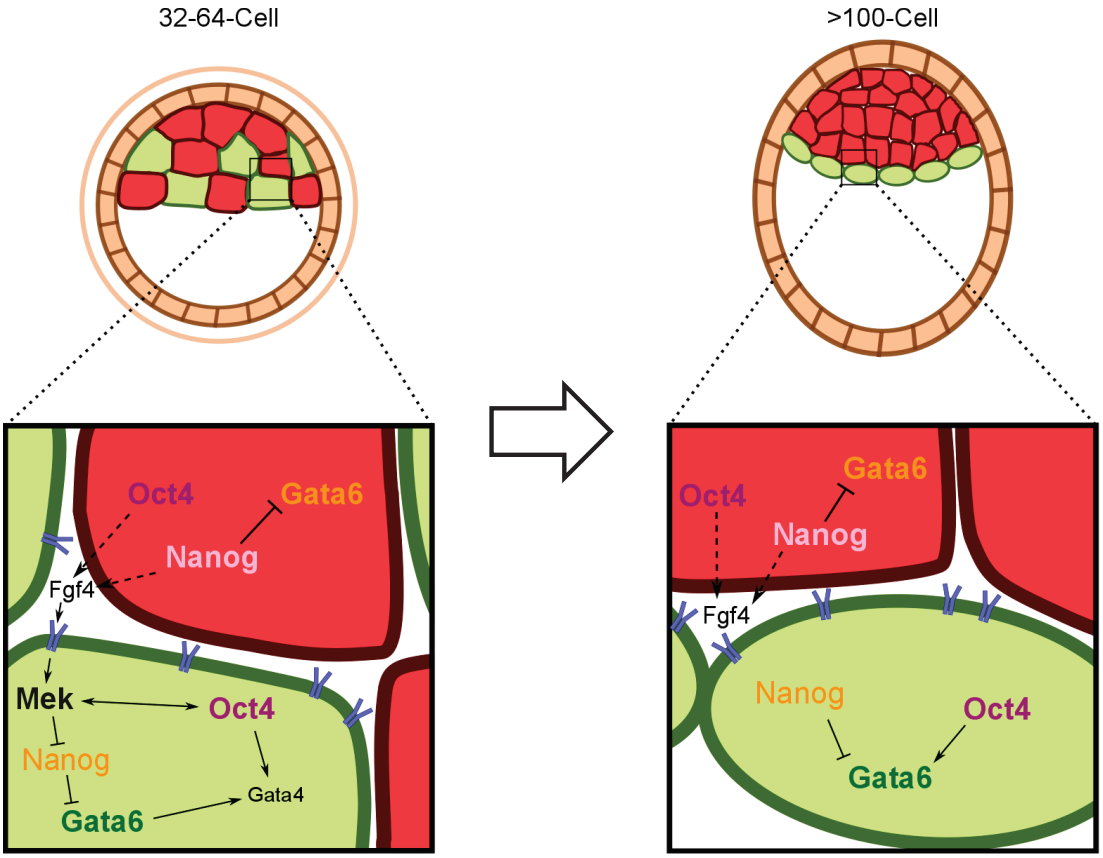

Figure 5: (Adapted from Posfai et al., 2014). Second lineage segregation generating Epi (red) and PE (green). The combined action of Fgf signalling, Nanog and Gata6 determines the specification of the two embryonic compartments. Oct4 contributes to the segregation as an additional level of regulation.

1.1.2. Capturing pluripotency *in vitro*

To study in detail pluripotency, during the past years many efforts have been made to generate *in vitro* cellular models recapitulating *in vivo* pluripotency. In 1981, the first embryonic pluripotent lines were derived: the embryonic stem cells (ESCs) (Evans and Kaufman, 1981; Martin, 1981). These cells are derived from the ICM at E3.25, they have a naïve pluripotent configuration and correspond to the pre-implantation pluripotent compartment. Later, in 2007, two parallel studies succeeded in deriving epiblast stem cells (EpiSCs) from the post-implantation epiblast, which show a primed pluripotent state (Brons et al., 2007; Tesar et al., 2007).

In the next part, I will describe the characteristics of these two cell models at the phenotypical, molecular and epigenetic levels, the signalling regulating their pluripotent states and the cellular conversions between pluripotent configurations.

1.1.2.1. Embryonic stem cells – model for naïve pluripotency

1.1.2.1.1. General characteristics

ESCs were originally derived from blastocyst isolation of the 129 mice strain (Evans and Kaufman, 1981). They were cultivated over a layer of irradiated fibroblasts (feeder cells), fundamental for cytokine dispersion in the medium, with conditioned media derived from ECs (embryonic carcinoma cells, the malignant counterparts of ESCs, previously isolated *in vitro*) (Evans and Kaufman, 1981; Kleinsmith and Pierce, 1964). Later, it was found that BMP4 treatment can compensate serum requirement and the combination of LIF and BMP renders the cell culture serum- and feeder-free (Smith et al., 1988; Williams et al., 1988; Ying et al., 2003a).

There are many characteristics linking ESCs to the pre-implantation epiblast and ICM. They are pluripotent, as proved by their competence to generate chimaera when injected in pre-implantation blastocyst of a donor mice: they can contribute extensively to the formation of adult tissues and to the germ line (Bradley et al., 1984). As ICM, female ESCs do not show X chromosome inactivation (Wutz and Jaenisch, 2000) and display a reduced expression of differentiation markers compared to post-implantation blastocyst.

1.1.2.1.2. ESCs molecular network.

Maintenance of pluripotency in ESCs is determined by the combined action of three transcription factors: Oct4, Sox2 and Nanog (OSN). They are considered the pluripotency core factors because their absence *in vivo* causes the failure in the formation of a complete epiblast (Avilion, 2003; Chambers et al., 2003; Nichols et al., 1998). The pluripotency core plays its role on three levels. Firstly, OSN bind together to enhancers of pluripotent genes and activate their transcription (X. Chen et al., 2008). Secondly, OSN recruit repressive complexes on the regulatory elements of differentiation genes (Bilodeau et al., 2009; Loh et al., 2006). Thirdly, OSN can also promote their own expression, determining the formation of a positive feedback loop that ensures pluripotency maintenance (Boyer et al., 2005; Cole et al., 2008). The OSN core is further supported by ancillary factors tuning and regulating pluripotency maintenance. On the contrary, it can be perturbated by external forces that favour exit from pluripotency and commitment. (Fig.6).

1.1.2.1.2.1. Oct4

Oct4, encoded by the Pou5f1 gene, is an octamer-binding TF fundamental to prevent ESCs differentiation *in vitro* and for ICM formation *in vivo* (Nichols et al., 1998). Its expression arises in blastomeres, then it is restricted to ICM and epiblast and in the adult it is maintained only in primordial germ cells (PGCs) after gastrulation (Pesce and Schöler, 2000). Its level is fine tuned in ESCS: its overexpression leads to primitive endoderm and mesoderm commitment, while its acute deletion induces progressively trophectodermal differentiation (Niwa et al., 2000). Moreover, limited levels of monoallelic Oct4, obtained using Oct4 heterozygous ESCs, showed a stabilized uniform naïve state (Karwacki-Neisius et al., 2013)

Together with Sox2, they are expressed in every pluripotent state and they orchestrate the acquisition and maintenance of pluripotency (Avilion, 2003; Masui et al., 2007; Nichols et al., 1998).

1.1.2.1.2.2. Sox2

Sex determining region Y-Box or Sox2 is a member of the Sox family, a class of TFs characterized by the HMG DNA-binding domain (Lefebvre et al., 2007). Sox2 deletion is embryonically lethal due to the failure in the formation of the pluripotent epiblast (Avilion, 2003). Its expression begins in the morula, and in the pre-implantation embryo it is specific of the pluripotent compartment (ICM and epiblast) (Avilion, 2003). However, after gastrulation, Sox2 is still expressed and plays a role in neural differentiation, antagonising other lineages differentiation (Zhao et al., 2004). In an opposite way, Oct4 favours meso-endodermal differentiation against neurectoderm lineage (Thomson et al., 2011).

In ESCs, Oct4 and Sox2 composes heterodimer complexes at juxtaposed Oct-Sox sites, formed by the octamers recognised by Oct4 followed shortly by Sox binding sites (Ambrosetti et al., 1997; Loh et al., 2006). Interestingly, deletion of Sox2 is not detrimental for ESCs maintenance if it is counter-balanced by Oct4 overexpression. This could suggest that the main role of Sox2 in the pluripotency core is to ensure Oct4 binding to specific target sites (Masui et al., 2007).

1.1.2.1.2.3. Nanog

Nanog belongs to the family of the homeobox TFs. *In vivo*, it is highly expressed until mid-blastocyst and it is quickly downregulated at the onset of implantation (Chambers et al., 2003). Its absence causes embryonic lethality due to the impaired development of the ICM towards Epi and PE (Mitsui et al., 2003). On the contrary, its deletion in ESCs doesn't induce differentiation and Nanog knock-out (KO) cells can self-renew, even if their tendency to differentiate is higher and they cannot contribute to the germ line (Chambers et al., 2007a). From these data, it seems that Nanog has a critical role in *in vivo* pluripotency, while *in vitro* KO ESCs can be amplified thanks to culture conditions. This is in line with the data showing that Nanog sustained expression in ESCs homogenizes the levels of Rex1, Klf4 and other naïve pluripotency markers, which constantly fluctuate at the single-cell level in the heterogeneous ESC population (MacArthur et al., 2012). Nanog sustained expression is sufficient to maintain cells in the pluripotent state upon withdrawal of cytokines required for ESCs self-renewal. These evidences consolidates the importance of this TF for the naïve pluripotency maintenance (Chambers et al., 2003). Interestingly, even if Oct4/Sox2 and Nanog has their own target sites, the

three transcription factors can interact together and bind common elements to govern pluripotency in ESCs (Loh et al., 2006).

1.1.2.1.2.4. Ancillary factors and differentiation signals

Other signals contribute to regulate the balance between pluripotency and differentiation. Ancillary factors, not strictly required for early pre-implantation development, can favour self-renewal and pluripotency maintenance. Above them, we can mention Esrrb, Tcfp2l1, Klf2, Klf4, Sall4 and Prdm14 (Hackett and Surani, 2014). For example, Esrrb, the estrogen-related receptor beta, interacts with Oct4 and positively regulates Nanog activity (van den Berg et al., 2008). Moreover, Esrrb is a Nanog target gene. Its overexpression can replace Nanog requirement in cytokine-independent ESCs culture and its deletion impacts severely the ESCs self-renewal (Festuccia et al., 2012).

On the contrary, some factors, even if expressed by ESCs, antagonize pluripotency and promote commitment and differentiation. For example, Tcf3 is one of the major negative regulators of pluripotency expressed in ESCs. It binds the same loci recognized by the OSN core, mediating an antagonistic effect (Cole et al., 2008). Other examples are the P-ERK and NuRD complex activities (see above for details about these two differentiation inducers).

Interestingly, these factors negatively regulating pluripotency are nonetheless expressed in ESCs. What is the biological significance of these “rebel” factors? Considering that *in vivo* pluripotency is a short developmental stage before differentiation onset, and that pluripotent cells are intrinsically poised to commitment, these factors could constitute a trigger for rapid differentiation and a buffer mechanism counteracting pluripotent factors to avoid an excessively slow exit from the naïve state.

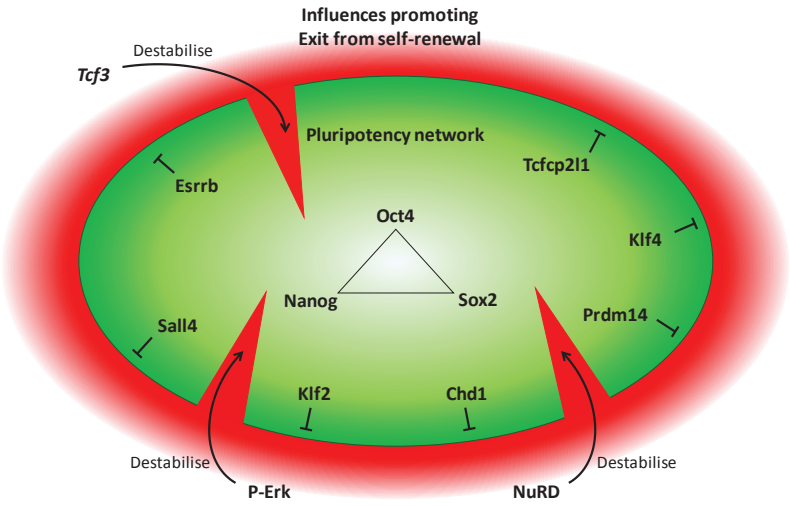

Figure 6: (Adapted from Hackett et al., 2014). Representation of the equilibrium between factors maintaining pluripotency against influences promoting differentiation. OSN core works together with ancillary factors (represented on the interior border) to avoid commitment induces by differentiating forces (represented on the outside).

1.1.2.1.3. Epigenetic landscape of ESCs

Epigenetic plays a fundamental role for ESCs maintenance at two levels. It is required for the establishment of a high transcription rate characteristic of ESCs and necessary for rapid proliferation. Moreover, epigenetic complexes, together with pluripotency transcription factors, regulate self-renewal and pluripotency.

ESCs are characterized by high transcriptional and translational rate, in line with the high demand of macromolecules to sustain their fast proliferation (Bulut-Karslioglu et al., 2018). This hyper-transcription is regulated by open chromatin: ESCs present a genome which is largely hypomethylated and the global DNA methylation is restored during differentiation (Leitch et al., 2013). Indeed, ESCs can be established and maintained in absence of DNA methylation: the combined deletion of DNA methyltransferase Dnmt1, Dnmt3a and Dnmt3n does not affect ESCs self-renewal and pluripotency (Meissner, 2005; Tsumura et al., 2006). However, the reacquisition of the epigenetic marks provided by Dnmts is fundamental for differentiation (Jackson et al., 2004). In a parallel way, DNA demethylases Tet are strongly expressed in ESCs and decreased during differentiation (Ito et al., 2010). There is a positive regulatory loop governing permissive chromatin, transcription

and translation in ESCs, where chromatin activators have short half-life and are constantly produced by growing cells. This loop is finely tuned by cellular growth: if cells stop to grow, the absence of growth signals (like mTOR and c-Myc) negatively impacts the activity of epigenetic activators, leading to a closer chromatin state and a reduction in the hyper-transcription and in translation of the epigenetic factors (Bulut-Karslioglu et al., 2018).

Moreover, epigenetic factors are required for the precise control of self-renewal and pluripotency in ESCs. We can distinguish different classes of epigenetic factors operating in ESCs: histone-modifying enzymes, ATP-dependent remodelling complexes and DNA methyltransferases.

Histone modifying enzymes deposit or erase epigenetic marks like methylation and acetylation on histones, the fundamental units of chromatin architecture. This class of enzymes plays an important role in the regulation of differentiation genes, repressing them and, at the same time, poising them for quick activation. This is reached thanks to the formation of bivalent marks at developmental genes promoters (Bernstein et al., 2006). These promoters are at the same time characterized by the activating H3K4me2/3 modifications, deposited by Trithorax group (TrxG) complex, and the repressive H3K27me3 marks, placed by the Polycomb repressive complex 2 (PRC2) (Ang et al., 2011; Azuara et al., 2006). In this way, rapid gene expression can be quickly achieved by erasing H3K27me3.

ATP-dependent remodelling complexes carry out their function using ATP as an energy source to modify nucleosome disposition. For example, the chromodomain factor Chd1 is fundamental for maintaining chromatin in an open state and it is required for ESCs self-renewal and pluripotency (Gaspar-Maia et al., 2009, p. 1). On the contrary, the NuRD complex forces ESCs to commitment. Thanks to its core subunit Mbd3, the complex recruits PRC2, which deposits H3K27me3 repressive marks on promoters of pluripotency genes, poising the cells towards exit from pluripotency and commitment (Reynolds et al., 2012).

DNA methyltransferases (Dnmts) are enzymes that promote the transfer of methyl groups on DNA, leading to gene activation or repression. Even if these enzymes are expressed in ESCs, the genome of these cells is globally hypomethylated (Leitch et

al., 2013), thanks to the action of opposite epigenetic factor hindering Dnmts action. For example, PRDM14 is an epigenetic factor inducing demethylation and preserving pluripotency: this PRC complex component represses the Fgf differentiation pathway and co-occupies the same genomic loci as Nanog and Esrrb, promoting a naïve transcriptome. At the same time, it represses de-novo methylation orchestrated by Dnmts, mediating a naïve epigenome (Yamaji et al., 2013) (Fig.7).

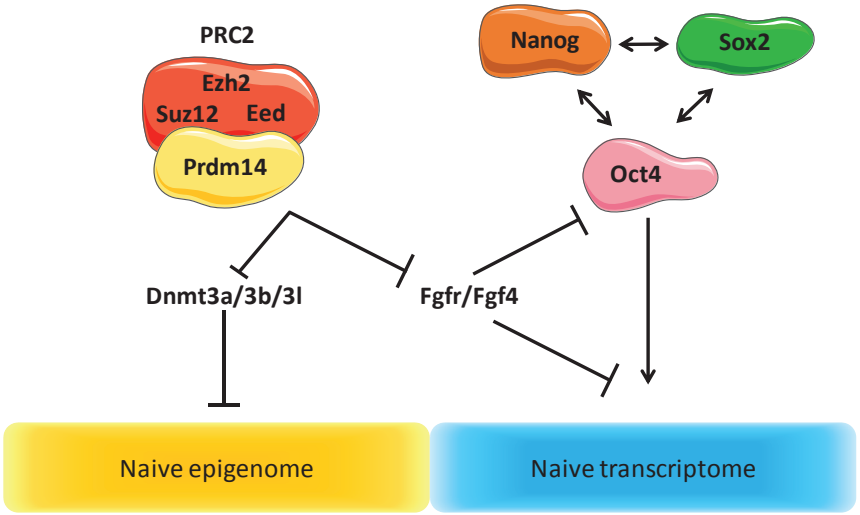

Figure 7: (Adapted from Yamaji et al., 20134). PRDM14 action in ESCs. The PRC2 component inhibits the Fgf pathway and repress Dnmts, promoting pluripotency through an induction of a naïve epigenome and transcriptome.

1.1.2.2. Epiblast stem cells – model for primed pluripotency

Epiblast stem cells or EpiSCs are primed pluripotent cells that recapitulate the post-implantation epiblast. They were derived for the first time in 2007 from the mouse post-implantation blastocyst, between day 5.5 and 6.5, in the presence of Fgf and Activin/Nodal. After their establishment, they are grown in the presence of both signals (Brons et al., 2007; Tesar et al., 2007). In contrast to dome-like and rounded ESCs colonies, they form large and flat colonies, similar to human ESCs.

They can give rise to the three germ layers, as suggested by *in vitro* and *in vivo* tests. They can contribute to chimaera when injected in the post-implantation blastocyst, but fail to colonize pre-implantation epiblast, highlighting the different molecular characteristics of

the naïve and primed configurations (Huang et al., 2012). Unlike ESCs, they show inactivation of X chromosome in female lines and they repress naïve markers, expressing primed pluripotency genes associated with the commitment initiation.

On a molecular level, compared to ESCs, Oct4 and Sox2 are similarly expressed, but Nanog levels are decreased and other naïve markers, such as Esrrb, Klf2, Klf4, Rex1 and Prdm14, are absent. (Tesar et al., 2007). However, Oct4 regulation differs between the two cellular models: while in ESCs Oct4 expression is driven from its distal element, in EpiSCs it is controlled by the proximal element (Choi et al., 2016). Concomitant with the loss of naïve markers, they acquire new expression of primed markers, such as Fgf5, Otx2, Gata6, Brachyury and Zic2. In particular, the Otx2 homeobox TF induces the redistribution of Oct4 towards previously inaccessible enhancers, leading to substantial transcription changes (Buecker et al., 2014).

At an epigenetic level, EpiSCs are similar to ESCs concerning global methylation levels. However, they have a more pronounced methylation pattern at germline-specific genes promoters or promoters which are bivalent or marked by H3K27me3 in ESCs (Hackett et al., 2013). Interestingly, during the switch from ESCs to EpiSCs, a reconfiguration of the enhancers of active genes takes place. Some genes, controlled by proximal enhancers in ESCs, switch to a distal regulation in EpiSCs. These distal elements have higher sequence conservation and their activity is maintained in differentiated cells (Factor et al., 2014).

1.1.3. Pathway dynamics in the pre- and post-implantation embryo

Several pathways dictate the development of the pluripotent compartment from the ICM until the post-implantation embryo. Indeed, the maintenance in culture of the *in vitro* models ESCs and EpiSCs is also dependent on signalling pathways. In the complexity of this regulation, three pathways boost pre-implantation/ICM state, Lif-Jak-Stat, BMP and Wnt. On the other hand, Fgf-Mapk-Erk and Activin/Nodal regulate the post-implantation/Late Epi (Posfai et al., 2014).

Interestingly, not all the pathways necessary *in vitro* are strictly required *in vivo.* How can we explain this difference? The *in vivo* environment is more complex, and the absence of a precise signal is probably compensated from redundant mechanisms. Another discrepancy relies on the time differences between the long culture of established ESCs compared to the rapid changes in the *in vivo* pluripotent compartment: according to this second hypothesis, some pathways would not be required *in vivo* because the rapid developmental kinetics

would not allow the emergence of the negative phenotypes. In this section, I will detail the mechanisms and function of these pathway, focusing my attention on their role in *in vitro* models, ESCs and EpiSCs.

1.1.3.1. LIF

Leukaemia inhibitor factor (Lif) is a member of the Interleukin 6 (Il6) family of cytokines. It is a fundamental signal for ESCs propagation *in vitro*, as far as its withdrawal induces a rapid differentiation in a population formed by mixed mesoderm and endoderm cells (Smith et al., 1988; Williams et al., 1988). This phenotype is attributed to its role in the stabilization of the core pluripotency network, formed by Oct4, Sox2 and Nanog (OSN), through two independent pathways (Nakai-Futatsugi and Niwa, 2013; Smith et al., 1988). In the first pathway, the Lif-Jak-Stat pathway, Lif binds its receptor Lifr and coreceptor Gp130 (Gearing et al., 1991). The binding induces the recruitment of the Jak kinase, which phosphorylates tyrosine residues on the heterodimeric receptor. The activated complex works as a docking platform and recruits Stat3 by its SH2 domain. In this site, Stat3 can be phosphorylated by Jak (Stahl et al., 1995). Once phosphorylated, Stat3 translocates into the nucleus, where it forms homodimers and binds to its target genes (Sasse et al., 1997). Among them, we can find the pluripotency transcription factor Klf4, which positively regulates Sox2 expression (Niwa et al., 2009). In ESCs, the Jak-Stat axis represents the major pathway for Lif signalling, as far as Lif fails to support ESCs maintenance in a Stat3-/- background (Hall et al., 2009a).

In parallel, Lif mediates the Pi3K (phosphoinositide 3-kinase)/Akt pathway. Pi3K is a lipid kinase which phosphorylates inositol phospholipids as substrate. In specific, it converts Pip2 (phosphatidylinositol-4,5-biphosphate) into Pip3 (phosphatidylinositol-3,4,5-triphosphate) (Cantley, 2002). Once phosphorylated, Pip3 recruits the serine/threonine kinase Akt1 at the inner cell membrane, where Akt1 is phosphorylated and activated by the Pi3k-dependent kinase-1 Pdk1. Once activated, Akt1 influences different signalling pathways through regulation of its substrates IKK, Mdm2 and mTOR. Tbx3 is a T-box transcription factor which control Nanog expression (Niwa et al., 2009). Interestingly, the pluripotency factor Tbx3 expression is dependent on the Pi3k/Akt pathway, and, in Lif-withdrawal condition, sustained expression of Akt1 is sufficient to ensure Tbx3 and Nanog expression (Niwa et al., 2009).

Thus, Lif signalling through two different pathways, Jak/Stat and Pi3/Akt, sustains the expression of Sox2 and Nanog, maintaining in a positive loop the pluripotency core circuit.

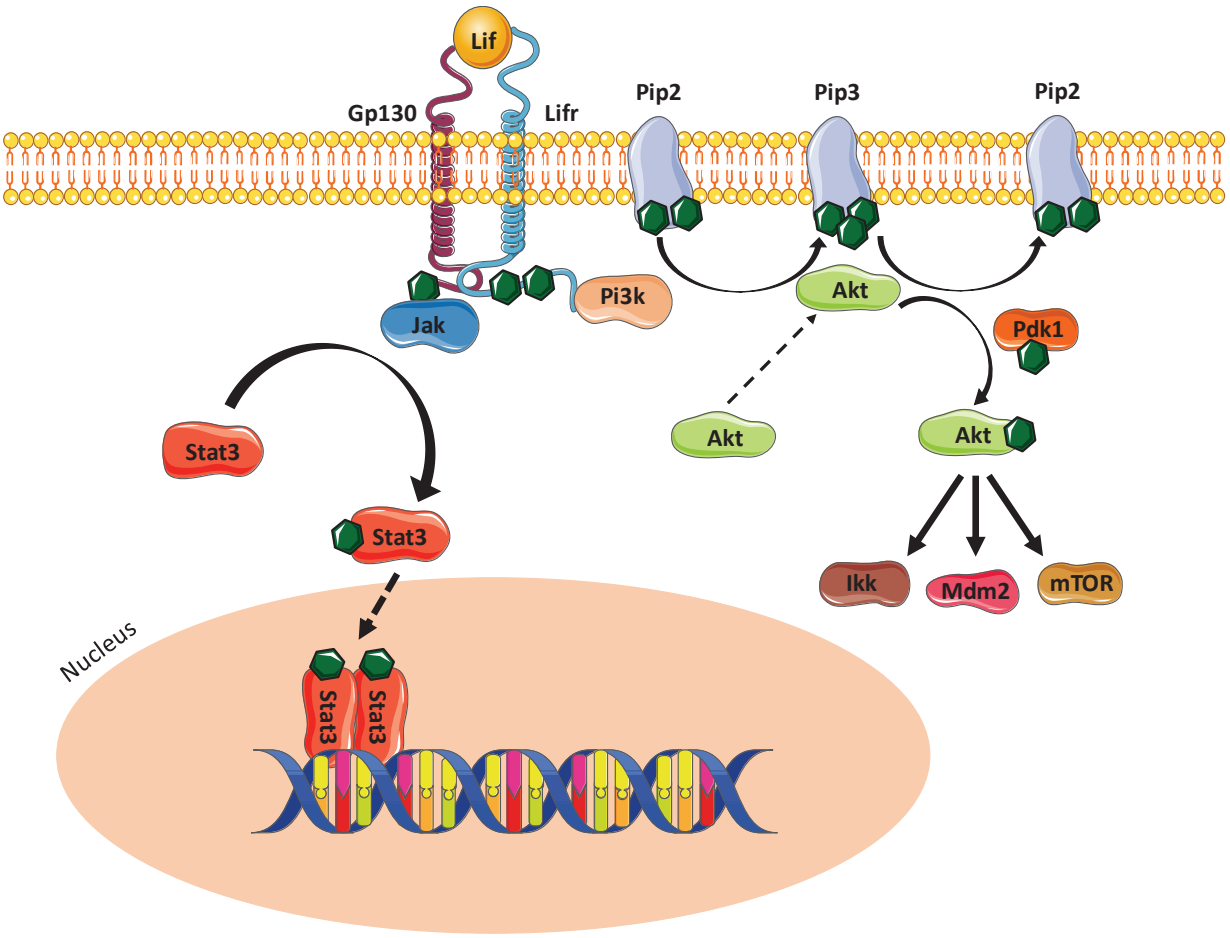

Figure 8: Lif signalling through Jak-Stat and Pi3k-Akt pathways leads to the activation of pluripotency genes (Sox2, Nanog) and maintenance of naïve ESCs.

Interestingly, Lif signalling induces a third pathway, the Mapk-Mek-Erk cascade (see below for the details of this pathway), a differentiation pathway which leads to ESCscommitment. Which is the role of this mechanism? Why does the same ligand activate pluripotency and commitment pathways? There are two explications for this apparently contradictory mechanism. First, in ESCs, low levels of Erk activity are fundamental for cell proliferation and cell cycle progression. Erk supresses cell apoptosis, it plays a role in telomerases activity and it safeguards genome stability (H. Chen et al., 2015; Guo et al., 2013). Lif signalling induces basal level of Erk, required to maintain these physiological roles. Indeed, Erk activates developmental genes and represses pluripotency genes only when it is highly induced by Fgf (Brumbaugh et al., 2014; Kim et

al., 2012; Lai et al., 2012). This differential signalling renders Erk a crucial sensor in ESCs biology. In fact, ESCs linger in an equilibrium state: they maintain self-renewal and pluripotency, and, at the same time, they need to quickly respond to external cues and differentiate. Taking into account the necessity of a rapid differentiation, Lif activation of the Mapk-Mek-Erk pathway constitutes a great advantage for ESCs, as far as the Mapk cascade is already basally active and ready to receive the Fgf differentiation signal. In line with this, Phospho-Erk (P-Erk) maintains in a poised state many promoters of developmental genes, binding their sites to avoid TFIIH occupancy and phosphorylating RNAPolII (Tee et al., 2014) (**Fig.9**).

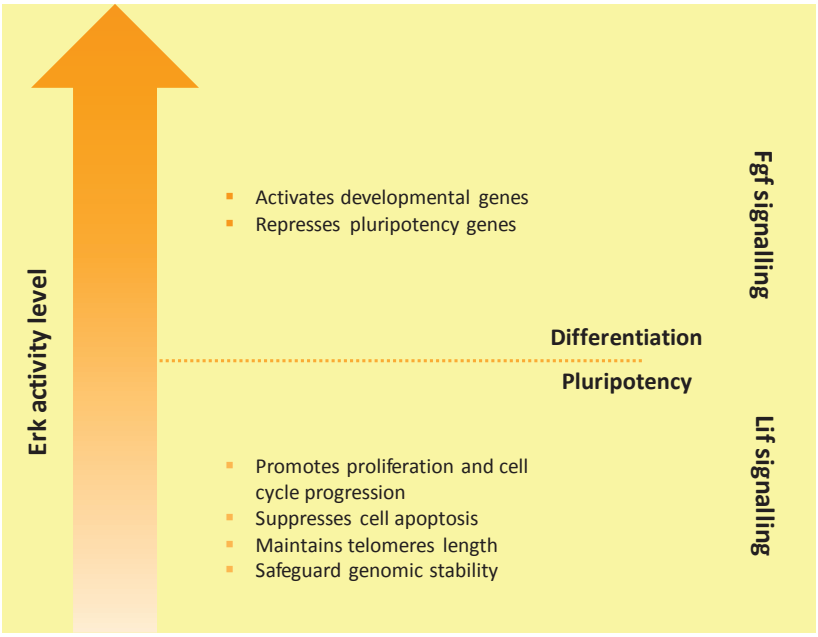

Figure 9: Erk activity in maintenance of pluripotency and commitment. Different levels of P-Erk induces opposite responses in ESCs. While low level of P-Erk favours ESCs homeostasis, higher levels mediate their differentiation.

1.1.3.2. BMP

Bone morphogenetic factor (Bmp) is a member of the transforming growth factor beta (TGFβ) superfamily. Its signalling is beneficial for ESCs maintenance: in serum-deprived conditions, Bmp is sufficient in combination with Lif to maintain the ESCs undifferentiated state (Ying et al., 2003a). There are two types of Bmp receptors, I and II: in ESCs, there is only one receptor of type 1, BmprII, and three receptors of classe II, Alk2, Alk3 and Alk6. BmprII interacts with one of the Alks to create a heterodimeric complex. In ESCs, Bmp4 binding induces the phosphorylation of BmprII by the Alk component. The activated receptor phosphorylates Smad proteins, Smad1,3 and 8, the principal effectors of the pathway. Smad proteins form heterotrimeric complexes with Smad4 and translocate to the nucleus where they act as transcription factors (Shi and Massagué, 2003) (**Fig.10**).

One of the principal targets of Bmp signalling is the Id TF family. Notably, Id2 is described to avoid neuronal differentiation in ESC, consistent with Bmp inducing non-neuronal differentiation. Interestingly, in serum-free conditions, Lif alone cannot maintain pluripotency, but ESCs differentiate towards neuronal lineage (Ying et al., 2003a). Indeed, complementary expression of Lif and Bmp in free-medium conditions creates an equilibrium that sustains pluripotency, with Lif preventing mesoderm and endoderm differentiation and Bmp interfering with the neuronal commitment. The Fgf-Mapk-Erk pathway can induce neuronal differentiation (Ying et al., 2003b). Bmp signalling inhibits this pathway: the Smad1,4,5 heterotrimer activates the diphosphatase Dusp9, which de-phosphorylates and inhibits Erk (Li et al., 2012). In response, Fgf-Mapk-Erk can inhibit the Bmp pathway phosphorylating Smad1 at the link region. This phosphorylation enables the interaction of the Smad1 effector domain with its intrinsic inhibitory domain, resulting in the abolition of Smad heterotrimers formation and Bmp signalling inhibition (Kretzschmar et al., 1997).

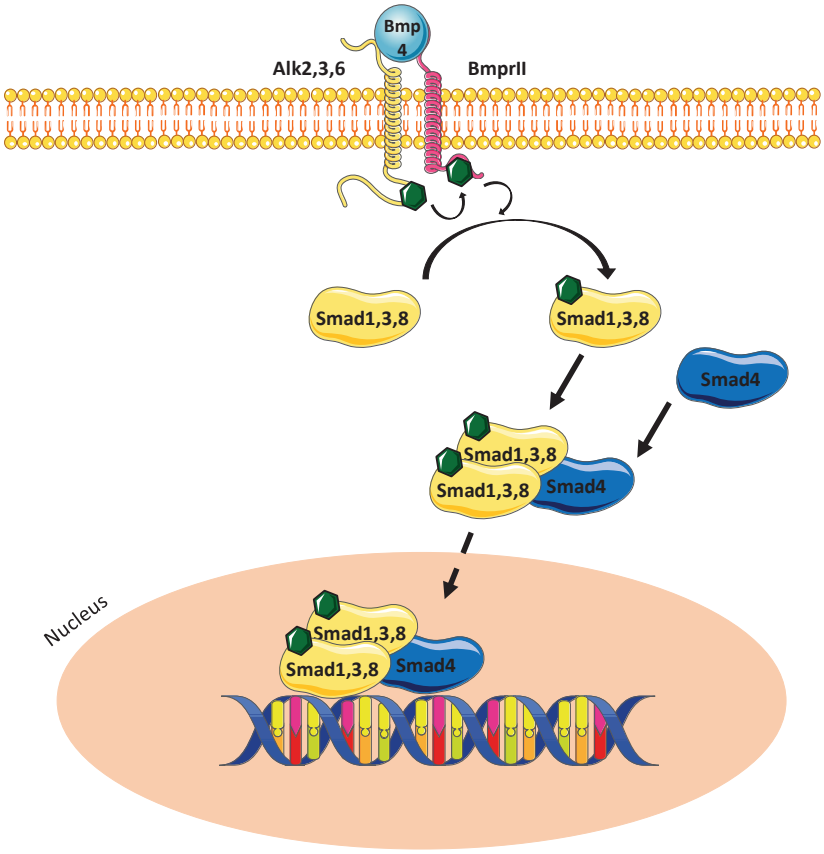

Figure 8: BMP signalling in ESCs. The activation of this pathway mediates neural differentiation repression. In combination with Lif, it can sustain ESCs in serum- and feeder-free conditions

1.1.3.3. WNT

Firstly discovered in Drosophila, as Wingless (Wg), Wnt is one of the principal pathways in embryonic development and adult tissue homeostasis (Wiese et al., 2018). In ESCs, Wnt plays a double role: while it contributes positively to ensure self-renewal, its activity is also fundamental to ensure the transition to post-implantation epiblast and the following developmental processes (in particular gastrulation (Haegel et al., 1995)). The major effector of Wnt is β-catenin. In absence of Wnt signalling, β-catenin levels are low, because the protein is phosphorylated by the destructor complex, formed by Axin, APC, and Gsk3α/β, and degraded via the SCFβ-TRCP E3-ubiquitin ligase, resulting in constant proteolysis of neo-synthesized β-catenin (Amit, 2002; Hart et al., 1998; Liu et al., 2002; Rubinfeld et al., 1993). After synthesis and palmitoylation, Wnt is secreted in the extracellular space (Bartscherer et al., 2006; Willert et al., 2003). Once secreted, Wnt binds its receptor Frizzled (Frz) and its coreceptor Lrp5/6 (Tamai et al., 2000). The formation of the Wnt-Frz-Lrp complex enables the recruitment of Dishevelled (Dsh) via the interaction of Frz with Dsh. In turn, Dsh recruits to the membrane the Axin,

destabilising the destructor complex (Cong, 2004). This destabilization leads to the phosphorylation of Gsk3 by Lrp5/6, and its consequent degradation, erasing the effects of the destructor complex on β-catenin, not anymore phosphorylated by Gsk3 (Piao et al., 2008; Stamos et al., 2014). In this way, β-catenin is able to translocate to the nucleus, where it acts as a transcriptional co-activator for the members of the DNA binding Tcf/Lef family (van de Wetering et al., 1997) (**Fig.9**).

In classical serum+Lif culture conditions, Wnt is not fundamental for ESCs self-renewal and maintenance: β-catenin KO ESCs display defects in focal adhesion of colonies, showing colonies with loose associated cells, but ESCs self-renew normally and form chimera when injected in the blastocyst (Haegel et al., 1995; Huelsken et al., 2000). However, Wnt signalling increase (obtained through Gsk3-inhibitor BIO or recombinant Wnt3a) renders ESCs cultures Lif-independent, suggesting a role of Wnt in ESCs self-renewal (Sato et al., 2004). Indeed, ESCs secrete Wnt in the medium (ten Berge et al., 2011), explaining the unnecessity of Wnt addition to the medium. Interestingly, blocking the ligand secretion by IWP2 leads to loss of ESC colonies morphology, downregulation of naïve markers Rex1, Pecam1 and Stella and upregulation of primed pluripotency markers Fgf5, Otx2, Dntm3b, supporting the idea that Wnt is fundamental for the maintenance of naïve ESCs and to prevent the switch to the primed state (ten Berge et al., 2011).

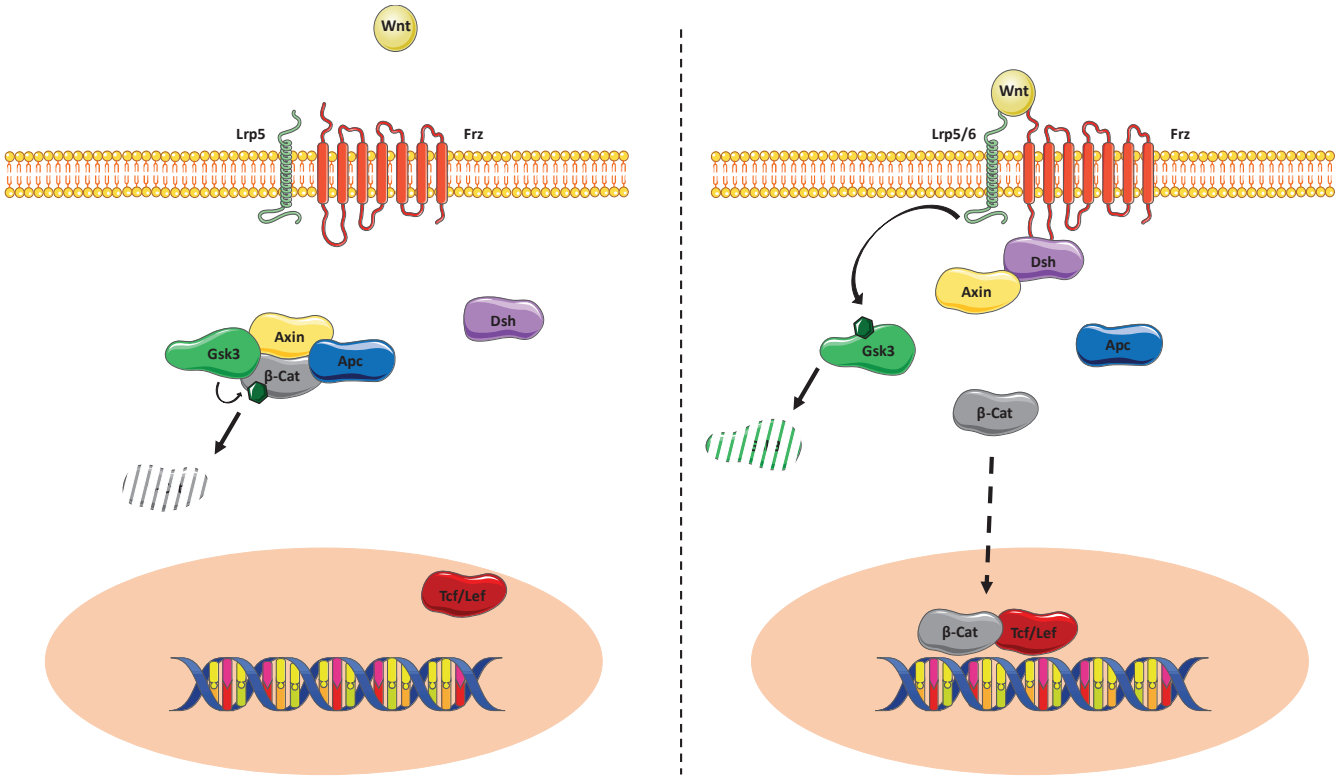

Figure 9: Wnt signalling in ESCs.. Left panel: in the absence of Wnt lignand, β-catenin is degraded by the destruction complex. Right panel: Wnt signalling induces Gsk3 degradation and β-catenin stabilization.

How does β-catenin mediate this self-renewal activity? To answer this question, we need to analyse β-catenin nuclear role. This protein works as a cofactor for the DNA binding Tcf/Lef TFs. The more abundant factor of the family expressed in ESCs is Tcf3 (Pereira et al., 2006), which act as a repressor of ESCs pluripotency and self-renewal: Tcf3-/- ESCs self-renew upon Lif withdrawal and show defects in exit from pluripotency, displaying a delayed differentiation (Yi et al., 2008). Furthermore, RNAi knockdown of Tcf3 favours the maintenance of Nanog-positive colonies upon induction of differentiation by retinoic acid (Schaniel et al., 2009). Moreover, Tcf3 binding sites are majorly co-occupied by OSN, but Tcf3 depletion have opposite phenotypes compared to OSN depletion (Cole et al., 2008; Loh et al., 2006; Marson et al., 2008).
Indeed, when Wnt is activated, high levels of nuclear β-catenin bind Tcf3, resulting in a displacement of this TF from its targets genes and inhibition of its repressing activity on pluripotency (Wray et al., 2011).

At the same time, Wnt is necessary for ESCs differentiation: knock-out of APC or double knock-out (DKO) of Gsk3α and Gsk3β show defects in *in vitro* and *in vivo* differentiation (Doble et al., 2007; Kielman et al., 2002). The phenotypes observed are related to an increase in the endogenous levels of β-catenin, which avoid proper differentiation (Kielman et al., 2002). Indeed, DKO for Gsk3 coupled with inhibition of β-catenin expression leads to rescue the DKO phenotypes (Kelly et al., 2011).

1.1.3.4. FGF

Fgf is one of the major pathways regulating early embryonic development. *In vivo*, its signalling is fundamental to establish the proper segregation in epiblast and PE: mice knock-out (KO) for Fgf4 die immediately after implantation (Feldman et al., 1995). Moreover, Fgf signalling is required for ESCs differentiation and EpiSCs maintenance *in vitro* (Kunath et al., 2007; Tesar et al., 2007). In ESCs, the Fgf4 ligand cooperates with the extracellular heparan sulfate proteoclygans (Hspgs) to bind the Fgfr2 receptor (Ornitz, 2000). The formation of the heterotrimeric complex Fgf-Fgfr-Hspg guides the homodimerization of two receptor molecules and their reciprocal trans-phosphorylation, creating the active receptor (Goetz and Mohammadi, 2013). The activated receptor

induces four different pathways: Ras-Mapk, Pi3k-Akt, Plcγ, and Stat pathways. In ESCs, the predominant signalling consists in the Ras-Mapk axis. In this pathway, Fgfr2 phosphorylates the major substrate Frs2α, which then recruits guanine nucleotide exchange factor Sos through the adaptor protein Grb2, leading to Sos activation (Kouhara et al., 1997, p.). Sos adds a guanine group to the GDPase Ras, activating it. The active GTPase Ras can induce the Mapk kinase cascade, characterized by a stepwise phosphorylation of Raf, Mek and finally Erk (Zhang and Liu, 2002). Erk, once phosphorylated, translocates to the nucleus and activates transcription factors downstream to the Fgf/Mapk/Erk pathway (Firnberg and Neubüser, 2002, p. 2) (**Fig.10**).

The activation of the FGF signalling leads to ESCs differentiation. Fgf4 KO ESCs do not have detrimental effects on cell proliferation, suggesting that Fgf4 is not necessary for self-renewal, while they exhibit defects in exit from pluripotency and engagement of commitment (Kunath et al., 2007; Wilder et al., 1997). In this direction, during neural differentiation, inhibition of Fgfr or Erk abolishes neural induction, with cells expressing the epiblast marker Fgf5 and pluripotency marker Nanog, suggesting that Fgf signalling is required for ESCs differentiation (Stavridis et al., 2007). In a parallel study, withdrawal of Lif from culture conditions induces neuronal differentiation of ESCs. In this set, Fgf-null ESCs were not able to differentiate, but the deficit was restored upon Fgf recombinant treatment, with ESCs giving rise to neural and also mesodermal lineages (Kunath et al., 2007). Similar results were obtained with Mek inhibitor, Fgfr inhibitor and ERK2-/- ESCs. The blocking of differentiation observed after Fgf suppression was also used in a practical way: Mek inhibition combined with Lif and Bmp4 led to derived mESCs from recalcitrant C57BL/6 and CBA strains (Batlle-Morera et al., 2008).
How does Fgf regulate exit from pluripotency and early differentiation? Erk phosphorylates Stat3 at the serine 727. This leads to its inactivation and to the blockade of Lif-Jak-Stat signalling, priming ESCs to differentiation (Huang et al., 2014). In a parallel way, Erk interacts with the activation domain of the naïve marker Klf4, inhibiting it by phosphorylation on the serine 123 (Kim et al., 2012).

ESCs in normal condition (serum + Lif) are characterized by a metastable state in which a dynamic heterogeneous expression of pluripotency and differentiation factors fluctuates in time at single-cell and population level. This has been well described in many studies, using reporter lines for pluripotency markers, as Nanog, Rex1 and Stella, which showed that at each moment, in the global ESCs population, a fraction of cells express naïve

pluripotency markers, while another fraction is primed to commitment, expressing differentiation markers like Brachyury, Gata6 and Sox17 (Chambers et al., 2007b; Hayashi et al., 2008; Toyooka et al., 2008). Indeed, Fgf plays an important role together with other pluripotency pathways to establish this equilibrium. To provide this fine-tuning, Fgf presents different negative feedbacks allowing quick reversion of primed ESCs to a naïve state. For example, ESCs treated with Fgf inhibitor revealed a downregulation of Dusp4 and Dusp6, known Fgf signalling inhibitors, and decrease of Spred1, a Ras/Erk inhibitor, suggesting that in normal condition Fgf modulates the expression of its own inhibitors (Lanner et al., 2009).

Combined action of Activin and Fgf signalling dictates the maintenance of EpiSCs, inhibiting differentiation to neural lineage and at the same time avoiding reversion to ESCs-like state (Greber et al., 2010). This is surprising, considering that Fgf has been previously described to being required for neural differentiation (Kunath et al., 2007). Indeed, although Fgf is important for the primary differentiation of ESCs to post-implantation EpiSCs, its activity inhibits further neuronal differentiation (Stavridis et al., 2010).

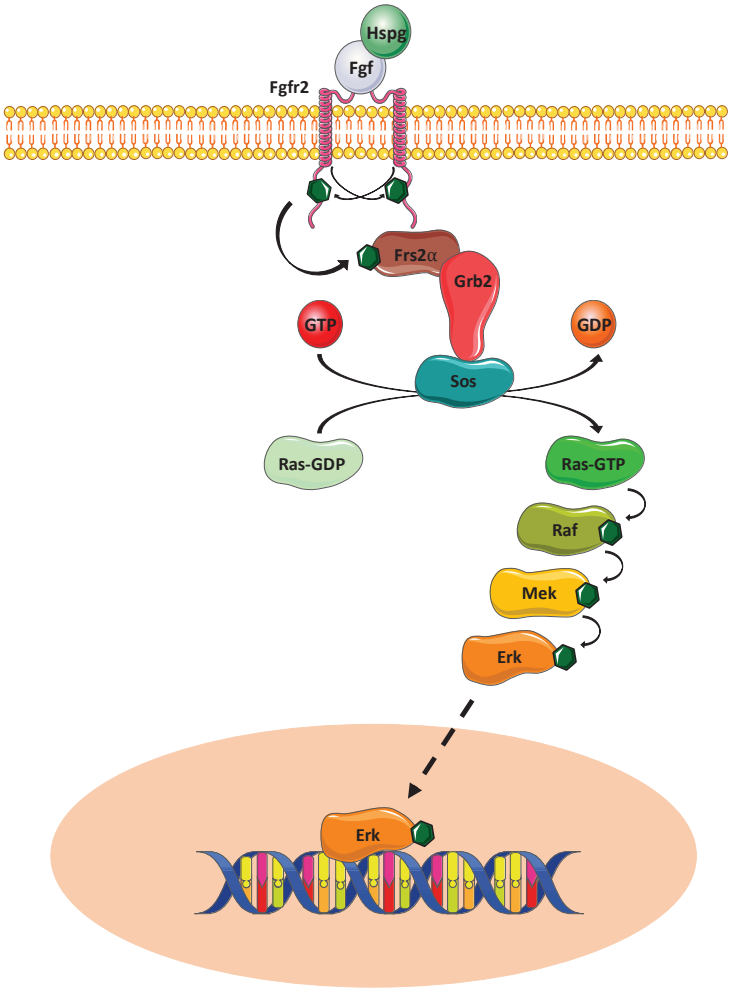

Figure 10: Fgf signalling in ESCs. The signalling activation induces ESCs differentiation, thus its levels are strictly controlled to avoid aberrant commitment. It is important for maintenance in culture of EpiSCs.

1.1.3.5. NODAL/ACTIVIN

Activin and Nodal are members of the transforming growth factor beta (TGFβ) superfamily. They can both bind the same receptors and induce the same response. For these reasons, we usually talk about Nodal/Activin pathway. *In vivo*, loss of their signalling causes hypo-proliferation, downregulation of pluripotent markers and expression of neuroectodermal genes in post-implantation embryos, leading to failure in mesoderm and definitive endoderm formation (Camus et al., 2006). *In vitro*, this pathway is sufficient and necessary to establish and maintain EpiSCs (Brons et al., 2007; Tesar et al., 2007). Concerning Nodal/Activin pathway, there is only a Nodal gene in mammals (Zhou et al., 1993). Nodal is translated as an inactive precursor, then cleaved by Spc1 and Spc4 (Constam and Robertson, 2000). Once activated, it forms homo-dimeric ligands through disulphide bounds. Activins are formed by the dimerization of Inhibin subunits (βa, βb, βc and βe). Concerning their receptors, Activin and Nodal recognize type II Activin receptors

and type I Alk receptors, particularly Alk4 (Tsuchida et al., 2004). As in Bmp signalling, activation of receptors phosphorylates Smad effectors and leads to the formation of the heterotrimeric Smad complexes, but, in this case, the Smad proteins involved are Smad2,3 and 4 (Massague, 2005) (**Fig.11**).

Nodal/Activin pathway covers a quite limited role in ESCs: its inhibition obtained by chemicals inhibitors, Smad7 upregulation or Smad2 knockdown has no evident effects on self-renewal and pluripotency network in serum+Lif conditions. However, when Lif is withdrawn, Nodal/Activin signalling ensures proliferation and propagation of ESCs (Ogawa et al., 2006). This is consistent with the binding of Smad2 on Oct4 promoter (always in Lif-withdrawal conditions) and with the activation of trophectodermal genes observed upon the pathway inhibition (Lee et al., 2011, p. 2).
Moreover, as Fgf induces neurectoderm differentiation (Stavridis et al., 2007), overexpression of Nodal in ESCs leads to mesodermal and definitive endodermal commitment, while inhibiting neurectoderm formation (Pfendler et al., 2005).

Nodal/Activin signal is fundamental for EpiSCs propagation: suppression of the pattern leads to loss of pluripotency and neurectodermal differentiation (Vallier et al., 2009). This is consistent with Oct4 and Nanog being two major target genes of the pathway (Lee et al., 2011; Vallier et al., 2009).

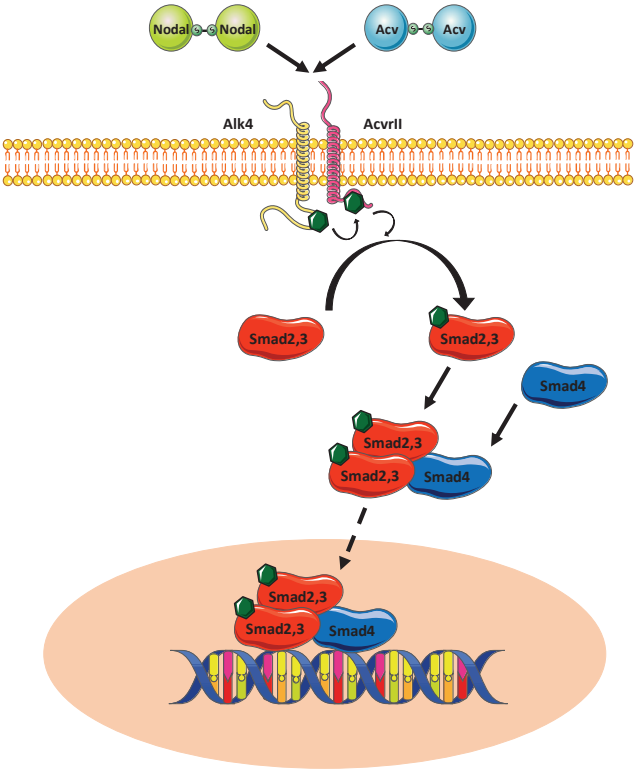

Figure 11: Nodal/Activin signalling maintains ESCs and EpiSCs. The signalling is fundamental for EpiSCs culture, while it is important to maintain pluripotency in ESCs only in Lif-depleted conditions.

1.1.4. Changes in cellular identity in the embryo until the post-implantation stage

Following the classical view, embryonic development is an unidirectional process, where cells become more and more specialized, and cellular plasticity is gradually and irreversibly lost.

However, the situation is not as simplistic as this description. Thanks to exterior signals or expression of TFs, cells can transit towards different states in a more plastic way and reconvert from a more committed state to a more naïve, highlighting the fallacy of the unidirectional and irreversible model.

Indeed, primed EpiSCs can revert to a ESC state thanks to different mechanisms (Guo et al., 2009; Hanna et al., 2009a), and heterogenous naïve ESCs can achieve a configuration where pluripotent markers are more homogeneous and cells are refractory to commitment, known as ground state (Ying et al., 2008). Interestingly, these two processes are reversible, with ESCs going back to EpiSCs and ground state-ESCs reverting to heterogeneous naïve ESCs.

1.1.4.1. From naive to ground state

The discovery of ground state was based on the fact that ESCs are present in a metastable state, where, at single-cell level, they both express transiently naïve and primed markers (Chambers et al., 2007b; Hayashi et al., 2008; Toyooka et al., 2008). Indeed, Erk and Tcf3, direct effectors of Fgf and Wnt pathways, are two of the major forces orchestrating commitment and driving the expression of primed genes (Brumbaugh et al., 2014; Cole et al., 2008; Kunath et al., 2007; Yi et al., 2008). On the other hand, the pluripotency core composed by OSN transcription factors antagonises the action of these differentiating signals.

Thus, Smith and colleagues postulated that isolation of ESCs by depriving them from external signals would allow the OSN core to work undisturbed and promotes a naïve homogeneous state. This hypothesis was consistent with studies showing that (i) inhibition of GSK3, and subsequent β-catenin stabilization and Tcf3 inactivation, have positive effects on ESCs self-renewal and pluripotent markers expression (Sato et al., 2004) and (ii) inhibition of MEK, which induces Erk dephosphorylation and inactivation, leads to similar positive phenotypes. Moreover, MEK inhibition allowed to derive ESCs from recalcitrant mice strains (Batlle-Morera et al., 2008).

Based on these observations, Smith and colleagues treated ESCs in deprived-serum condition with a combination of 3 inhibitors, SU5402, PD184352 and CHIR99021, inhibiting FGFR, Erk and GSK3 respectively. They found that, in these signal-deprived condition, ESCs could self-renew independently from Lif-Jak-Stat pathway and contribute to chimaera formation (Ying et al., 2008). The cocktail was later substituted by Lif+2i inhibitors, with CHIR99021 inhibiting GSK3 and PD0325901 for inhibition of MEK, due to the enhanced cell proliferation and ESCs clonogenicity observed in presence of Lif. Indeed, the characteristics of these culture conditions led to the *in vitro* derivation of rat and nonobese diabetic (NOD) mice ESCs (Buehr et al., 2008; Li et al., 2008; Jennifer Nichols et al., 2009).

Transcriptomic signatures of ESCs and 2i-ESCs display notable differences. Interestingly, different studies on 2i-ESCs assess different *in vivo* correspondence, clustering these cells with *in vivo* late morula/early ICM or the E4.5 pre-implantation epiblast (Boroviak et al., 2015; Bulut-Karslioglu et al., 2016). In both cases, these developmental stages represent a more naïve pluripotent compartment compared to the ICM (which correspond to the *in vivo* ESCs counterpart). This is consistent with the fact that 2i-ESCs, compared to ESCs, are characterized by repression of primed markers such as Pax6, Brachyury and Runx1, Nanog biallelic expression and, at the population level, they express uniformly naïve markers such

as Klf4, Rex1 and Nanog (Marks et al., 2012; Miyanari and Torres-Padilla, 2012). This leads to the homogeneous naïve profile and the loss of primed-associated gene expression characteristic of the ground state. Thanks to an approach based on modelling the ground state transcription circuit on an abstract Boolean network, it was possible to define the minimal circuit responsible for ground state maintenance. This model considers three input (Lif stimulation, Gsk3 inhibition and MEK inhibition) which regulate twelve nodes, bound one to another by positive or repressive links (Dunn et al., 2014) (**Fig.12**).

Notably, the switch in culture conditions from serum to 2i and 2i to serum gives rise to the same transcriptomic variations, showing that the two transcriptomes are interconvertible and highlighting the plasticity of ESCs to switch between the two cell states (Marks et al., 2012).

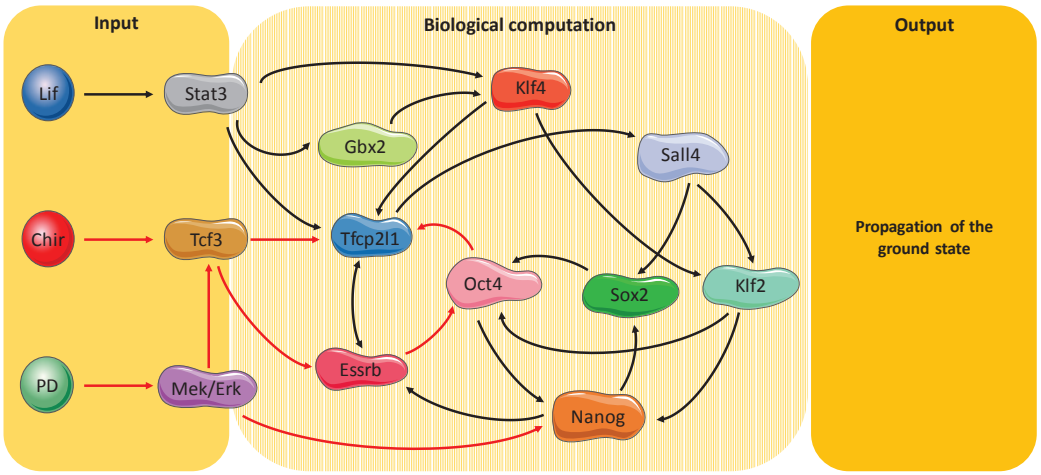

Figure 12: (Adapted from Dunn et al., 2014) Transcriptional circuit of the ground state. Three input are implied in the model (on the left, Lif, ChirON and PD.) Positive interactions are represented by black arrows, negative by red ones.

At an epigenetic level, the global distribution of epigenetic marks on the genome (such as the active mark H3K4me3 and H3K36me3, constitutive mark H3K9me3 and repressive H3K27me3) is similar between serum- and 2i-ESCs. However, in 2i-ESCs, the H3K27me3 mark is decreased at many promoters and this does not correlate with gene expression differences: for example, primed pluripotency genes are not expressed even if the repressive mark is erased from their promoters. In a parallel way, bivalent promoters are decreased for one third in 2i conditions, losing the repressive mark, but they are still not expressed. Indeed, in 2i-ESCs, RNA PolII is increased at transcription starting sites, suggesting an higher promoter proximal pausing, explaining why loss of repressive markers is not

sufficient to induce transcriptional initiation (Marks et al., 2012). Following the hypothesis that 2i-ESCs cluster with the pre-implantation epiblast, this peculiar epigenetic state, characterized by poised promoters of primed pluripotency genes and developmental genes, could constitute a rapid trigger to induce commitment and induction of lineage-specific transcription programs. Thus, RNA PolII pausingmay serve to ensure rapid, coordinated, and synchronous gene expression in response to differentiation signals (Boettiger and Levine, 2009; Nechaev and Adelman, 2011).

1.1.4.2. EpiSCs to ESCs reprogramming

EpiSCs can change their molecular and cellular characteristics and reprogram to ESCs thanks to culture condition and/or genetic modifications. The obtained ESCs show X reactivation and can contribute to chimaeras if injected in the pre-implantation blastocyst, suggesting that the reprogramming gives rise to full-potential ESCs (Bao et al., 2009). Overexpression of Klf2, Klf4 or c-Myc can induce this process together with the switch from Activin+Fgf medium to 2i+Lif medium (Guo et al., 2009; Hall et al., 2009b; Hanna et al., 2009a). Another mechanism for EpiSCs reprogramming requires the re-activation of the distal Oct4 promoter, which is normally preferentially active in ESCs, and, in this settings, switch from Activin+Fgf to serum+Lif conditions are sufficient to induce spontaneous reversion (Bao et al., 2009). Furthermore, reprogramming of EpiSCs is strongly increased by switch to 2i+Lif medium, consistent with the effects of Fgf signalling in EpiSCs in the silencing of Klf2 to avoid spontaneous reprogramming (Greber et al., 2010).

1.2. Transdifferentiation in the somatic cell

According to the classical view of development, once differentiated, a cell keeps its somatic identity, losing its plastic potential (Patel and Hobert, 2017) .

However, this initial inference was revolutionized in the last years: a terminally differentiated cell can lose its specific characteristics and directly convert to a new cell type in a biological process called transdifferentiation. This phenomenon can be accompanied by a reacquisition of cellular plasticity towards an intermediate state. However, this middle step is not required for every transdifferentiation and, in each case, the intermediate populations are instable and quickly differentiate to the new cellular somatic states. In the last decades, many studies have been accomplished showing this process both *in vitro* and *in vivo*.

1.2.1. *In vivo* transdifferentiation

In vivo, transdifferentiation has been described in invertebrates, amphibia and mammals. *C. Elegans* represents a perfect model to study differentiation thanks to the precisely known fate of each cell of the organism. In this animal, transdifferentiation occurs naturally during development, where one precise cell during the second larval stage transdifferentiates from a hindgut cell to a neuron in every animal observed (Jarriault et al., 2008). Changes in cell fate from a germ cell layer to another can also be induced artificially: for example, the transient overexpression of ELT-7 induces pharyngeal margin cells to transdifferentiate into intestinal cells (Riddle et al., 2013).

The amphibian adult newt eye represents a good model of cell fate conversion accompanied by a partial plasticity reacquisition. After lens injury, in a two-step process, pigmented epithelial cells go through an initial de-differentiation, characterized by expression of stem cell markers Klf4 and Sox2 (Maki et al., 2009), followed by a second phase of re-differentiation, defined by expression of γ-crystallin and other lens-specific markers (Mizuno et al., 2002).

In mammals, cell conversion can be observed principally by injury or forced expression of factors. A relevant model of mammal transdifferentiation is the liver. In this tissue, Notch ectopic expression and injuries induce hepatocytes (the principal cellular type of the liver) to transdifferentiate into biliary epithelia cells (BECs), which play a key role in bile secretion (Yanger et al., 2013).

1.2.2. *In vitro* transdifferentiation

In the last years, scientists have developed many protocols to induce transdifferentiation *in vitro*. Here, I will focus on three known examples:

1.2.2.1. Fibroblasts to myoblasts

In this first described model of *in vitro* transdifferentiation, a fibroblast, a mesenchymal precursor involved in ECM formation, connective tissue integrity and wound healing (Tracy et al., 2016), can convert into a myoblast, precursor of muscle cells.

In this first pioneer study, Davis and colleagues showed that fibroblasts transfected with the TF MyoD convert into stable myoblast populations, which contain myosin-positive multinucleate syncitia and express muscle differentiation markers (MHC, MLC1, MLC2) (Davis et al., 1987). Three years later, Choi et collegues showed that, starting from different cell types less and less related to the skeletal lineage (notably, dermal fibroblasts, chondroblasts, gizzard smooth muscle cells and retinal pigmented epithelial cells), the efficiency of myotubes generation changes depending on the initial cell type. Derived myotubes showed typical markers and morphological characteristics (shape, number of nuclei, density of myofibrils) and expressed in the sarcomeres structural proteins like MHC, myomesin and titin (Choi et al., 1990).

1.2.2.2. B cells to macrophages

In this second model, B lymphocytes, immune cells responsible for secreting specific antibodies against pathogens, can transdifferentiate into myeloid macrophages, cells constituting a more general barrier acting in the immune response. In this remarkable study, Xie and colleagues showed that it is possible to directly convert a B cell in a macrophage through a multi-step transdifferentiation process. (Xie et al., 2004).

During this cell fate conversion, C/EBPs proteins (C/EBPα and C/EBPβ) play a fundamental driving role. Indeed, sustained expression of these bZip TFs leads to downregulation of B-cell marker Pax5 and consequent decrease of CD19, E2A and EBF, leading to a loss of B-cell somatic identity. Moreover, cooperation of overexpressed C/EBPs with endogenous Pu1 drives the upregulation of the macrophage receptor Mac-1 and other macrophages markers (as F4/80 or M-CSFR), triggering the formation after 5 days of reprogrammed cells who share

same morphological features, immunoglobulin rearrangement and gene expression profiles of *bona fide* macrophages.

1.2.2.3. Fibroblasts to neurons

Firstly described by Wernig lab, a mouse embryonic fibroblast (MEF) can transdifferentiate to mature induced neuron (iN) thanks to the combined action of the three transcription factors Ascl1, Brn2 and Myt1l (BAM cocktail) (Vierbuchen et al., 2010). The study was performed with Tau:GFP reporter fibroblasts to identify Tau^+ neurons emergence. Already after 3 days of reprogramming, GFP^+ cells were detectable and displayed immature neuron-like shapes. At day 5, cells started to acquire more complex branching processes, with the complexity increasing until day 12, when well-developed neurons can be observed. However, from day 5 to day 12, there was no increase in the number of GFP+ cells, suggesting that, even if the neurons become more and more complex, there are no further events of *de novo* neurogenesis. These data suggest that BAM-mediated neuronal conversion is a rapid event that take places in the first 5 days of the MEF-to-neuron transdifferentiation.

A precise characterisation of these iN showed that they possess *bona fide* neuron characteristics: they express neuronal markers Tuj1, Tau, Map2 and Neun, depolarization of their membrane leads to an action potential burst, and they harbour inactivating inward and outward currents. They are also responsive to GABA and it is possible to observe VGlut1 puncta in their neurites, suggesting a co-presence in culture of inhibitory and excitatory neurons. They are also able to form synapsis, as detected by AMPA and NMDA receptor-mediated EPSCs.

To go further in the detail of the characterization of this process, following studies of Wernig lab focused on the single role of Ascl1, Brn2 and Myt1l during MEF-to-neuron transdifferentiation (Wapinski et al., 2013). The study showed that, unlike Brn2 and Myt1l, Ascl1 has the major impact in inducing the process. Indeed, overexpression of the TF in the beginning of reprogramming recapitulates significantly the differences observed in the MEFs upon BAM induction. Ascl1 works as a pioneer factor, it binds closed chromatin sites which are characterized by a trivalent signature composed from high enrichment in H3K4me1 and H3K27ac with an opposite low/intermediate enrichment of H3K9me3. To display in a functional way the importance of Ascl1 in MEF-to-neuron transdifferentiation, another study of the lab showed that Ascl1 alone can induce the formation of immature neuronal cells. Furthermore, thanks to culture with glial cells, important to neuronal complexity (Ullian,

2001) , immature cells derived from Ascl1 overexpression can give rise to complex iNs (Chanda et al., 2014).

1.3. Pluripotent reprogramming generates induced pluripotent stem cells

As introduced in the previous part, a somatic cell can dedifferentiate and convert in another somatic cell. Notably, in some cases, the process is associated to a transient reacquisition of a partial plasticity (van Oevelen et al., 2013).

Interestingly, a somatic cell can also revert to a complete pluripotent state, giving rise to induced pluripotent stem cells, or iPSCs. To achieve this state, cells are reprogrammed thanks to the combined action of four transcription factors, Oct4, Sox2, Klf4 and c-Myc. Together, they form the well-known Yamanaka cocktail and the process is known as pluripotent reprogramming (PR) (Takahashi and Yamanaka, 2006).

These cells represent powerful tools for different reasons. Before going in the detail of this exceptional reprogramming, in the next paragraph I will describe the possible uses of iPSCs.

1.3.1. iPSCs applications.

Human iPSCs were derived few years later using the same Yamanaka cocktail (Takahashi et al., 2007). These cells give the possibility to work on derived patient stem cells and can constitute a great tool for different reasons. Firstly, iPSCs could be used to regenerate patient-specific organs, avoiding the problems linked to histocompatibility. Secondly, as it is well described in neuropathology and cancer, drugs do not work in the same way on different patients. Having a personalized tool to recreate *in vitro* patient cells and tissues gives the possibility to perform drug or molecule screening in a patient-specific manner. Finally, in many cases, researchers cannot work on *in vivo* human organs, but hIPSCs can be differentiated into *in vitro* organoids to model diseases and test new therapies.

All of this could also be accomplished using human embryonic stem cells (hESCs), but the relative policy is strict and it leads to ethical issues. Thus, hiPSCs represent a valuable alternative.

1.3.1.1. iPS in regenerative medicine – stem cell therapies

In the last decades, translational and clinical investigation have shown the enormous potential of iPSCs for therapeutic applications. Stem-cell-based therapies displayed remarkable clinical results, with alleviation or healing of specific diseases and validated therapies for cornea, retina, hematopoietic, bone and skin diseases are now a reality (De Luca et al., 2019). Some of these stem-cell therapies use iPSC-derived multipotent

progenitors, capable of generate different organ-specific cell types; at the same time, other therapies use multipotent precursor cells obtained directly from the adult organism, where they are usually quiescent.

Takahasi group performed one of the first autologous iPSC-mediated stem-cell therapies in 2015. They transplanted a sheet of iPSC-derived retinal pigment epithelium (RPE) in the eye of a patient affected by neovascular age-related macular degeneration, which causes profound loss of central vision. One year after, even if the RPE patch was intact, there was no improvement in the patient condition, maybe due to the severe initial status of the disease (Mandai et al., 2017). Nevertheless, new studies are ongoing, using RPE directly derived from healthy donor, ESCs and IPSCs-derived RPE, and the first results obtained seem more promising (Zarbin et al., 2019)

Gene therapy represents an interesting tool for editing genome and, combined with stem-cell therapies, can bring wonderful results. This has been well established in hematopoietic diseases, where, instead of starting from hiPSCs, hematopoietic stem cells (HSCs) can be directly mobilized from bone marrow, collected after blood purification, genetically modified and re-injected in the patient. This technique has allowed to fight several hematopoietic diseases. For example, thanks to stem-cell therapies, it has been possible to heal 27 patients of ADA-SCID, who do not show negative side effects in the last 16 years (2000-2016, until the last published control) (Cicalese et al., 2016). For the treatment of ADA-SCID, Strimvelis has been the first stem-cell therapy approved by Europe in 2016 (Schimmer and Breazzano, 2016). With a similar pipeline, other therapies were efficient for hematopoietic diseases, such as X-linked adrenoleukodystrophy, Wiskott-Aldrich Syndrome and β-thalassemia (Aiuti et al., 2013; Ferrua et al., 2019; Hacein-Bey Abina et al., 2015; Sessa et al., 2016; Thompson et al., 2018).

iPSCs are currently being used for stem-cell therapies in pre-clinical studies and ongoing clinical studies, as the trial for iPSCs-based cell therapy in Parkinson Disease recently started in Takahashi lab (ID UNIM: UMIN000033564)

1.3.1.2. iPSCs in disease modelling – a promise from organoids

One of the challenges in the understanding of human diseases consists in the impossibility to genetically modulate *in vivo* samples. Even if mice models represent useful alternatives for many studies, species differences could be the origin of misleading results. For example, numerous rodent models has been derived for the study of Alzheimer disease, but no one can completely recapitulate the effects observed in humans, in particular the

decrease in neurons numbers (Onos et al., 2016). There is an evident demand to develop human platforms for a better and more direct study. Human iPSCs represent an interesting opportunity, with the idea to develop *in vitro* organoids recapitulating the molecular signature and functionality of the correspondent human organs. iPSCs can be induced to re-differentiate into 3D structures which mimic normal tissues, called organoids (Kadoshima et al., 2013; Mariani and Vaccarino, 2019). Many studies have been conducted in the last decade using organoids to dissect human diseases. For example, thanks to brain organoids (also known as mini-brain) it has been possible to identify an excess in neuronal production and a decrease of the non-neuronal populations in the mini-brains of macrocephalia patients (Mariani et al., 2015). Nevertheless, a big challenge in the domain consists in developing more complex organoids to recapitulate as much as possible human organs. In this context, absence of vascularisation is a main problem limiting the growth and maturation of these organoids. Interestingly, Xia lab has recently developed a new model of vascularized 3D kidney organoids, thanks to the precise tuning of Wnt signalling, which induces the emergence of a DR+ subpopulation, that starts to express CD31 and VEGFA, indicating vascular maturation (Low et al., 2019). Another issue consists in variability between different organoids coming from the same iPSC line. Arlota lab has lately derived dorsal forebrain organoids which recapitulate the complex diversity of human brain, but, at the same time, single-cell profiling shows that 95% of the produced organoids give rise to a similar neuronal repertoire, even with organoids generated from different lines, showing reproducible neuronal heterogeneity (Velasco et al., 2019).

1.3.1.3. iPSCs in drug discovery

iPSCs constitute also an important tool for the discovery of new drugs. Indeed, they allow to develop cellular models to perform large-scale screening of new molecules, with the aim to test efficiency and toxicity on the designed cells. This represents a relevant and less expensive platform to observe immediate phenotypes and test side effects on the cell type of interest. iPSC-derived models can correspond to 2D culture: for example, iPSCs can be mutated for the Tar DNA binding protein-43 (TDP-43) and induced into motor neurons, with the aim to mimic amyotrophic lateral sclerosis (ALS). A screening performed on these iPSC-derived neurons showed that the acetyltransferase inhibitor Anacardic acid rescues the negative phenotype of the mutated motor neurons (Egawa et al., 2012). Another IPSC-derived model used for drug discovery is “organs on a chip”,

engineered tissues designed with the aim of mimicking the minimal functional unit of an organ (Ronaldson-Bouchard and Vunjak-Novakovic, 2018). Finally, it is also possible to use organoids to perform drug discovery in a more complex set. For example, in the organoid model for achondroplasia, iPSCs mutated for the Fgfr3 receptor have defects in differentiation towards cartilage tissue. Using this system, molecules previously described for regulating Fgf3 signalling or chondrocyte differentiation have been screened. Data showed that the statin family rescues the defects in cartilage formation (Yamashita et al., 2014).

Giving the importance of iPSCs as promising means for medicine and development studies, it is important to understand the mechanisms of their generation to ensure proper iPSCs derivation.

2. FIRST PHD PROJECT:

PLURIPOTENT AND MALIGNANT REPROGRAMMING: ROUTES TOWARDS iPSCs GENERATION AND CANCER DEVELOPMENT

As introduced in the previous part, development is not a unidirectional process, but we can identify changes in cellular identity of differentiated cells, characterized by loss of somatic identity and in many cases reacquisition of cellular plasticity.

For my first PhD project, I have been particularly interested in the early steps of cellular reprogramming, asking how a cell loses its identity in the very beginning of cell conversion and which elements can constitute a roadblock towards reprogramming and trans-differentiation processes.

We decided to analyze more than one system of reprogramming, with the aim to identify global characteristics related to loss of somatic identity in different scenarios, and not specific features of one reprogramming.

We chose to work principally on the initial steps of iPSC generation and malignant transformation, as far as the two processes, despite the different outputs, share interesting analogies.

In particular, we focused our attention on studying the early processes which bring a cell to lose its somatic identity and become more sensible to OSKM action and oncogenic stimuli, the pluripotent and the malignant reprogramming (Ischenko et al., 2013; Takahashi and Yamanaka, 2006).

In this chapter, I will present some essential knowledge about iPSCs generation, malignant transformation and I will highlight the similarities of the two processes, which led us to choose pluripotent and malignant reprogramming as our model of study.

2.1. Pluripotent reprogramming and iPSCs generation

2.1.1. Before Yamanaka: Seminal experiments towards induced pluripotency

There had been many important studies that traced the route for the ground-breaking work of Takahashi and Yamanaka. In figure 13, it is possible to observe a timeline of these discoveries.

One of the first findings showed that nuclei of differentiated cells are able to erase their epigenetic memory and act in an equivalent way of nuclei of pluripotent cells. It was achieved by somatic cell nuclear transfer (SCNT) in amphibians: in 1950s and '60s, Briggs and King and later Gordon showed that nuclei obtained from Xenopus blastulae or intestinal epithelial cells were able to sustain cleavage and blastula development when injected in an enucleated egg (Briggs and King, 1952; Gurdon, n.d.).

This showed that, at a genetic level, a more differentiated cell is still competent to carry on early development. Hence, considering that the genome corresponds to the molecular basis of a cell, it suggests also that differentiated cells have intrinsically the possibility to switch back to pluripotency.

Another important contribution towards the discovery of iPSCs has been the establishment of pluripotent cell lines. In particular, this was started with studies on carcinoma-derived cell lines. Teratocarcinoma are benign tumor formed by chaotic arrays of differentiated tissues. Kleinsmith and Pierce in 1964 derived cellular lines form these teratocarcinoma. This and later studies showed that these embryonic carcinoma (ECs) lines, when injected *in vivo* in subcutaneous mice, formed teratocarinoma, tumors containing the three germ layers, and injected in blastocyst they could give rise to germ-line chimaeras (Bradley et al., 1984; Kleinsmith and Pierce, 1964). These experiments showed that adult tissues have still the competence of being pluripotent.

A third fundamental discovery was the pluripotent tetraploid hybrid cells formation. In the first application, Miller and Ruddle in 1976 fused pluripotent carcinoma cells with differentiated thymocytes, with the aim to understand which is the predominant fate between the pluripotent and somatic program. *In vivo* injections of these cells gave rise to tumors containing several differentiated tissues, reminiscent of teratocarcinoma derived tissues (Miller and Ruddle, 1976). These experiments not only demonstrated that the pluripotent program is dominant on the somatic one, but also that a differentiated cell can be modified to reprogram to an induced-pluripotent cell.

But what could mediate this pluripotent conversion? Further studies highlighted that TFs could play an important role in the process: for example, it was shown that somatic fusion of ESCs with neurosphere cells activated the expression of the transcription factor Oct4 (Do and Schöler, 2004). More evidences came from transdifferentiation experiments, which showed that TFs as Myod and Cebpα can drive cell conversion (Davis et al., 1987; Xie et al., 2004).

Taken together, these evidences showed that somatic cell has the intrinsic possibility to revert to pluripotency and that transcription factors play capital roles in changes of cellular identity. These studies posed the basis for the discovery of pluripotent reprogramming.

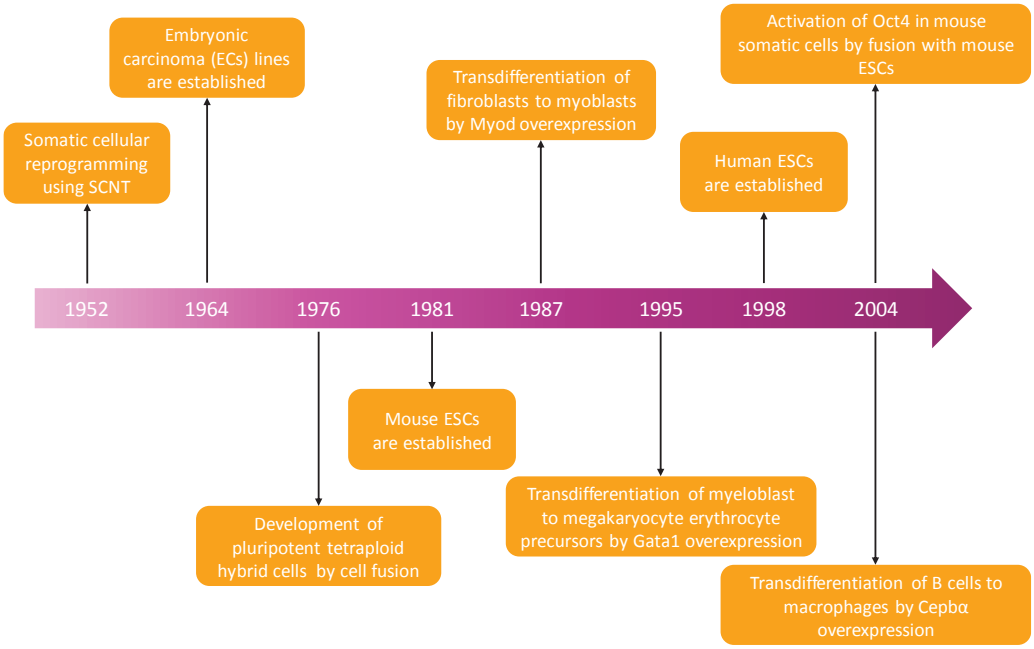

Figure 13: Timeline of fundamental studies that traced the path to iPSCs discovery.

2.1.2. Takahashi and Yamanaka, 2006:

All the seminal experiments listed in the previous part constituted the base of Yamanaka and Takahashi work on iPSCs generation.

In the study, they selected 24 genes which are expressed in ESCs and during blastocyst development and could potentially convert a somatic MEF to a pluripotent cell (Takahashi and Yamanaka, 2006).

To screen these factors, they developed a strategy based on geneticin resistance under the control of the Fbx15 promoter. Fbx15 is an ESCs marker not expressed in MEF, but not essential nor for pre-implantation development neither ESCs maintenance. Thus, its knock-out, applied

to insert in the Fbx15 locus the geneticin resistance βgeo cassette, is not detrimental to attend pluripotency. In this way, cells characterized by pluripotent features will activate the Fbx15 promoter, express the geneticin resistance and survive upon antibiotics treatment.

After the development of $Fbx15^{\beta geo/\beta geo}$ MEF, they screened the 24 candidates: MEFs infected with retroviral plasmids for the 24 candidates, infected one by one, did not generate any Fbx15 positive colony, suggesting that each factor alone cannot induce iPSCs formation, while the cocktail of the 24 factors together induced formation of G418-resistant colonies.

To determine which factors are required for iPSCs formation, they withdrew one by one the 24 factors. They identified 10 candidates whose absence was detrimental for iPSCs generation. With the same mechanism, starting from the 10 candidates, they isolated a combination of four factors which gave the higher reprogramming efficiencies: Oct4, Sox2, Klf4 and c-Myc. They were also able to obtain iPSCs with the OSKM cocktail starting with adult cells, the tail tip fibroblasts (TTPs).

Analysis performed on iPSCs showed radical similarities with ESCs: they express the same pluripotent markers, they are able to create teratoma once injected *in vivo* and some colonies showed proper karyotype. However, they were not able to obtain chimaera competence with the two tested colonies.

One year later, the same team succeeded in inducing human fibroblasts to reprogram into human induced pluripotent stem cells (hISPCs), which showed the same characteristics of human ESCs, like antigene profile, gene expression, epigenetic status and telomerase activity (Takahashi et al., 2007).

2.1.3. Technical development after 2006:

After these extraordinary discoveries, many studies were conducted, with the aim to produce iPSC of better quality suitable for regenerative medicine.

One of the major problems of Yamanaka study was the inability of iPSC to contribute to chimaera pups. Subsequent studies showed that Fbx15-based screening was not a perfectly reliable strategy, because it allowed isolating colonies which had proper morphology, Fbx15 expression but without an established pluripotency network. These colonies were called pre-IPSCs and they did not show the same characteristics as true-iPSCs and ESCs described before. Further studies took advantage of systems based on the Oct4 or Nanog promoters, more stringent than the Fbx1 one. Same studies also showed that a delay in the timing of OSKM induction gave rise to more faithful iPSCs colonies, more similar to ESCs at a molecular and

epigenetic level. These cells have a transcriptional pattern similar to ESCs, re-activation of the X chromosome, similar histone marks, DNA demethylation at Nanog and Oct4 loci and, importantly, are capable of giving rise to chimaera and are germ-line competent (Maherali et al., 2007; Wernig et al., 2007).

Another problem in Yamanaka experiments was related to the delivery system used for OSKM expression: retroviruses. Indeed, even if this class of viruses is usually silenced in ESCs and iPSCs (Jähner et al., 1982; Park et al., 2008; Stewart et al., 1982), the silencing may not always be completely efficient, leading to viral expression of OSKM TFs in iPSCs, something uncanny for regenerative medicine. Moreover, retroviruses infect only proliferating cells, limiting drastically the number of initial cell types available to reprogram. Another drawback consists in integrating at high frequency in the genome, increasing the possibility of integration in coding sequences or regulatory elements.

A first technical advance was represented by the use of lentivirus instead of retrovirus. In this way, it has been possible to obtain iPSCs starting from an higher number of somatic cells (Yu et al., 2007). Moreover, polycistronic vectors were derived to reduce the number of insertions, compared to the initial Yamanaka study where OSKM were separately delivered (Carey et al., 2009). Then, to solve the problem of random insertion in the genome, non-integrative delivery systems were derived. These methods comprise viral and non-viral techniques and they could represent a better perspective for regenerative medicine. In the first cases, virus that do not integrate in the genome, like adenovirus or Sendai viruses (SeV), were applied. However, in the case of adenoviruses, the strategy requires multiple infections, the process of virus production is laborious and the reprogramming efficiency is lower compared to integrative strategies (Zhou and Freed, 2009). In the second case, the Sendai RNA-viruses are very efficient in transfection (in the form of negative-strand single-strand RNA), but due to their constitutive replication, they may be difficult to degrade in the final iPSCs. They were thus engineered to be degraded by arising the culture temperature to 39°C. A new generation of Sendai viruses consists in SeV dp, which are replication-defective and erasable by siRNA administration, so more suitable for a medical use (Nishimura et al., 2011).

Another possibility is represented by non-integrative non-viral systems, like episomal vectors. These plasmids do not integrate in DNA but they are nevertheless actively replicated and transcribed (Okita et al., 2008). However, as for adenovirus, multiple infections are required, and reprogramming is less efficient.

It is also possible to administrate synthetic OSKM mRNA directly to the cells. Even if the RNA-based technique is the most efficient between the non-integrative possibilities, multiple

transfections are needed and it is highly immunogenic (Brouwer et al., 2016; Warren et al., 2010).

Furthermore, iPSCs generation has been performed in absence of OSKM induction, by reprogramming MEFs with seven small molecules, which mimics the Yamanaka cocktail effects: VPA, CHIR99021, E616452, Tranylcypromine, Forskolin, 3-deazaneplanocin A (DZNep), and PD0325901 (Hou et al., 2013).

Another alternative is represented by transgenic mice expressing OSKM in a Tet-on inducible strategy. Cells derived with this secondary system reprogram with higher efficiency compared to retrovirus infections (25- to 50-fold) and allows to induce OSKM expression upon doxycycline administration (Wernig et al., 2008a).

2.1.4. Phases of pluripotent reprogramming:

During reprogramming, MEFs go through profound remodelling induced by OSKM ectopic expression. We can distinguish principally three phases in the process. An initiation phase, in which most cells are subjected to the wide effects of OSKM action and undergo changes at morphological, molecular and epigenetic levels. A second phase, the maturation phase, in which only a small fraction of cells will acquire pluripotency features. And a third and last phase, the stabilization phase, which consists in the establishment of stable iPSC lines (**Fig.14**). During the first phase, the majority of cells respond to OSKM input, thus whole-population studies were used to study the initiation phase. On the contrary, during maturation and stabilization, only a tiny percentage of cells reprogram to pluripotency, thus studies have been focused on describing reprogramming intermediates by cell surface markers, single-cells RNASeq or tracing clonally-derived cells (see later for a more detailed explanation) (Golipour et al., 2012; Nefzger et al., 2014; Polo et al., 2012).

2.1.4.1. Initiation phase

This first phase is characterised by a rapid loss of expression of somatic markers, increase in cellular proliferation and decrease in cell size, consistent with the upregulation of c-Myc (Mikkelsen et al., 2008a; Smith et al., 2010). These really first modifications are followed by a change in the cellular morphology, called mesenchymal-to-epithelial transition (MET). Indeed, fibroblasts are elongated cells with typical mesenchymal shapes. On the contrary, iPSCs and ESCs form small cell clusters, tightly packed into

colonies, consistent with their epithelial status. Indeed, in MEFs, OSKM mediate this transition from a mesenchymal to an epithelial state by inhibiting Tgfβ pathway and in cooperation with Bmp, repressing Snail, Zeb and other mesenchymal factors and upregulating epithelial markers like E-Caderin and Epcam (Li et al., 2010; Samavarchi-Tehrani et al., 2010). MET is a first step of PR only if the departing cells are mesenchymal. Epithelial cells do not go through initial morphological changes. The requirement of the epithelial morphology is also highlighted by the fact that epithelial cells like keratinocytes reprogram at higher efficiencies compared to mesenchymal cells, such as MEFs (Aasen et al., 2008).

Interestingly, even if the transcriptional response to OSKM is wide, only a fraction of cells start to reprogram towards pluripotency (Smith et al., 2010). The other cells undergo apoptosis, senescence or cell-cycle arrest. These processes are induced as defence mechanisms counteracting the OSKM reprogramming action and constitute the principal reasons why so many cells are unable to generate iPSCs, explaining the poor efficiency of the PR.

In the cells prone to reprogram, OSKM play a fundamental role in inhibiting these physiological responses, in line with important regulators of these defence mechanisms (such as p53, p21 and the Ink4a/Arf locus) downregulated during reprogramming. Moreover, deletion of these regulators before the onset of reprogramming enhances its efficiency (Banito et al., 2009; Li et al., 2009, p. 4; Marión et al., 2009; Utikal et al., 2009).

Another change observed during the initiation phase is the beginning of a switch in the metabolic activity of cells. While MEFs are characterized by a strong impact of oxidative phosphorylation (OxPhos) on the cellular metabolism, in iPSCs the metabolism relies more on the glycolysis, reflecting the *in vivo* pre-implantation pluripotent cells, which are subjected to low dose of oxygen (Mohyeldin et al., 2010). Moreover, the glycolytic pathway is more suitable for self-renewing cells due to the enhanced speed of metabolite production compared to OxPhos. Thus, together with enhanced proliferation and morphological changes, we can observe from the beginning of reprogramming a gradual decrease in OxPhos and increase in glycolysis (Mathieu and Ruohola-Baker, 2017; Prigione et al., 2014).

On a molecular level, we can observe a large arrangement of transcriptome expression to support these various processes, involving genes necessary for proliferation, metabolism, cytoskeletal organization and developmental processes (Mikkelsen et al., 2008a). These

profound changes are mediated by a remodelling of the chromatin mediated by OSKM. Upon the four TFs induction, promoters of somatic genes starts to lose the active mark H3K4me2 and they are rapidly downregulated (Polo et al., 2012). It is also possible to observe an increasing depletion of the repressive mark H3K27me3 at the loci important for reprogramming. In parallel, in these loci, there is a new wave of H3K4me2 deposition, an epigenetic mark associated to transcription-factor binding. Indeed, this mark becomes particularly present at the promoters of pluripotency genes which contain Oct4 and Sox2 binding regions, but interestingly it does not co-occupy these sites with the activating mark H3K36me3, suggesting that these loci are ready for transcriptional activation but still not expressed (Koche et al., 2011). This is in line with the expression of pluripotent genes only starting at the later maturation phase.

2.1.4.2. Maturation phase

This second phase is characterized by the onset of the first pluripotency-associated genes expression, as Fbxo15, Sall4 and endogenous Oct4, followed by the naïve markers Nanog and Esrrb (Buganim et al., 2012). Overexpression of these early pluripotency markers enhances reprogramming efficiency, highlighting the importance of their activation (Han et al., 2010; Heng et al., 2010). We can also observe a reduction in the level of proteins related to electron chain transport system and a concomitant glycolytic enzymes upregulation, suggesting a gradual process of metabolic switch along the two first phases (Hansson et al., 2012; Zhang et al., 2012).

At the end of this phase, a key element for the transition to the stabilization phase is the silencing of the exogenous OSKM expression and the reliability of the newly re-activated pluripotency network (Polo et al., 2012).

On a molecular level, surprisingly, pluripotency factors are not the only factors driving transition to the last phase: a combination of pluripotent (Esrrb, Utf1, Lin28 and Dppa2), germline (Mnd1, Mutyh, Rad54b) and cytoskeletal (Tuba3a, Pdzk1, Itgb7, Kirrel2) genes mediates the exit from the maturation phase (Buganim et al., 2012; Golipour et al., 2012).

2.1.4.3. Stabilization phase

In this last phase, the establishment of stable iPSC lines is achieved.

Cells do not rely anymore on exogenous OSKM expression, but they are sustained by the endogenous molecular signature typical of the pluripotent state (Brambrink et al., 2008;

Wernig et al., 2007). They also undergo high-scale epigenetic modifications. For example, newly formed iPSCs are characterized by telomerase activation, which leads to telomeric elongation (Stadtfeld et al., 2008). At the same time, female iPSCs reactivate the inactive X chromosome. In ESCs, both X chromosome are active and, at the onset of differentiation, female ESCs silence one of the two chromosome in a process mediated by the long non coding RNA Xist, known as X chromosome inactivation (XCI) (Payer and Lee, 2008). In the last phase of pluripotent reprogramming, cells reactivate the inhibited X chromosome (Xi) and reset its heterochromatin state to equal levels of the activated X chromosome (Xa), leading to XaXa pattern, such as ESCs. This enables a random silencing of one of the two Xa chromosomes if iPSCs are induced to re-differentiate (Maherali et al., 2007).

In the stabilization phase, we can also observe a wave of DNA methylation rearrangement. This process is mediated by the reactivation of enzymes like AID, TETs and DNMTs (Polo et al., 2012). Modifications in methylation level are related to the erasing of the epigenetic memory observed at the end of reprogramming. During reprogramming, there is a reset of the epigenetic landscape present in the initial cells. If the reset is not complete, it can bias the differentiation potential of iPSCs (Kim et al., 2011) . Indeed, modification of DNA methylation obtained with cells passaging or using the 5-aza methylase inhibitor has been associated to a full epigenetic memory erasing (Ohi et al., 2011, p. 201). Moreover, AID has been shown to promote actively the epigenetic reset (Kumar et al., 2013).

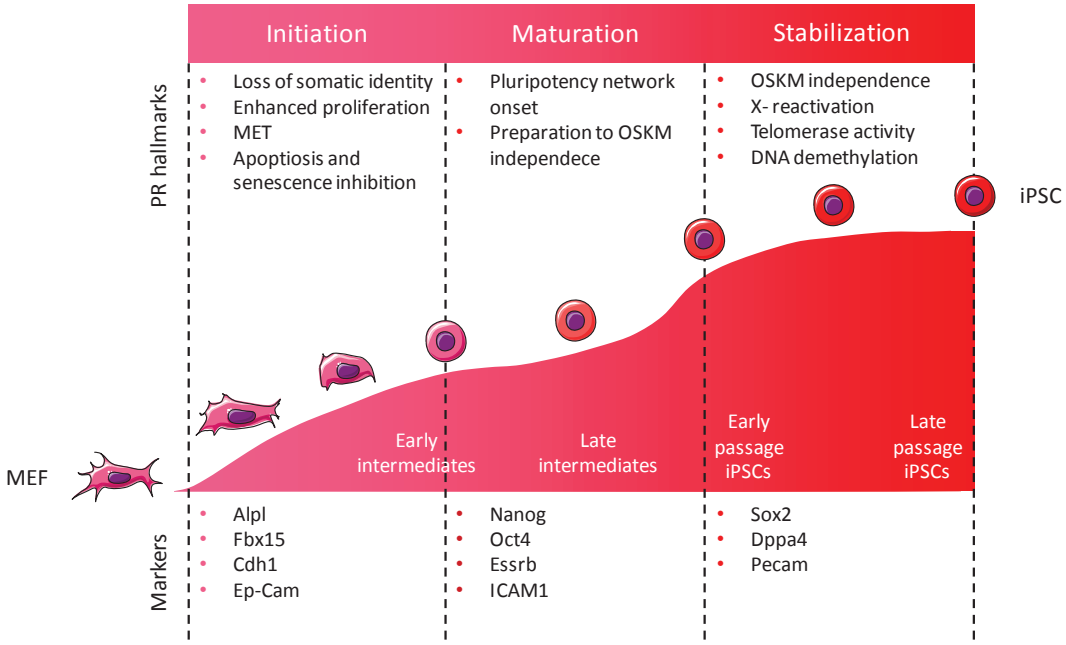

13: (Adapted from David et Polo, 2013) The three phases of pluripotent reprogramming, initiation, maturation and stabilization. They are displayed with the principal events and markers for each step.

2.1.5. Stochastic or deterministic?

During reprogramming, we can distinguish both a stochastic and a hierarchical pattern. In the first stochastic part, even if most cells acquire and express OSKM, only few of them will become iPSCs. Also reprogramming intermediates, more enriched to generate iPSCs compared to the total population, do not represent a pure population entirely generating iPSCs (Stadtfeld et al., 2008). Until now, it has not been possible to determine a specific subset of cells in the beginning of reprogramming that will become iPSCs, as it is proposed by the “elite” model. Following this theory, in the heterogeneous initial population, a group of cells possess stem properties and already harbour the potential to generate iPSCs. However, iPSCs were derived from terminally differentiated cell types, as B cells and T cells, excluding the requirement of a stem pool in the initial steps (Seki et al., 2010; Stadtfeld et al., 2012). Moreover, clonal experiments on B cells showed that more than 90% of cells can give rise to daughter cells that have the potential to become iPSCs (Hanna et al., 2009b). Furthermore, highlighting the stochasticity component, single-cell analyses showed that every cell from the same clone reach pluripotency at different kinetics and this stochastic emergence has an epigenetic base, with the Nurd/Mbd3 complex causing the delay in reprogramming (Buganim et al., 2012; Rais et al., 2013). From these evidences, it seems that the process is characterized by an initial stochastic pattern.

However, the slight percentage of cells that undergo reprogramming enter a second phase of hierarchical organisation, which begins with the activation of the endogenous Sox2. The activation of this transcription factor induces the expression of other pluripotency initiating factors (PIFs) that stabilize the iPSCs pluripotency network. The precise hierarchy of this second phase is highlighted by the fact that single-cell analysis, performed on cells coming from the same clone, shows a deep decrease in transcript heterogeneity after the onset of PIFs expression compared to the precedent phase (Buganim et al., 2012; Hanna et al., 2009b). The deterministic nature of the second part of reprogramming is also noticeable in the stabilization phase, when iPSCs go through precise processes such as late-pluripotency genes activation and many epigenetic rearrangements saw before to give rise to established iPSC lines (Mikkelsen et al., 2008a).

2.1.6. Capturing reprogramming heterogeneity in intermediates stages

As told before, the better way to study the maturation and stabilization phases does not consist in whole population studies, as far as most of the cells are blocked due to apoptosis, senescence and other reprogramming roadblocks. On the contrary, it is important to focus on the few cells that will become pluripotent, the intermediates prone to reprogram.

One of the first methods used to study them consisted in time-lapse microscopy (Araki et al., 2009; Smith et al., 2010). However, this approach gives information on morphological changes, but it does not give any knowledge about the molecular characteristics of the intermediates.

Another method allows to discriminate between refractory and reprogramming intermediates thanks to cell surface markers. This has been combined with the use of fluorescent reporter for early pluripotency markers, such as Pou5f1:GFP or Nanog:GFP, with the aim to capture their activation during reprogramming.

In this way, it has been possible to trace reprogramming maps following expression of cell surface markers and activation of endogenous pluripotency genes. For example, the Hochedlinger lab identified subpopulations where loss of the cell surface marker Thy1 and acquisition of SSEA1 lead to an enrichment in iPSCs formation, compared to the whole population. In the same study, they also showed that this rearrangement of cell surface markers consists in an early step of reprogramming, compared to expression of endogenous Sox2, telomerase and X chromosome reactivation, that they tracked thanks to GFP fluorescent reporters. All these data allowed them to create one of the first roadmaps of intermediates populations towards pluripotency (Stadtfeld et al., 2008). A later study of the lab used these identified intermediates to perform micro-array analysis, and identified two major waves of

changes in gene expression during reprogramming, which culminated with around 1'500 genes differentially expressed at day 12 of reprogramming (Polo et al., 2012). In parallel, Kaji lab developed another roadmap to follow reprogramming cells. In this study, they showed that decrease of the cell surface marker CD44 and upregulation of Icam are early event compared to the Nanog endogenous expression onset, measured with a GFP reporter. Using RNA-sequencing analysis they showed again this double wave of gene expression changes (O'Malley et al., 2013). Even if the roadmaps for MEF reprogramming are the most studied, attempts were performed to characterize pluripotent trajectories starting from other cellular types, as keratinocytes and neutrophils. Comparison between the transcriptome data obtained from the intermediates from the different cellular types highlighted that the two transcriptomic waves were shared among the three reprogramming types, while transient activation of developmental genes was specific of the cellular type (Nefzger et al., 2017).

Finally, the most recent roadmaps take advantage of single-cell RNASeq (sc-RNASeq) analyses, which allow to model single cell trajectories of reprogramming. This approach led to individuate non-reprogramming (NR) branches during PR. Within these NR branches, a disequilibrium between Klf4 and Sox2 exogenous expression leads to a Cd34+/Fxyd5+/Psca+ keratinocyte-like NR state (Guo et al., 2019). Other non-reprogramming branches comprise terminal stromal, neural and extra-embryonic fates (Schiebinger et al., 2019). Single cell analysis led also to the discovery of a first stochastic and later hierarchical phase during reprogramming (Buganim et al., 2012).

2.2. Malignant reprogramming and malignant transformation

2.2.1. Malignant transformation and cancer initiation

Organs development follows specific patterns and rules, in a process called morphogenesis. During morphogenesis, cells proliferate and differentiate in a precise manner to form tissues and organs. The plasticity conferred to pluripotent cells to differentiate into several tissues is underlined by the presence in each cell of a complete genome, containing the information required to generate a whole organism. Thus, the precise identity of a cell, determined by the genes expressed in it, is tightly regulated at a molecular and epigenetic level intracellularly but also by morphogens, signalling cues and mechanical forces at the intercellular level (Heisenberg and Bellaïche, 2013; Recasens-Alvarez et al., 2017; Tabata, 2004).

Thanks to this tight regulation, during development, multipotent cells receive precise temporal and spatial information that regulate their proliferation and the fate of their daughter cells. Even if the majority of cells lose this proliferation potential in the adult age, many organs keep pools of adult stem cells, that, in case of injury or for the normal turnover of the organ, can be activated, proliferate and generate new cells (Wagers and Weissman, 2004).

Thus, the processes driving morphogenesis and tissue repair are always tightly controlled to avoid atypical cell behaviours, primarily cellular hyperproliferation and formation of aspecific cell types. Otherwise, the versatility and autonomy of each cell, conferred by carrying a full-potential genome, can be detrimental.

One of the major risks is represented by mutations of the genome. Indeed, modifications to the DNA sequence by insertions, deletions, point-mutations or aberrant translocations, can potentially cause deregulation of gene expression with uncontrolled effects (Loewe and Hill, 2010). These mutations can arise following errors in DNA replication or can be induced by environmental factors, called mutagens. These mutagens can be of physical and chemical origin, for example UV radiations and cigarette chemical compounds (Godtfredsen, 2005; Green et al., 2011).

Indeed, malignant transformation begins with the accumulation of these mutations. Genes harbouring mutations which facilitate cancer development are classified as oncogenes, while genes whose mutation causes the loss of mechanisms acting against cancer are called onco-suppressors. Oncogenes and onco-suppressors are, thus, the major actors of malignant transformation (Bailey et al., 2018).

The accumulation of different mutations on oncogenes and onco-suppressors leads to the malignant transformation and cancer development. This characteristic of cancer shed light on two important characteristics of malignant transformation. Firstly, it is a multi-step process: the consequential accumulation of mutations during the organism life is fundamental for the development of the disease.

Second, this multi-step development pattern suggests that cancer has a partial stochastic origin. Mutations consist in stochastic events depending on cell proliferation or environmental factors (Tomasetti and Vogelstein, 2015). Moreover, the same mutagenic insults do not induce precise mutations on DNA in a systematic manner, but two different neighbour cells can be differentially affected from the same mutagen.

In the next part, we will focus on the hallmarks of cancer, which are responsible for cancer growth and escape from the control mechanisms active in normal cells.

2.2.2. Hallmarks of cancer

2.2.2.1. Inducing sustained proliferation

Normal cell proliferation is regulated by several growth factors in a precise manner to avoid hyperproliferation and deregulation of organ homeostasis. On the contrary, cancer cells are characterized by an uncontrolled proliferation (Preston-Martin et al., 1990).

One of the main ways of cancer cells to promote their continuous proliferation is ensuring a constant signalling of growth factor. There are many mechanisms that enable this continuous signalization in malignant cells.

Firstly, cancer cells can produce growth ligands in an autocrine way or can induce stromal cells forming the tumor microenvironment to produce similar signals, from which they can also take advantage (Zhang et al., 2010)

Deregulation of receptors can also induce constitutively the pathway activation: receptors in cancer cells can be overexpressed to sensitise cells and react at decreased levels of ligands, or their binding or intracellular domain can be mutated to induce a constitutive signalling. This in the case of the epithelial growth factor (Egf) receptor, which is overexpressed in many types of cancer, but it can also be mutated by a truncation of the ectodomain. In both cases, this leads to a sustained signalling of the Egf pathway (Sigismund et al., 2018).

Moreover, many oncogenes codify for growth pathway effectors. Mutations on these proteins induce signalling in a stable manner or avoid the negative feedback mechanisms that normally

tune pathways. For example, in Mapk and PI3k signalling pathways, the kinases B-Raf and PI3K are mutated to render the pathways active even in absence of their ligands (Holderfield et al., 2014; Jiang and Liu, 2009).

Concerning the disruption of negative feedbacks, the most known example consists in the Kristen-Ras (K-Ras), a member of the small GTPase superfamily, mutated in more than 90% of human pancreatic cancers (Collins et al., 2012). The proteins of this family are GTPase who bind and hydrolyse GTP to GDP. In normal conditions, the GTP-bound form of Ras can bind and locate to the membrane Raf, the first kinase of the Mapk pathway, for its activation. This induces the Mapk pathway, which leads to several phenotypes, such as cell proliferation. Once Ras had hydrolysed the GTP to GDP, the GDP-bound form of Ras cannot efficiently bind Raf, which is released in the cytoplasm, no longer activated, leading to the inhibition of the pathway. K-Ras GTP/GDP turnover constitutes a negative feedback regulating the Mapk pathway (Marshall, 1995). However, the mutation K-RasG12D on the twelfth aminoacid of K-Ras, which leads to a substitution of glycine to aspartate, leads to the loss of the hydrolysis activity of K-Ras. This induces a constitutive GTP-bound K-Ras, a constant recruitment of Raf to the membrane and MAPK signalling, which finally leads to stable cell proliferation (Vasan et al., 2014).

In a parallel way, as cancer cells need to maintain growth positive signals, they also must counteract the action of growth suppressor signals. Indeed, many of the genes controlling these proliferation mechanisms are veritable onco-suppressors.

The most known onco-suppressors involved are Rb and p53, they both control two complementary circuits which determine if cells proliferate or enter senescence and apoptosis. Concerning its ability of cell-cycle checkpoint, Rb plays its role in G1 phase of cell cycle by the inhibition of the E2F transcription factors, essential factors of the G1 to S phase transition (Weinberg, 1995). Additionally, it can associate with the cell-cycle inhibitor p27 via the APC complex to arrest cells in G1 (Ji et al., 2004, p. 2). Due to these characteristics, loss of Rb activity leads to cell cycle re-entry in quiescent stem cells and in post-mitotic differentiated cells (Sage, 2012).

In a complementary manner, p53 acts as an inner sensor of the cell and, in case of negative stress, it induces an arrest of cell cycle. In case of DNA damages or other types of stress, such as the decrease of important macromolecules and growth-promoting signals, p53 arrests cell cycle in G1 phase, driving the expression of the cell-cycle inhibitor p21 (Wade Harper, 1993). However, if the cell is too damaged and the time given by cycle arrest to fix the problem is not sufficient, p53 drives the cell towards senescence or apoptosis (Clarke et al., 1993; Serrano et al., 1997).

Loss of Rb and p53 finally leads to a decrease of the mechanisms safeguarding cellular homeostasis and strongly enhanced cellular proliferation. This, together with the increased signalling of growth pathways, leads to the hyperproliferation associated to cancer development.

Moreover, loss of these two factors induces a decrease in the control of DNA integrity, and an increased genome instability: for this reason p53 is also known as the guardian of genome (Lane, 1992). Together with an inflammation microenvironment, genome instability is one of the most important conditions for malignant transformation.

But why is genome instability so important for malignant transformation? As we will see in this chapter, cancer must bypass different obstacles to ensure its expansion. It needs to hijack growth suppressor, circumvent cellular programmes such as senescence and apoptosis and it also needs to escape immune system surveillance (Hanahan and Weinberg, 2011). Genome instability is fundamental for all of these activities: high rates in DNA mutations in the developing cancer give rise to a genetically high heterogeneous cell population, similarly to an accelerated Darwinian evolution (Salk et al., 2010). Among the several clones with differences in the mutations pattern, some of them will acquire advantageous mutations that allow them to bypass the multiple cellular barriers. In this way, we can look at the development of cancer as a history of continuous clonal expansions. At each barrier hijacked, the genome instability ensures new heterogeneity among the daughter cells of the winning clones, giving rise to new subclonal populations. Thus, at the next obstacle, some of the newly formed clones will own the advantageous mutations that permit them to bypass the next cellular barrier.

But how can this genome instability be achieved? Through the mutations of the care-takers of genome, genes of the DNA-maintenance machinery that codify for proteins important for genome integrity, involved in detecting DNA damages, repairing them or signalling towards senescence or acting in the deactivation of molecules potentially damaging DNA (Kinzler and Vogelstein, 1997).

Another characteristic related to cell proliferation in cancer is the loss of contact inhibition: as easily observed in *in vitro* culture, when normal primary cells reach confluence, they avoid formation of multiple cell layers and their proliferation is blocked by different signals, which give rise to the so-called “contact inhibition”.

On the contrary, this inhibition is lost in malignant transformation. One of the mechanisms responsible for this phenomenon consists in the loss-of-function mutations or deletion of the

onco-suppressor NF2 (Petrilli and Fernández-Valle, 2016). When NF2 is expressed, it mediates cell-inhibition by connecting cell-surface adhesion marker E-cadherin to growth EGF receptor, inhibiting EGFR internalisation and activation through the actomyosin cytoskeleton (Chiasson-MacKenzie et al., 2015). This leads to a decrease in cellular proliferation when cells are too dense. Thus, when the NF2 gene is mutated, the connection between E-Cadherin and EGFR is lost, and growth pathways are no longer under the negative regulation of adhesion proteins.

2.2.2.2. Erasing cell defence barriers to reach immortalization

To ensure strong proliferation and tumor growth, malignant cells rely on several mechanisms. Firstly, as seen before, they can enhance growth pathways and avoid their negative regulation. Moreover, malignant cells become able to counteract and hijack the cellular processes that constrain the uncontrolled proliferation, namely apoptosis and senescence. The ability to block these cellular responses is an essential feature of malignant transformation, considering that the cancer-associated genome instability is the cause of the activation of these cell defence mechanisms (Bartkova et al., 2006; Halazonetis et al., 2008; Lowe et al., 2004).

Concerning apoptosis, Bcl-2 proteins play an important role in the onset of this process. We can distinguish two different classes of Bcl-2 proteins: anti-apoptotic factor, as Bcl-2, Bcl-x(L), Bcl-w, Mcl-1 and A1, and pro-apoptotic Bcl2, as Bax and Bak. When cells receive apoptosis signals, Bax and Bak, usually inhibited to avoid an aberrant cell death, are not repressed anymore by the anti-apoptotic factors and induce the permeabilization of the mitochondrial outer membrane (MOMP). This phenomenon leads to the secretion of the mitochondrial cytochrome c in the cytoplasm, which activates a cascade of caspases, the proteases which act as principal effectors of apoptosis (Green, 2004). During malignant transformation, tumor cells avoid apoptosis in several ways, most importantly by p53 loss of function. Indeed, in a normal context, p53 can induce apoptosis upregulating the expression of the pro-apoptotic factors Noxa and Puma. Alternatively, cancer can bypass apoptosis thanks to upregulation of anti-apoptotic signals or downregulating mutations in pro-apoptotic signals (Adams and Cory, 2007).

Replicative potential of a normal cell is associated with two consecutive barriers: senescence, which drives cells to a non-proliferative but still viable condition, and crisis, in which most of the cells die.

During the first phase, cells that enter senescence are in a long-term cell cycle arrest. Thus, they are insensible to growth signals. Furthermore, they change their morphology, acquiring a large and flat shape, are characterize by telomeres shortening, DNA damages accumulation

and, at a molecular level, they strongly activate the CDKN2A locus, which encodes INK4A and ARF genes. Indeed, these two genes are two important tumor suppressors, respectively upstream to Rb and p53 (Lukas et al., 1995; Ouelle et al., 1995).

The second phase, the crisis, is strictly related to the status of telomeres in cells. At each round of amplification, daughter cells inherit chromosomes characterized by shorter telomeres compared to the mother cell. Cells which undergo several rounds of amplification, acquire shorter and shorter telomeres at each cell cycle. The cells that can bypass the first senescence barrier continue to proliferate until telomeres are so eroded that they cannot cover properly the chromosomes ends. This telomere attrition triggers the enter in the crisis phase, until autophagic death (Nassour et al., 2019).

However, during malignant transformation, cells can hijack these two barriers thanks to reactivation of telomerases. These enzymes, initially active during early development and almost absent in differentiated cells, are re-expressed in malignant cells and mediate telomeres elongation (Blasco, 2005). The action of the telomerases, thus, induces cancer cells to bypass both senescence and crisis, leading to an unlimited proliferation potential, known as immortalization.

2.2.2.3. Adapting to the environment

There are other additional characteristics that are required for tumor growth and expansion. Indeed, tumor needs nutriments and oxygen to sustain neoplastic massive growth. Thus, an important feature of cancer is the induction of new and aberrant angiogenesis. In organs homeostasis, angiogenesis is transiently activated for slow endothelial turn-over or for precise and controlled functions, such as female reproductive cycle. On the contrary, in cancer, angiogenesis becomes a constitutive trait, with continuous sprout of new vessels to irrigate the expanding tumor. The process is mediated by different mechanisms: the oncogenic-mediated activation of the angiogenesis inducer vascular endothelial growth factor-A (Vegf-A) (Carmeliet, 2005); the chronical upregulation of proangiogenic signals like fibroblast growth factor (Fgf) (Casanovas et al., 2005); and, depending on the state of the tumor, the precise regulation of the angiogenesis inhibitor thrombospondin-1 (TSP-1) (Kazerounian et al., 2008).

In this way, thanks to constant angiogenesis, cancer is always provided by new oxygen and nutrients. Considering the massive cell growth and division typical of malignant transformation, developing tumors must quickly re-employee nutrients received from the newly formed vessels, and transform them in energy and metabolite for cell growth and amplification. For this reason, in cancer we can observe an adaptation of metabolism, a switch from a metabolism

based on oxidative phosphorylation (OxPhos) towards glycolysis, a phenomenon known as Warburg effect (Warburg, 1956). The choice of glycolysis seems apparently inefficient, considering that glycolysis, compared to OxPhos, provides eighteen-fold less ATP molecules, the principal energetic source for the cells. However, high proliferating cells need many metabolites to create the several macromolecules and organelles required for cell division and the daughter cells. In this light, glycolysis seems a better option, because at the same time it creates ATP and generates different metabolic intermediates, that can be used in other biosynthetic pathways to produce the required macromolecules, including nucleotides and amino acids (Vander Heiden et al., 2009). Moreover, to counterbalance the deficit in ATP production, cancers develop alternative ways to increase the glucose uptake, such as enhanced expression of the glucose transporter Glut1 mediated by the c-Myc oncogene (Osthus et al., 2000).

All these characteristics are necessary for the cancer growth. However, if we forget the intrinsic aetiology of cancer and consider this disease as an independent being, it lives in a parasitism condition with its host. Indeed, as we saw before, the host tries to abolish this neoplastic growth by many cellular defence mechanisms. One of these essential barriers consists in the organism immunosurveillance. Another fundamental feature of cancer is the ability to evade the host immunosurveillance (Beatty and Gladney, 2015). In the beginning of cancer development, many cancer cells are erased by CD8+ cytotoxic T lymphocytes (CTLs) and natural killers (NK) cells. However, the immune suppression leads to selection of particularly resistant cancer clones derived from advantageous mutagenic patterns. These clones escape the immunosurveillance and grow undisturbed.

Nevertheless, even if immune system plays a fundamental role on contrasting expansion, the inflammation set off by immunosurveillance is favourable to cancer development. Indeed, together with genome instability, inflammation is one of the two conditions for malignant transformation (Hanahan and Weinberg, 2011a). Inflammation provides cancer of many molecules fundamental for its development: growth factors, survival factors, pro-angiogenic factors, cytokines, ROS which increase DNA damage of cancer genome and other molecules facilitating cancer development (Grivennikov et al., 2010).

2.2.2.4. Forming secondary tumors

Finally, the initial tumor can also migrate and colonize secondary organs, creating secondary tumors, called metastasis. Indeed, the metastasis is the most common cause of cancer death

(Mehlen and Puisieux, 2006). Cancer cells need to go through strong morphological adaptations to achieve metastasis formation. The majority of tumors are carcinoma, cancer composed by epithelial cells. During the metastatic process, malignant cells must abandon the crowded epithelia context of the primary tumor, enter in the flux of blood and lymphatic vessels and later extravasate in a second area to generate the secondary tumor. To enter the flux and migrate in the vessels, epithelial cancer cells need to acquire a more dynamic, spindly and fibroblastic shape, through acquisition of mesenchymal features, in a process called epithelial-to-mesenchymal transition or EMT. Thanks to the mesenchymal shape, cells can easily migrate into the vessels from the primary district and survive better under peristalsis and blood pressure. At a molecular level, EMT is characterized by downregulation of epithelial markers, as E-cadherin, and upregulation of mesenchymal transcription factors, EMT-TFs, as Snail, Slug and Twist (Yang and Weinberg, 2008). On the contrary, when cells extravasate to the parenchyma of secondary epithelia area, they need to perform a mirror process, the mesenchymal-to-epithelial transition or MET (Hugo et al., 2007). Indeed, repression of the transient mesenchymal phenotype is necessary for the accomplishment of metastasis and E-cadherin has been shown to be required in metastasis formation: even if its downregulation increases the initial malignant invasion, its depletion also induces defects in cellular proliferation, cancer survival, metastasis seeding and outgrowth (Padmanaban et al., 2019). After extravagations, cancer cells can give rise to small nodules known as micro-metastasis and, with different delays, start to proliferate and form new secondary tumors (Fidler, 2003).

Interestingly, an intermediate state, where cells express both epithelial and mesenchymal markers, has been associated with the higher degree of aggressivity, called partial EMT. In breast cancer, partial EMT leads to mammosphere formation independently of the tumor subtype and promotes stemness compared to mesenchymal cells (Grosse-Wilde et al., 2015). In a subset of ovarian cancer, cells co-expressing epithelial and mesenchymal markers drive tumor growth, giving rise to both epithelial-only and hybrid cells (Strauss et al., 2011).
Partial EMT was also associated with a poor patient survival and resistance to chemotherapy (Smith and Bhowmick, 2016; Thomas et al., 1999)

2.2.2.5. Hierarchical structure of tumors

The ability of switching from epithelial to mesenchymal morphology correlates in time with another important feature of cancer cells: cancer plasticity and emergence of cancer stem cells (CSC).

Indeed, in the high heterogeneity of the tumor mass, it is possible to identify few cells that display peculiar characteristic compared to the rest of the population, the CSC (Clevers, 2011). These cells constitute the core of cancer: they are the primary cause of therapy resistance and tumor recurrence, being able to self-renew and re-create the malignant mass after treatments. Another characteristic that explain their stem status is their ability to activate many differentiation pathways to reconstitute, after therapy, the original tumor heterogeneity (Al-Hajj et al., 2003; Lapidot et al., 1994; Singh et al., 2004). Surprisingly, this heterogeneity is not limited to the production of malignant cells, but CSCs can also generate non-tumor cells of the microenvironment in a process known as vascular mimicry. For example, in glioblastoma and breast cancer, tumor cells can transdifferentiate and give rise to pericytes and endothelial cells, which contribute to sustain neovascularization and consequently tumor growth (Cheng et al., 2013; Wagenblast et al., 2015; Wang et al., 2010).

On a molecular level, Aldh1 activity and Cd34, Cd133, Cd44, Cd166 and Cd24 expression can be used to identify CSCs from solid tumors, but each CSC coming from a different tumor has its own peculiar expression profile (Visvader and Lindeman, 2012). Embryonic stem cell markers are also partially re-acquired, for example Oct4 is aberrantly expressed in breast, thyroid, oesophagus and prostate cancer (de Resende et al., 2013; Madjd et al., 2009; Zhou et al., 2011), or Sox2 in lung, oesophagus, brain and breast cancers and Ewing sarcoma (Y. Chen et al., 2008; Riggi et al., 2014; Sarkar and Hochedlinger, 2013)

Indeed, the emergence of CSCs is correlated to the capacity of cancer cells to form metastasis: in different malignant contexts, upregulation of EMT-TFs leads to an increase of tumor-initiating potential (Mani et al., 2008; Wellner et al., 2009). However, this is not an universal rule, as far as, on the contrary, in prostate and bladder cancer the EMT-TF Snail induces EMT but at the same time decreases CSC properties (Celià-Terrassa et al., 2012). Moreover, in mice squamous cell carcinoma different levels of Twist1 correlate separately to stem cell properties or EMT induction (Beck et al., 2015). Considering all this information together, it seems that stemness correlates more with the acquisition of cellular morphological and phenotypical plasticity, more than expression of mesenchymal genes, important for migration and the beginning of the metastatic process.

2.2.3. Cancer: a reprogramming disease

For a long period, cancer has been considered a proliferation disease where driver mutations in important oncogenes and onco-supressors lead to the emergence of clonal populations that acquire major adaptative and proliferative advantages (Puisieux et al., 2018).

However, considering cancer development in its whole complexity, we can observe that not every feature derives directly from an increased proliferation or adaptation. This is, for example, the case for metastasis, in which a different characteristic, the morphological plasticity between epithelial and mesenchymal state, is required. The rapid loss of identity and acquisition of new features indicate the existence of a certain cellular plasticity associated to malignant development, a distinctive trait which is highlighted by the existence of the aforementioned CSCs. Furthermore, processes of dedifferentiation in cancer has been associated to enhanced metastasis potential and chemoresistance (Gupta et al., 2009; Mani et al., 2008).

Taking in account these evidences, the traditional idea of proliferation and adaptation as the main principles driving cancer development should be reformulated, considering that cellular plasticity may play an important role in cancer development. But what is the extent of this cellular plasticity? Does it play a role just in EMT/MET switch and in the transdifferentiation potential of CSCs or can it be observed in other and earlier steps of cancer development?

More importantly, can cellular plasticity work in parallel, or in substitution, to mutations to drive proliferation and cancer development? As said before, the traditional model of tumor formation is based on the stepwise accumulation of mutations, which induces genome instability and malignant transformation. In a practical way, Campbella and colleagues showed that the minimal number of driving mutations to cancer onset corresponds on average to four coding substitution (Martincorena et al., 2017). However, this model does not take in account pediatric cancers, where diseases arise too rapidly to be explained with a stepwise mutations model. Indeed, these cancers are characterized by one or few driving mutations sufficient for malignant onset (Vogelstein et al., 2013). This is the case of retinoblastoma, atypical teratoid/rhabdoid tumor (AT/RT) and neuroblastoma, where biallelic inactivation of RB1, of SMARCB1 and genomic amplification of NMYC are necessary and sufficient to drive malignant transformation (Han et al., 2016; Weiss, 1997; X. L. Xu et al., 2014).

How can we explain such aggressive cancers with so few mutations? How can we reconciliate the classical view of cancer with these developmental cancers?

The explanation probably resides in the initial differentiation grade of the cancer cell of origin. During development, chromatin is more permissive than in the adult, in line with the requirement of rapid responses to signalling cues driving organ development. On the contrary, in the adult

organs, most cells are differentiated, and the chromatin is closer, to avoid aberrant gene expression. For this reason, the chromatin plasticity of developing cells renders them sensitive to few oncogenic insults, while, in the adult, the differentiated status requires many mutations to render the cell more responsive to cancer development. (Puisieux et al., 2018).

This is highlighted by studies showing that, in the same organ, normal stem cells are more prone to give rise to malignant transformation compared to the differentiated cells (Barker et al., 2009). Indeed, a new concept is emerging in the field, proposed the first time by Dyer and colleagues: the concept of pliancy, an intrinsic sensibility of cells to react to oncogenic insult leading to malignant transformation depending on their degree of differentiation (X. Chen et al., 2015) . Furthermore, the path towards malignancy can differ depending on the level of pliancy of the cell of origin, as it has been recently shown by Puisieux lab. Taking advantage of subpopulations of normal epithelial mammary cells coming from the same mammoplasties, they showed that normal cells respond differently to oncogenic insults depending on their pliancy degree: mammary stem cells express the EMT-TF Zeb1, which protects this subpopulation from oncogenes-induced DNA damage, activating an antioxidant program. As a result, tumorigenesis is induced without high genomic instability. On the contrary, Zeb1 is absent from luminal progenitors and differentiated epithelial cells, which accumulate high DNA damages upon oncogenic insult and develop tumors characterized by chromosomal instability (Morel et al., 2017).

To sum up, the plasticity, characteristic of the developing embryo, creates an environment suitable for oncogenic insult and malignant transformation. But what about the adult? How does the differentiation state influence cancer development in mature tissues? Many cancers come from adult stem cells, as intestinal cancer and leukaemia (Barker et al., 2009; George et al., 2016). However, this is not the case of every cancer: lineage tracing experiments have shown that differentiated cells can initiate malignant transformation (Van Keymeulen et al., 2015). Moreover, in some cases, differentiated cells and the correspondent stem cell pool are equally permissive towards tumorigenesis, as is the case of glioblastoma (Bachoo et al., 2002). Pluripotent reprogramming towards iPSCs showed that a differentiated cell can lose its somatic identity and reacquire pluripotent features. In the oncogenic context, can we observe reacquisition of plasticity before malignant transformation? Not a full pluripotency, like in iPSCs, but a dedifferentiation process, which renders the cell more sensitive to oncogenic insult?

In this direction, different studies showed that, before cancer onset, differentiated cells can reprogram thanks to the action of oncogenes or other stress sources to a less differentiated state and become more sensible to malignant transformation (Roy and Hebrok, 2015). This reprogramming process includes a first step of dedifferentiation and loss of somatic identifiers and a second step of acquisition of new cellular markers, called transdifferentiation or, if the conversion

happens at the level of the entire tissue, metaplasia. The physiological role of metaplasia consists in a protective function, when cellular replacement is needed after chronic damage or to limit the advance of a negative condition. This is the case, for example, of Barret's esophagus, a chronic inflammation where esophagus squamous epithelial cells convert into intestine-like columnar cells, with the aim to defend the organ from the chronic gastroesophageal reflux (Spechler and Souza, 2014). However, this process has also been described in esophageal adenocarcinoma as an initial key event of malignant transformation (Hvid-Jensen et al., 2011).

Another important example of dedifferentiation and transdifferentiation at the onset of malignant transformation is represented by pancreatic ductal adenocarcinoma (PDAC). This cancer can arise from different types of pre-tumoral lesions, among which the most common are the pancreatic intraepithelial neoplasia (PanIN) (Hezel et al., 2006). Different cell types have been described as cell-of origin of these lesions. Considering the localization of PanIN, in contact with the pancreatic ductal tree, the most probable candidate as cell-of-origin was considered the pancreatic duct cells (PDCs). However, evidences suggest that PDCs are incapable to give rise to complete PanIN (Lee and Bar-Sagi, 2010; Pylayeva-Gupta et al., 2012; Ray et al., 2011) On the contrary, PanIN are initiated by acinar cells, which go through a conversion into ductal cells before forming PanIN, as demonstrated by lineage tracing experiments (Carriere et al., 2007). In the same direction, it was shown that induction of the oncogenic K-Ras specifically in acinar cells gives rise to lesions recapitulating the ones observed when K-Ras is activated in the whole pancreatic epithelium (De La O et al., 2008; Friedlander et al., 2009). Indeed, the process requires a first step, in which acinar cells, upon various insults, lose their somatic identity and enter a state of dedifferentiation, characterized by a loss of acinar markers Nr5a2, Mist1 and Ptf1a (von Figura et al., 2014). This state provides them with a plasticity required for the second step, the transdifferentiation towards ductal cells, known as ADM (acinar to ductal metaplasia) (De La O et al., 2008; Habbe et al., 2008; Shi et al., 2013), where expression of ductal markers such as Sox9 and Hnf6 arises (Krah et al., 2015; Pin et al., 2001). ADM can lead to premalignant lesions, as observed when acinar cells receive oncogenic insults orchestrated by EGFR, TGF-α, SV-40 T-antigen or K-RasG12D (Bockman and Merlino, 1992; Ornitz et al., 1987; Sandgren et al., 1990; Tuveson et al., 2006; Wagner et al., 1998). Dedifferentiation and reprogramming can be detected in many cases of malignant transformation. Loss of tumor-suppressors p53 and Nf1 in differentiated neuron and astrocytes leads to dedifferentiation and formation of gliobastomas. Indeed, these tumors are principally composed of Sox2 and Nestin positive cells, two markers of neural stem cells, and molecular characterization of this process shows an initial loss of differentiated markers followed by increase of Nestin expression (Friedmann-Morvinski et al., 2012).

Furthermore, in malignant transformation, we can also observe events of reprogramming of somatic cells into cancer stem cells. For example, in human basal breast cancer, non-CSCs can reprogram to CSC thanks to the action of ZEB1, which is stalled at bivalent promoters and induces gene activation depending on microenvironment signals (for example TGFβ inducing EMT) (Chaffer et al., 2013). Always in mammary context, *in vitro* analysis using transformed human mammary epithelial cells (HMEC) showed that a subpopulation of $Cd44^-$ non CSC can autonomously convert to $Cd44^+$ cancer stem cells, capable to give rise to mammospheres *in vitro* and tumor in NOD/SCID mice *in vivo* (Chaffer et al., 2011). This cellular plasticity can also explain the failure of cancer therapies targeting specifically CSCs to avoid disease relapse (Saygin et al., 2019)

Interestingly, in an opposite fashion, malignant cells can be differentiated into somatic, non-proliferating cells. This was shown in acute promyelitic leukemia (APML), where a reciprocal translocation of the chromosome 15 and 17 leads to the formation of the oncoprotein PML-RARa, a driver of malignant transformation, formed by the fusion of the protomyelocytic leukemia gene (PML) with the retinoic acid receptor gene RAR-a (Borrow et al., 1990). Interestingly, it has been shown that retinoic acid (RA) is essential for proper embryonic differentiation (Ross et al., 2000). In a similar manner, treating APML cells with all-trans retinoic acid can induce cancer cell differentiation leading sometimes to curative responses in patients (Breitman et al., 1981; Warrell et al., 1991).

Considering these many observations, even if dedifferentiation alone cannot account for the whole malignant transformation, it can provide an essential starting point. Oncogenic insults can follow dedifferentiation to induce malignant transformation. Indeed, in this model of cancer development, the precise combination of oncogenic insult and cell-of-origin is required for cancer development. For example, combined action of K-Ras and Sox9 in pancreatic acinar cells is required to give rise to PDAC pre-lesions, while K-Ras cooperates with the loss of Pten to drive intraductal papillary mucinous neoplasia starting from pancreatic ductal cells (Kopp et al., 2018, 2012).

Notably, Petrenko group developed an *in vitro* model of plasticity induced by oncogenic insult: in the study, they showed that the combined action of c-Myc and K-RasG12D can induce differentiated MEFs towards a rapid malignant transformation, independent of cell proliferation and mutation accumulation. In this multi-step process, K-RasG12D mediates a morphological reprogramming, characterized by the loss of MEF markers Thy1 and Sca1 and the generation of a double-negative (DN) non-tumorigenic cell population. The following co-operation with c-Myc drives DN cells into malignant transformation (Ischenko et al., 2013).

From these evidences, we can conclude that cancer is not just an evolution of clonal expansions mediated by proliferation and adaptation, but dedifferentiation and cellular plasticity influences

tumor initiation and progression. Interestingly, different levels of pliancy are associated to different roads to tumorigenesis.

It becomes prerogative to study which mechanisms drives the loss of somatic identity and leads to higher pliant state where cells become sensitive to oncogenic insults.

2.3. Similarities between pluripotent reprogramming and malignant transformation

Based on what have been described above, iPSCs generation and malignant transformation share many remarkable characteristics. They are both stochastic, heterogeneous and multi-step processes (Buganim et al., 2012; Dagogo-Jack and Shaw, 2018; Manian et al., 2015; Tomasetti and Vogelstein, 2015). Loss of somatic identity and reacquisition of developmental features have been described in both scenario (Mikkelsen et al., 2008b; Roy and Hebrok, 2015).

Moreover, several biological processes take place during both iPSC generation and malignant transformation, such as increase in proliferation, morphological changes (MET/EMT), metabolic switch, apoptosis and senescence inhibition and telomerase reactivation (David and Polo, 2014; Hanahan and Weinberg, 2011b).

Furthermore, we can observe an interplay between the factors determining PR and MR: PR-drivers Oct4, Sox2, Klf4 and c-Myc can act as *bona fide* oncogenes (Dang, 2012; de Jong and Looijenga, 2006; Herreros-Villanueva et al., 2013; Yu et al., 2011). On the contrary, known onco-suppressors such as Rb and p53 constitute a roadblock for iPSCs generation (Kareta et al., 2015; Kawamura et al., 2009). Same epigenetics events happen in both processes, such as DNA methylation remodelling and activity of chromatin regulators as Suv39h1, Setdb1, Ezh2 and Bmi1 (Suva et al., 2013).

The analogy between the two scenarios is also appreciable *in vivo*. Firstly described in Serrano lab, induction of *in vivo* reprogramming in OSKM doxycyline-inducible mice led to teratoma formation. The continuous induction for 15 days causes the emergence of these benign tumour, a veritable marker of *in vivo* pluripotency (Abad et al., 2013). Even if cyclic administration leads to amelioration of aging phenotypes, a partial reprogramming (7 days of OSKM expression) drives formation of carcinoma resembling the Wilms tumor, an aggressive pediatric kidney cancer (Ocampo et al., 2016; Ohnishi et al., 2014).

Studies in the lab also highlight similarities between these two processes (see appendix for the corresponding submitted manuscript, for which I am second author). We compared iPSCs generation and malignant transformation focusing on their early steps: pluripotent reprogramming (PR) and malignant reprogramming (MR) (using the model proposed by Petrenko group (Ischenko et al., 2013)). In both models, Thy1 is an interesting marker to trace reprogramming routes: this membrane protein, widely expressed in MEFs, is lost at early steps of the two processes, specifically in reprogramming intermediates prone to iPSCs generation and malignant transformation.

Since the reprogramming efficiency of the Thy1^{low} subpopulation is still very low for both PR and MR, we performed transcriptomic analyses to identify additional MEF markers commonly downregulated during PR and MR. We identified 55 genes commonly regulated in PR- and MR-

Thy1^{low} subpopulations. We selected the zinc finger TF Bcl11b, previously described as a cellular identity gatekeeper in T cells (Wakabayashi et al., 2003). Using a reporter line for Bcl11b (Bcl11b: tomato), we showed that Thy1^{low}Bcl11b^{low} subpopulations reprogram towards pluripotency and malignancy better than the single Thy1^{low} cells. Moreover, thanks to the combined analysis of the two proteins, it has been possible to identify a new roadmap of iPSCs generation and malignant transformation based on these reprogramming markers. We characterized reprogramming intermediates on an epigenomic and transcriptomic level. This characterization led us to identify other regulators of cellular identity that modulates PR and MR, Bcl11a and Fosl1.

Together with the previous results described in literature, our data highlight a similarity between the two reprogramming processes. Moreover, our study describes, for the first time, a comparative molecular roadmap of cellular identity lost during iPSCs generation and malignant transformation.

To go further in the description of these common characteristics, during my PhD I focused on the transcription factors c-Myc, extensively described in malignant transformation and iPSCs generation and present in both pluripotent and malignant reprogramming cocktails.

2.4. C-Myc

2.4.1. General characteristics

c-Myc is a basic helix loop helix (bHLH) transcription factor, a protein family described for its role during development. It belongs to the bHLH leucine-zipper (bHLHZ) subfamily, together with other members n-Myc and l-Myc. l-Myc function is poorly described and the n-Myc function is tissue-specific, for example regulating neurodevelopment (Knoepfler, 2002). On the contrary, c-Myc is widely expressed and acts as a cellular sensor, mediating pleiotropic effects on different cellular processes as proliferation, cell growth, apoptosis, energetic metabolism and biosynthetic pathways (Eilers and Eisenman, 2008). It also works as a node of many growth-promoting signals and is a commonly regulated effector of numerous biological pathways. Myc proteins were firstly discovered in chicken, where the oncogenic retrovirus v-Myc drives emergence of fulminant tumors known as myelocytomatosis (Duesberg and Vogt, 1979; Sheiness and Bishop, 1979).

2.4.2. c-Myc structure

c-Myc is formed by a large unstructured N-terminal region containing the MBI and MBII Myc boxes, followed by a middle region composed of MBIII, MBIV and a nuclear localization sequence rich in PEST (proline, glutamic acid, serine and threonine) residues. Finally, at the C-terminal, it displays a 100-amminoacid region comprising the bHLHZ domain, important for heterodimerization with other bHLH proteins and DNA binding (Carabet et al., 2019) (**Fig. 14**).
In normal conditions, c-Myc does not form homodimers, but creates heterodimers interacting with the bHLHZ Max (Amati et al., 1993; Blackwood and Eisenman, 1991). Once the heterodimer is formed, it can bind the DNA through the basic regions contained in the heterodimer, capable of opening the DNA double helix at the level of the major groove to allow the insertion of the heterodimer helixes (Ferré-D'Amaré et al., 1994, 1993).
While the bHLHZ domain is required for heterodimerization with Max and DNA binding, the Myc boxes are important for c-Myc regulation and interaction with other protein partners. MBI plays a key role for c-Myc stability and it is involved in the ubiquitylation and its proteasomal degradation. Many ubiquitin ligases involved in c-Myc regulation have been described, for example FBW7 (Yada et al., 2004).
MBII accounts for interaction with different proteins to mediate c-Myc principal functions (Stone et al., 1987). This includes components of the histone acetyltransferase (HAT)

complexes, as TRAPP-GCN5, Tip60 and Tip48, important for c-Myc role in histone acetylation and gene activation (McMahon et al., 1998). MBII also plays a role in c-Myc protein stability, binding at its site the E3 ligase SKP2, involved in c-Myc degradation (von der Lehr et al., 2003). Moreover, the loop region between MBI and MBII is also important for interaction with other effectors of Myc activity, as BRD4 and P-TEFb (Eberhardy and Farnham, 2002; Wu et al., 2013). MBIII is responsible for c-Myc mediated gene repression: it gives a docking site to histone deacetylase repressor complexes, such as SIN3 and HDAC3 (Garcia-Sanz et al., 2014, p. 3; Kurland and Tansey, 2008).

As MBII, MBIV is also important for c-Myc transcriptional activity. It also contains the interaction sites of p27, a c-Myc inhibitor, which phosphorylates the residue S62, inducing c-Myc degradation (Hydbring et al., 2017).

Apart from the control at the level of c-Myc protein stability, this TF is tightly regulated at the transcriptional level by different signalling pathways, transcription factors, chromatin regulators and cis-regulatory elements (Wierstra and Alves, 2008).

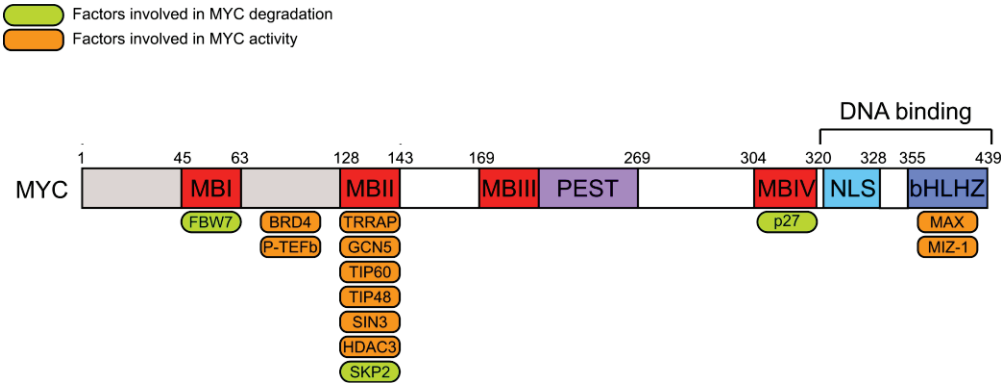

Figure 14: (Adapted from Conacci-Sorrell et al., 2014) Proteic structure of the bHLHZ c-Myc. Functional (blue) and regulation (red) domains are represented. On the bottom of the image, representation of a non-exhaustive list of factors involved in Myc degradation (green) and activity (orange).

2.4.3. Max interaction and mechanism of action

The principal interactor of c-Myc is Max. c-Myc and Max form preferably heterodimers, as far as the homodimers Max-Max associates more rarely and bind DNA with lower efficiency. Moreover, Max phosphorylation interferes with homodimer formation without impacting negatively heterodimerization (Berberich and Cole, 1992).

Interestingly, c-Myc-Max binding is not always associated to changes in transcriptional output of the bound regions. Coupled Chip-Seq and RNA-Seq analysis have shown that only a small

percentage of the bound regions undergoes transcriptional modifications (Perna et al., 2012; Seitz et al., 2011; Zeller et al., 2006). The discrepancy is due to the requirement of co-factors to induce changes in gene expression.

The c-Myc-Max heterodimer binds active chromatin sites characterized by histone marks H3K4me3 or H3K27ac (Guccione et al., 2006). The binding itself is mediated by H3K4me3-associated chromatin remodellers, such as Wdr5 and Bptf (Caforio et al., 2018; Thomas et al., 2015, p. 5). Together with its binding to DNA, c-Myc recruits Trapp via its MBII domain (McMahon et al., 1998). Trapp in turn interacts with HATs like Gcn5 and Tip60 to promote gene activation. Open chromatin is thus bound by bromodomain-containing proteins, such as Brd4, and other co-activators of bromodomain, which recruits the positive transcription elongation factor P-TEFb, with both Brd4 and P-TEFb interacting with c-Myc on the loop between MBI and MBII (Eberhardy and Farnham, 2002; Wu et al., 2013). Transcription activators recruited in the complex can then activate the kinase activity of P-TEFb, which phosphorylates the C-terminal of RNAPolII, causing its release and transcriptional elongation (Itzen et al., 2014, p. 4) (**Fig. 15**). c-Myc does not mediate only transcriptional activation, but also repression. To induce transcriptional repression, c-Myc-Max complex can interact with other transcription factors, such as the Myc-interacting zinc finger protein 1, Miz1 (Seoane et al., 2001; Staller et al., 2001). The complex formed with Miz1 leads principally to transcriptional repression, due to the recruitment of co-repressors, such as the DNA methyltransferase Dnmt3a (Brenner et al., 2005). Moreover, Miz1 plays a role in stabilizing c-Myc protein by inhibition of its ubiquitin-dependent degradation (Salghetti, 1999).

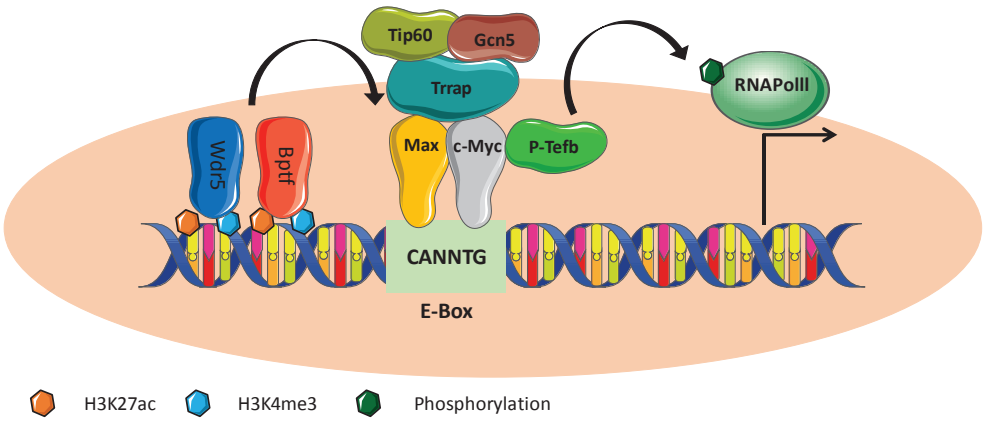

Figure 15: (Adapted from Dang et al., 2012) Mechanism of action of c-Myc mediating transcriptional activation. C-Myc upregulation drives RNAPolII-mediated transcriptional activation

2.4.4. Myc function

Myc covers different functions, principally acting as a sensor to signals, inducing cell proliferation and growth. This is well displayed in cancer, where malignant cells rely on c-Myc strong activity to ensure the energetic need linked to a massive proliferation (Pelengaris et al., 2002; Shachaf et al., 2004). On the contrary, an opposite example is provided by developmental diapause, an embryonic state, typical of many invertebrates and vertebrates, in which the development of the embryo is temporarily blocked before implantation, in case of disadvantageous environmental conditions (Hondo and Stewart, 2004; Renfree and Shaw, 2000). In this situation, the blastocyst enters a dormant phase characterized by proliferative and metabolic quiescence. In line with c-Myc function, it is not unexpected that c-Myc is strongly downregulated *in vivo* during mouse diapause. Moreover, inhibition of c-Myc and n-Myc in ESCs leads to *in vitro* dormancy similar to embryonic diapause (Scognamiglio et al., 2016).

To exploit its sensor activity and link growth signals to cellular responses, c-Myc modulates the transcription and production of key components of almost every biosynthetic pathway (Dang, 2013). This comprises control of DNA replication, cell cycle, ribosome biogenesis and protein synthesis, anabolites production and energy production.

2.4.4.1. c-Myc function in iPS generation

During iPSCs generation, c-Myc plays an essential role in the initial steps of pluripotent reprogramming. Its activity leads to the downregulation of somatic identity markers, as Snai1 and Snai2, de-differentiation and increase of proliferation and cell cycle, as highlighted by enhanced expression of Rfc4, Mcm5, Ccnd1, Ccnd2 (Mikkelsen et al., 2008a).

Moreover, during pluripotent reprogramming, it orchestrates a different function compared to the other Yamanaka factors. Oct4, Sox2 and Klf4 act as pioneer factors, binding together to closed regions of DNA to induce their transcriptional activation, preferentially acting on distal elements. On the contrary, c-Myc targets chromatin regions already opened in the somatic cell, binds at promoter sequences and drives direct changes in gene expression. In the first days of reprogramming, it binds promoter of somatic genes and induces the erasure of the epigenetic mark H3K4me2, associated with active transcription. Moreover, c-Myc recruits OSK in a fraction of its binding sites and can also work as an enhancer for OSK binding to inaccessible chromatin, resulting in the existence of “OSKM”, “OSK” and “only M” bound sites (Soufi et al., 2012). As expected for its described functions, genes associated with c-Myc binding (“M only” and

"OSKM") are involved in translation control, RNA splicing, cell cycle and energy production (Sridharan et al., 2009). It has been shown that c-Myc drives a similar regulatory network between ESCs and cancer cells, but the function of this c-Myc module is independent from the core pluripotency network, highlighting the difference between OSK and c-Myc (Kim et al., 2010). This suggests that c-Myc plays an important role both in reprogramming and pluripotency, but a different function compared to pluripotency factors (Kim et al., 2010)

Despite the c-Myc-associated functions in the beginning of PR, contrasting views were proposed for c-Myc requirement during iPSCs generation. It was shown that c-Myc presence in reprogramming cocktail is dispensable (Wernig et al., 2008b) and many variations of PR generate iPSCs through reprogramming cocktails, in which c-Myc is absent and can be substituted by HDAC inhibitors (Araki et al., 2011; Huangfu et al., 2008). However, the quality of OSK-derived iPSCs was questioned, as far as they show defects in re-differentiation ability, with less high-grade chimaera formation and defects in neuronal differentiation (Araki et al., 2011; Löhle et al., 2012). Indeed, recent studies have shown the necessity of c-Myc in pluripotent reprogramming concerning activation of glycolytic flux and induction of a hybrid energetic program, DNA synthesis, proliferation, DNA repair and chromatin reorganization (Prieto et al., 2018; Zviran et al., 2019). Moreover, highlighting the importance of endogenous c-Myc, in a study aimed to compare the transdifferentiation and the pluripotent reprogramming potential of pre-B cells, cells harbouring low levels of c-Myc transdifferentiate rapidly into macrophages, but fail to accomplish pluripotent reprogramming, while c-Myc-high pre-B cells reprogram efficiently to iPSCs (Francesconi et al., 2019).

2.4.4.2. c-Myc in malignant transformation

c-Myc is one of the most known oncogenes, contributing to more than 75% human cancers, such as prostate, breast, colon, cervical cancers, myeloid leukemia, lymphomas and small-cell lung carcinomas (Carabet et al., 2018). Also its paralog genes, n-Myc and l-Myc have been described to being mutated and acting as oncogenes for neuroblastoma and lung cancer respectively (Brodeur et al., 1984; Nau et al., 1985).

The first evidence of c-Myc oncogene function came from the Burkitt lymphoma, where it is always found altered due to chromosome translocation into the immunoglobulin alpha switch region (Taub et al., 1982). However, c-Myc is not only translocated, but can also be found amplified, mutated or upregulated as a downstream effect of the action of other oncogenes (Beroukhim et al., 2010; He, 1998; Shou et al., 2000). Stabilization of its mRNA in cancer is also

observed, with an elongated half-life, as well as alterations of its turnover rate (Kalkat et al., 2017). All these events lead to an increase expression and/or activity of the c-Myc protein.

Its function as oncogene has been shown in different *in vivo* models (Adams et al., 1985; Leder et al., 1986). However, even if c-Myc is associated to a broad range of tumors, it always works in cooperation with other oncogenes and onco-suppressors to drive malignant transformation: for example, c-Myc activity in mammary carcinoma leads to spontaneous mutations of K-Ras, and c-Myc-induced lymphoma lack onco-suppressors such as p53 or Arf (D'Cruz et al., 2001; Eischen et al., 1999). Moreover, in combination with other oncogenes, it can transform primary MEFs (Land et al., 1983).

It seems so that c-Myc is a mediator of tumor initiation and promotion, without being sufficient alone or strictly necessary. However, on the contrary, c-Myc expression is essential for progression of many tumors and its inhibition is detrimental for tumor growth, leading to blockage in cellular proliferation and induction of apoptosis (Pelengaris et al., 2002; Wang et al., 2008). Indeed, many tumor model regress once c-Myc expression is depleted, suggesting the existence of a tumoral addiction phenomenon to c-Myc (Gabay et al., 2014). Interestingly, c-Myc addiction takes places even when the cancer initiation is not driven by this bHLH TF, but from other oncogenes, like KrasG12D and SV40 viral antigens (Sodir et al., 2011; Soucek et al., 2008). Additionally, tumors addicted to c-Myc are also dependent on nutrients supply: glucose and glutamine withdrawal in c-Myc overexpressing malignant cells leads to their apoptosis (Shim et al., 1998; Yuneva et al., 2007). This can be associated to c-Myc role in biomass accumulation, with the deregulated growth induced by c-Myc causing this nutrient sensitivity.

Moreover, c-Myc is important also in late steps of cancer development, where it triggers metastasis formation by miR-9 mediated targeting of E-cadherin during EMT. Moreover it transactivates the polycomb complex protein Bmi-1, which induces EMT through repression of the onco-suppressor Pten (Ma et al., 2010, p. 9; Song et al., 2009).

2.4.5. c-Myc is a basic Helix-Loop-Helix transcription factor

c-Myc belongs to the family of basic helix-loop-helix protein (bHLH). This protein class has previously been described to play several functions during development and many genes of this class constitute veritable onco-suppressors and oncogenes (Bersten et al., 2013; Sun et al., 2007).

The proteins of this family are characterized by two high conserved domains that together form a region of 60 ammino-acids, the basic and the helix-loop-helix domains.

The basic domain mediates the DNA binding at the E-box consensus sequence (CANNTG), with the two central nucleotides and the surrounding ones giving the specificity of the binding. The HLH domain is composed by two alpha-helices connected by a non-conserved loop region and facilitates the interactions with other subunits to form homo- or hetero-dimers (Murre et al., 1989). bHLH TFs can hetero-dimerize with many partners and the multiple combination of the interactions, together with the differential specificity of the E-boxes, determine how bHLH TF complexes control different functions through transcriptional regulation (Fairman et al., 1993). Among the bHLH family, we can distinguish two major classes: class II bHLH TFs are tissue-specific and define DNA-binding specificity, while the class I bHLH TFs, also called E-proteins (such as E2A, HEB and E2-2), are constitutively expressed and help the first group to achieve DNA binding and transcriptional regulation (Berkes and Tapscott, 2005; Bertrand et al., 2002; Sun and Baltimore, 1991, p. 12). We can also identify a group of bHLH TFs, the Id proteins, which lack the DNA binding domain and act merely as antagonist of class II bHLH for the binding with E-proteins. Thus, they work as DNA-binding inhibitors of class II bHLH (Wang and Baker, 2015).

bHLH TFs play a fundamental role in neurodevelopment, where they mediate NPCs self-renewal and neuron, astrocytes and oligodendrocytes differentiation (Ross et al., 2003). NPCs maintenance rely on Hes factors (Hes1, Hes3 and Hes5): these bHLH TFs show their repressive action forming homodimers and binding DNA to repress expression of their target genes (Sasai et al., 1992). They maintain the precursor identity by inhibiting pro-neural genes such as Ascl1 and Neurog2 at different regulation levels: they can repress their expression and, at a post-transcriptional level, they can antagonise pro-neural bHLH TF activity physically interacting with them and displacing them by their canonical targets (Giagtzoglou, 2003; Imayoshi et al., 2008). They can also perturb heterodimers formed by pro-neural bHLH TFs and E-proteins: this is the case of Hes1, which binds E47 and avoids its recruitment by Ascl1, necessary for the formation of the heterodimer Ascl1-E47 and its DNA binding (Sasai et al., 1992). Similar function is accomplished also by Id TFs, which recruit E-proteins to avoid their interaction with pro-neural bHLH TFs, resulting in Ids acting as anti-differentiation dominant-negative antagonists of proneural bHLH transcription factors. Moreover, Id TFs block the auto-regulative negative loop formed by Hes1 on its own expression (Bai et al., 2007).
However, not all Hes genes are anti-differentiation factors: on the contrary, Hes6 interacts with Hes1 avoiding both its transcriptional repression activity and its ability to perturb the formation of the Ascl1-E47 pro-neural heterodimer (Bae et al., 2000) (**Fig.16**).

On the other hand, a second group of bHLH TFs drives the differentiation of neural precursor cells (NPCs) into the different neural cell types (Bertrand et al., 2002). During neuronal differentiation, Ngn1, Ngn2 and Ascl1 interact with bHLH E-proteins to form hetero-dimer complexes which transactivate expression of target genes, involved in cell-cycle exit, neurotransmitter biosynthesis and neurite outgrowth (Castro et al., 2011). While Olig1 and Olig2 have been described as the bHLH TFs mediating differentiation towards oligodendrocytes, for astrocytes a precise master regulator has not been yet described (Meijer et al., 2012).

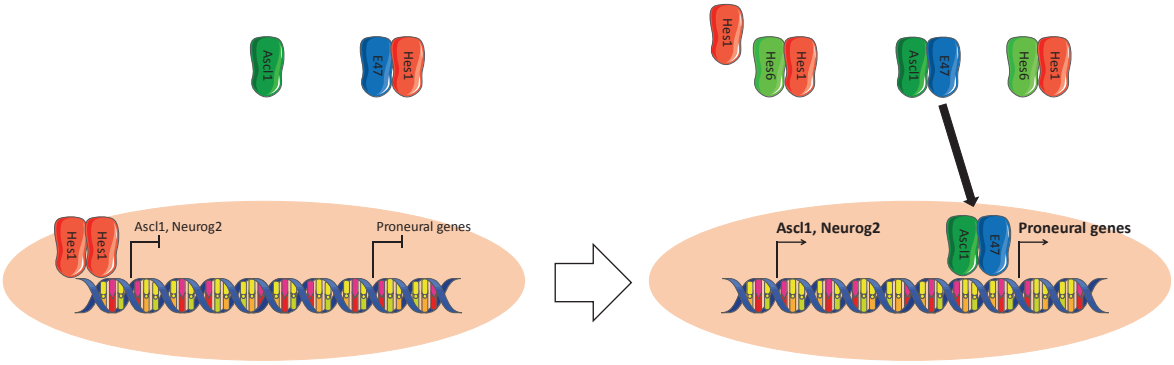

Figure 16: bHLH interactions during neural precursor cells (NPCs) differentiation. Left: Hes1 blocks differentiation in NPCs. Right: Hes6 repression activity on Hes1 induces pro-neural genes expression.

To sum-up, in neurodevelopment we can distinguish two different functions of bHLH TFs. On one end, they drive changes of cellular identity, like Ascl1 or Olig factors during the differentiation processes. On the other hand, they prevent cellular identity conversion and safeguard initial cellular identity, such as Hes1 in NPCs. Moreover, as mentioned above, bHLH TFs can obstacle one with each other at different levels, as it has been shown for the repression of Hes6 on Hes1 activity (Bae et al., 2000).

Interestingly, in our reprograming system, c-Myc has already been proposed as a bHLH TF driving loss of cellular identity and fate conversion during iPSCs generation and malignant transformation (Ischenko et al., 2013; Mikkelsen et al., 2008a)
We thus wonder if it could exist one or more bHLH TFs antagonising c-Myc activity, avoiding cellular identity reprogramming and behaving as gatekeepers of the somatic identity.

As described in the results section, a bHLH TFs screening identified Atoh8 as a protector of cellular identity and an obstacle towards reprogramming processes.

2.5. Atoh8

2.5.1. General characteristics

The atonal bHLH superfamily contains eight families: NeuroD, Neurogenin, Atonal, Oligo, Beta3, Mist and NET (Chen et al., 2011, p. 8). Within the group of the atonal bHLH TFs, Atoh8, also called Math6, is the sole mammalian member of the Net group (Rawnsley et al., 2013). Firstly described in neurodevelopment, following studies have shown that its expression is broadly distributed in the embryo after the beginning of gastrulation and that it is fundamental for many developmental processes. Being identified in 2001, there are few studies (around thirty) published on this bHLH TF. Thus, much information regarding its precise regulation, mechanisms and functions are still missing.

2.5.2. Expression pattern

In the central nervous system (CNS), Atoh8 is initially widely expressed between E12.5 and 16.5 in the pro-neural precursors of the ventricular zone, in the cortical plate and other regions of the brain, in the spinal cord and the dorsal root ganglia. Its expression is gradually restricted during neural differentiation to a subset of adult mature neurons present in the hippocampus, in the Purkinje cells of the cerebellum and weakly expressed in the adult retina (Inoue et al., 2001).

However, Atoh8 expression is not restricted to the CNS, but at different stages of development it is expressed in somitic muscles, kidney, heart, blood and vascular progenitors, lung, liver, pancreas, intestine, spleen and vascular smooth muscles (Balakrishnan-Renuka et al., 2014; Ejarque et al., 2013; Fang et al., 2014; Kautz et al., 2008; Lynn et al., 2008; Rawnsley et al., 2013; Ross et al., 2006; Yao et al., 2010).

For example, Atoh8 expression is observed in the developing kidney, where it is constantly expressed from E14.5 to birth (day 0); after birth, its expression in kidney arises and reaches its maximal level at day 7 post-birth. By day 13, its expression begins to decline and by day 40 low levels persist in adulthood, where Atoh8 is specifically expressed in the subset population of podocytes (Ross et al., 2006, p. 6).

Moreover, its expression is not limited to embryonic tissues: indeed, Atoh8 is strongly expressed in placenta at E8.5, it is still present at E10.5, while its level decreases at E13.5 and it is expressed in a subset of cells of the decidua region at E18.5 (Böing et al., 2018).

According to these expression patterns, it seems that Atoh8 is broadly expressed in several differentiating tissues, while its presence is restricted to specific cellular types in more mature tissues. This suggest that this bHLH TF could possibly play a double role during development: an initial role of general promoter of differentiation and a second role specific of precise cell subsets within several adult organs.

2.5.3. Structure

The structure of this bHLH TF is quite peculiar compared to the other Atoh bHLH TFs. It has a distant structural homology with the *Drosophila* atonal gene, thus it shows only 43-57% of homology in the bHLH domain with the other mammalian atonal genes, such as Neurog1, NeuroD1 and Atoh1. However, even if Atoh8 diverges from these atonal factors, all these genes are more similar compared to the non-atonal Mash1, classifying Atoh8 in the atonal family (Inoue et al., 2001). (**Fig.17**)

While the Atoh8 bHLH domain presents a 100% homology among many species, the N-terminal region of Atoh8 differs highly upon different evolutionary lineages (Chen et al., 2011, p. 8; Inoue et al., 2001).

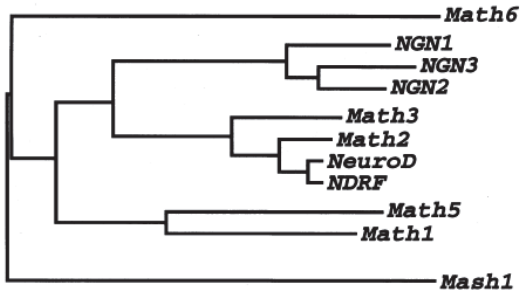

Figure 17: (Adapted from Inoue et al., 2001) Philogenetic tree of mouse atonal homologues. Atoh8/Math6 is more similar to other atonal factors than to Mash1

The peculiarity of this bHLH TF is also conferred by its exon-intron structure: while all the others atonal proteins are characterized by a sole exon, Atoh8 is composed of two long introns (the first one of around 11Kb and the second one longer than 12Kb) and three different exons, with two long exons 1 and 2, plus a third exon encoding just for one glutamic acid (Chen et al., 2011; Inoue et al., 2001).

In the N-terminal part of the protein, after the first one hundred amino acids, we can find a proline rich (Pro-rich) domain required for transcriptional repression (Ejarque et al., 2013). It is

followed by a serine rich (Ser-rich) domain and a predicted nuclear localization signal (NLS). In the C-terminal domain we can find the basic and the HLH domain, typical of the bHLH transcription factors (Chen et al., 2016) (**Fig.18**).

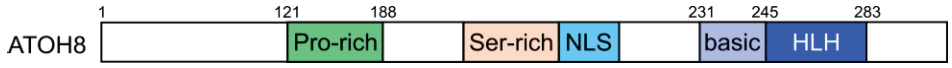

Figure 18: Protein structure of the bHLH Atoh8. The Pro-rich domain is important for Atoh8 gene repression, the basic and HLH domain for its DNA binding and dimerization.

2.5.4. Regulation

The 5'-UTR of Atoh8 constitutes a GC-rich element (72%) and is highly structured, suggesting that it can play an important role in Atoh8 regulation. The 1.0 Kb region upstream its coding sequence contains the basal promoter of the gene. This fragment contains four E-boxes, suggesting that its expression can be modulated by other bHLH TFs, as it has been described for the Neurog3 binding to the third E-box (Pujadas et al., 2011).

One of the major features of Atoh8 regulation consists in its bivalent promoter. Atoh8 is situated in a CpG island of 1.9Kb, which starts 0,7kb upstream its TSS (Pujadas et al., 2011). Indeed, a class of CpG-rich promoter consists in bivalent promoters, firstly described in ESCs (Bernstein et al., 2006). This chromatin configuration is mainly found at developmental genes that are quickly activated after ESCs differentiation and is characterized by two methylation marks with opposite effects: H3K4me2/3 and H3K27me3. While in ESCs the bivalent methylation maintains the promoter silenced, at the onset of differentiation, the loss of H3K27me3 drives a quick activation.

In the case of Atoh8, few factors have been described to induce the H3K27me3-mediated repression and these mechanisms are strongly activated in cancer. For example, long non-coding RNA PDZD7 mediates activation of EZH2, a methyltransferase that drives the H3K27me3 methylation of Atoh8 and its silencing (Zhang et al., 2019). In a similar way, the EBV-encoded latent membrane protein LMP1 overexpression, observed in nasopharyngeal carcinoma, impairs the H3K4me3 activating mark, enhancing the occupancy of the repressive H3K27me3 (Wang et al., 2016, p. 8).

On the contrary, Neurog3 binding on Atoh8 promoter mediates removal of the repressive H3K27me3 mark and activation of Atoh8 expression (Pujadas et al., 2011).

On a signalling level, Atoh8 seems to be a target gene of the Tgfβ superfamily, as it has been shown regulated by Gdf5 during retinal development and Bmp4 in the liver (Kautz et al., 2008; Li et al., 2019, p. 8).

2.5.5. Function

The lacking information on Atoh8 presented in the published studies do not allow to describe a unifying function of this bHLH TF. This could be related to the paucity of information on this protein, but Atoh8 could also play different roles in several organs, depending on other co-factors present in a tissue-specific manner.

First studies on Atoh8 showed a contribution of this factor in neurodevelopment: in the first seminal study, Inoue and colleagues showed that over-expression of Atoh8 in retinal explants at E17.5 biases the differentiation towards a neural fate against a glial fate, proposing Atoh8 as a neuronal differentiation factor (Inoue et al., 2001).
However, an opposite study, performed in chicken, showed that Atoh8 is expressed in the stem cell progenitors of the peripheral region of the retina, the ciliary marginal zone (CMZ), where it negatively regulates retinal ganglion cells differentiation (Kubo and Nakagawa, 2010), confusing the current knowledge on the Atoh8 role during neural development. The observed differences could be related to the molecular structure of the avian Atoh8, which lacks a large portion of the N-terminal (Chen et al., 2011, p. 8). Furthermore, a recent study confirmed the role in retina differentiation, as far as GDF5 signalling induces differentiation of retinal stem cells into neurons in an Atoh8-mediated manner (Li et al., 2019, p. 8).

Atoh8 plays important functions also outside of the CNS, identifying this protein as a pleiotropic factor, compared to many other bHLH TF which are tissue specific. Particularly, it plays an important role in development of mesoderm-derived organs, where it contributes to the onset of differentiation in the vascular system, the hypaxial myotome of the trunk, the heart and the skeletal chondrocytes (Balakrishnan-Renuka et al., 2014; Fang et al., 2014; Rawnsley et al., 2013; Schroeder et al., 2019).

Considering the pleiotropic effects accomplished by this molecule, the spontaneous question about its requirement during development has been arisen. Currently, there are opposing views on the necessity of Atoh8 during embryonic development. While a first group showed that this TF is fundamental during development and its deletions leads to lethality around

gastrulation, a second group showed no severe developmental defects in an Atoh8 KO mice (Böing et al., 2018; Lynn et al., 2008). This could be related to the different techniques used to knock-out the Atoh8 gene, as far as in the first study the KO was achieved by deletion of exon1, intron 1 and exon2, while the second group deleted the first exon (which contain 257 of the overall 322 amino acids). To date, Atoh8 requirement during development is still an open question.

Taking in account the broad expression during embryonic development, the bivalent structure of its promoter and the several functions described, the literature displays Atoh8 as a broad inducer of cellular differentiation.

2.5.6. Atoh8: cancer and stemness

Atoh8 is broadly lost in the major part of tumors (for example, hepatocellular carcinoma, nasopharyngeal carcinoma, and bladder cancer, oligodendroglioma) (Ducray et al., 2008; Freire et al., 2008; Song et al., 2015, p. 8; Wang et al., 2016; Ye et al., 2017; Zaravinos et al., 2011).
In hepatocellular carcinoma (HCC), Atoh8 has been largely described as an onco-supressor. Moreover, its downregulation leads to the acquisition of CSC features.
In cancer lines derived from this tumor, it has been shown that, when expressed, Atoh8 inhibits proliferation, tumor growth, invasive and migratory abilities. However, upon its depletion, expression of stemness- and CSC-associated genes like Oct4, Nanog, Sox2 and Cd133 is enhanced, suggesting acquisition of stem cells features. In particular, loss of Atoh8 expression increases the number of $Cd133^{+}$ cells, which constitute the cancer stem cell population of HCC, leading to an enhanced aggressiveness, self-renewal capability and chemoresistance (Song et al., 2015, p. 8).

The study identifies Atoh8 not only as an obstacle to cancer development, but it constitutes also a roadblock to acquisition of cancer stem properties. This could suggest a possible role of this factor as a cellular gatekeeper acting against cellular identity conversion.

3. FIRST PHD PROJECT PAPER:

A C-MYC/ATOH8/WNT AXIS ORCHESTRATES CELLULAR REPROGRAMMING IN IPSC GENERATION AND MALIGNANT TRANSFORMATION

Authors: G. Furlan[1], A. Huyghe[1], M. Siouda[2], F. Mugnier[1], L. De Matteo[1], P. Wajda[1], B. Gibert[3], N. Rama[3], R. Dante[3], R. Gasa[4], P. Mulligan[2], F. Lavial[1]*.

Affiliations : 1 Cellular reprogramming and oncogenesis Laboratory - Lyon University, Université Claude Bernard Lyon 1, INSERM 1052, CNRS 5286, Centre Léon Bérard, Cancer Research Center of Lyon, Lyon, France; 2 Epigenetics and cancer Laboratory - Lyon University, Université Claude Bernard Lyon 1, INSERM 1052, CNRS 5286, Centre Léon Bérard, Cancer Research Center of Lyon, Lyon, France; 3 Dependence receptors, cancer and development Laboratory - Lyon University, Université Claude Bernard Lyon 1, INSERM 1052, CNRS 5286, Centre Léon Bérard, Cancer Research Center of Lyon, Lyon, France; 4 Diabetes and Obesity Research Laboratory - IDIBAPS August Pi I Sunyer Biomedical Research

Contact Information: * F. Lavial: fabrice.lavial@lyon.unicancer.fr

Abstract

Restriction of cellular plasticity and determination of somatic identity are two fundamental processes during organism development. These events are reversed during pluripotent reprogramming (PR), when a differentiated cell loses its identity to reacquire pluripotent features and generate induced pluripotent stem cells (iPSCs), thanks to the combined action of Oct4, Sox2, Klf4 and c-Myc (OSKM). Loss of somatic identity and partial reacquisition of cellular plasticity are elements characterizing also the first steps of malignant transformation, where perturbation of cellular identity anticipates oncogenic insult, in a process called malignant reprogramming (MR). We propose to consider pluripotent and malignant reprogramming as two models to study the initial dedifferentiation and loss of somatic identity iPSCs generation and malignant transformation. Indeed, these two processes share valuable similarities: OSKM can act as *bona fide* oncogenes and known onco-suppressors constitute roadblocks to pluripotent reprogramming. Moreover, the same biological responses, such as apoptosis and senescence, obstacle iPSCs generation and malignant transformation.

We analysed the role of c-Myc in these scenarios. Indeed, this basic Helix Loop Helix transcription factor (bHLH TF) has already been shown to be veritable oncogene and is fundamental for pluripotent reprogramming. bHLH transcription factors represent a family of TFs initially identified for their role in development and cell differentiation. They are known to form heterodimeric complexes and to promote or antagonise each other activity. In this study, we identified a new bHLH TF antagonising c-Myc action during malignant transformation and iPSCs generation, Atoh8. Indeed, depletion of this bHLH TF enhance both PR and MR. Interestingly, we showed that c-Myc can directly repress the expression of Atoh8, and this repression leads to an activation of Wnt pathway, responsible for the phenotypes observed in iPSCs generation and malignant transformation.

Highlights

- The basic Helix-Hoop-Helix (bHLH) transcription factor c-Myc endogenous levels are fundamental to ensure iPSCs generation and malignant transformation
- A comprehensive bHLH transcription factor screening identifies Atoh8 as a novel obstacle towards iPSC formation and tumorigenesis
- Depletion of Atoh8 in the somatic cell before oncogenic insult results in a more aggressive malignant transformation correlated to a partial EMT state.
- Atoh8 is a broad gatekeeper of cellular identity antagonising to multiple reprogramming processes.
- c-Myc-mediated Atoh8 repression induces Wnt pathway activation.

Introduction:

Establishing and safeguarding cellular identity is a key objective for multicellular organisms. During development, embryonic stem cells (ESCs) differentiate into the three germ layers, where precursor stem cells give rise to tissues and organs (Bedzhov et al., 2014). Lineage segregation in the early embryo is accompanied by the progressive restriction of cellular plasticity and specialisation into different somatic identities (Patel and Hobert, 2017). Adult cells maintain their somatic identity thanks to precise molecular mechanisms that determine their specific cellular type and differentiation state.

However, somatic adult cells can dedifferentiate, losing their somatic identity and reacquiring cellular plasticity, to generate induced pluripotent stem cells (iPSCs), in a process known as pluripotent reprogramming (PR) (Takahashi and Yamanaka, 2006). The first phase of this process consists in an immediate response of downregulation of cell-specific genes and enhanced proliferation, leading to loss of somatic identity (Mikkelsen et al., 2008).

Loss of somatic identity is a characteristic of pluripotent reprogramming shared with malignant transformation. For a long period, cancer has been considered a merely proliferative disease, where advantageous mutational events promote expansion of clonal populations characterized by enhanced proliferation and survival advantages (Hahn and Weinberg, 2002). However, in the last years, cellular dedifferentiation has emerged as an important initial phase to render cells sensitive to oncogenes action (Roy and Hebrok, 2015; Yuan et al., 2019). This has been widely shown in several types of cancer, where a first phase of loss of somatic characteristics, known as transdifferentiation or metaplasia (depending if the process concerns some cells or the entire organ), leads to changes in the cellular identity that prepare cells to malignant transformation. In pancreatic ductal adenocarcinoma (PDAC), normal acinar cells loose expression of acinar markers before entering acinar to ductal metaplasia (ADM), where oncogenic insults initiates adenocarcinoma (De La O et al., 2008; Shi et al., 2013; von Figura et al., 2014). In Barret's esophagus, conversion of somatic identity from normal squamous epithelial cells to columnar epithelial cells consists in a first step towards esophageal adenocarcinoma (Hvid-Jensen et al., 2011). Moreover, loss of tumorsuppressors p53 and Nf1 in neurons and astrocytes leads to cellular dedifferentiation and formation of glioblastoma composed largely by cells expressing Sox2 and Nestin, typical markers of neural stem cells (Friedmann-Morvinski et al., 2012). These examples show that the loss of somatic markers is one of the first steps in tumorigenesis and, thus, mechanisms safeguarding somatic identity could represent a first obstacle towards malignant transformation.

In this context, the action of mutated K-Ras (K-RasG12D) and c-Myc oncogenes, combined with the loss of the oncosuppressor p53 (KMP cocktail), have been recently shown to trigger reprogramming and malignant transformation in somatic cells (Ischenko et al., 2013). This process, called malignant reprogramming (MR),

is emerging as a novel determinant of cancer development, acting at the early stage of the process, but its characterization is very limited.

Deciphering the regulatory networks that triggers the conversion of a somatic cell to a dedifferentiated state prone to tumorigenesis is crucial to broaden our knowledge of cancer initiation.

Interestingly, pluripotent reprogramming shares key features with malignant transformation: (i) the four pluripotent reprogramming factors OSKM represent independently *bona fide* oncogenes (Dang, 2012; de Jong and Looijenga, 2006; Herreros-Villanueva et al., 2013; Yu et al., 2011). (ii) tumor suppressors, such as p53 and Rb, act also as reprogramming roadblocks (Kareta et al., 2015; Kawamura et al., 2009). (iii) same cellular processes, such as senescence and apoptosis, constitute significant barriers to both PR and OR (Li et al., 2009; Sherr, 2001; Utikal et al., 2009). (iv) the premature termination of pluripotent reprogramming *in vivo* leads to tumorigenesis (Ohnishi et al., 2014). These evidences suggest that, among malignant transformation and iPSC generation, common events could render a cell susceptible to dedifferentiate and receive pluripotent induction or oncogenic insult.

We are particularly interested in deciphering the function of basic Helix-loop-Helix transcription factors (bHLH TFs) in the context of pluripotent reprogramming and malignant transformation. This family of transcription factors was initially identified for their role in development, where many bHLH TFs are fundamental for the processes of cell identity conversion and differentiation (Bertrand et al., 2002; Fujii et al., 2006; Gradwohl et al., 2000). In particular, we focused on the bHLH TF c-Myc function in these two reprogramming scenario, being c-Myc a well described oncogene and one factor of the Yamanaka reprogramming cocktail (Dang, 2012; Takahashi and Yamanaka, 2006). Indeed, c-Myc function in pluripotent reprogramming is debated and its endogenous requirement in pluripotent reprogramming and malignant transformation is unclear (Araki et al., 2011; Löhle et al., 2012; Wernig et al., 2008).

As well described in neurodevelopment, bHLH can have opposite roles antagonizing each other action (Bae et al., 2000; Imayoshi and Kageyama, 2014; Sasai et al., 1992).

In this study, with the aim to find bHLH TFs competing with c-Myc to safeguard somatic cellular identity, a systematic screening of bHLH TF expression kinetics during iPSC generation and malignant transformation led to identify the transcription factor Atoh8. We showed that its depletion renders cells more prone to both reprogramming processes, showing its novel role as an obstacle towards loss of somatic identity during iPSC generation and oncogenesis. We thus characterized the effects of Atoh8 depletion in iPSCs and transformed cells obtained at the end of reprogramming. While iPSCs are not negatively impacted by the initial Atoh8 downregulation, transformed cells derived in an Atoh8-null background are more aggressive and display a partial EMT state. Furthermore, we showed that Atoh8 plays a broader role as a general barrier to dedifferentiation and reprogramming in several scenarios. Moreover, c-Myc drive Atoh8 repression acting directly on its promoter. Finally, we demonstrated that Atoh8 depletion induces Wnt signalling activation, which accounts for the observed enhanced efficiencies in malignant transformation and iPSCs generation.

Results:

c-Myc function in iPS cells generation and malignant transformation

Somatic cells can be reprogrammed towards pluripotency thanks to the combined overexpression of the four transcription factors, Oct4, Sox2, Klf4 and c-Myc (Takahashi and Yamanaka, 2006). However, it was shown that fibroblasts can be reprogrammed to iPSCs through the exogenous expression of Oct4, Sox2 and Klf4 alone. In this perspective, c-Myc effect should be limited to an increased acceleration of the process and c-Myc presence in reprogramming cocktail would be dispensable (Wernig et al., 2008). However, further studies questioned the differentiation potential of OSK-derived iPSCs and showed that c-Myc low expression levels are detrimental to pluripotent reprogramming efficacy (Araki et al., 2011; Francesconi et al., 2019; Löhle et al., 2012). We revisited c-Myc function during iPS cells generation from mouse embryonic fibroblasts (MEF). In contrast to Oct4 and Sox2, c-Myc and Klf4 were found expressed in MEF (Fig1A). We therefore wondered whether c-Myc was found dispensable for iPS cells generation because its endogenous levels is sufficient to trigger the reactivation of the pluripotent program.

To assess the function of endogenous c-Myc in iPS cells generation, MEFs were infected with sh#c-Myc lentiviral particles (Fig. S1A) prior to OSK transduction (Fig 1B). In this setting, we found that c-Myc downregulation severely hindered the efficiency of alkaline phosphatase positive (AP+) iPSC colonies formation, demonstrating a critical function for endogenous c-Myc during PR (Fig 1C-D).

c-Myc has also been shown to cover an important role in malignant transformation. Not only it cooperates with other oncogenic events to induce tumor initiation, but established tumors also rely on its strong expression due to the advantages of cell growth and proliferation that it brings (Dang, 2012). Since c-Myc exogenous expression has been found to trigger malignant reprogramming (MR) (Ischenko et al., 2013), we next assessed whether, similarly as during iPSC formation, its endogenous expression critically regulates MR. In this context, c-Myc is already present in MEFs and its level increases during malignant transformation (Fig 1E). MEF harboring a Lox-Stop-Lox (LSL)-KRasG12D cassette were transduced with sh#c-Myc lentiviral particles prior to Cre and sh#p53 infection. We assessed the ability of MEFs to form immortalized foci using cresyl-violet staining 30 days after infection (Fig1F). Similarly to PR, downregulation of the endogenous c-Myc severely reduced the efficiency of foci formation, indicating that endogenous c-Myc levels control loss of contact inhibition during malignant transformation (Fig1G-H). Of note, similar results were obtained when c-Myc function was blocked using CAS403811-55-2, an inhibitor that avoids c-Myc heterodimerization with its partner Max and abolishes c-Myc transcriptional effects. (FigS1B-C). Altogether, the results demonstrate a driving role of endogenous c-Myc in iPSC generation and immortalization of MEFs.

Identification of BHLH transcription factors concomitantly downregulated during iPS cells formation and malignant transformation

c-Myc belongs to the family of basic Helix-Loop-Helix (bHLH) transcription factors (TFs) that have been shown to mediate reciprocal regulation, especially in neurodevelopment (Imayoshi and Kageyama, 2014). They can be divided into two groups with contrasting roles: drivers of cellular identity changes or gatekeepers of cellular identity. These factors can be expressed in equilibrium in many cell types and the imbalance of the expression of one or few of these factors can drive changes in cellular fate decision (Imayoshi and Kageyama, 2014). Due to the key function played by c-Myc in induced pluripotency and malignant transformation as a bHLH TF inducing identity changes, we next assessed whether it was possible to identify other bHLH antagonizing c-Myc reprogramming function and safeguarding MEF identity.

An exhaustive screening was performed on the bHLH TFs described so far. Starting from the 111 factors identified in literature, 49 were found expressed in the MEF using RNA-seq data (Fig S1E). Among those, in order to isolate candidates downregulated specifically in reprogramming intermediates, we took advantage of the cell surface marker Thy1 (Ischenko et al., 2013; Stadtfeld et al., 2008). Broadly expressed in initial MEF, thy1 is specifically downregulated in the early days of iPS cells generation by a subset of cells ($Thy1^{Low}$) that harbors high reprogramming efficiency when compared with cells maintaining thy1 ($Thy1^{High}$) (Stadtfeld et al., 2008). Interestingly, Thy1 is also downregulated in MEF undertaking transformation, with $Thy1^{Low}$ subpopulation more prone to give rise to *in vivo* tumor compared to the refractory $Thy1^{High}$ (Ischenko et al., 2013).

$Thy1^{Low}$ and $Thy1^{High}$ cells were FACS sorted at day 3 of PR and MR and subjected to RNASeq analysis (FigS1D, Huyghe et al., manuscript submitted). We clustered the 49 bHLH TFs based on the ratio of their expression between $Thy1^{Low}$ and $Thy1^{High}$ in both reprogramming scenarios using bioinformatic software to perform supervised hierarchical clustering of the 49 bHLH TFs with Thy1 (Fig 1I, S1E). This approach allowed us to identify three bHLH TFs, namely Atoh8, Id4 and Twist2, that exhibited a specific downregulation in $Thy1^{Low}$ reprogramming intermediates during both PR and MR. Interestingly, unlike Id4 and Twist2, Atoh8 was the only factor found downregulated in both $Thy1^{Low}$ subpopulations by Western blot, and the sole factor completely silenced in iPSC cells and malignant cells generated from MEFs (Fig 1J-K). We therefore selected this candidate for further investigation.

Interrogation of publicly available resources confirmed Atoh8 transcript expression in MEFs and its progressive downregulation during rodent iPSC cells generation (Fig1M, FigS1G, FigS1J) (Knaupp et al., 2017; Nefzger et al., 2017; Polo et al., 2012), in agreement with its lack of expression in mESCs or in the *in vivo* pluripotent embryonic compartment until post-implantation epiblast (embryonic day 5.5) (FigS2C) (Boroviak et al., 2015). Of note, Atoh8 expression is also downregulated during human iPS cells generation from immortalized secondary fibroblasts (FigS2D) (Cacchiarelli et al., 2015), in contrast with a recent published study (Divvela et al., 2019). Altogether, these data reinforce the view that Atoh8 could safeguard MEFs identity and act as a putative obstacle to PR.

We next assessed the Atoh8 expression level in malignant tissues compared to the somatic counterparts. Public database analyses were performed taking advantage of TGCA data for lung (LUSC, LUAD), breast (BRCA) and prostate (PRAD) cancers. Of note, Atoh8 is lost in several cancers when compared with healthy tissues, highlighting its potential role as a tumor suppressor (Fig 1L, S1F).

Together, these results showed that c-Myc endogenous level is fundamental for the proper occurrence of iPSCs generation and malignant transformation. Moreover, a bHLH TFs screening based on the Thy1 marker identified Atoh8 as a putative obstacle of the two reprogramming processes, possibly harboring opposite effects compared to the reprogramming role of c-Myc.

Atoh8 regulates the efficiency and the pace of iPS cells generation.

To assess whether Atoh8 regulates reprogramming efficiency, loss-of-function strategy were developed (Fig. S2A-B). MEFs harboring a doxycycline-inducible system for OSKM expression were used. Upon sh#Atoh8 lentiviral transduction, OSKM was induced by doxycycline treatment and iPSC colony number was assessed by AP+ staining after 15 days of reprogramming (Fig2A). The RNAi-mediated knockdown of Atoh8 (Fig S2B, 77,7% of KD on average) led to a 4.4-fold increase of reprogramming efficiency (Fig 2B-C), evaluated by AP+ colonies counting, indicating that Atoh8 constrains iPS cells generation. Of note, similar results were obtained using OSKM-doxycycline inducible Pou5F1-GFP reporter MEFs, counting the number of the GFP-positive colonies at the end of reprogramming (Fig 2D-F). Moreover, resembling results were obtained by targeting Atoh8 locus with 2 independent CRISPR guides (FigS2C), demonstrating that the bHLH TF Atoh8 limits pluripotent reprogramming efficiency (Fig2G-H, FigS2C-D).

Because Atoh8 is rapidly downregulated during iPS cells generation, we wondered whether it hinders the process in its early days. We therefore tracked the emergence of Pou5f1-GFP positive cells by FACS during iPS cells generation in presence or absence of Atoh8. As depicted in figure 2I-J, we noticed an increase of GFP+ cells in the sh#Atoh8 condition already at day 4 of reprogramming, indicating that Atoh8 depletion triggers an early phenotype during iPS cells generation.

We next wondered whether Atoh8 depletion could accelerate iPS cells generation. In the route towards pluripotency, reprogramming cells switch on the endogenous pluripotency network and become independent of the OSKM transgenes expression. We therefore assessed whether Atoh8 downregulation could accelerate the formation of transgene-independent cells. We again took advantage of OSKM-inducible Pou5f1-GFP reporter MEFs. Fibroblasts were exposed to OSKM induction for six days before doxycycline withdrawal and the reprogramming was carried on until day 15 without further OSKM transgene expression (Fig2K). In contrast to control cells, Atoh8-depleted cells became transgene independent as early as day 6 and, even upon doxycycline withdrawal, they could form AP+ colonies (Fig 2L-M).

Furthermore, when Pou5f1+ cells were FACS sorted at day 6 from the Atoh8-downregulated condition and put back in culture, they were able to give rise to Pou5f1+ iPSC colonies (FigS3F), that could be amplified for more than 10 passages and expressed pluripotency markers (Fig 2N-O).

The results obtained show that depletion of Atoh8 in MEFs induces an increase in the efficiency and pace of pluripotent reprogramming, demonstrating the role of Atoh8 as a somatic roadblock during iPSC generation.

Atoh8 loss increases the efficiency and accelerate malignant transformation

We next wondered if Atoh8 can safeguard somatic identity and interfere with the onset of malignant transformation. In tumorigenesis, a first step is represented by cellular immortalization, when cells bypass the proliferation limit imposed by telomeres shortening and acquire an aberrant enhanced proliferation (Bodnar, 1998). Immortalization is followed by transformation, the capability to give rise to aggressive tumors. To assess if Atoh8 acts as a roadblock of malignant transformation, we depleted Atoh8 and induced malignant reprogramming (MR) through c-Myc and Ras overexpression coupled to p53 shRNA-downregulation. We thus observed how Atoh8 depletion affects the two properties associated to the malignant state, immortalization and transformation.

To determine the effects of Atoh8 knock-down on immortalization, lentiviral sh#Atoh8 particles were transduced in MEFs prior to MR induction. Foci formation tests were then performed to assess immortalized cells anchorage-dependent growth. Immortalized foci were stained after 30 days with cresyl-violet staining (Fig3A). Notably, Atoh8 depletion induces a strong increase (10-fold) in the number of immortalization events (Fig3B-C).

We next investigated Atoh8 downregulation effects on acquisition of transformation characteristics. With this aim, we performed soft agar colonies tests, to estimate anchorage-independent growth of transformed cells: after Atoh8 depletion and induction of MR, cells were splitted for three passages before starting soft agar experiments. Transformed soft agar colonies were stained with cresyl-violet after 30 days (Fig3D). Data obtained showed that Atoh8 loss increases the frequency of transformation events (Fig3E-F).

Furthermore, we obtained comparable results using the two independent CRISPR/Cas9 guides, demonstrating that the bHLH TF Atoh8 limits immortalization and transformation in tumorigenesis (Fig3G-H, FigS2G-H).

Since Atoh8 loss leads to an increase in the pace of pluripotent reprogramming, in a parallel way we assessed whether its depletion could accelerate the acquisition of the malignant properties.

Control and Atoh8 depleted cells were transduced with c-Myc, Ras and sh#p53 lentiviral particles and subjected to soft agar assays as early as day 6 post transduction (Fig 3I). In these stringent settings, where the time given to cells to accumulate malignant properties was shortened, control cells nearly failed to form colonies. In contrast, Atoh8 depleted cells were already able to form colonies, demonstrating that those cells

require fewer days to acquire malignant properties, thus showing that Atoh8 depletion accelerate the malignant transformation (3J-K).

Consequences of Atoh8 depletion on the acquisition of pluripotent and malignant features

Modifying the initial state of a somatic cell could hinder the formation of *bona fide* iPSC or alter the sensitivity of somatic cells before malignant transformation. We next investigated whether Atoh8 downregulation induces differences in iPSC and cancer cell generated from pluripotent and malignant reprogramming.

In order to assess whether Atoh8 depletion prior to reprogramming modulates the acquisition of pluripotent features, two control and two sh#Atoh8 iPSC clones were isolated, amplified and biobanked. We did not detect significant changes in the expression of the pluripotency markers Oct4, Sox2, Nanog and SSEA1 between the four cell lines (Fig4A-B). In line with this, both control and sh#Atoh8 lines were able to differentiate into the three germ layers both *in vitro* in EBs (Fig S3A) and *in vivo* in teratoma (Fig 4C).

Altogether, these results indicate that the early Atoh8 loss does not significantly impact the pluripotency network establishment and the differentiation potential of iPS cells.

In a similar manner, we determined whether Atoh8 early depletion could trigger differences in the stepwise acquisition of malignant features. After control and sh#Atoh8 lentiviral particles infection, MR was induced as described above. Polyclonal cell lines were established after more than 10 passages upon MR induction.

Cancer cell lines were obtained and tested for immortalization and transformation properties. Notably, sh#Atoh8 depleted cells were more prone to grow in adherent and non-adherent conditions, as shown by foci formation and soft agar experiments (Fig 4D-G).

Based on these results, we next assessed the tumorigenic potential of the derived cancer cell lines *in vivo*. Cancer cells for control and sh#Atoh8 conditions were injected subcutaneously in immune-depressed mice. Consequently, tumor growth and survival rate of the injected mice were followed for 15 days after cell injections. Mice injected with sh#Atoh8 cancer cells developed tumor more quickly and of bigger size compared to the control mice, and showed a reduced overall survival (Fig4H, FigS3B). Histological analyses of the derived tumors showed that, as expected, they contained malignant proliferative cells giving rise to neoplastic hyperproliferative tissues (FigS4C). Proliferation rate for control and sh#Atoh8 lines showed significant but minor proliferation differences ruling out the possibility that the observed *in vivo* phenotype are merely associated to an enhanced proliferation (FigS4D).

To gain insight on the higher aggressiveness of sh#Atoh8 cancer cells, RNA-Seq was performed on control and sh#Atoh8 cancer cell established lines (FigS4E). Gene ontology for molecular function was performed using statistical overrepresentation test by Panther DB. GO results showed that the first most enriched gene family correspond to cell adhesion molecules (Fig4I). Indeed, as highlighted by phalloidin staining, sh#Atoh8 cancer cells formed dense and compact colonies compared to the more elongated and less clustered control line, suggesting a switch from a mesenchymal to a more epithelial state (Fig4J). Recent studies suggested

that a partial EMT state is strongly associated to an increased aggressiveness in cancer (Pastushenko et al., 2018). With this aim, we analyzed the expression of epithelial and mesenchymal markers in control and sh#Atoh8 lines. As expected, an increase of epithelial markers was observed in the sh#Atoh8 condition. However, interestingly, there was no decrease in mesenchymal markers expression, whose expression and protein level showed similar levels compared to the control (Fig4K, S4F). To avoid the possibility that data obtained were due to a specific clonal expansion in the polyclonal population, more polyclonal cell lines were derived upon two independent MR inductions. *In vitro* aggressiveness and EMT partial state were tested and results consistently recapitulated the data observed with the first polyclonal lines (FigS4G-I). To assess the kinetics of the acquisition of the epithelial characteristics, we performed Western blot analysis respectively after 1, 3 and 5 passages (p1, p3 and p5) upon MR induction (Fig4L). The epithelial marker E-cadherin was found increased in Atoh8-depleted cancer cells after 6 days (p1) only of malignant reprogramming and the differences became more and more pronounced at p3 and p5, showing that partial EMT status is a characteristic acquired in the beginning of malignant transformation (Fig4L).

Collectively, the data obtained showed that Atoh8 depletion in MEFs, not only enhances the efficiency of malignant transformation, but has also profound effects on the stepwise acquisition of malignant properties, resulting in transformed cells with different features. Indeed, cancer cells generated from Atoh8-depleted MEFs acquire a partial EMT phenotype and consistently become more aggressive, as tested both *in vitro* and *in vivo*.

Atoh8 is a broad-range gatekeeper of cellular identity

We next wondered if Atoh8 can act as a more general cellular reprogramming barrier in other contexts. To test another scenario of iPSC generation, we took advantage of human pluripotent reprogramming, due to the promising profile observed in published data, where Atoh8 is classified as an early somatic gene and its expression is quickly lost in the first phase of reprogramming (FigS1I) (Cacchiarelli et al., 2015). Upon sg#Atoh8 targeting, human dermal fibroblasts (HDF) were transduced with OSKM Sendai viruses to induced reprogramming. IPSC colonies were determined by AP+ staining or SSEA4 live immunofluorescence (Fig5A).

Data obtained showed that downregulation of Atoh8 leads to a significant increase of efficiency in human reprogramming (2.23-fold and 3.05-fold respectively for AP+ staining and SSEA4 IF) (Fig5B-E).

To exclude the possibility that Atoh8 downregulation has negative impacts on derived hIPS, one control and sg#Atoh8 monoclones were isolated, amplified in culture for more than 10 passages and tested for pluripotency marker expression and differentiation potential. Atoh8 depletion did not showed negative effects on derived hIPSC, as both monoclones expressed comparable levels of pluripotency markers and could differentiate into the three germ layers in a similar manner (FigS5A-C).

We then tested Atoh8 role in a direct reprogramming process, the MEF to neuron transdifferentation, accomplished by the combined action of Brn2, Ascl1 and Myt1 (BAM) (Vierbuchen et al., 2010). After

sh#Atoh8 lentiviral particles transduction, MEF were infected with doxycycline-inducible BAM lentiviruses and neuron formation was determined by MAP2 immunofluorescence after eight days of reprogramming (Fig5F). Atoh8-depletion leads to a 3.1-fold increase in MAP2+ induced neurons formation (Fig5G-H), suggesting that Atoh8 acts as a roadblock of this transdifferentiation process.

Finally, we investigated if Atoh8 could act as an obstacle in other scenarios of malignancy, precisely in the transition from immortalization to transformation. To address this question, we took advantage of NIH3T3 immortalized cell line. NIH3T3 can give rise to immortalized foci, but they are not tumorigenic and cannot form transformed soft agar colonies. However, oncogenes induction can induce transformation in this cell line (Moscatelli, 1989; Wang et al., 2017). Transformation of NIH3T3 was induced thanks to c-Myc upregulation (FigS5D). We wondered if downregulation of Atoh8 in NIH3T3 could sensitize the cells to c-Myc action and increase the efficiency of the transformation. Upon sh#Atoh8 lentiviral infection, c-Myc was overexpressed in NIH3T3 through retroviral particles. Soft agar experiments were started at the third cell splitting and soft agar colonies were stained by cresyl-violet 30 days after (Fig5I). Interestingly, Atoh8 depletion before oncogenic insult drives the increase in the frequency of soft agar emergence, indicating again that Atoh8 acts as an obstacle for the acquisition of transformed properties (Fig5J-K).

Altogether these data show that Atoh8 plays a role of roadblock towards different types of transdifferentiation and reprogramming, reinforcing the identification of Atoh8 as somatic identity guardian bHLH TF.

c-Myc driven Atoh8 repression leads to Wnt pathway activation

As described in neurodevelopment, bHLH acting in an antagonising way can regulate their reciprocal expression and action (Bae et al., 2000; Imayoshi and Kageyama, 2014). We next wondered if in our system c-Myc and Atoh8 can regulate each other expression to drive pluripotent and malignant reprogramming. Indeed, during PR and MR, c-Myc is consistently upregulated in both reprogramming cocktails. We wondered if the observed downregulation of Atoh8 in reprogramming intermediates and final products could be mediated by c-Myc upregulation. Retroviral upregulation of c-Myc in MEFs led to gradual decrease of Atoh8 protein level (Fig6A). We wondered if c-Myc could act at a transcriptional level to drive Atoh8 downregulation. Indeed, data obtained showed that c-Myc directly binds Atoh8 promoter and decreases its expression (Fig6B-C). To test the specificity of c-Myc induced downregulation among other reprogramming factors, single factors of PR and MR cocktails were induced in the initial MEFs by viral infection and Atoh8 transcript was quantified (FigS5A). Only KRasG12D mutation could induce Atoh8 downregulation, consistent with c-Myc being downstream to the MAPK pathway (Kerkhoff et al., 1998; Vaseva et al., 2018). Interestingly, Atoh8 depletion slightly increased the level of c-Myc at both RNA and protein level, suggesting the existence

of a feedback loop tuning the expression of these two bHLH TFs (Fig6D, S5B). Altogether, data obtained show that c-Myc mediates the Atoh8 repression observed in PR and MR.

We next aimed to understand why Atoh8 depletion increases MR and PR efficiencies. We depleted Atoh8 in the initial MEF and performed whole transcriptome analysis, to identify Atoh8 function in MEFs and assess if the loss of this function could explain the enhanced PR and MR efficiencies. We performed RNA-Seq on samples collected 5 days upon Atoh8 downregulation. PCA components showed that control and sh#Atoh8 samples clustered separately (Fig6E). 299 genes were differentially expressed between the two conditions (Fig6F). Panther DB analysis showed a strong enrichment in gene families correlated with Wnt pathway (Fig6G, S5C). To test a potential role of Atoh8 in Wnt pathway regulation, we depleted the bHLH TF and estimated levels of the active form of β-Catenin, the major effector of Wnt pathway, and of Phospho-Gsk3 (P-Gsk3), the Wnt inhibitor that, when phosphorylated, is degraded. Results obtained showed that Atoh8 knock-down led to active β-Catenin and P-Gsk3 protein levels increase, consistent with Wnt pathway induction (Fig 6H). Furthermore, to test the extent of Wnt induction, we performed Atoh8 depletion with concomitant chemical treatment with CHIR99021, a GSK3 inhibitor that leads to Wnt activation. Data obtained do not show an additional effect of Atoh8 knock-down and the CHIR99021 treatment, compared to the only depletion of Atoh8, suggesting that Atoh8 downregulation alone is sufficient to induce strongly Wnt pathway activation (Fig 6H).

We next wondered which genes of the Wnt pathway are directly affected by Atoh8 downregulation. Analysis of RNA-seq data showed that Atoh8 depletion leads to decrease in expression of Wnt inhibitors Dkk2, Tle2, Sfrp1 and Sfrp2 and increase in expression of Wnt effectors and activators c-Myc, Lef1, Wnt9a and Tcf7, highlighting again the function of Atoh8 as a Wnt pathway inhibitor (Fig6I). Identified Wnt target genes were validate at RNA and protein level (Fig6J, FigS5D).

We next investigated if Wnt activation could account for the increase of PR and MR efficiencies observed upon Atoh8 depletion. We chose to focus our attention on Wnt inhibitors with the aim to assess if their downregulation can mimic reprogramming phenotypes observed upon Atoh8 knock-down. shRNAs targeting Wnt candidates were designed and validated (FigS5E). Upon shRNA lentiviral particles transduction, PR and MR were induced as described before and evaluated respectively by AP+ staining at day 15 and immortalized foci formation at day 30.

sh#Dkk2 lentiviral transduction was incompatible with MEF survival. However, Tle2, Sfrp1 and Sfrp2 depletion induced an increase in iPSC generation efficiency (1.93-, 2.92- and 2.27-fold respectively for Tle2, Sfrp1, and Sfrp2) (Fig6K,M). Interestingly, Sfrp1 and Sfrp2 depletion induced also an increase in malignant transformation efficiency (2.73- and 3.05-fold for Sfrp1 and Sfrp2) (Fig6L,N).

Altogether our results showed that Atoh8 fine-tunes the degree of Wnt activation in MEFs. Its downregulation, mediated by c-Myc overexpression, leads to Wnt pathway induction, which brings to an increase in iPS generation and malignant transformation (Fig7).

Discussion:

In this study, we found that Atoh8 can act as a somatic barrier towards MR, PR and other processes of reprogramming, transdifferentiation and transformation. Indeed, increase in MR and PR efficiencies upon Atoh8 downregulation are consistent with (1) a general loss of this bHLH TF in many types of cancer compared to their respective normal tissue and (2) the absence of its expression in mouse and human IPSCs and ESCs. However, Atoh8 does not act directly as an oncosuppressor, but is more probably one of the first barrier erased during malignancy. To this end, Atoh8 is rarely mutated in cancer, while it is usually downregulated. Consistently, its downregulation alone in NIH3T3 is not sufficient to induce transformation (data not shown), while its depletion before c-Myc oncogenic insult leads to a strong increase in the oncogenic-induced transformation, highlighting its barrier role. Interestingly, its barrier action is independent from cell immortalization, suggesting again that the cellular plasticity obtain by Atoh8 downregulation is independent from the hyper-proliferation associated with immortalization and underlying again the multifactorial etiology of cancers as proliferation and plasticity driven diseases.

Atoh8 has been initially proposed as a key factor for neurodevelopment (Inoue et al., 2001). Unexpectedly, downregulation of Atoh8 leads to an increase in the efficiency of MEF to neuron transdifferentiation. However, Atoh8 seems to have a broader role during embryonic development (Lynn et al., 2008; Rawnsley et al., 2013; Ross et al., 2006; Yao et al., 2010), and, in neurodevelopment, a specific role in maturation of precise neuronal populations (Li et al., 2019). Moreover, published RNA-Seq data showed that Atoh8 is not specifically expressed in neuron compared to other brain cell type (Zhang et al., 2014), suggesting that, despite its first description, it does not act as a major neural commitment factor, but more likely plays a broad role duringdifferentiation.

We thus asked what the more general function of Atoh8 during embryonic development could be. Our results revealed a novel unexpected role of Atoh8 as a Wnt inhibitor. Wnt signaling is required at different stages of development (Sato et al., 2004; Takada et al., 1994; ten Berge et al., 2011), and it is fundamental during gastrulation (Haegel et al., 1995), where Wnt plays an important role for the proper antero-posterior axis patterning (Huelsken et al., 2000). Interestingly, Atoh8 KO mice are not viable, because of developmental defects accumulated at the onset or during gastrulation (Lynn et al., 2008). We speculate that the loss of Atoh8 induces a sustained Wnt signalling which, not modulated anymore, leads to defects during gastrulation. It would be interesting to develop *in vivo* model to assess it.

Notably, a correlation between Atoh1 and Wnt was highlighted in colorectal cancer (Tsuchiya et al., 2007), where Wnt drives tumorigenesis (Groden et al., 1991) while Atoh1 was described to play a role in counteracting malignancy (Leow et al., 2004). It would be interesting to study Atoh8 function in this type of cancer and assess its interplay with Wnt signaling.

We showed that c-Myc upregulation in MEFs leads to Atoh8 downregulation. On the contrary, upregulation of Atoh8 did not induce a decrease in c-Myc levels, suggesting that the regulation is unidirectional (data not shown). It would be interesting to know if Atoh8 and c-Myc share the same gene targets and if c-Myc can bind sites usually bound by Atoh8 in the case of c-Myc upregulation and consequent Atoh8 decrease.

bHLH TFs are described to interact with each-other to create heterodimers for DNA binding (Imayoshi and Kageyama, 2014). bHLH TFs can also bind other family members to sequestrate them and avoid their DNA binding or cooperation with other bHLH TFs (Sasai et al., 1992). Interestingly, a sequestering role has already been described for Atoh8 during pancreas development, where it binds E47, avoiding its interaction with Neurog3 (Ejarque et al., 2013). It would be interesting to investigate if Atoh8 can sequestrate other bHLH TF during pluripotent and malignant reprogramming, for example destabilize the c-Myc-Max complex.

In cancer biology, a crucial issue is to estimate the level of pliancy of a cell, to assess at which degree it is susceptible to become tumorigenic (Chen et al., 2015; Puisieux et al., 2018). A capital example of this concept can be observed in the gut, where, depending on the differentiation levels of intestinal cells, the oncogenic insult orchestrated by APC mutation has completely different output in cancer development (Barker et al., 2009). Interestingly, our data showed that the downregulation of Atoh8 alone 48 hours before the oncogenic insult is enough to increase drastically the pliancy of the cell. This can be easily observed analysing the obtained transformed cells which, even if coming from the same cell type of the control, show a strongly increased degree of malignancy and differences in the genomic expression.

In summary, our results described the fundamental requirement of c-Myc during pluripotent and malignant reprogramming. We also identified Atoh8 as a new bHLH TF counteracting c-Myc reprogramming role in PR and MR and acting as a somatic barrier in different scenarios. Notably, tumorigenic cells obtained in absence of Atoh8 are drastically more aggressive. We also showed that the observed phenotype in PR and MR are associated to a Wnt pathway activation induced upon c-Myc-mediated Atoh8 downregulation.

Bibliography:

Araki, R., Hoki, Y., Uda, M., Nakamura, M., Jincho, Y., Tamura, C., Sunayama, M., Ando, S., Sugiura, M., Yoshida, M.A., Kasama, Y., Abe, M., 2011. Crucial role of c-Myc in the generation of induced pluripotent stem cells. Stem Cells Dayt. Ohio 29, 1362–1370. https://doi.org/10.1002/stem.685

Bae, S., Bessho, Y., Hojo, M., Kageyama, R., 2000. The bHLH gene Hes6, an inhibitor of Hes1, promotes neuronal differentiation. Dev. Camb. Engl. 127, 2933–2943.

Barker, N., Ridgway, R.A., van Es, J.H., van de Wetering, M., Begthel, H., van den Born, M., Danenberg, E., Clarke, A.R., Sansom, O.J., Clevers, H., 2009. Crypt stem cells as the cells-of-origin of intestinal cancer. Nature 457, 608–611. https://doi.org/10.1038/nature07602

Bedzhov, I., Graham, S.J.L., Leung, C.Y., Zernicka-Goetz, M., 2014. Developmental plasticity, cell fate specification and morphogenesis in the early mouse embryo. Philos. Trans. R. Soc. B Biol. Sci. 369. https://doi.org/10.1098/rstb.2013.0538

Bertrand, N., Castro, D.S., Guillemot, F., 2002. Proneural genes and the specification of neural cell types. Nat. Rev. Neurosci. 3, 517–530. https://doi.org/10.1038/nrn874

Bodnar, A.G., 1998. Extension of Life-Span by Introduction of Telomerase into Normal Human Cells. Science 279, 349–352. https://doi.org/10.1126/science.279.5349.349

Boroviak, T., Loos, R., Lombard, P., Okahara, J., Behr, R., Sasaki, E., Nichols, J., Smith, A., Bertone, P., 2015. Lineage-Specific Profiling Delineates the Emergence and Progression of Naive Pluripotency in Mammalian Embryogenesis. Dev. Cell 35, 366–382. https://doi.org/10.1016/j.devcel.2015.10.011

Cacchiarelli, D., Trapnell, C., Ziller, M.J., Soumillon, M., Cesana, M., Karnik, R., Donaghey, J., Smith, Z.D., Ratanasirintrawoot, S., Zhang, X., Ho Sui, S.J., Wu, Z., Akopian, V., Gifford, C.A., Doench, J., Rinn, J.L., Daley, G.Q., Meissner, A., Lander, E.S., Mikkelsen, T.S., 2015. Integrative Analyses of Human Reprogramming Reveal Dynamic Nature of Induced Pluripotency. Cell 162, 412–424. https://doi.org/10.1016/j.cell.2015.06.016

Chen, X., Pappo, A., Dyer, M.A., 2015. Pediatric solid tumor genomics and developmental pliancy. Oncogene 34, 5207–5215. https://doi.org/10.1038/onc.2014.474

Dang, C.V., 2012. MYC on the path to cancer. Cell 149, 22–35. https://doi.org/10.1016/j.cell.2012.03.003

de Jong, J., Looijenga, L.H.J., 2006. Stem cell marker OCT3/4 in tumor biology and germ cell tumor diagnostics: history and future. Crit. Rev. Oncog. 12, 171–203.

De La O, J.-P., Emerson, L.L., Goodman, J.L., Froebe, S.C., Illum, B.E., Curtis, A.B., Murtaugh, L.C., 2008. Notch and Kras reprogram pancreatic acinar cells to ductal intraepithelial neoplasia. Proc. Natl. Acad. Sci. 105, 18907–18912. https://doi.org/10.1073/pnas.0810111105

Divvela, S.S.K., Nell, P., Napirei, M., Zaehres, H., Chen, J., Gerding, W.M., Nguyen, H.P., Gao, S., Brand-Saberi, B., 2019. bHLH Transcription Factor Math6 Antagonizes TGF-β Signalling in Reprogramming, Pluripotency and Early Cell Fate Decisions. Cells 8. https://doi.org/10.3390/cells8060529

Ejarque, M., Altirriba, J., Gomis, R., Gasa, R., 2013. Characterization of the transcriptional activity of the basic helix-loop-helix (bHLH) transcription factor Atoh8. Biochim. Biophys. Acta 1829, 1175–1183. https://doi.org/10.1016/j.bbagrm.2013.08.003

Francesconi, M., Di Stefano, B., Berenguer, C., de Andrés-Aguayo, L., Plana-Carmona, M., Mendez-Lago, M., Guillaumet-Adkins, A., Rodriguez-Esteban, G., Gut, M., Gut, I.G., Heyn, H., Lehner, B., Graf, T., 2019. Single cell RNA-seq identifies the origins of heterogeneity in efficient cell transdifferentiation and reprogramming. eLife 8, e41627. https://doi.org/10.7554/eLife.41627

Friedmann-Morvinski, D., Bushong, E.A., Ke, E., Soda, Y., Marumoto, T., Singer, O., Ellisman, M.H., Verma, I.M., 2012. Dedifferentiation of Neurons and Astrocytes by Oncogenes Can Induce Gliomas in Mice. Science 338, 1080–1084. https://doi.org/10.1126/science.1226929

Fujii, I., Matsukura, M., Ikezawa, M., Suzuki, S., Shimada, T., Miike, T., 2006. Adenoviral mediated MyoD gene transfer into fibroblasts: myogenic disease diagnosis. Brain Dev. 28, 420–425. https://doi.org/10.1016/j.braindev.2005.12.007

Gradwohl, G., Dierich, A., LeMeur, M., Guillemot, F., 2000. neurogenin3 is required for the development of the four endocrine cell lineages of the pancreas. Proc. Natl. Acad. Sci. U. S. A. 97, 1607–1611. https://doi.org/10.1073/pnas.97.4.1607

Groden, J., Thliveris, A., Samowitz, W., Carlson, M., Gelbert, L., Albertsen, H., Joslyn, G., Stevens, J., Spirio, L., Robertson, M., 1991. Identification and characterization of the familial adenomatous polyposis coli gene. Cell 66, 589–600. https://doi.org/10.1016/0092-8674(81)90021-0

Haegel, H., Larue, L., Ohsugi, M., Fedorov, L., Herrenknecht, K., Kemler, R., 1995. Lack of beta-catenin affects mouse development at gastrulation. Dev. Camb. Engl. 121, 3529–3537.

Hahn, W.C., Weinberg, R.A., 2002. Rules for Making Human Tumor Cells. N. Engl. J. Med. 347, 1593–1603. https://doi.org/10.1056/NEJMra021902

Herreros-Villanueva, M., Zhang, J.-S., Koenig, A., Abel, E.V., Smyrk, T.C., Bamlet, W.R., de Narvajas, A. a.-M., Gomez, T.S., Simeone, D.M., Bujanda, L., Billadeau, D.D., 2013. SOX2 promotes dedifferentiation and imparts stem cell-like features to pancreatic cancer cells. Oncogenesis 2, e61. https://doi.org/10.1038/oncsis.2013.23

Huelsken, J., Vogel, R., Brinkmann, V., Erdmann, B., Birchmeier, C., Birchmeier, W., 2000. Requirement for beta-catenin in anterior-posterior axis formation in mice. J. Cell Biol. 148, 567–578. https://doi.org/10.1083/jcb.148.3.567

Hvid-Jensen, F., Pedersen, L., Drewes, A.M., Sørensen, H.T., Funch-Jensen, P., 2011. Incidence of Adenocarcinoma among Patients with Barrett's Esophagus. N. Engl. J. Med. 365, 1375–1383. https://doi.org/10.1056/NEJMoa1103042

Imayoshi, I., Kageyama, R., 2014. bHLH factors in self-renewal, multipotency, and fate choice of neural progenitor cells. Neuron 82, 9–23. https://doi.org/10.1016/j.neuron.2014.03.018

Inoue, C., Bae, S.K., Takatsuka, K., Inoue, T., Bessho, Y., Kageyama, R., 2001. Math6, a bHLH gene expressed in the developing nervous system, regulates neuronal versus glial differentiation. Genes Cells Devoted Mol. Cell. Mech. 6, 977–986.

Ischenko, I., Zhi, J., Moll, U.M., Nemajerova, A., Petrenko, O., 2013. Direct reprogramming by oncogenic Ras and Myc. Proc. Natl. Acad. Sci. U. S. A. 110, 3937–3942. https://doi.org/10.1073/pnas.1219592110

Kareta, M.S., Gorges, L.L., Hafeez, S., Benayoun, B.A., Marro, S., Zmoos, A.-F., Cecchini, M.J., Spacek, D., Batista, L.F.Z., O'Brien, M., Ng, Y.-H., Ang, C.E., Vaka, D., Artandi, S.E., Dick, F.A., Brunet, A., Sage, J., Wernig, M., 2015. Inhibition of pluripotency networks by the Rb tumor suppressor restricts reprogramming and tumorigenesis. Cell Stem Cell 16, 39–50. https://doi.org/10.1016/j.stem.2014.10.019

Kawamura, T., Suzuki, J., Wang, Y.V., Menendez, S., Morera, L.B., Raya, A., Wahl, G.M., Izpisúa Belmonte, J.C., 2009. Linking the p53 tumour suppressor pathway to somatic cell reprogramming. Nature 460, 1140–1144. https://doi.org/10.1038/nature08311

Kerkhoff, E., Houben, R., Löffler, S., Troppmair, J., Lee, J.-E., Rapp, U.R., 1998. Regulation of c-myc expression by Ras/Raf signalling. Oncogene 16, 211–216. https://doi.org/10.1038/sj.onc.1201520

Knaupp, A.S., Buckberry, S., Pflueger, J., Lim, S.M., Ford, E., Larcombe, M.R., Rossello, F.J., de Mendoza, A., Alaei, S., Firas, J., Holmes, M.L., Nair, S.S., Clark, S.J., Nefzger, C.M., Lister, R., Polo, J.M., 2017. Transient and Permanent Reconfiguration of Chromatin and Transcription Factor Occupancy Drive Reprogramming. Cell Stem Cell 21, 834-845.e6. https://doi.org/10.1016/j.stem.2017.11.007

Leow, C.C., Romero, M.S., Ross, S., Polakis, P., Gao, W.-Q., 2004. Hath1, down-regulated in colon adenocarcinomas, inhibits proliferation and tumorigenesis of colon cancer cells. Cancer Res. 64, 6050–6057. https://doi.org/10.1158/0008-5472.CAN-04-0290

Li, H., Collado, M., Villasante, A., Strati, K., Ortega, S., Cañamero, M., Blasco, M.A., Serrano, M., 2009. The Ink4/Arf locus is a barrier for iPS cell reprogramming. Nature 460, 1136–1139. https://doi.org/10.1038/nature08290

Li, Y., Li, H., Zhang, L., Xiong, S., Wen, S., Xia, X., Zhou, X., 2019. Growth/differentiation 5 promotes the differentiation of retinal stem cells into neurons via Atoh8. J. Cell. Physiol. 234, 21307–21315. https://doi.org/10.1002/jcp.28735

Löhle, M., Hermann, A., Glaß, H., Kempe, A., Schwarz, S.C., Kim, J.B., Poulet, C., Ravens, U., Schwarz, J., Schöler, H.R., Storch, A., 2012. Differentiation Efficiency of Induced Pluripotent Stem Cells Depends on the Number of Reprogramming Factors. STEM CELLS 30, 570–579. https://doi.org/10.1002/stem.1016

Lynn, F.C., Sanchez, L., Gomis, R., German, M.S., Gasa, R., 2008. Identification of the bHLH factor Math6 as a novel component of the embryonic pancreas transcriptional network. PloS One 3, e2430. https://doi.org/10.1371/journal.pone.0002430

Mikkelsen, T.S., Hanna, J., Zhang, X., Ku, M., Wernig, M., Schorderet, P., Bernstein, B.E., Jaenisch, R., Lander, E.S., Meissner, A., 2008. Dissecting direct reprogramming through integrative genomic analysis. Nature 454, 49–55. https://doi.org/10.1038/nature07056

Moscatelli, D., 1989. Transformation of NIH 3T3 cells with basic fibroblast growth factor or the hst/K-fgf oncogene causes downregulation of the fibroblast growth factor receptor: reversal of morphological transformation and restoration of receptor number by suramin. J. Cell Biol. 109, 2519–2527. https://doi.org/10.1083/jcb.109.5.2519

Nefzger, C.M., Rossello, F.J., Chen, J., Liu, X., Knaupp, A.S., Firas, J., Paynter, J.M., Pflueger, J., Buckberry, S., Lim, S.M., Williams, B., Alaei, S., Faye-Chauhan, K., Petretto, E., Nilsson, S.K., Lister, R., Ramialison, M., Powell, D.R., Rackham, O.J.L., Polo, J.M., 2017. Cell Type of Origin Dictates the Route to Pluripotency. Cell Rep. 21, 2649–2660. https://doi.org/10.1016/j.celrep.2017.11.029

Ohnishi, K., Semi, K., Yamamoto, T., Shimizu, M., Tanaka, A., Mitsunaga, K., Okita, K., Osafune, K., Arioka, Y., Maeda, T., Soejima, H., Moriwaki, H., Yamanaka, S., Woltjen, K., Yamada, Y., 2014. Premature termination of reprogramming in vivo leads to cancer development through altered epigenetic regulation. Cell 156, 663–677. https://doi.org/10.1016/j.cell.2014.01.005

Pastushenko, I., Brisebarre, A., Sifrim, A., Fioramonti, M., Revenco, T., Boumahdi, S., Van Keymeulen, A., Brown, D., Moers, V., Lemaire, S., De Clercq, S., Minguijón, E., Balsat, C., Sokolow, Y., Dubois, C., De Cock, F., Scozzaro, S., Sopena, F., Lanas, A., D'Haene, N., Salmon, I., Marine, J.-C., Voet, T., Sotiropoulou, P.A., Blanpain, C., 2018. Identification of the tumour transition states occurring during EMT. Nature 556, 463–468. https://doi.org/10.1038/s41586-018-0040-3

Patel, T., Hobert, O., 2017. Coordinated control of terminal differentiation and restriction of cellular plasticity. eLife 6. https://doi.org/10.7554/eLife.24100

Polo, J.M., Anderssen, E., Walsh, R.M., Schwarz, B.A., Nefzger, C.M., Lim, S.M., Borkent, M., Apostolou, E., Alaei, S., Cloutier, J., Bar-Nur, O., Cheloufi, S., Stadtfeld, M., Figueroa, M.E., Robinton, D., Natesan, S., Melnick, A., Zhu, J., Ramaswamy, S., Hochedlinger, K., 2012. A molecular roadmap of reprogramming somatic cells into iPS cells. Cell 151, 1617–1632. https://doi.org/10.1016/j.cell.2012.11.039

Puisieux, A., Pommier, R.M., Morel, A.-P., Lavial, F., 2018. Cellular Pliancy and the Multistep Process of Tumorigenesis. Cancer Cell 33, 164–172. https://doi.org/10.1016/j.ccell.2018.01.007

Rawnsley, D.R., Xiao, J., Lee, J.S., Liu, X., Mericko-Ishizuka, P., Kumar, V., He, J., Basu, A., Lu, M., Lynn, F.C., Pack, M., Gasa, R., Kahn, M.L., 2013. The transcription factor Atonal homolog 8 regulates Gata4 and Friend of Gata-2 during vertebrate development. J. Biol. Chem. 288, 24429–24440. https://doi.org/10.1074/jbc.M113.463083

Ross, M.D., Martinka, S., Mukherjee, A., Sedor, J.R., Vinson, C., Bruggeman, L.A., 2006. Math6 expression during kidney development and altered expression in a mouse model of glomerulosclerosis. Dev. Dyn. Off. Publ. Am. Assoc. Anat. 235, 3102–3109. https://doi.org/10.1002/dvdy.20934

Roy, N., Hebrok, M., 2015. Regulation of Cellular Identity in Cancer. Dev. Cell 35, 674–684. https://doi.org/10.1016/j.devcel.2015.12.001

Sasai, Y., Kageyama, R., Tagawa, Y., Shigemoto, R., Nakanishi, S., 1992. Two mammalian helix-loop-helix factors structurally related to Drosophila hairy and Enhancer of split. Genes Dev. 6, 2620–2634. https://doi.org/10.1101/gad.6.12b.2620

Sato, N., Meijer, L., Skaltsounis, L., Greengard, P., Brivanlou, A.H., 2004. Maintenance of pluripotency in human and mouse embryonic stem cells through activation of Wnt signaling by a pharmacological GSK-3-specific inhibitor. Nat. Med. 10, 55–63. https://doi.org/10.1038/nm979

Sherr, C.J., 2001. The INK4a/ARF network in tumour suppression. Nat. Rev. Mol. Cell Biol. 2, 731–737. https://doi.org/10.1038/35096061

Shi, G., DiRenzo, D., Qu, C., Barney, D., Miley, D., Konieczny, S.F., 2013. Maintenance of acinar cell organization is critical to preventing Kras-induced acinar-ductal metaplasia. Oncogene 32, 1950–1958. https://doi.org/10.1038/onc.2012.210

Stadtfeld, M., Maherali, N., Breault, D.T., Hochedlinger, K., 2008. Defining Molecular Cornerstones during Fibroblast to iPS Cell Reprogramming in Mouse. Cell Stem Cell 2, 230–240. https://doi.org/10.1016/j.stem.2008.02.001

Takada, S., Stark, K.L., Shea, M.J., Vassileva, G., McMahon, J.A., McMahon, A.P., 1994. Wnt-3a regulates somite and tailbud formation in the mouse embryo. Genes Dev. 8, 174–189. https://doi.org/10.1101/gad.8.2.174

Takahashi, K., Yamanaka, S., 2006. Induction of pluripotent stem cells from mouse embryonic and adult fibroblast cultures by defined factors. Cell 126, 663–676. https://doi.org/10.1016/j.cell.2006.07.024

ten Berge, D., Kurek, D., Blauwkamp, T., Koole, W., Maas, A., Eroglu, E., Siu, R.K., Nusse, R., 2011. Embryonic stem cells require Wnt proteins to prevent differentiation to epiblast stem cells. Nat. Cell Biol. 13, 1070–1075. https://doi.org/10.1038/ncb2314

Tsuchiya, K., Nakamura, T., Okamoto, R., Kanai, T., Watanabe, M., 2007. Reciprocal targeting of Hath1 and beta-catenin by Wnt glycogen synthase kinase 3beta in human colon cancer. Gastroenterology 132, 208–220. https://doi.org/10.1053/j.gastro.2006.10.031

Utikal, J., Polo, J.M., Stadtfeld, M., Maherali, N., Kulalert, W., Walsh, R.M., Khalil, A., Rheinwald, J.G., Hochedlinger, K., 2009. Immortalization eliminates a roadblock during cellular reprogramming into iPS cells. Nature 460, 1145–1148. https://doi.org/10.1038/nature08285

Vaseva, A.V., Blake, D.R., Gilbert, T.S.K., Ng, S., Hostetter, G., Azam, S.H., Ozkan-Dagliyan, I., Gautam, P., Bryant, K.L., Pearce, K.H., Herring, L.E., Han, H., Graves, L.M., Witkiewicz, A.K., Knudsen, E.S., Pecot, C.V., Rashid, N., Houghton, P.J., Wennerberg, K., Cox, A.D., Der, C.J., 2018. KRAS Suppression-Induced Degradation of MYC Is Antagonized by a MEK5-ERK5 Compensatory Mechanism. Cancer Cell 34, 807-822.e7. https://doi.org/10.1016/j.ccell.2018.10.001

Vierbuchen, T., Ostermeier, A., Pang, Z.P., Kokubu, Y., Südhof, T.C., Wernig, M., 2010. Direct conversion of fibroblasts to functional neurons by defined factors. Nature 463, 1035–1041. https://doi.org/10.1038/nature08797

von Figura, G., Morris, J.P., Wright, C.V.E., Hebrok, M., 2014. Nr5a2 maintains acinar cell differentiation and constrains oncogenic Kras-mediated pancreatic neoplastic initiation. Gut 63, 656–664. https://doi.org/10.1136/gutjnl-2012-304287

Wang, C., Liu, H., Qiu, Q., Zhang, Z., Gu, Y., He, Z., 2017. TCRP1 promotes NIH/3T3 cell transformation by over-activating PDK1 and AKT1. Oncogenesis 6, e323–e323. https://doi.org/10.1038/oncsis.2017.18

Wernig, M., Meissner, A., Cassady, J.P., Jaenisch, R., 2008. c-Myc is dispensable for direct reprogramming of mouse fibroblasts. Cell Stem Cell 2, 10–12. https://doi.org/10.1016/j.stem.2007.12.001

Yao, J., Zhou, J., Liu, Q., Lu, D., Wang, L., Qiao, X., Jia, W., 2010. Atoh8, a bHLH transcription factor, is required for the development of retina and skeletal muscle in zebrafish. PloS One 5, e10945. https://doi.org/10.1371/journal.pone.0010945

Yu, F., Li, J., Chen, H., Fu, J., Ray, S., Huang, S., Zheng, H., Ai, W., 2011. Kruppel-like factor 4 (KLF4) is required for maintenance of breast cancer stem cells and for cell migration and invasion. Oncogene 30, 2161–2172. https://doi.org/10.1038/onc.2010.591

Yuan, S., Norgard, R.J., Stanger, B.Z., 2019. Cellular Plasticity in Cancer. Cancer Discov. 9, 837–851. https://doi.org/10.1158/2159-8290.CD-19-0015

Zhang, Y., Chen, K., Sloan, S.A., Bennett, M.L., Scholze, A.R., O'Keeffe, S., Phatnani, H.P., Guarnieri, P., Caneda, C., Ruderisch, N., Deng, S., Liddelow, S.A., Zhang, C., Daneman, R., Maniatis, T., Barres, B.A., Wu, J.Q., 2014. An RNA-sequencing transcriptome and splicing database of glia, neurons, and vascular cells of the cerebral cortex. J. Neurosci. Off. J. Soc. Neurosci. 34, 11929–11947. https://doi.org/10.1523/JNEUROSCI.1860-14.2014

Acknowledgements:

We are grateful to the Cytometry platform of the Cancer research center of Lyon and A. Paradisi, N. Combemorel, M. Ruel for technical assistance.

Fundings:

This work was supported by institutional grants from Inserm/Cnrs, Atip-avenir, Plan cancer, La ligue contre le cancer nationale et régionale (FL and GF), INCa (FL), Fondation ARC (FL), Centre Léon Bérard (FL and AH), Fondation pour la recherche médicale (FL ARF20170938622 and GF).

Author Contributions:

GF performed most of the experiments from figures 1-6. AH, FM and LDM performed experiments in figures 4 and 6. MS performed ChiP experiments. NR and RD performed bio-informatic analyses. BG and PW performed in vivo work. FL and GF designed experiments. GF wrote the manuscript. FL designed and supervised the study.

Methods:

Mice genotyping and MEFs derivation

R26rtTA;Col1a14F2A (21), LSL-K-rasG12D (22), R26-CREERT2, Oct4-EGFP, mice were housed under french national guidelines and crossed to obtained the genotypes of interest.

Genotyping was carried out upon genomic DNA extraction from adult tails and embryonic heads using the DirectPCR Lysis Reagent (102-T, Viagen Biotech). Genotypes PCR were performed with EconoTaq Plus Green 2X Master Mix (Lucigen). Primers used are listed in Table 1.

MEFs were isolated from E13.5 embryos after removal of ectodermal and endoderm tissues (head and bowels). The remaining tissues were dissociated with cutters and further with trypsin at 37°C for 10 min. Derived cells were resuspended in MEF medium.

Histology

Teratoma and xenograft were fixed in 10% buffered formalin and afterwards embedded in paraffin. 200 µm-thick tissue slices were obtained from paraffin-embedded tissue according to conventional procedures. Hematoxylin-eosin staining was performed on prepared sections and examined under a light microscope. Immunohistochemistry was carried out thanks to an automated immunostainer (Ventana Discovery XT, Roche, Meylan, France) using the Omnimap DAB Kit following manufacturer's instructions. Sections were incubated with a rabbit anti-Ki67 (F/RM-9106, Thermo Fisher Scientific) and later with an anti-rabbit HRP, followed by DAB solution with 3,3'-diaminobenzidine as a chromogenic substrate. Slides were scanned via the panoramic scan II (3D Histech) and the image analysis was performed with the CaseViewer software.

Teratoma

Teratoma formation assays were carried out by injection of 1x106 iPS cells into both testes of 7-week-old immunodeficient (SCID) mice (CB17/SCID, Charles River). Mice were sacrified 3-4 weeks after injection and teratoma were surgically extracted. Teratomas were incubated in 4% paraformaldehyde fix solution and sectioned for histological staining.

Xenografts

Xenograft assays were carried out by injection $3x10^6$ immortalized cells resuspended in PBS and matrigel (1:1) and injected subcutaneously into SCID mice (N = 6 for each group). The volume of the tumor was measured every 3 days until day 16. Upon sacrifice, xenograft were fixed in 4% paraformaldehyde and sectioned for histological staining.

Plasmids and constructs

pMXS-Oct4, pMXS-Sox2, pMXS-Klf4, pMXS-Myc, pLKO.1, Tet-O-FUW-Brn2, Tet-O-FUW-Ascl1, Tet-O-FUW-Myt1l and FUdeltaGW-rtTA plasmids were purchased from Addgene. shRNAs against Atoh8, Dkk2, Tle2, Sfrp1, Sfrp2 and Trp53 were developed using the MISSION shRNA library from Sigma-Aldrich and cloned using the Rapid DNA ligation kit (Sigma-Aldrich) into the pLKO.1 vector digested with AgeI and EcoRI. shRNA sequences are listed in Table 1. Single guide RNA targeting Atoh8 were designed with UCSC genome browser and CRISPOR program and inserted into the lentiCRISPRv2 plasmid upon BsmBI restriction.

Cell culture and viral production

MEFs, TCs, PlatE and 293FT were cultivated in MEF medium, prepared adding to DMEM high glucose: 10% fetal bovine serum (FBS), 100 U/mL penicillin / streptomycin (PS), 1 mM sodium pyruvate, 2 mM L-glutamine, 0.1 mM Non Essential Amino Acids (NEAA) and 0.1 mM β-mercaptoethanol.

Mouse iPSCs were cultivated in to DMEM high glucose: 15% knock-out serum (KSR), 100 U/mL penicillin / streptomycin (PS), 1 mM sodium pyruvate, 2 mM L-glutamine, 0.1 mM Non Essential Amino Acids (NEAA) and 0.1 mM β-mercaptoethanol and home-made LIF.

Human iPSCs were cultivated in TeSRTM-E8TM medium (STEMCELLS technologies).

Induced neurons were cultivated in DMEM/F12 complemented with 25 μg/ml Insulin, 50 μg/ml Transferrin, 30nM Sodium Selenite, 20nM Progesterone and 100mM Putrescine.

293FT cells and were used to produce pLKO.1-derived and FUW-derived lentiviral particles. Calcium phosphate transfection of the pLKO.1 vectors, together with VSV-G envelope and Gag-Pol plasmids, was performed using the CalPhos Mammalian Transfection kit (Ozyme). After 7 hours of incubation, medium was changed with 10 mL of fresh MEF medium. Medium was than collected after 48 hours and stored at -80°c or directly used to infect MEFs. pMXs-based retroviral particles were similarly generated with Plat-E cells (a packaging cell line constitutively expressing gag, pol and env genes).

Pluripotent reprogramming experiments

Reprogrammable R26rtTA;Col1a14F2A; Oct4-EGFP MEFs within three passages after derivation were plated in six-well plates at 60,000 cells per well. The day after, cells were infected overnight with lentiviral shRNA particles in the presence of 8 μg/ml Polybrene, and medium was then replaced by fresh medium. The following day, medium was additioned with 2 μg/ml doxycycline to induce OSKM expression. After 72 hours in MEF medium + Dox, MEFs were reseeded on 0.1% gelatin coated plates in iPSC medium. Medium was replaced or supplemented with Dox-containing fresh medium for 15 days. OCT4-GFP+ colonies were counted under an Axiovert 200 M microscope, while alkaline phosphatase (AP) staining was performed with the Leukocyte Alkaline Phosphatase kit (Sigma-Aldrich).

For OSK reprogramming, showed in figure 1, wild-type MEF were used and the Doxycyline treatment was substituted with an infection of retroviral particles for OSK overexpression.

Malignant reprogramming experiments

For MR, the LSL-K-RasG12D;R26-CreErt2 MEFs were similarly infected overnight with lentiviral shRNA particles in the presence of 8 μg/mL polybrene. 48 h later the cells MR was induced by co-infection overnight with sh#p53- and Myc-carrying viruses together with 4-hydroxitamoxifen treatment (1 μM) to induce K-RasG12D expression. 72 hours later, MEFs were replated in six-well plates at low density (500, 1,000 or 2,000 cells per well) in low-serum MEF medium (MEF medium with 5% FBS) for the foci formation assay. Medium was changed every 4 days for 30 days.

For soft-agar analysis, 72 hours after MR induction, cells were reseeded at normal concentrations and, after 1-3 passages, soft agar assays were performed: cells were plated at a density of 25,000-50,000 cells per well on an agarose-MEF medium layers.

Foci and soft agar colonies were stained between day 25 and 30 with a 0.5% cresyl violet solution in 20% methanol.

Immunofluorescence

Cells were fixed with 4% paraformaldehyde for 10 min at room temperature (RT°C), washed 3 times for 10 minutes with PBS, permeabilized with 0.1% Triton X-100 for 30 min at RT°C and blocked with 1% bovine serum albumin (BSA) for 1 h. After incubation with primary antibodies diluted in BSA over-night at 4°C, cells were washed 3 times, incubated with fluorophore-labeled secondary antibodies (Life technologies), washed again 3 times and stained with 2µg/ml Hoechst 33242 (H1399, Termofisher). Used primary antibodies were: Nanog (mouse: RCAB002P, Reprocell; human: AF1997, R&D), Ssea1 (sc-101462, Santa Cruz), Oct4 (sc-5279, Santa Cruz), Sox2 (ab97959, Abcam), Map2 (M4403, Sigma). Phalloidin staining was performed using GFP-coupled Phalloidin-Atto 488 (49409, Sigma-Aldrich). Live SSEA4 immunostaining was carried out with the GloLIVE Human Pluripotent Stem Cell Live Cell Imaging Kit (SC023B, R&D).

RNA extraction and RT-qPCR

RNA extraction was performed using Trizol reagent and 1 µg of RNA was reverse-transcribed with the RevertAid H Minus First Strand cDNA Synthesis kit (Life Technologies). RT-qPCR was performed with the LightCycler 480 SYBR Green I Master mix (Roche) on the LightCycler 96 machine (Roche). Gapdh and Actin were used as housekeeping genes. Used qPCR primers are listed in Table 1.

Protein extraction and Western blot

Cells were scrapped in RIPA buffer (150 mM NaCl, 1% Triton, 0.5% deoxycholate, 0.1% SDS and 50 mM Tris, pH 8.0) supplemented with protease inhibitor and phosphatase inhibitors. Scrapped cells were incubated 30 min on ice, lysed by sonication, and centrifugated for 10 min at 15,000g. Supernatants were collected and proteins were denatured 10 min at 95 °C in Laemmli sample buffer, separated on 4-15% or 12% polyacrylamide gels, and transferred onto a nitrocellulose membrane with the TransBlot Turbo Transfer System (Biorad). The membrane was blocked with 5% milk in T-BST (Tris-buffered saline, 0.1% Tween 20) for 1 h, incubated with primary antibody at 4°C overnight and secondary antibodies for 1 h at RT°C. Antigens were detected using ECL reagents. The following antibodies were used: mouse anti-Oct4 (sc-5279, Santa Cruz, 1:1,000), rabbit anti-Sox2 (ab97959, Abcam, 1:1,000), goat anti-Klf4 (AF3158, R&D, 1:1,000), mouse anti-c-Myc (sc-42, Santa-Cruz, 1:200), rabbit anti-K-Ras (8955, Cell signaling, 1:1000), rabbit anti-K-RasG12D (14429, Cell signaling, 1:1000), mouse anti-p53 (sc-126, Santa-Cruz, 1:200), rabbit-anti Atoh8 (PA5-20710, Termofisher, 1:1000), rabbit anti-Id4 (BCH-9/82-12, BioCheck, 1:1000), mouse anti-Twist2 (HOO7581-M01, Abnova, 1:250), rabbit anti-Nanog (RCAB002P, Reprocell,1:1000), mouse anti-Ssea1 (sc-101462, Santa Cruz, 1:1000), mouse anti-Cdh1 (610181, BD, 1:1000), rabbit anti-Snail (C15D3, Cell signaling, 1:1000), rabbit anti-

Vim (R28, Cell signaling, 1:1000), mouse anti-Twist1 (ab50887, Abcam, 1:250), goat anti-hSox2 (AF2018, R&D, 1:1000), rabbit anti-hNanog (3580, Cell signaling, 1:1000), mouse anti-Active β-Catenin (8E7, Millipore, 1:1000), mouse anti-β-Catenin (sc-7963, Santa-Cruz, 1:1000), rabbit anti-P-Gsk3a/b (9331, Cell signaling, 1:1000), rabbit anti-Gsk3b (9315, Cell signaling, 1:1000), mouse anti-Tle2 (sc-374226, Santa-Cruz, 1:500), rabbit anti-Lef1 (2230, Cell signaling, 1:1000), rabbit anti-Gapdh (sc-25778, Santa-Cruz, 1:4000) horse radish peroxidase (HRP)-conjugated anti-ACTIN (Sigma Aldrich, A3854, 1:10,000), HRP-conjugated goat anti-rabbit (Interchim, 111-035-144, 1:5,000), HRP-conjugated goat anti-mouse (Interchim, 115-035-075, 1:5,000), and HRP-conjugated goat anti-rat (Interchim, 112-035-143, 1:5,000).

FACS

Flow cytometry analysis were performed with the FACS Canto II (BD). The following antibody was used: anti-mouse CD90.2 (Thy-1.2) APC (eBioscience, 17-0902). FACS Sorting was performed on a BD FACS Aria.

NGS analyses

RNA quality was analysed using a Bioanalyser (Agilent). Libraries were constructed and sequenced on an illumina Hiseq 2000 by the cancer genomics platform on site.

Statistical analyses

All data are presented as mean ± SEM. Statistical analyses were performed using GraphPad Prism software. Student t tests were used for paired comparisons. Two-tales P-values are indicated on each graph.

Genotyping primers

Transgene	Primer 1	Primer 2	Primer 3
$Col1a1^{4F2A}$	CCCTCCATGTGTGACCAAGG	TTGCTCAGCGGTGCTGTCCA	GCACAGCATTGCGGACATG
$R26^{rtTA}$	GCGAAGAGTTTGTCCTCAACC	AAAGTCGCTCTGAGTTGTTAT	GGAGCGGGAGAAATGGATATG
LSL-$K\text{-}ras^{G12D}$	CCTTTACAAGCGCACGCAGACTGTAGA	AGCTAGCCACCATGGCTTGAGTAAGTCTGCA	
R26-CRE^{ERT2}	TGCCACGACCAAGTGACAGC	CCAGGTTACGGATATAGTTCATG	
OCT4-EGFP	CAAGGCAAGGGAGGTAGACA	TGCCAGACAATGGCTATGAG	CCAAAAGACGGCAATATGGT

shRNA sequences

	Forward sequence
sh#p53	CCCACTACAAGTACATGTGTAA
sh#Atoh8	CGTCAATTTCACACGTAATTT
sh#Tle2	AGAGCTGGATCAGGGATTTAC
sh#Sfrp1	ACTGGCCCGAGATGCTCAAAT
sh#Sfrp2	CGGCATCGAGTACCAGAACAT

Guide CRISPR sequences

	Forward sequence	Reverse sequence
sg#Atoh8_1	CACCGGAAGCACATCCCGGTCCTCG	AAACCGAGGACCGGGATGTGCTTCC
sg#Atoh8_2	CACCGCCGGGATGTGCTTCATGGCG	AAACCGCCATGAAGCACATCCCGGC

qPCR

primers

	Forward primer	Reverse primer
Gapdh	CATGGCCTTCCGTGTTCCTA	GCCTGCTTCACCACCTTCTT
Actin	GCTGTATTCCCCTCCATCGTG	CACGGTTGGCCTTAGGGTTCAG
Atoh8	CCTCAGCTTCTCCGAGTGTG	CAGGTCACTCCTTCCGTTTCT
c-Myc	CGCCCAGTGAGGATATCTGG	GTAGCGACCGCAACATAGGA
Cdh1	TGTATGTGTGTGGGTGCTGAT	GAGAACGGTTTCAATGGCTTACC
EPCam	GGCTGAGATAAAGGAGATGGGTG	CCCTTCGCAGGTCTTCATCT
Krt8	CGGCTACTCAGGAGGACT	CAGCTTCCCATCTCGGGTTT
Vim	AGACCAGAGATGGACAGGTGA	TTGCGCTCCTGAAAAACTGC
Snail	GTCCAGCTGTAACCATGCCT	TGTCACCAGGACAAATGGGG
h_Brachury	CAGGTCCCGAAAGATGCAGT	GTGCTCCTCCACTGCTTTGA
h_Eomes	AGCCATGTTTGCCCTAGTCC	GCTTGCTCTCTCCTGAGTCC
h_Gata4	TACATGTCTCTCCCCTGGCA	GAACGAAGGGTCTGCAGTGA
h_Sox17	TGGACCGCACGGAATTTGAA	GGACACCACCGAGGAAATGG
Dkk	GCTGTAGGGGGCATTTCCTT	TCCCTGTTCTTCAGCGTTCC
Tle2	CATCTGCTGCCTTTTCAGAGTG	TTGGTAAAGCCCACACCAGG
Sfrp1	GGAAGCCTCTAAGCCCCAAG	CATCCTCAGTGCAAACTCGC
Sfrp2	GTGTCCGAAAGGGACCTGAA	TGACCAGATACGGAGCGTTG
Lef1	CCAAGCAAGGCATGTCCAGA	GAAGTGTCGCCTGACAGTGA

Figures:

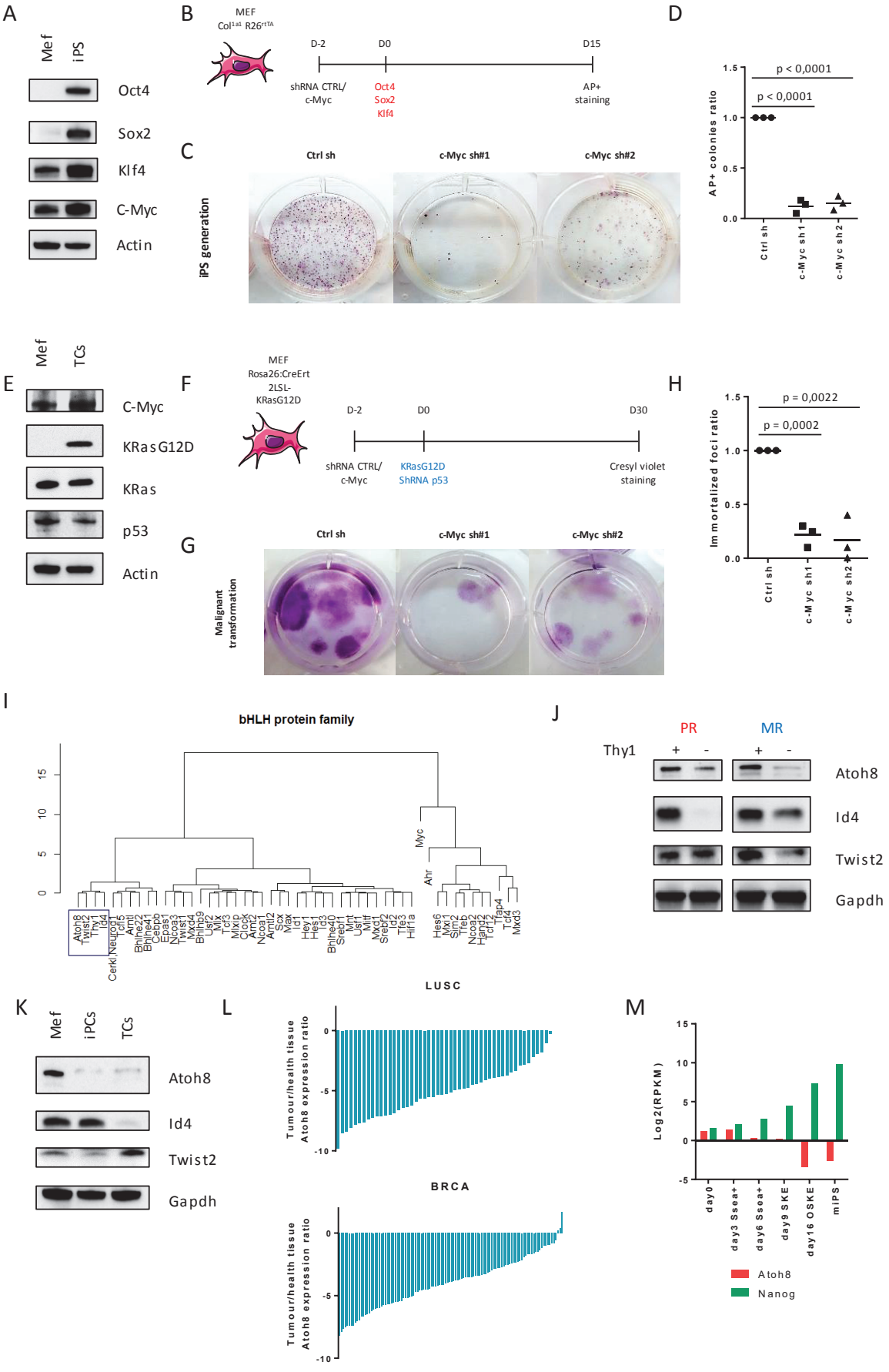
A
Mef
iPS
Oct4
Sox2
Klf4
C-Myc
Actin
B
MEF
Col1a1 R26rtTA
D-2
D0
D15
shRNA CTRL/
c-Myc
Oct4
Sox2
Klf4
AP+
staining
C
Ctrl sh
c-Myc sh#1
c-Myc sh#2
iPS generation
D
p < 0,0001
p < 0,0001
AP+ colonies ratio
Ctrl sh
c-Myc sh1
c-Myc sh2
E
Mef
TCs
C-Myc
KRasG12D
KRas
p53
Actin
F
MEF
Rosa26:CreErt
2LSL-
KRasG12D
D-2
D0
D30
shRNA CTRL/
c-Myc
KRasG12D
ShRNA p53
Cresyl violet
staining
G
Ctrl sh
c-Myc sh#1
c-Myc sh#2
Malignant
transformation
H
p = 0,0022
p = 0,0002
Immortalized foci ratio
Ctrl sh
c-Myc sh1
c-Myc sh2
I
bHLH protein family
Myc
Ahr
LUSC
BRCA
Tumour/health tissue
Atoh8 expression ratio
J
PR
MR
Thy1
Atoh8
Id4
Twist2
Gapdh
K
Mef
iPCs
TCs
Atoh8
Id4
Twist2
Gapdh
L
Tumour/health tissue
Atoh8 expression ratio
M
Log2(RPKM)
day0
day3 Ssea+
day6 Ssea+
day9 SKE
day16 OSKE
miPS
Atoh8
Nanog

Figure 1: Identification of a new obstacle towards c-Myc reprogramming activity. (a) Western blot showing expression levels of Oct4, Sox2, Klf4 and c-Myc in MEFs and iPSCs. (b) Scheme depicting pluripotent reprogramming in presence and absence of c-Myc endogenous expression. Cells were infected with lentiviral shRNA particles targeting control and c-Myc coding sequences. 48 hours later, retroviral particles were infected to induce Oct4, Sox2 and Klf4 over-expression. iPSC colonies were scored at day 15 by AP+ staining. (c) Picture representing AP+ colonies on the different conditions, representative of three independent experiments. (d) colony counting. Data are the mean ± s.d. (n=3 independent experiments). Student's t-test was used, and two-sided p-values are indicated (e) Western blot showing expression levels of c-Myc, K-RasG12D, K-Ras and p53 in MEFs and TCs. (f) Scheme depicting MR immortalization in presence and absence of c-Myc endogenous expression. Cells were infected with lentiviral particles targeting control and c-Myc coding sequences. 48 hours later, malignant reprogramming was induced by 4-OHT treatment (to induce K-RasG12D expression) and lentiviral shRNA particles targeting p53. Immortalized foci were scored at day 30 by Cresyl-violet staining. (g) Picture representing Cresyl-violet foci on the different conditions, representative of three independent experiments. (h) colony counting. Data are the mean ± s.d. (n=3 independent experiments). Student's t-test was used, and two-sided p-values are indicated. (i) Supervised hierarchical clustering, showing Thy1 and the 49 bHLH TFs expressed in MEF, based on transcript levels represented in Thy1-/Thy1+ expression ratio at day 3 of PR and MR. (j) Western blot showing expression level of Atoh8, Id4 and Twist2 in MEFs, Thy1- and Thy+ subpopulations at day 3 of PR and MR. (k) Western blot showing expression levels of Atoh8, Id4 and Twist2 in MEFs, IPSCs and TCs. (l) Histogram depicting Atoh8 transcript levels in LUSC and BRCA patients. Data are presented as a log2 of the ratio of Atoh8 FPKMs between malignant and healthy tissues. (m) Atoh8 (red) and Nanog (green) expression levels in MEF, PR intermediates and mIPSCs. Data, extracted from Nefzger. et al., 2017, present Atoh8 and Nanog transcripts level in log2 of FPKM.

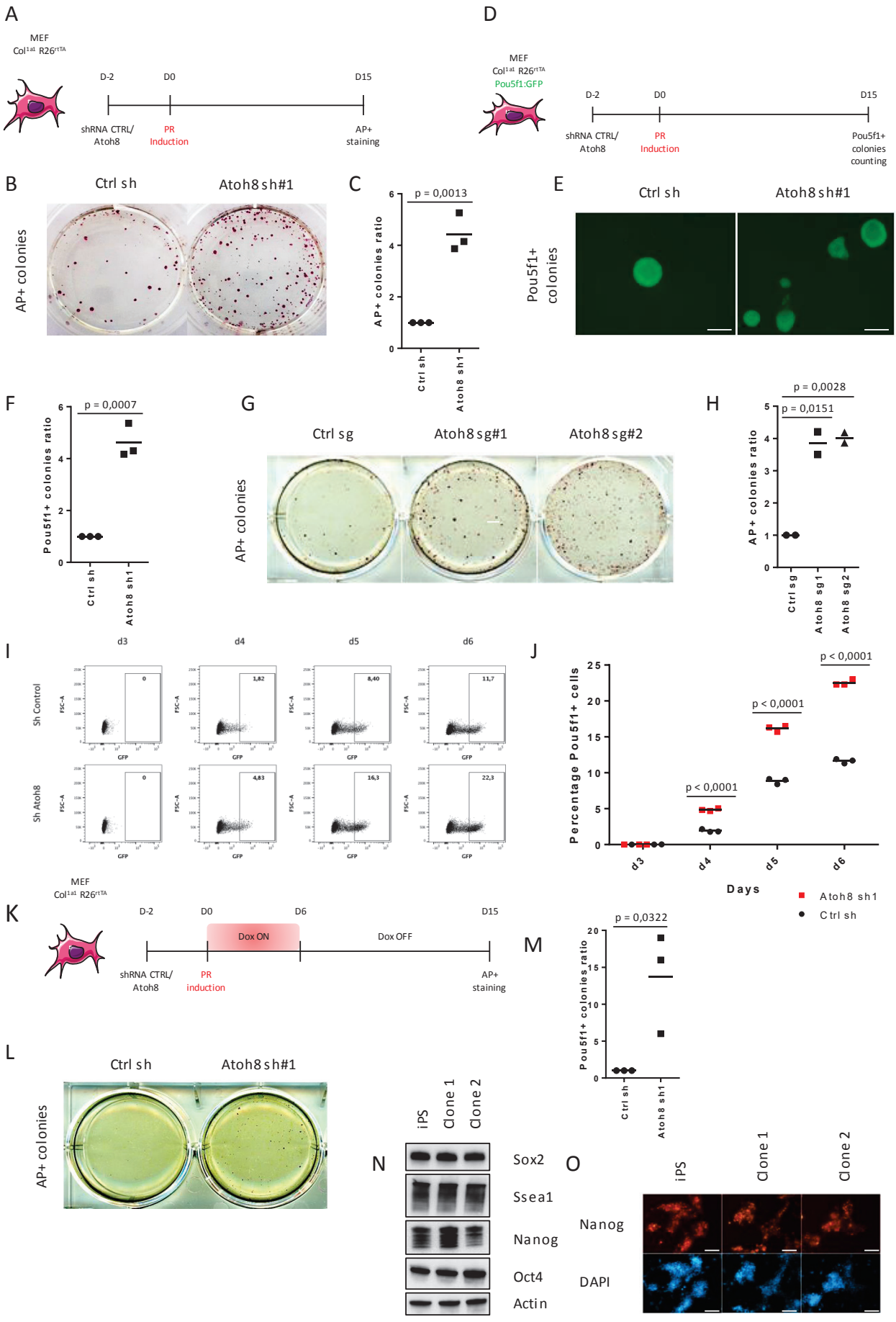
A
MEF
Col1a1 R26rtTA
D-2
D0
D15
shRNA CTRL/
Atoh8
PR
Induction
AP+
staining
D
MEF
Col1a1 R26rtTA
Pou5f1:GFP
D-2
D0
D15
shRNA CTRL/
Atoh8
PR
Induction
Pou5f1+
colonies
counting
B
Ctrl sh
Atoh8 sh#1
AP+ colonies
C
p = 0,0013
AP+ colonies ratio
Ctrl sh
Atoh8 sh1
E
Ctrl sh
Atoh8 sh#1
Pou5f1+
colonies
F
p = 0,0007
Pou5f1+ colonies ratio
Ctrl sh
Atoh8 sh1
G
Ctrl sg
Atoh8 sg#1
Atoh8 sg#2
AP+ colonies
H
p = 0,0028
p = 0,0151
AP+ colonies ratio
Ctrl sg
Atoh8 sg1
Atoh8 sg2
I
d3
d4
d5
d6
Sh Control
Sh Atoh8
FSC-A
GFP
0
1,82
8,40
11,7
0
4,83
16,3
22,3
J
p < 0,0001
p < 0,0001
p < 0,0001
p < 0,0001
Percentage Pou5f1+ cells
d3
d4
d5
d6
Days
Atoh8 sh1
Ctrl sh
K
MEF
Col1a1 R26rtTA
D-2
D0
D6
D15
Dox ON
Dox OFF
shRNA CTRL/
Atoh8
PR
induction
AP+
staining
M
p = 0,0322
Pou5f1+ colonies ratio
Ctrl sh
Atoh8 sh1
L
Ctrl sh
Atoh8 sh#1
AP+ colonies
N
iPS
Clone 1
Clone 2
Sox2
Ssea1
Nanog
Oct4
Actin
O
iPS
Clone 1
Clone 2
Nanog
DAPI

Figure 2: Atoh8 as a novel barrier towards pluripotent reprogramming. (a) Scheme depicting pluripotent reprogramming upon shRNA Atoh8 downregulation. Cells were infected with lentiviral shRNA particles targeting control or Atoh8 coding sequences. 48 hours later, pluripotent reprogramming was started by doxycycline treatment to induce the expression of the OSKM cocktail. iPSC colonies were scored at day 15 by AP+ staining. (b) Picture representing AP+ colonies at day 15 of PR in sh#control and sh#Atoh8 conditions, representative of three independent experiments. (c) AP+ iPSCs colony counting. Data are the mean ± s.d. (n=3 independent experiments). Student's t-test was used, and two-sided p-values are indicated. (d) Scheme depicting pluripotent reprogramming upon shRNA Atoh8 downregulation. Pou5f1-GFP reporter MEFs cells were were infected with lentiviral shRNA particles targeting control or Atoh8 coding sequences. Pluripotent reprogramming was induced as described in Fig. 2A. iPS colonies were scored at day 15 by GFP+ staining. (e) Picture representing Pou5f1-GFP+ colonies at day 15 of PR in sh#control and sh#Atoh8 conditions, representative of three independent experiments. (f) colony counting. Data are the mean ± s.d. (n=3 independent experiments). Student's t-test was used, and two-sided p-values are indicated. (g) Picture representing AP+ colonies at day 15 of PR upon Atoh8 downregulation using two different CRISPR guides, representative of two independent experiments. (h) colony counting. Data are the mean ± s.d. (n=2 independent experiments). Student's t-test was used, and two-sided p-values are indicated. (i) FACS analysis showing Pou5f1-GFP profile from day 3 to day 6 of pluripotent reprogramming perfomed in sh#Control and sh#Atoh8 background (j) Graph depicting Pou5f1-GFP+ percentage of cells in function of reprogramming day (from day 3 to day 6). Squares correspond to sh#control, circles to sh#Atoh8. Data are the mean ± s.d. (n=3 independent experiments). Student's t-test was used, and two-sided p-values are indicated (k) Scheme depicting acceleration test in pluripotent reprogramming. Cells were were infected with lentiviral shRNA particles targeting control or Atoh8 coding sequences. Pluripotent reprogramming was induced by doxycycline-mediated OSKM induction for 6 days, than cells were harvested in KSR+Lif medium without doxycycline for the remaining 9 days. iPSC colonies were scored at day 15 by AP+ staining. (l) Picture representing AP+ colonies at day 15 of PR in sh#control and sh#Atoh8 conditions, representative of three independent experiments. (m) colony counting. Data are the mean ± s.d. (n=2 independent experiments). Student's t-test was used, and two-sided p-values are indicated. (n) Western blot showing expression level of Ssea1, Sox2, Nanog and Oct4 in monoclonal lines obtained from full-15 days-reprogramming (iPS) and accelerated-6 days-reprogramming (Clone 1 and 2). (o) Nanog immunofluorescence of monoclonal lines obtained from full-15 days-reprogramming (iPS) and accelerated-6 days-reprogramming (Clone 1 and 2).

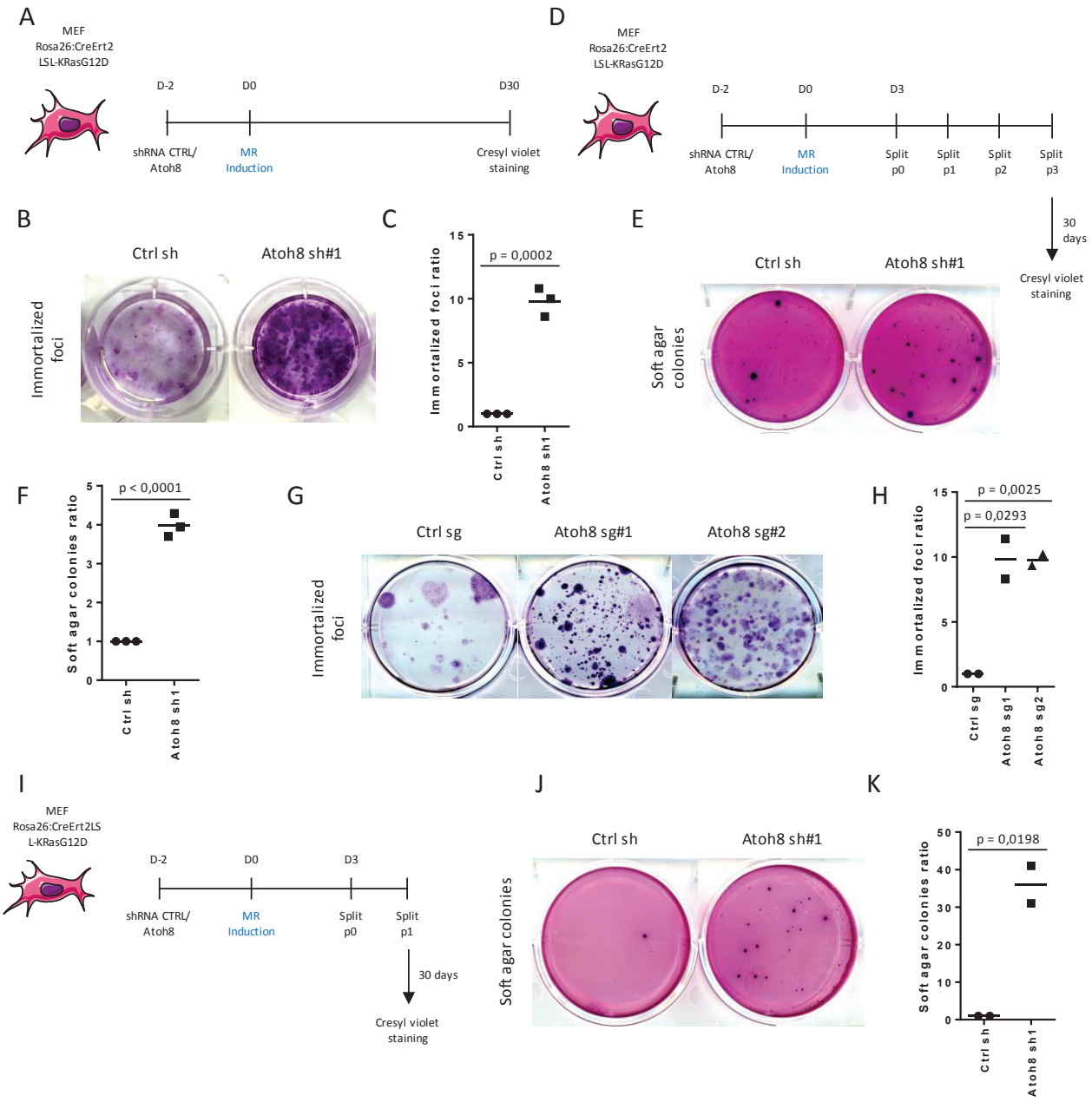
A
MEF
Rosa26:CreErt2
LSL-KRasG12D
D-2
D0
D30
shRNA CTRL/
Atoh8
MR
Induction
Cresyl violet
staining
D
MEF
Rosa26:CreErt2
LSL-KRasG12D
D-2
D0
D3
shRNA CTRL/
Atoh8
MR
Induction
Split
p0
Split
p1
Split
p2
Split
p3
30
days
Cresyl violet
staining
B
Ctrl sh
Atoh8 sh#1
Immortalized
foci
C
p = 0,0002
Immortalized foci ratio
Ctrl sh
Atoh8 sh1
E
Ctrl sh
Atoh8 sh#1
Soft agar
colonies
F
p < 0,0001
Soft agar colonies ratio
Ctrl sh
Atoh8 sh1
G
Ctrl sg
Atoh8 sg#1
Atoh8 sg#2
Immortalized
foci
H
p = 0,0025
p = 0,0293
Immortalized foci ratio
Ctrl sg
Atoh8 sg1
Atoh8 sg2
I
MEF
Rosa26:CreErt2LS
L-KRasG12D
D-2
D0
D3
shRNA CTRL/
Atoh8
MR
Induction
Split
p0
Split
p1
30 days
Cresyl violet
staining
J
Ctrl sh
Atoh8 sh#1
Soft agar colonies
K
p = 0,0198
Soft agar colonies ratio
Ctrl sh
Atoh8 sh1

Figure 3: Atoh8 as a novel barrier towards malignant reprogramming. (a) Scheme depicting MR immortalization upon Atoh8 downregulation. Cells were infected with lentiviral particles targeting control and c-Myc coding sequences. 48 hours later, malignant reprogramming was induced by 4-OHT treatment (to induce K-RasG12D expression), lentiviral shRNA particles targeting p53 and retroviral particles for induce c-Myc over-expression. Immortalized foci were scored at day 30 by Cresyl-violet staining. (b) Picture representing Cresyl-violet foci at day 30 of MR immortalization in sh#control and sh#Atoh8 conditions, representative of three independent experiments. (c) colony counting. Data are the mean ± s.d. (n=3 independent experiments). Student's t-test was used, and two-sided p-values are indicated. (d) Scheme depicting MR transformation upon Atoh8 downregulation. Cells were infected with lentiviral particles targeting control and c-Myc coding sequences. 48 hours later, malignant reprogramming was induced as described in Fig. 3A. Cells were then splitted three times before starting soft-agar tests. Transformed soft-agar colonies were scored at day 30 by Cresyl-violet staining. (e) Picture representing Cresyl-violet soft-agar colonies at day 30 of MR transformation in sh#control and sh#Atoh8 conditions, representative of three independent experiments. (f) colony counting. Data are the mean ± s.d. (n=3 independent experiments). Student's t-test was used, and two-sided p-values are indicated. (g) Picture representing Cresyl-violet immortalized foci at day 30 of MR immortalization upon Atoh8 downregulation using two different CRISPR guides. (h) colony counting. Data are the mean ± s.d. (n=2 independent experiments). Student's t-test was used, and two-sided p-values are indicated. (i) Scheme depicting acceleration test in malignant reprogramming Cells were infected with lentiviral particles targeting control and c-Myc coding sequences. 48 hours later, malignant reprogramming was induced as described in Fig. 3A. Cells were then splitted only once before starting soft-agar tests. Transformed soft-agar colonies were scored at day 30 by Cresyl-violet staining. (j) Picture representing Cresyl-violet soft-agar colonies at day 30 of MR transformation in sh#control and sh#Atoh8 conditions, representative of three independent experiments. (k) colony counting. Data are the mean ± s.d. (n=3 independent experiments). Student's t-test was used, and two-sided p-values are indicated.

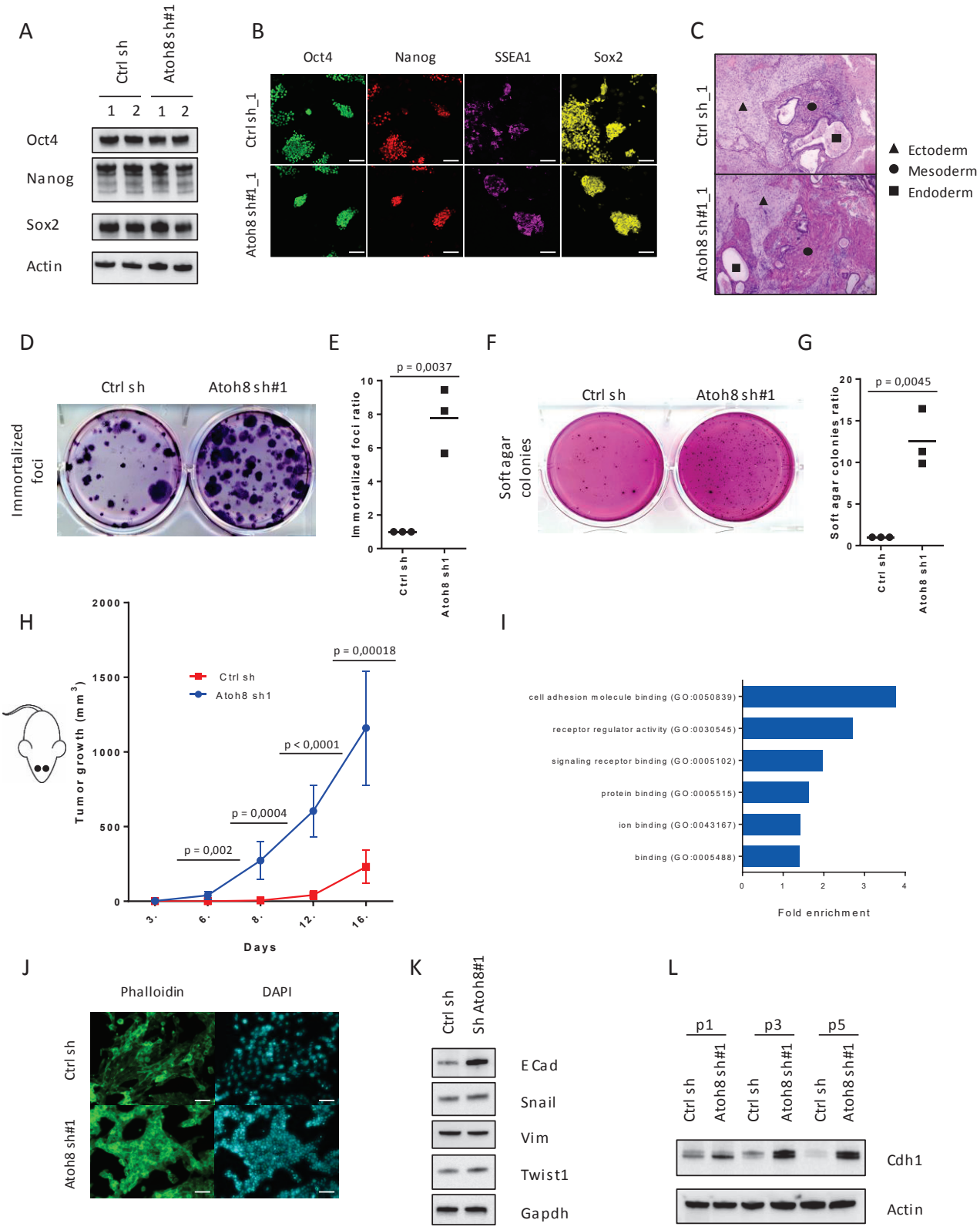
A
Ctrl sh
Atoh8 sh#1
1 2 1 2
Oct4
Nanog
Sox2
Actin
B
Oct4
Nanog
SSEA1
Sox2
Ctrl sh_1
Atoh8 sh#1_1
C
Ctrl sh_1
Atoh8 sh#1_1
Ectoderm
Mesoderm
Endoderm
D
Ctrl sh
Atoh8 sh#1
Immortalized foci
E
p = 0,0037
Immortalized foci ratio
Ctrl sh
Atoh8 sh1
F
Ctrl sh
Atoh8 sh#1
Soft agar colonies
G
p = 0,0045
Soft agar colonies ratio
Ctrl sh
Atoh8 sh1
H
Ctrl sh
Atoh8 sh1
p = 0,00018
p < 0,0001
p = 0,0004
p = 0,002
Tumor growth (mm3)
Days
I
cell adhesion molecule binding (GO:0050839)
receptor regulator activity (GO:0030545)
signaling receptor binding (GO:0005102)
protein binding (GO:0005515)
ion binding (GO:0043167)
binding (GO:0005488)
Fold enrichment
J
Phalloidin
DAPI
Ctrl sh
Atoh8 sh#1
K
Ctrl sh
Sh Atoh8#1
E Cad
Snail
Vim
Twist1
Gapdh
L
p1
p3
p5
Ctrl sh
Atoh8 sh#1
Cdh1
Actin

Figure 4: Atoh8 downregulation effects on PR and MR products, iPSCs and TCs: (a) Western blot showing expression levels of Oct4, Nanog and Sox2 in iPSC monoclonal lines obtained in sh#control and sh#Atoh8 background. (b) Immunofluorescence for Oct4, Nanog, Ssea4, Sox2 in iPS monoclonal lines obtained in sh#control and sh#Atoh8 background. (c) Picture depicts histological analysis of teratomas derived from sh#control and sh#Atoh8 iPSC monoclonal lines. 2 independent teratoma were analyzed per cell line. Triangle = ectodermal tissue; circle = mesodermal tissues; square = endodermal tissue. (d) Picture representing Cresyl-violet immortalized foci at day 30 of foci formation assay starting from TC polyclonal lines derived in sh#Control and sh#Atoh8 background. (e) colony counting. Data are the mean ± s.d. (n=3 independent experiments). Student's t-test was used, and two-sided p-values are indicated. (f) Picture representing Cresyl-violet transformed colonies at day 30 of soft-agar assay starting from TC polyclonal lines derived in sh#Control and sh#Atoh8 background. (g) colony counting. Data are the mean ± s.d. (n=2 independent experiments). Student's t-test was used, and two-sided p-values are indicated. (h) Xenograft tumor volume over time after injection of sh#control and sh#Atoh8 TCs. 6 independent mice per condition were analysed. Data are the mean ± s.d. (n=6 independent mice). Student's t-test was used, and two-sided p-values are indicated (i) Statistical overrepresentation analysis. The Panther DB tool was used to detect overrepresented family genes within the genes differentially expressed in sh#control and sh#Atoh8 TCs. A Fisher's exact two-sided test was used to calculate p-values. (j) Phalloidin immunofluorescence of TCs obtained in sh#control and sh#Atoh8 background. (k) Western blot showing expression level of Cdh1, Snail, Vim and Twist1 in sh#control and sh#Atoh8 polyclonal TCs. (l) Western blot showing expression level of Cdh1 in sh#control and sh#Atoh8 conditions at passage 1, 3 and 5 during malignant reprogramming.

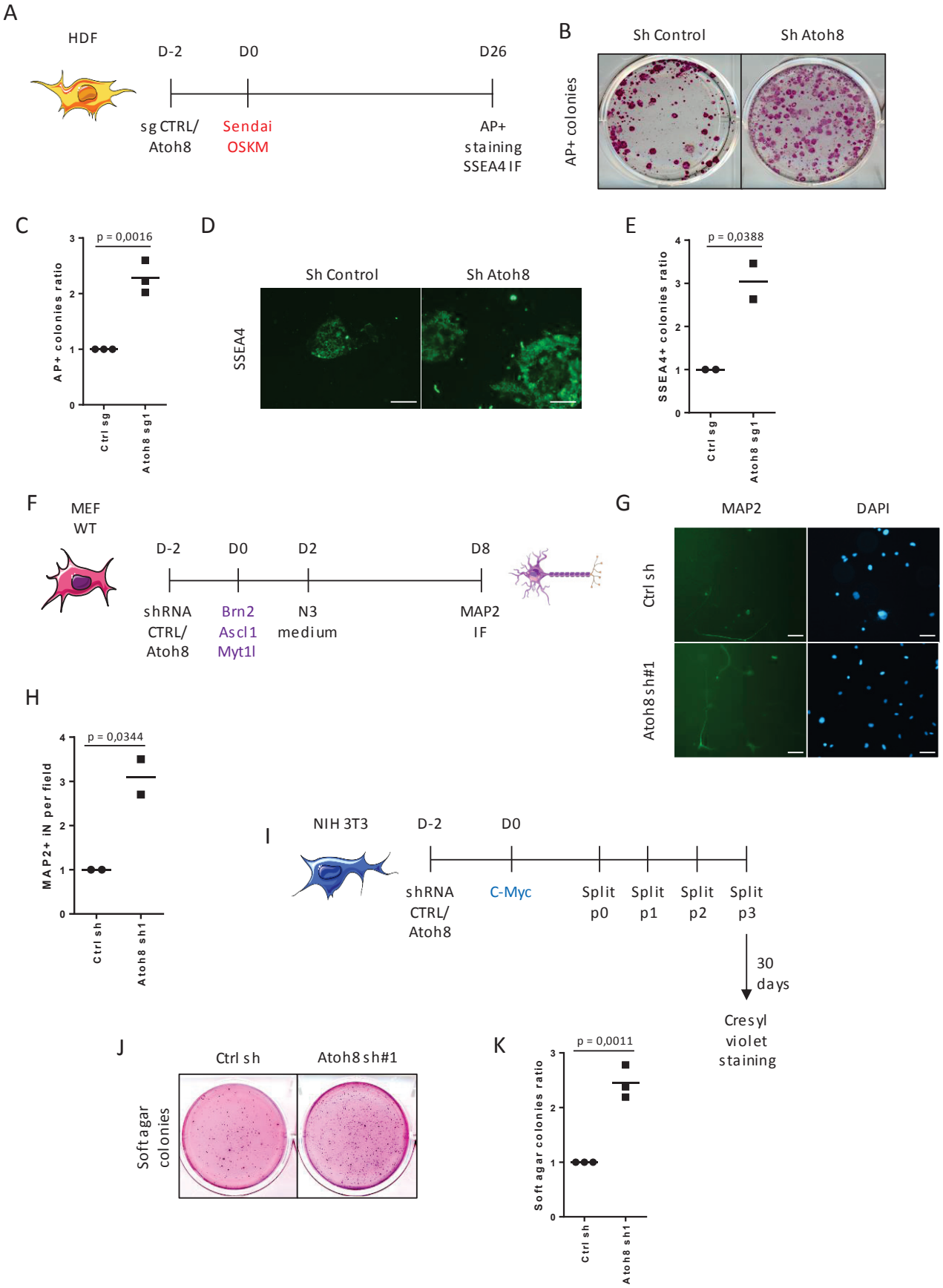
A
HDF
D-2
D0
D26
sg CTRL/
Atoh8
Sendai
OSKM
AP+
staining
SSEA4 IF
B
Sh Control
Sh Atoh8
AP+ colonies
C
p = 0,0016
AP+ colonies ratio
Ctrl sg
Atoh8 sg1
D
Sh Control
Sh Atoh8
SSEA4
E
p = 0,0388
SSEA4+ colonies ratio
Ctrl sg
Atoh8 sg1
F
MEF
WT
D-2
D0
D2
D8
shRNA
CTRL/
Atoh8
Brn2
Ascl1
Myt1l
N3
medium
MAP2
IF
G
MAP2
DAPI
Ctrl sh
Atoh8 sh#1
H
p = 0,0344
MAP2+ iN per field
Ctrl sh
Atoh8 sh1
I
NIH 3T3
D-2
D0
shRNA
CTRL/
Atoh8
C-Myc
Split
p0
Split
p1
Split
p2
Split
p3
30
days
Cresyl
violet
staining
J
Ctrl sh
Atoh8 sh#1
Soft agar
colonies
K
p = 0,0011
Soft agar colonies ratio
Ctrl sh
Atoh8 sh1

Figure 5: Atoh8 acts a general roadblock during cellular identity changes. (a) Scheme depicting human pluripotent reprogramming. Cells were infected with lentiviral sg#control and sg#Atoh8 particles. 48 hours later, pluripotent reprogramming was induced with OSKM Sendai viruses and iPSC colonies were scored at day 26 by AP+ staining or live SSEA4+ imaging. (b) Picture representing AP+ colonies at day 26 of human PR in sg#control and sg#Atoh8 conditions, representative of three independent experiments. (c) colony counting. Data are the mean ± s.d. (n=3 independent experiments). Student's t-test was used, and two-sided p-values are indicated. (d) Picture representing SSEA4+ colonies at day 26 of human PR in sg#control and sg#Atoh8 conditions, representative of two independent experiments. (e) colony counting. Data are the mean ± s.d. (n=2 independent experiments). Student's t-test was used, and two-sided p-values are indicated. (f) Scheme depicting MEF to neuron transdifferentiation. Cells were infected with lentiviral sh#control and sh#Atoh8 particles. 48 hours later, MEF to neuron reprogramming was induced through lentiviral infection of Brn2, Ascl1 and Mtyl1. Cells were changed from MEF to N3 medium at day 3 and induced neurons iNs scored at day 8 by MAP2 immunofluorescence. (g) Immunofluorescence for Map2 in induced neurons obtained in sh#control and sh#Atoh8 background, representative of two independent experiments. (h) iNS counting per field. Data are the mean ± s.d. (n=2 independent experiments). Student's t-test was used, and two-sided p-values are indicated. (i) Scheme depicting NIH3T3 transformation. Cells were infected with lentiviral sh#control and sh#Atoh8 particles. 48 hours later, NIH3T3 reprogramming was induced through retroviral infection of c-Myc. Cells were splitted for three passages before starting soft-agar experiments and transformed colonies were revealed after 30 additional days by Cresyl-violet staining. (j) Picture representing transformed soft-agar colonies at day 30 of NIH3T3 transformation in sh# control and sh#Atoh8 conditions, representative of three independent experiments. (k) colony counting. Data are the mean ± s.d. (n=3 independent experiments). Student's t-test was used, and two-sided p-values are indicated.

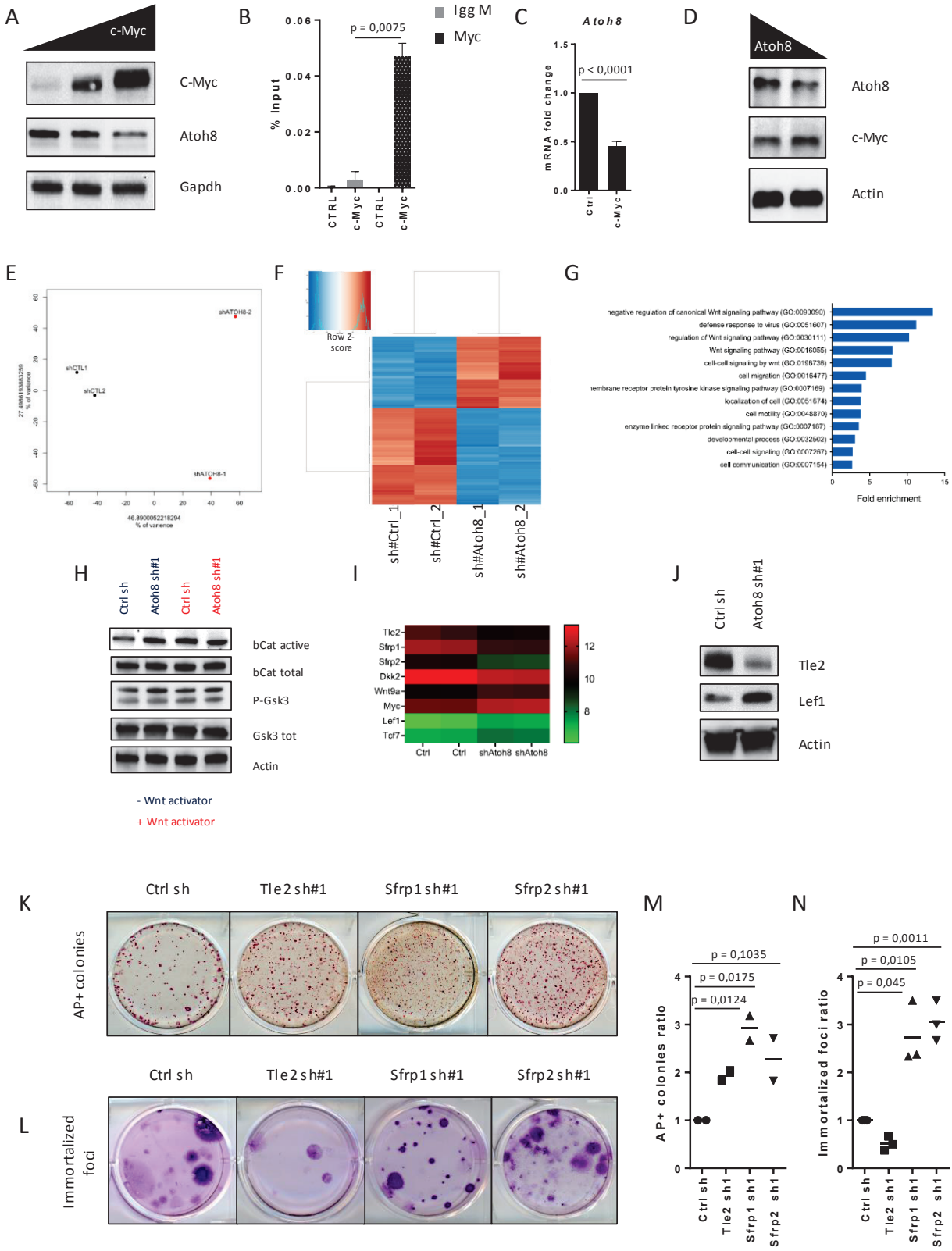
A
c-Myc
C-Myc
Atoh8
Gapdh
B
Igg M
Myc
p = 0,0075
% Input
CTRL
c-Myc
C
Atoh8
p < 0,0001
mRNA fold change
Ctrl
c-Myc
D
Atoh8
Atoh8
c-Myc
Actin
E
shCTL1
shCTL2
shATOH8-1
shATOH8-2
F
Row Z-score
sh#Ctrl_1
sh#Ctrl_2
sh#Atoh8_1
sh#Atoh8_2
G
negative regulation of canonical Wnt signaling pathway (GO:0090090)
defense response to virus (GO:0051607)
regulation of Wnt signaling pathway (GO:0030111)
Wnt signaling pathway (GO:0016055)
cell-cell signaling by wnt (GO:0198738)
cell migration (GO:0016477)
tembrane receptor protein tyrosine kinase signaling pathway (GO:0007169)
localization of cell (GO:0051674)
cell motility (GO:0048870)
enzyme linked receptor protein signaling pathway (GO:0007167)
developmental process (GO:0032502)
cell-cell signaling (GO:0007267)
cell communication (GO:0007154)
Fold enrichment
H
Ctrl sh
Atoh8 sh#1
Ctrl sh
Atoh8 sh#1
bCat active
bCat total
P-Gsk3
Gsk3 tot
Actin
- Wnt activator
+ Wnt activator
I
Tle2
Sfrp1
Sfrp2
Dkk2
Wnt9a
Myc
Lef1
Tcf7
Ctrl
Ctrl
shAtoh8
shAtoh8
J
Ctrl sh
Atoh8 sh#1
Tle2
Lef1
Actin
K
Ctrl sh
Tle2 sh#1
Sfrp1 sh#1
Sfrp2 sh#1
AP+ colonies
L
Ctrl sh
Tle2 sh#1
Sfrp1 sh#1
Sfrp2 sh#1
Immortalized foci
M
p = 0,1035
p = 0,0175
p = 0,0124
AP+ colonies ratio
Ctrl sh
Tle2 sh1
Sfrp1 sh1
Sfrp2 sh1
N
p = 0,0011
p = 0,0105
p = 0,045
Immortalized foci ratio
Ctrl sh
Tle2 sh1
Sfrp1 sh1
Sfrp2 sh1

Figure 6: c-Myc driven Atoh8 repression leads to Wnt pathway activation. (a) Western blot showing expression levels of c-Myc and Atoh8 in MEFs subjected to increasing doses of c-Myc. (b) q-RTPCR showing levels of Atoh8 DNA immunoprecipitated with control IggM or Myc antibody in control or c-Myc-overexpressing conditions. Data, represented as a percentage of Atoh8 DNA levels in ChiP input, are the mean +/- sd of 2 independent experiments. Student T-test was used, and two-sided p-values are indicated. (c) q-RTPCR showing Atoh8 expression levels upon c-Myc overexpression. Data, normalized to control vector, are the mean +/- sd of 3 independent experiments. Student T-test was used, and two-sided p-values are indicated. (d) Western blot showing expression level of c-Myc and Atoh8 in MEFs subjected to sh#-induced Atoh8 downregulation. (e) Principal component analysis of RNA-sequencing of two samples of MEFs wild-type after 5 days upon infection of lentiviral sh#control and of sh#Atoh8 particles. (f) Dendrogram presenting RNA-sequencing data of the 299 differentially expressed genes in sh#control and Atoh8#conditions. FPKM values are normalized to z-score and presented as Log2 values. Color scale is provided in the image. (g) Graphic depicting fold enrichment of statistical overrepresentation analysis. The Panther DB tool was used to detect overrepresented family genes within the genes differentially expressed in sh#control and sh#Atoh8 MEFs. A Fisher's exact two-sided test was used to calculate p-values. (h) Western blot showing expression level of Wnt pathway factors in MEFs upon 5 days of sh#control and sh#Atoh8 downregulation and treated for the last 48 hours with DMSO or Chir99021 inhibitor. (i) Dendrogram presenting RNA-sequencing data of the eight differentially expressed genes involved in Wnt pathway activation in sh#control and sh#Atoh8 conditions. FPKM values are presented as Log2 values. Color scale is provided. (j) Western blot showing expression levels of Tle2 and Lef1 after 5 days upon sh#control and sh#Atoh8 targeting. (k) Picture representing AP+ colonies at day 15 of PR in sh#control, sh#Tle2, sh#Sfrp1 and sh#Sfrp2 conditions, representative of two independent experiments. (l) colony counting. Data are the mean ± s.d. (n=2 independent experiments). Student's t-test was used, and two-sided p-values are indicated. (m) Picture representing Cresyl-violet foci formation colonies at day 30 of MR immortalization in sh#control, sh#Tle2, sh#Sfrp1 and sh#Sfrp2 conditions, representative of three independent experiments. (f) colony counting. Data are the mean ± s.d. (n=3 independent experiments). Student's t-test was used, and two-sided p-values are indicated.

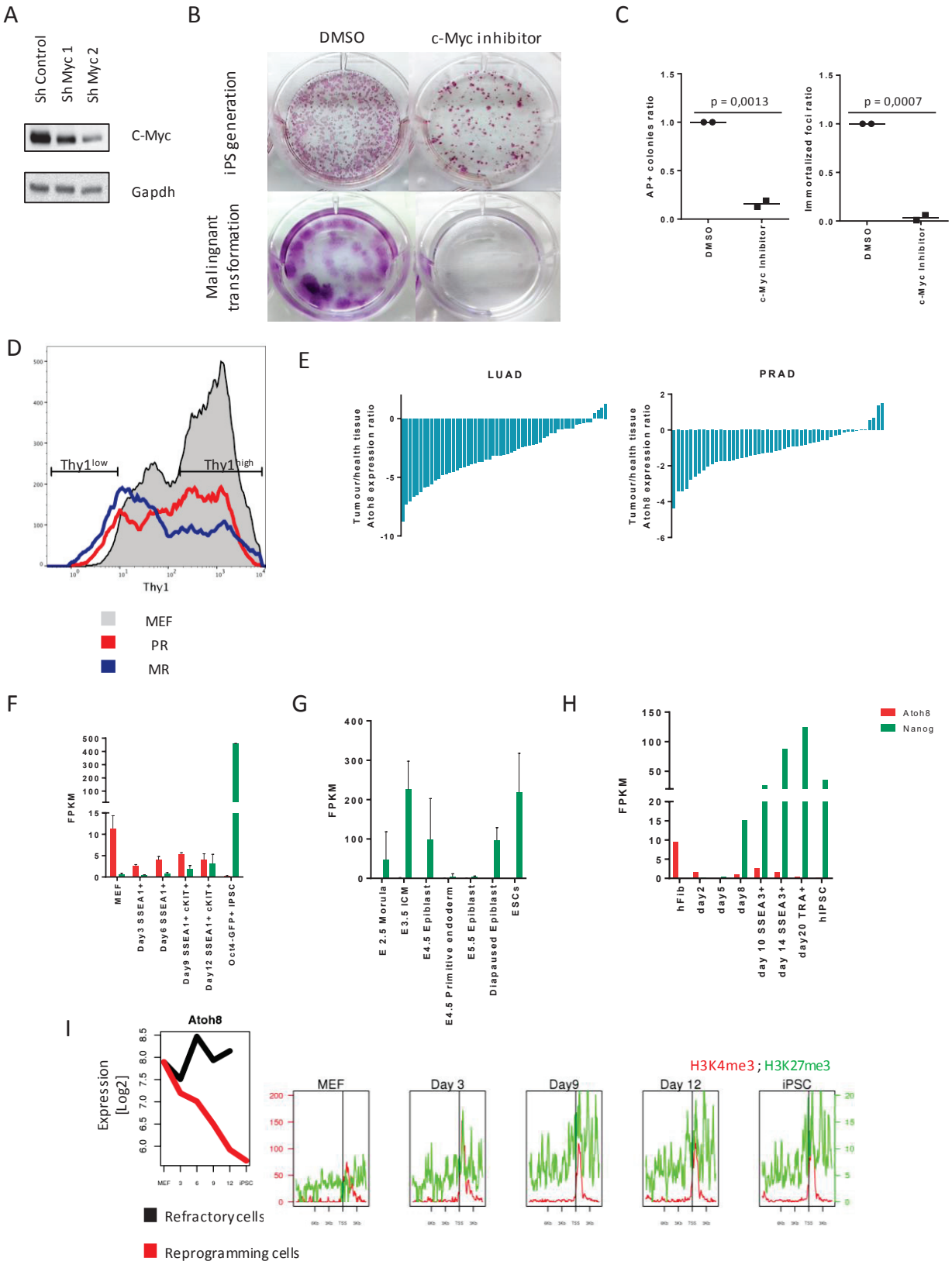
A
Sh Control
Sh Myc 1
Sh Myc 2
C-Myc
Gapdh
B
DMSO
c-Myc inhibitor
iPS generation
Malignant transformation
C
AP+ colonies ratio
p = 0,0013
Immortalized foci ratio
p = 0,0007
DMSO
c-Myc Inhibitor
D
Thy1low
Thy1high
Thy1
MEF
PR
MR
E
LUAD
PRAD
Tumour/health tissue Atoh8 expression ratio
F
FPKM
MEF
Day3 SSEA1+
Day6 SSEA1+
Day9 SSEA1+ cKIT+
Day12 SSEA1+ cKIT+
Oct4-GFP+ IPSC
G
FPKM
E 2.5 Morula
E3.5 ICM
E4.5 Epiblast
E4.5 Primitive endoderm
E5.5 Epiblast
Diapaused Epiblast
ESCs
H
Atoh8
Nanog
FPKM
hFib
day2
day5
day8
day 10 SSEA3+
day 14 SSEA3+
day20 TRA+
hIPSC
I
Atoh8
Expression [Log2]
MEF
3
6
9
12
iPSC
H3K4me3 ; H3K27me3
MEF
Day 3
Day9
Day 12
iPSC
Refractory cells
Reprogramming cells

Supplementary Figure 1: Atoh8 expression in pluripotent reprogramming and malignant transformation. (a) Knockdown efficiency of c-Myc in MEFs. Western blot showing c-Myc expression level upon downregulation with two independent shRNA (sh Myc1 and sh Myc2). (b) Picture representing AP+ colonies (upper panels) and Cresyl-violet immortalized foci (lower panels) derived upon PR and MR in DMSO or c-Myc inhibitor conditions, representative of two independent experiments. (c) AP+ iPS colonies and Cresyl-violet immortalized foci countings. Data are the mean ± s.d. (n=2 independent experiments). Student's t-test was used, and two-sided p-values are indicated. (d) FACS profile showing gating strategy for Thy1 sorting. Thy profiles corresponding to MEF (black), day 3 of PR (red) and day 3 of MR (blue). (e) Histogram depicting Atoh8 transcript levels in LUAD and PRAD patients. Data are presented as a log2 of the ratio of Atoh8 FPKMs between malignant and healthy tissues. (f) Atoh8 (red) and Nanog (green) expression levels in MEF, PR intermediates and mIPSCs. Data, extracted from Knaupp. et al., 2017, present Atoh8 and Nanog transcripts level in FPKM. (g) Atoh8 (red) and Nanog (green) expression levels in embryonic stem cells (ESCs) and *in vivo* totipotent and pluripotent compartments. Data, extracted from Boroviak. et al., 2015, present Atoh8 and Nanog transcripts level in FPKM. (h) Atoh8 (red) and Nanog (green) expression levels in human fibroblasts, human PR intermediates and hIPSCs. Data, extracted from Chacchiarelli. et al., 2015, present Atoh8 and Nanog transcripts level in FPKM. (i) Left panel: Atoh8 expression levels in MEF, PR intermediates and iPSCs in prone (red) and refractory (black) populations. Data, extracted from Polo. et al., 2012, are presented as a log2 of Atoh8 transcripts levels in microarray analysis. Right panel: H3K4m3 (red) and H3K27me3 (green) methylation profile in MEFs, PR intermediates and iPSCs extracted from Polo. et al., 2012.

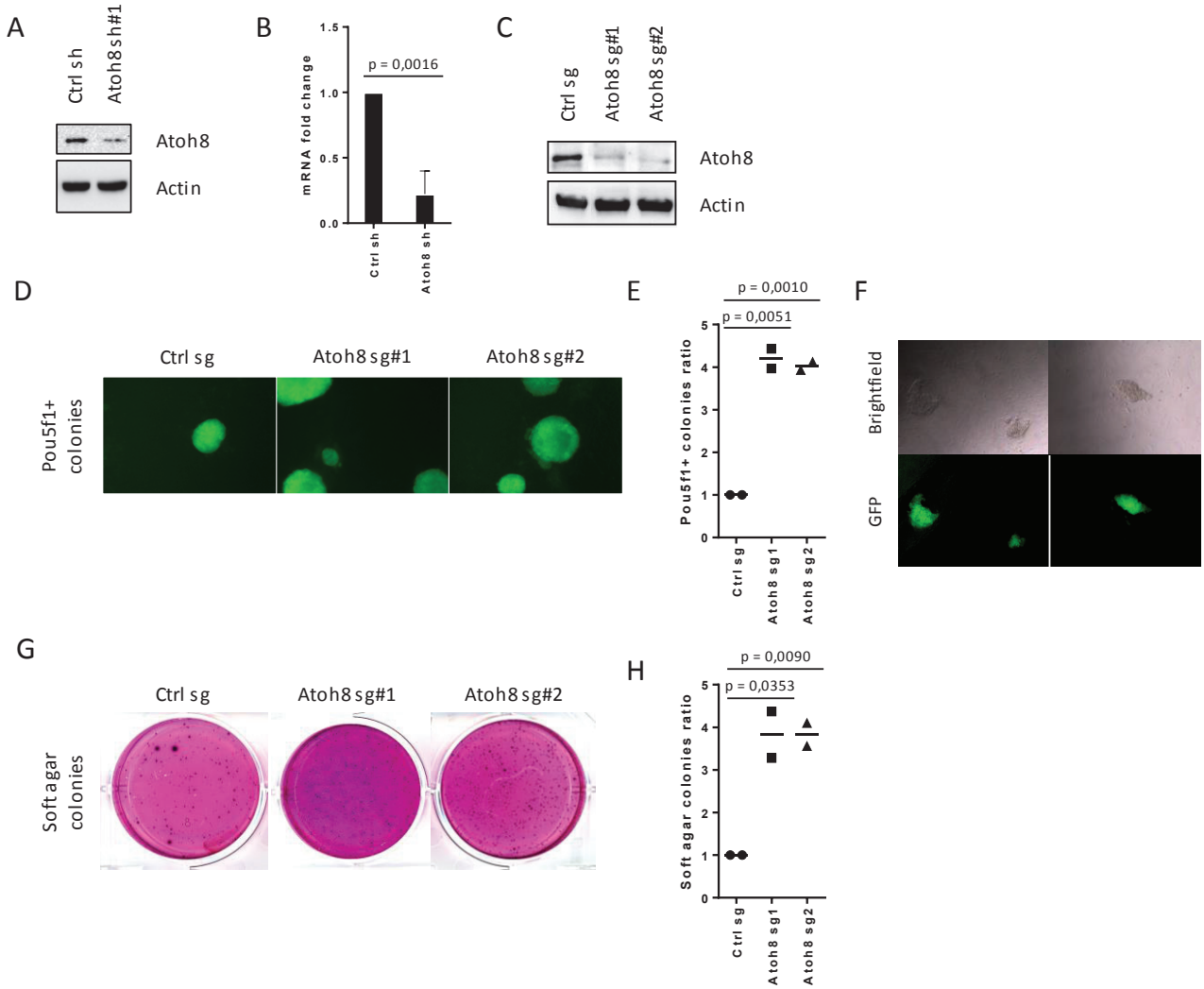

Supplementary Figure 2: Atoh8 as a novel barrier towards pluripotent and malignant reprogramming. (a-b) sh#Atoh8 knockdown efficiency in MEFs. (a) Western blot showing Atoh8 expression level upon infection with lentiviral shRNA particles targeting control and Atoh8 coding sequences. (b) q-RTPCR showing Atoh8 expression levels upon downregulation with sh#Atoh8. Data, normalized to sh#control, are the mean +/- sd of 3 independent experiments. Student T-test was used, and two-sided p-values are indicated. (c) sg#Atoh8 targeting efficiency of Atoh8 in MEFs. Western blot showing Atoh8 expression level upon downregulation with two different sgRNA targeting Atoh8 (sg Atoh8-1 and sg Atoh8-2). (d) Picture representing Pou5f1-GFP+ colonies at day 15 of PR upon Atoh8 downregulation using two different CRISPR guides, representative of two independent experiments. (e) colony counting. Data are the mean ± s.d. (n=2 independent experiments). Student's t-test was used, and two-sided p-values are indicated. (f) Epifluorescence microscope images showing iPSCs Pou5f1-GFP+ colonies derived from a partia-6-days pluripotent reprogramming. Brightfield and GFP represented. (g) Picture representing Cresyl-violet transformed soft-agar colonies at day 30 of MR transformation upon Atoh8 downregulation using two different CRISPR guides. (h) colony counting. Data are the mean ± s.d. (n=2 independent experiments). Student's t-test was used, and two-sided p-values are indicated.

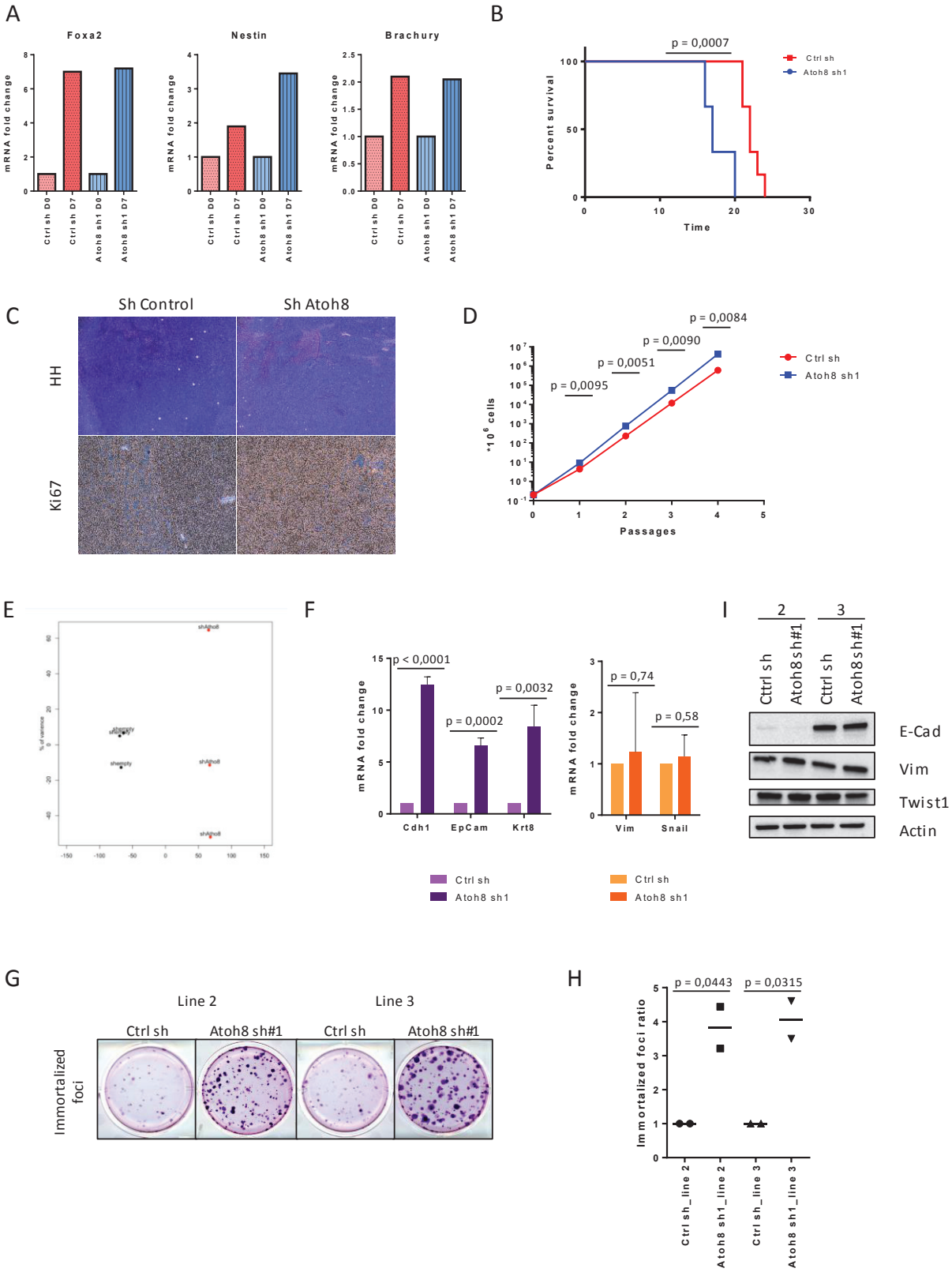
A
Foxa2
Nestin
Brachury
mRNA fold change
Ctrl sh D0
Ctrl sh D7
Atoh8 sh1 D0
Atoh8 sh1 D7
B
p = 0,0007
Ctrl sh
Atoh8 sh1
Percent survival
Time
C
Sh Control
Sh Atoh8
HH
Ki67
D
p = 0,0084
p = 0,0090
p = 0,0051
p = 0,0095
Ctrl sh
Atoh8 sh1
*10^6 cells
Passages
E
F
p < 0,0001
p = 0,0002
p = 0,0032
p = 0,74
p = 0,58
mRNA fold change
Cdh1
EpCam
Krt8
Vim
Snail
Ctrl sh
Atoh8 sh1
I
2
3
Cttrl sh
Atoh8 sh#1
E-Cad
Vim
Twist1
Actin
G
Line 2
Line 3
Ctrl sh
Atoh8 sh#1
Immortalized foci
H
p = 0,0443
p = 0,0315
Immortalized foci ratio
Ctrl sh_line 2
Atoh8 sh1_line 2
Ctrl sh_line 3
Atoh8 sh1_line 3

Supplementary Figure 3: Effects on final iPSCs and TCs upon initial Atoh8 knock-down. (a) q-RTPCR showing three germ layers markers Foxa2, Nestin and Brachury expression levels after 7 days of differentiation of sh#control and sh#Atoh8 iPSC monoclonals lines into embryonic-bodies. Data, normalized to day0 of differentiation, are the representation of 1 experiment. (b) Survival growth of mice injected with sh#control and sh#Atoh8 TCs to perform xenografts described in figure 4H. Data are the mean ± s.d. (n=6 independent mice). Student's t-test was used, and two-sided p-values are indicated. (c) Picture depicts hematoxylin-eosin and KI67 staining histological analysis of xenograft derived from sh#control and sh#Atoh8 TC polyclonal lines. (d) Proliferation curve of sh#control and sh#Atoh8 TCs over time. Data are the mean ± s.d. (n=3 independent experiments). Student's t-test was used, and two-sided p-values are indicated. (e) Principal compontent analysis of RNA-sequencing of three samples of sh#control and of sh#Atoh8 TCs samples. (f) q-RTPCR showing Cdh1, EpCam, Krt8, Vim and Snail expression in sh#control and sh#Atoh8 TCs. Data, normalized to sh#control, are the mean ± sd (n=3 independent experiments). Student's t-test was used, and two-sided p-values are indicated. (g) Picture representing Cresyl-violet immortalized foci at day 30 of foci formation assay starting from TC polyclonal lines 2 and 3 obtained in sh#control and sh#Atoh8 background. (h) colony counting. Data are the mean ± s.d. (n=3 independent experiments). Student's t-test was used, and two-sided p-values are indicated. (i) Western blot showing expression level of Cdh1, Vim and Twist1 in sh#control and sh#Atoh8 TC polyclonal lines 2 and 3.

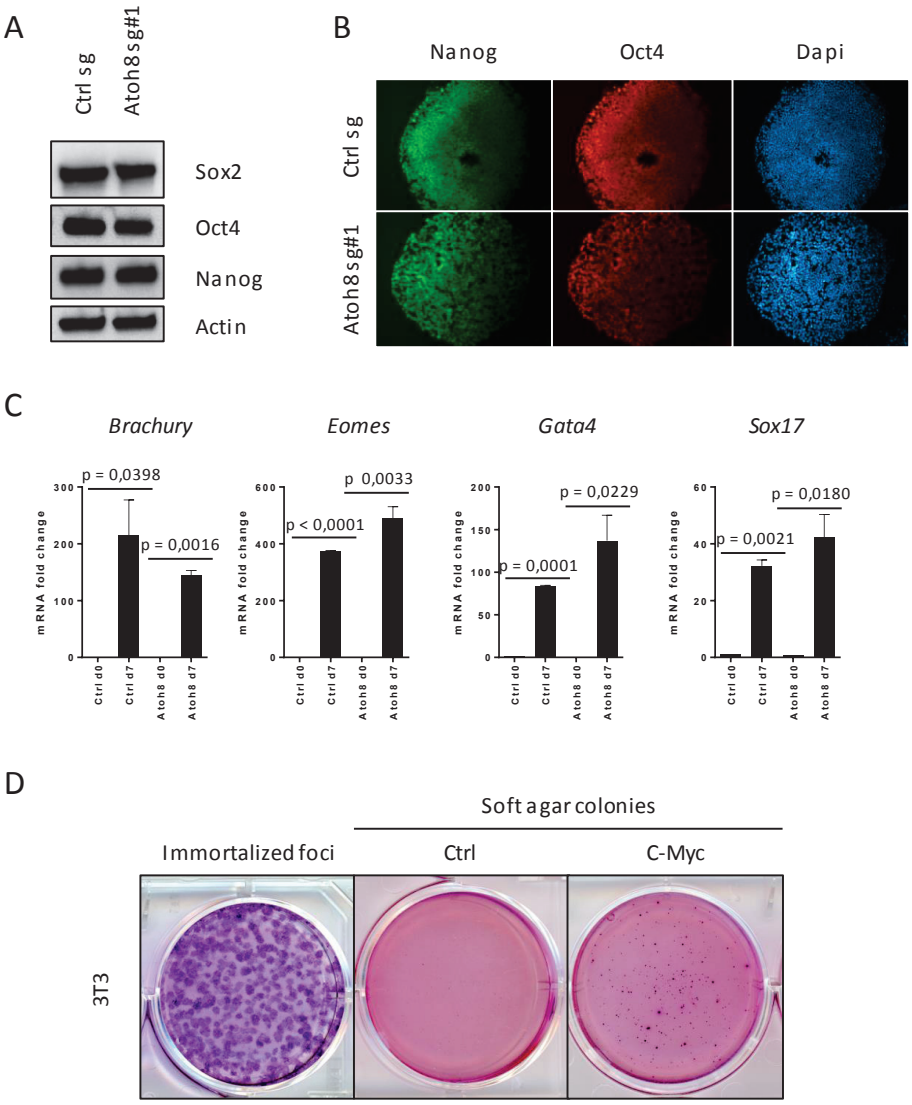

Figure 4 Supplementary: Characterization of hIPS monoclonal line obtained upon Atoh8 downregulation. (a) Western blot showing expression level of Sox2, Nanog and Oct4 in hiPS monoclonal lines obtained in a sg#control and sg#Atoh8 background. (b) Immunofluorescence for Oct4 and Nanog in hiPS sg#control and sg#Atoh8 monoclonal lines. (c) q-RTPCR showing three germ layers markers Foxa2, Nestin and Brachury expression levels after 11 days of sg#control and sg#Atoh8 monoclonal lines differentiation to embryonic-bodies. Data, normalized to day 0 of differentiation, are the mean +/- sd of 3 independent experiments. Student T-test was used, and two-sided p-values are indicated. (e) Picture representing immortalized foci and transformed soft-agar colonies obtained from NIH3T3. First panel: immortalized foci obtained after 15 days of foci formation test in control conditions, stained with Cresyl-violet. Second panel: Cresyl-violet staining after 30 days of soft agar experiment in control conditions: no detectable transformed colonies. Third panel: transformed colonies obtained after 30 days of soft agar experiment in c-Myc overexpressing conditions, stained with Cresyl-violet.

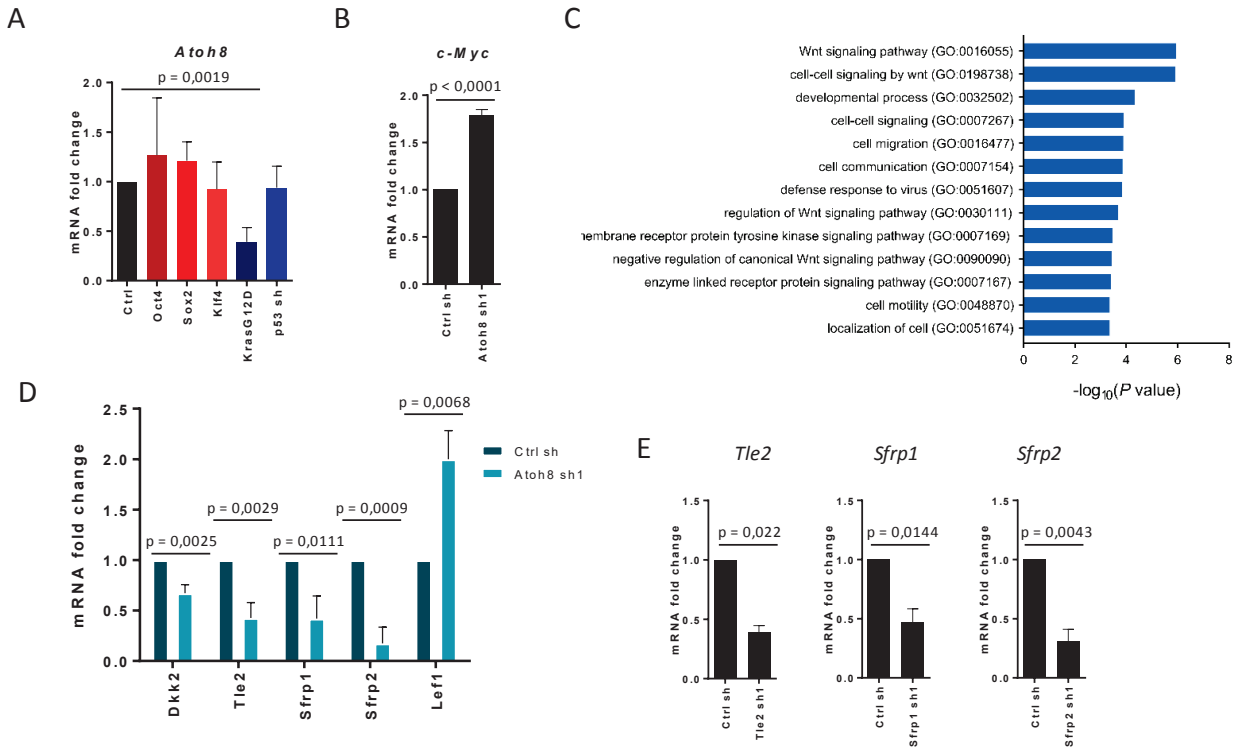

Supplementary Figure 5: Atoh8 c-Myc driven inhibition activates Wnt pathway. (a) q-RTPCR showing Atoh8 expression levels after 3 days of Oct4, Sox2, Klf4 over-expression, p53 downregulation or KRasG12D induction in MEF. Data, normalized to control, are the mean +/- sd of 3 independent experiments. Student T-test was used, and two-sided p-values are indicated. (b) q-RTPCR showing c-Myc expression levels after 5 days of Atoh8 downregulation in MEF. Data, normalized to control, are the mean +/- sd of 3 independent experiments. Student T-test was used, and two-sided p-values are indicated. (c) Graphic depicting statistical significance of fold enrichment observed in statistical overrepresentation analysis. The Panther DB tool was used to detect overrepresented family genes within the genes differentially expressed in sh#control and sh#Atoh8 MEFs. A Fisher's exact two-sided test was used to calculate p-values. (d) q-RTPCR showing Dkk2, Tle2, Sfrp1, Sfrp2 and Lef1 expression levels after 5 days of Atoh8 downregulation in MEF. Data, normalized to control, are the mean +/- sd of 3 independent experiments. Student T-test was used, and two-sided p-values are indicated. (e) q-RTPCR showing Tle2, Sfrp1 and Sfrp2 expression levels upon downregulation with sh#Tle2, sh#Sfrp1 and sh#Sfrp2. Data, normalized to sh#control, are the mean +/- sd of 3 independent experiments. Student T-test was used, and two-sided p-values are indicated.

4. SECOND PHD PROJECT:

NETRIN-1 SIGNALLING MODULATION PROVIDES A NON-CHEMICAL ALTERNATIVE TO 2i EMPLOYMENT IN THE CONTROL OF NAÏVE PLURIPOTENCY

Combined activation of Wnt pathway and reduction of Fgf signalling through 2i (GSK3 and MEK) inhibitors constituted a powerful tool for theorical and practical advances in the pluripotency field. The culture of ESCs in 2i+Lif conditions leads to homogenized naïve *in vitro* cultures. This has allowed to produce ESCs with greater differentiation potential, higher chimaera formation and more efficient CRISPR gene editing (Wray et al., 2010). Among the different advantages provided by 2i, the use of these inhibitors, in combination with Lif, led to a better comprehension of circuits regulating ESCs maintenance, an enhanced knowledge of Wnt and Fgf effectors in pluripotency and promoted the derivation of ESC lines from rats and recalcitrant mice strain, as the non-obese diabetic (NOD) mice (Buehr et al., 2008; Dunn et al., 2014; Li et al., 2008; Martello et al., 2012; Jennifer Nichols et al., 2009).

However, 2i employment presents a considerable drawback. When cultivated for long periods in 2i+Lif conditions, ESCs presents genomic integrity defects, which lead to developmental potential impairment (Choi et al., 2017).

Alternatives to the 2i use have been proposed: combined action of Lif, Mek inhibitor and the atypical protein kinase C (aPKCi) inhibitor can be used to derive rat ESCs in a more efficient way compared to the 2i+Lif conditions (Shimizu et al., 2012). However, this second cocktail again contains Mek inhibitor, which has been identified as the responsible for the observed epigenetic alterations (Choi et al., 2017).

It thus becomes relevant to think to alternative strategies that brings the same advantages offered by 2i+Lif, without the genomic alterations that cause developmental defects (Choi et al., 2017).

A recent work of the lab showed that the axon guidance Netrin-1 regulates pluripotent reprogramming through apoptosis blockage (Ozmadenci et al., 2015). We next wondered if this secreted ligand could play a role in pluripotency maintenance, particularly focusing our attention on a possible induction of a homogeneous naïve state.

4.1. Netrin discovery

Netrins form a family of ligands firstly described for their involvement in the axon guidance, the process by which neurons extend their axons towards their target regions (Stoeckli, 2018).

The first form of Netrin, named Uncoordinated-6 (Unc-6), was discovered in *C. elegans* following a screening performed to identify key factors of neuronal migration and axon guidance (Hedgecock et al., 1990). The first vertebrate homologues discovered were the chicken Netrin-1 and Netrin-2, which promote and guide the out-growth of the commissural axons of the spinal cord (Serafini et al., 1994).

In mammals, we can find six forms of Netrin. Four of them constitute a group of secreted proteins, Netrin-1, -3, -4 and -5, while the other two, Netrin-G1 and -G2, are sequestered to the membrane through a GPI anchor (Nakashiba et al., 2002; Serafini et al., 1994; Wang et al., 1999; Yamagishi et al., 2015; Yin et al., 2000).

4.2. Netrins structure

Netrins constitute a family of extracellular proteins who belong structurally to the laminin family. Laminins are heterotrimeric proteins composed by three aminoacidic chains, (α-,β-, and γ-chain) essential for the composition of the extracellular matrix (ECM), (Timpl et al., 1979).

With a molecular weight of about 70KDa, netrins are formed by three distinct domains: the N-terminal globular domain, called domain VI, the central domain constituted by the EGF repeats (V1, V2 and V3) called domain V, and the C-terminal domain, called domain C for the secreted Netrins and C' for the GPI-anchored (Cirulli and Yebra, 2007). An exception is represented by Netrin-5, which does not present a VI domain and contains just two EGF repetitions in the central domain (Yamagishi et al., 2015) (**Fig.19**)

Compared to laminins, domains VI and V of netrins are respectively homologous to the domains VI and V of these secreted proteins, with Netrin-1, -3 similar to laminin γ-chain and Netrin-4, -G1 and -G2 to laminin β-chain. On the other hand, netrins C-terminal domains do not show any homology with laminins (Rajasekharan and Kennedy, 2009). Highly enriched in positive-charged amminoacids, C domains constitute a possible platform for interactions with extracellular heparan-sulphate (Kappler et al., 2000).

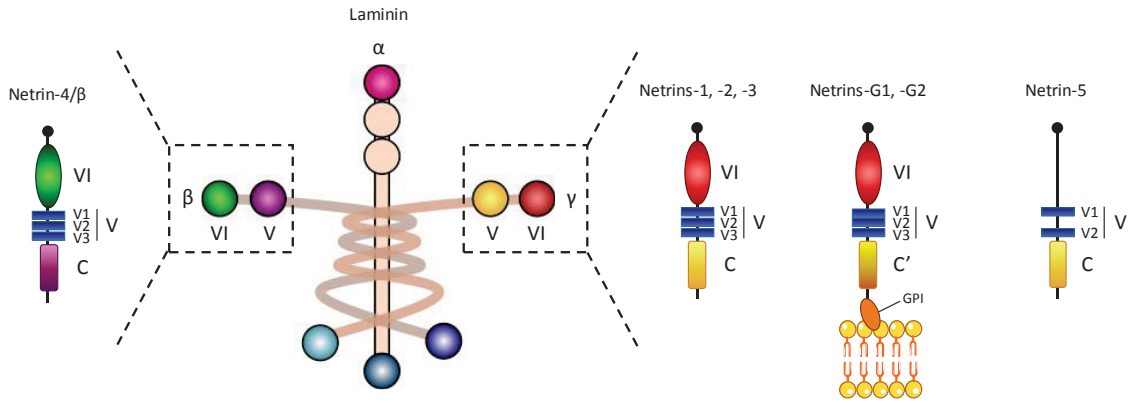

Figure 19: Netrins family structures. In the Netrins family, we can find four secreted molecules (Netrin-1,-2,-3,-4) and two GPI-anchored members. They are principally formed by an N-terminal globular domain (red/green), a central domain containing EGFs repeats (blue) and a "domain C" C-terminal domain (yellow/purple).

The most studied member of the family is Netrin-1. This pleiotropic molecule is expressed in the developing embryo and in a large spectrum of adult tissues and organs, in particular highly expressed in the central nervous system (CNS) (Alcántara et al., 2000). Interestingly, the average expression observed in the adult results decreased compared to the levels observed in the embryo, suggesting a relevance of the ligand in embryonic development.

4.3. Netrin-1 and its receptors

Netrin-1 has been showed to bind several receptors in different models. Interestingly, depending on the selected receptor, Netrin-1 can signal through different pathways and express distinct facets of its pleiotropic function. Its most described receptors are Dcc, Neogenin and the Unc family, but Netrin-1 can bind also less studied membrane receptors, as Dscam, A2b and some integrines (α6β4 and α3β1) (**Fig.20**).

4.3.1. DCC: Deleted in Colorectal Cancer

Dcc was described for the first time in human by a screening aimed to identify genes present in the region of the chromosome 18q21 that show a loss of heterozygosity in 70% of colorectal cancers (Fearon et al., 1990).

First evidences of the interaction of Netrin with Dcc comes from the first studies on *C. Elegans*, where Hedgecock and colleagues showed that the same defects in ventral and dorsal axonal

projections observed in the Unc-6 mutant (homologous on Netrin-1) were recapitulated in Unc-40 and Unc-5, respectively corresponding to the vertebrates Dcc and Unc-5 family (Chan et al., 1996, p. 40). Moreover, Dcc is expressed in the developing embryo in the commissural neurons of the spinal cord, where their axon projections respond to the Netrin-1 presence. Indeed, in this model, an antibody blocking Dcc receptor activity erases the effects of Netrin-1 on axon out-growth (Keino-Masu et al., 1996; Serafini et al., 1996). Furthermore, knock-out mice for Netrin-1 and Dcc show the same phenotype, with pups dying few hours after birth (Dominici et al., 2017; Fazeli et al., 1997; Yung et al., 2015).

As Netrin-1, during embryonic development, Dcc is mainly and strongly expressed in the CNS, but its expression is observed also in the peripheric nervous system (Gad et al., 1997, p. 199; Jiang et al., 2003). On the contrary, in the adult the expression of Dcc is relatively low, still observed in the CNS, but in a smaller number of neural structures compared to the developing embryo (Gad et al., 1997; Osborne et al., 2005, p. 200).

At the molecular level, the Dcc receptor belongs to the Immunoglobulin superfamily. Composed of around 175-190 KDa, depending on its isoform, it is formed by a long extracellular N-terminal domain, organized in four immunoglobulin domains and six type III fibronectin domains, and a shorter intarcellular C-terminal domain, constituted by three domains with no homology recognized with other described proteins, the domains P1, P2 and P3, fundamental for Dcc signalling transduction (Finci et al., 2015). The fourth and fifth fibronectin domain represent the binding site for Netrin-1 interaction (Geisbrecht et al., 2003; K. Xu et al., 2014).

The signalling of Netrin-1 through Dcc was principally described in the axonal growth cones, mobile structures formed at the extremity of axons which drive their expansion. Here, Netrin-1 bind the extracellular portion of Dcc inducing its heterodimerization through the internal P3 domain (Stein, 2001). The heterodimerization of the receptor enables its interaction with several intracellular proteins, as the tyrosine kinases FAK and Fyn, the scaffold protein Nck1 and actin-binding proteins Ena/Vasp and N-WASP (Lebrand et al., 2004; Li et al., 2004, 2002, p. 1; Shekarabi, 2005). The recruitment of these proteins leads to several signalling pathways that mediates cytoskeletal reorganization to promote axonal growth, as the Rho GTPase and the MAPK/Mek/Erk pathways (Forcet et al., 2002; Shekarabi and Kennedy, 2002).

4.3.2. Neogenin

After Dcc, Neogenin (Neo-1) has been the second vertebrate homologous identified for the *C. Elegans* gene Unc-40. Belonging too to the immunoglobuline superfamily, Neo-1 share the 50% of homology with the Dcc gene and displays a similar secondary structure (Vielmetter, 1994).

Unlike Dcc and Netrin-1 KO, which present neural defects that lead to perinatal death, KO mice for Neo-1 do not present alteration in neuronal axon guidance and are perfectly viable, with slight defects in myogenic differentiation (Bae et al., 2009).
During the embryonic development, contrary to Dcc, Neo-1 has been described to be expressed in different organs, as gut, pancreas, lung and kidney, usually restricted to precise tissues, possibly playing a role during organogenesis (Fitzgerald et al., 2006). Neo-1 is also expressed in several adult tissues (Gad et al., 1997; Keeling et al., 1997). In the CNS, Neo-1 is principally present in regions of neuronal maturation, which host processes of axogenesis and dendritic arborization (Gad et al., 1997). Interestingly, the axon guidance process orchestrated by Neo-1 in these structures is not mediated by Netrin-1, but by another Neogenin ligand, ten-fold more efficient than Netrin-1, Repulsive Guidance Molecule a (or RGMa) (Rajagopalan et al., 2004).

Like Dcc, Neo-1 contains an extracellular domain organized in four immunoglobulin and six fibronectin domains, particularly conserved with Dcc aminoacidic sequence. On the other hand, the intracellular domain is divergent compared to Dcc, a part from the P1-3 domains which are conserved across all vertebrates (Cole et al., 2007).
The interaction with Netrin-1 is mediated by the binding between the domains VI and V of Netrin-1 and the fourth and fifth fibronectin domain of Neo-1 (Keino-Masu et al., 1996). Even if it shows the same binding of the Netrin-1/Dcc interaction, the Netrin-1/Neo-1 binding is characterized by distinct structural and stochiometric features (K. Xu et al., 2014).

Signalling of Netrin-1 through Neo-1 has been less studied compared to the homologous Dcc and little is known about this pathway. However, it has been shown that Neo-1, as Dcc, can interact with FAK and PTP-α, suggesting a possible redundancy in their function (Ren et al., 2004).
In this direction, Netrin-1 induces chemioattractive migration inside and outside the CNS, determinates cell adhesion and mediate differentiation through Neo-1 (Kang et al., 2004; Park et al., 2004; Srinivasan et al., 2003; Wilson and Key, 2006).

4.3.3. Unc-5 family

As anticipated before, the same screening which led to the identification of Unc-6 and Unc-40 (Netrin and Dcc) showed that the *C. Elegans* Unc-5, coding for the Unc-5 family in vertebrates, is fundamental for proper axon guidance (Hedgecock et al., 1990). Considering that the Unc-5 mutant recapitulated the phenotype of Unc-6 mutant, it was hypothesized that Unc-5 is a Netrin-1 receptor involved in the neuronal migration and axon projection in regions far from the Netrin-1 source.

Interestingly, the same study showed opposite effects of Netrin-1 depending on the bound receptor: while Netrin-1 have an attractive effect for axons of neurons expressing Dcc, it plays a repulsive role for axonal branching of neurons expressing Unc-5. This bifunctionality, dependent on the engaged receptor, was soon after demonstrated also in vertebrates (Colamarino and Tessier-Lavigne, 1995).

Four Unc-5 homologous has been identified in vertebrates: Unc5-a, -b, -c and -d. During the embryonic development, they are all particularly expressed in the developing CNS (Leonardo et al., 1997). However, while expression of Unc5-a is merely restricted to the CNS, Unc5-b, -c and -d are present in other embryonic tissues, during blood vessel formation, retina development, bud limp and mammary gland patterning (Engelkamp, 2002). Regarding their requirement during development, while Unc5-a and -d KO mice are vital, Unc5-b KO showed embryonic lethality at E12.5 and Unc5-c KO mice in the few hours after birth (Burgess, 2006; Lu et al., 2004; Williams et al., 2006; Zhu et al., 2013).

In the adult, Unc5-a and -c are strongly expressed in the spinal cord, while, outside the CNS their expression, of Unc5-b in particular, seem to be more ubiquitous (Manitt et al., 2004; Thiebault et al., 2003).

On a structural level, members of the Unc5 family are type I transmembrane receptors. Containing around 110KDa, they belong too to the superfamily of Immunoglobulins.

Their N-terminal extracellular region contains two Immunoglobulin domains followed by two type I Thrombospondines domains, while the C-terminal intracellular portion is formed by three different components: a ZU-5 domain (Zona Occludens-1/Unc5 homology domain), homologous to the ones found in the tight junctions-associated zona occludens proteins, an UPA domain (Unc-Pidd-Ankyrins) capable of interacting with the intercellular Dcc domain P3, and finally a Death domain (DD), homologous to the ones found in the death receptor family Tnf (Grandin et al., 2016).

The interaction with Netrin-1 concerns the IV and V Netrin-1 domain and the two Ig domains of Unc5.

In the CNS, Netrin signalling through the Unc5 receptors drives a repulsive effect for neuronal axon guidance (Colamarino and Tessier-Lavigne, 1995). The process of repulsion mediated by the Netrin-1/Unc-5 axis is unclear: only the tyrosine phosphatase Shp2 has been identified in the process, and Unc5 receptors phosphorylation on the ZU-5 domains is required for its recruitment. At a functional level, it is hypothesized that the recruited Shp2 could interact with Rho GTPases and induce cytoskeletal reorganisation (Tong et al., 2001). Repulsive roles of the Netrin-1/Unc5-b signalling has been shown also outside the CNS, where the signalling hinders inappropriate lateral branching during lung morphogenesis, constitutes a repulsive cue in angiogenesis pathfinding and promotes placental vascularization (Liu et al., 2004; Lu et al., 2004; Navankasattusas et al., 2008).

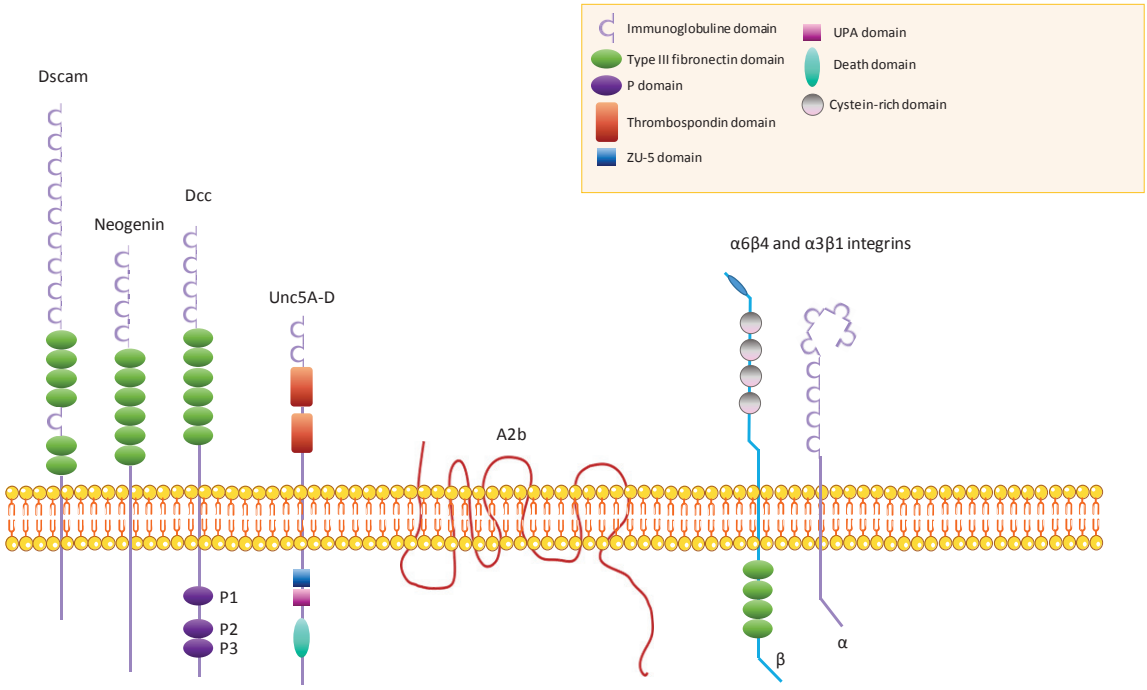

Figure 20: Netrins receptors structures. Netrins can bind different receptors to mediate different functions. In the figure, the most described receptors are illustrated, with a legend depicting the structural domains composing them.

4.4. Netrin-1 function

During embryonic development, Netrin-1 and its receptors are strongly expressed in many regions in the CNS, where they play important roles. However, Netrin-1 is a pleiotropic molecule covering essential functions in many aspects of development and adult homeostasis. Moreover, Netrin-1 and its receptors have also been shown to be involved in cancer development through the model of dependence receptors

4.4.1. Netrin-1 as a driver of axon guidance.

During spinal cord development, Netrin-1 is particularly expressed in a medio-ventral structure known as floor plate and in the neuronal progenitors, which are situated in the medial centro-ventral zone of the spinal cord and whose radial axons take contact with the dorsal surface of the spinal cord, the pia mater (Serafini et al., 1996).

In this structure, Netrin-1 plays a fundamental role in the proper formation of the dorso-ventral projections of commissural neurons (Serafini et al., 1996). During this process, commissural axons from neurons present in the dorsal region of the spinal cord project towards the ventral floor plate, where they cross the median line and expand towards the anterior and posterior directions of the spinal cord (Wentworth, 1984). Particularly, the Netrin-1/Dcc axis mediates the first step of the process, where it guides the projections towards the floor plate thanks to is chemoattraction properties (Keino-Masu et al., 1996). Indeed, organisms deficient for Netrin-1 and Dcc present major defects in axonal growth and in projections of commissural axons (Dominici et al., 2017; Fazeli et al., 1997; Serafini et al., 1996). Unexpectedly, the Netrin-1 required for this chemoattraction is not produced by the floor plate, but by the neuronal progenitors (Dominici et al., 2017; Varadarajan et al., 2017).

Notably, like other axon guidance ephrines, Netrin-1 is a bifunctional molecule: while it can mediate chemoattraction via signalling through the Dcc receptor, it plays a repulsive role in certain neurons expressing the Unc5 receptors (Alcántara et al., 2000). Moreover, interestingly, while the short-distance repulsion requires signalling through the Unc5 receptors, Dcc is required in addition for long-distance repulsion, suggesting that different stoichiometry and composition of receptor complexes mediate opposite effects of the Netrin-1 signalling (Hong et al., 1999; Varela-Echavarría et al., 1997).

4.4.2. Netrin-1 as a driver of neuronal migration

Neuronal migration is indispensable for the correct positioning of neurons during development to ensure a functional neuronal circuit. Produced at the level of the ventricular zone (VZ), new-born neurons migrate towards their correct position through radial or tangential migration. Netrin-1 is involved specifically in tangential migration, where neurons migrate perpendicularly to the direction of radial glial projections thanks to the action of attractive or repulsive signals (Nadarajah and Parnavelas, 2002). Netrin-1/Dcc signalling mediates tangential migration of a set of dorsal interneurons of the spinal cord, while signalling through Integrin α3β1 is required for cortical interneurons (Junge et al., 2016; Stanco et al., 2009). Indeed, Netrin-1 KO leads to several defects in neuronal migration, as absent formation of pontine nuceli, responsible for the connection between cortex and cerebellum (Serafini et al., 1996; Yee et al., 1999).

4.4.3. Netrin-1 functions outside the CNS

Outside the CNS, Netrin-1 has many pleiotropic effects with different functions depending on the bound receptor.

During embryonic development, Netrin-1 participates to morphogenesis of several organs. For example, the Netrin-1/Unc5-b axis regulates lung morphogenesis by inhibiting formation of aberrant alveolar budding, while in the inner ear Netrin-1 is required in the optic epithelium for the formation of semi-circular canals possibly through interaction with Integrin α3β1 (Liu et al., 2004; Matilainen et al., 2007; Salminen et al., 2000).

Netrin-1 regulates also cellular adhesion through Neogenin signalling in the developing mammary gland. The combined action of the ligand-receptor improves the stabilization of the precise interaction between the prelumenal cells and the cap cells of the terminal end buds (Srinivasan et al., 2003).

The role of Netrin-1 in migration and cellular adhesion has been shown also during the embryonic development of pancreas. Indeed, cells composing the pancreatic epithelium expressing the Integrins α3β1 and α6β4 migrate in the direction of cells secreting Netrin-1. Thanks to this attraction, they can adhere to the basal membrane (Yebra et al., 2003).

Netrin-1 has been shown to regulate cellular proliferation in the adult kidney via its receptor Unc5-b, while in *in vitro* culture of mesenchymal stem cells, derived from the umbilical cord, the effects on proliferation seem to be mediated by Integrin α6β4 (Lee et al., 2016; Wang et al., 2009).

Moreover, the Netrin-1/Unc5-b couple seems to modulate angiogenesis. However, the data on this function are contrasting, with some studies proposing a pro-angiogenic role and other an anti-angiogenic effect (Castets et al., 2009; Larrivee et al., 2007; Lu et al., 2004; Park et al., 2004).

4.4.4. Netrin-1 in cancer

Netrin-1 has been described to accomplish a role also in cancer biology. The action of Netrin-1 and its receptor Dcc represents the first example of the model of dependence receptors (Goldschneider and Mehlen, 2010). According to this theory, some receptors can induce distinct pathways depending on the presence or absence of their ligands in the extracellular environment. In the presence of the ligand, receptors induce their canonical positive pathways, including for the aforementioned cases regulation of cellular migration, cellular adhesion, proliferation, etc… On the other hand, when the ligand is absent in the extracellular space, the same receptors can induce their negative pathways, actively driving apoptotic cell death. Following this model, these receptors are called dependence receptors, being the cells dependent to the ligand presence for their survival (Mehlen et al., 1998).

Nowadays, the family of dependence receptor corresponds to a functional family composed by many receptors. This family encloses many Netrin-1 receptors, as Dcc (the first described), Unc5 receptors, and Neogenin (even if, in this case, responding to the RGMa ligand), and other known receptors as Notch-3 and c-Kit (Lin et al., 2017; Llambi, 2001; Matsunaga et al., 2004; Wang et al., 2018).

Thanks to their characteristics, dependence receptors constitute a valid mechanism of anti-tumoral surveillance. The negative pathways of these receptors can induce apoptosis in aberrantly proliferating cells where the ligand quantity become insufficient, controlling, in this way, the cell number in the tissues where the receptors are expressed.
Cancer cells can bypass these barriers in several ways: by upregulating the ligands production or by downregulating or mutating receptors and effectors of the negative pathways to abolish their onco-suppressor activity.
In line with this idea, Netrin-1 expression has been found increased in several types of breast, prostate, lung, pancreas, gastric cancers, glioblastomas and neuroblastomas (Bernet and Fitamant, 2008; Delloye-Bourgeois et al., 2009; Fitamant et al., 2008; Kefeli et al., 2017; Latil et

al., 2003). In the same way, Netrin-1 receptors has been found downregulated in cancer, for example Dcc and Unc5-b, lost in colorectal, prostate, breast and ovary cancers (Bernet et al., 2007; Fearon et al., 1990; Thiebault et al., 2003).

4.4.5. Netrin in reprogramming and stemness

Among the different functions orchestrated by this pleiotropic molecule, Netrin-1 has been recently proposed to play a fundamental role in iPSCs generation and cancer plasticity (Ozmadenci et al., 2015; Sung et al., 2019).

In our lab, it has been recently shown that, during pluripotent reprogramming, Netrin-1 is expressed in a biphasic fashion, transiently downregulated during the early steps of the process and upregulated after day 6. This peculiar expression was further analysed at a functional level: Ozmadenci and colleagues showed that RNAi-induced downregulation of Netrin-1 expression impairs drastically the efficiency of iPSCs generation. Furthermore, in a mirror way, treatment with recombinant Netrin-1 induces an increase in the efficiencies of both mouse and human pluripotent reprogramming. Notably, the enhanced iPSCs generation is due to the presence of recombinant Netrin-1 in the first days of reprogramming, which is capable to limit the apoptosis induced by the activation of Dcc negative pathway observed during the transient decrease of Netrin-1 expression. Indeed, during the first days of reprogramming, while Netrin-1 level decreases, Dcc level remains steady. The decrease of ligand leads to Dcc negative pathway induction and consequent cell death, particularly in the reprogramming intermediates more prone to generate iPSCs.

Association of Netrin-1 with increased stemness has also been showed in the context of cancer (Sung et al., 2019). Indeed, in human colorectal cancer Netrin-1 and Unc5-b expression have been associated to a stromal signature, more precisely a cancer associated fibroblast (CAF) signature. Indeed, when co-cultured with colon and lung cancer cells, CAFs showed a strong increase of both Netrin-1 and Unc5-b expression. Moreover, the inhibition of Netrin-1 signalling, mediated by a blocking antibody that avoids Netrin-1 interaction with Unc5-b, led to a downregulation of cancer stem cell markers Nanog, Oct4 and ALDH1A1, and decreased the *in vitro* clonogenicity and *in vivo* engraftment of cancer cells. Sung et colleagues furtherly showed that Netrin-1 regulates the acquisition of stem cell features by increasing levels of secreted cues previously described as cancer stem cells mediators, Il6 and Il8 (L. Chen et al., 2015; Kim et al., 2013).

5. SECOND PHD PROJECT PAPER:

CONTROL OF NAÏVE PLURIPOTENCY BY THE NETRIN-1/NEO1/UNC5B SIGNALLING AXIS.

Authors: A. Huyghe[1†], G. Furlan[1†], D. Ozmadenci[1†], C. Galonska[2], J. Charlton[2], X. Gaume[1], N. Combémorel[1], N. Allegre[3], J.Y. Zhang[4], P. Wajda[1], N. Rama[5], P. Vieugué[5], I. Durand[6], M. Brevet[7], N. Gadot[8], T. Imhof[9], B.J. Merrill[4], M. Koch[9], P. Mehlen[5,8], C. Chazaud[3], A. Meissner[2] and F. Lavial[1*].

Affiliations : [1]Cellular reprogramming and oncogenesis Laboratory - Univ Lyon, Université Claude Bernard Lyon 1, INSERM 1052, CNRS 5286, Centre Léon Bérard, Centre de recherche en cancérologie de Lyon, 69008 Lyon, France; [2]Broad Institute of MIT and Harvard, Cambridge, MA 02142, USA; Harvard Stem Cell Institute, Cambridge, MA 02138, USA; Department of Stem Cell and Regenerative Biology, Harvard University, Cambridge, MA 02138, USA; [3]GReD, Université Clermont Auvergne, CNRS, INSERM, BP38, 63001 Clermont-Ferrand, France; [4]Department of Biochemistry and Molecular Genetics, University of Illinois, Chicago, IL 60607, USA; [5]Apoptosis, Cancer and Development Laboratory - Univ Lyon, Université Claude Bernard Lyon 1, INSERM 1052, CNRS 5286, Centre Léon Bérard, Centre de recherche en cancérologie de Lyon, 69008 Lyon, France; [6]Cytometry Facility, Univ Lyon, Université Claude Bernard Lyon 1, INSERM 1052, CNRS 5286, Centre Léon Bérard, Centre de recherche en cancérologie de Lyon, 69008 Lyon, France; [7]Department of pathology, HCL Cancer Institute and Lyon1 University, France; [8]Department of Translational Research and Innovation, Centre Léon Bérard, France; [9]Institute for Dental Research and Oral Musculoskeletal Research, Center for Biochemistry, University of Cologne, 50931 Cologne, Germany.

Contact Information : [*]Correspondence to: F. Lavial: fabrice.lavial@lyon.unicancer.fr

[†]Contributed equally to this work

Short title: netrin-1 controls pluripotent features *in vitro* and *in vivo*.

Abstract:

In mouse embryonic stem cells (mESCs), the chemical blockade of Gsk3α/β and Mek1/2 (2i) instructs a self-renewing ground state whose endogenous inducers are unknown. Here we showed that the axon guidance cue netrin-1 promotes naive pluripotency by triggering signalling, transcriptomic and epigenetic changes partially overlapping with 2i. Furthermore, we demonstrated that netrin-1 can substitute 2i to sustain mESCs self-renewal in combination with Lif and regulates the formation of the pluripotent epiblast *in vivo*. Mechanistically, we revealed how netrin-1 and the balance of its receptors Neo1 and Unc5B co-regulate Wnt and Mapk pathways in both mouse and human ESCs. Netrin-1 signalling (i) induces Fak kinase to inactivate Gsk3α/β and stabilize β-Catenin and (ii) increases the phosphatase activity of a PR55γ-containing PP2A complex to reduce Erk1/2 activity. Collectively, this work identifies netrin-1 as a regulator of *in vitro* and *in vivo* pluripotent features and reveals that a unique ligand can mediate different effects in stem cells depending on its receptors dosage, opening perspectives for balancing self-renewal and lineage commitment.

Keywords: netrin-1, Neo1, Unc5B, ground state, pluripotency, Pp2A, Gsk3α/β, Wnt, Mapk.

Introduction:

Mouse embryonic stem cells (mESC) are endowed with unlimited self-renewal and characterized by a regulatory circuitry composed of a few key transcription factors, mainly regulated by four signaling cues[1-3]. Lif[4], Wnt3a[5] and Bmp4[6] sustain self-renewal while Fgf4 is the primary signal to exit self-renewal and acquire competence to differentiate via Erk1/2 activation[7]. Conventional culture conditions require Lif and serum/KSR (referred hereafter as serum/Lif) to maintain a self-renewing state. In this setting, the Fgf/Mapk and the repressive Gsk3α/β/Tcf7l1 pathways remain active, leading to a heterogeneous cell population. These metastable mESCs exhibit fluctuating expression of pluripotency factors such as Nanog and detectable levels of early lineage genes[8]. The concomitant suppression of Mapk signalling, *via* Mek1/2 blockade, and activation of the Wnt pathway, *via* Gsk3α/β blockade (described as 2i), supports mESCs self-renewal and instructs cells toward a ground state of pluripotency[9,8,10]. The 2i mESCs display relatively uniform expression of pluripotency factors and negligible levels of most lineage-affiliated genes, therefore resembling the naive epiblast. This finding of a pluripotent ground state has led to conceptual and practical advances, including the establishment of germline-competent ESCs from recalcitrant mouse strains and from rat[11,12]. However, the prolonged chemical blockade of Mek1/2 and the resulting global DNA hypomethylation have recently been shown to compromise the genomic stability of mESCs, calling into question the use of these inhibitors[13]. Hence, the identification of endogenous signalling pathway(s) controlling self-renewal and ground state pluripotency is not only crucial to advance our understanding of early embryonic development but also for best developing strategies to generate stable human naive pluripotent stem cells.

Netrins are secreted proteins initially described for their crucial role in axon guidance during the development of the nervous system[14,15]. Netrin-1, purified by Tessier-Lavigne and colleagues as a soluble laminin-related molecule able to elicit the growth of commissural axons, is now considered as a pleiotropic ligand involved in development and pathologies[14,16,17]. Most of netrin-1 functions are mediated by signalling through the receptors deleted in colorectal carcinoma (Dcc) and Unc5-homologs (Unc5h, i.e., Unc5A, Unc5B, Unc5C, Unc5D), though Neogenin (Neo1) also constitutes an effective receptor for netrin-1[18-20]. Mechanistically, the characterization of this repertoire led to identify netrin-1 as a bifunctional molecule able to exert opposite effects - attracting or repulsing - neurons, endothelial or immune cells depending on the receptors it engages[21,22,23]. Our recent work showed that netrin-1 constrains apoptosis early during somatic cell reprogramming[24] yet the precise function of this pathway in stem cells self-renewal and lineage commitment remains unknown.

In this study, we revealed an early developmental function for the axon guidance cue netrin-1 in the control of naive pluripotency. By combining embryo and cellular models with signalling, transcriptomic and epigenomic analyses, we found that netrin-1 and its receptors Neo1 and Unc5B activate a complex signalling cascade to control Wnt and Mapk in mESCs and support self-renewal in combination with Lif. *In vivo*, we

reported an early function for netrin-1 in the formation of the pluripotent compartment of pre-implantation embryos. Our findings shed light on a novel regulator of *in vitro* and *in vivo* pluripotent features and revealed that a unique ligand can have diverse effects in stem cells depending on its receptors balance.

Results:

Netrin-1 is regulated by Wnt and Mapk signalling in mouse and human pluripotent stem cells.

In order to identify regulator(s) of pluripotent features, we compared the transcriptomes of serum/Lif mESCs supplemented with inhibitors of Gsk3α/β (CHIR99021), Mek1/2 (PD0325901) or both (2i) for 48 hours. Among the transcripts affected by Wnt and Mapk signalling modulation, netrin-1 was induced by Gsk3α/β inhibition and 2i but repressed by Mek1/2 blockade at both transcript and protein levels (Fig. 1a-b), whereas other netrin family members (netrin 4, -5, and -G1 and -G2)[25] remained unaffected (Supplementary Fig. 1a). Since netrin-1 is expressed at basal levels in serum/Lif conditions but particularly elevated following Gsk3α/β inhibition (Fig. 1a-b), we asked whether it constitutes a target of the Wnt pathway in pluripotent cells. Consistently, mESCs treated with recombinant Wnt3a elevated netrin-1 expression while treatment with Lif and Bmp4 had no significant effect (Fig. 1c). A similar netrin-1 induction was observed in human induced pluripotent stem (hiPS) cells in response to Gsk3α/β inhibition or Wnt3a (Supplementary Fig. 1b). Since canonical Wnt pathway stimulation, or Gsk3α/β inhibition, have been shown to stabilize pluripotency by alleviating the repressive effect of Tcf7l1 on the core pluripotency network[26], we evaluated netrin-1 expression in Tcf7L1/Lef1 knockout mESCs (Zhang J. et al., manuscript in revision). netrin-1 expression was released in absence of TcF7l1 but drastically reduced if both Tcf7l1 and Lef1 are depleted, indicating that Tcf7l1 acts as a main repressor of netrin-1 activation by Lef1 (Supplementary Fig. 1c-d). Collectively, these results demonstrate that the ligand netrin-1, expressed at basal levels in serum/Lif conditions, is regulated by Wnt and Mapk signalling in pluripotent stem cells.

The activation of the netrin-1/Neo1/Unc5B signalling axis sustains Nanog and mESC undifferentiated state.

The distribution of naive pluripotency factors such as Nanog is heterogeneous in serum/Lif mESCs and becomes homogeneous in 2i[9]. To characterize netrin-1 expression, we derived mESCs from *netrin-1 βgeo* knock-in reporter blastocysts[27]. We found that netrin-1 is heterogeneously expressed and confined to 8% of serum/Lif mESCs, confirming its basal expression in this setting. This βgal-positive fraction increased to 26 and 23% in presence of Gsk3α/β inhibitor and 2i, respectively (Fig. 1d). Exploration of single-cell transcriptomic data[28] provided similar results on *netrin-1* transcript heterogeneity (Supplementary Fig. 1e) but also revealed that the mean *netrin-1* expression level *per* cell is significantly higher in 2i (Supplementary Fig. 1f).

Due to its strong induction in 2i, we asked whether netrin-1 could actively instruct ground state pluripotency features. Most netrin-1 functions are mediated by the receptors Dcc, Neo1 and Unc5A, B, C and D[18-20]. In serum/Lif mESCs and miPSCs as well as in pre-implantation embryos, *Dcc* was absent but *Unc5B* and *Neo1* were detected (Supplementary Fig. 2a-b). We therefore generated mESCs exogenously expressing different HA-tagged netrin-1 forms from cre-excisable transgenes (Fig. 1e), wild-type (netrin-1^{WT}) or mutated on residues known to be critical for its interaction with Dcc/Neo1 (netrin-$1^{Neo1\text{-}mut}$) or Unc5B (netrin-$1^{Unc5B\text{-}mut}$) (Fig. 1f-g)[17,20]. We established mESC monoclones expressing the netrin-1 versions at similar levels (Supplementary Fig. 2c), comparable to its endogenous levels in 2i (Supplementary Fig. 2d). Strikingly, FACS analysis showed that the size and granulometry of netrin-1^{WT} cells became homogeneous with a prominent contribution of the receptor Unc5B (Supplementary Fig. 2e). Similarly to 2i, we next showed that Nanog heterogeneity was drastically reduced in netrin-1^{WT} mESCs grown in serum/Lif, as shown by immunofluorescence and quantification of the Nanog/Oct4 ratio (Fig. 1h-i). This observation was correlated with elevated levels of Esrrb and Sox2 while Oct4 remained constant (Fig. 1j). Importantly, both netrin-1 mutants fail to confer the same profile, highlighting the complementary roles of Neo1 and Unc5B (Fig. 1h-j). Interrogation of transcriptomic data of single mESCs grown in serum/Lif revealed a significant correlation between *netrin-1* and *Esrrb* levels (Supplementary Fig. 2f).

We next assessed whether netrin-1 signalling activation, by sustaining Nanog, safeguards the undifferentiated state. When cells were grown without Lif for 7 days and replated for 7 days with Lif (Fig. 1k), we found that netrin-1^{WT} conferred strong resistance to differentiation while both mutants failed, reinforcing the involvement of both Neo1 and Unc5B in netrin-1 function (Fig. 1l-m). As expected, TAT-Cre-mediated excision of the netrin-1 transgene led to the abrogation of this ability in revertant cells (Fig. 1n-o). We next generated netrin-1 dox-inducible mESCs that also presented enhanced resistance to differentiation upon Dox addition (Supplementary Fig. 2g-i), confirming netrin-1 effect on pluripotency.

We next demonstrated that sustained expression of netrin-1 severely impairs mESCs differentiation both *in vitro* and *in vivo*. We first evaluated whether netrin-1 maintains the expression of naive pluripotency markers in differentiation conditions. Nanog and Esrrb were still expressed in netrin-1^{WT} mESCs after 6 days in N2B27-Lif while it was extinguished in control cells (Fig. 1p). Immunofluorescence showed that, in contrast to control cells, a significant amount of netrin-1^{WT} mESCs sustains Nanog and Esrrb expression in differentiation-promoting conditions (Fig. 1q-r). Similarly, after 7 days in non-adherent culture conditions, EBs derived from netrin-1^{WT} mESCs failed to repress Nanog and Esrrb (Fig. 1s) or to induce the differentiation genes *Wnt3*, *Mixl1*, *Foxa2*, *Amn*, *Nes* and *Cdh2* (Supplementary Fig. 2j). Teratoma generated with control or netrin-1^{WT} cells were analysed 6 weeks after injection in the testis of immunocompromised mice and revealed a severe differentiation defect caused by netrin-1 sustained expression (Fig. 1t). Finally, when control and netrin-1^{WT} mESCs were grown at clonal density on laminin in N2B27+Lif for 5 passages, we found that netrin-1 expression increased significantly mESC self-renewal ability, as indicated by AP+ colonies counting (Fig. 1u-v). Collectively,

these data showed that the netrin-1/Neo1/Unc5B signalling axis sustains Nanog and protects mESCs from *in vitro* and *in vivo* differentiation.

The activation of the netrin-1/Neo1/Unc5B signalling axis induces transcriptomic and epigenetic changes partially overlapping with 2i

To gain insight into netrin-1 function, we compared the transcriptomes of control and netrin-1^{WT} mESCs grown in serum/Lif by RNA-seq. Netrin-1^{WT} expression impacted 434 genes (fc >1.5 or <-1.5 at adjusted p-value<0.05), with a striking repression of differentiation genes such as *Gata6* and *Gata4* (Fig. 2a). Functional annotation clustering of differentially expressed genes by gene ontology (GO) Panther (protein analysis through evolutionary relationships) analysis revealed strong association with "embryo development", "endoderm development" and "regulation of Mapk cascade" (Fig. 2b). Significant differences were also apparent for genes related to cell proliferation, in agreement with the slightly accelerated growth of netrin-1^{WT} mESCs without differences in cell cycle features (Supplementary Fig. 2k-l). Because similar GO terms are modulated in 2i mESCs[8], we wondered whether netrin-1 triggered the acquisition of ground state pluripotency features. We compared the transcriptomes of control and netrin-1^{WT} mESCs grown in serum/Lif to previously published datasets (see Methods)[29,30]. While serum/Lif and control samples clustered together as expected, the transcriptome of netrin-1^{WT} cells acquired limited but significant similarities with 2i mESCs (Fig. 2c). To evaluate the respective role of the receptors Neo1 and Unc5B in netrin-1 function, we next compared the transcriptomic effects of the wild-type form of netrin-1 and its mutants by RNA-seq (Fig. 2d-e). Both mutant forms failed at conferring the full transcriptomic signature, reinforcing that netrin-1 ability to interact with both Neo1 and Unc5B is required to modulate mESCs physiology.

We next assessed whether netrin-1 signalling also instructs ground state-related epigenomic modifications, in particular enhancers activity, histone and DNA methylation landscapes. We found that netrin-1^{WT} mESCs displayed increased activity of the naïve Oct4 distal enhancer (DE), Jarid2 and Prdm14 enhancers, described to be induced in 2i (Fig. 2f)[31]. ChIP-seq analyses revealed a global decrease in both H3K4me3 and H3K27me3 histone marks in netrin-1^{WT} mESCs compared with control cells (global enrichment for H3K27me3 ctrl=3.729 versus netrin-1=2.12 and Fig. 2g-h for H3K4me3), similarly to 2i[8]. Enriched H3K4me3 was however detected at pluripotency genes such as *Nanog* and *Sox2* (Fig. 2i), in agreement with their induction in netrin-1^{WT} mESCs. In addition, we showed that H3K27me3 was significantly reduced at bivalent domains (Fig. 2j-k), as reported for 2i[8]. In 2i, the reduction of the expression of the *de novo* methyltransferases *Dnmt3A*, *B* and *L* by Mek1/2 inhibition, coupled with the reduction of the Uhrf1 protein, triggers genome-wide DNA hypomethylation in male ESC[32,10,13,33]. In striking contrast to 2i, restricted representation bisulphite sequencing (RRBS) revealed that netrin-1^{WT} mESCs (grown for >30 passsages in presence of the transgene) display similar DNA methylation levels to control cells (mean = 0.25+/-0.003 and 0.24+/-0.004 respectively) (Fig. 2l and Supplementary Fig. 2m).

In addition, even if *Dnmt3A* level was found slightly reduced in netrin-1^{WT} mESCs (Supplementary Fig. 2n), Uhrf1 protein level was rather induced (Fig. 2m). Other critical differences were found between netrin-1^{WT} and 2i mESCs. While 2i mESCs are characterized by a repression of early differentiation genes of the three germ layers[8], we did not detect downregulation of early ectodermal genes in netrin-1^{WT} mESCs grown in serum/Lif, suggesting that spontaneous differentiation toward ectoderm is not repressed (Fig. 2n). Collectively, these results indicate that the netrin-1/Neo1/Unc5B signalling axis induces profound transcriptomic and epigenomic changes in mESC. The resulting configuration shares some features with 2i such as enhancer activity but also severely differs on some aspects such as global DNA methylation.

Netrin-1 controls Wnt and Mapk signalling by modulating Gsk3α/β and Erk1/2 activities in mouse and human pluripotent stem cells.

We next dissected molecularly how netrin-1 instructs pluripotency features partially related to the ground state. With 2i, the chemical blockade of Gsk3α/β leads to Wnt pathway activation while Mek1/2 inhibition suppresses Mapk signalling[9]. We detected a strong activation of the Wnt pathway in netrin-1^{WT} mESCs, as illustrated by accumulation of active β-catenin, dephosphorylated on Ser37 and Thr41 and therefore no longer targeted for destruction (Fig. 3a). Of note, point mutants showed that netrin-1 interactions with both Neo1 and Unc5B are required for β-catenin stabilization (Fig. 3a). When we assessed the level of the β-catenin destruction complex members in netrin-1^{WT} mESCs, Gsk3α/β activity was severely reduced, as revealed by elevated levels of its inactive form, phosphorylated on Ser21 and Ser9[34] (p-Gsk3α/β)(Fig. 3a). In addition, we showed that the p-Gsk3α/β level reached in netrin-1^{WT} mESCs is equivalent to control cells treated with recombinant Wnt3a, and can not be significantly elevated by Wnt3a addition (Fig. 3b).

Netrin-1 has been linked to different kinases such as Fak, Dapk[35], Fyn[36,37], Pka[38] and c-Jnk1[39] that could be involved in Gsk3α/β phosphorylation. Among those, we found increased levels of active Fak (phosphorylated on Tyr 397) in netrin-1^{WT} mESCs (Fig. 3c). The fact that Fak has been shown to phosphorylate Gsk3α/β[40] prompted us to investigate whether netrin-1 promoting effect on Wnt is mediated by Fak. RNAi-mediated depletion of Fak in netrin-1^{WT} mESCs (>80%, Supplementary Fig. 3a) reduced p-Gsk3α/β, therefore diminishing Wnt pathway activation, as shown by β-catenin (Fig. 3d).

We next showed that netrin-1^{WT} mESCs harbour reduced phospho-Erk1/2 (p-Erk1/2) levels while p-Mek1/2 remained constant (Fig. 3e), and this decrease required both Neo1 and Unc5B, as revealed by the point mutants. Because Mapk is controlled by Lif and Fgf, we next determined whether netrin-1 signalling modulated mESCs sensitivity to these cytokines. Deprivation/stimulation experiments indicated that the responsiveness to Fgf4 was significantly reduced in netrin-1^{WT} mESCs, as illustrated by p-Erk1/2 (Fig. 3f). In contrast, in similar settings, Lif-mediated p-Erk1/2 and p-Stat3 inductions were not affected (Supplementary Fig. 3b). The link between Unc5B and the phosphatase complex Pp2a[35] next prompted us to investigate whether it is involved

in p-Erk1/2 decrease in mESC. Pp2a is a heterotrimeric complex comprising scaffolding, regulatory and catalytic subunits[41]. We demonstrated first by immunoprecipitation of the catalytic subunit Pp2acα that netrin-1 signalling activation led to a significant increase of its phosphatase activity (Fig. 3g). In line with the fact that the qualitative composition of the complex has been shown to modulate its activity[42], we noticed an induction of the regulatory subunit *PR55γ* in netrin-1^{WT} mESCs (Fig. 3h). To evaluate whether the Pp2a complex is responsible for Mapk signalling attenuation, we attempted to rescue p-Erk1/2 levels by RNAi-mediated depletion of the catalytic Pp2acα or the regulatory PR55γ subunits. Using 2 independent siRNA, we showed that the efficient knockdown (>80%, Supplementary Fig. 3c) of both subunits solely rescued p-Erk1/2 level while leaving p-Mek1/2 and p-Gsk3α/β steady (Fig. 3i).

We next developed other strategies to deliver netrin-1. First, we generated netrin-1 dox-inducible mESCs that showed similar and dose-dependent changes in Wnt and Mapk signalling following dox addition (Fig. 3j). Netrin-1 dox-inducible feeder line was next generated by stable transfection. When mESCs were plated on these irradiated feeders, treated or not with dox, we noticed that netrin-1 triggers similar signalling changes, indicating that netrin-1 can act in a paracrine manner on pluripotency (Fig. 3k).

Finally, the generation of human iPS cells expressing exogenously netrin-1 revealed that the activation of the pathway triggers similar effects in human pluripotent stem cells - elevation of Wnt activity triggered by Gsk3α/β inactivation and reduction of Mapk by Erk1/2 dephosphorylation - but it was not sufficient to elevate the expression of naive pluripotency factors such as Nanog (Fig. 3l).

Collectively, we showed that netrin-1 signalling activation promotes Wnt signalling by activating Fak kinase that triggers Gsk3α/β inactivation and β-catenin stabilization. Netrin-1 also modifies Pp2a complex activity that triggers Erk1/2 dephosphorylation.

Netrin-1 supports mESC self-renewal in combination with Lif

To compare the magnitude of the changes induced by netrin-1 and 2i, control and netrin-1^{WT} mESCs were subjected to 2i treatment for 48 hours in serum/Lif (Fig. 4a). The basal levels of p-Gsk3α/β, Nanog and Esrrb in serum/Lif netrin-1^{WT} mESCs was nearly comparable to 2i-treated mESCs. However, Mapk alleviation was significantly lower, as evidenced by 30% decrease of Erk1/2 (Fig. 4a). As expected, Mapk activity was still responsive to 2i treatment, confirming that netrin-1 only partially mimicks signalling changes induced by 2i.

We next assessed whether recombinant netrin-1 (r-netrin-1 - see methods for production) triggers similar changes as transgenes in mESCs. First, we showed that a 48 hrs treatment of mESCs with increasing doses of r-netrin-1 led to gradual Nanog induction, demonstrating a paracrine effect of r-netrin-1 on the pluripotent network (Fig. 4b-c). This treatment also led to dose-dependent changes of β-catenin, p-Gsk3α/β and p-Erk1/2 levels, confirming the effect of netrin-1 on those pathways (Fig. 4d). In order to decipher the sequence of events triggered by r-netrin-1, we performed a time-course analysis by treating mESCs for 24 and 48 hours.

The changes on signalling appeared with different kinetics - pErk1/2 decrease was detectable at 24h while β-catenin induction was observed at 48 hours (Fig. 4e). Paralleled transcriptomic analyses allowed to define a heatmap clustering early and late responders to r-netrin-1 (Fig. 4f). At 24h, within a very limited response to netrin-1 (35 genes differentially expressed genes (DEGs), log2 fold change <1 or >1 and adjusted p-value <0.05), significant downregulations were detected for the pluripotency genes *c-Myc* and *Utf1*, as described in 2i. Differentiation genes such as *Hand1* and Fgf targets *Etv4*, *Spry4* and *Dusp6* were also repressed, in agreement with the rapid changes of p-Erk1/2. At 48h, a larger transcriptomic response was evident (193 DEGs), encompassing *Tfap2c*, *Prdm14* and *Dppa3* upregulations. Of note, most of the early endoderm and mesoderm genes repressed in netrin-1^{WT} mESCs (Fig. 2n) were not repressed at these early time points, suggesting that netrin-1 induces signalling changes prior to repress differentiation.

We next asked whether r-netrin-1 can support mESCs self-renewal in combination with Lif, as reported for 2i. The mESCs were grown at clonal density on laminin in N2B27+Lif with r-netrin-1 or 2i for 6 passages (18 days) (Fig. 4g-h). Colony formation assays, performed at various passages, confirmed that Lif is not sufficient to maintain self-renewal in serum-free media (Fig. 4g-h). However, the sole addition of r-netrin-1 to Lif allowed to sustain self-renewal as 2i (Fig. 4g-h). When replated in serum/Lif after 5 passages in N2B27+Lif+r-netrin-1 or N2B27+Lif+2i, mESCs harboured similar Nanog and Esrrb levels (Fig. 4i). Altogether, these data showed that r-netrin-1 can be used to co-regulate Wnt/Mapk and to sustain mESC self-renewal, in combination with Lif.

<u>The Neo1 and Unc5b receptors are required for endogenous netrin-1 function in mESCs</u>

Because netrin-1 is also expressed at basal levels in serum/Lif conditions (Fig. 1b), we assessed its endogenous function in pluripotent cells. We generated netrin-1 conditional knockout mESCs by crossing netrin-$1^{fl/fl}$ [43] and Rosa26 CreERT2 mice (Fig. 5a). Because feeder cells secrete netrin-1, netrin-$1^{fl/fl}$ mESCs were adapted onto gelatin surfaces and netrin-1 depletion confirmed after TAM treatment (Supplementary Fig. 4a). After 48 hrs, netrin-1 deletion induces changes on signalling and pluripotency that mainly mirrored gain-of-function. Wnt pathway activation, as evidenced by β-catenin, was reduced while Mapk activity was induced *via* p-Erk1/2 (Fig. 5b). Nanog and Esrrb levels were also reduced (Fig. 5b), confirming netrin-1 action on those signalling pathways *in vitro*. However, the expression of epiblast (*Fgf5*, *Otx2*) or primitive endoderm (*Gata4*, *Gata6*) transcripts was not significantly induced (Supplementary Fig. 4b). Of note, netrin-1 acute deletion also led to a significant decrease of mESC self-renewal ability (Fig. 5c-d) with no significant changes of proliferation and cell death (Supplementary Fig. 4c-d). Importantly, these defects, observed in the first days following netrin-1 deletion, were rapidly compensated and netrin-1Δ/Δ mESCs could be maintained at high density for >20 passages (Supplementary Fig. 4e).

To decipher the respective contribution of each receptor to netrin-1 function, we generated netrin-1, Neo1 and Unc5B KO mESCs by Crispr/Cas9 genome editing using 2 independent sgRNA (Fig. 5e and Supplementary

Fig. 4f-g). Crispr/Cas9-mediated netrin-1 loss led to similar changes in p-Erk1/2 and β-catenin levels as the conditional KO strategy (Fig. 5f), and these changes were partially rescued by r-netrin-1 treatment of netrin-1^{KO} mESCs (Fig. 5g). Netrin-1 loss triggered a self-renewal defect (Fig. 5h-i), and this effect was compensated when cells were grown in 2i, in agreement with netrin-1 mode of action on Wnt and Mapk signalling (Supplementary Fig. 4h). Importantly, in serum/Lif conditions, Unc5B and Neo1 single KO induced signalling and clonogenicity changes that largely mimicked netrin-1 loss (Fig. 5f-i), indicating that a tight dosage of the receptors is required to co-regulate Wnt/Mapk and therefore self-renewal.

Netrin-1 regulates cell fate allocation in pre-implantating embryos

Netrin-1 depletion was reported to cause embryonic lethality at E14.5[44] but no function has been reported in pre-implantating embryos. Due to the unexpected function we described in mESCs, we assessed whether this axon guidance cue could be expressed and play an earlier function than previously thought. *In vivo*, the naive pluripotent compartment gradually develops within the mouse inner cell mass (ICM) between E3.5 and E4.5 and becomes separated from the primitive endoderm (PrE) progenitors. *netrin-1/Oct4 in situ* hybridization revealed a confined *netrin-1* expression in the naive epiblast while no signal was detected in the adjacent PrE (Fig. 6a). Interrogation of published single-cell transcriptomic data confirmed a significantly higher *netrin-1* expression in epiblastic cells than in PrE in E4.5 embryos[45] (Supplementary Fig. 4i). The use of *netrin-1 βgeo* embryos also showed a specific βgal activity in the epiblast of blastocysts, indicating that netrin-1 is expressed in pluripotent blastomeres *in vivo* (Fig. 6b).

Due to its specific expression in pluripotent blastomeres, we next examined whether netrin-1 regulates the formation of the epiblast. To assess the consequences of netrin-1 depletion, we analysed E3.75 and E4.5 (E3.75 grown *in vitro* for 24 hrs) embryos from intercrosses between netrin-$1^{fl/fl}$ males and netrin-$1^{fl/wt}$; EIIa-$cre^{+/-}$ females (Fig. 6c). This experimental strategy was selected because EIIa-cre has been shown to be active at the 1 cell-stage and offsprings inheriting EIIa-cre maternally was shown to exhibit a widespread reporter expression[46]. Netrin-1 depletion led to a significant reduction of the number of ICM cells, defined as Dapi positive/Cdx2 negative, in E3.75 embryos, indicating a function for netrin-1 in the homeostasis of the ICM (Fig. 6d-e). This defect was compensated when embryos were grown *in vitro* and analysed 24hrs later, in adequation with the fact that netrin-1 is not absolutely required at these embryonic stages (Fig. 6f-g).

We finally assessed whether netrin-1 controls mESCs derivation efficiency. Starting from blastocysts obtained through netrin-$1^{+/βgeo}$ mice crosses[27] (Fig. 6h), 18 expanded blastocysts outgrowths were subsequently amplified and netrin-1 status analysed. Among those, a single netrin-$1^{βgeo/βgeo}$ mESC line was detected (Fig. 6i), shedding light on a significant deviation from the 1:2:1 expected genotype frequency. Similar derivations performed in presence of r-netrin-1 allowed to rescue the genotype deviation (Fig. 6i), indicating that netrin-1 controls optimal pluripotency capture. Altogether, these approaches revealed an unexpected function for netrin-1 during pre-implantation development.

Netrin-1 exerts different effects in mESCs depending on the Neo1/Unc5B stoichiometry.

netrin-1 has been shown to trigger opposite responses depending on its receptors dosage in neurons, endothelial or immune cells[21,22,23]. We therefore asked whether netrin-1 can also exert different functions depending on the Neo1/Unc5B stoichiometry in mESCs and differentiated derivatives. Interestingly, while netrin-1 and both receptors are expressed in mESCs, EB differentiation induces netrin-1 and affected the dosage toward a Neo1^{low}/Unc5B^{high} ratio (Fig. 7a). Of note, *Unc5b* inductions was already detected when mESCs were converted in an epiblast-like (EpiLC) state[47] (Supplementary Fig. 5a). To alter experimentally the ligand and receptors ratio, we engineered control and netrin-1^{WT} mESCs to express Neo1 or Unc5B upon dox addition (Fig. 7b). We found that p-Erk1/2 decrease triggered by netrin-1 is even more pronounced when Neo1 is exogenously expressed (Fig. 7c). On the contrary, when the receptors ratio is switched toward Neo1^{low}/Unc5B^{high} by inducing Unc5B, p-Erk1/2 is significantly increased by netrin-1, indicating that the ligand has different effects on Mapk depending on its receptors balance (Fig. 7d). In line with p-Erk1/2 function in lineage commitment, we found that this experimental setting (netrin-1^{high}/Neo1^{low}/Unc5B^{high}) triggered Nanog and Esrrb downregulation (Fig. 7e) and a severe reduction of mESCs resistance to differentiation (Fig. 7f-g). In line with this view, by subjecting mESCs expressing solely Unc5B (Neo1^{KO}) or Neo1 (Unc5B^{KO}) to differentiation in N2B27-Lif, we found that mESCs expressing Unc5B presented an enhanced induction of the differentiation genes *Nestin* and *βIII-tubulin* when compared with control or Neo1-expressing cells (Fig. 7h). Collectively, these data indicate that netrin-1 effect on self-renewal is tightly regulated by its receptors balance.

Netrin-1 coordinates differentiation in vitro and in vivo.

Loss of a pro-self-renewal signal in mESCs leads to their accelerated differentiation, as shown for Lif[4], Wnt[48] and Bmp[6]. However, because we found that netrin-1 can repress or induce p-Erk1/2, we assessed whether and how its loss impacted mESC differentiation *in vitro* and *in vivo*. We subjected netrin-1$^{fl/fl}$ mESCs, treated or not with TAM, to various differentiation assays. In EBs, netrin-1 deletion led to a delay, rather than an acceleration, in the induction of early differentiation genes of the 3 germ layers (Fig. 7i), indicating that netrin-1 contributes to coordinated differentiation. In line with this, netrin-1 depleted cells generated smaller-size teratomas than control cells (Supplementary Fig. 5b). To assess whether these defects were associated with differentiation and/or proliferation and/or cell death, we performed guided neural differentiation in N2B27-Lif. In this setting, netrin-1 is induced and a similar switch of receptors as in EBs occurs (Fig. 7j). After 8 days, we observed a reduced induction of the differentiation transcripts *Nestin* and *βIII-tubulin* in absence of netrin-1 (Supplementary Fig. 5c). This difference was accompanied by a reduction of proliferation observed as early as day2 (Fig. 7k) but no significant difference of cell death (Supplementary Fig. 5d), indicating that netrin-1

controls differentiation and proliferation *in vitro*. *In vivo*, when injected into blastocysts, netrin-1-depleted mESCs harboured a reduced ability to give rise to color-coated chimera (Fig. 7l-m). To better characterize this defect, GFP-labelled netrin-$1^{fl/fl}$ mESCs, treated or not with TAM, were aggregated with morulas. Immunofluorescence analyses for GFP and cleaved Caspase3 conducted on late blastocysts revealed a significant increase in the number of apoptotic cells in embryos injected with netrin-1 depleted cells, suggesting that netrin-1 promotes cell survival, as described previously (Fig. 7n-o). Altogether, these results demonstrate that netrin-1 deregulation induces differentiation, proliferation and survival defects.

Discussion:

In this study, we document that the neuronal guidance cue netrin-1, expressed in the epiblast and in mESCs, is an autocrine/paracrine factor that promotes pluripotent features. In particular, netrin-1 controls mESCs self-renewal and trigger signaling, transcriptomic and epigenetic features that partially overlaps with the ground state of pluripotency (Fig. 8)[9]. Even if we showed that netrin-1 signalling acts by reducing Mapk and promoting Wnt in a similar manner than 2i, it targets a different effector of the Mapk pathway - namely Erk1/2 - *via* Pp2a. In line with this difference and in contrast to prolonged Mek1/2 blockade, we did not observe a global DNA hypomethylation in netrin-1^{WT} mESCs[13]. Due to the facts that the use of a Src inhibitor also preserves mESCs epigenetic integrity, and that Src and Fak are interconnected[49], it will be interesting to assess whether Src inhibition triggers a similar cascade as described here.

We revealed that netrin-1 signalling co-regulates Mapk and Wnt signalling in both mouse and human pluripotent stem cells (PSC). Even if netrin-1 exogenous expression is solely not sufficient to confer naive properties to human PSCs (Fig. 3l), subsequent developments should investigate whether the combination of recently described protocols with netrin-1 signalling modulation could help in deriving and/or sustaining naive human pluripotent stem cells.

Using genetic models, we revealed that this signalling pathway influences cell fate allocation during pre-implantation development (Fig. 6). Despite such effect, mouse embryos lacking zygotic netrin-1 expression develop normally through the epiblast stage and die at embryonic day 14.5 (E14.5)[44]. The cause of the embryonic death is currently unknown, but it coincides with the embryonic lethality of mice null for Unc5B[23]. It remains to be investigated whether, as with gp130 stimulation, such role may be accentuated in the context of delayed implantation[50].

Self-renewal and lineage commitment are classically triggered by distinct signalling molecules in a given stem cell type. Murine ESC self-renewal is sustained by Lif[4], Wnt3a[5] and Bmp4[6] while Fgf4 is considered as the primary signal to exit self-renewal and differentiate[7]. A pro-differentiation function has been suggested for Bmp4 during mESCs differentiation but seems to reflect a late suppression of neural fate rather than an active mesodermal induction[7,51]. Here, we showed that netrin-1 can exert different effects on Mapk depending on

the Neo1/Unc5B dosage. In particular, we showed that the repressive activity of netrin-1 on Mapk cascade is converted into a promoting one by Unc5B induction but some questions remain to be answered. First, the factors responsible for Unc5B induction during lineage priming remain to be identified. Interrogation of publically available resources[52] indicated that transcription factors associated with primed pluripotency such as Otx2 or with differentiated derivatives such as Cdx2, MyoD and Gata3 trigger *Unc5B* transcript induction when exogenously expressed in mESCs (GEO accession number GSE31381). Second, the molecular mechanisms responsible for the differential effect of netrin-1 on p-Erk1/2 remain to be dissected. Because we showed that these effects are mediated by the Pp2a subunit PR55γ, and that its paralogues PR55α and PR55δ have been shown to affect the Nodal pathway in opposite ways[42], it will be interesting to assess whether Pp2a subunits composition is also responsible for netrin-1 opposite effect on Mapk in mESCs. Finally, while netrin-1 has been shown to mediate different responses - attracting or repelling neurons, endothelial or immune cells[21,22], our study suggests that this ability of netrin-1 reflects a fundamental characteristic of this protein, which manifests earlier in development than previously proposed, and which might govern other cellular responses than cell migration such as cell fate decisions.

Collectively, our work positions netrin-1 as a crucial signalling pathway that feedback loops with Wnt and Mapk in pluripotent cells *in vitro* and *in vivo*, and demonstrates that a unique ligand can trigger different effects in stem cells depending on its receptors stoichiometry, opening fascinating perspectives for regenerative medicine and cancer biology.

Author Contributions:

AH and GF performed most of the experiments from figures 1-7. DO performed experiments in figures 1, 5 and 7. XG and NC performed experiments in figures 1, 3 and 5. CG performed ChIP-seq experiments. JC and NR carried out the bio-informatic analyses. PW did teratoma experiments. FL, AH, GF and DO designed experiments. FL supervised the study and wrote the manuscript. This work was supported by institutional grants from Inserm/Cnrs, Atip-avenir, Plan cancer, La ligue contre le cancer nationale et régionale (FL), INCa (FL), Fondation ARC (FL, GF and DO), Centre Léon Bérard (FL and AH), Fondation pour la recherche médicale (FL ARF20170938622), National Institutes of Health [R01-HD081534 B.J.M], ANR (PM), ERC (PM) and the DFG Forschergruppe 2722 (MK).

Acknowledgements:

We are grateful to the PBES lyon for technical assistance. We thank V. Azuara and D. Stupack for critical readings of the manuscript and L. Favre-Louis for technical assistance.

References:

1 Evans, M. J. & Kaufman, M. H. Establishment in culture of pluripotential cells from mouse embryos. *Nature* **292**, 154-156 (1981).

2 Martin, G. R. Isolation of a pluripotent cell line from early mouse embryos cultured in medium conditioned by teratocarcinoma stem cells. *Proceedings of the National Academy of Sciences of the United States of America* **78**, 7634-7638 (1981).

3 Dunn, S. J., Martello, G., Yordanov, B., Emmott, S. & Smith, A. G. Defining an essential transcription factor program for naive pluripotency. *Science* **344**, 1156-1160, doi:10.1126/science.1248882 (2014).

4 Williams, R. L. *et al.* Myeloid leukaemia inhibitory factor maintains the developmental potential of embryonic stem cells. *Nature* **336**, 684-687, doi:10.1038/336684a0 (1988).

5 Sato, N., Meijer, L., Skaltsounis, L., Greengard, P. & Brivanlou, A. H. Maintenance of pluripotency in human and mouse embryonic stem cells through activation of Wnt signaling by a pharmacological GSK-3-specific inhibitor. *Nat Med* **10**, 55-63, doi:10.1038/nm979 (2004).

6 Ying, Q. L., Nichols, J., Chambers, I. & Smith, A. BMP induction of Id proteins suppresses differentiation and sustains embryonic stem cell self-renewal in collaboration with STAT3. *Cell* **115**, 281-292 (2003).

7 Kunath, T. *et al.* FGF stimulation of the Erk1/2 signalling cascade triggers transition of pluripotent embryonic stem cells from self-renewal to lineage commitment. *Development* **134**, 2895-2902, doi:10.1242/dev.02880 (2007).

8 Marks, H. *et al.* The transcriptional and epigenomic foundations of ground state pluripotency. *Cell* **149**, 590-604, doi:10.1016/j.cell.2012.03.026 (2012).

9 Ying, Q. L. *et al.* The ground state of embryonic stem cell self-renewal. *Nature* **453**, 519-523, doi:10.1038/nature06968 (2008).

10 Ficz, G. *et al.* FGF signaling inhibition in ESCs drives rapid genome-wide demethylation to the epigenetic ground state of pluripotency. *Cell stem cell* **13**, 351-359, doi:10.1016/j.stem.2013.06.004 (2013).

11 Buehr, M. *et al.* Capture of authentic embryonic stem cells from rat blastocysts. *Cell* **135**, 1287-1298, doi:10.1016/j.cell.2008.12.007 (2008).

12 Li, P. *et al.* Germline competent embryonic stem cells derived from rat blastocysts. *Cell* **135**, 1299-1310, doi:10.1016/j.cell.2008.12.006 (2008).

13 Choi, J. *et al.* Prolonged Mek1/2 suppression impairs the developmental potential of embryonic stem cells. *Nature*, doi:10.1038/nature23274 (2017).

14 Serafini, T. *et al.* The netrins define a family of axon outgrowth-promoting proteins homologous to C. elegans UNC-6. *Cell* **78**, 409-424 (1994).

15 Kennedy, T. E., Serafini, T., de la Torre, J. R. & Tessier-Lavigne, M. Netrins are diffusible chemotropic factors for commissural axons in the embryonic spinal cord. *Cell* **78**, 425-435 (1994).

16 Cirulli, V. & Yebra, M. Netrins: beyond the brain. *Nature reviews. Molecular cell biology* **8**, 296-306, doi:10.1038/nrm2142 (2007).

17 Grandin, M. *et al.* Structural Decoding of the Netrin-1/UNC5 Interaction and its Therapeutical Implications in Cancers. *Cancer cell* **29**, 173-185, doi:10.1016/j.ccell.2016.01.001 (2016).

18 Bell, C. H. *et al.* Structure of the repulsive guidance molecule (RGM)-neogenin signaling hub. *Science* **341**, 77-80, doi:10.1126/science.1232322 (2013).

19 Rajagopalan, S. *et al.* Neogenin mediates the action of repulsive guidance molecule. *Nature cell biology* **6**, 756-762, doi:10.1038/ncb1156 (2004).

20 Xu, K. *et al.* Neural migration. Structures of netrin-1 bound to two receptors provide insight into its axon guidance mechanism. *Science* **344**, 1275-1279, doi:10.1126/science.1255149 (2014).

21 Ko, S. Y., Dass, C. R. & Nurgali, K. Netrin-1 in the developing enteric nervous system and colorectal cancer. *Trends Mol Med* **18**, 544-554, doi:10.1016/j.molmed.2012.07.001 (2012).

22 Hong, K. *et al.* A ligand-gated association between cytoplasmic domains of UNC5 and DCC family receptors converts netrin-induced growth cone attraction to repulsion. *Cell* **97**, 927-941 (1999).

23 Lu, X. *et al.* The netrin receptor UNC5B mediates guidance events controlling morphogenesis of the vascular system. *Nature* **432**, 179-186, doi:10.1038/nature03080 (2004).

24 Ozmadenci, D. *et al.* Netrin-1 regulates somatic cell reprogramming and pluripotency maintenance. *Nature communications* **6**, 7398, doi:10.1038/ncomms8398 (2015).

25 Rajasekharan, S. & Kennedy, T. E. The netrin protein family. *Genome Biol* **10**, 239, doi:10.1186/gb-2009-10-9-239 (2009).

26 Wray, J. *et al.* Inhibition of glycogen synthase kinase-3 alleviates Tcf3 repression of the pluripotency network and increases embryonic stem cell resistance to differentiation. *Nature cell biology* **13**, 838-845, doi:10.1038/ncb2267 (2011).

27 Skarnes, W. C., Moss, J. E., Hurtley, S. M. & Beddington, R. S. Capturing genes encoding membrane and secreted proteins important for mouse development. *Proceedings of the National Academy of Sciences of the United States of America* **92**, 6592-6596 (1995).

28 Kumar, R. M. *et al.* Deconstructing transcriptional heterogeneity in pluripotent stem cells. *Nature* **516**, 56-61, doi:10.1038/nature13920 (2014).

29 Bulut-Karslioglu, A. *et al.* Inhibition of mTOR induces a paused pluripotent state. *Nature* **540**, 119-123, doi:10.1038/nature20578 (2016).

30 Boroviak, T. *et al.* Lineage-Specific Profiling Delineates the Emergence and Progression of Naive Pluripotency in Mammalian Embryogenesis. *Developmental cell* **35**, 366-382, doi:10.1016/j.devcel.2015.10.011 (2015).

31 Galonska, C., Ziller, M. J., Karnik, R. & Meissner, A. Ground State Conditions Induce Rapid Reorganization of Core Pluripotency Factor Binding before Global Epigenetic Reprogramming. *Cell stem cell* **17**, 462-470, doi:10.1016/j.stem.2015.07.005 (2015).

32 Habibi, E. *et al.* Whole-genome bisulfite sequencing of two distinct interconvertible DNA methylomes of mouse embryonic stem cells. *Cell stem cell* **13**, 360-369, doi:10.1016/j.stem.2013.06.002 (2013).

33 von Meyenn, F. *et al.* Impairment of DNA Methylation Maintenance Is the Main Cause of Global Demethylation in Naive Embryonic Stem Cells. *Molecular cell* **62**, 848-861, doi:10.1016/j.molcel.2016.04.025 (2016).

34 Beurel, E., Grieco, S. F. & Jope, R. S. Glycogen synthase kinase-3 (GSK3): regulation, actions, and diseases. *Pharmacol Ther* **148**, 114-131, doi:10.1016/j.pharmthera.2014.11.016 (2015).

35 Guenebeaud, C. *et al.* The dependence receptor UNC5H2/B triggers apoptosis via PP2A-mediated dephosphorylation of DAP kinase. *Molecular cell* **40**, 863-876, doi:10.1016/j.molcel.2010.11.021 (2010).

36 Ren, X. R. *et al.* Focal adhesion kinase in netrin-1 signaling. *Nat Neurosci* **7**, 1204-1212, doi:10.1038/nn1330 (2004).

37 Liu, G. *et al.* Netrin requires focal adhesion kinase and Src family kinases for axon outgrowth and attraction. *Nat Neurosci* **7**, 1222-1232, doi:10.1038/nn1331 (2004).

38 Moore, S. W. & Kennedy, T. E. Protein kinase A regulates the sensitivity of spinal commissural axon turning to netrin-1 but does not switch between chemoattraction and chemorepulsion. *J Neurosci* **26**, 2419-2423, doi:10.1523/JNEUROSCI.5419-05.2006 (2006).

39 Qu, C. *et al.* c-Jun N-terminal kinase 1 (JNK1) is required for coordination of netrin signaling in axon guidance. *The Journal of biological chemistry* **288**, 1883-1895, doi:10.1074/jbc.M112.417881 (2013).

40 Gao, C. *et al.* FAK/PYK2 promotes the Wnt/beta-catenin pathway and intestinal tumorigenesis by phosphorylating GSK3beta. *Elife* **4**, doi:10.7554/eLife.10072 (2015).

41 Sangodkar, J. *et al.* All roads lead to PP2A: exploiting the therapeutic potential of this phosphatase. *FEBS J* **283**, 1004-1024, doi:10.1111/febs.13573 (2016).

42 Batut, J. *et al.* Two highly related regulatory subunits of PP2A exert opposite effects on TGF-beta/Activin/Nodal signalling. *Development* **135**, 2927-2937, doi:10.1242/dev.020842 (2008).

43 Dominici, C. *et al.* Floor-plate-derived netrin-1 is dispensable for commissural axon guidance. *Nature*, doi:10.1038/nature22331 (2017).

44 Bin, J. M. *et al.* Complete Loss of Netrin-1 Results in Embryonic Lethality and Severe Axon Guidance Defects without Increased Neural Cell Death. *Cell Rep* **12**, 1099-1106, doi:10.1016/j.celrep.2015.07.028 (2015).

45 Nakamura, T. *et al.* A developmental coordinate of pluripotency among mice, monkeys and humans. *Nature* **537**, 57-62, doi:10.1038/nature19096 (2016).

46 Heffner, C. S. *et al.* Supporting conditional mouse mutagenesis with a comprehensive cre characterization resource. *Nature communications* **3**, 1218, doi:10.1038/ncomms2186 (2012).

47 Hayashi, K., Ohta, H., Kurimoto, K., Aramaki, S. & Saitou, M. Reconstitution of the mouse germ cell specification pathway in culture by pluripotent stem cells. *Cell* **146**, 519-532, doi:10.1016/j.cell.2011.06.052 (2011).

48 ten Berge, D. *et al.* Embryonic stem cells require Wnt proteins to prevent differentiation to epiblast stem cells. *Nature cell biology* **13**, 1070-1075, doi:10.1038/ncb2314 (2011).

49 Mitra, S. K. & Schlaepfer, D. D. Integrin-regulated FAK-Src signaling in normal and cancer cells. *Curr Opin Cell Biol* **18**, 516-523, doi:10.1016/j.ceb.2006.08.011 (2006).

50 Nichols, J., Chambers, I., Taga, T. & Smith, A. Physiological rationale for responsiveness of mouse embryonic stem cells to gp130 cytokines. *Development* **128**, 2333-2339 (2001).

51 Kawasaki, H. *et al.* Induction of midbrain dopaminergic neurons from ES cells by stromal cell-derived inducing activity. *Neuron* **28**, 31-40 (2000).

52 Correa-Cerro, L. S. *et al.* Generation of mouse ES cell lines engineered for the forced induction of transcription factors. *Sci Rep* **1**, 167, doi:10.1038/srep00167 (2011).

53 Cusanovich, D. A. *et al.* Multiplex single cell profiling of chromatin accessibility by combinatorial cellular indexing. *Science* **348**, 910-914, doi:10.1126/science.aab1601 (2015).

Methods:

Cell culture and embryos. *Netrin-1*$^{\beta geo}$ reporter[27] and netrin-1 conditional knockout (netrin-1$^{fl/fl}$)[43] mice were derived from C57/bl6 mixed background in N2B27/2i+Lif on feeders for 5 days and then transferred in serum/LIF. Netrin-1 depletion in netrin-1$^{fl/fl}$ mESCs is induced by treatment with 4'OH-tamoxifen (TAM) at 0.2µM for 48 hours. Cgr8 and E14Tg2a ES cells were cultured on gelatin as previously described[24]. Control, netrin-1, netrin-1$^{Unc5B\text{-}mut}$ and netrin-1$^{Neo1\text{-}mut}$ were established from the same starting Cgr8 population. The netrin-1^{KO}, Neo1^{KO} and Unc5B^{KO} and netrin-1 dox-inducible mESCs were generated by stable transfection of Cgr8 mESCs using FugeneHD reagent (Promega) or lipofectamine 2000 (Life technologies). Netrin-1 revertant mESCs were obtained by treating cells with 100 units TAT-Cre (SCR-508, Millipore) for 24 hours followed by FACS cell sorting of GFP expressing cells. Control Neo1-doxi, netrin-1 Neo1-doxi, control Unc5B-doxi and netrin-1 Unc5B-doxi mESCs were generated by infecting control and netrin-1 mESCs with dox-inducible plasmids (kind gift from Mehlen lab). The siRNA (Dharmacon) were reverse transfected in Cgr8 ES cells at a final concentration of 30nM using lipofectamine 2000. Silenced Negative Control siRNA (Life technologies) was used as negative control for siRNA transfection. Cells were harvested 2-3 days post transfection. siRNA sequences are detailed in supplementary table 1. The hiPS cells, generated using Sendai viruses, were cultured in complete TeSR-E8 medium on Vitronectin-coated plates (StemCell Technologies). Medium was changed

daily and cells were chemically passaged once a week in the presence of 10µM ROCK inhibitor Y-27632 (Sigma-Aldrich) with Ultra-Pure EDTA solution (Invitrogen). All cell lines used in the study were tested mycoplasma-free (Mycoalert kit). The following recombinant proteins were used as follows: Mouse Wnt3a (R&D Systems, 1324-WN) 50ng/ml, Human Fgf4 (Peprotech, 100-31) 10ng/ml, Human Activin (Invitrogen, PHG9014). 293T and plat-E cells were grown in DMEM supplemented with 10% FCS and penicillin/streptomycin. PD0325901 (Millipore, 444968) and CHIR99021 (Millipore, 361571) were purchased from Merck Millipore. Luciferase assays were performed using dual luciferase reporter assay system (Promega E1910). Wild type netrin-1 from Gallus gallus lacking the C-terminal domain (NP_990750, aa: 26-458) was cloned into a modified PCEP vector with an C-terminal Strep-II tag. HEK293 cells were stably transfected and secreted netrin-1 purified by Streptavidin chromatography (IBA) followed by the removal of the tag by thrombin digestion. Purified netrin-1 was then dialyzed against PBS and passed through a sterile filter. Protein concentration was corrected by the calculated extinction coefficients for netrin-1 (ProtParam utility available on the ExPaSy server). Embryos were flushed in M2 medium (Sigma) and grown ON in KSOM (Sigma) or sequential blast (Origio) media. Genotyping of netrin-$1^{fl/fl}$ embryos was performed as previously described[43]. X-gal was detected in blastocysts using secondary antibodies coupled with biotin and the vectastain ABC kit and DAB (vector system).

Self-renewal and exit from pluripotency assays. For colony formation assay, mESCs are plated at clonal density (60-100 cells per cm^2 depending on the strain) in serum/LIF on gelatin-coated plates. Media was changed every day during 7 days before detection of alkaline phosphatase positive colonies detection (AP0100-1KT, Sigma). For exit from pluripotency assays, mESCs were grown for 7 days in serum minus LIF on gelatin, then split and replated for 7 additional days in serum/LIF. For self-renewal assays (Fig. 4), E14Tg2a mESCs were plated at clonal density on laminin-coated dishes and split every 3 days.

Differentiation assays *in vitro* and *in vivo*.

Serum deprivation/stimulation experiments were conducted by growing mESCs overnight in N2B27 media without cytokines followed by exposure to the appropriate molecules for the times indicated in the figures. Control Neo1-doxi and netrin-1 Neo1-doxi mESCs were grown in N2B27+dox media for 24h prior to collection and Embryoid body (EB) formation assays were carried out by growing mESCs in non adherent culture conditions in non-treated plastic plates for the indicated times. Epiblast-like (EpiLC) induction was performed as previously described[18]. Teratoma formation assays were performed by injecting $1x10^6$ mESCs in the testis of 7-week-old severe combined immunodeficient (SCID) mice (CB17/SCID, Charles River). After 3-4 weeks, the mice were euthanized and lesions were surgically removed and fixed in formol or in 4% paraformaldehyde for sections. For blastocyst injections, netrin-$1^{fl/fl}$, treated or not with Tamoxifen (TAM) for 48 hours, were injected into BALB/cANRj blastocysts. The day before injection, frozen BALB/cANRj morulas from Quickblasto (JANVIER, France) were thawed according to the manufacturer's instructions and incubated overnight in KSOM medium (millipore, France) at 37°C, 5% CO2. Between 5 and 15 cells were injected into expanded blastocysts in M2

medium (Sigma) using standard blastocyst injection techniques. Blastocysts were then allowed to recover for a period of 1–3 hours prior to being implanted into pseudo pregnant females. All animal procedures were performed in accordance with institutional guidelines (French ceccapp project 01369.01).

Constructs. To perform *in situ* hybridization on mouse embryos, a netrin-1 probe was cloned from mESC cDNA into pGEMTeasy (Promega) (sequence available on request) and in situ hybridization performed as previously described. Point mutations were introduced into the pcagg-netrin-1-ires-puro vector to generate netrin-1 mutant versions using the quick site directed mutagenesis kit (Agilent). CRISPR KO plasmids were engineered using the backbone pSpCas9 (BB)-2A-Puro and the protocol from the Zhang lab (Ran et al., 2013). The small guides (sg) were designed using the UCSC genome browser and CRISPOR (Haeussler et al., 2016) websites. Guides are detailed in supplementary table 1. Neo1 and Unc5B Dox inductible pITR vectors are kind gifts from Mehlen lab.

Antibodies, Q-RTPCR and biochemical assays. Primary antibodies used in this study are detailed in supplementary table 1. The main antibodies were validated using gain- and loss-of-function approaches. Membrane Fractionation was performed by using Mem-PER Plus Membrane Protein Extraction Kit (Thermofisher 89842). Nuclear and cytoplasmic extraction was performed with the NE-PER Nuclear and Cytoplasmic Extraction Reagents Kit (Thermofisher 78833). Pp2a activity was measured using an immunoprecipitation-based method (Millipore 17-313). Q-RTPCR, immunofluorescence and western blot were performed as previously described[24]. Primers are available upon request.

Deep-sequencing. RNA quality was analysed using a Bioanalyser (Agilent). Libraries were constructed and sequenced on an illumina Hiseq 2000 by the Beckman Coulter Genomics and Genewiz companies. ChIP-seq experiments were performed as previously described[31]. For ChIP-seq analysis, BWA was used for alignment of data to the mm9 genome with de-duplication performed using Picard tools, followed by peak calling using macs2 with narrow peak settings. To compare between control and netrin-1 conditions, homer annotatePeaks.pl was used with size = 2000, hist = 10 and –ghist used to generate read enrichments from both the control and netrin-1 sample using the control macs2 peaks. Data was then plotted in R using custom scripts. For analysis of RRBS data, UCSC liftOver was used to convert co-ordinates from mm10 to mm9 and the two replicates for control and netrin-1 samples were averaged at matching CpGs. For comparison to 2i conditions, WGBS data from GSM1027572 was used. Control, netrin-1 and 2i data were then merged so that only matched CpGs with coverage of at least 5X (for control and netrin-1) and 1X (2i) were used. Violin plots were generated in R using the library 'Vioplot' V0.2 and heatmaps were made using custom scripts in R. BedTools V2.25.0 was used to intersect CpGs with the following genomic features: high CpG promoters (HCP), CpG islands (CGI), low CpG promoters (LCP), CGI shores, exons, introns, long interspersed nuclear elements[53],

short interspersed nuclear elements (SINE), long terminal repeats and intracisternal A-particle elements, with all annotation downloaded from UCSC with the exception of CGI and LCP/HCP which were computationally assigned. For any CpGs located within these features, mean methylation was calculated and plotted in R. NGS data are deposited on GEO (record number series GSE102831, secure token for reviewers access ybgpggqmxfublid).

Hierarchical clustering. Control and netrin-1 mESCs datasets were processed as follows. The "primary assembly" Mus musculus genome sequence (release GRCm38.p5) and transcriptome annotations (Ensembl release 87) were downloaded from the GENCODE website. Raw read data (fastq files) were mapped to these sequences using STAR (with parameters --outFilterType BySJout, --outSAMtype BAM Unsorted, and --quantMode GeneCounts). This last parameter allows direct conversion of the mappings into gene counts. These gene counts were transformed into FPKM and combined with the table provided by ref. 7. Only gene names present in both datasets were kept. The following process was applied: 1. keep genes with at least an average FPKM of 10 in at least one cell type (resulting in, as reported, 9639 genes); 2. normalize between datasets by subtracting, for each gene, the average log2 (FPKM + 1) in each dataset from this gene log2 (FPKM + 1) in the corresponding samples (geometric mean); 3. compute a dissimilarity matrix between samples by using the 1 – Spearman correlation between samples; 4. generate a hierarchical clustering using the "average" agglomeration method.

FACS. Analysis was performed on a BD LSRFortessa. Sorting was performed on a BD FACSDiVa. Cells were sorted, washed immediately and centrifuged before being plated directly in fresh medium or frozen for RNA extraction and gene expression analysis.

Quantifications and Statistics. Western blot quantifications were performed with ImageJ. Statistical analyses of mean and variance were performed with Prism 6 (GraphPad Software) and Student's t-test or Wilcoxon tests when indicated.

Figures:

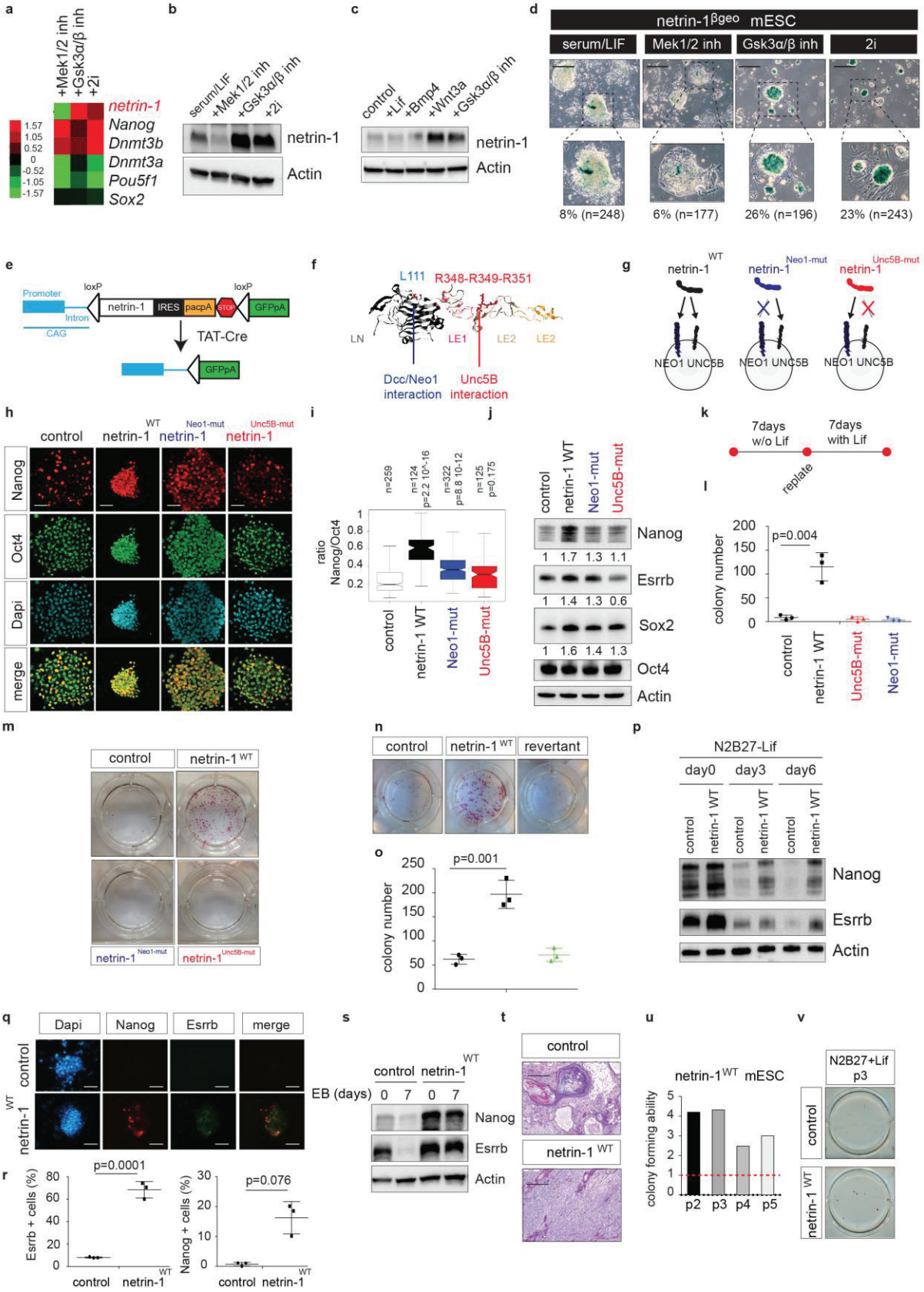
a
+Mek1/2 inh
+Gsk3α/β inh
+2i
netrin-1
Nanog
Dnmt3b
Dnmt3a
Pou5f1
Sox2
1.57
1.05
0.52
0
-0.52
-1.05
-1.57
b
serum/LIF
+Mek1/2 inh
+Gsk3α/β inh
+2i
netrin-1
Actin
c
control
+Lif
+Bmp4
+Wnt3a
+Gsk3α/β inh
netrin-1
Actin
d
netrin-1βgeo mESC
serum/LIF
Mek1/2 inh
Gsk3α/β inh
2i
8% (n=248)
6% (n=177)
26% (n=196)
23% (n=243)
e
Promoter
loxP
netrin-1
IRES
pacpA
loxP
GFPpA
Intron
CAG
TAT-Cre
GFPpA
f
L111
R348-R349-R351
LN
LE1
LE2
LE2
Dcc/Neo1 interaction
Unc5B interaction
g
WT
netrin-1
Neo1-mut
netrin-1
Unc5B-mut
netrin-1
NEO1 UNC5B
NEO1 UNC5B
NEO1 UNC5B
h
control
WT
netrin-1
Neo1-mut
netrin-1
Unc5B-mut
netrin-1
Nanog
Oct4
Dapi
merge
i
n=259
n=124
p=2.2 10^-16
n=322
p=8.8 10-12
n=125
p=0.175
ratio Nanog/Oct4
1
0.8
0.6
0.4
0.2
control
netrin-1 WT
Neo1-mut
Unc5B-mut
j
control
netrin-1 WT
Neo1-mut
Unc5B-mut
Nanog
1 1.7 1.3 1.1
Esrrb
1 1.4 1.3 0.6
Sox2
1 1.6 1.4 1.3
Oct4
Actin
k
7days w/o Lif
7days with Lif
replate
l
colony number
200
150
100
50
0
p=0.004
control
netrin-1 WT
Unc5B-mut
Neo1-mut
m
control
netrin-1 WT
netrin-1 Neo1-mut
netrin-1 Unc5B-mut
n
control
netrin-1 WT
revertant
o
colony number
250
200
150
100
50
0
p=0.001
p
N2B27-Lif
day0
day3
day6
control
netrin-1 WT
control
netrin-1 WT
control
netrin-1 WT
Nanog
Esrrb
Actin
q
Dapi
Nanog
Esrrb
merge
control
WT netrin-1
r
Esrrb + cells (%)
80
60
40
20
0
p=0.0001
control
netrin-1 WT
Nanog + cells (%)
30
20
10
0
p=0.076
control
netrin-1 WT
s
control
netrin-1 WT
EB (days)
0
7
0
7
Nanog
Esrrb
Actin
t
control
netrin-1 WT
u
netrin-1 WT mESC
colony forming ability
5
4
3
2
1
0
p2
p3
p4
p5
v
N2B27+Lif
p3
control
netrin-1 WT

Figure 1. netrin-1 signalling controls pluripotency features. (a) Dendogram depicting *netrin-1* and pluripotency transcript level in serum/Lif mESCs supplemented with Mek1/2-inh, Gsk3α/β-inh or both (2i) for 48 hours. Data are log2 FPKM values normalized to serum/Lif mESCs. (b) Western blot showing netrin-1 level in similar settings. 3 independent experiments gave similar results. (c) Western blot for netrin-1 level in mESCs grown in serum treated for 24 hours with the indicated molecules. 3 independent experiments gave similar results. (d) Representative brightfield pictures of *netrin-1 βgeo* mESCs grown in serum/Lif or with inhibitors for 48h. Bars, 250µm. Percentages of positive cells are indicated. n= total number of cells counted. (e) Schematic of the transgenic approach to express netrin-1 in mESCs. TAT-cre treatment excises netrin-1 transgene and turns on GFP expression. (f) netrin-1 protein structure depicting residues critical for the interaction with Unc5B and Dcc/Neo1. LN: Laminin-like domain; LE: EGF repeats. (g) Representation of the different netrin-1 mESC models. netrin-$1^{Neo1\text{-}mut}$ express a netrin-1 version carrying the L111E mutation while netrin-$1^{Unc5B\text{-}mut}$ express a netrin-1 version carrying R348A-R349A-R351A mutations. (h) Immunofluorescence for Nanog and Oct4 in control, netrin-1^{WT}, netrin-$1^{Neo1\text{-}mut}$ and netrin-$1^{Unc5B\text{-}mut}$ mESCs grown in serum/Lif. Bars: 50 µm. (i) Quantification of the Nanog/Oct4 ratio intensity in single cells of the different populations. n corresponds to the number of cells. The line that divides the box into 2 parts represents the median of the data. The end of the box shows the upper and lower quartiles. The extreme lines show the highest and lowest value excluding outliers. T-test was used, two-tailed p-value is indicated. (j) Western blot of pluripotent factors level in cell lines from (g). 3 independent experiments gave similar results. (k) Scheme depicting exit from pluripotency assays. Cells were plated at clonal density (60-100 cells/cm^2), grown for 7 days without Lif, split and replated at clonal density for 6 additional days, before scoring AP+ colonies. (l) Colony counting. Data are the mean ± s.d. (n=3 independent experiments). Student's t-test was used. Two-tailed p-value is indicated. (m) Pictures of a single experiment representative of three independent ones. Colonies were stained for alkaline phosphatase (AP) activity. (n) Pictures of a single experiment representative of two independent ones performed with netrin-1 revertant mESCs. Similar settings as (k). (o) Colony countings. Data are the mean ± s.d. (n=3 independent experiments). Student's t-test was used, two-tailed p-value is indicated. (p) Western blot for Nanog and Esrrb during N2B27-Lif differentiation of control and netrin-1^{WT} mESCs. 3 independent experiments gave similar results. (q-r) Nanog and Esrrb immunofluorescence after 6 days in N2B27-Lif. (q) Representative pictures. Bars: 50 µm. (r) Countings of Nanog and Esrrb positive cells. Data are the mean ± s.d. (n=3 independent experiments) of Nanog and Esrrb positive cells. Student's t-test was used, two-tailed p-values are indicated. 488 control and 416 netrin-1^{WT} mESCs were counted. (s) Embryoid body formation. Western blot on control and netrin-1^{WT} mESCs at day0 and day7 of EB formation. 3 independent experiments gave similar results. (t) Teratoma formation. Picture depicts histological analysis of teratomas derived from control and netrin-1^{WT} mESCs. Bars = 0,2mm. 4 independent teratoma were analysed per cell line. (u-v) Long-term self-renewal assays. (u) Colony counting. After each passage, cells were plated at clonal density in serum/Lif and AP colonies scored. Value 1 is given to the number of colonies formed by control cells, for each passage (red dotted line). (v) Pictures of a single

experiment representative of two independent ones. Colonies were stained for alkaline phosphatase (AP) activity.

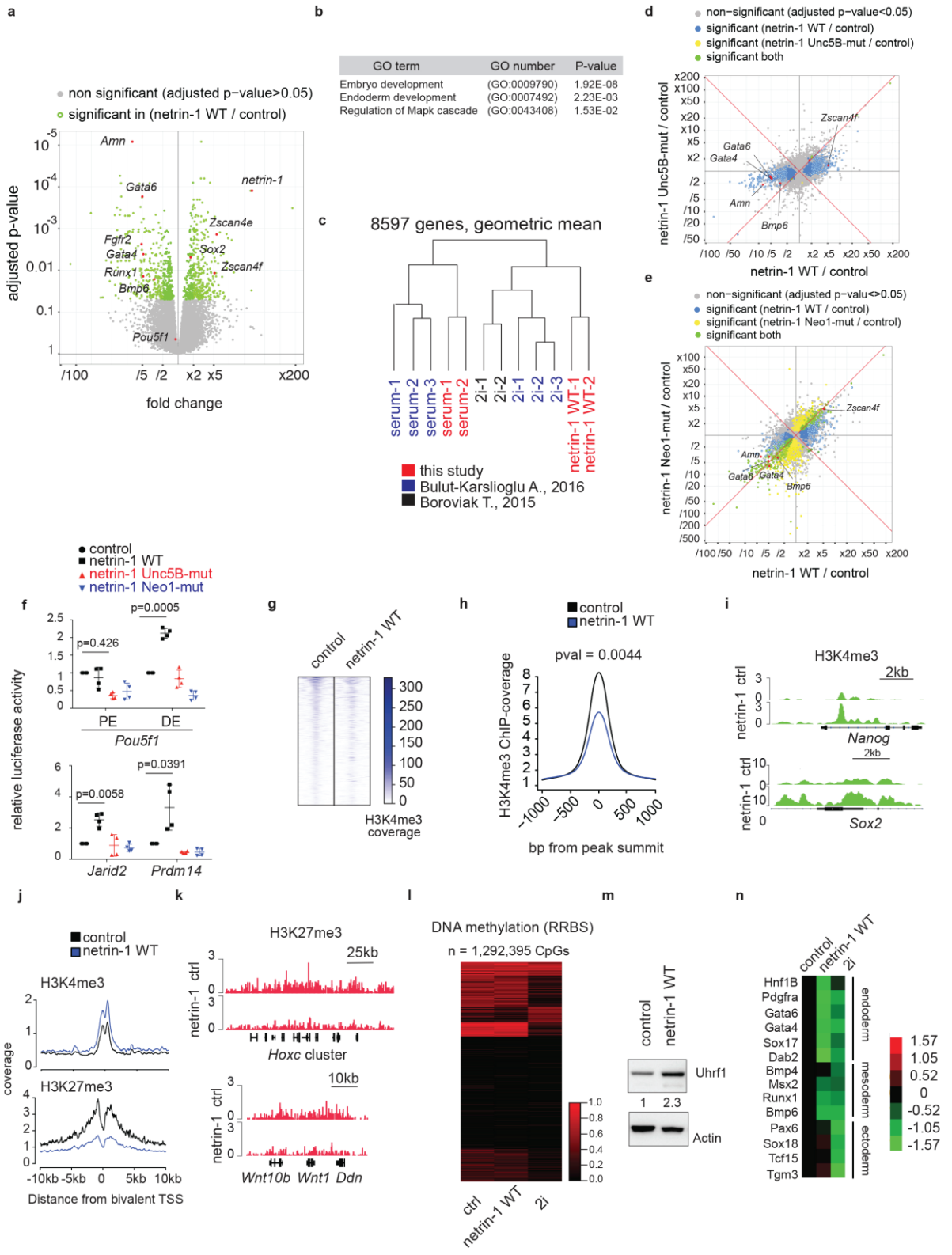

Figure 2. netrin-1 signalling triggers transcriptomic and epigenetic changes in mESCs. (a) Volcano plot comparing the transcriptomes of control and netrin-1^{WT} mESCs. Each dot corresponds to a transcript. n=3 independent samples. Benjamini-Hochberg adjusted p-values of the comparisons were computed using the limma-voom workflow. (b) Statistical overrepresentation analysis. The Panther DB tool was used to detect overrepresented GO within the genes differentially expressed in control and netrin-1^{WT} mESCs. A Fisher's exact two-sided test

was used to calculate p-values. (c) Hierarchical clustering of control and netrin-1^{WT} transcriptomes with serum/Lif and 2i mESCs published datasets. Datasets from Bulut-karslioglu. et al., 2016, are used (see methods for details). (d-e) Plot comparing netrin-1^{WT} and netrin-$1^{Unc5B\text{-}mut}$ (d) or netrin-$1^{Neo1\text{-}mut}$ (e) effects on mESCs transcriptome. Each dot corresponds to a transcript. n=3 independent samples. Benjamini-Hochberg adjusted p-values of the comparisons were computed using the limma-voom workflow. (f) Specific enhancer activity characterizes netrin-1^{WT} mESCs. Luciferase data are normalized to Renilla activity and expressed as the mean ± s.d. (n=4 independent experiments). Student's t-test was used and 2-sided p-values are indicated. (g-k) H3K4Me3 and H3K27Me3 distribution in control and netrin-1^{WT} mESCs. Data representative of 2 independent experiments. (g) Heatmap displaying the H3K4me3 ChIP read enrichment for control and netrin-1^{WT} mESCs for regions defined as H3K4me3 peaks in control cells. For every peak, the summit (at 0) +/- 1000 bp is shown. Only peaks with q-value < 0.01 and mean enrichment for the region in the top third quantile are displayed (*n* = 11,131). The read enrichment is described by the color key to the right. Peaks were called using MACS2, which uses a Poisson test and the Benjamini-Hochberg model to derive q-values. (h) For all significant (qvalue < 0.01) H3K4me3 peaks in control cells (*n* = 44,486), the H3K4me3 ChIP read enrichment is displayed for control and netrin-1^{WT} mESCs. (p= 0.0044; t.test). q-values were derived from MACS2. (i) Representative browser shots of H3K4me3 enrichment at *Nanog* and *Sox2* loci. (j) H3K4Me3 and H3K27Me3 enrichment at bivalent domains in control and netrin-1^{WT} mESCs. (k) Representative browser shots of H3K27me3 enrichment at bivalent loci. (l) Heatmap displays methylation levels for 1.3M matched CpGs in control, netrin-1^{WT} mESCs grown in serum/Lif and 2i mESCs. Each horizontal line is one CpG. n=2 independent experiments. (m) Western blot for Uhrf1 in indicated mESCs grown in serum/Lif. 3 independent experiments gave similar results. (n) Differentiation-related genes expression in control, 2i and netrin-1^{WT} mESCs. Dendogram presents RNA-seq data. FPKM values are normalised to control mESCs and presented as Log2 values. Color scale is provided.

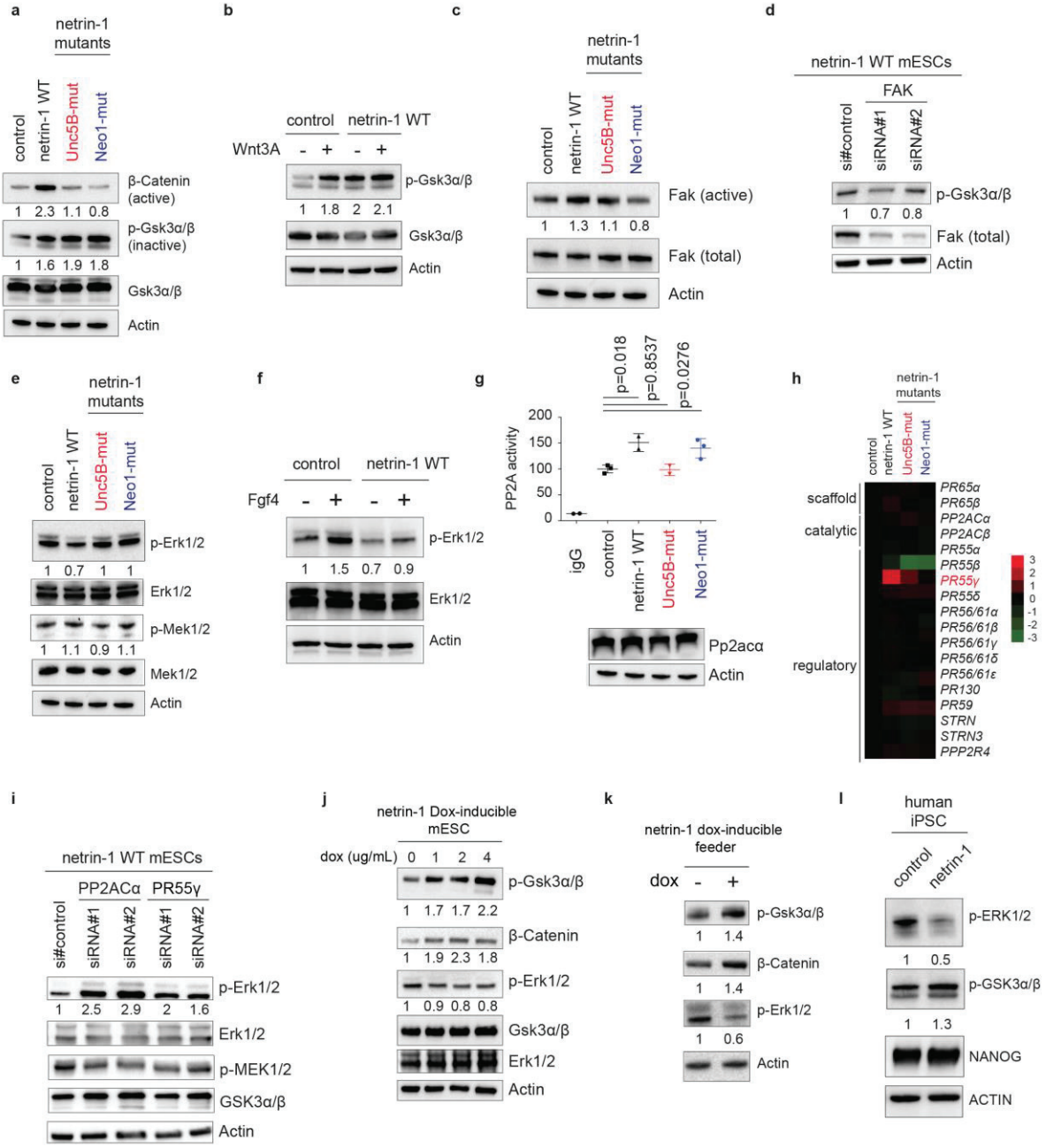

Figure 3: netrin-1 regulates Gsk3α/β and Erk1/2 activities in mouse and human pluripotent stem cells. (a) Effect of netrin-1 signalling on the Wnt pathway. Western blot of Wnt pathway members levels in control and netrin-1 expressing (WT or mutant) mESCs grown in serum/Lif. 3 independent experiments gave similar results. (b) Effect of netrin-1 signalling on Wnt3a sensitivity. Control and netrin-1^{WT} mESCs serum starved ON and

stimulated with recombinant Wnt3a for 6 hours prior to samples collection. 3 independent experiments gave similar results. (c) Effect of netrin-1 signalling on Fak kinase. Western blot of phospho- (active) and total Fak levels in control and netrin-1^{WT} mESCs. 3 independent experiments gave similar results. (d) Fak silencing rescues Wnt activity in netrin-1^{WT} mESCs. Western blot of netrin-1^{WT} mESCs transfected with control siRNA or 2 independent siRNA targeting Fak. 3 independent experiments gave similar results. (e) Effect of netrin-1 signalling on Mapk status. Western blot of Mapk members levels in control and netrin-1 expressing (WT or mutant) mESCs grown in serum/Lif. 3 independent experiments gave similar results. (f) Effect of netrin-1 on Fgf4 sensitivity. Control and netrin-1^{WT} mESCs were serum starved ON and stimulated with recombinant Fgf4 for 20 mins prior to samples collection. 3 independent experiments gave similar results. (g) Modulation of Pp2a activity by netrin-1 signalling in mESCs. Top panel - The phosphatase activity of the complex is assessed in control and netrin-1 expressing mESCs following immunoprecipitation of Pp2acα (or control IgG). Data are the mean ± s.d. (n=3 independent experiments). T-test was used and two-sided p-values are indicated. Bottom panel - western blot depicts Pp2acα levels in the corresponding mESC populations. 3 independent experiments gave similar results. (h) Dendogram depicting *Pp2a* subunits transcript level in control and netrin-1^{WT} mESCs. The raw FPKM data are normalized to control mESCs and presented as log2. n=3 independent samples. (i) Pp2a subunits silencing rescue p-Erk1/2 levels in netrin-1^{WT} mESCs. Western blot of p-Erk1/2 levels in netrin-1^{WT} mESCs transfected with control siRNA or 2 independent siRNA targeting *Pp2acα* or *PR55γ*. 3 independent experiments gave similar results. (j) Western blot depicting Wnt and Mapk activation levels in netrin-1 dox-inducible mESCs. Dox is added at the indicated concentrations for 48 hrs. 3 independent experiments gave similar results. (k) Netrin-1-expressing feeder triggers similar signalling changes in mESCs. The irradiated feeder was plated and treated or not with dox for 24 hours at 2µg/mL. The next day, mESCs were plated on those feeders and grown for 3 days before collection for WB. 3 independent experiments gave similar results. (l) Netrin-1 signalling function in human pluripotent stem cells. Western blot of Wnt and Mapk members in control and netrin-1^{WT} human iPS cells. 3 independent experiments gave similar results.

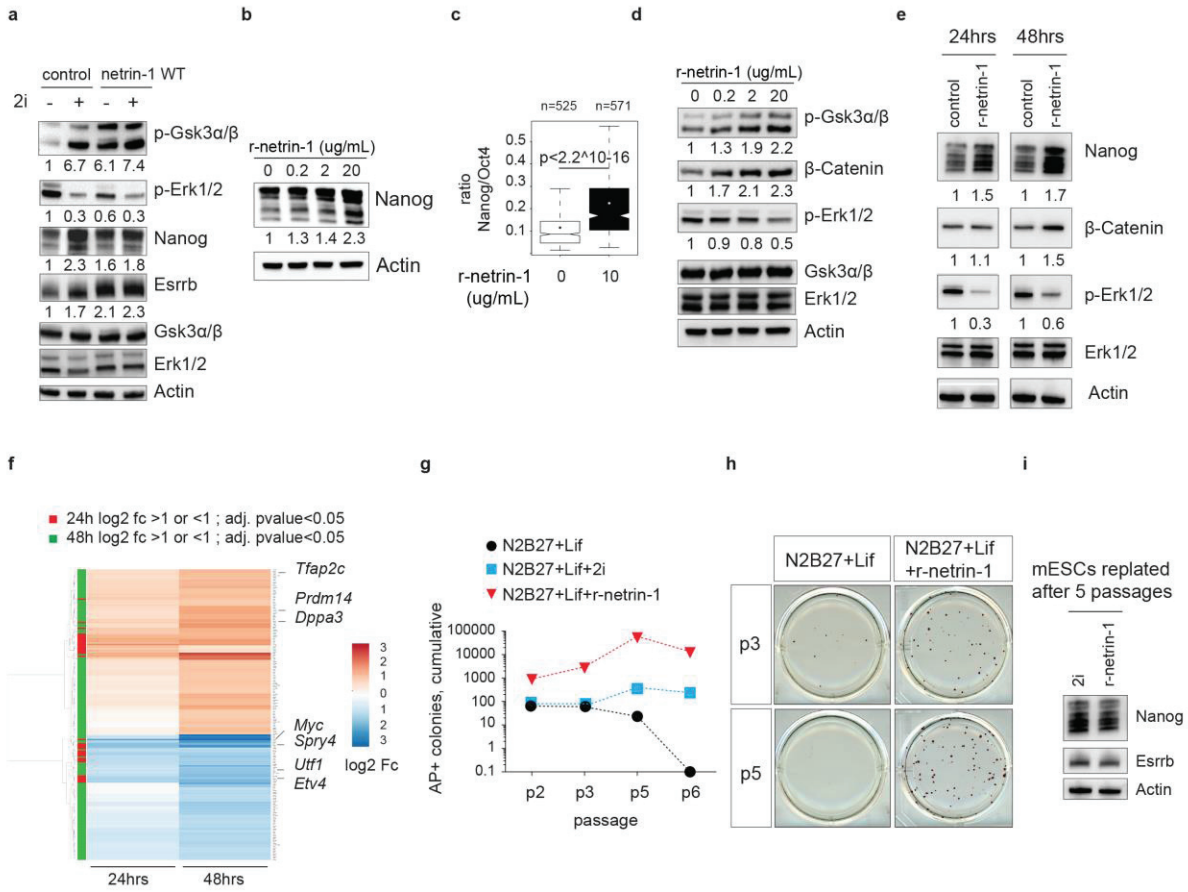

Figure 4: Recombinant netrin-1 supports mESC self-renewal in combination with LIF. (a) Western blot comparing signalling and pluripotency changes induced by netrin-1 and 2i. Control and netrin-1^{WT} mESCs are grown in serum/Lif and treated with 2i for 2 days. 3 independent experiments gave similar results. (b) Western blot depicts Nanog levels in response to increasing doses of r-netrin-1. Cells are treated with indicated concentrations for 48 hrs. 3 independent experiments gave similar results. (c) Quantification of the Nanog/Oct4 ratio intensity in single cells of the different populations. n corresponds to the number of cells. The line that divides the box into 2 parts represents the median of the data. The end of the box shows the upper and lower quartiles. The extreme lines show the highest and lowest value excluding outliers. T-test was used, two-tailed p-value is indicated. (d) Western blot for Wnt and Mapk members in similar settings as (b). Similar results were obtained from 3 independent experiments. (e) Western blot of pluripotency and signalling changes occurring after 24 and 48 hrs of r-netrin-1 treatment at 20µg/mL. 3 independent experiments gave similar results. (f) Heatmap presenting differentially expressed genes. RNA-seq is performed on mESCs treated or not with r-netrin-1. n=4 independent samples. A two-sided wald test was used for p-value calculation and a two-sided Benjamini-Hochberg for adjustement. (g) Self-renewal assays. E14Tg2a mESCs are maintained for 6 passages in the indicated conditions. After splitting at p2, 3, 5 and 6, cells are counted and similar numbers are plated at clonal density in serum/Lif for 7 days and the number of AP+ colonies counted to evaluate the self-renewal potential of the cells. Data present a single experiment representative of 2 independent ones. (h)

Pictures presenting the self-renewal abilities of mESCs grown in the indicated conditions for 3 and 5 passages. Similar results were obtained from 3 independent experiments. (i) Western blot of pluripotency factors. mESCs grown in N2B27+Lif+2i or N2B27+Lif+r-netrin-1 for 5 passages (15 days) are grown in serum/Lif for 7 days before collection. 3 independent experiments gave similar results.

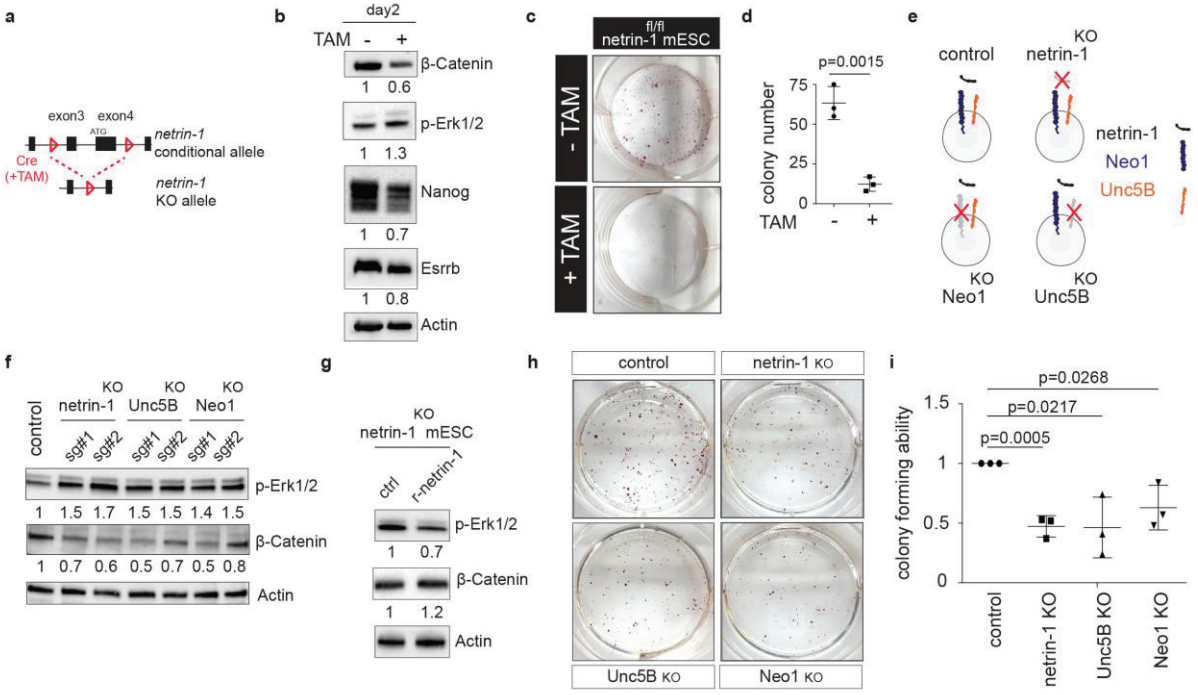

Figure 5: Endogenous netrin-1 controls pluripotency. (a) Schematic of the *netrin-1* conditional allele. KO, knockout. (b) Western blot for Wnt and Mapk members in netrin-1$^{fl/fl}$ mESCs treated ON or not with tamoxifen (TAM) in N2B27+Lif for 48 hrs before collection. 3 independent experiments gave similar results. (c) Colony formation assays. Similar results were obtained from 3 independent experiments. (d) Colony countings. Data are expressed as the mean ± s.d. (n=3 independent experiments). T-test was used and two-sided p-value is indicated. (e) Scheme depicting the netrin-1^{KO}, Neo1^{KO}, Unc5B^{KO} mESCs generated by crispr/cas9. (f) Effect of netrin-1, Neo1 and Unc5B depletion on Wnt and Mapk pathways by western blot. 3 independent experiments gave similar results. (g) Western blot for Wnt and Mapk members. Netrin-1^{KO} mESCs were treated for 48hrs with r-netrin-1 (20µg/mL) before collection. 3 independent experiments gave similar results. (h-i) Effect of ligand/receptors depletion on mESC self-renewal ability. Cell lines from (e) were subjected to colony formation assay. (h) Brightfield pictures of a single experiment representative of three independent ones. (i) Colony counting. Data are the mean ± s.d. (n=3 independent experiments). Student's t-test was used and two-sided p-values are indicated.

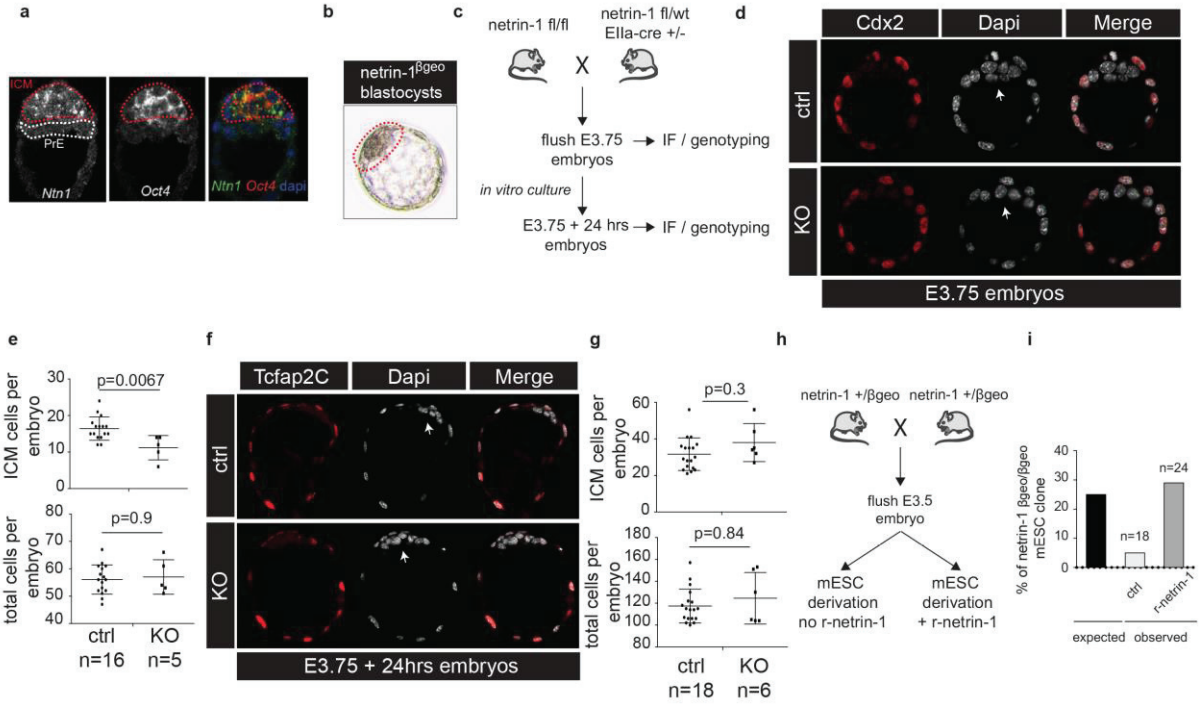

Figure 6: Netrin-1 regulates cell fate allocation in pre-implantating embryos. (a) *Netrin-1/Oct4 in situ* hybridization on E4.5 embryo. n=17 E4.5-E4.75 embryos from 3 independent experiments. (b) X-gal activity in blastocyst-stage embryos. netrin-1-*βgeo* reporter embryos were flushed at E3.5 and grown *in vitro* for 24 hrs before fixation. n=9 embryos from 3 independent experiments. (c) Scheme depicting the intercrosses. (d) Picture of control and netrin-1 KO E3.75 embryos. Immunofluorescence for Cdx2 marks trophectoderm cells. Arrows indicate ICM cells. n=4 independent experiments. (e) Countings. The graph depicts the average number of ICM cells per embryo and sd: ((Dapi+ cells) - (Cdx2+ cells)). n=number of embryos analysed. Ctrl: netrin-1+/+ and netrin-1+/- embryos. KO: netrin-1-/- embryos. The p-values of a two-sided non-parametrical wilcoxon test are indicated. (f) Picture of control and netrin-1 KO E3.75 embryos grown for 24 additional hours *in vitro*. Immunofluorescence for Tcfap2C marks trophectoderm cells. Arrows indicate epiblast cells. n=3 independent experiments. (g) Counting. The graph depicts the average number of ICM cells per embryo and sd: ((Dapi+ cells) - (Tcfap2c+ cells)). n=number of embryos analysed. Ctrl: netrin-1+/+ and netrin-1+/- embryos. KO: netrin-1-/- embryos. The p-values of a two-sided non parametrical wilcoxon test are indicated. (h) Scheme of the intercrosses. (i) Graph depicting the percentage of *netrin-1βgeo/βgeo* mESCs lines obtained from *netrin-1+/βgeo* heterozygous crosses. n=number of lines generated. Embryos were flushed at E3.5, grown on feeders in N2B27+Lif+2i for 3 days and then in serum/Lif. Netrin-1 status was evaluated by Western blot.

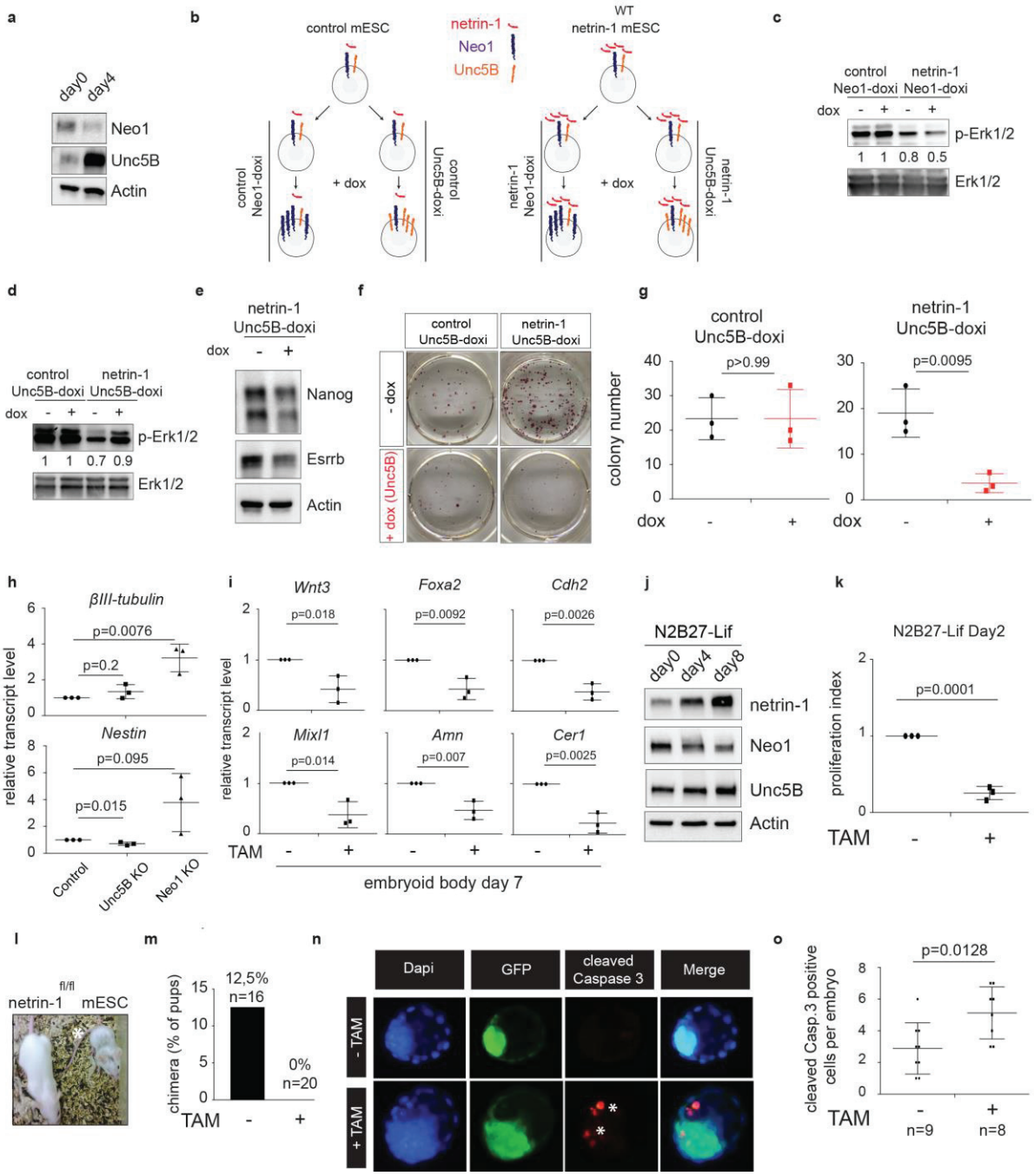

Figure 7: netrin-1 exerts different effects in mESCs depending on its receptors balance. (a) Western blot in mESCs and day4 EBs. 3 independent experiments gave similar results. (b) Schematic of the generation of control, control Neo1-doxi, netrin-1 Neo1-doxi, control Unc5B-doxi and netrin-1 Unc5B-doxi mESCs. (c) Neo1 exogenous expression reduces p-Erk1/2 in presence of netrin-1. 3 independent experiments gave similar results. (d) Unc5B exogenous expression induces p-Erk1/2 in presence of netrin-1. 3 independent experiments gave similar results. (e) Unc5B exogenous expression reduces pluripotency factor level in presence of netrin-1. 3 independent experiments gave similar results. (f-g) Unc5B reduces resistance to differentiation in presence of high netrin-1 level. Exit from pluripotency assays are performed with control Unc5B-doxi and netrin-1 Unc5B-doxi mESCs treated or not with doxycycline. (f) Representative pictures of a single experiment

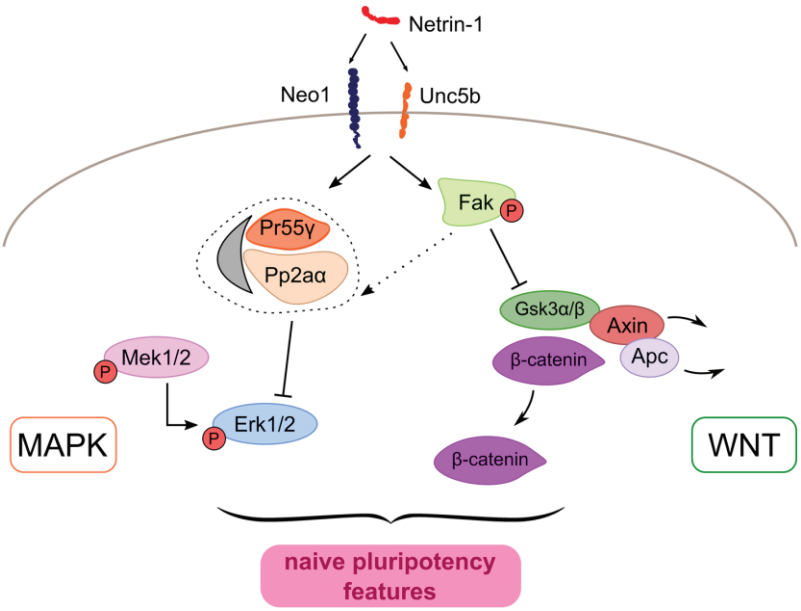

representative of three independent ones. (g) Colony counting. Data are the mean ± s.d. (n=3 independent experiments). Student's t-test was used and two-sided p-values are indicated. (h) Q-RTPCR depicts *Nestin* and *βIII-tubulin* levels at day 8 of differentiation in N2B27-Lif. Data are normalized to housekeeping genes and value 1 is given to day8 Ctrl mESCs. Data are the mean ± s.d. (n=3 independent experiments). Student's T test was used and two-sided p-values are indicated. (i) Q-RTPCR depicts *Wnt3a, Mixl1*, *Foxa2*, *Amn*, *Cdh2* and *Cer1* transcript level in day7 EBs generated with netrin-$1^{fl/fl}$ mESCs treated or not with TAM. Data are the mean ± s.d. (n=3 independent experiments) and value 1 is given to -TAM mESCs. Student's T test was used and two-sided p-values are indicated. (j) Netrin-1, Unc5b and Neo1 expression during neural differentiation. 3 independent experiments gave similar results. (k) Netrin-1 depletion triggers a proliferation defect during differentiation. The netrin-$1^{fl/fl}$ mESCs, treated or not with TAM, are grown for 2 days in N2B27-Lif and cell number counted. Data are the mean ± s.d. (n=3 independent experiments). Two-sided p-values of a student's t-test are indicated. (l-m) netrin-1 depletion impairs mESCs developmental potential. Blastocyst injections were performed with netrin-$1^{fl/fl}$ mESCs treated or not with TAM prior to injection. (l) Example of color-coated chimera obtained following injection of netrin-$1^{fl/fl}$ mESCs. (m) Percentage of chimera obtained are shown, n=number of live pups obtained. (n) Picture of representative embryos immunostained for GFP and cleaved Caspase 3. Morulas are aggregated with 5-10 netrin-$1^{fl/fl}$ mESCs treated or not with TAM and blastocysts fixed 36hrs post-aggregation. Asterisks mark apoptotic cells. 3 independent experiments gave similar results. (o) Countings. Cleaved Caspase 3 positive cells are scored. Data are the mean ± s.d. (3 independent experiments). n=number of embryos analysed. T-test was used and two-sided p-values are indicated.

Figure 8: Graphical summary of the results. The binding of netrin-1 to its receptors Neo1 and Unc5B modifies the composition and the activity of the Pp2a complex with a strong induction of the regulatory PR55γ subunit,

leading to Erk1/2 dephosphorylation and Mapk signalling attenuation. Activated Fak kinase triggers Gsk3α/β inactivation by phosphorylation, leading to β-Catenin stabilization and Wnt signalling promotion. The combined promotion of Wnt and alleviation of Mapk triggers the acquisition of naive pluripotency features partially overlapping with the ground state.

Supplementary information:

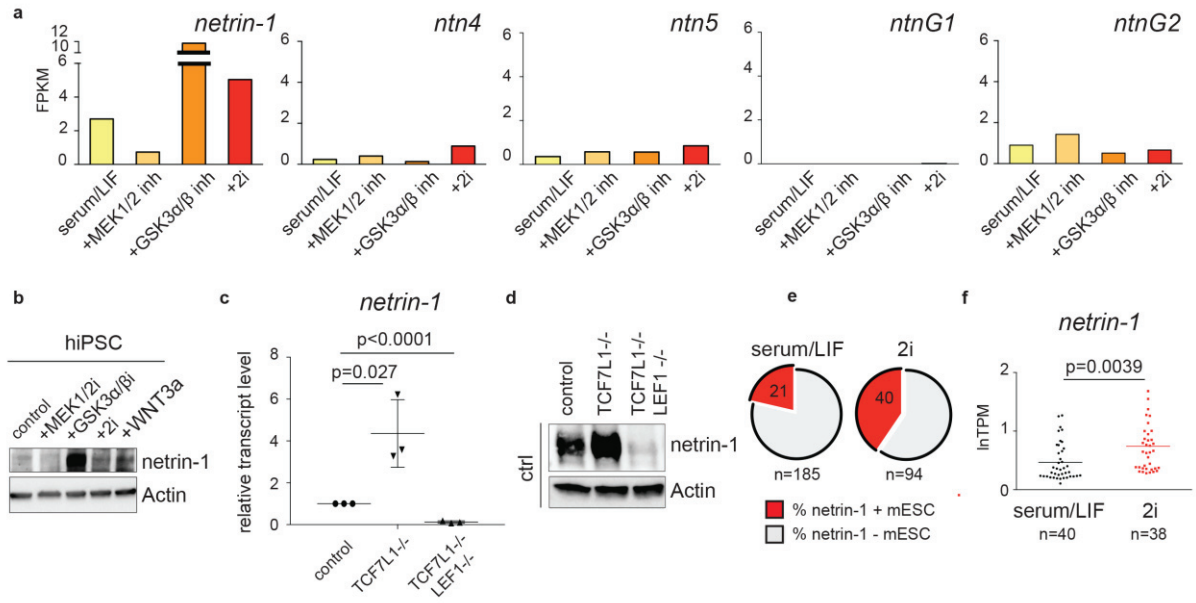

Supplementary Figure 1. netrin-1 is expressed in naive pluripotent cells *in vitro.* (a) Data present FPKM values for *netrin-1*, *Ntn4*, *Ntn5*, *NtnG1* and *NtnG2* in serum/Lif mESCs treated or not with Mek1/2-inh (PD), Gsk3α/β-inh (CHIR) or both (2i). (b) Western blot depicting netrin-1 levels in human iPS cells treated similarly as (a). 3 independent experiments gave similar results. (c) *Netrin-1* and *Oct4* transcripts level in indicated mESCs. Q-RTPCR data are expressed relative to mESCs as the mean ± s.d. (n=3 independent experiments). Student's t-test was used and two-tailed p-values are indicated. (d) Netrin-1 western blot in indicated mESCs. 3 independent experiments gave similar results. (e) *Netrin-1* expression in single mESCs in Serum/Lif and 2i. Single-cell transcriptomic data are extracted from Kumar et al., 2014. n=number of cells analysed in each condition. (f) *Netrin-1* mean expression in single mESCs. Data are extracted from Kumar et al., 2014 n=number of cells analysed in each condition. The bar represents the mean ± s.d. of *netrin-1* expression in the 2 conditions. Student t-test was used and two-sided p-value is indicated.

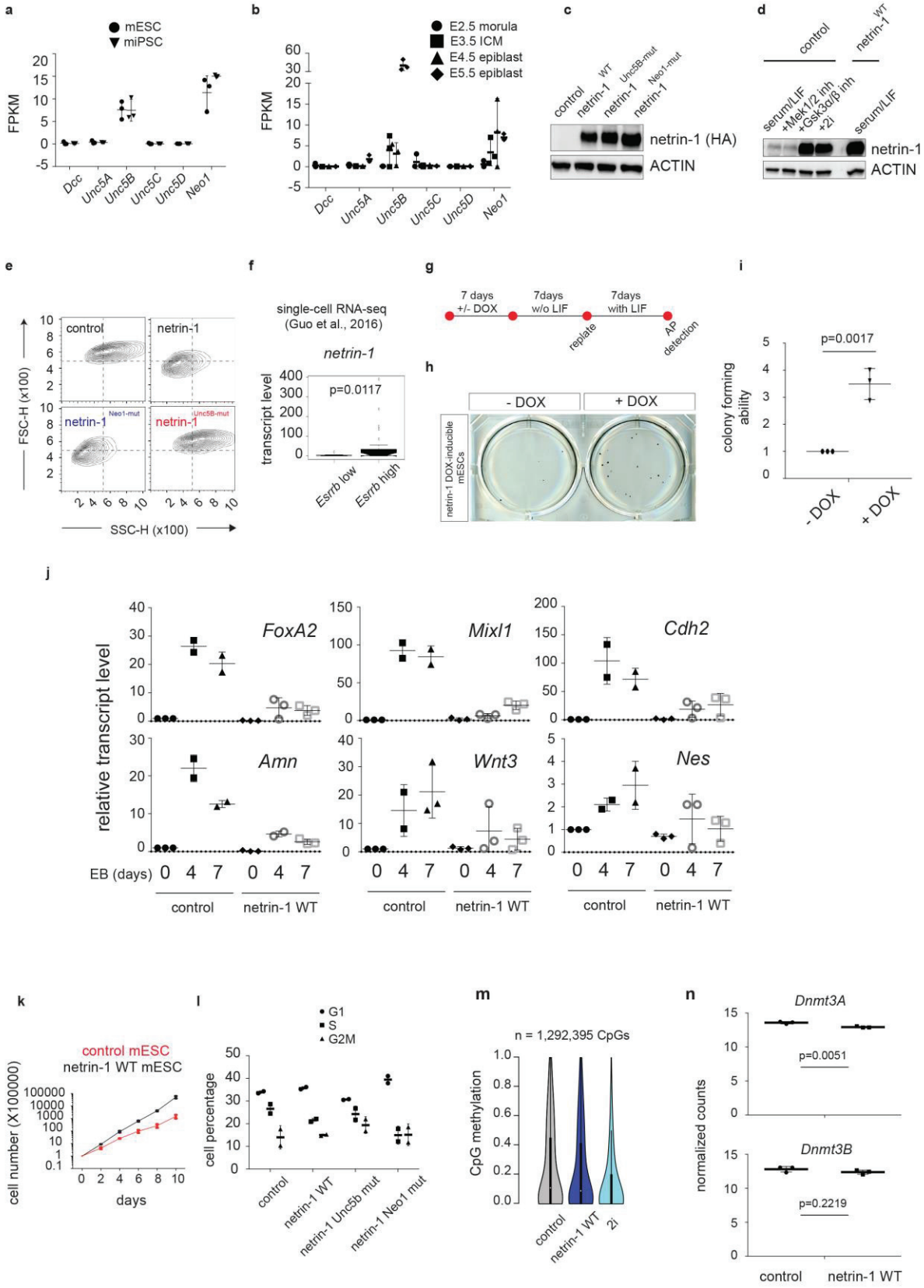

Supplementary Figure 2. netrin-1 triggers pluripotency features partially overlapping with the ground state. (a) Graph of netrin-1 receptors transcript levels in mouse ES and iPS cells. RNA-seq data are presented as FPKM values and expressed as the mean ± s.d. (n=3 independent experiments). (b) netrin-1 receptors expression

during early mouse development. Data, extracted from Boroviak. et al., 2015, present transcripts level in FPKM. Data are presented as the mean ± s.d. (n=3 independent experiments). (c) Western blot depicts exogenous netrin-1 (HA) levels in control, netrin-1^{WT}, netrin-$1^{Unc5B\text{-}mut}$ and netrin-$1^{Neo1\text{-}mut}$ mESCs. 3 independent experiments gave similar results. (d) Western blot depicts netrin-1 levels in control mESCs supplemented with Mek1/2-inh, Gsk3α/β-inh or 2i alongside netrin-1^{WT} mESCs grown in serum/LIF. 3 independent experiments gave similar results. (e) FACS analysis (FSC/SSC) of the different populations grown in serum/Lif. 3 independent experiments gave similar results. (f) netrin-1 expression in ES cells subpopulations. Data are extracted from Guo et al. 2016. *Esrrb* expression is used to distinguish quartiles of $Esrrb^{high}$ (>Q1) and $Esrrb^{low}$ (<Q1) cells. netrin-1 expression is analysed in the corresponding quartile. 48 total cells were analysed, 12 cells for <Q1 and 36 cells for >Q1. Student's t-test was used and two-tailed p-value is indicated. (g) Scheme depicting exit from pluripotency assays. (h) Pictures of a single experiment representative of three independent ones. Cells were plated and induced with or without Dox for 7 days. They were then plated at clonal density (60-100 cells/cm^2), grown for 7 days without Lif and replating at similar density for 7 additional days, before scoring AP+ colonies. (i) Colony counting. Data are the mean ± s.d. (n=3 independent experiments). Student's t-test was used and two-sided p-values are indicated. (j) Q-RTPCR depicts mesoderm (*Wnt3a* and *Mixl1*), endoderm (*FoxA2* and *Amn*) and ectoderm (*Nes* and *Cdh2*) transcript level in mESCs and day4 and day7 EBs generated with control or netrin-1^{WT} mESCs. Data are the mean ± s.d. (n=3 independent experiments). (k) Control and netrin-1^{WT} mESCs proliferation curves. Data are the mean ± s.d. of 2 independent experiments. (l) Cell cycle features of control and netrin-1^{WT} mESCs. Data are the mean ± s.d. (n=2 independent experiments). (m) Violin plots displaying methylation levels for control, netrin-1^{WT} and 2i mESCs for 1.3M matched CpGs. Bold line indicates 25-75th percentile, white dot indicates median. (n) Dnmt3A and Dnmt3B expression levels in netrin-1^{WT} mESCs. Data are the mean ± s.d. (n=3 independent experiments) of normalized counts. Student's T test was used and two-sided p-values are indicated.

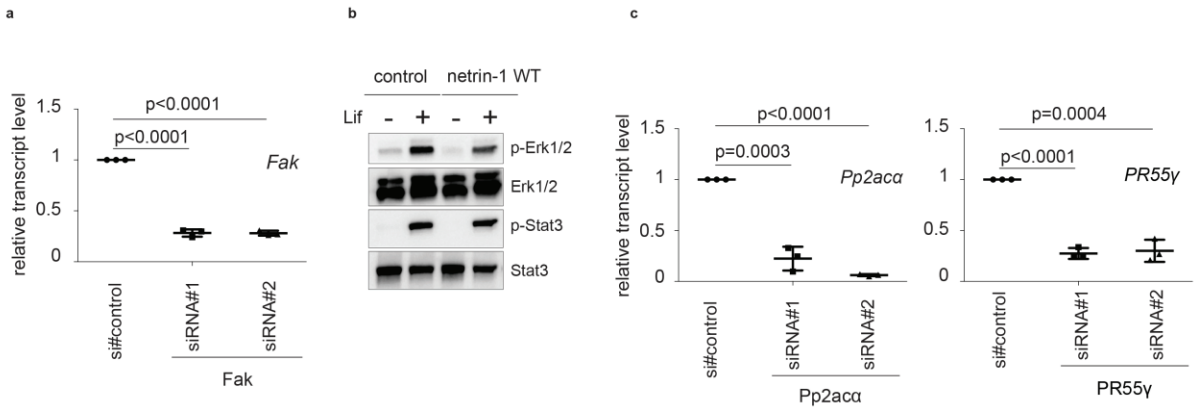

Supplementary Figure 3. Molecular cascade downstream of netrin-1 in mESCs. (a) Knockdown efficiency of Fak in mESCs. Q-RTPCR depicts *Fak* transcript level following transfection of netrin-1 mESCs with independent siRNA. Data, normalised to si#control mESCs, are the mean +/- sd of 3 independent experiments. Student T-test was used and two-sided p-values are indicated. (b) Effect of netrin-1 signalling on Lif sensitivity. Control and netrin-1^{WT} mESCs were serum starved ON and stimulated with Lif for 10 mins prior to samples collection. 3 independent experiments gave similar results. (c) Knockdown efficiency of Pp2acα and PR55γ in mESCs. Similar settings as (a).

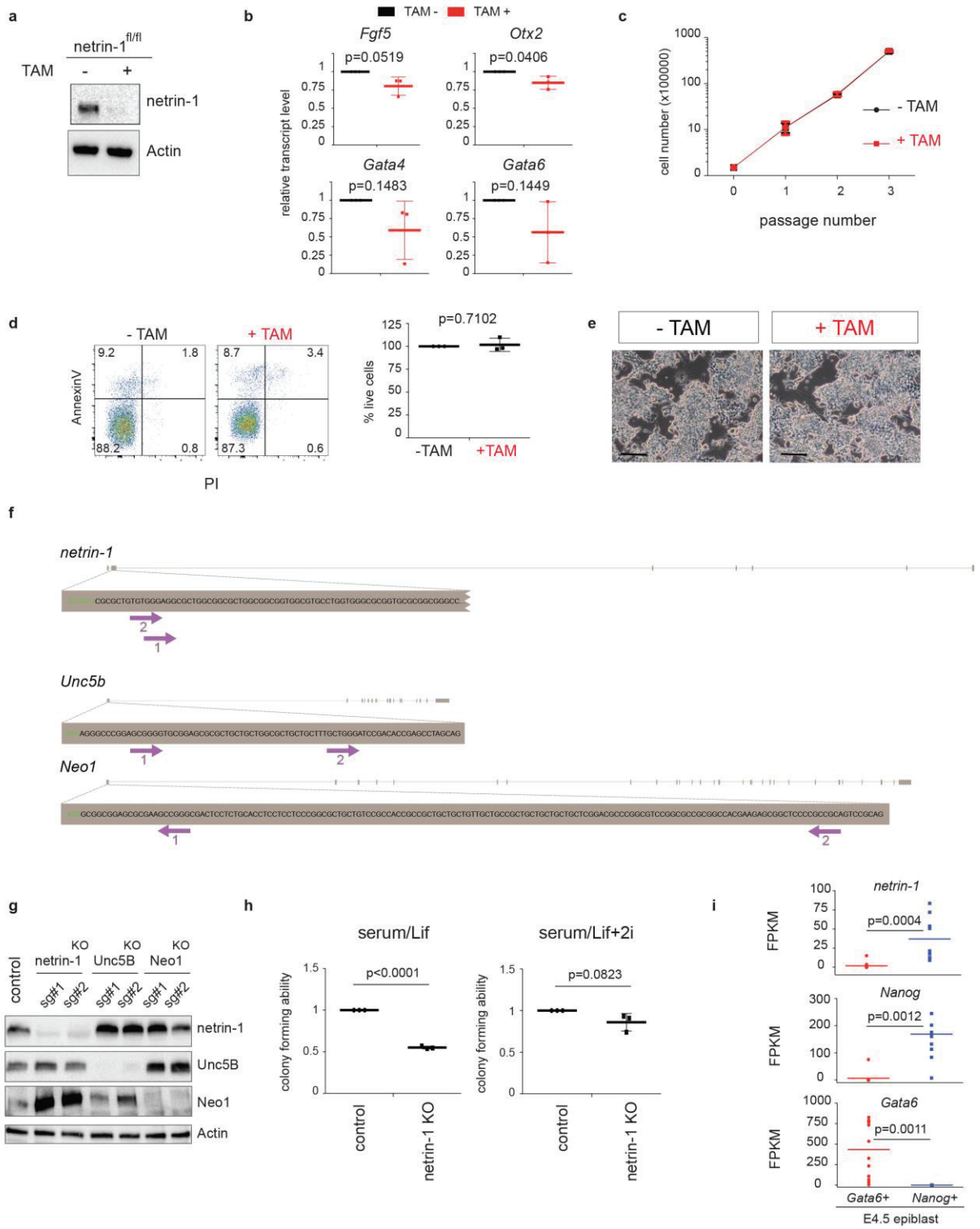

Supplementary Figure 4. Endogenous netrin-1 controls pluripotency features. (a) Western blot for netrin-1 in netrin-$1^{fl/fl}$ mESCs treated or not with 4'OH-tamoxifen (TAM) for 3 days before collection. 4 independent experiments gave similar results. (b) Effect of netrin-1 depletion on differentiation genes. Q-RTPCR depicts *Fgf5, Otx2, Gata4* and *Gata6* transcript level following netrin-1 depletion in mESCs. Data are the mean +/- sd of 3 independent experiments. Student T-test was used and two-sided p-values are indicated. (c) netrin-$1^{fl/fl}$ mESCs proliferation curves. The netrin-$1^{fl/fl}$ mESCs, treated or not with TAM, were counted at each passage in

serum/Lif. Data are the mean +/- sd of 3 independent experiments. (d) Cell death analysis. The netrin-$1^{fl/fl}$ mESCs, treated or not with TAM, were grown for 2 days in N2B27+Lif before PI-AnnexinV staining was performed. The left panel presents a representative FACS profile and the right panel a graph of mean data ± s.d. (n=3 independent experiments). Value 100% is given to the percentage of live cells in untreated netrin-$1^{fl/fl}$ mESCs. (e) Brightfiled pictures of netrin-$1^{fl/fl}$ mESCs treated or not with 4'OH-tamoxifen and subsequently maintained in culture for 22 passages. Bars: 50 µm. (f) Scheme depicting the position of the guides used to target netrin-1, Unc5B and Neo1 loci by crispr/cas9. The grey boxes correspond to exons, and pink arrows indicate the 2 independent guides for each locus. (g) Western blot of netrin-1, Unc5B and Neo1 levels in the corresponding mESC lines. 3 independent experiments gave similar results. (h) Self-renewal assay. Control and netrin-1^{KO} mESCs are plated at clonal density in serum+Lif (left panel) or serum+Lif+2i (right panel) for 7 days before AP positive colonies was scored. Data are the mean ± s.d. (n=3 independent experiments). Student's t-test was used and two-sided p-values are indicated. (i) *Netrin-1*, *Nanog* and *Gata6* expression in single blastomeres. Data, extracted from Nakamura et al., 2016, correspond to FPKM values for 9 nanog positive cells and 12 gata6 positive blastomeres. Each dot corresponds to a cell, the bar is the mean ± s.d. Student T-test was used and two-sided p-values are indicated.

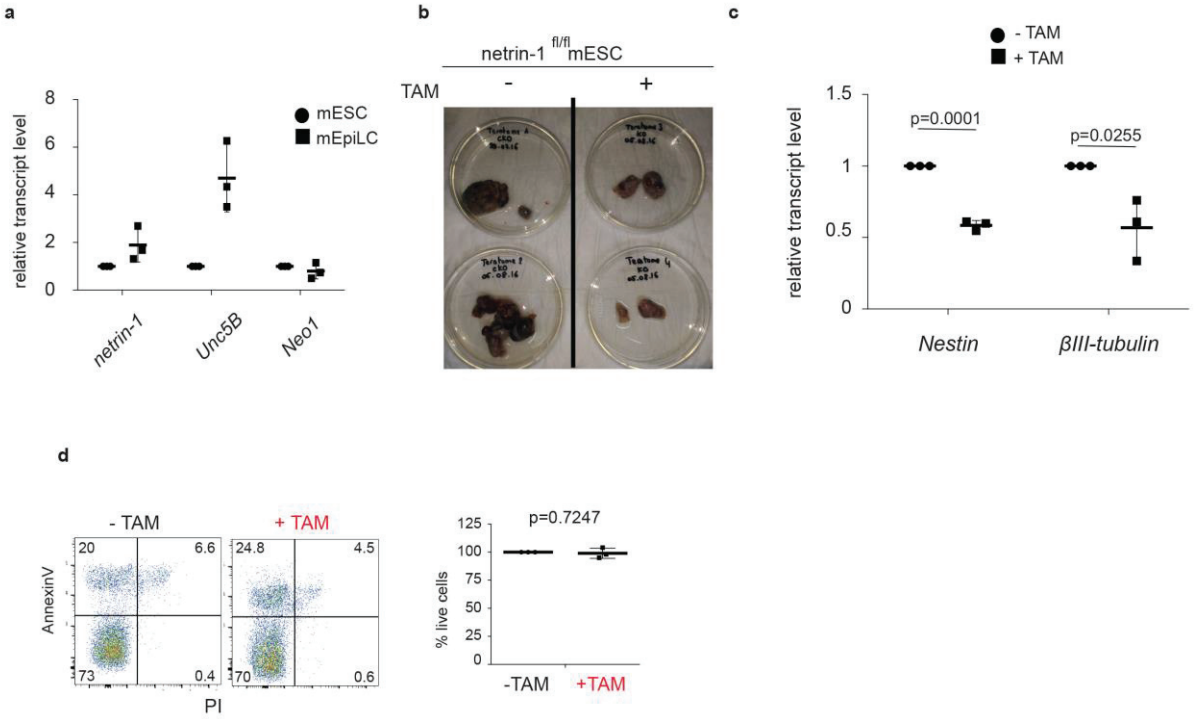

Supplementary Figure 5. netrin-1 controls coordinated differentiation. (a) *Neo1* and *Unc5B* expression in epiblast-like cells (EpiLC). Q-RTPCR data are expressed relative to mESCs as the mean ± s.d. (n=3 independent experiments). (b) Pictures of teratoma obtained following injection of netrin-$1^{fl/fl}$ mESCs treated (right panel) or not (left panel) with TAM 24 hours prior to injection. 4 independent teratoma per condition were analysed. (c) Q-RTPCR depicts *Nestin* and *βIII-tubulin* levels at day 8 of differentiation in N2B27-Lif. Data are normalized to housekeeping genes and value 1 is given to day8 Ctrl mESCs. Data are the mean ± s.d. (n=3 independent experiments). Student's t-test was used and two-sided p-values are indicated. (d) Cell death analysis. The netrin-$1^{fl/fl}$ mESCs, treated or not with TAM ON, were grown for 2 days in N2B27-Lif before PI-AnnexinV staining was performed. The left panel present a representative FACS profile and the right panel a graph of mean data ± s.d. (n=3 independent experiments). Value 100% is given to the percentage of live cells in untreated netrin-$1^{fl/fl}$ mESCs.

Supplementary Table 1

siRNA	
siGENOME Mouse Ptk2 (14083)	D-041099-01-0002
siGENOME Mouse Ptk2 (14083)	D-041099-02-0002
siGENOME Mouse Dapk1 (69635)	D-040260-01-0002
siGENOME Mouse Dapk1 (69635)	D-040260-02-0002
siGENOME Mouse Ppp2ca (19052)	D-040657-01-0002
siGENOME Mouse Ppp2ca (19052)	D-040657-02-0002
siGENOME Mouse Ppp2r2c (269643)	D-055606-01-0002
siGENOME Mouse Ppp2r2c (269643)	D-055606-02-0002

antibodies	
OCT4	Santa Cruz, sc5279
NANOG	Cosmobio, RCA B000 2P-F
SOX2	Abcam, ab9759
ESRRB	R&D Systems, PP-H6705-00
ACTIN	Sigma, A3854
NEO1	Cell signalling, 39447
UNC5B	Cell signalling, 13851
netrin-1	R&D Systems, AF-6419
p-ERK1/2	Cell Signaling, T202, Y204-9101
total ERK1/2	Sigma, M5670
p-STAT3	Cell Signalling, Tyr705-D3A7
STAT3	Cell Signaling, 79D7
β-CATENIN	Millipore, 05-665
TCF7L1	kind gift from B. Merrill lab
H3K27Me3	Diagenode #C15410195-10
H3K4Me3	Active Motif #61379
GSK3	Cell signalling, 9315
p-GSK3 (inactif)	Cell signalling, 9331
MEK1/2	Cell signalling, 9122
p-MEK1/2	Cell signalling, 9121
FAK	Cell signalling, 3285

p-FAK	Cell signalling, 3283
pp2AC	Millipore, 05-421, clone 1D6,
GFP	Abcam, ab13970
X-gal	Abcam, ab9361
cleaved Caspase 3	Cell signalling, 9664

sg sequences for crispr/cas9 targeting	
netrin-1 sg#1	CAGCATGATGCGCGCTGTGT
netrin-1 sg#2	GCGCGCTGTGTGGGAGGCGC
Neo1 sg#1	GGAGGTGCAGAGGAGTCGCC
Neo1 sg#2	CTTACCTGCGGACTGCGGCG
Unc5B sg#1	GAGCATGAGGGCCCGGAGCG
Unc5B sg#2	GCTGGCGCTGCTGCTTTGCT

6. DISCUSSION AND FUTURE PERSPECTIVES

During my PhD, I have been interested in deciphering processes controlling cellular identity in different contexts. A first project was focused on deciphering the mechanisms that drive loss of somatic identity and dedifferentiation during malignant transformation and iPSCs generation. The results obtained allowed to us to identify a novel balance between two basic Helix Loop Helix transcription factors determining cellular reprogramming: while c-Myc drives iPSCs generation and malignant transformation, we identified Atoh8 as a novel roadblock of the two processes.

A second study led us to explore changes in cellular identity among pluripotency. We identified Netrin-1 and its receptors Neo-1 and Unc5-b as new regulators of naïve pluripotency. We showed that the Netrin-1 pathway converts heterogeneous ESCs to a homogeneous naïve state sharing partial homologies with the 2i-induced ground state.

In this last part, I will discuss separately the results obtained for the two projects and I will propose some ideas to continue the two studies.

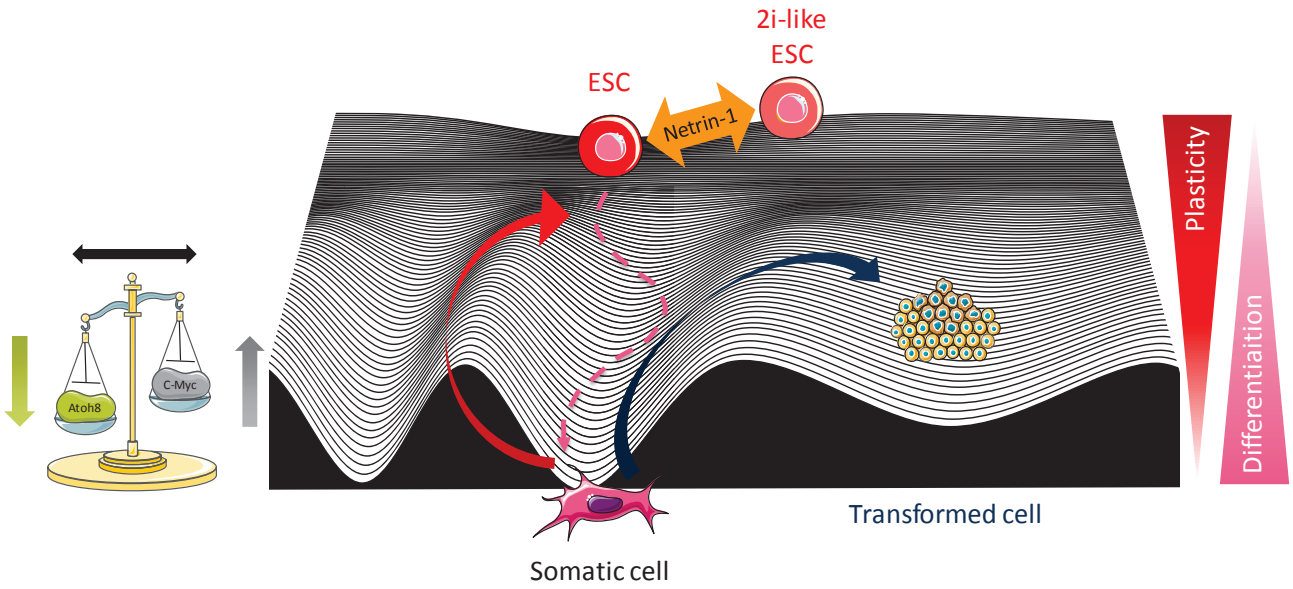

Figure 21: Recapitulative scheme of results obtained during the PhD. C-Myc is fundamental for pluripotent reprogramming and malignant transformation, while Atoh8 is an obstacle for both processes, highlighting the importance of bHLH TFs in regulating loss of somatic identity and reprogramming.

The Netrin-1 ligand and its receptors Unc5-b and Neo-1 drives change of cellular identity in the heterogeneous ESCs population. Their action leads to homogeneous naïve ESCs, resembling for many aspects the ground state 2i-induced ESCs.

6.1. Atoh8 project

Our data highlight the requirement for c-Myc during pluripotent and malignant reprogramming. Even if its exogenous expression is dispensable for iPSCs generation and malignant transformation, its endogenous level is fundamental for both processes accomplishment. This is in line with recent reports showing the importance of endogenous c-Myc in the early steps of pluripotent reprogramming (Prieto et al., 2018; Zviran et al., 2019).

Interestingly, Klf4 is also expressed as c-Myc in the initial MEFs. However, the over-expression of Oct4, Sox2 and c-Myc in combination with the endogenous Klf4 is not sufficient to induce iPSCs generation, with cells senescing and dying few days after OSM infection (data not shown). Thus, it seems that, unlike c-Myc, Klf4 endogenous levels are not sufficient to mediate pluripotent reprogramming, suggesting different requirements in Yamanaka factor stoichiometry, as previously described (Carey et al., 2011).

Our results have interesting repercussions also for cancer biology. Even if the combined action of K-RasG12D and p53 loss are sufficient to drive malignant immortalization, their effect is erased by the depletion of the endogenous c-Myc (Bailey et al., 2016; O'Dell et al., 2012). These results show an important role of this factors in the first steps of malignant transformation. These evidences are also in line with the dependence of some tumors to c-Myc expression levels (Myc-addicted tumors) (Dang, 2012).

C-Myc has been described as a target of K-Ras activity through Erk1/2 and Erk5 signalling (Vaseva et al., 2018). Moreover, our data show that induction of the K-RasG12D mutation in MEFs has the same effects of c-Myc over-expression on Atoh8 transcript levels (FigS5A, paper 1). It would be interesting to address which is the relevance of c-Myc as a K-Ras effector and at which level c-Myc endogenous depletion influences the effects of K-Ras in malignant transformation.

We also described a new role for Atoh8 as an obstacle to iPSCs generation and malignant transformation. In the screening to isolate Atoh8, based on the Thy1 marker, Id4 and Twist2 were also identified. The same functional experiments to test Atoh8 role in PR and MR were carried out for these two candidates. Downregulation of Twist2 and Id4 did not show any increase in efficiency of iPSCs generation, we thus decided to focus on Atoh8. Cumulative effects were observed when Atoh8 was downregulated in combination with Id4, but the differences were not significant. However, we cannot completely exclude a combinatory effect, due to the difficulty to downregulate both genes at the same time with a significant efficiency (data not shown).

However, depletion of Twist2 and Id4 induced an enhanced malignant transformation and over-expression of c-Myc led to downregulation of Twist2 and Id4 at RNA and protein level (data not

shown). It would be interesting to investigate if c-Myc can play a role of master regulator of a bHLH network in the onset of malignant transformation.

Atoh8 depletion increases also the efficiency of malignant transformation. Notably, the enhanced malignant reprogramming associated to the downregulation of this developmental gene highlights the link between developmental processes and malignant transformation. Interestingly, depletion of Atoh8 in the initial MEFs not only increases the efficiency of malignant transformation but have also profound effects on the subsequent acquisition of malignant properties and the final characteristics of the transformed cells, emerging at the end of the process: transformed cells obtained from Atoh8 depleted MEFs present a different EMT state and a more aggressive behaviour. Interestingly, the perturbation of the somatic MEF by depleting Atoh8, one of its somatic gatekeepers, has dramatic effects on malignant transformation. This is in line with the concept of pliancy, which postulates that diversity in the somatic state at the beginning of oncogenesis causes differences in the routes towards malignancy and in the final transformed cells (Puisieux et al., 2018).
In this context, we showed that the enhanced aggressiveness of transformed cells derived in an Atoh8-depleted background is related to a partial EMT state. It would be intriguing to explore the metastatic potential of these cells via *in vitro* migration experiments and *in vivo* tail vein injection tests. Changes in EMT state has been previously associated with cancer stemness and chemoresistance. Moreover, loss of Atoh8 in hepatocellular carcinoma leads to acquisition of CSC markers and enhanced chemoresistance (Song et al., 2015). It would be relevant to address the expression of stemness-associated markers also in our transformed cells.

In the study, we propose to consider Atoh8 as a novel cellular gatekeeper against reprogramming phenomena. It would be important to assess which are the long-term effects of the downregulation of this bHLH TF on the MEF, without inducing reprogramming: if it is a veritable protector of the cellular identity, it is possible that its loss on the long term leads to a decrease of the cellular fitness. Analysis on cellular proliferation, apoptosis and cell cycle could give us some clues for this open question.

Atoh8 plays an important obstacle role not only in iPSCs generation and malignant transformation, but also in other scenario of reprogramming (MEF-to-neuron transdifferentiation, human pluripotent reprogramming, NIH3T3 immortalization-to-transformation). Even if these data highlight a role of Atoh8 as a general roadblock, a limit of the actual work consists in the fact that the several reprogrammings tested were performed starting with fibroblasts. It would be interesting

to reprogram other cellular types to broaden the message, but Atoh8 is not expressed in the initial cells of many reprogramming scenarios (lymphocytes T, lymphocytes B, neutrophils and keratinocytes). This is in line with published data on Atoh8 broad expression during development and restriction to few cell types in the adult.

Our data showed also show that c-Myc downregulates Atoh8 RNA and protein leves. c-Myc-mediated repression of this bHLH TF is consistent with the action of c-Myc in the early steps of pluripotent reprogramming and the classification of Atoh8 as an early somatic marker lost in the beginning of iPSCs generation (Cacchiarelli et al., 2015; Mikkelsen et al., 2008a). Interestingly, bHLH TFs have been shown to interact in two ways to regulate each other function. In the case of negative regulation, as we observed in our case, bHLH TFs can bind promoters and repress the transcription of other bHLH factors. Alternatively, they can compete for the same proteins to form heterodimers, sequestrating co-factors to other members of the family to avoid their action (see introduction).

In our case, we showed that c-Myc can bind Atoh8 promoter, and this binding leads to Atoh8 transcriptional repression (Fig6B-C, paper 1). The mechanisms of this repression are still unknown and further experiments are needed to address this point. Interestingly, as described before, Atoh8 has a bivalent promoter (Pujadas et al., 2011), which is silenced during reprogramming due the H3K27me3 methylation accumulation (Fig. S1, paper 1) (Wang et al., 2016; Zhang et al., 2019). It has been shown in other models that this repression is mediated by the PCR-component Ezh2 (Zhang et al., 2019). Notably, Ezh2 has been proposed as a c-Myc co-factor, essential for its transcriptional repression during pluripotent reprogramming (Rao et al., 2015, p. 2). It is important to test if the c-Myc-mediated Atoh8 repression is correlated to an increase of the H3K27me3 mark deposited by the c-Myc/Ezh2 complex.

Furthermore, c-Myc could also obstacle Atoh8 action by sequestrating other bHLH TFs that could potentially heterodimerize with Atoh8. An interaction of Atoh8 with the Class I bHLH TF E47 has been described (Ejarque et al., 2013). C-Myc could sequestrate this bHLH TF and avoid its interaction with Atoh8. Moreover, it could also directly mediate E47 repression, but differences in E47 expression were not detectable upon c-Myc over-expression (data not shown).

We also showed that, in a feed-back mechanism, Atoh8 downregulation increases the levels of c-Myc RNA and protein, suggesting that Atoh8 negatively regulates it. Recently, precise functions for c-Myc in pluripotent reprogramming has been described, such as metabolic rewiring and tRNA codon usage (Prieto et al., 2018; Zviran et al., 2019). It would be interesting to test if sustained expression of Atoh8 can avoid these phenotypes associated to c-Myc action during reprogramming.

On a functional level, we showed that loss of Atoh8 induces Wnt activation by downregulating Wnt inhibitors expression (Dkk2, Tle2, Sfrp1 and Sfrp2). However, the mechanisms mediating this regulation are still unknown. It is now important to know if these Wnt inhibitors are direct targets of Atoh8 binding on their promoter or if their activation is indirect. In this direction, it is crucial to perform Chip-PCR experiments to test Atoh8 binding on their promoters.
Moreover, consistent with our data, one of Atoh8 knock-out models shows major developmental defects at gastrulation (Ejarque et al., 2016). At this embryonic stage, precise tuning of Wnt signalling is fundamental for antero-posterior axis patterning (Haegel et al., 1995; Huelsken et al., 2000). It would be fascinating to study the effects of Atoh8 downregulation during gastrulation, to see if the *in vivo* observed phenotypes of the Atoh8 KO are related to a deregulation of Wnt signalling, establishing a link between Atoh8 and Wnt also during embryonic development.

To have a better understanding of how c-Myc antagonises Atoh8 somatic function, it would be crucial to assess if c-Myc can hinder Atoh8 activation of Wnt inhibitors. To address this issue, Chip-PCR of Atoh8 on Wnt inhibitors promoters could be performed with increasing doses of c-Myc, with the aim to observe if c-Myc over-expression can disturb Atoh8 binding. More generally, it would be fascinating to see if c-Myc and Atoh8 can compete for the same binding domain at a broader level. With this aim, RNA-sequencing analyses should be performed upon c-Myc overexpression or Atoh8 depletion, to identify genes commonly regulated by these two TFs. Moreover, thanks to Chip-Seq analysis, it would be possible to describe the distribution of these two factors. The data obtained from these analyses would be of great impact to address the mechanisms orchestrating Atoh8 and c-Myc antagonism. Focusing the attention on bHLH TFs, the same results could also give some indications for the hypothesis that proposes c-Myc as a master gene regulating a bHLH TFs network during iPSCs generation and malignant transformation.

6.2. Netrin project

In this second project, we showed that Netrin-1 and its receptors Neo-1 and Unc5-b mediate a homogenous naïve pluripotent state, recapitulating some features of the 2i-induced ground state.

Our data show that Netrin-1 induction in ESCs drives an increase and homogenization of naïve markers as Sox2, Nanog and Esrrb, which are usually expressed heterogeneously in the normal culture conditions (serum + LIF). We suggest that this increase is due to an activation of Wnt and repression of Mapk signalling, as shown by the induction of the active form of β-catenin and decrease of Erk phosphorylation. However, we cannot exclude that Netrin-1 enhances the expression of naïve markers via alternative pathways. It is important to test if we can observe the same phenotypes on naive markers even when effects on Wnt and Mapk pathways are inhibited (for example by silencing Pp2a and Fak).
We showed that Netrin-1 expression changes in ground state: ChirON and 2i treatment increase the level of Netrin-1, while PD reduces it, identifying Netrin-1 as a target of both the Wnt and Fgf pathways (Fig1B, paper 2). The double regulation from Wnt and Fgf, the former related to pluripotency and the latter to commitment, matches the bipotent role of Netrin-1 in induction of naïve pluripotency and regulation of differentiation, as demonstrated by the fact that both over-expressing cells and KO cells show differentiation defects (Fig1T, 7L-M, paper 2).

Notably, Wnt activates Netrin-1 expression and Netrin-1 induces Wnt pathway, highlighting a positive interplay between these two factors. This is in line with the cooperation of Netrin-1 and Wnt signallings observed in axon guidance. In *C. Elegans*, Netrin-1 and Wnt work together to guide axon migration respectively on the dorso-vetral and antero-posterior axis. Moreover, it has been recently demonstrated that these two pathways act in a redundant way, working in parallel in the determination of the two axis (Levy-Strumpf and Culotti, 2014). This redundancy is consistent with our data showing that Netrin-1 and Wnt3a induction do not show an additional effect on Wnt pathway activation (Fig3B, paper 2). It would be interesting to know if Wnt, in a mirror way, can also activate the Netrin-1/Unc5-b/Neo-1 pathway, but the Netrin-1 signalization is poorly understood and most of the effectors are unknown. Notably, it has been shown that Wnt activity through MOM-5/Frizzled can regulate negatively Unc-5 expression (Levy-Strumpf et al., 2015).

The link between Netrins and Fgf has been reported in many studies: both signalling pathways play determinant roles in angiogenesis and lymphangiogenesis (Larrieu-Lahargue et al., 2010; Park et al., 2004). Moreover, on a molecular level, Dcc can activate Mapk signalling through a direct recruitment

and activation of Erk1/2 (Forcet et al., 2002). Also in our case, we observe an activation of the Mapk/Mek/Erk pathway and the effect is mediated by the Pp2a complex. The signalling through Pp2a could reflect differential mechanisms down-stream the Dcc and Neo-1 pathways.

The Fgf regulation on Netrin-1, highlighted by the decreased expression of Netrin-1 upon PD treatment (Fig1B, paper 2), denotes the role of this ligand in ESCs differentiation. Indeed, Netrin-1 levels are increased during differentiation. From these observations, we speculate that, while in pluripotency the expression of Netrin-1 is regulated majorly by Wnt activity, during the differentiation the increase in Fgf signalling drives the enhanced Netrin-1 expression.

To test this hypothesis, we could inhibit Wnt signalling in ESCs and observe if Netrin-1 expression changes. If differences in expression are noticed, it would be interesting to study at a mechanistic level how the regulation of Netrin-1 by this pathway is orchestrated.

Moreover, while Mapk has a positive effect on Netrin-1 expression in ESCs (as highlighted by Netrin-1 decrease upon PD treatment), Netrin-1 mediates a repression of the Mapk signalling. This auto-regulatory negative loop is maybe one of the mechanisms required to avoid differentiation of ESCs. During differentiation, both FGF activity and Netrin-1 expression increases: It would be interesting to assess if Netrin-1 plays this buffer role also after the onset of commitment.

During differentiation, not only Netrin-1 levels increase, but we can also observe changes in stoichiometry of its receptors (increase of Unc5-b and decrease of Neo-1). This can explain the differential action of Netrin-1 as a pluripotent and differentiation factor (Fig 7A, 7J, paper 2). Indeed, combined over-expression of Netrin-1 and Unc5-b leads to a in induction of P-Erk, while the over-expression of the ligand with Neo-1 reduced the levels of phosphorylation of this factor (Fig7C-D, paper 2).

Thus, during differentiation, Unc5b and Neo1 receptors change their expression level and have an opposite effect. On the contrary, in pluripotency, where they are both expressed, both receptors are required for Wnt activation, Mapk inhibition and naive pluripotency maintenance.

It thus seems that, depending on the stoichiometry of receptors, Netrin-1 can cover different functions. This model has already been proposed in axon guidance, where Dcc-mediated signalling induces chemoattraction, Unc-5 signalling chemorepulsion on short distances, while the combination of Dcc and Unc-5 drives long-distance chemorepulsion (Finci et al., 2015). It would be interesting in the future to identify specifically the stoichiometry of Netrin and its receptors in ESCs and during differentiation at a single cell level, to understand which configurations of ligand/receptor are associated to a naïve or to a differentiated state. Moreover, from our results, it emerges that the increase of Unc5-b levels is correlated to a switch in the Netrin role from pluripotency to differentiation regulator. In the study we did not focus on the regulation of receptors

expression, but it is crucial to understand what causes the enhanced expression of Unc5-b and the decrease in Neo-1 level at the onset of differentiation.

In the study, we reported that Netrin-1 signalling mediates Wnt activation via Fak and Fgf decrease through Pp2a, as shown by inhibition of Fak and Pp2a experiments (Fig3D, 3I, paper 2). Indeed, it has been reported that the Netrin-1 axis can induce Fak to promote the Pp2a complex activity (An et al., 2016). Moreover, other studies showed Fak activation of Mapk pathway (Bechara et al., 2008; Webb et al., 2004). For having better insights on the precise order of the effectors of Netrin-1 pathway, it would be crucial to assess if Fak modulation can induce differences also in Mapk signalling.

Fak is a tyrosine kinase that has important cellular functions, primarily through regulation of the cytoskeleton. It has been shown that mechanotransduction mediated by Fak is a fundamental feature of Netrin-1-induced chemoattraction in axon guidance (Moore et al., 2012). Many extracellular proteins, such as Cochlin, R-spondin and IGFBP, have been reported to play important roles in maintaining stemness in ESCs and other multipotent stem cells (de Lau et al., 2011; Huynh et al., 2011; Zhang et al., 2013). It would be intriguing to explore the link between Netrin-1/FAK mechanotransduction and the maintenance of the pluripotent state in ESCs.

Notably, nor FAK neither Pp2a could be detected co-immunoprecipitated with Unc5-b or Neo-1 (data not shown). This makes us wonder which are the first effectors directly interacting with receptors at the beginning of the signalling pathway. To address this question, it would be important to perform mass spectrometry analysis to identify the factors directly interacting with the receptors and describe in a deep way the mechanisms of Netrin-1 pathway in ESCs. Moreover, it would be interesting to perform the same analyses during differentiation, to understand how the differences in receptors stoichiometry impact downstream pathways.

Our data show that, as 2i, Netrin can activate Wnt pathway and repress Mapk signalling, driving a homogenous expression of naïve markers. However, the extent of Netrin-1 action does not recapitulate completely the effects of 2i. One of the major differences consists in the extent of Mapk repression, as far as 2i is more efficient than Netrin-1 to reduce P-Erk levels (Fig4A, paper 2). However, long-term ESCs culture in 2i has been correlated to DNA instability and decrease in chimaera generation potential due to an excessive repression of MEK (Choi et al., 2017). It would be interesting to test if long term cultures with recombinant Netrin-1 present the same phenotype or if the reduced repression on Mapk signalling can avoid the genome instability observed in 2i conditions.

Our data show that Netrin-1 expression can be activated by 2i and that Netrin-1 have similar effects of 2i, regarding pathway activation and stabilization of a homogenous naïve state. From these results, we wonder if Netrin-1 acts as an effector of 2i induction. In this optic, recombinant Netrin-1 could be used in substitution to 2i, possibly avoiding the negative effects on DNA integrity.

Thanks to the use of feeder-secreting Netrin-1 and the recombinant protein, we showed that Netrin-1 can act in a paracrine way. It would be intriguing to address which is the extent of its paracrine effect on the distance range. Due to the absence of commercial antibody to detect efficiently Netrin-1 by immunofluorescence in ESCs, it would be interesting to develop a reporter line for Netrin-1 expression and perform IF for naïve markers, to observe if the cells adjacent to Netrin-1 expressing cells express naïve makers at higher levels.
The paracrine effects observed with the treatment of recombinant Netrin-1 open interesting practical applications. In particular, it would be interesting to test if it can be used to derive ESCs from rat or mouse recalcitrant strains.

Our data show that, in serum-deprived conditions, recombinant Netrin-1 and Lif treatment are sufficient for ESCs self-renewal along multiple lineages. It has been described that Lif mediates specific repression of mesodermal and endodermal differentiation. Interestingly, over-expression of Netrin-1 in ESCs induces a decrease in the level of the heterogeneous expression of mesodermal and endodermal markers, suggesting that Netrin-1 and Lif can block ESCs differentiation in similar way. Notably, the Lif KO mice do not present defects in the epiblast development, and Netrin-1 depletion effects are compensated by other mechanisms (Fig6D-G, paper 2) (Stewart et al., 1992). It would be intriguing to test if Netrin-1 can compensate Lif absence in activating the Jak-Stat pathway. Moreover, it would be interesting to address the phenotype of the double KO for Netrin-1 and Lif in the embryonic pluripotent compartment.

7. BIBLIOGRAPHY

Aasen, T., Raya, A., Barrero, M.J., Garreta, E., Consiglio, A., Gonzalez, F., Vassena, R., Bilić, J., Pekarik, V., Tiscornia, G., Edel, M., Boué, S., Belmonte, J.C.I., 2008. Efficient and rapid generation of induced pluripotent stem cells from human keratinocytes. Nat. Biotechnol. 26, 1276–1284. https://doi.org/10.1038/nbt.1503

Abad, M., Mosteiro, L., Pantoja, C., Cañamero, M., Rayon, T., Ors, I., Graña, O., Megías, D., Domínguez, O., Martínez, D., Manzanares, M., Ortega, S., Serrano, M., 2013. Reprogramming in vivo produces teratomas and iPS cells with totipotency features. Nature 502, 340–345. https://doi.org/10.1038/nature12586

Adams, J.M., Cory, S., 2007. The Bcl-2 apoptotic switch in cancer development and therapy. Oncogene 26, 1324–1337. https://doi.org/10.1038/sj.onc.1210220

Adams, J.M., Harris, A.W., Pinkert, C.A., Corcoran, L.M., Alexander, W.S., Cory, S., Palmiter, R.D., Brinster, R.L., 1985. The c-myc oncogene driven by immunoglobulin enhancers induces lymphoid malignancy in transgenic mice. Nature 318, 533–538. https://doi.org/10.1038/318533a0

Aiuti, A., Biasco, L., Scaramuzza, S., Ferrua, F., Cicalese, M.P., Baricordi, C., Dionisio, F., Calabria, A., Giannelli, S., Castiello, M.C., Bosticardo, M., Evangelio, C., Assanelli, A., Casiraghi, M., Di Nunzio, S., Callegaro, L., Benati, C., Rizzardi, P., Pellin, D., Di Serio, C., Schmidt, M., Von Kalle, C., Gardner, J., Mehta, N., Neduva, V., Dow, D.J., Galy, A., Miniero, R., Finocchi, A., Metin, A., Banerjee, P.P., Orange, J.S., Galimberti, S., Valsecchi, M.G., Biffi, A., Montini, E., Villa, A., Ciceri, F., Roncarolo, M.G., Naldini, L., 2013. Lentiviral Hematopoietic Stem Cell Gene Therapy in Patients with Wiskott-Aldrich Syndrome. Science 341, 1233151–1233151. https://doi.org/10.1126/science.1233151

Aksoy, I., Jauch, R., Chen, J., Dyla, M., Divakar, U., Bogu, G.K., Teo, R., Leng Ng, C.K., Herath, W., Lili, S., Hutchins, A.P., Robson, P., Kolatkar, P.R., Stanton, L.W., 2013. Oct4 switches partnering from Sox2 to Sox17 to reinterpret the enhancer code and specify endoderm. EMBO J. 32, 938–953. https://doi.org/10.1038/emboj.2013.31

Alcántara, S., Ruiz, M., De Castro, F., Soriano, E., Sotelo, C., 2000. Netrin 1 acts as an attractive or as a repulsive cue for distinct migrating neurons during the development of the cerebellar system. Dev. Camb. Engl. 127, 1359–1372.

Al-Hajj, M., Wicha, M.S., Benito-Hernandez, A., Morrison, S.J., Clarke, M.F., 2003. Prospective identification of tumorigenic breast cancer cells. Proc. Natl. Acad. Sci. 100, 3983–3988. https://doi.org/10.1073/pnas.0530291100

Amati, B., Brooks, M.W., Levy, N., Littlewood, T.D., Evan, G.I., Land, H., 1993. Oncogenic activity of the c-Myc protein requires dimerization with Max. Cell 72, 233–245. https://doi.org/10.1016/0092-8674(93)90663-B

Ambrosetti, D.C., Basilico, C., Dailey, L., 1997. Synergistic activation of the fibroblast growth factor 4 enhancer by Sox2 and Oct-3 depends on protein-protein interactions facilitated by a specific spatial arrangement of factor binding sites. Mol. Cell. Biol. 17, 6321–6329. https://doi.org/10.1128/MCB.17.11.6321

Amit, S., 2002. Axin-mediated CKI phosphorylation of beta -catenin at Ser 45: a molecular switch for the Wnt pathway. Genes Dev. 16, 1066–1076. https://doi.org/10.1101/gad.230302

An, X.-Z., Zhao, Z.-G., Luo, Y.-X., Zhang, R., Tang, X.-Q., Hao, D.-L., Zhao, X., Lv, X., Liu, D.-P., 2016. Netrin-1 suppresses the MEK/ERK pathway and ITGB4 in pancreatic cancer. Oncotarget 7, 24719–24733. https://doi.org/10.18632/oncotarget.8348

Ang, Y.-S., Tsai, S.-Y., Lee, D.-F., Monk, J., Su, J., Ratnakumar, K., Ding, J., Ge, Y., Darr, H., Chang, B., Wang, J., Rendl, M., Bernstein, E., Schaniel, C., Lemischka, I.R., 2011. Wdr5 Mediates Self-Renewal and Reprogramming via the Embryonic Stem Cell Core Transcriptional Network. Cell 145, 183–197. https://doi.org/10.1016/j.cell.2011.03.003

Araki, R., Hoki, Y., Uda, M., Nakamura, M., Jincho, Y., Tamura, C., Sunayama, M., Ando, S., Sugiura, M., Yoshida, M.A., Kasama, Y., Abe, M., 2011. Crucial role of c-Myc in the generation of induced pluripotent stem cells. Stem Cells Dayt. Ohio 29, 1362–1370. https://doi.org/10.1002/stem.685

Araki, R., Jincho, Y., Hoki, Y., Nakamura, M., Tamura, C., Ando, S., Kasama, Y., Abe, M., 2009. Conversion of Ancestral Fibroblasts to Induced Pluripotent Stem Cells. STEM CELLS N/A-N/A. https://doi.org/10.1002/stem.282

Avilion, A.A., 2003. Multipotent cell lineages in early mouse development depend on SOX2 function. Genes Dev. 17, 126–140. https://doi.org/10.1101/gad.224503

Azuara, V., Perry, P., Sauer, S., Spivakov, M., Jørgensen, H.F., John, R.M., Gouti, M., Casanova, M., Warnes, G., Merkenschlager, M., Fisher, A.G., 2006. Chromatin signatures of pluripotent cell lines. Nat. Cell Biol. 8, 532–538. https://doi.org/10.1038/ncb1403

Bachoo, R.M., Maher, E.A., Ligon, K.L., Sharpless, N.E., Chan, S.S., You, M.J., Tang, Y., DeFrances, J., Stover, E., Weissleder, R., Rowitch, D.H., Louis, D.N., DePinho, R.A., 2002. Epidermal growth factor receptor and Ink4a/Arf: convergent mechanisms governing terminal differentiation and transformation along the neural stem cell to astrocyte axis. Cancer Cell 1, 269–277.

Bae, G.-U., Yang, Y.-J., Jiang, G., Hong, M., Lee, H.-J., Tessier-Lavigne, M., Kang, J.-S., Krauss, R.S., 2009. Neogenin regulates skeletal myofiber size and focal adhesion kinase and extracellular signal-regulated kinase activities in vivo and in vitro. Mol. Biol. Cell 20, 4920–4931. https://doi.org/10.1091/mbc.e09-06-0491

Bae, S., Bessho, Y., Hojo, M., Kageyama, R., 2000. The bHLH gene Hes6, an inhibitor of Hes1, promotes neuronal differentiation. Dev. Camb. Engl. 127, 2933–2943.

Bai, G., Sheng, N., Xie, Z., Bian, W., Yokota, Y., Benezra, R., Kageyama, R., Guillemot, F., Jing, N., 2007. Id Sustains Hes1 Expression to Inhibit Precocious Neurogenesis by Releasing Negative Autoregulation of Hes1. Dev. Cell 13, 283–297. https://doi.org/10.1016/j.devcel.2007.05.014

Bailey, J.M., Hendley, A.M., Lafaro, K.J., Pruski, M.A., Jones, N.C., Alsina, J., Younes, M., Maitra, A., McAllister, F., Iacobuzio-Donahue, C.A., Leach, S.D., 2016. p53 mutations cooperate with oncogenic Kras to promote adenocarcinoma from pancreatic ductal cells. Oncogene 35, 4282–4288. https://doi.org/10.1038/onc.2015.441

Bailey, M.H., Tokheim, C., Porta-Pardo, E., Sengupta, S., Bertrand, D., Weerasinghe, A., Colaprico, A., Wendl, M.C., Kim, J., Reardon, B., Ng, P.K.-S., Jeong, K.J., Cao, S., Wang, Zixing, Gao, J., Gao, Q., Wang, F., Liu, E.M., Mularoni, L., Rubio-Perez, C., Nagarajan, N., Cortés-Ciriano, I., Zhou, D.C., Liang, W.-W., Hess, J.M., Yellapantula, V.D., Tamborero, D., Gonzalez-Perez, A., Suphavilai, C., Ko, J.Y., Khurana, E., Park, P.J., Van Allen, E.M., Liang, H., Lawrence, M.S., Godzik, A., Lopez-Bigas, N., Stuart, J., Wheeler, D., Getz, G., Chen, K., Lazar, A.J., Mills, G.B., Karchin, R., Ding, L., Caesar-Johnson, S.J., Demchok, J.A., Felau, I., Kasapi, M., Ferguson, M.L., Hutter, C.M., Sofia, H.J., Tarnuzzer, R., Wang, Zhining, Yang, L., Zenklusen, J.C., Zhang, J. (Julia), Chudamani, S., Liu, J., Lolla, L., Naresh, R., Pihl, T., Sun, Q., Wan, Y., Wu, Y., Cho, J., DeFreitas, T., Frazer, S., Gehlenborg, N., Getz, G., Heiman, D.I., Kim, J., Lawrence, M.S., Lin, P., Meier, S., Noble, M.S., Saksena, G., Voet, D., Zhang, Hailei, Bernard, B., Chambwe, N., Dhankani, V., Knijnenburg, T., Kramer, R., Leinonen, K., Liu, Y., Miller, M., Reynolds, S., Shmulevich, I., Thorsson, V., Zhang, W., Akbani, R., Broom, B.M., Hegde, A.M., Ju, Z., Kanchi, R.S., Korkut, A., Li, J., Liang, H., Ling, S., Liu, W., Lu, Y., Mills, G.B., Ng, K.-S., Rao, A., Ryan, M., Wang, Jing, Weinstein, J.N., Zhang, J., Abeshouse, A., Armenia, J., Chakravarty, D., Chatila, W.K., de Bruijn, I., Gao, J., Gross, B.E., Heins, Z.J., Kundra, R., La, K., Ladanyi, M., Luna, A., Nissan, M.G., Ochoa, A., Phillips, S.M., Reznik, E., Sanchez-Vega, F., Sander, C., Schultz, N., Sheridan, R., Sumer, S.O., Sun, Y., Taylor, B.S., Wang, Jioajiao, Zhang, Hongxin, Anur, P., Peto, M., Spellman, P., Benz, C., Stuart, J.M., Wong, C.K., Yau, C., Hayes, D.N., Parker, J.S., Wilkerson, M.D., Ally, A., Balasundaram, M., Bowlby, R., Brooks, D., Carlsen, R., Chuah, E., Dhalla, N., Holt, R., Jones, S.J.M., Kasaian, K., Lee, D., Ma, Y., Marra, M.A., Mayo, M., Moore, R.A., Mungall, A.J., Mungall, K., Robertson, A.G., Sadeghi, S., Schein, J.E., Sipahimalani, P., Tam, A., Thiessen, N., Tse, K., Wong, T., Berger, A.C., Beroukhim, R., Cherniack, A.D., Cibulskis, C., Gabriel, S.B., Gao, G.F., Ha, G., Meyerson, M., Schumacher, S.E., Shih, J., Kucherlapati, M.H., Kucherlapati, R.S., Baylin, S., Cope, L., Danilova, L., Bootwalla, M.S., Lai, P.H., Maglinte, D.T., Van Den Berg, D.J., Weisenberger, D.J., Auman, J.T., Balu, S., Bodenheimer, T., Fan, C., Hoadley, K.A., Hoyle, A.P., Jefferys, S.R., Jones, C.D., Meng, S., Mieczkowski, P.A., Mose, L.E., Perou, A.H., Perou, C.M., Roach, J., Shi, Y., Simons, J.V., Skelly, T., Soloway, M.G., Tan, D., Veluvolu, U., Fan, H., Hinoue, T., Laird, P.W., Shen, H., Zhou, W., Bellair, M., Chang, K., Covington, K., Creighton, C.J., Dinh, H., Doddapaneni, H., Donehower, L.A., Drummond, J., Gibbs, R.A., Glenn, R., Hale, W., Han, Y., Hu, J., Korchina, V., Lee, S., Lewis, L., Li, W., Liu, X., Morgan, M., Morton, D., Muzny, D., Santibanez, J., Sheth, M., Shinbrot, E., Wang, L., Wang, M., Wheeler, D.A., Xi, L., Zhao, F., Hess, J., Appelbaum, E.L., Bailey, M., Cordes, M.G., Ding, L., Fronick, C.C., Fulton, L.A., Fulton, R.S., Kandoth, C., Mardis, E.R., McLellan, M.D., Miller, C.A., Schmidt, H.K., Wilson, R.K., Crain, D., Curley, E., Gardner, J., Lau, K., Mallery, D., Morris, S., Paulauskis, J., Penny, R., Shelton, C., Shelton, T., Sherman, M., Thompson, E., Yena, P., Bowen, J., Gastier-Foster, J.M., Gerken, M., Leraas, K.M., Lichtenberg, T.M., Ramirez, N.C., Wise, L., Zmuda, E., Corcoran, N., Costello, T., Hovens, C., Carvalho, A.L., de Carvalho, A.C., Fregnani, J.H., Longatto-Filho, A., Reis, R.M., Scapulatempo-Neto, C., Silveira, H.C.S., Vidal, D.O., Burnette, A., Eschbacher, J., Hermes, B., Noss, A., Singh, R., Anderson, M.L., Castro, P.D., Ittmann, M., Huntsman, D., Kohl, B., Le, X., Thorp, R., Andry, C., Duffy, E.R., Lyadov, V., Paklina, O.,

Setdikova, G., Shabunin, A., Tavobilov, M., McPherson, C., Warnick, R., Berkowitz, R., Cramer, D., Feltmate, C., Horowitz, N., Kibel, A., Muto, M., Raut, C.P., Malykh, A., Barnholtz-Sloan, J.S., Barrett, W., Devine, K., Fulop, J., Ostrom, Q.T., Shimmel, K., Wolinsky, Y., Sloan, A.E., De Rose, A., Giuliante, F., Goodman, M., Karlan, B.Y., Hagedorn, C.H., Eckman, J., Harr, J., Myers, J., Tucker, K., Zach, L.A., Deyarmin, B., Hu, H., Kvecher, L., Larson, C., Mural, R.J., Somiari, S., Vicha, A., Zelinka, T., Bennett, J., Iacocca, M., Rabeno, B., Swanson, P., Latour, M., Lacombe, L., Têtu, B., Bergeron, A., McGraw, M., Staugaitis, S.M., Chabot, J., Hibshoosh, H., Sepulveda, A., Su, T., Wang, T., Potapova, O., Voronina, O., Desjardins, L., Mariani, O., Roman-Roman, S., Sastre, X., Stern, M.-H., Cheng, F., Signoretti, S., Berchuck, A., Bigner, D., Lipp, E., Marks, J., McCall, S., McLendon, R., Secord, A., Sharp, A., Behera, M., Brat, D.J., Chen, A., Delman, K., Force, S., Khuri, F., Magliocca, K., Maithel, S., Olson, J.J., Owonikoko, T., Pickens, A., Ramalingam, S., Shin, D.M., Sica, G., Van Meir, E.G., Zhang, Hongzheng, Eijckenboom, W., Gillis, A., Korpershoek, E., Looijenga, L., Oosterhuis, W., Stoop, H., van Kessel, K.E., Zwarthoff, E.C., Calatozzolo, C., Cuppini, L., Cuzzubbo, S., DiMeco, F., Finocchiaro, G., Mattei, L., Perin, A., Pollo, B., Chen, C., Houck, J., Lohavanichbutr, P., Hartmann, A., Stoehr, C., Stoehr, R., Taubert, H., Wach, S., Wullich, B., Kycler, W., Murawa, D., Wiznerowicz, M., Chung, K., Edenfield, W.J., Martin, J., Baudin, E., Bubley, G., Bueno, R., De Rienzo, A., Richards, W.G., Kalkanis, S., Mikkelsen, T., Noushmehr, H., Scarpace, L., Girard, N., Aymerich, M., Campo, E., Giné, E., Guillermo, A.L., Van Bang, N., Hanh, P.T., Phu, B.D., Tang, Y., Colman, H., Evason, K., Dottino, P.R., Martignetti, J.A., Gabra, H., Juhl, H., Akeredolu, T., Stepa, S., Hoon, D., Ahn, K., Kang, K.J., Beuschlein, F., Breggia, A., Birrer, M., Bell, D., Borad, M., Bryce, A.H., Castle, E., Chandan, V., Cheville, J., Copland, J.A., Farnell, M., Flotte, T., Giama, N., Ho, T., Kendrick, M., Kocher, J.-P., Kopp, K., Moser, C., Nagorney, D., O'Brien, D., O'Neill, B.P., Patel, T., Petersen, G., Que, F., Rivera, M., Roberts, L., Smallridge, R., Smyrk, T., Stanton, M., Thompson, R.H., Torbenson, M., Yang, J.D., Zhang, L., Brimo, F., Ajani, J.A., Gonzalez, A.M.A., Behrens, C., Bondaruk, J., Broaddus, R., Czerniak, B., Esmaeli, B., Fujimoto, J., Gershenwald, J., Guo, C., Lazar, A.J., Logothetis, C., Meric-Bernstam, F., Moran, C., Ramondetta, L., Rice, D., Sood, A., Tamboli, P., Thompson, T., Troncoso, P., Tsao, A., Wistuba, I., Carter, C., Haydu, L., Hersey, P., Jakrot, V., Kakavand, H., Kefford, R., Lee, K., Long, G., Mann, G., Quinn, M., Saw, R., Scolyer, R., Shannon, K., Spillane, A., Stretch, J., Synott, M., Thompson, J., Wilmott, J., Al-Ahmadie, H., Chan, T.A., Ghossein, R., Gopalan, A., Levine, D.A., Reuter, V., Singer, S., Singh, B., Tien, N.V., Broudy, T., Mirsaidi, C., Nair, P., Drwiega, P., Miller, J., Smith, J., Zaren, H., Park, J.-W., Hung, N.P., Kebebew, E., Linehan, W.M., Metwalli, A.R., Pacak, K., Pinto, P.A., Schiffman, M., Schmidt, L.S., Vocke, C.D., Wentzensen, N., Worrell, R., Yang, H., Moncrieff, M., Goparaju, C., Melamed, J., Pass, H., Botnariuc, N., Caraman, I., Cernat, M., Chemencedji, I., Clipca, A., Doruc, S., Gorincioi, G., Mura, S., Pirtac, M., Stancul, I., Tcaciuc, D., Albert, M., Alexopoulou, I., Arnaout, A., Bartlett, J., Engel, J., Gilbert, S., Parfitt, J., Sekhon, H., Thomas, G., Rassl, D.M., Rintoul, R.C., Bifulco, C., Tamakawa, R., Urba, W., Hayward, N., Timmers, H., Antenucci, A., Facciolo, F., Grazi, G., Marino, M., Merola, R., de Krijger, R., Gimenez-Roqueplo, A.-P., Piché, A., Chevalier, S., McKercher, G., Birsoy, K., Barnett, G., Brewer, C., Farver, C., Naska, T., Pennell, N.A., Raymond, D., Schilero, C., Smolenski, K., Williams, F., Morrison, C., Borgia, J.A., Liptay, M.J., Pool, M., Seder, C.W., Junker, K., Omberg, L., Dinkin, M., Manikhas, G., Alvaro, D., Bragazzi, M.C., Cardinale, V., Carpino, G., Gaudio, E., Chesla, D., Cottingham, S., Dubina, M., Moiseenko, F., Dhanasekaran, R., Becker, K.-F., Janssen, K.-P., Slotta-Huspenina, J., Abdel-Rahman, M.H., Aziz, D., Bell, S., Cebulla, C.M., Davis, A., Duell, R., Elder, J.B., Hilty, J., Kumar, B., Lang, J., Lehman, N.L., Mandt, R., Nguyen, P., Pilarski, R., Rai, K., Schoenfield, L., Senecal, K., Wakely, P., Hansen, P., Lechan, R., Powers, J., Tischler, A., Grizzle, W.E., Sexton, K.C., Kastl, A., Henderson, J., Porten, S., Waldmann, J., Fassnacht, M., Asa, S.L., Schadendorf, D., Couce, M., Graefen, M., Huland, H., Sauter, G., Schlomm, T., Simon, R., Tennstedt, P., Olabode, O., Nelson, M., Bathe, O., Carroll, P.R., Chan, J.M., Disaia, P., Glenn, P., Kelley, R.K., Landen, C.N., Phillips, J., Prados, M., Simko, J., Smith-McCune, K., VandenBerg, S., Roggin, K., Fehrenbach, A., Kendler, A., Sifri, S., Steele, R., Jimeno, A., Carey, F., Forgie, I., Mannelli, M., Carney, M., Hernandez, B., Campos, B., Herold-Mende, C., Jungk, C., Unterberg, A., von Deimling, A., Bossler, A., Galbraith, J., Jacobus, L., Knudson, M., Knutson, T., Ma, D., Milhem, M., Sigmund, R., Godwin, A.K., Madan, R., Rosenthal, H.G., Adebamowo, C., Adebamowo, S.N., Boussioutas, A., Beer, D., Giordano, T., Mes-Masson, A.-M., Saad, F., Bocklage, T., Landrum, L., Mannel, R., Moore, K., Moxley, K., Postier, R., Walker, J., Zuna, R., Feldman, M., Valdivieso, F., Dhir, R., Luketich, J., Pinero, E.M.M., Quintero-Aguilo, M., Carlotti, C.G., Dos Santos, J.S., Kemp, R., Sankarankuty, A., Tirapelli, D., Catto, J., Agnew, K., Swisher, E., Creaney, J., Robinson, B., Shelley, C.S., Godwin, E.M., Kendall, S., Shipman, C., Bradford, C., Carey, T., Haddad, A., Moyer, J., Peterson, L., Prince, M., Rozek, L., Wolf, G., Bowman, R., Fong, K.M., Yang, I., Korst, R., Rathmell, W.K., Fantacone-Campbell, J.L., Hooke, J.A., Kovatich, A.J., Shriver, C.D., DiPersio, J., Drake, B., Govindan, R., Heath, S., Ley, T., Van Tine, B., Westervelt, P., Rubin, M.A., Lee, J.I., Aredes, N.D., Mariamidze, A., 2018. Comprehensive

Characterization of Cancer Driver Genes and Mutations. Cell 173, 371-385.e18. https://doi.org/10.1016/j.cell.2018.02.060

Balakrishnan-Renuka, A., Morosan-Puopolo, G., Yusuf, F., Abduelmula, A., Chen, J., Zoidl, G., Philippi, S., Dai, F., Brand-Saberi, B., 2014. ATOH8, a regulator of skeletal myogenesis in the hypaxial myotome of the trunk. Histochem. Cell Biol. 141, 289–300. https://doi.org/10.1007/s00418-013-1155-0

Banito, A., Rashid, S.T., Acosta, J.C., Li, S., Pereira, C.F., Geti, I., Pinho, S., Silva, J.C., Azuara, V., Walsh, M., Vallier, L., Gil, J., 2009. Senescence impairs successful reprogramming to pluripotent stem cells. Genes Dev. 23, 2134–2139. https://doi.org/10.1101/gad.1811609

Bao, S., Tang, F., Li, X., Hayashi, K., Gillich, A., Lao, K., Surani, M.A., 2009. Epigenetic reversion of post-implantation epiblast to pluripotent embryonic stem cells. Nature 461, 1292–1295. https://doi.org/10.1038/nature08534

Barker, N., Ridgway, R.A., van Es, J.H., van de Wetering, M., Begthel, H., van den Born, M., Danenberg, E., Clarke, A.R., Sansom, O.J., Clevers, H., 2009. Crypt stem cells as the cells-of-origin of intestinal cancer. Nature 457, 608–611. https://doi.org/10.1038/nature07602

Bartkova, J., Rezaei, N., Liontos, M., Karakaidos, P., Kletsas, D., Issaeva, N., Vassiliou, L.-V.F., Kolettas, E., Niforou, K., Zoumpourlis, V.C., Takaoka, M., Nakagawa, H., Tort, F., Fugger, K., Johansson, F., Sehested, M., Andersen, C.L., Dyrskjot, L., Ørntoft, T., Lukas, J., Kittas, C., Helleday, T., Halazonetis, T.D., Bartek, J., Gorgoulis, V.G., 2006. Oncogene-induced senescence is part of the tumorigenesis barrier imposed by DNA damage checkpoints. Nature 444, 633–637. https://doi.org/10.1038/nature05268

Bartscherer, K., Pelte, N., Ingelfinger, D., Boutros, M., 2006. Secretion of Wnt Ligands Requires Evi, a Conserved Transmembrane Protein. Cell 125, 523–533. https://doi.org/10.1016/j.cell.2006.04.009

Batlle-Morera, L., Smith, A., Nichols, J., 2008. Parameters influencing derivation of embryonic stem cells from murine embryos. genesis 46, 758–767. https://doi.org/10.1002/dvg.20442

Beatty, G.L., Gladney, W.L., 2015. Immune Escape Mechanisms as a Guide for Cancer Immunotherapy. Clin. Cancer Res. 21, 687–692. https://doi.org/10.1158/1078-0432.CCR-14-1860

Bechara, A., Nawabi, H., Moret, F., Yaron, A., Weaver, E., Bozon, M., Abouzid, K., Guan, J.-L., Tessier-Lavigne, M., Lemmon, V., Castellani, V., 2008. FAK-MAPK-dependent adhesion disassembly downstream of L1 contributes to semaphorin3A-induced collapse. EMBO J. 27, 1549–1562. https://doi.org/10.1038/emboj.2008.86

Beck, B., Lapouge, G., Rorive, S., Drogat, B., Desaedelaere, K., Delafaille, S., Dubois, C., Salmon, I., Willekens, K., Marine, J.-C., Blanpain, C., 2015. Different Levels of Twist1 Regulate Skin Tumor Initiation, Stemness, and Progression. Cell Stem Cell 16, 67–79. https://doi.org/10.1016/j.stem.2014.12.002

Bedzhov, I., Graham, S.J.L., Leung, C.Y., Zernicka-Goetz, M., 2014. Developmental plasticity, cell fate specification and morphogenesis in the early mouse embryo. Philos. Trans. R. Soc. B Biol. Sci. 369. https://doi.org/10.1098/rstb.2013.0538

Berberich, S.J., Cole, M.D., 1992. Casein kinase II inhibits the DNA-binding activity of Max homodimers but not Myc/Max heterodimers. Genes Dev. 6, 166–176. https://doi.org/10.1101/gad.6.2.166

Berkes, C.A., Tapscott, S.J., 2005. MyoD and the transcriptional control of myogenesis. Semin. Cell Dev. Biol. 16, 585–595. https://doi.org/10.1016/j.semcdb.2005.07.006

Bernet, A., Fitamant, J., 2008. Netrin-1 and its receptors in tumour growth promotion. Expert Opin. Ther. Targets 12, 995–1007. https://doi.org/10.1517/14728222.12.8.995

Bernet, A., Mazelin, L., Coissieux, M.-M., Gadot, N., Ackerman, S.L., Scoazec, J.-Y., Mehlen, P., 2007. Inactivation of the UNC5C Netrin-1 receptor is associated with tumor progression in colorectal malignancies. Gastroenterology 133, 1840–1848. https://doi.org/10.1053/j.gastro.2007.08.009

Bernstein, B.E., Mikkelsen, T.S., Xie, X., Kamal, M., Huebert, D.J., Cuff, J., Fry, B., Meissner, A., Wernig, M., Plath, K., Jaenisch, R., Wagschal, A., Feil, R., Schreiber, S.L., Lander, E.S., 2006. A Bivalent Chromatin Structure Marks Key Developmental Genes in Embryonic Stem Cells. Cell 125, 315–326. https://doi.org/10.1016/j.cell.2006.02.041

Beroukhim, R., Mermel, C.H., Porter, D., Wei, G., Raychaudhuri, S., Donovan, J., Barretina, J., Boehm, J.S., Dobson, J., Urashima, M., Mc Henry, K.T., Pinchback, R.M., Ligon, A.H., Cho, Y.-J., Haery, L., Greulich, H., Reich, M., Winckler, W., Lawrence, M.S., Weir, B.A., Tanaka, K.E., Chiang, D.Y., Bass, A.J., Loo, A., Hoffman, C., Prensner, J., Liefeld, T., Gao, Q., Yecies, D., Signoretti, S., Maher, E., Kaye, F.J., Sasaki, H., Tepper, J.E., Fletcher, J.A., Tabernero, J., Baselga, J., Tsao, M.-S., Demichelis, F., Rubin, M.A., Janne, P.A., Daly, M.J., Nucera, C., Levine, R.L., Ebert, B.L., Gabriel, S., Rustgi, A.K., Antonescu, C.R., Ladanyi, M., Letai, A., Garraway, L.A., Loda, M., Beer, D.G., True, L.D., Okamoto, A., Pomeroy, S.L., Singer, S., Golub, T.R., Lander, E.S., Getz, G., Sellers, W.R., Meyerson, M., 2010. The landscape of somatic copy-number alteration across human cancers. Nature 463, 899–905. https://doi.org/10.1038/nature08822

Bersten, D.C., Sullivan, A.E., Peet, D.J., Whitelaw, M.L., 2013. bHLH-PAS proteins in cancer. Nat. Rev. Cancer 13, 827–841. https://doi.org/10.1038/nrc3621

Bertrand, N., Castro, D.S., Guillemot, F., 2002. Proneural genes and the specification of neural cell types. Nat. Rev. Neurosci. 3, 517–530. https://doi.org/10.1038/nrn874

Bilodeau, S., Kagey, M.H., Frampton, G.M., Rahl, P.B., Young, R.A., 2009. SetDB1 contributes to repression of genes encoding developmental regulators and maintenance of ES cell state. Genes Dev. 23, 2484–2489. https://doi.org/10.1101/gad.1837309

Blackwood, E., Eisenman, R., 1991. Max: a helix-loop-helix zipper protein that forms a sequence-specific DNA-binding complex with Myc. Science 251, 1211–1217. https://doi.org/10.1126/science.2006410

Blasco, M.A., 2005. Telomeres and human disease: ageing, cancer and beyond. Nat. Rev. Genet. 6, 611–622. https://doi.org/10.1038/nrg1656

Bockman, D.E., Merlino, G., 1992. Cytological changes in the pancreas of transgenic mice overexpressing transforming growth factor α. Gastroenterology 103, 1883–1892. https://doi.org/10.1016/0016-5085(92)91448-D

Bodnar, A.G., 1998. Extension of Life-Span by Introduction of Telomerase into Normal Human Cells. Science 279, 349–352. https://doi.org/10.1126/science.279.5349.349

Boettiger, A.N., Levine, M., 2009. Synchronous and Stochastic Patterns of Gene Activation in the *Drosophila* Embryo. Science 325, 471–473. https://doi.org/10.1126/science.1173976

Böing, M., Brand-Saberi, B., Napirei, M., 2018. Murine transcription factor Math6 is a regulator of placenta development. Sci. Rep. 8, 14997. https://doi.org/10.1038/s41598-018-33387-x

Boroviak, T., Loos, R., Lombard, P., Okahara, J., Behr, R., Sasaki, E., Nichols, J., Smith, A., Bertone, P., 2015. Lineage-Specific Profiling Delineates the Emergence and Progression of Naive Pluripotency in Mammalian Embryogenesis. Dev. Cell 35, 366–382. https://doi.org/10.1016/j.devcel.2015.10.011

Borrow, J., Goddard, A., Sheer, D., Solomon, E., 1990. Molecular analysis of acute promyelocytic leukemia breakpoint cluster region on chromosome 17. Science 249, 1577–1580. https://doi.org/10.1126/science.2218500

Boyer, L.A., Lee, T.I., Cole, M.F., Johnstone, S.E., Levine, S.S., Zucker, J.P., Guenther, M.G., Kumar, R.M., Murray, H.L., Jenner, R.G., Gifford, D.K., Melton, D.A., Jaenisch, R., Young, R.A., 2005. Core Transcriptional Regulatory Circuitry in Human Embryonic Stem Cells. Cell 122, 947–956. https://doi.org/10.1016/j.cell.2005.08.020

Bradley, A., Evans, M., Kaufman, M.H., Robertson, E., 1984. Formation of germ-line chimaeras from embryo-derived teratocarcinoma cell lines. Nature 309, 255–256. https://doi.org/10.1038/309255a0

Brambrink, T., Foreman, R., Welstead, G.G., Lengner, C.J., Wernig, M., Suh, H., Jaenisch, R., 2008. Sequential Expression of Pluripotency Markers during Direct Reprogramming of Mouse Somatic Cells. Cell Stem Cell 2, 151–159. https://doi.org/10.1016/j.stem.2008.01.004

Breitman, T.R., Collins, S.J., Keene, B.R., 1981. Terminal differentiation of human promyelocytic leukemic cells in primary culture in response to retinoic acid. Blood 57, 1000–1004.

Brenner, C., Deplus, R., Didelot, C., Loriot, A., Vir, E., De Smet, C., Gutierrez, A., Danovi, D., Bernard, D., Boon, T., Giuseppe Pelicci, P., Amati, B., Kouzarides, T., de Launoit, Y., Di Croce, L., Fuks, F., 2005. Myc represses transcription through recruitment of DNA methyltransferase corepressor. EMBO J. 24, 336–346. https://doi.org/10.1038/sj.emboj.7600509

Briggs, R., King, T.J., 1952. Transplantation of living nuclei from blastula cells into enucleated frogs' eggs. Proc. Natl. Acad. Sci. 38, 455–463. https://doi.org/10.1073/pnas.38.5.455

Brodeur, G., Seeger, R., Schwab, M., Varmus, H., Bishop, J., 1984. Amplification of N-myc in untreated human neuroblastomas correlates with advanced disease stage. Science 224, 1121–1124. https://doi.org/10.1126/science.6719137

Brons, I.G.M., Smithers, L.E., Trotter, M.W.B., Rugg-Gunn, P., Sun, B., Chuva de Sousa Lopes, S.M., Howlett, S.K., Clarkson, A., Ahrlund-Richter, L., Pedersen, R.A., Vallier, L., 2007. Derivation of pluripotent epiblast stem cells from mammalian embryos. Nature 448, 191–195. https://doi.org/10.1038/nature05950

Brouwer, M., Zhou, H., Nadif Kasri, N., 2016. Choices for Induction of Pluripotency: Recent Developments in Human Induced Pluripotent Stem Cell Reprogramming Strategies. Stem Cell Rev. Rep. 12, 54–72. https://doi.org/10.1007/s12015-015-9622-8

Brumbaugh, J., Russell, J.D., Yu, P., Westphall, M.S., Coon, J.J., Thomson, J.A., 2014. NANOG Is Multiply Phosphorylated and Directly Modified by ERK2 and CDK1 In Vitro. Stem Cell Rep. 2, 18–25. https://doi.org/10.1016/j.stemcr.2013.12.005

Buecker, C., Srinivasan, R., Wu, Z., Calo, E., Acampora, D., Faial, T., Simeone, A., Tan, M., Swigut, T., Wysocka, J., 2014. Reorganization of Enhancer Patterns in Transition from Naive to Primed Pluripotency. Cell Stem Cell 14, 838–853. https://doi.org/10.1016/j.stem.2014.04.003

Buehr, M., Meek, S., Blair, K., Yang, J., Ure, J., Silva, J., McLay, R., Hall, J., Ying, Q.-L., Smith, A., 2008. Capture of Authentic Embryonic Stem Cells from Rat Blastocysts. Cell 135, 1287–1298. https://doi.org/10.1016/j.cell.2008.12.007

Buganim, Y., Faddah, D.A., Cheng, A.W., Itskovich, E., Markoulaki, S., Ganz, K., Klemm, S.L., van Oudenaarden, A., Jaenisch, R., 2012. Single-Cell Expression Analyses during Cellular Reprogramming Reveal an Early Stochastic and a Late Hierarchic Phase. Cell 150, 1209–1222. https://doi.org/10.1016/j.cell.2012.08.023

Bulut-Karslioglu, A., Biechele, S., Jin, H., Macrae, T.A., Hejna, M., Gertsenstein, M., Song, J.S., Ramalho-Santos, M., 2016. Inhibition of mTOR induces a paused pluripotent state. Nature 540, 119–123. https://doi.org/10.1038/nature20578

Bulut-Karslioglu, A., Macrae, T.A., Oses-Prieto, J.A., Covarrubias, S., Percharde, M., Ku, G., Diaz, A., McManus, M.T., Burlingame, A.L., Ramalho-Santos, M., 2018. The Transcriptionally Permissive Chromatin State of Embryonic Stem Cells Is Acutely Tuned to Translational Output. Cell Stem Cell 22, 369-383.e8. https://doi.org/10.1016/j.stem.2018.02.004

Burgess, R.W., 2006. Motor Axon Guidance of the Mammalian Trochlear and Phrenic Nerves: Dependence on the Netrin Receptor Unc5c and Modifier Loci. J. Neurosci. 26, 5756–5766. https://doi.org/10.1523/JNEUROSCI.0736-06.2006

Cacchiarelli, D., Trapnell, C., Ziller, M.J., Soumillon, M., Cesana, M., Karnik, R., Donaghey, J., Smith, Z.D., Ratanasirintrawoot, S., Zhang, X., Ho Sui, S.J., Wu, Z., Akopian, V., Gifford, C.A., Doench, J., Rinn, J.L., Daley, G.Q., Meissner, A., Lander, E.S., Mikkelsen, T.S., 2015. Integrative Analyses of Human Reprogramming Reveal Dynamic Nature of Induced Pluripotency. Cell 162, 412–424. https://doi.org/10.1016/j.cell.2015.06.016

Caforio, M., Sorino, C., Iacovelli, S., Fanciulli, M., Locatelli, F., Folgiero, V., 2018. Recent advances in searching c-Myc transcriptional cofactors during tumorigenesis. J. Exp. Clin. Cancer Res. 37, 239. https://doi.org/10.1186/s13046-018-0912-2

Camus, A., Perea-Gomez, A., Moreau, A., Collignon, J., 2006. Absence of Nodal signaling promotes precocious neural differentiation in the mouse embryo. Dev. Biol. 295, 743–755. https://doi.org/10.1016/j.ydbio.2006.03.047

Cantley, L.C., 2002. The Phosphoinositide 3-Kinase Pathway. Science 296, 1655–1657. https://doi.org/10.1126/science.296.5573.1655

Carabet, L., Leblanc, E., Lallous, N., Morin, H., Ghaidi, F., Lee, J., Rennie, P., Cherkasov, A., 2019. Computer-Aided Discovery of Small Molecules Targeting the RNA Splicing Activity of hnRNP A1 in Castration-Resistant Prostate Cancer. Molecules 24, 763. https://doi.org/10.3390/molecules24040763

Carabet, L., Rennie, P., Cherkasov, A., 2018. Therapeutic Inhibition of Myc in Cancer. Structural Bases and Computer-Aided Drug Discovery Approaches. Int. J. Mol. Sci. 20, 120. https://doi.org/10.3390/ijms20010120

Carey, B.W., Markoulaki, S., Beard, C., Hanna, J., Jaenisch, R., 2010. Single-gene transgenic mouse strains for reprogramming adult somatic cells. Nat. Methods 7, 56–59. https://doi.org/10.1038/nmeth.1410

Carey, B.W., Markoulaki, S., Hanna, J., Saha, K., Gao, Q., Mitalipova, M., Jaenisch, R., 2009. Reprogramming of murine and human somatic cells using a single polycistronic vector. Proc. Natl. Acad. Sci. 106, 157–162. https://doi.org/10.1073/pnas.0811426106

Carey, B.W., Markoulaki, S., Hanna, J.H., Faddah, D.A., Buganim, Y., Kim, J., Ganz, K., Steine, E.J., Cassady, J.P., Creyghton, M.P., Welstead, G.G., Gao, Q., Jaenisch, R., 2011. Reprogramming Factor Stoichiometry Influences the Epigenetic State and Biological Properties of Induced Pluripotent Stem Cells. Cell Stem Cell 9, 588–598. https://doi.org/10.1016/j.stem.2011.11.003

Carmeliet, P., 2005. VEGF as a Key Mediator of Angiogenesis in Cancer. Oncology 69, 4–10. https://doi.org/10.1159/000088478

Carriere, C., Seeley, E.S., Goetze, T., Longnecker, D.S., Korc, M., 2007. The Nestin progenitor lineage is the compartment of origin for pancreatic intraepithelial neoplasia. Proc. Natl. Acad. Sci. 104, 4437–4442. https://doi.org/10.1073/pnas.0701117104

Casanovas, O., Hicklin, D.J., Bergers, G., Hanahan, D., 2005. Drug resistance by evasion of antiangiogenic targeting of VEGF signaling in late-stage pancreatic islet tumors. Cancer Cell 8, 299–309. https://doi.org/10.1016/j.ccr.2005.09.005

Castets, M., Coissieux, M.-M., Delloye-Bourgeois, C., Bernard, L., Delcros, J.-G., Bernet, A., Laudet, V., Mehlen, P., 2009. Inhibition of Endothelial Cell Apoptosis by Netrin-1 during Angiogenesis. Dev. Cell 16, 614–620. https://doi.org/10.1016/j.devcel.2009.02.006

Castro, D.S., Martynoga, B., Parras, C., Ramesh, V., Pacary, E., Johnston, C., Drechsel, D., Lebel-Potter, M., Garcia, L.G., Hunt, C., Dolle, D., Bithell, A., Ettwiller, L., Buckley, N., Guillemot, F., 2011. A novel function of the proneural factor Ascl1 in progenitor proliferation identified by genome-wide characterization of its targets. Genes Dev. 25, 930–945. https://doi.org/10.1101/gad.627811

Celià-Terrassa, T., Meca-Cortés, Ó., Mateo, F., Martínez de Paz, A., Rubio, N., Arnal-Estapé, A., Ell, B.J., Bermudo, R., Díaz, A., Guerra-Rebollo, M., Lozano, J.J., Estarás, C., Ulloa, C., plvarez-Simón, D., Milà, J., Vilella, R., Paciucci, R., Martínez-Balbás, M., García de Herreros, A., Gomis, R.R., Kang, Y., Blanco, J., Fernández, P.L., Thomson, T.M., 2012. Epithelial-mesenchymal transition can suppress major attributes of human epithelial tumor-initiating cells. J. Clin. Invest. 122, 1849–1868. https://doi.org/10.1172/JCI59218

Chaffer, C.L., Brueckmann, I., Scheel, C., Kaestli, A.J., Wiggins, P.A., Rodrigues, L.O., Brooks, M., Reinhardt, F., Su, Y., Polyak, K., Arendt, L.M., Kuperwasser, C., Bierie, B., Weinberg, R.A., 2011. Normal and neoplastic nonstem cells can spontaneously convert to a stem-like state. Proc. Natl. Acad. Sci. 108, 7950–7955. https://doi.org/10.1073/pnas.1102454108

Chaffer, C.L., Marjanovic, N.D., Lee, T., Bell, G., Kleer, C.G., Reinhardt, F., D'Alessio, A.C., Young, R.A., Weinberg, R.A., 2013. Poised Chromatin at the ZEB1 Promoter Enables Breast Cancer Cell Plasticity and Enhances Tumorigenicity. Cell 154, 61–74. https://doi.org/10.1016/j.cell.2013.06.005

Chambers, I., Colby, D., Robertson, M., Nichols, J., Lee, S., Tweedie, S., Smith, A., 2003. Functional expression cloning of Nanog, a pluripotency sustaining factor in embryonic stem cells. Cell 113, 643–655. https://doi.org/10.1016/s0092-8674(03)00392-1

Chambers, I., Silva, J., Colby, D., Nichols, J., Nijmeijer, B., Robertson, M., Vrana, J., Jones, K., Grotewold, L., Smith, A., 2007a. Nanog safeguards pluripotency and mediates germline development. Nature 450, 1230–1234. https://doi.org/10.1038/nature06403

Chambers, I., Silva, J., Colby, D., Nichols, J., Nijmeijer, B., Robertson, M., Vrana, J., Jones, K., Grotewold, L., Smith, A., 2007b. Nanog safeguards pluripotency and mediates germline development. Nature 450, 1230–1234. https://doi.org/10.1038/nature06403

Chan, S.S.-Y., Zheng, H., Su, M.-W., Wilk, R., Killeen, M.T., Hedgecock, E.M., Culotti, J.G., 1996. UNC-40, a C. elegans Homolog of DCC (Deleted in Colorectal Cancer), Is Required in Motile Cells Responding to UNC-6 Netrin Cues. Cell 87, 187–195. https://doi.org/10.1016/S0092-8674(00)81337-9

Chanda, S., Ang, C.E., Davila, J., Pak, C., Mall, M., Lee, Q.Y., Ahlenius, H., Jung, S.W., Südhof, T.C., Wernig, M., 2014. Generation of Induced Neuronal Cells by the Single Reprogramming Factor ASCL1. Stem Cell Rep. 3, 282–296. https://doi.org/10.1016/j.stemcr.2014.05.020

Chen, H., Guo, R., Zhang, Q., Guo, H., Yang, M., Wu, Z., Gao, S., Liu, L., Chen, L., 2015. Erk signaling is indispensable for genomic stability and self-renewal of mouse embryonic stem cells. Proc. Natl. Acad. Sci. 112, E5936–E5943. https://doi.org/10.1073/pnas.1516319112

Chen, Jingchen, Balakrishnan-Renuka, A., Hagemann, N., Theiss, C., Chankiewitz, V., Chen, Jinzhong, Pu, Q., Erdmann, K.S., Brand-Saberi, B., 2016. A novel interaction between ATOH8 and PPP3CB. Histochem. Cell Biol. 145, 5–16. https://doi.org/10.1007/s00418-015-1368-5

Chen, Jingchen, Dai, F., Balakrishnan-Renuka, A., Leese, F., Schempp, W., Schaller, F., Hoffmann, M.M., Morosan-Puopolo, G., Yusuf, F., Bisschoff, I.J., Chankiewitz, V., Xue, J., Chen, Jingzhong, Ying, K., Brand-Saberi, B., 2011. Diversification and Molecular Evolution of ATOH8, a Gene Encoding a bHLH Transcription Factor. PLoS ONE 6, e23005. https://doi.org/10.1371/journal.pone.0023005

Chen, L., Fan, J., Chen, H., Meng, Z., Chen, Z., Wang, P., Liu, L., 2015. The IL-8/CXCR1 axis is associated with cancer stem cell-like properties and correlates with clinical prognosis in human pancreatic cancer cases. Sci. Rep. 4, 5911. https://doi.org/10.1038/srep05911

Chen, X., Pappo, A., Dyer, M.A., 2015. Pediatric solid tumor genomics and developmental pliancy. Oncogene 34, 5207–5215. https://doi.org/10.1038/onc.2014.474

Chen, X., Xu, H., Yuan, P., Fang, F., Huss, M., Vega, V.B., Wong, E., Orlov, Y.L., Zhang, W., Jiang, J., Loh, Y.-H., Yeo, H.C., Yeo, Z.X., Narang, V., Govindarajan, K.R., Leong, B., Shahab, A., Ruan, Y., Bourque, G., Sung, W.-K., Clarke, N.D., Wei, C.-L., Ng, H.-H., 2008. Integration of External Signaling Pathways with the Core Transcriptional Network in Embryonic Stem Cells. Cell 133, 1106–1117. https://doi.org/10.1016/j.cell.2008.04.043

Chen, Y., Shi, L., Zhang, L., Li, R., Liang, J., Yu, W., Sun, L., Yang, X., Wang, Y., Zhang, Y., Shang, Y., 2008. The Molecular Mechanism Governing the Oncogenic Potential of SOX2 in Breast Cancer. J. Biol. Chem. 283, 17969–17978. https://doi.org/10.1074/jbc.M802917200

Cheng, L., Huang, Z., Zhou, W., Wu, Q., Donnola, S., Liu, J.K., Fang, X., Sloan, A.E., Mao, Y., Lathia, J.D., Min, W., McLendon, R.E., Rich, J.N., Bao, S., 2013. Glioblastoma stem cells generate vascular pericytes to support vessel function and tumor growth. Cell 153, 139–152. https://doi.org/10.1016/j.cell.2013.02.021

Chiasson-MacKenzie, C., Morris, Z.S., Baca, Q., Morris, B., Coker, J.K., Mirchev, R., Jensen, A.E., Carey, T., Stott, S.L., Golan, D.E., McClatchey, A.I., 2015. NF2/Merlin mediates contact-dependent inhibition of EGFR mobility and internalization via cortical actomyosin. J. Cell Biol. 211, 391–405. https://doi.org/10.1083/jcb.201503081

Choi, H.W., Joo, J.Y., Hong, Y.J., Kim, J.S., Song, H., Lee, J.W., Wu, G., Schöler, H.R., Do, J.T., 2016. Distinct Enhancer Activity of Oct4 in Naive and Primed Mouse Pluripotency. Stem Cell Rep. 7, 911–926. https://doi.org/10.1016/j.stemcr.2016.09.012

Choi, J., Costa, M.L., Mermelstein, C.S., Chagas, C., Holtzer, S., Holtzer, H., 1990. MyoD converts primary dermal fibroblasts, chondroblasts, smooth muscle, and retinal pigmented epithelial cells into striated mononucleated myoblasts and multinucleated myotubes. Proc. Natl. Acad. Sci. U. S. A. 87, 7988–7992. https://doi.org/10.1073/pnas.87.20.7988

Choi, J., Huebner, A.J., Clement, K., Walsh, R.M., Savol, A., Lin, K., Gu, H., Di Stefano, B., Brumbaugh, J., Kim, S.-Y., Sharif, J., Rose, C.M., Mohammad, A., Odajima, J., Charron, J., Shioda, T., Gnirke, A., Gygi, S., Koseki, H., Sadreyev, R.I., Xiao, A., Meissner, A., Hochedlinger, K., 2017. Prolonged Mek1/2 suppression impairs the developmental potential of embryonic stem cells. Nature 548, 219–223. https://doi.org/10.1038/nature23274

Cicalese, M.P., Ferrua, F., Castagnaro, L., Pajno, R., Barzaghi, F., Giannelli, S., Dionisio, F., Brigida, I., Bonopane, M., Casiraghi, M., Tabucchi, A., Carlucci, F., Grunebaum, E., Adeli, M., Bredius, R.G., Puck, J.M., Stepensky, P., Tezcan, I., Rolfe, K., De Boever, E., Reinhardt, R.R., Appleby, J., Ciceri, F., Roncarolo, M.G., Aiuti, A., 2016. Update on the safety and efficacy of retroviral gene therapy for immunodeficiency due to adenosine deaminase deficiency. Blood 128, 45–54. https://doi.org/10.1182/blood-2016-01-688226

Cirulli, V., Yebra, M., 2007. Netrins: beyond the brain. Nat. Rev. Mol. Cell Biol. 8, 296–306. https://doi.org/10.1038/nrm2142

Clarke, A.R., Purdie, C.A., Harrison, D.J., Morris, R.G., Bird, C.C., Hooper, M.L., Wyllie, A.H., 1993. Thymocyte apoptosis induced by p53-dependent and independent pathways. Nature 362, 849–852. https://doi.org/10.1038/362849a0

Clevers, H., 2011. The cancer stem cell: premises, promises and challenges. Nat. Med. 17, 313–319. https://doi.org/10.1038/nm.2304

Colamarino, S.A., Tessier-Lavigne, M., 1995. The axonal chemoattractant netrin-1 is also a chemorepellent for trochlear motor axons. Cell 81, 621–629. https://doi.org/10.1016/0092-8674(95)90083-7

Cole, M.F., Johnstone, S.E., Newman, J.J., Kagey, M.H., Young, R.A., 2008. Tcf3 is an integral component of the core regulatory circuitry of embryonic stem cells. Genes Dev. 22, 746–755. https://doi.org/10.1101/gad.1642408

Cole, S.J., Bradford, D., Cooper, H.M., 2007. Neogenin: A multi-functional receptor regulating diverse developmental processes. Int. J. Biochem. Cell Biol. 39, 1569–1575. https://doi.org/10.1016/j.biocel.2006.11.009

Collins, M.A., Bednar, F., Zhang, Y., Brisset, J.-C., Galbán, S., Galbán, C.J., Rakshit, S., Flannagan, K.S., Adsay, N.V., Pasca di Magliano, M., 2012. Oncogenic Kras is required for both the initiation and maintenance of pancreatic cancer in mice. J. Clin. Invest. 122, 639–653. https://doi.org/10.1172/JCI59227

Cong, F., 2004. Wnt signals across the plasma membrane to activate the -catenin pathway by forming oligomers containing its receptors, Frizzled and LRP. Development 131, 5103–5115. https://doi.org/10.1242/dev.01318

Constam, D.B., Robertson, E.J., 2000. Tissue-specific requirements for the proprotein convertase furin/SPC1 during embryonic turning and heart looping. Dev. Camb. Engl. 127, 245–254.

Dagogo-Jack, I., Shaw, A.T., 2018. Tumour heterogeneity and resistance to cancer therapies. Nat. Rev. Clin. Oncol. 15, 81–94. https://doi.org/10.1038/nrclinonc.2017.166

Dang, C.V., 2013. MYC, Metabolism, Cell Growth, and Tumorigenesis. Cold Spring Harb. Perspect. Med. 3, a014217–a014217. https://doi.org/10.1101/cshperspect.a014217

Dang, C.V., 2012. MYC on the path to cancer. Cell 149, 22–35. https://doi.org/10.1016/j.cell.2012.03.003

David, L., Polo, J.M., 2014. Phases of reprogramming. Stem Cell Res. 12, 754–761. https://doi.org/10.1016/j.scr.2014.03.007

Davis, R.L., Weintraub, H., Lassar, A.B., 1987. Expression of a single transfected cDNA converts fibroblasts to myoblasts. Cell 51, 987–1000. https://doi.org/10.1016/0092-8674(87)90585-x

D'Cruz, C.M., Gunther, E.J., Boxer, R.B., Hartman, J.L., Sintasath, L., Moody, S.E., Cox, J.D., Ha, S.I., Belka, G.K., Golant, A., Cardiff, R.D., Chodosh, L.A., 2001. c-MYC induces mammary tumorigenesis by means of a preferred pathway involving spontaneous Kras2 mutations. Nat. Med. 7, 235–239. https://doi.org/10.1038/84691

de Jong, J., Looijenga, L.H.J., 2006. Stem cell marker OCT3/4 in tumor biology and germ cell tumor diagnostics: history and future. Crit. Rev. Oncog. 12, 171–203.

De La O, J.-P., Emerson, L.L., Goodman, J.L., Froebe, S.C., Illum, B.E., Curtis, A.B., Murtaugh, L.C., 2008. Notch and Kras reprogram pancreatic acinar cells to ductal intraepithelial neoplasia. Proc. Natl. Acad. Sci. 105, 18907–18912. https://doi.org/10.1073/pnas.0810111105

de Lau, W., Barker, N., Low, T.Y., Koo, B.-K., Li, V.S.W., Teunissen, H., Kujala, P., Haegebarth, A., Peters, P.J., van de Wetering, M., Stange, D.E., van Es, J.E., Guardavaccaro, D., Schasfoort, R.B.M., Mohri, Y., Nishimori, K., Mohammed, S., Heck, A.J.R., Clevers, H., 2011. Lgr5 homologues associate with Wnt receptors and mediate R-spondin signalling. Nature 476, 293–297. https://doi.org/10.1038/nature10337

De Luca, M., Aiuti, A., Cossu, G., Parmar, M., Pellegrini, G., Robey, P.G., 2019. Advances in stem cell research and therapeutic development. Nat. Cell Biol. 21, 801–811. https://doi.org/10.1038/s41556-019-0344-z

de Resende, M.F., Chinen, L.T.D., Vieira, S., Jampietro, J., da Fonseca, F.P., Vassallo, J., Campos, L.C., Guimarães, G.C., Soares, F.A., Rocha, R.M., 2013. Prognostication of OCT4 isoform expression in prostate cancer. Tumor Biol. 34, 2665–2673. https://doi.org/10.1007/s13277-013-0817-9

Delloye-Bourgeois, C., Fitamant, J., Paradisi, A., Cappellen, D., Douc-Rasy, S., Raquin, M.-A., Stupack, D., Nakagawara, A., Rousseau, R., Combaret, V., Puisieux, A., Valteau-Couanet, D., Bénard, J., Bernet, A., Mehlen, P., 2009. Netrin-1 acts as a survival factor for aggressive neuroblastoma. J. Exp. Med. 206, 833–847. https://doi.org/10.1084/jem.20082299

Dietrich, J.-E., Hiiragi, T., 2007. Stochastic patterning in the mouse pre-implantation embryo. Dev. Camb. Engl. 134, 4219–4231. https://doi.org/10.1242/dev.003798

Divvela, S.S.K., Nell, P., Napirei, M., Zaehres, H., Chen, J., Gerding, W.M., Nguyen, H.P., Gao, S., Brand-Saberi, B., 2019. bHLH Transcription Factor Math6 Antagonizes TGF-β Signalling in Reprogramming, Pluripotency and Early Cell Fate Decisions. Cells 8. https://doi.org/10.3390/cells8060529

Do, J.T., Schöler, H.R., 2004. Nuclei of Embryonic Stem Cells Reprogram Somatic Cells. Stem Cells 22, 941–949. https://doi.org/10.1634/stemcells.22-6-941

Doble, B.W., Patel, S., Wood, G.A., Kockeritz, L.K., Woodgett, J.R., 2007. Functional Redundancy of GSK-3α and GSK-3β in Wnt/β-Catenin Signaling Shown by Using an Allelic Series of Embryonic Stem Cell Lines. Dev. Cell 12, 957–971. https://doi.org/10.1016/j.devcel.2007.04.001

Dominici, C., Moreno-Bravo, J.A., Puiggros, S.R., Rappeneau, Q., Rama, N., Vieugue, P., Bernet, A., Mehlen, P., Chédotal, A., 2017. Floor-plate-derived netrin-1 is dispensable for commissural axon guidance. Nature 545, 350–354. https://doi.org/10.1038/nature22331

Ducibella, T., Ukena, T., Karnovsky, M., Anderson, E., 1977. Changes in cell surface and cortical cytoplasmic organization during early embryogenesis in the preimplantation mouse embryo. J. Cell Biol. 74, 153–167. https://doi.org/10.1083/jcb.74.1.153

Ducray, F., Idbaih, A., de Reyniès, A., Bièche, I., Thillet, J., Mokhtari, K., Lair, S., Marie, Y., Paris, S., Vidaud, M., Hoang-Xuan, K., Delattre, O., Delattre, J.-Y., Sanson, M., 2008. Anaplastic oligodendrogliomas with 1p19q codeletion have a proneural gene expression profile. Mol. Cancer 7, 41. https://doi.org/10.1186/1476-4598-7-41

Duesberg, P.H., Vogt, P.K., 1979. Avian acute leukemia viruses MC29 and MH2 share specific RNA sequences: Evidence for a second class of transforming genes. Proc. Natl. Acad. Sci. 76, 1633–1637. https://doi.org/10.1073/pnas.76.4.1633

Dunn, S.-J., Martello, G., Yordanov, B., Emmott, S., Smith, A.G., 2014. Defining an essential transcription factor program for naive pluripotency. Science 344, 1156–1160. https://doi.org/10.1126/science.1248882

Eberhardy, S.R., Farnham, P.J., 2002. Myc Recruits P-TEFb to Mediate the Final Step in the Transcriptional Activation of the *cad* Promoter. J. Biol. Chem. 277, 40156–40162. https://doi.org/10.1074/jbc.M207441200

Egawa, N., Kitaoka, S., Tsukita, K., Naitoh, M., Takahashi, K., Yamamoto, T., Adachi, F., Kondo, T., Okita, K., Asaka, I., Aoi, T., Watanabe, A., Yamada, Y., Morizane, A., Takahashi, J., Ayaki, T., Ito, H., Yoshikawa, K., Yamawaki, S., Suzuki, S., Watanabe, D., Hioki, H., Kaneko, T., Makioka, K., Okamoto, K., Takuma, H., Tamaoka, A., Hasegawa, K., Nonaka, T., Hasegawa, M., Kawata, A., Yoshida, M., Nakahata, T., Takahashi, R., Marchetto, M.C.N., Gage, F.H., Yamanaka, S., Inoue, H., 2012. Drug Screening for ALS Using Patient-Specific Induced Pluripotent Stem Cells. Sci. Transl. Med. 4, 145ra104-145ra104. https://doi.org/10.1126/scitranslmed.3004052

Eilers, M., Eisenman, R.N., 2008. Myc's broad reach. Genes Dev. 22, 2755–2766. https://doi.org/10.1101/gad.1712408

Eischen, C.M., Weber, J.D., Roussel, M.F., Sherr, C.J., Cleveland, J.L., 1999. Disruption of the ARF-Mdm2-p53 tumor suppressor pathway in Myc-induced lymphomagenesis. Genes Dev. 13, 2658–2669. https://doi.org/10.1101/gad.13.20.2658

Ejarque, M., Altirriba, J., Gomis, R., Gasa, R., 2013. Characterization of the transcriptional activity of the basic helix-loop-helix (bHLH) transcription factor Atoh8. Biochim. Biophys. Acta 1829, 1175–1183. https://doi.org/10.1016/j.bbagrm.2013.08.003

Ejarque, M., Mir-Coll, J., Gomis, R., German, M.S., Lynn, F.C., Gasa, R., 2016. Generation of a Conditional Allele of the Transcription Factor Atonal Homolog 8 (Atoh8). PloS One 11, e0146273. https://doi.org/10.1371/journal.pone.0146273

Engelkamp, D., 2002. Cloning of three mouse Unc5 genes and their expression patterns at mid-gestation. Mech. Dev. 118, 191–197. https://doi.org/10.1016/S0925-4773(02)00248-4

Evans, M.J., Kaufman, M.H., 1981. Establishment in culture of pluripotential cells from mouse embryos. Nature 292, 154–156. https://doi.org/10.1038/292154a0

Factor, D.C., Corradin, O., Zentner, G.E., Saiakhova, A., Song, L., Chenoweth, J.G., McKay, R.D., Crawford, G.E., Scacheri, P.C., Tesar, P.J., 2014. Epigenomic Comparison Reveals Activation of "Seed" Enhancers during Transition from Naive to Primed Pluripotency. Cell Stem Cell 14, 854–863. https://doi.org/10.1016/j.stem.2014.05.005

Fairman, R., Beran-Steed, R.K., Anthony-Cahill, S.J., Lear, J.D., Stafford, W.F., DeGrado, W.F., Benfield, P.A., Brenner, S.L., 1993. Multiple oligomeric states regulate the DNA binding of helix-loop-helix peptides. Proc. Natl. Acad. Sci. 90, 10429–10433. https://doi.org/10.1073/pnas.90.22.10429

Fang, F., Wasserman, S.M., Torres-Vazquez, J., Weinstein, B., Cao, F., Li, Z., Wilson, K.D., Yue, W., Wu, J.C., Xie, X., Pei, X., 2014. The role of Hath6, a newly identified shear-stress-responsive transcription factor, in endothelial cell differentiation and function. J. Cell Sci. 127, 1428–1440. https://doi.org/10.1242/jcs.136358

Fazeli, A., Dickinson, S.L., Hermiston, M.L., Tighe, R.V., Steen, R.G., Small, C.G., Stoeckli, E.T., Keino-Masu, K., Masu, M., Rayburn, H., Simons, J., Bronson, R.T., Gordon, J.I., Tessier-Lavigne, M., Weinberg, R.A., 1997. Phenotype of mice lacking functional Deleted in colorectal cancer (Dcc) gene. Nature 386, 796–804. https://doi.org/10.1038/386796a0

Fearon, E., Cho, K., Nigro, J., Kern, S., Simons, J., Ruppert, J., Hamilton, Preisinger, A., Thomas, G., Kinzler, K., et, al., 1990. Identification of a chromosome 18q gene that is altered in colorectal cancers. Science 247, 49–56. https://doi.org/10.1126/science.2294591

Feldman, B., Poueymirou, W., Papaioannou, V., DeChiara, T., Goldfarb, M., 1995. Requirement of FGF-4 for postimplantation mouse development. Science 267, 246–249. https://doi.org/10.1126/science.7809630

Ferré-D'Amaré, A.R., Pognonec, P., Roeder, R.G., Burley, S.K., 1994. Structure and function of the b/HLH/Z domain of USF. EMBO J. 13, 180–189.

Ferré-D'Amaré, A.R., Prendergast, G.C., Ziff, E.B., Burley, S.K., 1993. Recognition by Max of its cognate DNA through a dimeric b/HLH/Z domain. Nature 363, 38–45. https://doi.org/10.1038/363038a0

Ferrua, F., Cicalese, M.P., Galimberti, S., Giannelli, S., Dionisio, F., Barzaghi, F., Migliavacca, M., Bernardo, M.E., Calbi, V., Assanelli, A.A., Facchini, M., Fossati, C., Albertazzi, E., Scaramuzza, S., Brigida, I., Scala, S., Basso-Ricci, L., Pajno, R., Casiraghi, M., Canarutto, D., Salerio, F.A., Albert, M.H., Bartoli, A., Wolf, H.M., Fiori, R., Silvani, P., Gattillo, S., Villa, A., Biasco, L., Dott, C., Culme-Seymour, E.J., van Rossem, K., Atkinson, G., Valsecchi, M.G., Roncarolo, M.G., Ciceri, F., Naldini, L., Aiuti, A., 2019. Lentiviral haemopoietic stem/progenitor cell gene therapy for treatment of Wiskott-Aldrich syndrome: interim results of a non-randomised, open-label, phase 1/2 clinical study. Lancet Haematol. 6, e239–e253. https://doi.org/10.1016/S2352-3026(19)30021-3

Festuccia, N., Osorno, R., Halbritter, F., Karwacki-Neisius, V., Navarro, P., Colby, D., Wong, F., Yates, A., Tomlinson, S.R., Chambers, I., 2012. Esrrb Is a Direct Nanog Target Gene that Can Substitute for Nanog Function in Pluripotent Cells. Cell Stem Cell 11, 477–490. https://doi.org/10.1016/j.stem.2012.08.002

Fidler, I.J., 2003. The pathogenesis of cancer metastasis: the "seed and soil" hypothesis revisited. Nat. Rev. Cancer 3, 453–458. https://doi.org/10.1038/nrc1098

Finci, L., Zhang, Y., Meijers, R., Wang, J.-H., 2015. Signaling mechanism of the netrin-1 receptor DCC in axon guidance. Prog. Biophys. Mol. Biol. 118, 153–160. https://doi.org/10.1016/j.pbiomolbio.2015.04.001

Firnberg, N., Neubüser, A., 2002. FGF Signaling Regulates Expression of Tbx2, Erm, Pea3, and Pax3 in the Early Nasal Region. Dev. Biol. 247, 237–250. https://doi.org/10.1006/dbio.2002.0696

Fitamant, J., Guenebeaud, C., Coissieux, M.-M., Guix, C., Treilleux, I., Scoazec, J.-Y., Bachelot, T., Bernet, A., Mehlen, P., 2008. Netrin-1 expression confers a selective advantage for tumor cell survival in metastatic breast cancer. Proc. Natl. Acad. Sci. U. S. A. 105, 4850–4855. https://doi.org/10.1073/pnas.0709810105

Fitzgerald, D.P., Seaman, C., Cooper, H.M., 2006. Localization of Neogenin protein during morphogenesis in the mouse embryo. Dev. Dyn. 235, 1720–1725. https://doi.org/10.1002/dvdy.20744

Forcet, C., Stein, E., Pays, L., Corset, V., Llambi, F., Tessier-Lavigne, M., Mehlen, P., 2002. Netrin-1-mediated axon outgrowth requires deleted in colorectal cancer-dependent MAPK activation. Nature 417, 443–447. https://doi.org/10.1038/nature748

Francesconi, M., Di Stefano, B., Berenguer, C., de Andrés-Aguayo, L., Plana-Carmona, M., Mendez-Lago, M., Guillaumet-Adkins, A., Rodriguez-Esteban, G., Gut, M., Gut, I.G., Heyn, H., Lehner, B., Graf, T., 2019. Single cell RNA-seq identifies the origins of heterogeneity in efficient cell transdifferentiation and reprogramming. eLife 8, e41627. https://doi.org/10.7554/eLife.41627

Frankenberg, S., Gerbe, F., Bessonnard, S., Belville, C., Pouchin, P., Bardot, O., Chazaud, C., 2011. Primitive Endoderm Differentiates via a Three-Step Mechanism Involving Nanog and RTK Signaling. Dev. Cell 21, 1005–1013. https://doi.org/10.1016/j.devcel.2011.10.019

Freire, P., Vilela, M., Deus, H., Kim, Y.-W., Koul, D., Colman, H., Aldape, K.D., Bogler, O., Yung, W.K.A., Coombes, K., Mills, G.B., Vasconcelos, A.T., Almeida, J.S., 2008. Exploratory Analysis of the Copy Number Alterations in Glioblastoma Multiforme. PLoS ONE 3, e4076. https://doi.org/10.1371/journal.pone.0004076

Friedlander, S.Y.G., Chu, G.C., Snyder, E.L., Girnius, N., Dibelius, G., Crowley, D., Vasile, E., DePinho, R.A., Jacks, T., 2009. Context-Dependent Transformation of Adult Pancreatic Cells by Oncogenic K-Ras. Cancer Cell 16, 379–389. https://doi.org/10.1016/j.ccr.2009.09.027

Friedmann-Morvinski, D., Bushong, E.A., Ke, E., Soda, Y., Marumoto, T., Singer, O., Ellisman, M.H., Verma, I.M., 2012. Dedifferentiation of Neurons and Astrocytes by Oncogenes Can Induce Gliomas in Mice. Science 338, 1080–1084. https://doi.org/10.1126/science.1226929

Frum, T., Halbisen, M.A., Wang, C., Amiri, H., Robson, P., Ralston, A., 2013. Oct4 Cell-Autonomously Promotes Primitive Endoderm Development in the Mouse Blastocyst. Dev. Cell 25, 610–622. https://doi.org/10.1016/j.devcel.2013.05.004

Fujii, I., Matsukura, M., Ikezawa, M., Suzuki, S., Shimada, T., Miike, T., 2006. Adenoviral mediated MyoD gene transfer into fibroblasts: myogenic disease diagnosis. Brain Dev. 28, 420–425. https://doi.org/10.1016/j.braindev.2005.12.007

Gabay, M., Li, Y., Felsher, D.W., 2014. MYC Activation Is a Hallmark of Cancer Initiation and Maintenance. Cold Spring Harb. Perspect. Med. 4, a014241–a014241. https://doi.org/10.1101/cshperspect.a014241

Gad, J.M., Keeling, S.L., Wilks, A.F., Tan, S.-S., Cooper, H.M., 1997. The Expression Patterns of Guidance Receptors, DCC and Neogenin, Are Spatially and Temporally Distinct throughout Mouse Embryogenesis. Dev. Biol. 192, 258–273. https://doi.org/10.1006/dbio.1997.8756

Garcia-Sanz, P., Quintanilla, A., Lafita, M.C., Moreno-Bueno, G., García-Gutierrez, L., Tabor, V., Varela, I., Shiio, Y., Larsson, L.-G., Portillo, F., Leon, J., 2014. Sin3b Interacts with Myc and Decreases Myc Levels. J. Biol. Chem. 289, 22221–22236. https://doi.org/10.1074/jbc.M113.538744

Gaspar-Maia, A., Alajem, A., Polesso, F., Sridharan, R., Mason, M.J., Heidersbach, A., Ramalho-Santos, J., McManus, M.T., Plath, K., Meshorer, E., Ramalho-Santos, M., 2009. Chd1 regulates open chromatin and pluripotency of embryonic stem cells. Nature 460, 863–868. https://doi.org/10.1038/nature08212

Gearing, D.P., Thut, C.J., VandeBos, T., Gimpel, S.D., Delaney, P.B., King, J., Price, V., Cosman, D., Beckmann, M.P., 1991. Leukemia inhibitory factor receptor is structurally related to the IL-6 signal transducer, gp130. EMBO J. 10, 2839–2848.

Geisbrecht, B.V., Dowd, K.A., Barfield, R.W., Longo, P.A., Leahy, D.J., 2003. Netrin Binds Discrete Subdomains of DCC and UNC5 and Mediates Interactions between DCC and Heparin. J. Biol. Chem. 278, 32561–32568. https://doi.org/10.1074/jbc.M302943200

George, J., Uyar, A., Young, K., Kuffler, L., Waldron-Francis, K., Marquez, E., Ucar, D., Trowbridge, J.J., 2016. Leukaemia cell of origin identified by chromatin landscape of bulk tumour cells. Nat. Commun. 7, 12166. https://doi.org/10.1038/ncomms12166

Giagtzoglou, N., 2003. Two modes of recruitment of E(spl) repressors onto target genes. Development 130, 259–270. https://doi.org/10.1242/dev.00206

Godtfredsen, N.S., 2005. Effect of Smoking Reduction on Lung Cancer Risk. JAMA 294, 1505. https://doi.org/10.1001/jama.294.12.1505

Goetz, R., Mohammadi, M., 2013. Exploring mechanisms of FGF signalling through the lens of structural biology. Nat. Rev. Mol. Cell Biol. 14, 166–180. https://doi.org/10.1038/nrm3528

Goldschneider, D., Mehlen, P., 2010. Dependence receptors: a new paradigm in cell signaling and cancer therapy. Oncogene 29, 1865–1882. https://doi.org/10.1038/onc.2010.13

Golipour, A., David, L., Liu, Y., Jayakumaran, G., Hirsch, C.L., Trcka, D., Wrana, J.L., 2012. A Late Transition in Somatic Cell Reprogramming Requires Regulators Distinct from the Pluripotency Network. Cell Stem Cell 11, 769–782. https://doi.org/10.1016/j.stem.2012.11.008

Gradwohl, G., Dierich, A., LeMeur, M., Guillemot, F., 2000. neurogenin3 is required for the development of the four endocrine cell lineages of the pancreas. Proc. Natl. Acad. Sci. U. S. A. 97, 1607–1611. https://doi.org/10.1073/pnas.97.4.1607

Grandin, M., Meier, M., Delcros, J.G., Nikodemus, D., Reuten, R., Patel, T.R., Goldschneider, D., Orriss, G., Krahn, N., Boussouar, A., Abes, R., Dean, Y., Neves, D., Bernet, A., Depil, S., Schneiders, F., Poole, K., Dante, R., Koch, M., Mehlen, P., Stetefeld, J., 2016. Structural Decoding of the Netrin-1/UNC5 Interaction and its Therapeutical Implications in Cancers. Cancer Cell 29, 173–185. https://doi.org/10.1016/j.ccell.2016.01.001

Greber, B., Wu, G., Bernemann, C., Joo, J.Y., Han, D.W., Ko, K., Tapia, N., Sabour, D., Sterneckert, J., Tesar, P., Schöler, H.R., 2010. Conserved and Divergent Roles of FGF Signaling in Mouse Epiblast Stem Cells and Human Embryonic Stem Cells. Cell Stem Cell 6, 215–226. https://doi.org/10.1016/j.stem.2010.01.003

Green, A.C., Williams, G.M., Logan, V., Strutton, G.M., 2011. Reduced Melanoma After Regular Sunscreen Use: Randomized Trial Follow-Up. J. Clin. Oncol. 29, 257–263. https://doi.org/10.1200/JCO.2010.28.7078

Green, D.R., 2004. The Pathophysiology of Mitochondrial Cell Death. Science 305, 626–629. https://doi.org/10.1126/science.1099320

Grivennikov, S.I., Greten, F.R., Karin, M., 2010. Immunity, Inflammation, and Cancer. Cell 140, 883–899. https://doi.org/10.1016/j.cell.2010.01.025

Groden, J., Thliveris, A., Samowitz, W., Carlson, M., Gelbert, L., Albertsen, H., Joslyn, G., Stevens, J., Spirio, L., Robertson, M., 1991. Identification and characterization of the familial adenomatous polyposis coli gene. Cell 66, 589–600. https://doi.org/10.1016/0092-8674(81)90021-0

Grosse-Wilde, A., Fouquier d'Hérouël, A., McIntosh, E., Ertaylan, G., Skupin, A., Kuestner, R.E., del Sol, A., Walters, K.-A., Huang, S., 2015. Stemness of the hybrid Epithelial/Mesenchymal State in Breast Cancer and Its Association with Poor Survival. PLOS ONE 10, e0126522. https://doi.org/10.1371/journal.pone.0126522

Guccione, E., Martinato, F., Finocchiaro, G., Luzi, L., Tizzoni, L., Dall' Olio, V., Zardo, G., Nervi, C., Bernard, L., Amati, B., 2006. Myc-binding-site recognition in the human genome is determined by chromatin context. Nat. Cell Biol. 8, 764–770. https://doi.org/10.1038/ncb1434

Guo, G., Huss, M., Tong, G.Q., Wang, C., Li Sun, L., Clarke, N.D., Robson, P., 2010. Resolution of Cell Fate Decisions Revealed by Single-Cell Gene Expression Analysis from Zygote to Blastocyst. Dev. Cell 18, 675–685. https://doi.org/10.1016/j.devcel.2010.02.012

Guo, G., Yang, J., Nichols, J., Hall, J.S., Eyres, I., Mansfield, W., Smith, A., 2009. Klf4 reverts developmentally programmed restriction of ground state pluripotency. Development 136, 1063–1069. https://doi.org/10.1242/dev.030957

Guo, L., Lin, L., Wang, X., Gao, M., Cao, S., Mai, Y., Wu, F., Kuang, J., Liu, H., Yang, J., Chu, S., Song, H., Li, D., Liu, Y., Wu, K., Liu, Jiadong, Wang, J., Pan, G., Hutchins, A.P., Liu, Jing, Pei, D., Chen, J., 2019. Resolving Cell Fate Decisions during Somatic Cell Reprogramming by Single-Cell RNA-Seq. Mol. Cell 73, 815-829.e7. https://doi.org/10.1016/j.molcel.2019.01.042

Guo, W., Hao, B., Wang, Q., Lu, Y., Yue, J., 2013. Requirement of B-Raf, C-Raf, and A-Raf for the growth and survival of mouse embryonic stem cells. Exp. Cell Res. 319, 2801–2811. https://doi.org/10.1016/j.yexcr.2013.09.006

Gupta, P.B., Onder, T.T., Jiang, G., Tao, K., Kuperwasser, C., Weinberg, R.A., Lander, E.S., 2009. Identification of Selective Inhibitors of Cancer Stem Cells by High-Throughput Screening. Cell 138, 645–659. https://doi.org/10.1016/j.cell.2009.06.034

Gurdon, J.B., n.d. The Developmental Capacity of Nuclei taken from Intestinal Epithelium Cells of Feeding Tadpoles 20.

Habbe, N., Shi, G., Meguid, R.A., Fendrich, V., Esni, F., Chen, H., Feldmann, G., Stoffers, D.A., Konieczny, S.F., Leach, S.D., Maitra, A., 2008. Spontaneous induction of murine pancreatic intraepithelial neoplasia (mPanIN) by acinar cell targeting of oncogenic Kras in adult mice. Proc. Natl. Acad. Sci. 105, 18913–18918. https://doi.org/10.1073/pnas.0810097105

Hacein-Bey Abina, S., Gaspar, H.B., Blondeau, J., Caccavelli, L., Charrier, S., Buckland, K., Picard, C., Six, E., Himoudi, N., Gilmour, K., McNicol, A.-M., Hara, H., Xu-Bayford, J., Rivat, C., Touzot, F., Mavilio, F., Lim, A., Treluyer, J.-M., Héritier, S., Lefrère, F., Magalon, J., Pengue-Koyi, I., Honnet, G., Blanche, S., Sherman, E.A., Male, F., Berry, C., Malani, N., Bushman, F.D., Fischer, A., Thrasher, A.J., Galy, A., Cavazzana, M., 2015. Outcomes Following Gene Therapy in Patients With Severe Wiskott-Aldrich Syndrome. JAMA 313, 1550. https://doi.org/10.1001/jama.2015.3253

Hackett, J.A., Dietmann, S., Murakami, K., Down, T.A., Leitch, H.G., Surani, M.A., 2013. Synergistic Mechanisms of DNA Demethylation during Transition to Ground-State Pluripotency. Stem Cell Rep. 1, 518–531. https://doi.org/10.1016/j.stemcr.2013.11.010

Hackett, J.A., Surani, M.A., 2014. Regulatory Principles of Pluripotency: From the Ground State Up. Cell Stem Cell 15, 416–430. https://doi.org/10.1016/j.stem.2014.09.015

Haegel, H., Larue, L., Ohsugi, M., Fedorov, L., Herrenknecht, K., Kemler, R., 1995. Lack of beta-catenin affects mouse development at gastrulation. Dev. Camb. Engl. 121, 3529–3537.

Haeussler, M., Schönig, K., Eckert, H., Eschstruth, A., Mianné, J., Renaud, J.-B., Schneider-Maunoury, S., Shkumatava, A., Teboul, L., Kent, J., Joly, J.-S., Concordet, J.-P., 2016. Evaluation of off-target and on-target scoring algorithms and integration into the guide RNA selection tool CRISPOR. Genome Biol. 17, 148. https://doi.org/10.1186/s13059-016-1012-2

Hahn, W.C., Weinberg, R.A., 2002. Rules for Making Human Tumor Cells. N. Engl. J. Med. 347, 1593–1603. https://doi.org/10.1056/NEJMra021902

Halazonetis, T.D., Gorgoulis, V.G., Bartek, J., 2008. An Oncogene-Induced DNA Damage Model for Cancer Development. Science 319, 1352–1355. https://doi.org/10.1126/science.1140735

Hall, J., Guo, G., Wray, J., Eyres, I., Nichols, J., Grotewold, L., Morfopoulou, S., Humphreys, P., Mansfield, W., Walker, R., Tomlinson, S., Smith, A., 2009a. Oct4 and LIF/Stat3 Additively Induce Krüppel Factors to Sustain Embryonic Stem Cell Self-Renewal. Cell Stem Cell 5, 597–609. https://doi.org/10.1016/j.stem.2009.11.003

Hall, J., Guo, G., Wray, J., Eyres, I., Nichols, J., Grotewold, L., Morfopoulou, S., Humphreys, P., Mansfield, W., Walker, R., Tomlinson, S., Smith, A., 2009b. Oct4 and LIF/Stat3 Additively Induce Krüppel Factors to Sustain Embryonic Stem Cell Self-Renewal. Cell Stem Cell 5, 597–609. https://doi.org/10.1016/j.stem.2009.11.003

Han, J., Yuan, P., Yang, H., Zhang, J., Soh, B.S., Li, P., Lim, S.L., Cao, S., Tay, J., Orlov, Y.L., Lufkin, T., Ng, H.-H., Tam, W.-L., Lim, B., 2010. Tbx3 improves the germ-line competency of induced pluripotent stem cells. Nature 463, 1096–1100. https://doi.org/10.1038/nature08735

Han, Z.-Y., Richer, W., Fréneaux, P., Chauvin, C., Lucchesi, C., Guillemot, D., Grison, C., Lequin, D., Pierron, G., Masliah-Planchon, J., Nicolas, A., Ranchère-Vince, D., Varlet, P., Puget, S., Janoueix-Lerosey, I., Ayrault, O., Surdez, D., Delattre, O., Bourdeaut, F., 2016. The occurrence of intracranial rhabdoid tumours in mice depends on temporal control of Smarcb1 inactivation. Nat. Commun. 7, 10421.

Hanahan, D., Weinberg, R.A., 2011a. Hallmarks of Cancer: The Next Generation. Cell 144, 646–674. https://doi.org/10.1016/j.cell.2011.02.013

Hanahan, D., Weinberg, R.A., 2011b. Hallmarks of Cancer: The Next Generation. Cell 144, 646–674. https://doi.org/10.1016/j.cell.2011.02.013

Hanna, J., Markoulaki, S., Mitalipova, M., Cheng, A.W., Cassady, J.P., Staerk, J., Carey, B.W., Lengner, C.J., Foreman, R., Love, J., Gao, Q., Kim, J., Jaenisch, R., 2009a. Metastable Pluripotent States in NOD-Mouse-Derived ESCs. Cell Stem Cell 4, 513–524. https://doi.org/10.1016/j.stem.2009.04.015

Hanna, J., Saha, K., Pando, B., van Zon, J., Lengner, C.J., Creyghton, M.P., van Oudenaarden, A., Jaenisch, R., 2009b. Direct cell reprogramming is a stochastic process amenable to acceleration. Nature 462, 595–601. https://doi.org/10.1038/nature08592

Hansson, J., Rafiee, M.R., Reiland, S., Polo, J.M., Gehring, J., Okawa, S., Huber, W., Hochedlinger, K., Krijgsveld, J., 2012. Highly Coordinated Proteome Dynamics during Reprogramming of Somatic Cells to Pluripotency. Cell Rep. 2, 1579–1592. https://doi.org/10.1016/j.celrep.2012.10.014

Hart, M.J., de los Santos, R., Albert, I.N., Rubinfeld, B., Polakis, P., 1998. Downregulation of β-catenin by human Axin and its association with the APC tumor suppressor, β-catenin and GSK3β. Curr. Biol. 8, 573–581. https://doi.org/10.1016/S0960-9822(98)70226-X

Hayashi, K., Lopes, S.M.C. de S., Tang, F., Surani, M.A., 2008. Dynamic Equilibrium and Heterogeneity of Mouse Pluripotent Stem Cells with Distinct Functional and Epigenetic States. Cell Stem Cell 3, 391–401. https://doi.org/10.1016/j.stem.2008.07.027

He, T., 1998. Identification of c-MYC as a Target of the APC Pathway. Science 281, 1509–1512. https://doi.org/10.1126/science.281.5382.1509

Hedgecock, E.M., Culotti, J.G., Hall, D.H., 1990. The unc-5, unc-6, and unc-40 genes guide circumferential migrations of pioneer axons and mesodermal cells on the epidermis in C. elegans. Neuron 4, 61–85. https://doi.org/10.1016/0896-6273(90)90444-K

Heisenberg, C.-P., Bellaïche, Y., 2013. Forces in Tissue Morphogenesis and Patterning. Cell 153, 948–962. https://doi.org/10.1016/j.cell.2013.05.008

Heng, J.-C.D., Feng, B., Han, J., Jiang, J., Kraus, P., Ng, J.-H., Orlov, Y.L., Huss, M., Yang, L., Lufkin, T., Lim, B., Ng, H.-H., 2010. The Nuclear Receptor Nr5a2 Can Replace Oct4 in the Reprogramming of Murine Somatic Cells to Pluripotent Cells. Cell Stem Cell 6, 167–174. https://doi.org/10.1016/j.stem.2009.12.009

Hermitte, S., Chazaud, C., 2014. Primitive endoderm differentiation: from specification to epithelium formation. Philos. Trans. R. Soc. B Biol. Sci. 369, 20130537. https://doi.org/10.1098/rstb.2013.0537

Herreros-Villanueva, M., Zhang, J.-S., Koenig, A., Abel, E.V., Smyrk, T.C., Bamlet, W.R., de Narvajas, A. a.-M., Gomez, T.S., Simeone, D.M., Bujanda, L., Billadeau, D.D., 2013. SOX2 promotes dedifferentiation and imparts stem cell-like features to pancreatic cancer cells. Oncogenesis 2, e61. https://doi.org/10.1038/oncsis.2013.23

Hezel, A.F., Kimmelman, A.C., Stanger, B.Z., Bardeesy, N., Depinho, R.A., 2006. Genetics and biology of pancreatic ductal adenocarcinoma. Genes Dev. 20, 1218–1249. https://doi.org/10.1101/gad.1415606

Hirate, Y., Hirahara, S., Inoue, K., Suzuki, A., Alarcon, V.B., Akimoto, K., Hirai, T., Hara, T., Adachi, M., Chida, K., Ohno, S., Marikawa, Y., Nakao, K., Shimono, A., Sasaki, H., 2013. Polarity-Dependent Distribution of Angiomotin Localizes Hippo Signaling in Preimplantation Embryos. Curr. Biol. 23, 1181–1194. https://doi.org/10.1016/j.cub.2013.05.014

Hochedlinger, K., Plath, K., 2009. Epigenetic reprogramming and induced pluripotency. Development 136, 509–523. https://doi.org/10.1242/dev.020867

Holderfield, M., Deuker, M.M., McCormick, F., McMahon, M., 2014. Targeting RAF kinases for cancer therapy: BRAF-mutated melanoma and beyond. Nat. Rev. Cancer 14, 455–467. https://doi.org/10.1038/nrc3760

Hondo, E., Stewart, C.L., 2004. Profiling gene expression in growth-arrested mouse embryos in diapause. Genome Biol. 6, 202. https://doi.org/10.1186/gb-2004-6-1-202

Hong, K., Hinck, L., Nishiyama, M., Poo, M., Tessier-Lavigne, M., Stein, E., 1999. A Ligand-Gated Association between Cytoplasmic Domains of UNC5 and DCC Family Receptors Converts Netrin-Induced Growth Cone Attraction to Repulsion. Cell 97, 927–941. https://doi.org/10.1016/S0092-8674(00)80804-1

Hou, P., Li, Y., Zhang, X., Liu, C., Guan, J., Li, H., Zhao, T., Ye, J., Yang, W., Liu, K., Ge, J., Xu, J., Zhang, Q., Zhao, Y., Deng, H., 2013. Pluripotent Stem Cells Induced from Mouse Somatic Cells by Small-Molecule Compounds. Science 341, 651–654. https://doi.org/10.1126/science.1239278

Huang, G., Yan, H., Ye, S., Tong, C., Ying, Q.-L., 2014. STAT3 Phosphorylation at Tyrosine 705 and Serine 727 Differentially Regulates Mouse ESC Fates: STAT3 Phosphorylation Regulates ESC Fates. STEM CELLS 32, 1149–1160. https://doi.org/10.1002/stem.1609

Huang, Y., Osorno, R., Tsakiridis, A., Wilson, V., 2012. In Vivo Differentiation Potential of Epiblast Stem Cells Revealed by Chimeric Embryo Formation. Cell Rep. 2, 1571–1578. https://doi.org/10.1016/j.celrep.2012.10.022

Huangfu, D., Maehr, R., Guo, W., Eijkelenboom, A., Snitow, M., Chen, A.E., Melton, D.A., 2008. Induction of pluripotent stem cells by defined factors is greatly improved by small-molecule compounds. Nat. Biotechnol. 26, 795–797. https://doi.org/10.1038/nbt1418

Huelsken, J., Vogel, R., Brinkmann, V., Erdmann, B., Birchmeier, C., Birchmeier, W., 2000. Requirement for beta-catenin in anterior-posterior axis formation in mice. J. Cell Biol. 148, 567–578. https://doi.org/10.1083/jcb.148.3.567

Hugo, H., Ackland, M.L., Blick, T., Lawrence, M.G., Clements, J.A., Williams, E.D., Thompson, E.W., 2007. Epithelial—mesenchymal and mesenchymal—epithelial transitions in carcinoma progression. J. Cell. Physiol. 213, 374–383. https://doi.org/10.1002/jcp.21223

Huynh, H., Zheng, J., Umikawa, M., Zhang, C., Silvany, R., Iizuka, S., Holzenberger, M., Zhang, W., Zhang, C.C., 2011. IGF binding protein 2 supports the survival and cycling of hematopoietic stem cells. Blood 118, 3236–3243. https://doi.org/10.1182/blood-2011-01-331876

Hvid-Jensen, F., Pedersen, L., Drewes, A.M., Sørensen, H.T., Funch-Jensen, P., 2011. Incidence of Adenocarcinoma among Patients with Barrett's Esophagus. N. Engl. J. Med. 365, 1375–1383. https://doi.org/10.1056/NEJMoa1103042

Hydbring, P., Castell, A., Larsson, L.-G., 2017. MYC Modulation around the CDK2/p27/SKP2 Axis. Genes 8, 174. https://doi.org/10.3390/genes8070174

Imayoshi, I., Kageyama, R., 2014. bHLH factors in self-renewal, multipotency, and fate choice of neural progenitor cells. Neuron 82, 9–23. https://doi.org/10.1016/j.neuron.2014.03.018

Imayoshi, I., Shimogori, T., Ohtsuka, T., Kageyama, R., 2008. Hes genes and neurogenin regulate non-neural versus neural fate specification in the dorsal telencephalic midline. Development 135, 2531–2541. https://doi.org/10.1242/dev.021535

Inoue, C., Bae, S.K., Takatsuka, K., Inoue, T., Bessho, Y., Kageyama, R., 2001. Math6, a bHLH gene expressed in the developing nervous system, regulates neuronal versus glial differentiation. Genes Cells Devoted Mol. Cell. Mech. 6, 977–986.

Ischenko, I., Zhi, J., Moll, U.M., Nemajerova, A., Petrenko, O., 2013. Direct reprogramming by oncogenic Ras and Myc. Proc. Natl. Acad. Sci. U. S. A. 110, 3937–3942. https://doi.org/10.1073/pnas.1219592110

Ito, S., D'Alessio, A.C., Taranova, O.V., Hong, K., Sowers, L.C., Zhang, Y., 2010. Role of Tet proteins in 5mC to 5hmC conversion, ES-cell self-renewal and inner cell mass specification. Nature 466, 1129–1133. https://doi.org/10.1038/nature09303

Itzen, F., Greifenberg, A.K., Bösken, C.A., Geyer, M., 2014. Brd4 activates P-TEFb for RNA polymerase II CTD phosphorylation. Nucleic Acids Res. 42, 7577–7590. https://doi.org/10.1093/nar/gku449

Jackson, E.L., Willis, N., Mercer, K., Bronson, R.T., Crowley, D., Montoya, R., Jacks, T., Tuveson, D.A., 2001. Analysis of lung tumor initiation and progression using conditional expression of oncogenic K-ras. Genes Dev. 15, 3243–3248. https://doi.org/10.1101/gad.943001

Jackson, M., Krassowska, A., Gilbert, N., Chevassut, T., Forrester, L., Ansell, J., Ramsahoye, B., 2004. Severe Global DNA Hypomethylation Blocks Differentiation and Induces Histone Hyperacetylation in Embryonic Stem Cells. Mol. Cell. Biol. 24, 8862–8871. https://doi.org/10.1128/MCB.24.20.8862-8871.2004

Jähner, D., Stuhlmann, H., Stewart, C.L., Harbers, K., Löhler, J., Simon, I., Jaenisch, R., 1982. De novo methylation and expression of retroviral genomes during mouse embryogenesis. Nature 298, 623–628. https://doi.org/10.1038/298623a0

Jarriault, S., Schwab, Y., Greenwald, I., 2008. A Caenorhabditis elegans model for epithelial-neuronal transdifferentiation. Proc. Natl. Acad. Sci. 105, 3790–3795. https://doi.org/10.1073/pnas.0712159105

Ji, P., Jiang, H., Rekhtman, K., Bloom, J., Ichetovkin, M., Pagano, M., Zhu, L., 2004. An Rb-Skp2-p27 Pathway Mediates Acute Cell Cycle Inhibition by Rb and Is Retained in a Partial-Penetrance Rb Mutant. Mol. Cell 16, 47–58. https://doi.org/10.1016/j.molcel.2004.09.029

Jiang, B.-H., Liu, L.-Z., 2009. PI3K/PTEN signaling in angiogenesis and tumorigenesis. Adv. Cancer Res. 102, 19–65. https://doi.org/10.1016/S0065-230X(09)02002-8

Jiang, Y., Liu, M., Gershon, M.D., 2003. Netrins and DCC in the guidance of migrating neural crest-derived cells in the developing bowel and pancreas. Dev. Biol. 258, 364–384. https://doi.org/10.1016/S0012-1606(03)00136-2

Junge, H.J., Yung, A.R., Goodrich, L.V., Chen, Z., 2016. Netrin1/DCC signaling promotes neuronal migration in the dorsal spinal cord. Neural Develop. 11, 19. https://doi.org/10.1186/s13064-016-0074-x

Kadoshima, T., Sakaguchi, H., Nakano, T., Soen, M., Ando, S., Eiraku, M., Sasai, Y., 2013. Self-organization of axial polarity, inside-out layer pattern, and species-specific progenitor dynamics in human ES cell-derived neocortex. Proc. Natl. Acad. Sci. 110, 20284–20289. https://doi.org/10.1073/pnas.1315710110

Kalkat, M., De Melo, J., Hickman, K., Lourenco, C., Redel, C., Resetca, D., Tamachi, A., Tu, W., Penn, L., 2017. MYC Deregulation in Primary Human Cancers. Genes 8, 151. https://doi.org/10.3390/genes8060151

Kang, J.-S., Yi, M.-J., Zhang, W., Feinleib, J.L., Cole, F., Krauss, R.S., 2004. Netrins and neogenin promote myotube formation. J. Cell Biol. 167, 493–504. https://doi.org/10.1083/jcb.200405039

Kang, M., Piliszek, A., Artus, J., Hadjantonakis, A.-K., 2013. FGF4 is required for lineage restriction and salt-and-pepper distribution of primitive endoderm factors but not their initial expression in the mouse. Development 140, 267–279. https://doi.org/10.1242/dev.084996

Kappler, J., Franken, S., Junghans, U., Hoffmann, R., Linke, T., Müller, H.W., Koch, K.-W., 2000. Glycosaminoglycan-Binding Properties and Secondary Structure of the C-Terminus of Netrin-1. Biochem. Biophys. Res. Commun. 271, 287–291. https://doi.org/10.1006/bbrc.2000.2583

Kareta, M.S., Gorges, L.L., Hafeez, S., Benayoun, B.A., Marro, S., Zmoos, A.-F., Cecchini, M.J., Spacek, D., Batista, L.F.Z., O'Brien, M., Ng, Y.-H., Ang, C.E., Vaka, D., Artandi, S.E., Dick, F.A., Brunet, A., Sage, J., Wernig, M., 2015. Inhibition of pluripotency networks by the Rb tumor suppressor restricts reprogramming and tumorigenesis. Cell Stem Cell 16, 39–50. https://doi.org/10.1016/j.stem.2014.10.019

Karwacki-Neisius, V., Göke, J., Osorno, R., Halbritter, F., Ng, J.H., Weiße, A.Y., Wong, F.C.K., Gagliardi, A., Mullin, N.P., Festuccia, N., Colby, D., Tomlinson, S.R., Ng, H.-H., Chambers, I., 2013. Reduced Oct4 Expression Directs a Robust Pluripotent State with Distinct Signaling Activity and Increased Enhancer Occupancy by Oct4 and Nanog. Cell Stem Cell 12, 531–545. https://doi.org/10.1016/j.stem.2013.04.023

Kautz, L., Meynard, D., Monnier, A., Darnaud, V., Bouvet, R., Wang, R.-H., Deng, C., Vaulont, S., Mosser, J., Coppin, H., Roth, M.-P., 2008. Iron regulates phosphorylation of Smad1/5/8 and gene expression of Bmp6, Smad7, Id1, and Atoh8 in the mouse liver. Blood 112, 1503–1509. https://doi.org/10.1182/blood-2008-03-143354

Kawamura, T., Suzuki, J., Wang, Y.V., Menendez, S., Morera, L.B., Raya, A., Wahl, G.M., Izpisúa Belmonte, J.C., 2009. Linking the p53 tumour suppressor pathway to somatic cell reprogramming. Nature 460, 1140–1144. https://doi.org/10.1038/nature08311

Kazerounian, S., Yee, K.O., Lawler, J., 2008. Thrombospondins: from structure to therapeutics: Thrombospondins in cancer. Cell. Mol. Life Sci. 65, 700–712. https://doi.org/10.1007/s00018-007-7486-z

Keeling, S.L., Gad, J.M., Cooper, H.M., 1997. Mouse Neogenin, a DCC-like molecule, has four splice variants and is expressed widely in the adult mouse and during embryogenesis. Oncogene 15, 691–700. https://doi.org/10.1038/sj.onc.1201225

Kefeli, U., Ucuncu Kefeli, A., Cabuk, D., Isik, U., Sonkaya, A., Acikgoz, O., Ozden, E., Uygun, K., 2017. Netrin-1 in cancer: Potential biomarker and therapeutic target? Tumor Biol. 39, 101042831769838. https://doi.org/10.1177/1010428317698388

Keino-Masu, K., Masu, M., Hinck, L., Leonardo, E.D., Chan, S.S.-Y., Culotti, J.G., Tessier-Lavigne, M., 1996. Deleted in Colorectal Cancer (DCC) Encodes a Netrin Receptor. Cell 87, 175–185. https://doi.org/10.1016/S0092-8674(00)81336-7

Kelly, K.F., Ng, D.Y., Jayakumaran, G., Wood, G.A., Koide, H., Doble, B.W., 2011. β-Catenin Enhances Oct-4 Activity and Reinforces Pluripotency through a TCF-Independent Mechanism. Cell Stem Cell 8, 214–227. https://doi.org/10.1016/j.stem.2010.12.010

Kerkhoff, E., Houben, R., Löffler, S., Troppmair, J., Lee, J.-E., Rapp, U.R., 1998. Regulation of c-myc expression by Ras/Raf signalling. Oncogene 16, 211–216. https://doi.org/10.1038/sj.onc.1201520

Kielman, M.F., Rindapää, M., Gaspar, C., van Poppel, N., Breukel, C., van Leeuwen, S., Taketo, M.M., Roberts, S., Smits, R., Fodde, R., 2002. Apc modulates embryonic stem-cell differentiation by controlling the dosage of β-catenin signaling. Nat. Genet. 32, 594–605. https://doi.org/10.1038/ng1045

Kim, J., Woo, A.J., Chu, J., Snow, J.W., Fujiwara, Y., Kim, C.G., Cantor, A.B., Orkin, S.H., 2010. A Myc Network Accounts for Similarities between Embryonic Stem and Cancer Cell Transcription Programs. Cell 143, 313–324. https://doi.org/10.1016/j.cell.2010.09.010

Kim, K., Zhao, R., Doi, A., Ng, K., Unternaehrer, J., Cahan, P., Hongguang, H., Loh, Y.-H., Aryee, M.J., Lensch, M.W., Li, H., Collins, J.J., Feinberg, A.P., Daley, G.Q., 2011. Donor cell type can influence the epigenome and differentiation potential of human induced pluripotent stem cells. Nat. Biotechnol. 29, 1117–1119. https://doi.org/10.1038/nbt.2052

Kim, M.O., Kim, S.-H., Cho, Y.-Y., Nadas, J., Jeong, C.-H., Yao, K., Kim, D.J., Yu, D.-H., Keum, Y.-S., Lee, K.-Y., Huang, Z., Bode, A.M., Dong, Z., 2012. ERK1 and ERK2 regulate embryonic stem cell self-renewal through phosphorylation of Klf4. Nat. Struct. Mol. Biol. 19, 283–290. https://doi.org/10.1038/nsmb.2217

Kim, S.-Y., Kang, J.W., Song, X., Kim, B.K., Yoo, Y.D., Kwon, Y.T., Lee, Y.J., 2013. Role of the IL-6-JAK1-STAT3-Oct-4 pathway in the conversion of non-stem cancer cells into cancer stem-like cells. Cell. Signal. 25, 961–969. https://doi.org/10.1016/j.cellsig.2013.01.007

Kinzler, K.W., Vogelstein, B., 1997. Gatekeepers and caretakers. Nature 386, 761–763. https://doi.org/10.1038/386761a0

Kleinsmith, L.J., Pierce, G.B., 1964. Multipotentiality of Single Embryonal Carcinoma Cells. Cancer Res. 24, 1544–1551.

Knaupp, A.S., Buckberry, S., Pflueger, J., Lim, S.M., Ford, E., Larcombe, M.R., Rossello, F.J., de Mendoza, A., Alaei, S., Firas, J., Holmes, M.L., Nair, S.S., Clark, S.J., Nefzger, C.M., Lister, R., Polo, J.M., 2017. Transient and Permanent Reconfiguration of Chromatin and Transcription Factor Occupancy Drive Reprogramming. Cell Stem Cell 21, 834-845.e6. https://doi.org/10.1016/j.stem.2017.11.007

Knoepfler, P.S., 2002. N-myc is essential during neurogenesis for the rapid expansion of progenitor cell populations and the inhibition of neuronal differentiation. Genes Dev. 16, 2699–2712. https://doi.org/10.1101/gad.1021202

Koche, R.P., Smith, Z.D., Adli, M., Gu, H., Ku, M., Gnirke, A., Bernstein, B.E., Meissner, A., 2011. Reprogramming Factor Expression Initiates Widespread Targeted Chromatin Remodeling. Cell Stem Cell 8, 96–105. https://doi.org/10.1016/j.stem.2010.12.001

Kopp, J.L., Dubois, C.L., Schaeffer, D.F., Samani, A., Taghizadeh, F., Cowan, R.W., Rhim, A.D., Stiles, B.L., Valasek, M., Sander, M., 2018. Loss of Pten and Activation of Kras Synergistically Induce Formation of Intraductal Papillary Mucinous Neoplasia From Pancreatic Ductal Cells in Mice. Gastroenterology 154, 1509-1523.e5. https://doi.org/10.1053/j.gastro.2017.12.007

Kopp, J.L., von Figura, G., Mayes, E., Liu, F.-F., Dubois, C.L., Morris, J.P., Pan, F.C., Akiyama, H., Wright, C.V.E., Jensen, K., Hebrok, M., Sander, M., 2012. Identification of Sox9-Dependent Acinar-to-Ductal Reprogramming as the Principal Mechanism for Initiation of Pancreatic Ductal Adenocarcinoma. Cancer Cell 22, 737–750. https://doi.org/10.1016/j.ccr.2012.10.025

Kouhara, H., Hadari, Y.R., Spivak-Kroizman, T., Schilling, J., Bar-Sagi, D., Lax, I., Schlessinger, J., 1997. A Lipid-Anchored Grb2-Binding Protein That Links FGF-Receptor Activation to the Ras/MAPK Signaling Pathway. Cell 89, 693–702. https://doi.org/10.1016/S0092-8674(00)80252-4

Koutsourakis, M., Langeveld, A., Patient, R., Beddington, R., Grosveld, F., 1999. The transcription factor GATA6 is essential for early extraembryonic development. Dev. Camb. Engl. 126, 723–732.

Krah, N.M., De La O, J.-P., Swift, G.H., Hoang, C.Q., Willet, S.G., Chen Pan, F., Cash, G.M., Bronner, M.P., Wright, C.V., MacDonald, R.J., Murtaugh, L.C., 2015. The acinar differentiation determinant PTF1A inhibits initiation of pancreatic ductal adenocarcinoma. eLife 4, e07125. https://doi.org/10.7554/eLife.07125

Kretzschmar, M., Doody, J., Massagu, J., 1997. Opposing BMP and EGF signalling pathways converge on the TGF-β family mediator Smad1. Nature 389, 618–622. https://doi.org/10.1038/39348

Kubo, F., Nakagawa, S., 2010. Cath6, a bHLH atonal family proneural gene, negatively regulates neuronal differentiation in the retina. Dev. Dyn. 239, 2492–2500. https://doi.org/10.1002/dvdy.22381
Kumar, R., DiMenna, L., Schrode, N., Liu, T.-C., Franck, P., Muñoz-Descalzo, S., Hadjantonakis, A.-K., Zarrin, A.A., Chaudhuri, J., Elemento, O., Evans, T., 2013. AID stabilizes stem-cell phenotype by removing epigenetic memory of pluripotency genes. Nature 500, 89–92. https://doi.org/10.1038/nature12299
Kunath, T., Saba-El-Leil, M.K., Almousailleakh, M., Wray, J., Meloche, S., Smith, A., 2007. FGF stimulation of the Erk1/2 signalling cascade triggers transition of pluripotent embryonic stem cells from self-renewal to lineage commitment. Development 134, 2895–2902. https://doi.org/10.1242/dev.02880
Kurland, J.F., Tansey, W.P., 2008. Myc-Mediated Transcriptional Repression by Recruitment of Histone Deacetylase. Cancer Res. 68, 3624–3629. https://doi.org/10.1158/0008-5472.CAN-07-6552
Lai, Y.-S., Chang, C.-W., Pawlik, K.M., Zhou, D., Renfrow, M.B., Townes, T.M., 2012. SRY (sex determining region Y)-box2 (Sox2)/poly ADP-ribose polymerase 1 (Parp1) complexes regulate pluripotency. Proc. Natl. Acad. Sci. 109, 3772–3777. https://doi.org/10.1073/pnas.1108595109
Land, H., Parada, L.F., Weinberg, R.A., 1983. Tumorigenic conversion of primary embryo fibroblasts requires at least two cooperating oncogenes. Nature 304, 596–602. https://doi.org/10.1038/304596a0
Lane, D.P., 1992. p53, guardian of the genome. Nature 358, 15–16. https://doi.org/10.1038/358015a0
Lanner, F., Lee, K.L., Sohl, M., Holmborn, K., Yang, H., Wilbertz, J., Poellinger, L., Rossant, J., Farnebo, F., 2009. Heparan Sulfation Dependent FGF Signalling Maintains Embryonic Stem Cells Primed for Differentiation in a Heterogeneous State. Stem Cells N/A-N/A. https://doi.org/10.1002/stem.265
Lapidot, T., Sirard, C., Vormoor, J., Murdoch, B., Hoang, T., Caceres-Cortes, J., Minden, M., Paterson, B., Caligiuri, M.A., Dick, J.E., 1994. A cell initiating human acute myeloid leukaemia after transplantation into SCID mice. Nature 367, 645–648. https://doi.org/10.1038/367645a0
Larrieu-Lahargue, F., Welm, A.L., Thomas, K.R., Li, D.Y., 2010. Netrin-4 induces lymphangiogenesis in vivo. Blood 115, 5418–5426. https://doi.org/10.1182/blood-2009-11-252338
Larrivee, B., Freitas, C., Trombe, M., Lv, X., DeLafarge, B., Yuan, L., Bouvree, K., Breant, C., Del Toro, R., Brechot, N., Germain, S., Bono, F., Dol, F., Claes, F., Fischer, C., Autiero, M., Thomas, J.-L., Carmeliet, P., Tessier-Lavigne, M., Eichmann, A., 2007. Activation of the UNC5B receptor by Netrin-1 inhibits sprouting angiogenesis. Genes Amp Dev. 21, 2433–2447. https://doi.org/10.1101/gad.437807
Latil, A., Chêne, L., Cochant-Priollet, B., Mangin, P., Fournier, G., Berthon, P., Cussenot, O., 2003. Quantification of expression of netrins, slits and their receptors in human prostate tumors: Netrins, Slits and Prostate Cancer. Int. J. Cancer 103, 306–315. https://doi.org/10.1002/ijc.10821
Lebrand, C., Dent, E.W., Strasser, G.A., Lanier, L.M., Krause, M., Svitkina, T.M., Borisy, G.G., Gertler, F.B., 2004. Critical Role of Ena/VASP Proteins for Filopodia Formation in Neurons and in Function Downstream of Netrin-1. Neuron 42, 37–49. https://doi.org/10.1016/S0896-6273(04)00108-4
Leder, A., Pattengale, P.K., Kuo, A., Stewart, T.A., Leder, P., 1986. Consequences of widespread deregulation of the c-myc gene in transgenic mice: Multiple neoplasms and normal development. Cell 45, 485–495. https://doi.org/10.1016/0092-8674(86)90280-1
Lee, K.L., Lim, S.K., Orlov, Y.L., Yit, L.Y., Yang, H., Ang, L.T., Poellinger, L., Lim, B., 2011. Graded Nodal/Activin Signaling Titrates Conversion of Quantitative Phospho-Smad2 Levels into Qualitative Embryonic Stem Cell Fate Decisions. PLoS Genet. 7, e1002130. https://doi.org/10.1371/journal.pgen.1002130
Lee, S.S., Lee, S.-J., Lee, S.H., Ryu, J.M., Lim, H.S., Kim, J.S., Song, E.J., Jung, Y.H., Lee, H.J., Kim, C.H., Han, H.J., 2016. Netrin-1-Induced Stem Cell Bioactivity Contributes to the Regeneration of Injured Tissues via the Lipid Raft-Dependent Integrin α6β4 Signaling Pathway. Sci. Rep. 6, 37526. https://doi.org/10.1038/srep37526
Lefebvre, V., Dumitriu, B., Penzo-Méndez, A., Han, Y., Pallavi, B., 2007. Control of cell fate and differentiation by Sry-related high-mobility-group box (Sox) transcription factors. Int. J. Biochem. Cell Biol. 39, 2195–2214. https://doi.org/10.1016/j.biocel.2007.05.019
Leitch, H.G., McEwen, K.R., Turp, A., Encheva, V., Carroll, T., Grabole, N., Mansfield, W., Nashun, B., Knezovich, J.G., Smith, A., Surani, M.A., Hajkova, P., 2013. Naive pluripotency is associated with global DNA hypomethylation. Nat. Struct. Mol. Biol. 20, 311–316. https://doi.org/10.1038/nsmb.2510
Leonardo, E.D., Hinck, L., Masu, M., Keino-Masu, K., Ackerman, S.L., Tessier-Lavigne, M., 1997. Vertebrate homologues of C. elegans UNC-5 are candidate netrin receptors. Nature 386, 833–838. https://doi.org/10.1038/386833a0
Leow, C.C., Romero, M.S., Ross, S., Polakis, P., Gao, W.-Q., 2004. Hath1, down-regulated in colon adenocarcinomas, inhibits proliferation and tumorigenesis of colon cancer cells. Cancer Res. 64, 6050–6057. https://doi.org/10.1158/0008-5472.CAN-04-0290

Levy-Strumpf, N., Culotti, J.G., 2014. Netrins and Wnts Function Redundantly to Regulate Antero-Posterior and Dorso-Ventral Guidance in C. elegans. PLoS Genet. 10, e1004381. https://doi.org/10.1371/journal.pgen.1004381

Levy-Strumpf, N., Krizus, M., Zheng, H., Brown, L., Culotti, J.G., 2015. The Wnt Frizzled Receptor MOM-5 Regulates the UNC-5 Netrin Receptor through Small GTPase-Dependent Signaling to Determine the Polarity of Migrating Cells. PLOS Genet. 11, e1005446. https://doi.org/10.1371/journal.pgen.1005446

Li, H., Collado, M., Villasante, A., Strati, K., Ortega, S., Cañamero, M., Blasco, M.A., Serrano, M., 2009. The Ink4/Arf locus is a barrier for iPS cell reprogramming. Nature 460, 1136–1139. https://doi.org/10.1038/nature08290

Li, P., Tong, C., Mehrian-Shai, R., Jia, L., Wu, N., Yan, Y., Maxson, R.E., Schulze, E.N., Song, H., Hsieh, C.-L., Pera, M.F., Ying, Q.-L., 2008. Germline Competent Embryonic Stem Cells Derived from Rat Blastocysts. Cell 135, 1299–1310. https://doi.org/10.1016/j.cell.2008.12.006

Li, R., Liang, J., Ni, S., Zhou, T., Qing, X., Li, H., He, W., Chen, J., Li, F., Zhuang, Q., Qin, B., Xu, J., Li, W., Yang, J., Gan, Y., Qin, D., Feng, S., Song, H., Yang, D., Zhang, B., Zeng, L., Lai, L., Esteban, M.A., Pei, D., 2010. A Mesenchymal-to-Epithelial Transition Initiates and Is Required for the Nuclear Reprogramming of Mouse Fibroblasts. Cell Stem Cell 7, 51–63. https://doi.org/10.1016/j.stem.2010.04.014

Li, W., Lee, J., Vikis, H.G., Lee, S.-H., Liu, G., Aurandt, J., Shen, T.-L., Fearon, E.R., Guan, J.-L., Han, M., Rao, Y., Hong, K., Guan, K.-L., 2004. Activation of FAK and Src are receptor-proximal events required for netrin signaling. Nat. Neurosci. 7, 1213–1221. https://doi.org/10.1038/nn1329

Li, X., Meriane, M., Triki, I., Shekarabi, M., Kennedy, T.E., Larose, L., Lamarche-Vane, N., 2002. The Adaptor Protein Nck-1 Couples the Netrin-1 Receptor DCC (Deleted in Colorectal Cancer) to the Activation of the Small GTPase Rac1 through an Atypical Mechanism. J. Biol. Chem. 277, 37788–37797. https://doi.org/10.1074/jbc.M205428200

Li, Y., Li, H., Zhang, L., Xiong, S., Wen, S., Xia, X., Zhou, X., 2019. Growth/differentiation 5 promotes the differentiation of retinal stem cells into neurons via Atoh8. J. Cell. Physiol. 234, 21307–21315. https://doi.org/10.1002/jcp.28735

Li, Z., Fei, T., Zhang, J., Zhu, G., Wang, L., Lu, D., Chi, X., Teng, Y., Hou, N., Yang, X., Zhang, H., Han, J.-D.J., Chen, Y.-G., 2012. BMP4 Signaling Acts via Dual-Specificity Phosphatase 9 to Control ERK Activity in Mouse Embryonic Stem Cells. Cell Stem Cell 10, 171–182. https://doi.org/10.1016/j.stem.2011.12.016

Lin, S., Negulescu, A., Bulusu, S., Gibert, B., Delcros, J.-G., Ducarouge, B., Rama, N., Gadot, N., Treilleux, I., Saintigny, P., Meurette, O., Mehlen, P., 2017. Non-canonical NOTCH3 signalling limits tumour angiogenesis. Nat. Commun. 8, 16074. https://doi.org/10.1038/ncomms16074

Liu, C., Li, Y., Semenov, M., Han, C., Baeg, G.-H., Tan, Y., Zhang, Z., Lin, X., He, X., 2002. Control of β-Catenin Phosphorylation/Degradation by a Dual-Kinase Mechanism. Cell 108, 837–847. https://doi.org/10.1016/S0092-8674(02)00685-2

Liu, Y., Stein, E., Oliver, T., Li, Y., Brunken, W.J., Koch, M., Tessier-Lavigne, M., Hogan, B.L.M., 2004. Novel Role for Netrins in Regulating Epithelial Behavior during Lung Branching Morphogenesis. Curr. Biol. 14, 897–905. https://doi.org/10.1016/j.cub.2004.05.020

Llambi, F., 2001. Netrin-1 acts as a survival factor via its receptors UNC5H and DCC. EMBO J. 20, 2715–2722. https://doi.org/10.1093/emboj/20.11.2715

Loewe, L., Hill, W.G., 2010. The population genetics of mutations: good, bad and indifferent. Philos. Trans. R. Soc. B Biol. Sci. 365, 1153–1167. https://doi.org/10.1098/rstb.2009.0317

Loh, Y.-H., Wu, Q., Chew, J.-L., Vega, V.B., Zhang, W., Chen, X., Bourque, G., George, J., Leong, B., Liu, J., Wong, K.-Y., Sung, K.W., Lee, C.W.H., Zhao, X.-D., Chiu, K.-P., Lipovich, L., Kuznetsov, V.A., Robson, P., Stanton, L.W., Wei, C.-L., Ruan, Y., Lim, B., Ng, H.-H., 2006. The Oct4 and Nanog transcription network regulates pluripotency in mouse embryonic stem cells. Nat. Genet. 38, 431–440. https://doi.org/10.1038/ng1760

Löhle, M., Hermann, A., Glaß, H., Kempe, A., Schwarz, S.C., Kim, J.B., Poulet, C., Ravens, U., Schwarz, J., Schöler, H.R., Storch, A., 2012. Differentiation Efficiency of Induced Pluripotent Stem Cells Depends on the Number of Reprogramming Factors. STEM CELLS 30, 570–579. https://doi.org/10.1002/stem.1016

Low, J.H., Li, P., Chew, E.G.Y., Zhou, B., Suzuki, K., Zhang, T., Lian, M.M., Liu, M., Aizawa, E., Rodriguez Esteban, C., Yong, K.S.M., Chen, Q., Campistol, J.M., Fang, M., Khor, C.C., Foo, J.N., Izpisua Belmonte, J.C., Xia, Y., 2019. Generation of Human PSC-Derived Kidney Organoids with Patterned Nephron Segments and a De Novo Vascular Network. Cell Stem Cell S1934590919302735. https://doi.org/10.1016/j.stem.2019.06.009

Lowe, S.W., Cepero, E., Evan, G., 2004. Intrinsic tumour suppression. Nature 432, 307–315. https://doi.org/10.1038/nature03098

Lu, X., le Noble, F., Yuan, L., Jiang, Q., de Lafarge, B., Sugiyama, D., Bréant, C., Claes, F., De Smet, F., Thomas, J.-L., Autiero, M., Carmeliet, P., Tessier-Lavigne, M., Eichmann, A., 2004. The netrin receptor UNC5B mediates

guidance events controlling morphogenesis of the vascular system. Nature 432, 179–186. https://doi.org/10.1038/nature03080
Lukas, J., Parry, D., Aagaard, L., Mann, D.J., Bartkova, J., Strauss, M., Peters, G., Bartek, J., 1995. Retinoblastoma-protein-dependent cell-cycle inhibition by the tumour suppressor p16. Nature 375, 503–506. https://doi.org/10.1038/375503a0
Lynn, F.C., Sanchez, L., Gomis, R., German, M.S., Gasa, R., 2008. Identification of the bHLH factor Math6 as a novel component of the embryonic pancreas transcriptional network. PloS One 3, e2430. https://doi.org/10.1371/journal.pone.0002430
Ma, L., Young, J., Prabhala, H., Pan, E., Mestdagh, P., Muth, D., Teruya-Feldstein, J., Reinhardt, F., Onder, T.T., Valastyan, S., Westermann, F., Speleman, F., Vandesompele, J., Weinberg, R.A., 2010. miR-9, a MYC/MYCN-activated microRNA, regulates E-cadherin and cancer metastasis. Nat. Cell Biol. 12, 247–256. https://doi.org/10.1038/ncb2024
MacArthur, B.D., Sevilla, A., Lenz, M., Müller, F.-J., Schuldt, B.M., Schuppert, A.A., Ridden, S.J., Stumpf, P.S., Fidalgo, M., Ma'ayan, A., Wang, J., Lemischka, I.R., 2012. Nanog-dependent feedback loops regulate murine embryonic stem cell heterogeneity. Nat. Cell Biol. 14, 1139–1147. https://doi.org/10.1038/ncb2603
Madjd, Z., Hashemi, F., Shayanfar, N., Farahani, A., Zarnani, A., Shrifi, A., Akbari, M., 2009. OCT-4, an Embryonic Stem Cell Marker Expressed in Breast, Brain and Thyroid Carcinomas Compared to Testicular Carcinoma. Iran. J. Cancer Prev. 2.
Maherali, N., Sridharan, R., Xie, W., Utikal, J., Eminli, S., Arnold, K., Stadtfeld, M., Yachechko, R., Tchieu, J., Jaenisch, R., Plath, K., Hochedlinger, K., 2007. Directly Reprogrammed Fibroblasts Show Global Epigenetic Remodeling and Widespread Tissue Contribution. Cell Stem Cell 1, 55–70. https://doi.org/10.1016/j.stem.2007.05.014
Maki, N., Suetsugu-Maki, R., Tarui, H., Agata, K., Del Rio-Tsonis, K., Tsonis, P.A., 2009. Expression of stem cell pluripotency factors during regeneration in newts. Dev. Dyn. 238, 1613–1616. https://doi.org/10.1002/dvdy.21959
Mandai, M., Watanabe, A., Kurimoto, Y., Hirami, Y., Morinaga, C., Daimon, T., Fujihara, M., Akimaru, H., Sakai, N., Shibata, Y., Terada, M., Nomiya, Y., Tanishima, S., Nakamura, M., Kamao, H., Sugita, S., Onishi, A., Ito, T., Fujita, K., Kawamata, S., Go, M.J., Shinohara, C., Hata, K., Sawada, M., Yamamoto, M., Ohta, S., Ohara, Y., Yoshida, K., Kuwahara, J., Kitano, Y., Amano, N., Umekage, M., Kitaoka, F., Tanaka, A., Okada, C., Takasu, N., Ogawa, S., Yamanaka, S., Takahashi, M., 2017. Autologous Induced Stem-Cell–Derived Retinal Cells for Macular Degeneration. N. Engl. J. Med. 376, 1038–1046. https://doi.org/10.1056/NEJMoa1608368
Mani, S.A., Guo, W., Liao, M.-J., Eaton, E.Ng., Ayyanan, A., Zhou, A.Y., Brooks, M., Reinhard, F., Zhang, C.C., Shipitsin, M., Campbell, L.L., Polyak, K., Brisken, C., Yang, J., Weinberg, R.A., 2008. The Epithelial-Mesenchymal Transition Generates Cells with Properties of Stem Cells. Cell 133, 704–715. https://doi.org/10.1016/j.cell.2008.03.027
Manian, K.V., Aalam, S.M.M., Bharathan, S.P., Srivastava, A., Velayudhan, S.R., 2015. Understanding the Molecular Basis of Heterogeneity in Induced Pluripotent Stem Cells. Cell. Reprogramming 17, 427–440. https://doi.org/10.1089/cell.2015.0013
Manitt, C., Thompson, K.M., Kennedy, T.E., 2004. Developmental shift in expression of netrin receptors in the rat spinal cord: Predominance of UNC-5 homologues in adulthood. J. Neurosci. Res. 77, 690–700. https://doi.org/10.1002/jnr.20199
Mariani, J., Coppola, G., Zhang, P., Abyzov, A., Provini, L., Tomasini, L., Amenduni, M., Szekely, A., Palejev, D., Wilson, M., Gerstein, M., Grigorenko, E.L., Chawarska, K., Pelphrey, K.A., Howe, J.R., Vaccarino, F.M., 2015. FOXG1-Dependent Dysregulation of GABA/Glutamate Neuron Differentiation in Autism Spectrum Disorders. Cell 162, 375–390. https://doi.org/10.1016/j.cell.2015.06.034
Mariani, J., Vaccarino, F.M., 2019. Breakthrough Moments: Yoshiki Sasai's Discoveries in the Third Dimension. Cell Stem Cell 24, 837–838. https://doi.org/10.1016/j.stem.2019.05.007
Marión, R.M., Strati, K., Li, H., Murga, M., Blanco, R., Ortega, S., Fernandez-Capetillo, O., Serrano, M., Blasco, M.A., 2009. A p53-mediated DNA damage response limits reprogramming to ensure iPS cell genomic integrity. Nature 460, 1149–1153. https://doi.org/10.1038/nature08287
Marks, H., Kalkan, T., Menafra, R., Denissov, S., Jones, K., Hofemeister, H., Nichols, J., Kranz, A., Francis Stewart, A., Smith, A., Stunnenberg, H.G., 2012. The Transcriptional and Epigenomic Foundations of Ground State Pluripotency. Cell 149, 590–604. https://doi.org/10.1016/j.cell.2012.03.026
Marshall, M., 1995. Interactions between Ras and Raf: Key regulatory proteins in cellular transformation. Mol. Reprod. Dev. 42, 493–499. https://doi.org/10.1002/mrd.1080420418
Marson, A., Levine, S.S., Cole, M.F., Frampton, G.M., Brambrink, T., Johnstone, S., Guenther, M.G., Johnston, W.K., Wernig, M., Newman, J., Calabrese, J.M., Dennis, L.M., Volkert, T.L., Gupta, S., Love, J., Hannett, N., Sharp,

P.A., Bartel, D.P., Jaenisch, R., Young, R.A., 2008. Connecting microRNA Genes to the Core Transcriptional Regulatory Circuitry of Embryonic Stem Cells. Cell 134, 521–533. https://doi.org/10.1016/j.cell.2008.07.020
Martello, G., Sugimoto, T., Diamanti, E., Joshi, A., Hannah, R., Ohtsuka, S., Göttgens, B., Niwa, H., Smith, A., 2012. Esrrb Is a Pivotal Target of the Gsk3/Tcf3 Axis Regulating Embryonic Stem Cell Self-Renewal. Cell Stem Cell 11, 491–504. https://doi.org/10.1016/j.stem.2012.06.008
Martin, G.R., 1981. Isolation of a pluripotent cell line from early mouse embryos cultured in medium conditioned by teratocarcinoma stem cells. Proc. Natl. Acad. Sci. 78, 7634–7638. https://doi.org/10.1073/pnas.78.12.7634
Martincorena, I., Raine, K.M., Gerstung, M., Dawson, K.J., Haase, K., Van Loo, P., Davies, H., Stratton, M.R., Campbell, P.J., 2017. Universal Patterns of Selection in Cancer and Somatic Tissues. Cell 171, 1029-1041.e21. https://doi.org/10.1016/j.cell.2017.09.042
Massague, J., 2005. Smad transcription factors. Genes Dev. 19, 2783–2810. https://doi.org/10.1101/gad.1350705
Masui, S., Nakatake, Y., Toyooka, Y., Shimosato, D., Yagi, R., Takahashi, K., Okochi, H., Okuda, A., Matoba, R., Sharov, A.A., Ko, M.S.H., Niwa, H., 2007. Pluripotency governed by Sox2 via regulation of Oct3/4 expression in mouse embryonic stem cells. Nat. Cell Biol. 9, 625–635. https://doi.org/10.1038/ncb1589
Mathieu, J., Ruohola-Baker, H., 2017. Metabolic remodeling during the loss and acquisition of pluripotency. Development 144, 541–551. https://doi.org/10.1242/dev.128389
Matilainen, T., Haugas, M., Kreidberg, J.A., Salminen, M., 2007. Analysis of Netrin 1 receptors during inner ear development. Int. J. Dev. Biol. 51, 409–414. https://doi.org/10.1387/ijdb.072273tm
Matsunaga, E., Tauszig-Delamasure, S., Monnier, P.P., Mueller, B.K., Strittmatter, S.M., Mehlen, P., Chédotal, A., 2004. RGM and its receptor neogenin regulate neuronal survival. Nat. Cell Biol. 6, 749–755. https://doi.org/10.1038/ncb1157
McMahon, S.B., Van Buskirk, H.A., Dugan, K.A., Copeland, T.D., Cole, M.D., 1998. The novel ATM-related protein TRRAP is an essential cofactor for the c-Myc and E2F oncoproteins. Cell 94, 363–374. https://doi.org/10.1016/s0092-8674(00)81479-8
Mehlen, P., Puisieux, A., 2006. Metastasis: a question of life or death. Nat. Rev. Cancer 6, 449–458. https://doi.org/10.1038/nrc1886
Mehlen, P., Rabizadeh, S., Snipas, S.J., Assa-Munt, N., Salvesen, G.S., Bredesen, D.E., 1998. The DCC gene product induces apoptosis by a mechanism requiring receptor proteolysis. Nature 395, 801–804. https://doi.org/10.1038/27441
Meijer, D.H., Kane, M.F., Mehta, S., Liu, H., Harrington, E., Taylor, C.M., Stiles, C.D., Rowitch, D.H., 2012. Separated at birth? The functional and molecular divergence of OLIG1 and OLIG2. Nat. Rev. Neurosci. 13, 819–831. https://doi.org/10.1038/nrn3386
Meissner, A., 2005. Reduced representation bisulfite sequencing for comparative high-resolution DNA methylation analysis. Nucleic Acids Res. 33, 5868–5877. https://doi.org/10.1093/nar/gki901
Mikkelsen, T.S., Hanna, J., Zhang, X., Ku, M., Wernig, M., Schorderet, P., Bernstein, B.E., Jaenisch, R., Lander, E.S., Meissner, A., 2008a. Dissecting direct reprogramming through integrative genomic analysis. Nature 454, 49–55. https://doi.org/10.1038/nature07056
Mikkelsen, T.S., Hanna, J., Zhang, X., Ku, M., Wernig, M., Schorderet, P., Bernstein, B.E., Jaenisch, R., Lander, E.S., Meissner, A., 2008b. Dissecting direct reprogramming through integrative genomic analysis. Nature 454, 49–55. https://doi.org/10.1038/nature07056
Miller, R.A., Ruddle, F.H., 1976. Pluripotent teratocarcinoma-thymus somatic cell hybrids. Cell 9, 45–55. https://doi.org/10.1016/0092-8674(76)90051-9
Mitsui, K., Tokuzawa, Y., Itoh, H., Segawa, K., Murakami, M., Takahashi, K., Maruyama, M., Maeda, M., Yamanaka, S., 2003. The homeoprotein Nanog is required for maintenance of pluripotency in mouse epiblast and ES cells. Cell 113, 631–642. https://doi.org/10.1016/s0092-8674(03)00393-3
Miyanari, Y., Torres-Padilla, M.-E., 2012. Control of ground-state pluripotency by allelic regulation of Nanog. Nature 483, 470–473. https://doi.org/10.1038/nature10807
Mizuno, N., Agata, K., Sawada, K., Mochii, M., Eguchi, G., 2002. Expression of crystallin genes in embryonic and regenerating newt lenses. Dev. Growth Differ. 44, 251–256.
Mohyeldin, A., Garzón-Muvdi, T., Quiñones-Hinojosa, A., 2010. Oxygen in Stem Cell Biology: A Critical Component of the Stem Cell Niche. Cell Stem Cell 7, 150–161. https://doi.org/10.1016/j.stem.2010.07.007
Molotkov, A., Mazot, P., Brewer, J.R., Cinalli, R.M., Soriano, P., 2017. Distinct Requirements for FGFR1 and FGFR2 in Primitive Endoderm Development and Exit from Pluripotency. Dev. Cell 41, 511-526.e4. https://doi.org/10.1016/j.devcel.2017.05.004
Moore, S.W., Zhang, X., Lynch, C.D., Sheetz, M.P., 2012. Netrin-1 attracts axons through FAK-dependent mechanotransduction. J. Neurosci. Off. J. Soc. Neurosci. 32, 11574–11585. https://doi.org/10.1523/JNEUROSCI.0999-12.2012

Morel, A.-P., Ginestier, C., Pommier, R.M., Cabaud, O., Ruiz, E., Wicinski, J., Devouassoux-Shisheboran, M., Combaret, V., Finetti, P., Chassot, C., Pinatel, C., Fauvet, F., Saintigny, P., Thomas, E., Moyret-Lalle, C., Lachuer, J., Despras, E., Jauffret, J.-L., Bertucci, F., Guitton, J., Wierinckx, A., Wang, Q., Radosevic-Robin, N., Penault-Llorca, F., Cox, D.G., Hollande, F., Ansieau, S., Caramel, J., Birnbaum, D., Vigneron, A.M., Tissier, A., Charafe-Jauffret, E., Puisieux, A., 2017. A stemness-related ZEB1–MSRB3 axis governs cellular pliancy and breast cancer genome stability. Nat. Med. 23, 568.

Moscatelli, D., 1989. Transformation of NIH 3T3 cells with basic fibroblast growth factor or the hst/K-fgf oncogene causes downregulation of the fibroblast growth factor receptor: reversal of morphological transformation and restoration of receptor number by suramin. J. Cell Biol. 109, 2519–2527. https://doi.org/10.1083/jcb.109.5.2519

Murre, C., McCaw, P.S., Vaessin, H., Caudy, M., Jan, L.Y., Jan, Y.N., Cabrera, C.V., Buskin, J.N., Hauschka, S.D., Lassar, A.B., Weintraub, H., Baltimore, D., 1989. Interactions between heterologous helix-loop-helix proteins generate complexes that bind specifically to a common DNA sequence. Cell 58, 537–544. https://doi.org/10.1016/0092-8674(89)90434-0

Nadarajah, B., Parnavelas, J.G., 2002. Modes of neuronal migration in the developing cerebral cortex. Nat. Rev. Neurosci. 3, 423–432. https://doi.org/10.1038/nrn845

Nakai-Futatsugi, Y., Niwa, H., 2013. Transcription Factor Network in Embryonic Stem Cells: Heterogeneity under the Stringency. Biol. Pharm. Bull. 36, 166–170. https://doi.org/10.1248/bpb.b12-00958

Nakashiba, T., Nishimura, S., Ikeda, T., Itohara, S., 2002. Complementary expression and neurite outgrowth activity of netrin-G subfamily members. Mech. Dev. 111, 47–60. https://doi.org/10.1016/S0925-4773(01)00600-1

Nassour, J., Radford, R., Correia, A., Fusté, J.M., Schoell, B., Jauch, A., Shaw, R.J., Karlseder, J., 2019. Autophagic cell death restricts chromosomal instability during replicative crisis. Nature 565, 659–663. https://doi.org/10.1038/s41586-019-0885-0

Nau, M.M., Brooks, B.J., Battey, J., Sausville, E., Gazdar, A.F., Kirsch, I.R., McBride, O.W., Bertness, V., Hollis, G.F., Minna, J.D., 1985. L-myc, a new myc-related gene amplified and expressed in human small cell lung cancer. Nature 318, 69–73. https://doi.org/10.1038/318069a0

Navankasattusas, S., Whitehead, K.J., Suli, A., Sorensen, L.K., Lim, A.H., Zhao, J., Park, K.W., Wythe, J.D., Thomas, K.R., Chien, C.-B., Li, D.Y., 2008. The netrin receptor UNC5B promotes angiogenesis in specific vascular beds. Development 135, 659–667. https://doi.org/10.1242/dev.013623

Nechaev, S., Adelman, K., 2011. Pol II waiting in the starting gates: Regulating the transition from transcription initiation into productive elongation. Biochim. Biophys. Acta BBA - Gene Regul. Mech. 1809, 34–45. https://doi.org/10.1016/j.bbagrm.2010.11.001

Nefzger, C.M., Alaei, S., Knaupp, A.S., Holmes, M.L., Polo, J.M., 2014. Cell Surface Marker Mediated Purification of iPS Cell Intermediates from a Reprogrammable Mouse Model. J. Vis. Exp. 51728. https://doi.org/10.3791/51728

Nefzger, C.M., Rossello, F.J., Chen, J., Liu, X., Knaupp, A.S., Firas, J., Paynter, J.M., Pflueger, J., Buckberry, S., Lim, S.M., Williams, B., Alaei, S., Faye-Chauhan, K., Petretto, E., Nilsson, S.K., Lister, R., Ramialison, M., Powell, D.R., Rackham, O.J.L., Polo, J.M., 2017. Cell Type of Origin Dictates the Route to Pluripotency. Cell Rep. 21, 2649–2660. https://doi.org/10.1016/j.celrep.2017.11.029

Niakan, K.K., Ji, H., Maehr, R., Vokes, S.A., Rodolfa, K.T., Sherwood, R.I., Yamaki, M., Dimos, J.T., Chen, A.E., Melton, D.A., McMahon, A.P., Eggan, K., 2010. Sox17 promotes differentiation in mouse embryonic stem cells by directly regulating extraembryonic gene expression and indirectly antagonizing self-renewal. Genes Dev. 24, 312–326. https://doi.org/10.1101/gad.1833510

Nichols, Jennifer, Jones, K., Phillips, J.M., Newland, S.A., Roode, M., Mansfield, W., Smith, A., Cooke, A., 2009. Validated germline-competent embryonic stem cell lines from nonobese diabetic mice. Nat. Med. 15, 814–818. https://doi.org/10.1038/nm.1996

Nichols, J., Silva, J., Roode, M., Smith, A., 2009. Suppression of Erk signalling promotes ground state pluripotency in the mouse embryo. Development 136, 3215–3222. https://doi.org/10.1242/dev.038893

Nichols, J., Smith, A., 2012. Pluripotency in the embryo and in culture. Cold Spring Harb. Perspect. Biol. 4, a008128. https://doi.org/10.1101/cshperspect.a008128

Nichols, J., Zevnik, B., Anastassiadis, K., Niwa, H., Klewe-Nebenius, D., Chambers, I., Schöler, H., Smith, A., 1998. Formation of Pluripotent Stem Cells in the Mammalian Embryo Depends on the POU Transcription Factor Oct4. Cell 95, 379–391. https://doi.org/10.1016/S0092-8674(00)81769-9

Nishimura, K., Sano, M., Ohtaka, M., Furuta, B., Umemura, Y., Nakajima, Y., Ikehara, Y., Kobayashi, T., Segawa, H., Takayasu, S., Sato, H., Motomura, K., Uchida, E., Kanayasu-Toyoda, T., Asashima, M., Nakauchi, H., Yamaguchi, T., Nakanishi, M., 2011. Development of Defective and Persistent Sendai Virus Vector: A

UNIQUE GENE DELIVERY/EXPRESSION SYSTEM IDEAL FOR CELL REPROGRAMMING. J. Biol. Chem. 286, 4760–4771. https://doi.org/10.1074/jbc.M110.183780
Niwa, H., Miyazaki, J., Smith, A.G., 2000. Quantitative expression of Oct-3/4 defines differentiation, dedifferentiation or self-renewal of ES cells. Nat. Genet. 24, 372–376. https://doi.org/10.1038/74199
Niwa, H., Ogawa, K., Shimosato, D., Adachi, K., 2009. A parallel circuit of LIF signalling pathways maintains pluripotency of mouse ES cells. Nature 460, 118–122. https://doi.org/10.1038/nature08113
Niwa, H., Toyooka, Y., Shimosato, D., Strumpf, D., Takahashi, K., Yagi, R., Rossant, J., 2005. Interaction between Oct3/4 and Cdx2 determines trophectoderm differentiation. Cell 123, 917–929. https://doi.org/10.1016/j.cell.2005.08.040
Ocampo, A., Reddy, P., Martinez-Redondo, P., Platero-Luengo, A., Hatanaka, F., Hishida, T., Li, M., Lam, D., Kurita, M., Beyret, E., Araoka, T., Vazquez-Ferrer, E., Donoso, D., Roman, J.L., Xu, J., Rodriguez Esteban, C., Nuñez, G., Nuñez Delicado, E., Campistol, J.M., Guillen, I., Guillen, P., Izpisua Belmonte, J.C., 2016. In Vivo Amelioration of Age-Associated Hallmarks by Partial Reprogramming. Cell 167, 1719-1733.e12. https://doi.org/10.1016/j.cell.2016.11.052
O'Dell, M.R., Li Huang, J., Whitney-Miller, C.L., Deshpande, V., Rothberg, P., Grose, V., Rossi, R.M., Zhu, A.X., Land, H., Bardeesy, N., Hezel, A.F., 2012. KrasG12D and p53 Mutation Cause Primary Intrahepatic Cholangiocarcinoma. Cancer Res. 72, 1557–1567. https://doi.org/10.1158/0008-5472.CAN-11-3596
Ogawa, K., Saito, A., Matsui, H., Suzuki, H., Ohtsuka, S., Shimosato, D., Morishita, Y., Watabe, T., Niwa, H., Miyazono, K., 2006. Activin-Nodal signaling is involved in propagation of mouse embryonic stem cells. J. Cell Sci. 120, 55–65. https://doi.org/10.1242/jcs.03296
Ohi, Y., Qin, H., Hong, C., Blouin, L., Polo, J.M., Guo, T., Qi, Z., Downey, S.L., Manos, P.D., Rossi, D.J., Yu, J., Hebrok, M., Hochedlinger, K., Costello, J.F., Song, J.S., Ramalho-Santos, M., 2011. Incomplete DNA methylation underlies a transcriptional memory of somatic cells in human iPS cells. Nat. Cell Biol. 13, 541–549. https://doi.org/10.1038/ncb2239
Ohnishi, K., Semi, K., Yamamoto, T., Shimizu, M., Tanaka, A., Mitsunaga, K., Okita, K., Osafune, K., Arioka, Y., Maeda, T., Soejima, H., Moriwaki, H., Yamanaka, S., Woltjen, K., Yamada, Y., 2014. Premature termination of reprogramming in vivo leads to cancer development through altered epigenetic regulation. Cell 156, 663–677. https://doi.org/10.1016/j.cell.2014.01.005
Okita, K., Nakagawa, M., Hyenjong, H., Ichisaka, T., Yamanaka, S., 2008. Generation of Mouse Induced Pluripotent Stem Cells Without Viral Vectors. Science 322, 949–953. https://doi.org/10.1126/science.1164270
O'Malley, J., Skylaki, S., Iwabuchi, K.A., Chantzoura, E., Ruetz, T., Johnsson, A., Tomlinson, S.R., Linnarsson, S., Kaji, K., 2013. High-resolution analysis with novel cell-surface markers identifies routes to iPS cells. Nature 499, 88–91. https://doi.org/10.1038/nature12243
Onos, K.D., Sukoff Rizzo, S.J., Howell, G.R., Sasner, M., 2016. Toward more predictive genetic mouse models of Alzheimer's disease. Brain Res. Bull. 122, 1–11. https://doi.org/10.1016/j.brainresbull.2015.12.003
Ornitz, D., Hammer, R., Messing, A., Palmiter, R., Brinster, R., 1987. Pancreatic neoplasia induced by SV40 T-antigen expression in acinar cells of transgenic mice. Science 238, 188–193. https://doi.org/10.1126/science.2821617
Ornitz, D.M., 2000. FGFs, heparan sulfate and FGFRs: complex interactions essential for development. BioEssays News Rev. Mol. Cell. Dev. Biol. 22, 108–112. https://doi.org/10.1002/(SICI)1521-1878(200002)22:2<108::AID-BIES2>3.0.CO;2-M
Osborne, P.B., Halliday, G.M., Cooper, H.M., Keast, J.R., 2005. Localization of immunoreactivity for Deleted in Colorectal Cancer (DCC), the receptor for the guidance factor netrin-1, in ventral tier dopamine projection pathways in adult rodents. Neuroscience 131, 671–681. https://doi.org/10.1016/j.neuroscience.2004.11.043
Osthus, R.C., Shim, H., Kim, S., Li, Q., Reddy, R., Mukherjee, M., Xu, Y., Wonsey, D., Lee, L.A., Dang, C.V., 2000. Deregulation of Glucose Transporter 1 and Glycolytic Gene Expression by c-Myc. J. Biol. Chem. 275, 21797–21800. https://doi.org/10.1074/jbc.C000023200
Ouelle, D.E., Zindy, F., Ashmun, R.A., Sherr, C.J., 1995. Alternative reading frames of the INK4a tumor suppressor gene encode two unrelated proteins capable of inducing cell cycle arrest. Cell 83, 993–1000. https://doi.org/10.1016/0092-8674(95)90214-7
Ozmadenci, D., Féraud, O., Markossian, S., Kress, E., Ducarouge, B., Gibert, B., Ge, J., Durand, I., Gadot, N., Plateroti, M., Bennaceur-Griscelli, A., Scoazec, J.-Y., Gil, J., Deng, H., Bernet, A., Mehlen, P., Lavial, F., 2015. Netrin-1 regulates somatic cell reprogramming and pluripotency maintenance. Nat. Commun. 6, 7398. https://doi.org/10.1038/ncomms8398
Padmanaban, V., Krol, I., Suhail, Y., Szczerba, B.M., Aceto, N., Bader, J.S., Ewald, A.J., 2019. E-cadherin is required for metastasis in multiple models of breast cancer. Nature. https://doi.org/10.1038/s41586-019-1526-3

Park, I.-H., Zhao, R., West, J.A., Yabuuchi, A., Huo, H., Ince, T.A., Lerou, P.H., Lensch, M.W., Daley, G.Q., 2008. Reprogramming of human somatic cells to pluripotency with defined factors. Nature 451, 141–146. https://doi.org/10.1038/nature06534

Park, K.W., Crouse, D., Lee, M., Karnik, S.K., Sorensen, L.K., Murphy, K.J., Kuo, C.J., Li, D.Y., 2004. The axonal attractant Netrin-1 is an angiogenic factor. Proc. Natl. Acad. Sci. 101, 16210–16215. https://doi.org/10.1073/pnas.0405984101

Pastushenko, I., Brisebarre, A., Sifrim, A., Fioramonti, M., Revenco, T., Boumahdi, S., Van Keymeulen, A., Brown, D., Moers, V., Lemaire, S., De Clercq, S., Minguijón, E., Balsat, C., Sokolow, Y., Dubois, C., De Cock, F., Scozzaro, S., Sopena, F., Lanas, A., D'Haene, N., Salmon, I., Marine, J.-C., Voet, T., Sotiropoulou, P.A., Blanpain, C., 2018. Identification of the tumour transition states occurring during EMT. Nature 556, 463–468. https://doi.org/10.1038/s41586-018-0040-3

Patel, T., Hobert, O., 2017. Coordinated control of terminal differentiation and restriction of cellular plasticity. eLife 6. https://doi.org/10.7554/eLife.24100

Payer, B., Lee, J.T., 2008. X Chromosome Dosage Compensation: How Mammals Keep the Balance. Annu. Rev. Genet. 42, 733–772. https://doi.org/10.1146/annurev.genet.42.110807.091711

Pelengaris, S., Khan, M., Evan, G.I., 2002. Suppression of Myc-Induced Apoptosis in β Cells Exposes Multiple Oncogenic Properties of Myc and Triggers Carcinogenic Progression. Cell 109, 321–334. https://doi.org/10.1016/S0092-8674(02)00738-9

Pereira, L., Yi, F., Merrill, B.J., 2006. Repression of Nanog Gene Transcription by Tcf3 Limits Embryonic Stem Cell Self-Renewal. Mol. Cell. Biol. 26, 7479–7491. https://doi.org/10.1128/MCB.00368-06

Perna, D., Fagà, G., Verrecchia, A., Gorski, M.M., Barozzi, I., Narang, V., Khng, J., Lim, K.C., Sung, W.-K., Sanges, R., Stupka, E., Oskarsson, T., Trumpp, A., Wei, C.-L., Müller, H., Amati, B., 2012. Genome-wide mapping of Myc binding and gene regulation in serum-stimulated fibroblasts. Oncogene 31, 1695–1709. https://doi.org/10.1038/onc.2011.359

Pesce, M., Schöler, H.R., 2000. Oct-4: control of totipotency and germline determination. Mol. Reprod. Dev. 55, 452–457. https://doi.org/10.1002/(SICI)1098-2795(200004)55:4<452::AID-MRD14>3.0.CO;2-S

Petrilli, A.M., Fernández-Valle, C., 2016. Role of Merlin/NF2 inactivation in tumor biology. Oncogene 35, 537–548. https://doi.org/10.1038/onc.2015.125

Pfendler, K.C., Catuar, C.S., Meneses, J.J., Pedersen, R.A., 2005. Overexpression of *Nodal* Promotes Differentiation of Mouse Embryonic Stem Cells into Mesoderm and Endoderm at the Expense of Neuroectoderm Formation. Stem Cells Dev. 14, 162–172. https://doi.org/10.1089/scd.2005.14.162

Piao, S., Lee, S.-H., Kim, H., Yum, S., Stamos, J.L., Xu, Y., Lee, S.-J., Lee, J., Oh, S., Han, J.-K., Park, B.-J., Weis, W.I., Ha, N.-C., 2008. Direct Inhibition of GSK3β by the Phosphorylated Cytoplasmic Domain of LRP6 in Wnt/β-Catenin Signaling. PLoS ONE 3, e4046. https://doi.org/10.1371/journal.pone.0004046

Pin, C.L., Rukstalis, J.M., Johnson, C., Konieczny, S.F., 2001. The bHLH transcription factor Mist1 is required to maintain exocrine pancreas cell organization and acinar cell identity. J. Cell Biol. 155, 519–530. https://doi.org/10.1083/jcb.200105060

Polo, Jose M., Anderssen, E., Walsh, R.M., Schwarz, B.A., Nefzger, C.M., Lim, S.M., Borkent, M., Apostolou, E., Alaei, S., Cloutier, J., Bar-Nur, O., Cheloufi, S., Stadtfeld, M., Figueroa, M.E., Robinton, D., Natesan, S., Melnick, A., Zhu, J., Ramaswamy, S., Hochedlinger, K., 2012. A Molecular Roadmap of Reprogramming Somatic Cells into iPS Cells. Cell 151, 1617–1632. https://doi.org/10.1016/j.cell.2012.11.039

Polo, Jose M., Anderssen, E., Walsh, R.M., Schwarz, B.A., Nefzger, C.M., Lim, S.M., Borkent, M., Apostolou, E., Alaei, S., Cloutier, J., Bar-Nur, O., Cheloufi, S., Stadtfeld, M., Figueroa, M.E., Robinton, D., Natesan, S., Melnick, A., Zhu, J., Ramaswamy, S., Hochedlinger, K., 2012. A molecular roadmap of reprogramming somatic cells into iPS cells. Cell 151, 1617–1632. https://doi.org/10.1016/j.cell.2012.11.039

Posfai, E., Tam, O.H., Rossant, J., 2014. Mechanisms of Pluripotency In Vivo and In Vitro, in: Current Topics in Developmental Biology. Elsevier, pp. 1–37. https://doi.org/10.1016/B978-0-12-416022-4.00001-9

Preston-Martin, S., Pike, M.C., Ross, R.K., Jones, P.A., Henderson, B.E., 1990. Increased cell division as a cause of human cancer. Cancer Res. 50, 7415–7421.

Prieto, J., Seo, A.Y., León, M., Santacatterina, F., Torresano, L., Palomino-Schätzlein, M., Giménez, K., Vallet-Sánchez, A., Ponsoda, X., Pineda-Lucena, A., Cuezva, J.M., Lippincott-Schwartz, J., Torres, J., 2018. MYC Induces a Hybrid Energetics Program Early in Cell Reprogramming. Stem Cell Rep. 11, 1479–1492. https://doi.org/10.1016/j.stemcr.2018.10.018

Prigione, A., Rohwer, N., Hoffmann, S., Mlody, B., Drews, K., Bukowiecki, R., Blümlein, K., Wanker, E.E., Ralser, M., Cramer, T., Adjaye, J., 2014. HIF1α Modulates Cell Fate Reprogramming Through Early Glycolytic Shift and Upregulation of PDK1-3 and PKM2: HIF1α Associated Metabolic Switch in iPSCs. STEM CELLS 32, 364–376. https://doi.org/10.1002/stem.1552

Puisieux, A., Pommier, R.M., Morel, A.-P., Lavial, F., 2018. Cellular Pliancy and the Multistep Process of Tumorigenesis. Cancer Cell 33, 164–172. https://doi.org/10.1016/j.ccell.2018.01.007

Pujadas, G., Felipe, F., Ejarque, M., Sanchez, L., Cervantes, S., Lynn, F.C., Gomis, R., Gasa, R., 2011. Sequence and epigenetic determinants in the regulation of the Math6 gene by Neurogenin3. Differentiation 82, 66–76. https://doi.org/10.1016/j.diff.2011.05.006

Rais, Y., Zviran, A., Geula, S., Gafni, O., Chomsky, E., Viukov, S., Mansour, A.A., Caspi, I., Krupalnik, V., Zerbib, M., Maza, I., Mor, N., Baran, D., Weinberger, L., Jaitin, D.A., Lara-Astiaso, D., Blecher-Gonen, R., Shipony, Z., Mukamel, Z., Hagai, T., Gilad, S., Amann-Zalcenstein, D., Tanay, A., Amit, I., Novershtern, N., Hanna, J.H., 2013. Deterministic direct reprogramming of somatic cells to pluripotency. Nature 502, 65–70. https://doi.org/10.1038/nature12587

Rajagopalan, S., Deitinghoff, L., Davis, D., Conrad, S., Skutella, T., Chedotal, A., Mueller, B.K., Strittmatter, S.M., 2004. Neogenin mediates the action of repulsive guidance molecule. Nat. Cell Biol. 6, 756–762. https://doi.org/10.1038/ncb1156

Ran, F.A., Hsu, P.D., Wright, J., Agarwala, V., Scott, D.A., Zhang, F., 2013. Genome engineering using the CRISPR-Cas9 system. Nat. Protoc. 8, 2281–2308. https://doi.org/10.1038/nprot.2013.143

Rao, R.A., Dhele, N., Cheemadan, S., Ketkar, A., Jayandharan, G.R., Palakodeti, D., Rampalli, S., 2015. Ezh2 mediated H3K27me3 activity facilitates somatic transition during human pluripotent reprogramming. Sci. Rep. 5, 8229. https://doi.org/10.1038/srep08229

Rawnsley, D.R., Xiao, J., Lee, J.S., Liu, X., Mericko-Ishizuka, P., Kumar, V., He, J., Basu, A., Lu, M., Lynn, F.C., Pack, M., Gasa, R., Kahn, M.L., 2013. The transcription factor Atonal homolog 8 regulates Gata4 and Friend of Gata-2 during vertebrate development. J. Biol. Chem. 288, 24429–24440. https://doi.org/10.1074/jbc.M113.463083

Recasens-Alvarez, C., Ferreira, A., Milán, M., 2017. JAK/STAT controls organ size and fate specification by regulating morphogen production and signalling. Nat. Commun. 8, 13815. https://doi.org/10.1038/ncomms13815

Ren, X.-R., Ming, G.-L., Xie, Y., Hong, Y., Sun, D.-M., Zhao, Z.-Q., Feng, Z., Wang, Q., Shim, S., Chen, Z.-F., Song, H.-J., Mei, L., Xiong, W.-C., 2004. Focal adhesion kinase in netrin-1 signaling. Nat. Neurosci. 7, 1204–1212. https://doi.org/10.1038/nn1330

Renfree, M.B., Shaw, G., 2000. Diapause. Annu. Rev. Physiol. 62, 353–375. https://doi.org/10.1146/annurev.physiol.62.1.353

Reynolds, N., Latos, P., Hynes-Allen, A., Loos, R., Leaford, D., O'Shaughnessy, A., Mosaku, O., Signolet, J., Brennecke, P., Kalkan, T., Costello, I., Humphreys, P., Mansfield, W., Nakagawa, K., Strouboulis, J., Behrens, A., Bertone, P., Hendrich, B., 2012. NuRD Suppresses Pluripotency Gene Expression to Promote Transcriptional Heterogeneity and Lineage Commitment. Cell Stem Cell 10, 583–594. https://doi.org/10.1016/j.stem.2012.02.020

Riddle, M.R., Weintraub, A., Nguyen, K.C.Q., Hall, D.H., Rothman, J.H., 2013. Transdifferentiation and remodeling of post-embryonic C. elegans cells by a single transcription factor. Development 140, 4844–4849. https://doi.org/10.1242/dev.103010

Riggi, N., Knoechel, B., Gillespie, S.M., Rheinbay, E., Boulay, G., Suvà, M.L., Rossetti, N.E., Boonseng, W.E., Oksuz, O., Cook, E.B., Formey, A., Patel, A., Gymrek, M., Thapar, V., Deshpande, V., Ting, D.T., Hornicek, F.J., Nielsen, G.P., Stamenkovic, I., Aryee, M.J., Bernstein, B.E., Rivera, M.N., 2014. EWS-FLI1 Utilizes Divergent Chromatin Remodeling Mechanisms to Directly Activate or Repress Enhancer Elements in Ewing Sarcoma. Cancer Cell 26, 668–681. https://doi.org/10.1016/j.ccell.2014.10.004

Ronaldson-Bouchard, K., Vunjak-Novakovic, G., 2018. Organs-on-a-Chip: A Fast Track for Engineered Human Tissues in Drug Development. Cell Stem Cell 22, 310–324. https://doi.org/10.1016/j.stem.2018.02.011

Ross, M.D., Martinka, S., Mukherjee, A., Sedor, J.R., Vinson, C., Bruggeman, L.A., 2006. Math6 expression during kidney development and altered expression in a mouse model of glomerulosclerosis. Dev. Dyn. Off. Publ. Am. Assoc. Anat. 235, 3102–3109. https://doi.org/10.1002/dvdy.20934

Ross, S.A., McCaffery, P.J., Drager, U.C., De Luca, L.M., 2000. Retinoids in Embryonal Development. Physiol. Rev. 80, 1021–1054. https://doi.org/10.1152/physrev.2000.80.3.1021

Ross, S.E., Greenberg, M.E., Stiles, C.D., 2003. Basic Helix-Loop-Helix Factors in Cortical Development. Neuron 39, 13–25. https://doi.org/10.1016/S0896-6273(03)00365-9

Roy, N., Hebrok, M., 2015. Regulation of Cellular Identity in Cancer. Dev. Cell 35, 674–684. https://doi.org/10.1016/j.devcel.2015.12.001

Rubinfeld, B., Souza, B., Albert, I., Muller, O., Chamberlain, S., Masiarz, F., Munemitsu, S., Polakis, P., 1993. Association of the APC gene product with beta-catenin. Science 262, 1731–1734. https://doi.org/10.1126/science.8259518

Sage, J., 2012. The retinoblastoma tumor suppressor and stem cell biology. Genes Dev. 26, 1409–1420. https://doi.org/10.1101/gad.193730.112
Salghetti, S.E., 1999. Destruction of Myc by ubiquitin-mediated proteolysis: cancer-associated and transforming mutations stabilize Myc. EMBO J. 18, 717–726. https://doi.org/10.1093/emboj/18.3.717
Salk, J.J., Fox, E.J., Loeb, L.A., 2010. Mutational Heterogeneity in Human Cancers: Origin and Consequences. Annu. Rev. Pathol. Mech. Dis. 5, 51–75. https://doi.org/10.1146/annurev-pathol-121808-102113
Salminen, M., Meyer, B.I., Bober, E., Gruss, P., 2000. Netrin 1 is required for semicircular canal formation in the mouse inner ear. Dev. Camb. Engl. 127, 13–22.
Samavarchi-Tehrani, P., Golipour, A., David, L., Sung, H., Beyer, T.A., Datti, A., Woltjen, K., Nagy, A., Wrana, J.L., 2010. Functional Genomics Reveals a BMP-Driven Mesenchymal-to-Epithelial Transition in the Initiation of Somatic Cell Reprogramming. Cell Stem Cell 7, 64–77. https://doi.org/10.1016/j.stem.2010.04.015
Sandgren, E.P., Luetteke, N.C., Palmiter, R.D., Brinster, R.L., Lee, D.C., 1990. Overexpression of TGFα in transgenic mice: Induction of epithelial hyperplasia, pancreatic metaplasia, and carcinoma of the breast. Cell 61, 1121–1135. https://doi.org/10.1016/0092-8674(90)90075-P
Sarkar, A., Hochedlinger, K., 2013. The sox family of transcription factors: versatile regulators of stem and progenitor cell fate. Cell Stem Cell 12, 15–30. https://doi.org/10.1016/j.stem.2012.12.007
Sasai, Y., Kageyama, R., Tagawa, Y., Shigemoto, R., Nakanishi, S., 1992. Two mammalian helix-loop-helix factors structurally related to Drosophila hairy and Enhancer of split. Genes Dev. 6, 2620–2634. https://doi.org/10.1101/gad.6.12b.2620
Sasse, J., Hemmann, U., Schwartz, C., Schniertshauer, U., Heesel, B., Landgraf, C., Schneider-Mergener, J., Heinrich, P.C., Horn, F., 1997. Mutational analysis of acute-phase response factor/Stat3 activation and dimerization. Mol. Cell. Biol. 17, 4677–4686. https://doi.org/10.1128/MCB.17.8.4677
Sato, N., Meijer, L., Skaltsounis, L., Greengard, P., Brivanlou, A.H., 2004a. Maintenance of pluripotency in human and mouse embryonic stem cells through activation of Wnt signaling by a pharmacological GSK-3-specific inhibitor. Nat. Med. 10, 55–63. https://doi.org/10.1038/nm979
Sato, N., Meijer, L., Skaltsounis, L., Greengard, P., Brivanlou, A.H., 2004b. Maintenance of pluripotency in human and mouse embryonic stem cells through activation of Wnt signaling by a pharmacological GSK-3-specific inhibitor. Nat. Med. 10, 55–63. https://doi.org/10.1038/nm979
Saygin, C., Matei, D., Majeti, R., Reizes, O., Lathia, J.D., 2019. Targeting Cancer Stemness in the Clinic: From Hype to Hope. Cell Stem Cell 24, 25–40. https://doi.org/10.1016/j.stem.2018.11.017
Schaniel, C., Ang, Y.-S., Ratnakumar, K., Cormier, C., James, T., Bernstein, E., Lemischka, I.R., Paddison, P.J., 2009. Smarcc1/Baf155 Couples Self-Renewal Gene Repression with Changes in Chromatin Structure in Mouse Embryonic Stem Cells. Stem Cells N/A-N/A. https://doi.org/10.1002/stem.223
Schiebinger, G., Shu, J., Tabaka, M., Cleary, B., Subramanian, V., Solomon, A., Gould, J., Liu, S., Lin, S., Berube, P., Lee, L., Chen, J., Brumbaugh, J., Rigollet, P., Hochedlinger, K., Jaenisch, R., Regev, A., Lander, E.S., 2019. Optimal-Transport Analysis of Single-Cell Gene Expression Identifies Developmental Trajectories in Reprogramming. Cell 176, 928-943.e22. https://doi.org/10.1016/j.cell.2019.01.006
Schimmer, J., Breazzano, S., 2016. Investor Outlook: Rising from the Ashes; GSK's European Approval of Strimvelis for ADA-SCID. Hum. Gene Ther. Clin. Dev. 27, 57–61. https://doi.org/10.1089/humc.2016.29010.ind
Schroeder, N., Wuelling, M., Hoffmann, D., Brand-Saberi, B., Vortkamp, A., 2019. Atoh8 acts as a regulator of chondrocyte proliferation and differentiation in endochondral bones. PLOS ONE 14, e0218230. https://doi.org/10.1371/journal.pone.0218230
Scognamiglio, R., Cabezas-Wallscheid, N., Thier, M.C., Altamura, S., Reyes, A., Prendergast, Á.M., Baumgärtner, D., Carnevalli, L.S., Atzberger, A., Haas, S., von Paleske, L., Boroviak, T., Wörsdörfer, P., Essers, M.A.G., Kloz, U., Eisenman, R.N., Edenhofer, F., Bertone, P., Huber, W., van der Hoeven, F., Smith, A., Trumpp, A., 2016. Myc Depletion Induces a Pluripotent Dormant State Mimicking Diapause. Cell 164, 668–680. https://doi.org/10.1016/j.cell.2015.12.033
Seitz, V., Butzhammer, P., Hirsch, B., Hecht, J., Gütgemann, I., Ehlers, A., Lenze, D., Oker, E., Sommerfeld, A., von der Wall, E., König, C., Zinser, C., Spang, R., Hummel, M., 2011. Deep Sequencing of MYC DNA-Binding Sites in Burkitt Lymphoma. PLoS ONE 6, e26837. https://doi.org/10.1371/journal.pone.0026837
Seki, T., Yuasa, S., Oda, M., Egashira, T., Yae, K., Kusumoto, D., Nakata, H., Tohyama, S., Hashimoto, H., Kodaira, M., Okada, Y., Seimiya, H., Fusaki, N., Hasegawa, M., Fukuda, K., 2010. Generation of induced pluripotent stem cells from human terminally differentiated circulating T cells. Cell Stem Cell 7, 11–14. https://doi.org/10.1016/j.stem.2010.06.003
Seoane, J., Pouponnot, C., Staller, P., Schader, M., Eilers, M., Massagué, J., 2001. TGFβ influences Myc, Miz-1 and Smad to control the CDK inhibitor p15INK4b. Nat. Cell Biol. 3, 400–408. https://doi.org/10.1038/35070086

Serafini, T., Colamarino, S.A., Leonardo, E.D., Wang, H., Beddington, R., Skarnes, W.C., Tessier-Lavigne, M., 1996. Netrin-1 is required for commissural axon guidance in the developing vertebrate nervous system. Cell 87, 1001–1014. https://doi.org/10.1016/s0092-8674(00)81795-x

Serafini, T., Kennedy, T.E., Gaiko, M.J., Mirzayan, C., Jessell, T.M., Tessier-Lavigne, M., 1994. The netrins define a family of axon outgrowth-promoting proteins homologous to C. elegans UNC-6. Cell 78, 409–424. https://doi.org/10.1016/0092-8674(94)90420-0

Serrano, M., Lin, A.W., McCurrach, M.E., Beach, D., Lowe, S.W., 1997. Oncogenic ras Provokes Premature Cell Senescence Associated with Accumulation of p53 and p16INK4a. Cell 88, 593–602. https://doi.org/10.1016/S0092-8674(00)81902-9

Sessa, M., Lorioli, L., Fumagalli, F., Acquati, S., Redaelli, D., Baldoli, C., Canale, S., Lopez, I.D., Morena, F., Calabria, A., Fiori, R., Silvani, P., Rancoita, P.M.V., Gabaldo, M., Benedicenti, F., Antonioli, G., Assanelli, A., Cicalese, M.P., del Carro, U., Sora, M.G.N., Martino, S., Quattrini, A., Montini, E., Di Serio, C., Ciceri, F., Roncarolo, M.G., Aiuti, A., Naldini, L., Biffi, A., 2016. Lentiviral haemopoietic stem-cell gene therapy in early-onset metachromatic leukodystrophy: an ad-hoc analysis of a non-randomised, open-label, phase 1/2 trial. The Lancet 388, 476–487. https://doi.org/10.1016/S0140-6736(16)30374-9

Shachaf, C.M., Kopelman, A.M., Arvanitis, C., Karlsson, Å., Beer, S., Mandl, S., Bachmann, M.H., Borowsky, A.D., Ruebner, B., Cardiff, R.D., Yang, Q., Bishop, J.M., Contag, C.H., Felsher, D.W., 2004. MYC inactivation uncovers pluripotent differentiation and tumour dormancy in hepatocellular cancer. Nature 431, 1112–1117. https://doi.org/10.1038/nature03043

Sheiness, D., Bishop, J.M., 1979. DNA and RNA from uninfected vertebrate cells contain nucleotide sequences related to the putative transforming gene of avian myelocytomatosis virus. J. Virol. 31, 514–521.

Shekarabi, M., 2005. Deleted in Colorectal Cancer Binding Netrin-1 Mediates Cell Substrate Adhesion and Recruits Cdc42, Rac1, Pak1, and N-WASP into an Intracellular Signaling Complex That Promotes Growth Cone Expansion. J. Neurosci. 25, 3132–3141. https://doi.org/10.1523/JNEUROSCI.1920-04.2005

Shekarabi, M., Kennedy, T.E., 2002. The Netrin-1 Receptor DCC Promotes Filopodia Formation and Cell Spreading by Activating Cdc42 and Rac1. Mol. Cell. Neurosci. 19, 1–17. https://doi.org/10.1006/mcne.2001.1075

Sheng, G., 2015. Epiblast morphogenesis before gastrulation. Dev. Biol. 401, 17–24. https://doi.org/10.1016/j.ydbio.2014.10.003

Sheng, G., Foley, A.C., 2012. Diversification and conservation of the extraembryonic tissues in mediating nutrient uptake during amniote development: Nutrient uptake during amniote development. Ann. N. Y. Acad. Sci. 1271, 97–103. https://doi.org/10.1111/j.1749-6632.2012.06726.x

Sherr, C.J., 2001. The INK4a/ARF network in tumour suppression. Nat. Rev. Mol. Cell Biol. 2, 731–737. https://doi.org/10.1038/35096061

Shi, G., DiRenzo, D., Qu, C., Barney, D., Miley, D., Konieczny, S.F., 2013. Maintenance of acinar cell organization is critical to preventing Kras-induced acinar-ductal metaplasia. Oncogene 32, 1950–1958. https://doi.org/10.1038/onc.2012.210

Shi, Y., Massagué, J., 2003. Mechanisms of TGF-β Signaling from Cell Membrane to the Nucleus. Cell 113, 685–700. https://doi.org/10.1016/S0092-8674(03)00432-X

Shim, H., Chun, Y.S., Lewis, B.C., Dang, C.V., 1998. A unique glucose-dependent apoptotic pathway induced by c-Myc. Proc. Natl. Acad. Sci. 95, 1511–1516. https://doi.org/10.1073/pnas.95.4.1511

Shimizu, T., Ueda, J., Ho, J.C., Iwasaki, K., Poellinger, L., Harada, I., Sawada, Y., 2012. Dual Inhibition of Src and GSK3 Maintains Mouse Embryonic Stem Cells, Whose Differentiation Is Mechanically Regulated by Src Signaling. STEM CELLS 30, 1394–1404. https://doi.org/10.1002/stem.1119

Shirayoshi, Y., Okada, T.S., Takeichi, M., 1983. The calcium-dependent cell-cell adhesion system regulates inner cell mass formation and cell surface polarization in early mouse development. Cell 35, 631–638. https://doi.org/10.1016/0092-8674(83)90095-8

Shou, Y., Martelli, M.L., Gabrea, A., Qi, Y., Brents, L.A., Roschke, A., Dewald, G., Kirsch, I.R., Bergsagel, P.L., Kuehl, W.M., 2000. Diverse karyotypic abnormalities of the c-myc locus associated with c-myc dysregulation and tumor progression in multiple myeloma. Proc. Natl. Acad. Sci. 97, 228–233. https://doi.org/10.1073/pnas.97.1.228

Sigismund, S., Avanzato, D., Lanzetti, L., 2018. Emerging functions of the EGFR in cancer. Mol. Oncol. 12, 3–20. https://doi.org/10.1002/1878-0261.12155

Singh, S.K., Hawkins, C., Clarke, I.D., Squire, J.A., Bayani, J., Hide, T., Henkelman, R.M., Cusimano, M.D., Dirks, P.B., 2004. Identification of human brain tumour initiating cells. Nature 432, 396–401. https://doi.org/10.1038/nature03128

Smith, A.G., Heath, J.K., Donaldson, D.D., Wong, G.G., Moreau, J., Stahl, M., Rogers, D., 1988. Inhibition of pluripotential embryonic stem cell differentiation by purified polypeptides. Nature 336, 688–690. https://doi.org/10.1038/336688a0

Smith, B., Bhowmick, N., 2016. Role of EMT in Metastasis and Therapy Resistance. J. Clin. Med. 5, 17. https://doi.org/10.3390/jcm5020017

Smith, Z.D., Nachman, I., Regev, A., Meissner, A., 2010. Dynamic single-cell imaging of direct reprogramming reveals an early specifying event. Nat. Biotechnol. 28, 521–526. https://doi.org/10.1038/nbt.1632

Sodir, N.M., Swigart, L.B., Karnezis, A.N., Hanahan, D., Evan, G.I., Soucek, L., 2011. Endogenous Myc maintains the tumor microenvironment. Genes Dev. 25, 907–916. https://doi.org/10.1101/gad.2038411

Song, L.-B., Li, J., Liao, W.-T., Feng, Y., Yu, C.-P., Hu, L.-J., Kong, Q.-L., Xu, L.-H., Zhang, X., Liu, W.-L., Li, M.-Z., Zhang, L., Kang, T.-B., Fu, L.-W., Huang, W.-L., Xia, Y.-F., Tsao, S.W., Li, M., Band, V., Band, H., Shi, Q.-H., Zeng, Y.-X., Zeng, M.-S., 2009. The polycomb group protein Bmi-1 represses the tumor suppressor PTEN and induces epithelial-mesenchymal transition in human nasopharyngeal epithelial cells. J. Clin. Invest. 119, 3626–3636. https://doi.org/10.1172/JCI39374

Song, Y., Pan, G., Chen, L., Ma, S., Zeng, T., Man Chan, T.H., Li, L., Lian, Q., Chow, R., Cai, X., Li, Yan, Li, Yan, Liu, M., Li, Yun, Zhu, Y., Wong, N., Yuan, Y.-F., Pei, D., Guan, X.-Y., 2015. Loss of ATOH8 Increases Stem Cell Features of Hepatocellular Carcinoma Cells. Gastroenterology 149, 1068-1081.e5. https://doi.org/10.1053/j.gastro.2015.06.010

Soucek, L., Whitfield, J., Martins, C.P., Finch, A.J., Murphy, D.J., Sodir, N.M., Karnezis, A.N., Swigart, L.B., Nasi, S., Evan, G.I., 2008. Modelling Myc inhibition as a cancer therapy. Nature 455, 679–683. https://doi.org/10.1038/nature07260

Soufi, A., Donahue, G., Zaret, K.S., 2012. Facilitators and Impediments of the Pluripotency Reprogramming Factors' Initial Engagement with the Genome. Cell 151, 994–1004. https://doi.org/10.1016/j.cell.2012.09.045

Spechler, S.J., Souza, R.F., 2014. Barrett's Esophagus. N. Engl. J. Med. 371, 836–845. https://doi.org/10.1056/NEJMra1314704

Sridharan, R., Tchieu, J., Mason, M.J., Yachechko, R., Kuoy, E., Horvath, S., Zhou, Q., Plath, K., 2009. Role of the Murine Reprogramming Factors in the Induction of Pluripotency. Cell 136, 364–377. https://doi.org/10.1016/j.cell.2009.01.001

Srinivasan, K., Strickland, P., Valdes, A., Shin, G.C., Hinck, L., 2003. Netrin-1/neogenin interaction stabilizes multipotent progenitor cap cells during mammary gland morphogenesis. Dev. Cell 4, 371–382.

Stadtfeld, M., Apostolou, E., Ferrari, F., Choi, J., Walsh, R.M., Chen, T., Ooi, S.S.K., Kim, S.Y., Bestor, T.H., Shioda, T., Park, P.J., Hochedlinger, K., 2012. Ascorbic acid prevents loss of Dlk1-Dio3 imprinting and facilitates generation of all-iPS cell mice from terminally differentiated B cells. Nat. Genet. 44, 398–405, S1-2. https://doi.org/10.1038/ng.1110

Stadtfeld, M., Maherali, N., Breault, D.T., Hochedlinger, K., 2008. Defining Molecular Cornerstones during Fibroblast to iPS Cell Reprogramming in Mouse. Cell Stem Cell 2, 230–240. https://doi.org/10.1016/j.stem.2008.02.001

Stahl, N., Farruggella, T., Boulton, T., Zhong, Z., Darnell, J., Yancopoulos, G., 1995. Choice of STATs and other substrates specified by modular tyrosine-based motifs in cytokine receptors. Science 267, 1349–1353. https://doi.org/10.1126/science.7871433

Staller, P., Peukert, K., Kiermaier, A., Seoane, J., Lukas, J., Karsunky, H., Möröy, T., Bartek, J., Massagué, J., Hänel, F., Eilers, M., 2001. Repression of p15INK4b expression by Myc through association with Miz-1. Nat. Cell Biol. 3, 392–399. https://doi.org/10.1038/35070076

Stamos, J.L., Chu, M.L.-H., Enos, M.D., Shah, N., Weis, W.I., 2014. Structural basis of GSK-3 inhibition by N-terminal phosphorylation and by the Wnt receptor LRP6. eLife 3, e01998. https://doi.org/10.7554/eLife.01998

Stanco, A., Szekeres, C., Patel, N., Rao, S., Campbell, K., Kreidberg, J.A., Polleux, F., Anton, E.S., 2009. Netrin-1- 3 1 integrin interactions regulate the migration of interneurons through the cortical marginal zone. Proc. Natl. Acad. Sci. 106, 7595–7600. https://doi.org/10.1073/pnas.0811343106

Stavridis, M.P., Collins, B.J., Storey, K.G., 2010. Retinoic acid orchestrates fibroblast growth factor signalling to drive embryonic stem cell differentiation. Development 137, 881–890. https://doi.org/10.1242/dev.043117

Stavridis, M.P., Lunn, J.S., Collins, B.J., Storey, K.G., 2007. A discrete period of FGF-induced Erk1/2 signalling is required for vertebrate neural specification. Development 134, 2889–2894. https://doi.org/10.1242/dev.02858

Stein, E., 2001. Binding of DCC by Netrin-1 to Mediate Axon Guidance Independent of Adenosine A2B Receptor Activation. Science 291, 1976–1982. https://doi.org/10.1126/science.1059391

Stephenson, R.O., Rossant, J., Tam, P.P.L., 2012. Intercellular Interactions, Position, and Polarity in Establishing Blastocyst Cell Lineages and Embryonic Axes. Cold Spring Harb. Perspect. Biol. 4, a008235–a008235. https://doi.org/10.1101/cshperspect.a008235

Stewart, C.L., Kaspar, P., Brunet, L.J., Bhatt, H., Gadi, I., Köntgen, F., Abbondanzo, S.J., 1992. Blastocyst implantation depends on maternal expression of leukaemia inhibitory factor. Nature 359, 76–79. https://doi.org/10.1038/359076a0

Stewart, C.L., Stuhlmann, H., Jahner, D., Jaenisch, R., 1982. De novo methylation, expression, and infectivity of retroviral genomes introduced into embryonal carcinoma cells. Proc. Natl. Acad. Sci. 79, 4098–4102. https://doi.org/10.1073/pnas.79.13.4098

Stoeckli, E.T., 2018. Understanding axon guidance: are we nearly there yet? Development 145, dev151415. https://doi.org/10.1242/dev.151415

Stone, J., de Lange, T., Ramsay, G., Jakobovits, E., Bishop, J.M., Varmus, H., Lee, W., 1987. Definition of regions in human c-myc that are involved in transformation and nuclear localization. Mol. Cell. Biol. 7, 1697–1709. https://doi.org/10.1128/MCB.7.5.1697

Strauss, R., Li, Z.-Y., Liu, Y., Beyer, I., Persson, J., Sova, P., Möller, T., Pesonen, S., Hemminki, A., Hamerlik, P., Drescher, C., Urban, N., Bartek, J., Lieber, A., 2011. Analysis of Epithelial and Mesenchymal Markers in Ovarian Cancer Reveals Phenotypic Heterogeneity and Plasticity. PLoS ONE 6, e16186. https://doi.org/10.1371/journal.pone.0016186

Strumpf, D., 2005. Cdx2 is required for correct cell fate specification and differentiation of trophectoderm in the mouse blastocyst. Development 132, 2093–2102. https://doi.org/10.1242/dev.01801

Sun, H., Ghaffari, S., Taneja, R., 2007. bHLH-Orange Transcription Factors in Development and Cancer. Transl. Oncogenomics 2, 107–120.

Sun, X.-H., Baltimore, D., 1991. An inhibitory domain of E12 transcription factor prevents DNA binding in E12 homodimers but not in E12 heterodimers. Cell 64, 459–470. https://doi.org/10.1016/0092-8674(91)90653-G

Sung, P.-J., Rama, N., Imbach, J., Fiore, S., Ducarouge, B., Neves, D., Chen, H.-W., Bernard, D., Yang, P.-C., Bernet, A., Depil, S., Mehlen, P., 2019. Cancer-Associated Fibroblasts Produce Netrin-1 to Control Cancer Cell Plasticity. Cancer Res. 79, 3651–3661. https://doi.org/10.1158/0008-5472.CAN-18-2952

Suva, M.L., Riggi, N., Bernstein, B.E., 2013. Epigenetic Reprogramming in Cancer. Science 339, 1567–1570. https://doi.org/10.1126/science.1230184

Tabata, T., 2004. Morphogens, their identification and regulation. Development 131, 703–712. https://doi.org/10.1242/dev.01043

Takada, S., Stark, K.L., Shea, M.J., Vassileva, G., McMahon, J.A., McMahon, A.P., 1994. Wnt-3a regulates somite and tailbud formation in the mouse embryo. Genes Dev. 8, 174–189. https://doi.org/10.1101/gad.8.2.174

Takahashi, K., Tanabe, K., Ohnuki, M., Narita, M., Ichisaka, T., Tomoda, K., Yamanaka, S., 2007. Induction of Pluripotent Stem Cells from Adult Human Fibroblasts by Defined Factors. Cell 131, 861–872. https://doi.org/10.1016/j.cell.2007.11.019

Takahashi, K., Yamanaka, S., 2006. Induction of pluripotent stem cells from mouse embryonic and adult fibroblast cultures by defined factors. Cell 126, 663–676. https://doi.org/10.1016/j.cell.2006.07.024

Tamai, K., Semenov, M., Kato, Y., Spokony, R., Liu, C., Katsuyama, Y., Hess, F., Saint-Jeannet, J.-P., He, X., 2000. LDL-receptor-related proteins in Wnt signal transduction. Nature 407, 530–535. https://doi.org/10.1038/35035117

Taub, R., Kirsch, I., Morton, C., Lenoir, G., Swan, D., Tronick, S., Aaronson, S., Leder, P., 1982. Translocation of the c-myc gene into the immunoglobulin heavy chain locus in human Burkitt lymphoma and murine plasmacytoma cells. Proc. Natl. Acad. Sci. 79, 7837–7841. https://doi.org/10.1073/pnas.79.24.7837

Tee, W.-W., Shen, S.S., Oksuz, O., Narendra, V., Reinberg, D., 2014. Erk1/2 Activity Promotes Chromatin Features and RNAPII Phosphorylation at Developmental Promoters in Mouse ESCs. Cell 156, 678–690. https://doi.org/10.1016/j.cell.2014.01.009

ten Berge, D., Kurek, D., Blauwkamp, T., Koole, W., Maas, A., Eroglu, E., Siu, R.K., Nusse, R., 2011a. Embryonic stem cells require Wnt proteins to prevent differentiation to epiblast stem cells. Nat. Cell Biol. 13, 1070–1075. https://doi.org/10.1038/ncb2314

ten Berge, D., Kurek, D., Blauwkamp, T., Koole, W., Maas, A., Eroglu, E., Siu, R.K., Nusse, R., 2011b. Embryonic stem cells require Wnt proteins to prevent differentiation to epiblast stem cells. Nat. Cell Biol. 13, 1070–1075. https://doi.org/10.1038/ncb2314

Tesar, P.J., Chenoweth, J.G., Brook, F.A., Davies, T.J., Evans, E.P., Mack, D.L., Gardner, R.L., McKay, R.D.G., 2007. New cell lines from mouse epiblast share defining features with human embryonic stem cells. Nature 448, 196–199. https://doi.org/10.1038/nature05972

Thiebault, K., Mazelin, L., Pays, L., Llambi, F., Joly, M.-O., Scoazec, J.-Y., Saurin, J.-C., Romeo, G., Mehlen, P., 2003. The netrin-1 receptors UNC5H are putative tumor suppressors controlling cell death commitment. Proc. Natl. Acad. Sci. 100, 4173–4178. https://doi.org/10.1073/pnas.0738063100

Thomas, L.R., Wang, Q., Grieb, B.C., Phan, J., Foshage, A.M., Sun, Q., Olejniczak, E.T., Clark, T., Dey, S., Lorey, S., Alicie, B., Howard, G.C., Cawthon, B., Ess, K.C., Eischen, C.M., Zhao, Z., Fesik, S.W., Tansey, W.P., 2015. Interaction with WDR5 Promotes Target Gene Recognition and Tumorigenesis by MYC. Mol. Cell 58, 440–452. https://doi.org/10.1016/j.molcel.2015.02.028

Thomas, P.A., Kirschmann, D.A., Cerhan, J.R., Folberg, R., Seftor, E.A., Sellers, T.A., Hendrix, M.J., 1999. Association between keratin and vimentin expression, malignant phenotype, and survival in postmenopausal breast cancer patients. Clin. Cancer Res. Off. J. Am. Assoc. Cancer Res. 5, 2698–2703.

Thompson, A.A., Walters, M.C., Kwiatkowski, J., Rasko, J.E.J., Ribeil, J.-A., Hongeng, S., Magrin, E., Schiller, G.J., Payen, E., Semeraro, M., Moshous, D., Lefrere, F., Puy, H., Bourget, P., Magnani, A., Caccavelli, L., Diana, J.-S., Suarez, F., Monpoux, F., Brousse, V., Poirot, C., Brouzes, C., Meritet, J.-F., Pondarré, C., Beuzard, Y., Chrétien, S., Lefebvre, T., Teachey, D.T., Anurathapan, U., Ho, P.J., von Kalle, C., Kletzel, M., Vichinsky, E., Soni, S., Veres, G., Negre, O., Ross, R.W., Davidson, D., Petrusich, A., Sandler, L., Asmal, M., Hermine, O., De Montalembert, M., Hacein-Bey-Abina, S., Blanche, S., Leboulch, P., Cavazzana, M., 2018. Gene Therapy in Patients with Transfusion-Dependent β-Thalassemia. N. Engl. J. Med. 378, 1479–1493. https://doi.org/10.1056/NEJMoa1705342

Thomson, M., Liu, S.J., Zou, L.-N., Smith, Z., Meissner, A., Ramanathan, S., 2011. Pluripotency Factors in Embryonic Stem Cells Regulate Differentiation into Germ Layers. Cell 145, 875–889. https://doi.org/10.1016/j.cell.2011.05.017

Timpl, R., Rohde, H., Robey, P.G., Rennard, S.I., Foidart, J.M., Martin, G.R., 1979. Laminin--a glycoprotein from basement membranes. J. Biol. Chem. 254, 9933–9937.

Tomasetti, C., Vogelstein, B., 2015. Variation in cancer risk among tissues can be explained by the number of stem cell divisions. Science 347, 78–81. https://doi.org/10.1126/science.1260825

Tong, J., Killeen, M., Steven, R., Binns, K.L., Culotti, J., Pawson, T., 2001. Netrin Stimulates Tyrosine Phosphorylation of the UNC-5 Family of Netrin Receptors and Induces Shp2 Binding to the RCM Cytodomain. J. Biol. Chem. 276, 40917–40925. https://doi.org/10.1074/jbc.M103872200

Toyooka, Y., Shimosato, D., Murakami, K., Takahashi, K., Niwa, H., 2008. Identification and characterization of subpopulations in undifferentiated ES cell culture. Development 135, 909–918. https://doi.org/10.1242/dev.017400

Tracy, L.E., Minasian, R.A., Caterson, E.J., 2016. Extracellular Matrix and Dermal Fibroblast Function in the Healing Wound. Adv. Wound Care 5, 119–136. https://doi.org/10.1089/wound.2014.0561

Tsuchida, K., Nakatani, M., Yamakawa, N., Hashimoto, O., Hasegawa, Y., Sugino, H., 2004. Activin isoforms signal through type I receptor serine/threonine kinase ALK7. Mol. Cell. Endocrinol. 220, 59–65. https://doi.org/10.1016/j.mce.2004.03.009

Tsuchiya, K., Nakamura, T., Okamoto, R., Kanai, T., Watanabe, M., 2007. Reciprocal targeting of Hath1 and beta-catenin by Wnt glycogen synthase kinase 3beta in human colon cancer. Gastroenterology 132, 208–220. https://doi.org/10.1053/j.gastro.2006.10.031

Tsumura, A., Hayakawa, T., Kumaki, Y., Takebayashi, S., Sakaue, M., Matsuoka, C., Shimotohno, K., Ishikawa, F., Li, E., Ueda, H.R., Nakayama, J., Okano, M., 2006. Maintenance of self-renewal ability of mouse embryonic stem cells in the absence of DNA methyltransferases Dnmt1, Dnmt3a and Dnmt3b. Genes Cells 11, 805–814. https://doi.org/10.1111/j.1365-2443.2006.00984.x

Tuveson, D.A., Zhu, L., Gopinathan, A., Willis, N.A., Kachatrian, L., Grochow, R., Pin, C.L., Mitin, N.Y., Taparowsky, E.J., Gimotty, P.A., Hruban, R.H., Jacks, T., Konieczny, S.F., 2006. *Mist1-Kras ^{G12D}* Knock-In Mice Develop Mixed Differentiation Metastatic Exocrine Pancreatic Carcinoma and Hepatocellular Carcinoma. Cancer Res. 66, 242–247. https://doi.org/10.1158/0008-5472.CAN-05-2305

Ullian, E.M., 2001. Control of Synapse Number by Glia. Science 291, 657–661. https://doi.org/10.1126/science.291.5504.657

Utikal, J., Polo, J.M., Stadtfeld, M., Maherali, N., Kulalert, W., Walsh, R.M., Khalil, A., Rheinwald, J.G., Hochedlinger, K., 2009a. Immortalization eliminates a roadblock during cellular reprogramming into iPS cells. Nature 460, 1145–1148. https://doi.org/10.1038/nature08285

Utikal, J., Polo, J.M., Stadtfeld, M., Maherali, N., Kulalert, W., Walsh, R.M., Khalil, A., Rheinwald, J.G., Hochedlinger, K., 2009b. Immortalization eliminates a roadblock during cellular reprogramming into iPS cells. Nature 460, 1145–1148. https://doi.org/10.1038/nature08285

Vallier, L., Mendjan, S., Brown, S., Chng, Z., Teo, A., Smithers, L.E., Trotter, M.W.B., Cho, C.H.-H., Martinez, A., Rugg-Gunn, P., Brons, G., Pedersen, R.A., 2009. Activin/Nodal signalling maintains pluripotency by controlling Nanog expression. Development 136, 1339–1349. https://doi.org/10.1242/dev.033951

van de Wetering, M., Cavallo, R., Dooijes, D., van Beest, M., van Es, J., Loureiro, J., Ypma, A., Hursh, D., Jones, T., Bejsovec, A., Peifer, M., Mortin, M., Clevers, H., 1997. Armadillo Coactivates Transcription Driven by the Product of the Drosophila Segment Polarity Gene dTCF. Cell 88, 789–799. https://doi.org/10.1016/S0092-8674(00)81925-X

Van Keymeulen, A., Lee, M.Y., Ousset, M., Brohée, S., Rorive, S., Giraddi, R.R., Wuidart, A., Bouvencourt, G., Dubois, C., Salmon, I., Sotiriou, C., Phillips, W.A., Blanpain, C., 2015. Reactivation of multipotency by oncogenic PIK3CA induces breast tumour heterogeneity. Nature 525, 119–123. https://doi.org/10.1038/nature14665

van Oevelen, C., Kallin, E., Graf, T., 2013. Transcription factor-induced enhancer modulations during cell fate conversions. Curr. Opin. Genet. Dev. 23, 562–567. https://doi.org/10.1016/j.gde.2013.07.003

Vander Heiden, M.G., Cantley, L.C., Thompson, C.B., 2009. Understanding the Warburg Effect: The Metabolic Requirements of Cell Proliferation. Science 324, 1029–1033. https://doi.org/10.1126/science.1160809

Varadarajan, S.G., Kong, J.H., Phan, K.D., Kao, T.-J., Panaitof, S.C., Cardin, J., Eltzschig, H., Kania, A., Novitch, B.G., Butler, S.J., 2017. Netrin1 Produced by Neural Progenitors, Not Floor Plate Cells, Is Required for Axon Guidance in the Spinal Cord. Neuron 94, 790-799.e3. https://doi.org/10.1016/j.neuron.2017.03.007

Varela-Echavarría, A., Tucker, A., Püschel, A.W., Guthrie, S., 1997. Motor Axon Subpopulations Respond Differentially to the Chemorepellents Netrin-1 and Semaphorin D. Neuron 18, 193–207. https://doi.org/10.1016/S0896-6273(00)80261-5

Vasan, N., Boyer, J.L., Herbst, R.S., 2014. A RAS Renaissance: Emerging Targeted Therapies for KRAS-Mutated Non-Small Cell Lung Cancer. Clin. Cancer Res. 20, 3921–3930. https://doi.org/10.1158/1078-0432.CCR-13-1762

Vaseva, A.V., Blake, D.R., Gilbert, T.S.K., Ng, S., Hostetter, G., Azam, S.H., Ozkan-Dagliyan, I., Gautam, P., Bryant, K.L., Pearce, K.H., Herring, L.E., Han, H., Graves, L.M., Witkiewicz, A.K., Knudsen, E.S., Pecot, C.V., Rashid, N., Houghton, P.J., Wennerberg, K., Cox, A.D., Der, C.J., 2018. KRAS Suppression-Induced Degradation of MYC Is Antagonized by a MEK5-ERK5 Compensatory Mechanism. Cancer Cell 34, 807-822.e7. https://doi.org/10.1016/j.ccell.2018.10.001

Velasco, S., Kedaigle, A.J., Simmons, S.K., Nash, A., Rocha, M., Quadrato, G., Paulsen, B., Nguyen, L., Adiconis, X., Regev, A., Levin, J.Z., Arlotta, P., 2019. Individual brain organoids reproducibly form cell diversity of the human cerebral cortex. Nature 570, 523–527. https://doi.org/10.1038/s41586-019-1289-x

Vielmetter, J., 1994. Neogenin, an avian cell surface protein expressed during terminal neuronal differentiation, is closely related to the human tumor suppressor molecule deleted in colorectal cancer. J. Cell Biol. 127, 2009–2020. https://doi.org/10.1083/jcb.127.6.2009

Vierbuchen, T., Ostermeier, A., Pang, Z.P., Kokubu, Y., Südhof, T.C., Wernig, M., 2010. Direct conversion of fibroblasts to functional neurons by defined factors. Nature 463, 1035–1041. https://doi.org/10.1038/nature08797

Visvader, J.E., Lindeman, G.J., 2012. Cancer Stem Cells: Current Status and Evolving Complexities. Cell Stem Cell 10, 717–728. https://doi.org/10.1016/j.stem.2012.05.007

Vogelstein, B., Papadopoulos, N., Velculescu, V.E., Zhou, S., Diaz, L.A., Kinzler, K.W., 2013. Cancer Genome Landscapes. Science 339, 1546–1558. https://doi.org/10.1126/science.1235122

von der Lehr, N., Johansson, S., Wu, S., Bahram, F., Castell, A., Cetinkaya, C., Hydbring, P., Weidung, I., Nakayama, K., Nakayama, K.I., Söderberg, O., Kerppola, T.K., Larsson, L.-G., 2003. The F-box protein Skp2 participates in c-Myc proteosomal degradation and acts as a cofactor for c-Myc-regulated transcription. Mol. Cell 11, 1189–1200.

von Figura, G., Morris, J.P., Wright, C.V.E., Hebrok, M., 2014. Nr5a2 maintains acinar cell differentiation and constrains oncogenic Kras-mediated pancreatic neoplastic initiation. Gut 63, 656–664. https://doi.org/10.1136/gutjnl-2012-304287

Wade Harper, J., 1993. The p21 Cdk-interacting protein Cip1 is a potent inhibitor of G1 cyclin-dependent kinases. Cell 75, 805–816. https://doi.org/10.1016/0092-8674(93)90499-G

Wagenblast, E., Soto, M., Gutiérrez-Ángel, S., Hartl, C.A., Gable, A.L., Maceli, A.R., Erard, N., Williams, A.M., Kim, S.Y., Dickopf, S., Harrell, J.C., Smith, A.D., Perou, C.M., Wilkinson, J.E., Hannon, G.J., Knott, S.R.V., 2015. A model of breast cancer heterogeneity reveals vascular mimicry as a driver of metastasis. Nature 520, 358–362. https://doi.org/10.1038/nature14403

Wagers, A.J., Weissman, I.L., 2004. Plasticity of Adult Stem Cells. Cell 116, 639–648. https://doi.org/10.1016/S0092-8674(04)00208-9

Wagner, M., Lopez, M.E., Cahn, M., Korc, M., 1998. Suppression of fibroblast growth factor receptor signaling inhibits pancreatic cancer growth in vitro and in vivo. Gastroenterology 114, 798–807. https://doi.org/10.1016/S0016-5085(98)70594-3

Wakabayashi, Y., Watanabe, H., Inoue, J., Takeda, N., Sakata, J., Mishima, Y., Hitomi, J., Yamamoto, T., Utsuyama, M., Niwa, O., Aizawa, S., Kominami, R., 2003. Bcl11b is required for differentiation and survival of alphabeta T lymphocytes. Nat. Immunol. 4, 533–539. https://doi.org/10.1038/ni927

Wang, C., Liu, H., Qiu, Q., Zhang, Z., Gu, Y., He, Z., 2017. TCRP1 promotes NIH/3T3 cell transformation by over-activating PDK1 and AKT1. Oncogenesis 6, e323–e323. https://doi.org/10.1038/oncsis.2017.18

Wang, H., Boussouar, A., Mazelin, L., Tauszig-Delamasure, S., Sun, Y., Goldschneider, D., Paradisi, A., Mehlen, P., 2018. The Proto-oncogene c-Kit Inhibits Tumor Growth by Behaving as a Dependence Receptor. Mol. Cell 72, 413-425.e5. https://doi.org/10.1016/j.molcel.2018.08.040

Wang, H., Copeland, N.G., Gilbert, D.J., Jenkins, N.A., Tessier-Lavigne, M., 1999. Netrin-3, a mouse homolog of human NTN2L, is highly expressed in sensory ganglia and shows differential binding to netrin receptors. J. Neurosci. Off. J. Soc. Neurosci. 19, 4938–4947.

Wang, H., Mannava, S., Grachtchouk, V., Zhuang, D., Soengas, M.S., Gudkov, A.V., Prochownik, E.V., Nikiforov, M.A., 2008. c-Myc depletion inhibits proliferation of human tumor cells at various stages of the cell cycle. Oncogene 27, 1905–1915. https://doi.org/10.1038/sj.onc.1210823

Wang, L.-H., Baker, N.E., 2015. E Proteins and ID Proteins: Helix-Loop-Helix Partners in Development and Disease. Dev. Cell 35, 269–280. https://doi.org/10.1016/j.devcel.2015.10.019

Wang, R., Chadalavada, K., Wilshire, J., Kowalik, U., Hovinga, K.E., Geber, A., Fligelman, B., Leversha, M., Brennan, C., Tabar, V., 2010. Glioblastoma stem-like cells give rise to tumour endothelium. Nature 468, 829–833. https://doi.org/10.1038/nature09624

Wang, W., Reeves, W.B., Ramesh, G., 2009. Netrin-1 increases proliferation and migration of renal proximal tubular epithelial cells via the UNC5B receptor. Am. J. Physiol.-Ren. Physiol. 296, F723–F729. https://doi.org/10.1152/ajprenal.90686.2008

Wang, Z., Xie, J., Yan, M., Wang, J., Wang, X., Zhang, J., Zhang, Y., Li, P., Lei, X., Huang, Q., Lin, S., Guo, X., Liu, Q., 2016. Downregulation of ATOH8 induced by EBV-encoded LMP1 contributes to the malignant phenotype of nasopharyngeal carcinoma. Oncotarget 7. https://doi.org/10.18632/oncotarget.8503

Wapinski, O.L., Vierbuchen, T., Qu, K., Lee, Q.Y., Chanda, S., Fuentes, D.R., Giresi, P.G., Ng, Y.H., Marro, S., Neff, N.F., Drechsel, D., Martynoga, B., Castro, D.S., Webb, A.E., Südhof, T.C., Brunet, A., Guillemot, F., Chang, H.Y., Wernig, M., 2013. Hierarchical Mechanisms for Direct Reprogramming of Fibroblasts to Neurons. Cell 155, 621–635. https://doi.org/10.1016/j.cell.2013.09.028

Warburg, O., 1956. On respiratory impairment in cancer cells. Science 124, 269–270.

Warrell, R.P., Frankel, S.R., Miller, W.H., Scheinberg, D.A., Itri, L.M., Hittelman, W.N., Vyas, R., Andreeff, M., Tafuri, A., Jakubowski, A., 1991. Differentiation therapy of acute promyelocytic leukemia with tretinoin (all-trans-retinoic acid). N. Engl. J. Med. 324, 1385–1393. https://doi.org/10.1056/NEJM199105163242002

Warren, L., Manos, P.D., Ahfeldt, T., Loh, Y.-H., Li, H., Lau, F., Ebina, W., Mandal, P.K., Smith, Z.D., Meissner, A., Daley, G.Q., Brack, A.S., Collins, J.J., Cowan, C., Schlaeger, T.M., Rossi, D.J., 2010. Highly Efficient Reprogramming to Pluripotency and Directed Differentiation of Human Cells with Synthetic Modified mRNA. Cell Stem Cell 7, 618–630. https://doi.org/10.1016/j.stem.2010.08.012

Webb, D.J., Donais, K., Whitmore, L.A., Thomas, S.M., Turner, C.E., Parsons, J.T., Horwitz, A.F., 2004. FAK-Src signalling through paxillin, ERK and MLCK regulates adhesion disassembly. Nat. Cell Biol. 6, 154–161. https://doi.org/10.1038/ncb1094

Weinberg, R.A., 1995. The retinoblastoma protein and cell cycle control. Cell 81, 323–330. https://doi.org/10.1016/0092-8674(95)90385-2

Weinberger, L., Ayyash, M., Novershtern, N., Hanna, J.H., 2016. Dynamic stem cell states: naive to primed pluripotency in rodents and humans. Nat. Rev. Mol. Cell Biol. 17, 155–169. https://doi.org/10.1038/nrm.2015.28

Weiss, W.A., 1997. Targeted expression of MYCN causes neuroblastoma in transgenic mice. EMBO J. 16, 2985–2995. https://doi.org/10.1093/emboj/16.11.2985

Wellner, U., Schubert, J., Burk, U.C., Schmalhofer, O., Zhu, F., Sonntag, A., Waldvogel, B., Vannier, C., Darling, D., Hausen, A. zur, Brunton, V.G., Morton, J., Sansom, O., Schüler, J., Stemmler, M.P., Herzberger, C., Hopt, U., Keck, T., Brabletz, S., Brabletz, T., 2009. The EMT-activator ZEB1 promotes tumorigenicity by repressing stemness-inhibiting microRNAs. Nat. Cell Biol. 11, 1487–1495. https://doi.org/10.1038/ncb1998

Wentworth, L.E., 1984. The development of the cervical spinal cord of the mouse embryo. I. A Golgi analysis of ventral root neuron differentiation. J. Comp. Neurol. 222, 81–95. https://doi.org/10.1002/cne.902220108

Wernig, M., Lengner, C.J., Hanna, J., Lodato, M.A., Steine, E., Foreman, R., Staerk, J., Markoulaki, S., Jaenisch, R., 2008a. A drug-inducible transgenic system for direct reprogramming of multiple somatic cell types. Nat. Biotechnol. 26, 916–924. https://doi.org/10.1038/nbt1483

Wernig, M., Meissner, A., Cassady, J.P., Jaenisch, R., 2008b. c-Myc is dispensable for direct reprogramming of mouse fibroblasts. Cell Stem Cell 2, 10–12. https://doi.org/10.1016/j.stem.2007.12.001

Wernig, M., Meissner, A., Foreman, R., Brambrink, T., Ku, M., Hochedlinger, K., Bernstein, B.E., Jaenisch, R., 2007. In vitro reprogramming of fibroblasts into a pluripotent ES-cell-like state. Nature 448, 318–324. https://doi.org/10.1038/nature05944

Wierstra, I., Alves, J., 2008. The c-myc Promoter: Still MysterY and Challenge, in: Advances in Cancer Research. Elsevier, pp. 113–333. https://doi.org/10.1016/S0065-230X(07)99004-1

Wiese, K.E., Nusse, R., van Amerongen, R., 2018. Wnt signalling: conquering complexity. Development 145, dev165902. https://doi.org/10.1242/dev.165902

Wilder, P.J., Kelly, D., Brigman, K., Peterson, C.L., Nowling, T., Gao, Q.-S., McComb, R.D., Capecchi, M.R., Rizzino, A., 1997. Inactivation of the FGF-4 Gene in Embryonic Stem Cells Alters the Growth and/or the Survival of Their Early Differentiated Progeny. Dev. Biol. 192, 614–629. https://doi.org/10.1006/dbio.1997.8777

Willert, K., Brown, J.D., Danenberg, E., Duncan, A.W., Weissman, I.L., Reya, T., Yates, J.R., Nusse, R., 2003. Wnt proteins are lipid-modified and can act as stem cell growth factors. Nature 423, 448–452. https://doi.org/10.1038/nature01611

Williams, M.E., Lu, X., McKenna, W.L., Washington, R., Boyette, A., Strickland, P., Dillon, A., Kaprielian, Z., Tessier-Lavigne, M., Hinck, L., 2006. UNC5A promotes neuronal apoptosis during spinal cord development independent of netrin-1. Nat. Neurosci. 9, 996–998. https://doi.org/10.1038/nn1736

Williams, R.L., Hilton, D.J., Pease, S., Willson, T.A., Stewart, C.L., Gearing, D.P., Wagner, E.F., Metcalf, D., Nicola, N.A., Gough, N.M., 1988. Myeloid leukaemia inhibitory factor maintains the developmental potential of embryonic stem cells. Nature 336, 684–687. https://doi.org/10.1038/336684a0

Wilson, N.H., Key, B., 2006. Neogenin interacts with RGMa and Netrin-1 to guide axons within the embryonic vertebrate forebrain. Dev. Biol. 296, 485–498. https://doi.org/10.1016/j.ydbio.2006.06.018

Wray, J., Kalkan, T., Gomez-Lopez, S., Eckardt, D., Cook, A., Kemler, R., Smith, A., 2011. Inhibition of glycogen synthase kinase-3 alleviates Tcf3 repression of the pluripotency network and increases embryonic stem cell resistance to differentiation. Nat. Cell Biol. 13, 838–845. https://doi.org/10.1038/ncb2267

Wray, J., Kalkan, T., Smith, A.G., 2010. The ground state of pluripotency. Biochem. Soc. Trans. 38, 1027–1032. https://doi.org/10.1042/BST0381027

Wu, S.-Y., Lee, A.-Y., Lai, H.-T., Zhang, H., Chiang, C.-M., 2013. Phospho Switch Triggers Brd4 Chromatin Binding and Activator Recruitment for Gene-Specific Targeting. Mol. Cell 49, 843–857. https://doi.org/10.1016/j.molcel.2012.12.006

Wutz, A., Jaenisch, R., 2000. A shift from reversible to irreversible X inactivation is triggered during ES cell differentiation. Mol. Cell 5, 695–705.

Xie, H., Ye, M., Feng, R., Graf, T., 2004. Stepwise reprogramming of B cells into macrophages. Cell 117, 663–676. https://doi.org/10.1016/s0092-8674(04)00419-2

Xu, K., Wu, Z., Renier, N., Antipenko, A., Tzvetkova-Robev, D., Xu, Y., Minchenko, M., Nardi-Dei, V., Rajashankar, K.R., Himanen, J., Tessier-Lavigne, M., Nikolov, D.B., 2014. Structures of netrin-1 bound to two receptors provide insight into its axon guidance mechanism. Science 344, 1275–1279. https://doi.org/10.1126/science.1255149

Xu, X.L., Singh, H.P., Wang, L., Qi, D.-L., Poulos, B.K., Abramson, D.H., Jhanwar, S.C., Cobrinik, D., 2014. Rb suppresses human cone-precursor-derived retinoblastoma tumours. Nature 514, 385.

Yada, M., Hatakeyama, S., Kamura, T., Nishiyama, M., Tsunematsu, R., Imaki, H., Ishida, N., Okumura, F., Nakayama, K., Nakayama, K.I., 2004. Phosphorylation-dependent degradation of c-Myc is mediated by the F-box protein Fbw7. EMBO J. 23, 2116–2125. https://doi.org/10.1038/sj.emboj.7600217

Yagi, R., Kohn, M.J., Karavanova, I., Kaneko, K.J., Vullhorst, D., DePamphilis, M.L., Buonanno, A., 2007. Transcription factor TEAD4 specifies the trophectoderm lineage at the beginning of mammalian development. Development 134, 3827–3836. https://doi.org/10.1242/dev.010223

Yamagishi, S., Yamada, K., Sawada, M., Nakano, S., Mori, N., Sawamoto, K., Sato, K., 2015. Netrin-5 is highly expressed in neurogenic regions of the adult brain. Front. Cell. Neurosci. 9, 146. https://doi.org/10.3389/fncel.2015.00146

Yamaji, M., Ueda, J., Hayashi, K., Ohta, H., Yabuta, Y., Kurimoto, K., Nakato, R., Yamada, Y., Shirahige, K., Saitou, M., 2013. PRDM14 Ensures Naive Pluripotency through Dual Regulation of Signaling and Epigenetic Pathways in Mouse Embryonic Stem Cells. Cell Stem Cell 12, 368–382. https://doi.org/10.1016/j.stem.2012.12.012

Yamanaka, Y., Lanner, F., Rossant, J., 2010. FGF signal-dependent segregation of primitive endoderm and epiblast in the mouse blastocyst. Development 137, 715–724. https://doi.org/10.1242/dev.043471
Yamashita, A., Morioka, M., Kishi, H., Kimura, T., Yahara, Y., Okada, M., Fujita, K., Sawai, H., Ikegawa, S., Tsumaki, N., 2014. Statin treatment rescues FGFR3 skeletal dysplasia phenotypes. Nature 513, 507–511. https://doi.org/10.1038/nature13775
Yang, J., Weinberg, R.A., 2008. Epithelial-Mesenchymal Transition: At the Crossroads of Development and Tumor Metastasis. Dev. Cell 14, 818–829. https://doi.org/10.1016/j.devcel.2008.05.009
Yanger, K., Zong, Y., Maggs, L.R., Shapira, S.N., Maddipati, R., Aiello, N.M., Thung, S.N., Wells, R.G., Greenbaum, L.E., Stanger, B.Z., 2013. Robust cellular reprogramming occurs spontaneously during liver regeneration. Genes Dev. 27, 719–724. https://doi.org/10.1101/gad.207803.112
Yao, J., Zhou, J., Liu, Q., Lu, D., Wang, L., Qiao, X., Jia, W., 2010. Atoh8, a bHLH transcription factor, is required for the development of retina and skeletal muscle in zebrafish. PloS One 5, e10945. https://doi.org/10.1371/journal.pone.0010945
Ye, M., He, Y., Lin, H., Yang, S., Zhou, Y., Zhou, L., Zhong, J., Lu, G., Zheng, J., Xue, Z.-X., Cai, Z.-Z., 2017. High expression of atonal homolog 8 predicts a poor clinical outcome in patients with colorectal cancer and contributes to tumor progression. Oncol. Rep. 37, 2955–2963. https://doi.org/10.3892/or.2017.5554
Yebra, M., Montgomery, A.M.P., Diaferia, G.R., Kaido, T., Silletti, S., Perez, B., Just, M.L., Hildbrand, S., Hurford, R., Florkiewicz, E., Tessier-Lavigne, M., Cirulli, V., 2003. Recognition of the neural chemoattractant Netrin-1 by integrins alpha6beta4 and alpha3beta1 regulates epithelial cell adhesion and migration. Dev. Cell 5, 695–707.
Yee, K.T., Simon, H.H., Tessier-Lavigne, M., O'Leary, D.D.M., 1999. Extension of Long Leading Processes and Neuronal Migration in the Mammalian Brain Directed by the Chemoattractant Netrin-1. Neuron 24, 607–622. https://doi.org/10.1016/S0896-6273(00)81116-2
Yi, F., Pereira, L., Merrill, B.J., 2008. Tcf3 Functions as a Steady-State Limiter of Transcriptional Programs of Mouse Embryonic Stem Cell Self-Renewal. Stem Cells 26, 1951–1960. https://doi.org/10.1634/stemcells.2008-0229
Yin, Y., Sanes, J.R., Miner, J.H., 2000. Identification and expression of mouse netrin-4. Mech. Dev. 96, 115–119. https://doi.org/10.1016/s0925-4773(00)00369-5
Ying, Q.-L., Nichols, J., Chambers, I., Smith, A., 2003a. BMP Induction of Id Proteins Suppresses Differentiation and Sustains Embryonic Stem Cell Self-Renewal in Collaboration with STAT3. Cell 115, 281–292. https://doi.org/10.1016/S0092-8674(03)00847-X
Ying, Q.-L., Stavridis, M., Griffiths, D., Li, M., Smith, A., 2003b. Conversion of embryonic stem cells into neuroectodermal precursors in adherent monoculture. Nat. Biotechnol. 21, 183–186. https://doi.org/10.1038/nbt780
Ying, Q.-L., Wray, J., Nichols, J., Batlle-Morera, L., Doble, B., Woodgett, J., Cohen, P., Smith, A., 2008. The ground state of embryonic stem cell self-renewal. Nature 453, 519–523. https://doi.org/10.1038/nature06968
Yu, F., Li, J., Chen, H., Fu, J., Ray, S., Huang, S., Zheng, H., Ai, W., 2011. Kruppel-like factor 4 (KLF4) is required for maintenance of breast cancer stem cells and for cell migration and invasion. Oncogene 30, 2161–2172. https://doi.org/10.1038/onc.2010.591
Yu, F.-X., Guan, K.-L., 2013. The Hippo pathway: regulators and regulations. Genes Dev. 27, 355–371. https://doi.org/10.1101/gad.210773.112
Yu, J., Vodyanik, M.A., Smuga-Otto, K., Antosiewicz-Bourget, J., Frane, J.L., Tian, S., Nie, J., Jonsdottir, G.A., Ruotti, V., Stewart, R., Slukvin, I.I., Thomson, J.A., 2007. Induced Pluripotent Stem Cell Lines Derived from Human Somatic Cells. Science 318, 1917–1920. https://doi.org/10.1126/science.1151526
Yuan, S., Norgard, R.J., Stanger, B.Z., 2019. Cellular Plasticity in Cancer. Cancer Discov. 9, 837–851. https://doi.org/10.1158/2159-8290.CD-19-0015
Yuneva, M., Zamboni, N., Oefner, P., Sachidanandam, R., Lazebnik, Y., 2007. Deficiency in glutamine but not glucose induces MYC-dependent apoptosis in human cells. J. Cell Biol. 178, 93–105. https://doi.org/10.1083/jcb.200703099
Yung, A.R., Nishitani, A.M., Goodrich, L.V., 2015. Phenotypic analysis of mice completely lacking netrin 1. Dev. Camb. Engl. 142, 3686–3691. https://doi.org/10.1242/dev.128942
Zaravinos, A., Lambrou, G.I., Boulalas, I., Delakas, D., Spandidos, D.A., 2011. Identification of common differentially expressed genes in urinary bladder cancer. PloS One 6, e18135. https://doi.org/10.1371/journal.pone.0018135
Zarbin, M., Sugino, I., Townes-Anderson, E., 2019. Concise Review: Update on Retinal Pigment Epithelium Transplantation for Age-Related Macular Degeneration. STEM CELLS Transl. Med. 8, 466–477. https://doi.org/10.1002/sctm.18-0282

Zeller, K.I., Zhao, X., Lee, C.W.H., Chiu, K.P., Yao, F., Yustein, J.T., Ooi, H.S., Orlov, Y.L., Shahab, A., Yong, H.C., Fu, Y., Weng, Z., Kuznetsov, V.A., Sung, W.-K., Ruan, Y., Dang, C.V., Wei, C.-L., 2006. Global mapping of c-Myc binding sites and target gene networks in human B cells. Proc. Natl. Acad. Sci. 103, 17834–17839. https://doi.org/10.1073/pnas.0604129103

Zhang, J., Fei, T., Li, Z., Zhu, G., Wang, L., Chen, Y.-G., 2013. BMP induces cochlin expression to facilitate self-renewal and suppress neural differentiation of mouse embryonic stem cells. J. Biol. Chem. 288, 8053–8060. https://doi.org/10.1074/jbc.M112.433995

Zhang, J., Nuebel, E., Daley, G.Q., Koehler, C.M., Teitell, M.A., 2012. Metabolic Regulation in Pluripotent Stem Cells during Reprogramming and Self-Renewal. Cell Stem Cell 11, 589–595. https://doi.org/10.1016/j.stem.2012.10.005

Zhang, W., Liu, H.T., 2002. MAPK signal pathways in the regulation of cell proliferation in mammalian cells. Cell Res. 12, 9–18. https://doi.org/10.1038/sj.cr.7290105

Zhang, X., Nie, D., Chakrabarty, S., 2010. Growth factors in tumor microenvironment. Front. Biosci. Landmark Ed. 15, 151–165. https://doi.org/10.2741/3612

Zhang, Y., Chen, K., Sloan, S.A., Bennett, M.L., Scholze, A.R., O'Keeffe, S., Phatnani, H.P., Guarnieri, P., Caneda, C., Ruderisch, N., Deng, S., Liddelow, S.A., Zhang, C., Daneman, R., Maniatis, T., Barres, B.A., Wu, J.Q., 2014. An RNA-sequencing transcriptome and splicing database of glia, neurons, and vascular cells of the cerebral cortex. J. Neurosci. Off. J. Soc. Neurosci. 34, 11929–11947. https://doi.org/10.1523/JNEUROSCI.1860-14.2014

Zhang, Y., Tang, B., Song, J., Yu, S., Li, Y., Su, H., He, S., 2019. Lnc-PDZD7 contributes to stemness properties and chemosensitivity in hepatocellular carcinoma through EZH2-mediated ATOH8 transcriptional repression. J. Exp. Clin. Cancer Res. CR 38, 92. https://doi.org/10.1186/s13046-019-1106-2

Zhao, S., Nichols, J., Smith, A.G., Li, M., 2004. SoxB transcription factors specify neuroectodermal lineage choice in ES cells. Mol. Cell. Neurosci. 27, 332–342. https://doi.org/10.1016/j.mcn.2004.08.002

Zhou, W., Freed, C.R., 2009. Adenoviral Gene Delivery Can Reprogram Human Fibroblasts to Induced Pluripotent Stem Cells. Stem Cells 27, 2667–2674. https://doi.org/10.1002/stem.201

Zhou, X., Huang, G.-R., Hu, P., 2011. Over-expression of Oct4 in human esophageal squamous cell carcinoma. Mol. Cells 32, 39–45. https://doi.org/10.1007/s10059-011-2315-5

Zhou, X., Sasaki, H., Lowe, L., Hogan, B.L.M., Kuehn, M.R., 1993. Nodal is a novel TGF-β-like gene expressed in the mouse node during gastrulation. Nature 361, 543–547. https://doi.org/10.1038/361543a0

Zhu, Y., Li, Y., Haraguchi, S., Yu, M., Ohira, M., Ozaki, T., Nakagawa, A., Ushijima, T., Isogai, E., Koseki, H., Nakamura, Y., Kong, C., Mehlen, P., Arakawa, H., Nakagawara, A., 2013. Dependence receptor UNC5D mediates nerve growth factor depletion–induced neuroblastoma regression. J. Clin. Invest. 123, 2935–2947. https://doi.org/10.1172/JCI65988

Zviran, A., Mor, N., Rais, Y., Gingold, H., Peles, S., Chomsky, E., Viukov, S., Buenrostro, J.D., Scognamiglio, R., Weinberger, L., Manor, Y.S., Krupalnik, V., Zerbib, M., Hezroni, H., Jaitin, D.A., Larastiaso, D., Gilad, S., Benjamin, S., Gafni, O., Mousa, A., Ayyash, M., Sheban, D., Bayerl, J., Aguilera-Castrejon, A., Massarwa, R., Maza, I., Hanna, S., Stelzer, Y., Ulitsky, I., Greenleaf, W.J., Tanay, A., Trumpp, A., Amit, I., Pilpel, Y., Novershtern, N., Hanna, J.H., 2019. Deterministic Somatic Cell Reprogramming Involves Continuous Transcriptional Changes Governed by Myc and Epigenetic-Driven Modules. Cell Stem Cell 24, 328-341.e9. https://doi.org/10.1016/j.stem.2018.11.014

8. APPENDIX 1:

The molecular roadmaps of reprogramming to pluripotency and malignancy identify Bcl11b as a broad-range regulator of cellular identity.

Authors: A. Huyghe[1], G. Furlan[1], J. Schroeder[2], J. Wang[3], Y. Yu[3], N. Rama[4], B. Gibert[4], P. Wajda[1], I. Goddard[5], N. Gadot[6], M. Brevet[7], P. Liu[3], J. Polo[2] and F. Lavial[1*].

Affiliations : [1]Cellular reprogramming and oncogenesis Laboratory - Lyon University, Université Claude Bernard Lyon 1, INSERM 1052, CNRS 5286, Centre Léon Bérard, Cancer Research Center of Lyon, Lyon, France; [2]Department of Anatomy and Developmental Biology, Monash University, Clayton, VIC 3800, Australia; [3]Wellcome Trust Sanger Institute, Hinxton, Cambridge, UK; [4]Apoptosis, Cancer and Development Laboratory - Lyon University, Université Claude Bernard Lyon 1, INSERM 1052, CNRS 5286, Centre Léon Bérard, Cancer Research Center of Lyon, Lyon, France; [5]Tumoral models laboratory - Lyon University, Université Claude Bernard Lyon 1, INSERM 1052, CNRS 5286, Centre Léon Bérard, Cancer Research Center of Lyon, Lyon, France; [6]Research Pathology Platform, Department of Translational Research and Innovation, Centre Léon Bérard, Lyon, France. Department of Translational Research and Innovation, Centre Léon Bérard, France; [7]Department of pathology, HCL Cancer Institute and Lyon1 University, France.

Contact Information: * F. Lavial: fabrice.lavial@lyon.unicancer.fr

One-sentence summary: Comparative roadmaps of cellular identity loss during iPS cell generation and malignant transformation.

Abstract

Loss of somatic cell identity during reprogramming is a critical step during both induced pluripotent stem (iPS) cell generation and malignant transformation. However, the molecular circuitries involved in both processes, and their degree of analogy, remain poorly characterized. In this study, we dissected the early cellular, transcriptomic and epigenomic changes occurring during pluripotent reprogramming (PR) - mediated by Oct4, Sox2, Klf4, c-Myc (OSKM) - and malignant reprogramming/transformation (MRT) - mediated by oncogenic K-Ras and c-Myc - in mouse embryonic fibroblasts (MEF). We demonstrated that loss of cellular identity during PR and MRT follows orderly sequences of intermediate stages, marked by changes in the cell surface marker Thy1 and the transcription factor (TF) Bcl11b. RNA- and ATAC-seq analyses of these reprogramming intermediates led to (i) defining shared but also specific transcriptomic and epigenomic features of PR/MRT and to (ii) identifying crucial regulators. Among them, we revealed antagonistic functions for the TFs Bcl11a and Bcl11b during both iPS cell generation and malignant transformation. Unexpectedly, we finally revealed that, upon an oncogenic insult, the initial susceptibility of MEF to lose identity has profound consequences on the subsequent acquisition of malignant properties *in vitro* and *in vivo*. Collectively, this comprehensive analysis enables the mapping of the reprogramming routes leading to iPS and malignant cells formation, and shed light on novel insights into reprogramming, induced pluripotency and cancer biology.

Highlights

-Molecular roadmaps of cellular identity loss during reprogramming to pluripotency and malignancy

-Comparing the transcriptomic and epigenomic reconfigurations occurring during reprogramming toward pluripotency and malignancy reveals shared and specific features.

-Bcl11a and Bcl11b regulate iPS cells generation and malignant transformation.

-The initial susceptibility of MEF to lose identity and reprogram profoundly impacts the subsequent acquisition of malignant properties.

-Cyclic OSKM expression constrains the development of K-Ras driven tumors in the lung.

Introduction

During development, cells within multicellular organisms progressively differentiate into functionally and phenotypically distinct fates. These cellular identities, established by cell type-specific gene expression programs, are remarkably stable and can be sustained over many cell divisions throughout an organism's lifespan. However, this view of cellular identity as an irreversible state has been extensively challenged by the discovery of pluripotent reprogramming (PR). In their seminal report, Takahashi and Yamanaka demonstrated that differentiated cell identity can be fully converted to pluripotency by a defined set of transcription factors (TFs) (Oct4, Sox2, Klf4, and c-Myc; thereafter named OSKM) (*1*). Mechanistically, OSKM trigger an early and widespread reconfiguration of chromatin states and TFs occupancy to orchestrate somatic identity loss in mouse embryonic fibroblasts (MEF), while gradual activation of the pluripotency-related transcriptional network is observed later during the process of induced pluripotent stem (iPS) cell generation (*2*–*5*). Cellular reprogramming is therefore critical for induced pluripotency.

Cellular reprogramming recently emerged as a critical regulator of malignant transformation. Cancer formation frequently relies on the activation of developmental signaling programs and the acquisition of self-renewal potential (*6*). Somatic stem cells have been considered to be relevant candidates of transformation due to their inherent self-renewing capacity and longevity, which would permit the acquisition of the combination of genetic and epigenetic aberrations sufficient for cell transformation (*7*). Nevertheless, recent studies demonstrated that, upon oncogenic alterations, progenitors or committed cells can act as tumor-initiating cells by reprogramming and re-acquiring stem cell-like traits (*8*, *9*). Cellular reprogramming triggered by oncogenes has therefore emerged as an alternative route toward malignancy *in vitro* and *in vivo* (*6*, *10*). *In vitro*, malignant transformation orchestrated by c-Myc and oncogenic K-Ras (K-Ras^{G12D}) in MEF is initiated by a malignant reprogramming process characterized by somatic identity loss, stochasticity and latency (*11*). *In vivo*, the concomitant activation of K-Ras and NF-κB in differentiated cells of the intestine induces their reprogramming and the initiation of tumors re-expressing the stem cell marker Lgr5 (*9*). In the adult pancreas, acinar cells have been shown to adopt an intermediate dedifferentiation state following an oncogenic insult. They then acquire ductal features through a reprogramming process, called acinar-to-ductal metaplasia, leading to premalignant lesions (*12*, *13*). Altogether, these studies unveil that cellular reprogramming constitutes a critical step of malignant transformation in certain contexts.

The processes of induced pluripotency and malignant transformation share some features. They are both constrained by oncogenic barriers, such as cell death and senescence, and are both considered to be stochastic and subjected to significant latencies (*11*, *14*, *15*). In line with this view, cyclic OSKM expression *in vivo* reduces hallmarks of aging (*16*) while prolonged OSKM induction induces teratoma formation (*17*) and fosters tumorigenesis (*18*, *19*), in agreement with their genuine oncoprotein functions (*20*).

Despite the crucial role of cellular reprogramming in induced pluripotency and malignant transformation and the degree of analogy between both processes, the molecular circuitries and in particular the intermediate states controlling both programs have never been compared, yet their knowledge might have equally profound implications for regenerative medicine and cancer biology. In this study, we compared the early steps of PR - mediated by OSKM - and malignant reprogramming/transformation (MRT) - mediated by oncogenic Ras (K-Ras^{G12D} or H-Ras^{G12V}) and c-Myc. Transcriptomic analyses led to the identification of a set of somatic markers, namely Bcl11b and Thy1 (*3*, *11*), that enabled us to compare the intermediate stages and define the reprogramming routes by which cells transit to lose their identity during PR and MRT. By characterizing the global reconfigurations of the transcriptome and of chromatin accessibility in these intermediates, we defined common and specific features of pluripotent and malignant reprogramming. We also identified a switch between the expression of the TFs Bcl11a and Bcl11b that critically controls both PR and MRT. Finally, we revealed that the initial susceptibility of somatic cells to lose identity has unexpected and profound consequences on the subsequent acquisition of malignant properties, while OSKM cycles *in vivo* constrain the development of K-Ras driven tumors in the lung.

Results

A genetic strategy to compare iPS cell generation and malignant transformation.

OSKM is the prototypical cocktail for iPS cell generation (*1*) and the cooperation between c-Myc and oncogenic K-Ras (K-Ras^{G12D}) has been reported to trigger malignant reprogramming and subsequent transformation (MRT) in MEF (*11*). To compare the early events of PR (induced by OSKM) and MRT (induced by c-Myc/K-Ras^{G12D}), MEF were derived from intercrosses between R26^{rtTA};Col1a1^{4F2A} (*21*) and LSL-K-Ras^{G12D};R26$^{cre/ERT2}$ (*22*) mice (Fig. 1A). The treatment of these reprogrammable MEF with doxycycline (Dox) for 14 days led to the emergence of iPS colonies at an efficiency of 0,208 +/-0,102%. As expected, these cells expressed Nanog and Ssea1 (Fig. S1A) and were able to undergo *in vivo* multilineage differentiation (Fig. 1B). In contrast, MRT was achieved by the treatment of reprogrammable MEF with tamoxifen (TAM) to induce K-Ras^{G12D} expression (by excision of a Lox-Stop-Lox cassette) and by c-Myc exogenous expression (Fig. 1A). Under these conditions, 21 days were required for the generation of cells harbouring malignant features *in vitro* and *in vivo*. Foci formation assay illustrated the clonal loss of contact inhibition at an efficiency of 0.662 +/-0.327% (Fig. 1C) while soft agar formation assay showed the acquisition of anchorage-independent growth potential (Fig. 1D). Finally, the injection of these cells in nude mice led to the formation of "liposarcoma-like" tumors (Fig. 1E).

Based on this genetic strategy, PR and MRT can be induced in the same population of reprogrammable MEF. We thus compared the early transcriptomic and cellular responses to the induction of each

reprogramming program (PR or MRT) and the combination of both (PR+MRT) (Fig. 1F). We conducted RNA-seq analysis on MEF, untreated or undergoing 5 days of PR, MRT or PR+MRT. Principal component analysis (PCA) illustrated how the OSKM and K-Ras^{G12D}/c-Myc cocktails triggered different transcriptomic responses. Interestingly, the concomitant induction of PR and MRT seemed to have a cumulative effect on the MEF transcriptome (Fig. S1B). At the cellular level, MEF proliferation was increased by PR and MRT with different kinetics, and this effect was also found to be cumulative (Fig. 1G). In contrast, cell cycle features appeared to be specifically modified by MRT induction (Fig. S1C). We next evaluated DNA damage after short inductions (5 days) of reprogramming. MRT induction triggered the formation of H2AX phosphorylation (γH2AX) foci in 45.1+/-10.0% of the cells (Fig. 1H-I). Of note, similar results were obtained with other oncogenic cocktails including p53 depletion and/or Cyclin E and H-Ras^{G12V} exogenous expression (Fig. S1D-E). In contrast, Dox-induced OSKM expression did not significantly increase the number of γH2AX foci (10.6+/-5.7% γH2AX positive cells). Interestingly, when PR and MRT were both induced in MEF, we found that OSKM significantly prevented γH2AX foci formation triggered by K-Ras^{G12D} and c-Myc (Fig. 1H-I). OSKM also prevented significantly apoptosis, as revealed by AnnexinV-PI staining (Fig. S1F-G). Altogether, these data indicate that PR and MRT trigger different transcriptomic and cellular responses in MEF and that OSKM unexpectedly prevent hallmarks of MRT-induced DNA damage and apoptosis.

Identification of somatic markers commonly downregulated in the early steps of iPS cell generation and malignant transformation

We next attempted to track MEF identity loss during iPS cell generation (PR) and malignant reprogramming/transformation (MRT). Because the early steps of both processes are highly inefficient (*1*, *11*), the design of a strategy to capture reprogramming intermediates (RI) on their way to pluripotency or malignancy was necessary. During PR, RI are tracked by combining markers of somatic identity loss (such as thy1) and markers of pluripotency network activation (such as SSEA1) (*23*, *24*). Due to the fact that these pluripotent genes are not reactivated during MRT, we attempted to identify a set of somatic markers commonly downregulated during PR and MRT that could be used in combination to track RI. We initially FACS profiled cell surface markers described for PR (CD73, CD49d and Thy1) (*23*, *25*) and MRT (Sca1, Thy1) (*11*, *26*) (data not shown). Among those, thy1 was the sole factor being downregulated in a subset of cells at day 5 of PR and MRT (Fig. S2A). We next assessed whether the loss of thy1 correlated with enhanced reprogramming potential during both PR and MRT. For iPS cell generation, thy1^{low} and thy1^{high} subpopulations were FACS sorted at day 5 of PR and replated at similar densities in reprogramming conditions. In those conditions, thy1^{low} cells formed 2-fold more alkaline phosphatase (AP) positive iPS colonies than thy1^{high} cells, in adequation with previous reports (*23*) (Fig. S2B-C). For MRT, a similar FACS sorting strategy was conducted to subject thy1^{low} and thy1^{high} cells to foci formation assay. The thy1^{low} cells

formed 4-fold more foci than thy1^{high} cells, indicating that thy1^{low} cells are more prone to lose contact inhibition (Fig. S2D-E), demonstrating that thy1 is a pertinent indicator of the reprogramming potential for PR and MRT.

Since the reprograming efficiency of the thy1^{low} subpopulation was still very low for both PR and MRT, we performed transcriptomic analyses to identify additional MEF markers commonly downregulated during PR and MRT. RNA-seq was conducted on untreated MEF, thy1^{low} cells (prone) and thy1^{high} cells (refractory) sorted by FACS at day5 of PR, MRT and PR+MRT (Fig. 2A). PCA showed a similar distribution of the samples as in Fig. S1B, based on the reprogramming program (Fig. 2B). Next, we compared, for each reprogramming scenario, untreated MEF and thy1^{low} cells prone to reprogramming. We identified respectively 116 and 376 genes modulated in thy1^{low} cells during PR and MRT (adjusted p-value< 10^-10; log2 FC >2.5 or <-2.5) (Fig. 2C). Statistical overrepresentation tests performed on the differentially expressed genes with Pantherdb revealed strong association of the PR-associated genes with "regulation of cell differentiation", "cell adhesion" and "cell-cell signalling", in agreement with the loss of MEF identity (Fig. 2D). For MRT-associated genes, we found enrichments for genes related to "muscle system process" and mesoderm identity but also "cell adhesion", similarly as PR. By overlapping both sets of genes, we identified 55 genes commonly regulated in PR- and MRT- thy1^{low} cells (Fig. 2E). Among them, we noticed the presence of several genes implicated in cellular adhesion (*Col7a1* (*27*), *Ncam1* (*28*), *Ctgf* (*29*), *Postn* (*30*)), cancer progression (*Podxl* (*31*)) and embryonic morphogenesis (*Grem2* (*32*)*)*. We selected the zinc finger TF Bcl11b described as a cellular identity gatekeeper in T cells (*33*). We showed by Q-RTPCR and Western blot that Bcl11b expression is high in MEF, specifically decreased in thy1^{low} cells during PR and MRT and silenced in iPS and malignant cells (Fig. 2F-G). Of interest, in both cases, Bcl11b expression was maintained or even induced in thy1^{high} cells, refractory to reprogram. Next, to assess whether Bcl11b loss could be used as an indicator of the reprogramming potential of a cell, we derived MEF from Bcl11b-tdTomato reporter knock-in mice (*34*) (Fig. 2H and S2F). FACS analysis confirmed that the majority (90%) of MEF expressed Bcl11b-tdTomato (Fig. 2I). In the absence of reprogramming, MEF stably maintained their Bcl11b distribution in culture (data not shown). After 5 days of PR or MRT, we noticed the emergence of a Bcl11b^{low} subpopulation of cells representing 28% and 51% of the population, respectively (Fig. 2I). We subsequently assessed the capacity of these subpopulations to form iPS cells during PR and malignant cells during MRT. For PR, we showed that Bcl11b^{low} cells, sorted by FACS at day 5 of reprogramming, formed 7-fold more AP+ iPS colonies than their Bcl11b^{high} counterparts (Fig. 2J-K). For MRT, Bcl11b^{low} cells formed foci at a 10-fold higher efficiency than Bcl11b^{high} (Fig. 2L-M), demonstrating that the loss of Bcl11b was correlated with increased capacities to form pluripotent or malignant cells. Altogether, these results showed that Bcl11b is a MEF marker and that its downregulation is correlated with enhanced reprograming potential toward pluripotency and malignancy.

Sequential loss of identity during reprogramming toward pluripotency and malignancy

The previous findings prompted us to investigate whether Bcl11b and thy1 could be used in combination to identify RI emerging during iPS cell generation and malignant transformation. To begin the experiments with an homogeneous population, Bcl11b-tdTomato^{high}/thy1^{high} MEF were FACS sorted to purity. In the absence of reprogramming induction, sorted MEF stably maintained a Bcl11b-tdtomato^{high}/thy1^{high} phenotype in culture (data not shown). Bcl11b/thy1 changes were next profiled during PR and MRT by FACS (Fig. 3A). By day 17, most of the cells displayed downregulation of both markers, similarly to iPS and malignant cells, as expected. Interestingly, the minor Bcl11b^{low}/thy1^{low} subpopulation that emerged by day5-7 of reprogramming harboured a strong reprogramming potential compared to the Bcl11b^{high}/thy1^{high} fraction. For PR, Bcl11b^{low}/thy1^{low} cells (hereafter entitled PRP for Pluripotent Reprogramming Prone) formed 13-fold higher iPS colonies than Bcl11b^{high}/thy1^{high} cells (hereafter entitled PRR for Pluripotent Reprogramming Refractory) (Fig. 3B-D). For MRT, Bcl11b^{low}/thy1^{low} cells (hereafter entitled MRP for Malignant Reprogramming Prone) formed foci at a 4-fold higher rate than Bcl11b^{high}/thy1^{high} cells (hereafter entitled MRR for Malignant Reprogramming Refractory) (Fig. 3E-G). These data indicate that the combined use of thy1 and Bcl11b allowed the isolation of early RI harboring a strong propensity to form pluripotent or malignant derivatives.

We next sought to define an orderly sequence of events leading to Bcl11b and thy1 downregulation during iPS cells generation and malignant transformation. For PR, the 4 following subpopulations were FACS sorted at day7 of reprogramming: Bcl11b^{high}/thy1^{high} (PRR), Bcl11b^{low}/thy1^{high} (PR1 = Pluripotent Reprogramming Intermediate 1), Bcl11b^{high}/thy1^{low} (PR2 = Pluripotent Reprogramming Intermediate 2), Bcl11b^{low}/thy1^{low} (PRP) (Fig. 3H). To demonstrate that the Bcl11b/thy1 profile changes observed in Fig. 3A reflected the transition of individual cells from one stage to the next, and not merely the loss of one major population and expansion of another minor population, each fraction was sorted, replated in reprogramming conditions for 48 hours before FACS analysis (Fig. 3H). The progression of cellular fates and the corresponding transition rates revealed the routes of cellular identity loss triggered by OSKM. First, we observed that the PRP state, characterized by the common downregulation of Bcl11b and thy1, is stable. Indeed, cells that reached the PRP state did not transit efficiently into other states. Secondly, we found that the PRR and PR2 states generated PRP cells at very low rate while PR1 cells transit into PRP very efficiently (35%). This suggests that reaching the PR1 state, characterized by Bcl11b extinction, is a rate-limiting step of iPS cell generation. Importantly, these progressions were strongly correlated with the relative capacities of the corresponding populations to form AP-positive colonies (Fig. 3I-J).

When a similar analysis was conducted with MRT, we observed that the MRP state is also quite stable (Fig. 3K). However, unlike PR, the MRR and MR1 cells were poorly efficient at generating MRP while MR2 cells

did transit toward this state at high efficiency, indicating that the loss of thy1 could constitute a rate-limiting step, in agreement with the relative ability of these subpopulations to form foci (Fig. 3L-M).
On the basis of total cell numbers in each gate, we generated the reprogramming trajectories presented in Figure 3N. Owing to the Bcl11b/thy1-based strategy we developed, we revealed hierarchical steps and cellular transition states leading to MEF identity loss during reprogramming toward pluripotency or malignancy.

Epigenomic and transcriptomic reconfigurations in pluripotent and malignant reprogramming intermediates

To investigate the dynamics of chromatin accessibility and transcriptome in cells refractory or poised to become pluripotent or malignant, ATAC-seq and RNA-seq analyses were conducted on untreated MEF alongside PRP, MRP (both $Bcl11b^{low}$/$thy1^{low}$), PRR, MRR (both $Bcl11b^{high}$/$thy1^{high}$) at 5 days of reprogramming, and iPS and malignant cells (Fig. 4A). PCA performed on ATAC-seq data showed that PRP and MRP cells, prone to generate iPS and malignant cells, respectively, segregated together on the X-axis (dim1) (Fig. 4B and S3A), indicating the existence of common chromatin accessibility changes in these RI.
We next classified the chromatin peaks in clusters defined by regions that (1) became accessible in both PRP/MRP over MEF (Cluster 1, n=3015); (2) were accessible in MEF but that exhibit loss of accessibility in both PRP/MRP over MEF (Cluster 2, n=4522); (3) were specifically gained in PRP over MEF and MRP (Cluster 3, n=5464) or MRP over MEF and PRP (Cluster 4, n=17282); (4) were specifically lost in PRP over MEF and MRP (Cluster 5, n=3776) or MRP over MEF and PRP (Cluster 6, n=13245) (Fig. 4C). This clustering highlighted that the number of peak modifications shared by PRP and MRP (C1+C2=7537) is close to the PRP-specific modifications (C3+C5=9240) but lower than MRT-specific ones (C4+C6=30527). These results also indicated that the early steps of PR and MRT trigger similar and specific changes in chromatin accessibility.
Analysis of DNA motif enrichment in the ATAC-seq clusters revealed different families of TF-binding motifs (Fig. 4D and S3B). Among those, we assessed whether the TF FosL1, present in different clusters, could potentially control PR and MRT efficiency. Interestingly, FosL1 downregulation, prior to PR induction, led to a 6-fold increase in reprogramming efficiency, as revealed by AP+ staining (Fig. 4E-F). In contrast, when a similar approach was induced prior to MRT, FosL1 depletion led to a 4-fold reduction in the number of immortalized foci (Fig. 4G-H). Altogether, these data indicate that the TF FosL1 antagonistically regulates PR and MRT efficiency.
We next conducted RNA-seq on similar samples (Fig. 4A). PCA revealed, similarly as ATAC-seq, that PRP and MRP segregated together on the X-axis (Fig. 4I). Volcano plot showed that 410 genes were differentially expressed between PRP (prone) and PRR (refractory) and 1389 genes between MRP (prone) and MRR

(refractory) (Fig. 4J). We therefore defined the common molecular signature of genes commonly regulated in PRP and MRP (Fig. 4K). GO analysis of this signature, comprising 301 genes (170 down and 131 up, adjusted p-value< 5.10^-2; log2 FC >1 or <-1), revealed enrichments in stem cell differentiation but also unexpectedly T cell activation and differentiation (Fig. 4L). In the latter category, we identified an induction of genes implicated in T cell migration (Dock8) (*35*), adhesion (Itgb2) (*36*) and activation (Clec4d, Ptprc and Lcp1) (*37*–*39*). Among these genes, we also noticed an induction of the Bcl11b paralog Bcl11a, involved in B lymphocyte differentiation, in the RI processing toward pluripotency and malignancy (*40*). Importantly, these genes were found silenced in both iPS and malignant cells (data not shown). Altogether, these data highlight the existence of specific and common reconfigurations of chromatin accessibility and transcriptome, encompassing a transient induction of a "T cell-like signature", in pluripotent and malignant RI.

A Bcl11b/Bcl11a switch regulates cellular identity changes during PR

The previous results revealed an induction of Bcl11a in RI prone to form iPS cells (PRP). Western blot analysis confirmed an inverse expression of Bcl11a and Bcl11b in cells prone (PRP) or refractory (PRR) to form iPS cells (Fig. 5A). In addition, profiling *Bcl11a* changes during iPS cells generation revealed that its induction is a transient event preceding its downregulation in iPS cells (Fig. S4A). Interrogation of publically available RNA-seq resources broadened the occurrence of Bcl11b loss and Bcl11a transient induction to the reprogramming of other murine somatic cells such as neutrophils and keratinocytes (*41*) (Fig. 5B).
To assess whether Bcl11a and Bcl11b functionally regulate iPS cell generation, gain- and loss-of-function approaches were conducted in MEF, prior to PR inductions. Bcl11b knockdown (Fig. S4B) improved significantly the efficiency of generation of AP+ iPS colonies, demonstrating its role as a MEF identity gatekeeper (Fig. 5C-D). Of note, Bcl11b-KD iPS cell lines were capable of *in vivo* differentiation into the three germ layers in teratoma (Fig. 5E), showing that Bcl11b loss does not deeply interfere with the acquisition of pluripotent features. Similar results were obtained by genetically depleting Bcl11b in conditional KO MEF (Fig. S4C-D). However, exogenous Bcl11b expression did not significantly impact PR efficiency (Fig. 5C-D and S4E). In striking contrast, when Bcl11a was depleted (Fig. S4F), we observed a significant reduction of iPS cell generation efficiency (Fig. 5F-G), demonstrating that the transient expression of Bcl11a that we observed (Fig. 5A) positively regulates PR.
These inverse effects of Bcl11a and Bcl11b on PR were even more pronounced when Oct4-GFP reporter MEF were used. Under these conditions, the loss of Bcl11b led to a 4-fold induction, and Bcl11a depletion to a 9-fold reduction, in the number of Oct4-GFP+ iPS colonies (Fig. 5H). Altogether, these data indicate opposite functions for the TFs Bcl11a and Bcl11b in iPS cell generation.

Next, we wondered whether Bcl11b controls iPS cell generation from other mouse somatic cells-of-origin. Because Bcl11b is expressed in T Lymphocytes (*33*), we isolated T cells from Bcl11b conditional KO mice (Fig. 5I-J). T-cell reprogramming into iPS cells was next performed in the presence or absence of Bcl11b. Bcl11b loss led to the formation of 2-3 fold more iPS colonies generated from T cells, as revealed by AP staining (Fig. 5K), broadening the role of Bcl11b as a reprogramming barrier. Altogether, these findings demonstrate antagonistic functions for the transcription factors Bcl11a and Bcl11b during various pluripotent and malignant reprogramming scenarii.

A Bcl11b/Bcl11a switch regulates cellular identity changes during malignant transformation

The previous findings revealed an induction of Bcl11a in RI prone to form malignant cells (MRP) that was confirmed by Western blot (Fig. 5L). Profiling *Bcl11a* changes during MEF malignant transformation revealed a similar transient induction of *Bcl11a* transcript than during iPS cell formation (Fig. S4G). We therefore investigated whether these TFs played similar roles during MRT. Bcl11b loss, triggered by RNAi or genetic depletion, significantly increased the efficiency of foci formation while its exogenous expression severely hindered the process, indicating that a tight level of Bcl11b safeguards MEF identity from MRT (Fig. 5M-N and S4H-I). In contrast, Bcl11a loss significantly hindered foci formation while its exogenous expression had no effect on MRT efficiency (Fig. 5O-P). The consequences of Bcl11a/b deletion on the acquisition of malignant properties were next examined. To do so, Control, Bcl11b and Bcl11a KD polyclonal cell lines were established and subjected to soft agar assays. In this context, we showed that Bcl11b loss enhanced, while Bcl11a limited, the ability to form colonies (Fig. 5Q-R).
The impact of Bcl11b on the epigenome during MRT was assessed by performing ATAC-seq on crispr sg#control and sg#Bcl11b MEF after 5 days of MRT (Fig. 5S). Bioinformatic analyses led to the identification of 20266 upregulated and 14866 downregulated peaks in the absence of Bcl11b (Fig. S4J). Analysis of DNA motif enrichment in the ATAC-seq clusters revealed different families of TF-binding motifs (Fig. 5T) such as the TFs Tead1, 3 and 4. The TEAD family of transcription factors plays a key role in the Hippo signaling pathway, a pathway involved in organ size control and tumor suppression by restricting proliferation and promoting apoptosis (*42*). Altogether, these data indicate that Bcl11b acts as a gatekeeper of MEF identity while the transient induction of its paralogue Bcl11a promotes reprogramming and the acquisition of malignant properties.

The initial susceptibility of MEF to lose Bcl11b and thy1 impacts the acquisition of malignant properties

It has been shown that cells respond differently to an oncogenic insult depending on their differentiation status (*7*, *10*). Here, using the Bcl11b/thy1-based strategy we developed, we questioned whether the early

propensity of somatic cells to lose their identity impacted the subsequent acquisition of malignant features. To do so, MEF were induced for MRT combining H-Ras^{G12V}, c-Myc expression and p53 knockdown. After 7 days, MRR (refractory to reprogram) and MRP (prone to reprogram) cells were FACS sorted, replated at similar densities and independent polyclonal cell lines established after >5 passages (Fig. 6A). Of note, these MRR- and MRP-derived cell lines did not express Bcl11b and thy1 and presented similar growth curves in 2D cultures (Fig. S5A). However, we found that the 3 independent MRP-derived cell lines formed colonies in soft agar at a 7-fold higher efficiency than the MRR-derived ones, indicating a higher potential for anchorage-independent growth (Fig. 6B-C).

RNA-seq analyses of the MRP- and MRR-derived cell lines showed that 1149 genes (adjusted p-value<0.05, log2 FC <-1 or >1) genes were expressed differentially, demonstrating that the initial susceptibility of somatic cells triggers profound transcriptomic changes in the transformed population (Fig. 6D). Statistical overrepresentation assays performed with Panther db showed enrichment for genes related to "cell migration" and "cell adhesion" in MRP-derived cells (Fig. 6E). In line with this view, the transcripts of the cell migration-related genes *Sema4d* (*43*) and *Pdgfb* (*44*) were significantly upregulated in MRP-derived cells while the cell adhesion-related transcripts *Itga4* (*45*) and *Cdh11* (*46*) were downregulated (Fig. 6F). We therefore assessed whether the aggressiveness of these cells was different *in vivo*. We employed the chick chorioallantoic membrane (CAM) assay as an *in vivo* model of tumor development (Fig. 6G). GFP-labelled MRR- and MRP-cells were seeded on the upper CAM of day11 chick embryos and the surface area of the primary tumors calculated 7 days later. The size of the GFP+ tumors generated with MRP-derived cells was more than 2-fold higher than those generated with MRR-derived cells (Fig. 6H-I and S5B), indicating an accelerated tumor growth *in vivo*. To strengthen this finding, we performed xenograft assays by injecting MRR- and MRP-derived cells into immunocompromised mice (Fig 6J). We found that the tumor growth of MRP-derived cells was significantly faster than MRR-derived cells (Fig. 6K) and the mice survival rate significantly reduced (Fig. 6L). Collectively, these results showed that the early propensity of somatic cells to lose identity *via* Bcl11b and thy1 expression has a profound impact on the subsequent acquisition of tumorigenic properties.

Cyclic OSKM expression constrains Erk1/2 activation and tumor development triggered by K-Ras in the lung.

Having assessed the effects of PR and MRT separately in MEFs, we finally explored their potential interaction *in vivo*. OSKM expression *in vivo* has already been shown to induce teratoma (*17*), trigger tumorigenesis (*18*) and facilitate K-Ras induced cancer development in the pancreas (*19*). However, cyclic OSKM expression triggers a partial reprogramming that has been shown to alleviate hallmarks of aging without triggering tumorigenesis (*16*). As short OSKM expression appeared to protect cells from DNA damage and apoptosis induced by oncogenic K-Ras (Fig. 1L), we wondered whether cycles of partial

reprogramming could constrain the development of K-Ras driven tumors in the lung, an organ described as refractory to OSKM-mediated teratoma formation (*47*). To do so, we crossed OSKM Dox-inducible mice ($R26^{rtTA}$;$Col1a1^{4F2A}$) (*21*) with KrasLA2/+ mice (*48*) that carry an activable oncogenic K-Ras allele and are highly predisposed to developing lung cancer. Groups of 8 weeks-old mice were subjected or not to cycles of OSKM induction (2 days ON/5 days OFF) by addition of Dox in the drinking water (Fig. 7A). Of note, Dox treatment could not be induced earlier because it triggered a high rate of morbidity in younger mice (data not shown). Histopathological analysis of 18 weeks-old mice showed a significant reduction in the number (Fig. 7B-C) and in the size (Fig. 7D-E) of tumors of the Dox-treated group, indicating that OSKM cycles hinder tumor development. A similar decrease in the size of tumors was observed by live *in vivo* monitoring of lung tumors using X-ray tomography (Fig. S5C-D) but these effects were not correlated with a significant difference in overall survival (Fig. S5E). It has been demonstrated that genetic alterations that affect the MAPK upstream components such as Ras, observed in many cancers, frequently involve Erk1/2 pathway impairment (*49*). Furthermore, it has been shown that short OSKM expression in pancreatic cells of K-Ras mutant mice induces the rapid formation of pancreatic ductal adenocarcinoma by a persistent activation of Erk1/2 (*19*). To further investigate the effects of cycles of partial reprogramming on tumorigenesis, we evaluated Erk1/2 activation degree in the lung tumors by immunostaining and revealed a significant reduction in the dox-treated group (Fig. 7F). Altogether, these data showed that cycles of partial reprogramming constrain p-Erk1/2 activation and the subsequent emergence and proliferation of K-ras driven tumors in the lung.

Discussion

Despite the critical function of cellular reprogramming in both induced pluripotency and cancer development, the associated molecular circuitries and their degree of analogy remain poorly characterized, yet their knowledge might have equally profound implications for regenerative medicine and cancer biology. Characterization of bulk populations has provided some insights, but as most cells fail to generate iPS or malignant cells, those analyses are necessarily biased toward measurement of unproductive reprogramming events. The heterogeneous and asynchronous nature of reprogramming required the identification of accurate markers or reporters to isolate pure populations of dedifferentiating cells. Here we developed a Bcl11b/thy1-based strategy to trace molecular route maps of cellular identity loss during reprogramming toward pluripotency and malignancy, a critical step toward the elucidation of the precise molecular mechanisms triggering specifically, or commonly, both processes. As an example of such potential, epigenomic analyses of pluripotent and malignant RI led to the identification of opposite functions for the TF FosL1 (*50*), hindering PR but facilitating MRT. In this sense, our study paves the way to design strategies aiming at promoting the direct induction of pluripotent reprogramming (PR) *in vivo* while

limiting malignant transformation. In addition, because the rare intermediate stages we isolated using the Bcl11b/thy1 strategy probably still exhibit some degree of heterogeneity, it will be of great interest to conduct high-resolution single cell level analyses on those RI to predict the trajectories employed by somatic cells during reprogramming toward pluripotency or malignancy.

Epigenome analyses allowed us to identify a T-cell signature, comprising the Clec4d, Lcp1, Ptprp and Itgb2 genes, that is transiently induced in both pluripotent and malignant RI. In a similar manner, Kaji and colleagues reported the existence of a transient epidermis signature during PR (*24*). This result challenged the dogmatic view of reprogramming as a two-step process and demonstrated the existence of intermediate and transient phases sharing analogies during iPS cell generation and malignant transformation.

We identified a transient switch between the expression of the TFs Bcl11a and Bcl11b that controls both PR and MRT. Due to the fact that Bcl11a and Bcl11b have recently been identified as part of the SWI/SNF chromatin remodeling complex (*51*), it will be of great interest to assess whether their stoichiometry controls the proper function of this complex during iPS cell generation and malignant transformation.

The differentiation status of a somatic cell is an important determinant of the phenotype of its reprogrammed or transformed derivatives (*52*, *53*). Adult stem cells generate iPS cells more efficiently than terminally differentiated cells (*54*, *55*) while several lines of evidence demonstrated that malignant cells originating from adult stem cells are more aggressive than from differentiated cells in the same genetic context (*7*, *56*–*58*). Here we demonstrated that, within the same population, the initial propensity of somatic cells to reprogram has profound consequences on the subsequent acquisition of malignant properties. Using the Bcl11b/thy1-based strategy to isolate RI, we showed that cells with an early propensity to reprogramming generate highly aggressive malignant cell lines while cells initially refractory to reprogramming form poorly aggressive ones. It will be of upmost importance to decipher the molecular and epigenetic determinants allowing somatic cells, within the same population, to engage toward different routes to malignancy depending on their initial propensity to reprogram.

Finally we also showed that cyclic OSKM expression constrains tumor development and p-Erk1/2 activation triggered by K-ras in the lung. To better apprehend OSKM function in lung cancer development, it remains to be investigated whether the observed phenotype resulted from lung-specific or systemic expression using cre-specific promoters driving OSKM expression.

By deciphering molecular routes of the loss of cellular identity during iPS cell generation and malignant transformation, our work opens fascinating perspectives for regenerative medicine and cancer biology.

References and Notes:

1. K. Takahashi, S. Yamanaka, Induction of pluripotent stem cells from mouse embryonic and adult fibroblast cultures by defined factors. *Cell*. 126, 663–676 (2006).

2. Y. Buganim, D. A. Faddah, A. W. Cheng, E. Itskovich, S. Markoulaki, K. Ganz, S. L. Klemm, A. van Oudenaarden, R. Jaenisch, Single-cell expression analyses during cellular reprogramming reveal an early stochastic and a late hierarchic phase. *Cell*. 150, 1209–1222 (2012).

3. J. M. Polo, E. Anderssen, R. M. Walsh, B. A. Schwarz, C. M. Nefzger, S. M. Lim, M. Borkent, E. Apostolou, S. Alaei, J. Cloutier, O. Bar-Nur, S. Cheloufi, M. Stadtfeld, M. E. Figueroa, D. Robinton, S. Natesan, A. Melnick, J. Zhu, S. Ramaswamy, K. Hochedlinger, A molecular roadmap of reprogramming somatic cells into iPS cells. *Cell*. 151, 1617–1632 (2012).

4. A. Soufi, G. Donahue, K. S. Zaret, Facilitators and impediments of the pluripotency reprogramming factors' initial engagement with the genome. *Cell*. 151, 994–1004 (2012).

5. R. Sridharan, J. Tchieu, M. J. Mason, R. Yachechko, E. Kuoy, S. Horvath, Q. Zhou, K. Plath, Role of the murine reprogramming factors in the induction of pluripotency. *Cell*. 136, 364–377 (2009).

6. N. Roy, M. Hebrok, Regulation of Cellular Identity in Cancer. *Dev. Cell*. 35, 674–684 (2015).

7. N. Barker, R. A. Ridgway, J. H. van Es, M. van de Wetering, H. Begthel, M. van den Born, E. Danenberg, A. R. Clarke, O. J. Sansom, H. Clevers, Crypt stem cells as the cells-of-origin of intestinal cancer. *Nature*. 457, 608–611 (2009).

8. D. Friedmann-Morvinski, E. A. Bushong, E. Ke, Y. Soda, T. Marumoto, O. Singer, M. H. Ellisman, I. M. Verma, Dedifferentiation of neurons and astrocytes by oncogenes can induce gliomas in mice. *Science*. 338, 1080–1084 (2012).

9. S. Schwitalla, A. A. Fingerle, P. Cammareri, T. Nebelsiek, S. I. Göktuna, P. K. Ziegler, O. Canli, J. Heijmans, D. J. Huels, G. Moreaux, R. A. Rupec, M. Gerhard, R. Schmid, N. Barker, H. Clevers, R. Lang, J. Neumann, T. Kirchner, M. M. Taketo, G. R. van den Brink, O. J. Sansom, M. C. Arkan, F. R. Greten, Intestinal tumorigenesis initiated by dedifferentiation and acquisition of stem-cell-like properties. *Cell*. 152, 25–38 (2013).

10. A. Puisieux, R. M. Pommier, A.-P. Morel, F. Lavial, Cellular Pliancy and the Multistep Process of Tumorigenesis. *Cancer Cell*. 33, 164–172 (2018).

11. I. Ischenko, J. Zhi, U. M. Moll, A. Nemajerova, O. Petrenko, Direct reprogramming by oncogenic Ras and Myc. *Proc. Natl. Acad. Sci. U.S.A.* 110, 3937–3942 (2013).

12. P. J. Grippo, P. S. Nowlin, M. J. Demeure, D. S. Longnecker, E. P. Sandgren, Preinvasive pancreatic neoplasia of ductal phenotype induced by acinar cell targeting of mutant Kras in transgenic mice. *Cancer Res.* 63, 2016–2019 (2003).

13. J. L. Kopp, G. von Figura, E. Mayes, F.-F. Liu, C. L. Dubois, J. P. Morris, F. C. Pan, H. Akiyama, C. V. E. Wright, K. Jensen, M. Hebrok, M. Sander, Identification of Sox9-dependent acinar-to-ductal reprogramming as the principal mechanism for initiation of pancreatic ductal adenocarcinoma. *Cancer Cell*. 22, 737–750 (2012).

14. J. Hanna, K. Saha, B. Pando, J. van Zon, C. J. Lengner, M. P. Creyghton, A. van Oudenaarden, R. Jaenisch, Direct cell reprogramming is a stochastic process amenable to acceleration. *Nature*. 462, 595–601 (2009).

15. R. M. Marión, K. Strati, H. Li, M. Murga, R. Blanco, S. Ortega, O. Fernandez-Capetillo, M. Serrano, M. A. Blasco, A p53-mediated DNA damage response limits reprogramming to ensure iPS cell genomic integrity. *Nature*. 460, 1149–1153 (2009).

16. A. Ocampo, P. Reddy, P. Martinez-Redondo, A. Platero-Luengo, F. Hatanaka, T. Hishida, M. Li, D. Lam, M. Kurita, E. Beyret, T. Araoka, E. Vazquez-Ferrer, D. Donoso, J. L. Roman, J. Xu, C. Rodriguez Esteban, G. Nuñez, E. Nuñez Delicado, J. M. Campistol, I. Guillen, P. Guillen, J. C. Izpisua Belmonte, In Vivo Amelioration of Age-Associated Hallmarks by Partial Reprogramming. *Cell*. 167, 1719-1733.e12 (2016).

17. M. Abad, L. Mosteiro, C. Pantoja, M. Cañamero, T. Rayon, I. Ors, O. Graña, D. Megías, O. Domínguez, D. Martínez, M. Manzanares, S. Ortega, M. Serrano, Reprogramming in vivo produces teratomas and iPS cells with totipotency features. *Nature*. 502, 340–345 (2013).

18. K. Ohnishi, K. Semi, T. Yamamoto, M. Shimizu, A. Tanaka, K. Mitsunaga, K. Okita, K. Osafune, Y. Arioka, T. Maeda, H. Soejima, H. Moriwaki, S. Yamanaka, K. Woltjen, Y. Yamada, Premature termination of reprogramming in vivo leads to cancer development through altered epigenetic regulation. *Cell*. 156, 663–677 (2014).

19. H. Shibata, S. Komura, Y. Yamada, N. Sankoda, A. Tanaka, T. Ukai, M. Kabata, S. Sakurai, B. Kuze, K. Woltjen, H. Haga, Y. Ito, Y. Kawaguchi, T. Yamamoto, Y. Yamada, In vivo reprogramming drives Kras-induced cancer development. *Nat Commun*. 9, 2081 (2018).

20. M. L. Suvà, N. Riggi, B. E. Bernstein, Epigenetic reprogramming in cancer. *Science*. 339, 1567–1570 (2013).

21. B. W. Carey, S. Markoulaki, C. Beard, J. Hanna, R. Jaenisch, Single-gene transgenic mouse strains for reprogramming adult somatic cells. *Nat. Methods*. 7, 56–59 (2010).

22. E. L. Jackson, N. Willis, K. Mercer, R. T. Bronson, D. Crowley, R. Montoya, T. Jacks, D. A. Tuveson, Analysis of lung tumor initiation and progression using conditional expression of oncogenic K-ras. *Genes Dev.* 15, 3243–3248 (2001).

23. M. Stadtfeld, N. Maherali, D. T. Breault, K. Hochedlinger, Defining molecular cornerstones during fibroblast to iPS cell reprogramming in mouse. *Cell Stem Cell*. 2, 230–240 (2008).

24. J. O'Malley, S. Skylaki, K. A. Iwabuchi, E. Chantzoura, T. Ruetz, A. Johnsson, S. R. Tomlinson, S. Linnarsson, K. Kaji, High-resolution analysis with novel cell-surface markers identifies routes to iPS cells. *Nature*. 499, 88–91 (2013).

25. E. Lujan, E. R. Zunder, Y. H. Ng, I. N. Goronzy, G. P. Nolan, M. Wernig, Early reprogramming regulators identified by prospective isolation and mass cytometry. *Nature*. 521, 352–356 (2015).

26. B. A. Schwarz, M. Cetinbas, K. Clement, R. M. Walsh, S. Cheloufi, H. Gu, J. Langkabel, A. Kamiya, H. Schorle, A. Meissner, R. I. Sadreyev, K. Hochedlinger, Prospective Isolation of Poised iPSC Intermediates Reveals Principles of Cellular Reprogramming. *Cell Stem Cell*. 23, 289-305.e5 (2018).

27. S. Heinonen, M. Männikkö, J. F. Klement, D. Whitaker-Menezes, G. F. Murphy, J. Uitto, Targeted inactivation of the type VII collagen gene (Col7a1) in mice results in severe blistering phenotype: a model for recessive dystrophic epidermolysis bullosa. *J. Cell. Sci.* 112 (Pt 21), 3641–3648 (1999).

28. A. M. Hinsby, V. Berezin, E. Bock, Molecular mechanisms of NCAM function. *Front. Biosci.* 9, 2227–2244 (2004).

29. A. M. Babic, C.-C. Chen, L. F. Lau, Fisp12/Mouse Connective Tissue Growth Factor Mediates Endothelial Cell Adhesion and Migration through Integrin αvβ3, Promotes Endothelial Cell Survival, and Induces Angiogenesis In Vivo. *Mol Cell Biol*. 19, 2958–2966 (1999).

30. K. Horiuchi, N. Amizuka, S. Takeshita, H. Takamatsu, M. Katsuura, H. Ozawa, Y. Toyama, L. F. Bonewald, A. Kudo, Identification and characterization of a novel protein, periostin, with restricted expression to periosteum and periodontal ligament and increased expression by transforming growth factor beta. *J. Bone Miner. Res.* 14, 1239–1249 (1999).

31. R. Doyonnas, D. B. Kershaw, C. Duhme, H. Merkens, S. Chelliah, T. Graf, K. M. McNagny, Anuria, omphalocele, and perinatal lethality in mice lacking the CD34-related protein podocalyxin. *J. Exp. Med.* 194, 13–27 (2001).

32. A. Ran, L. Guan, J. Wang, Y. Wang, GREM2 maintains stem cell-like phenotypes in gastric cancer cells by regulating the JNK signaling pathway. *Cell Cycle* (2019), doi:10.1080/15384101.2019.1646561.

33. Y. Wakabayashi, H. Watanabe, J. Inoue, N. Takeda, J. Sakata, Y. Mishima, J. Hitomi, T. Yamamoto, M. Utsuyama, O. Niwa, S. Aizawa, R. Kominami, Bcl11b is required for differentiation and survival of alphabeta T lymphocytes. *Nat. Immunol.* 4, 533–539 (2003).

34. P. Li, S. Burke, J. Wang, X. Chen, M. Ortiz, S.-C. Lee, D. Lu, L. Campos, D. Goulding, B. L. Ng, G. Dougan, B. Huntly, B. Gottgens, N. A. Jenkins, N. G. Copeland, F. Colucci, P. Liu, Reprogramming of T cells to natural killer-like cells upon Bcl11b deletion. *Science*. 329, 85–89 (2010).

35. X. Xu, L. Han, G. Zhao, S. Xue, Y. Gao, J. Xiao, S. Zhang, P. Chen, Z.-Y. Wu, J. Ding, R. Hu, B. Wei, H. Wang, LRCH1 interferes with DOCK8-Cdc42-induced T cell migration and ameliorates experimental autoimmune encephalomyelitis. *J. Exp. Med.* 214, 209–226 (2017).

36. B. N. Simpson, N. Hogg, L. M. Svensson, A. McDowall, W. Daley, K. Yarbrough, O. A. Abdul-Rahman, A new leukocyte hyperadhesion syndrome of delayed cord separation, skin infection, and nephrosis. *Pediatrics*. 133, e257-262 (2014).

37. Y. Miyake, K. Toyonaga, D. Mori, S. Kakuta, Y. Hoshino, A. Oyamada, H. Yamada, K.-I. Ono, M. Suyama, Y. Iwakura, Y. Yoshikai, S. Yamasaki, C-type lectin MCL is an FcRγ-coupled receptor that mediates the adjuvanticity of mycobacterial cord factor. *Immunity*. 38, 1050–1062 (2013).

38. T. Katagiri, M. Ogimoto, K. Hasegawa, Y. Arimura, K. Mitomo, M. Okada, M. R. Clark, K. Mizuno, H. Yakura, CD45 negatively regulates lyn activity by dephosphorylating both positive and negative regulatory tyrosine residues in immature B cells. *J. Immunol.* 163, 1321–1326 (1999).

39. G. H. Wabnitz, T. Köcher, P. Lohneis, C. Stober, M. H. Konstandin, B. Funk, U. Sester, M. Wilm, M. Klemke, Y. Samstag, Costimulation induced phosphorylation of L-plastin facilitates surface transport of the T cell activation molecules CD69 and CD25. *Eur. J. Immunol.* 37, 649–662 (2007).

40. P. Liu, J. R. Keller, M. Ortiz, L. Tessarollo, R. A. Rachel, T. Nakamura, N. A. Jenkins, N. G. Copeland, Bcl11a is essential for normal lymphoid development. *Nat. Immunol.* 4, 525–532 (2003).

41. C. M. Nefzger, F. J. Rossello, J. Chen, X. Liu, A. S. Knaupp, J. Firas, J. M. Paynter, J. Pflueger, S. Buckberry, S. M. Lim, B. Williams, S. Alaei, K. Faye-Chauhan, E. Petretto, S. K. Nilsson, R. Lister, M. Ramialison, D. R. Powell, O. J. L. Rackham, J. M. Polo, Cell Type of Origin Dictates the Route to Pluripotency. *Cell Rep*. 21, 2649–2660 (2017).

42. A. V. Pobbati, W. Hong, Emerging roles of TEAD transcription factors and its coactivators in cancers. *Cancer Biol. Ther.* 14, 390–398 (2013).

43. E. Flannery, M. Duman-Scheel, Semaphorins at the interface of development and cancer. *Curr Drug Targets*. 10, 611–619 (2009).

44. M. Arar, Y. C. Xu, I. Elshihabi, J. L. Barnes, G. G. Choudhury, H. E. Abboud, Platelet-derived growth factor receptor beta regulates migration and DNA synthesis in metanephric mesenchymal cells. *J. Biol. Chem.* 275, 9527–9533 (2000).

45. A.-C. Luissint, P. G. Lutz, D. A. Calderwood, P.-O. Couraud, S. Bourdoulous, JAM-L-mediated leukocyte adhesion to endothelial cells is regulated in cis by alpha4beta1 integrin activation. *J. Cell Biol.* 183, 1159–1173 (2008).

46. A. Jeanes, C. J. Gottardi, A. S. Yap, Cadherins and cancer: how does cadherin dysfunction promote tumor progression? *Oncogene*. 27, 6920–6929 (2008).

47. A. Chiche, I. Le Roux, M. von Joest, H. Sakai, S. B. Aguín, C. Cazin, R. Salam, L. Fiette, O. Alegria, P. Flamant, S. Tajbakhsh, H. Li, Injury-Induced Senescence Enables In Vivo Reprogramming in Skeletal Muscle. *Cell Stem Cell*. 20, 407-414.e4 (2017).

48. L. Johnson, K. Mercer, D. Greenbaum, R. T. Bronson, D. Crowley, D. A. Tuveson, T. Jacks, Somatic activation of the K-ras oncogene causes early onset lung cancer in mice. *Nature*. 410, 1111–1116 (2001).

49. F. Marampon, C. Ciccarelli, B. M. Zani, Biological Rationale for Targeting MEK/ERK Pathways in Anti-Cancer Therapy and to Potentiate Tumour Responses to Radiation. *Int J Mol Sci*. 20 (2019), doi:10.3390/ijms20102530.

50. C. Chronis, P. Fiziev, B. Papp, S. Butz, G. Bonora, S. Sabri, J. Ernst, K. Plath, Cooperative Binding of Transcription Factors Orchestrates Reprogramming. *Cell*. 168, 442-459.e20 (2017).

51. C. Kadoch, D. C. Hargreaves, C. Hodges, L. Elias, L. Ho, J. Ranish, G. R. Crabtree, Proteomic and bioinformatic analysis of mammalian SWI/SNF complexes identifies extensive roles in human malignancy. *Nat. Genet.* 45, 592–601 (2013).

52. T. A. Ince, A. L. Richardson, G. W. Bell, M. Saitoh, S. Godar, A. E. Karnoub, J. D. Iglehart, R. A. Weinberg, Transformation of different human breast epithelial cell types leads to distinct tumor phenotypes. *Cancer Cell*. 12, 160–170 (2007).

53. E. Lim, F. Vaillant, D. Wu, N. C. Forrest, B. Pal, A. H. Hart, M.-L. Asselin-Labat, D. E. Gyorki, T. Ward, A. Partanen, F. Feleppa, L. I. Huschtscha, H. J. Thorne, kConFab, S. B. Fox, M. Yan, J. D. French, M. A. Brown, G. K. Smyth, J. E. Visvader, G. J. Lindeman, Aberrant luminal progenitors as the candidate target population for basal tumor development in BRCA1 mutation carriers. *Nat. Med.* 15, 907–913 (2009).

54. S. Eminli, A. Foudi, M. Stadtfeld, N. Maherali, T. Ahfeldt, G. Mostoslavsky, H. Hock, K. Hochedlinger, Differentiation stage determines potential of hematopoietic cells for reprogramming into induced pluripotent stem cells. *Nat. Genet.* 41, 968–976 (2009).

55. K. Y. Tan, S. Eminli, S. Hettmer, K. Hochedlinger, A. J. Wagers, Efficient generation of iPS cells from skeletal muscle stem cells. *PLoS ONE*. 6, e26406 (2011).

56. G. Lapouge, K. K. Youssef, B. Vokaer, Y. Achouri, C. Michaux, P. A. Sotiropoulou, C. Blanpain, Identifying the cellular origin of squamous skin tumors. *Proc. Natl. Acad. Sci. U.S.A.* 108, 7431–7436 (2011).

57. A. C. White, K. Tran, J. Khuu, C. Dang, Y. Cui, S. W. Binder, W. E. Lowry, Defining the origins of Ras/p53-mediated squamous cell carcinoma. *Proc. Natl. Acad. Sci. U.S.A.* 108, 7425–7430 (2011).

58. L. Zhu, P. Gibson, D. S. Currle, Y. Tong, R. J. Richardson, I. T. Bayazitov, H. Poppleton, S. Zakharenko, D. W. Ellison, R. J. Gilbertson, Prominin 1 marks intestinal stem cells that are susceptible to neoplastic transformation. *Nature*. 457, 603–607 (2009).

Acknowledgements:

We are grateful to the Laboratoire des modèles tumoraux (LMT) and A. Lalande for technical assistance. We thank P. Mehlen and V. Azuara for critical readings of the manuscript.

Fundings:

This work was supported by institutional grants from Inserm/Cnrs, Atip-avenir, Plan cancer, La ligue contre le cancer nationale et régionale (FL), INCa (FL), Fondation ARC (FL), Centre Léon Bérard (FL and AH), Fondation pour la recherche médicale (FL ARF20170938622).

Author Contributions:

AH performed most of the experiments from figures 1-7. NR, JS and JP performed bio-informatic analyses. BG performed *in vivo* work. FL and AH designed experiments and wrote the manuscript. FL designed and supervised the study.

Methods

Mice and MEFs

$R26^{rtTA}$;$Col1a1^{4F2A}$ (*21*), LSL-K-ras^{G12D} (*22*), K-ras^{LA2} (*48*), R26-CRE^{ERT2}, Oct4-EGFP, Bcl11b-tdTomato (*34*) and $Bcl11b^{flox/flox}$ (*34*) mice were housed under standard conditions and bred in accordance with french national guidelines.

Genotyping was carried out on genomic DNA derived from adult and embryonic tails using the DirectPCR Lysis Reagent (102-T, Viagen Biotech) and EconoTaq Plus Green 2X Master Mix (Lucigen). Primers used are listed in Table 1.

MEFs were isolated from E13.5 embryos after removal of the head and internal organs. The remaining tissues were physically dissociated and incubated in trypsin at 37°C for 10 min after which cells were resuspended in MEF medium.

Doxycycline (Dox) was given to the $R26^{rtTA}$;$Col1a1^{4F2A}$;K-ras^{LA2} mice in the drinking water at 0.2 mg/ml starting at 8 weeks of age. The cycles of treatment consisted of 2 days with doxycycline and 5 days without.

The mice were analysed after 10 weeks of treatment or until the limit time point was achieved. (APAFIS#10379-2017022514315224 v5).
The *in vivo* monitoring of the lung tumors were performed by X-ray tomography (Quantum FX, Perkin Elmer).

Histology

For histological examination, lungs were fixed in 10% buffered formalin and embedded in paraffin. 200 µm-thick tissue sections of formalin-fixed, paraffin-embedded tissue were prepared according to conventional procedures. Sections were then stained with hematoxylin and eosin and examined under a light microscope. Immunohistochemistry was performed on an automated immunostainer (Ventana Discovery XT, Roche, Meylan, France) using the Omnimap DAB Kit according to the manufacturer's instructions. Sections were incubated with a rabbit anti-Ki67 (F/RM-9106, Thermo Fisher Scientific) and pERK1/2 (4370, Cell Signaling Technology) prior to adding an anti-rabbit HRP. Staining was visualized with DAB solution with 3,3'-diaminobenzidine as a chromogenic substrate. Finally, the sections were counterstained with Gill's hematoxylin. The slides were scanned using the panoramic scan II (3D Histech) and the images were analyzed with the CaseViewer software and halo image analysis platform (Indica Labs).

Teratoma

Teratoma formation assays were performed by injecting $1x10^6$ iPS cells into the testes of 7-week-old severe combined immunodeficient (SCID) mice (CB17/SCID, Charles River). After 3-4 weeks, the mice were euthanized and lesions were surgically removed and fixed in 4% paraformaldehyde for sectioning and hematoxylin-eosin staining.

Plasmids and constructs

pMXS-Oct4, pMXS-Sox2, pMXS-Klf4, pMXS-Myc, pLKO.1 and MSCV plasmids were purchased from Addgene. shRNAs against Bcl11a, Bcl11b,Trp53 and FosL1 were designed using the MISSION shRNA library from Sigma-Aldrich and ligated using the Rapid DNA ligation kit (Sigma-Aldrich) into the pLKO.1 vector digested with AgeI and EcoRI. shRNA sequences are listed in Table 1. Bcl11a and Bcl11b cDNA were amplified from MEFs and cloned into the MSCV expression vector at Pac1 and Sal1 restriction sites. Single guide RNA targeting Bcl11b (designed with CRISPOR program) were cloned into the lentiCRISPRv2 plasmid at a BsmBI restriction site. pWPIR Hras G12V and cyclinE plasmids were kindly supplied by A. Puisieux's lab. Tet-O-FUW-Brn2, Tet-O-FUW-Ascl1, Tet-O-FUW-Myt1l and FUdeltaGW-rtTA plasmids were purchased from Addgene.

Cell culture and viral production

MEF medium consists of DMEM supplemented with 10% fetal bovine serum (FBS), 100 U/mL penicillin / streptomycin (PS), 1 mM sodium pyruvate, 2 mM L-glutamine, 0.1 mM Non Essential Amino Acids (NEAA) and 0.1 mM β-mercaptoethanol.

293FT cells, grown in MEF medium, were used to produce pLKO.1-derived and *Hras*G12V-carrying lentiviral particles. Briefly, calcium phosphate transfection of the pLKO.1 vectors, along with plasmids encoding the envelope G glycoprotein of the vesicular stomatitis virus (VSV-G) and Gag-Pol, was performed with the CalPhos Mammalian Transfection kit (Ozyme) in 10-cm dishes. Medium was changed with 10 mL of MEF medium after 7 h of incubation. The lentivirus-containing supernatants were collected 48 h later and stored at -80 °C. pMXs- and MSCV-based retroviral vectors were similarly generated with Plat-E cells (a retroviral packaging cell line constitutively expressing *gag*, *pol* and *env* genes).

Pluripotent reprogramming experiments

For Dox-induced PR, reprogrammable $R26^{rtTA}$;$Col1a1^{4F2A}$; Oct4-EGFP MEFs within three passages were plated in six-well plates at 80,000-100,000 cells per well in MEF medium. The following day, cells were infected overnight with shRNA-carrying lentiviral stocks in the presence of 8 μg/ml polybrene, and medium was then replaced by fresh medium with 2 μg/ml Dox. MEFs were reseeded 72 h after infection on 0.1% gelatin coated plates in iPSC medium (DMEM containing 15% KnockOut Serum Replacement, 1,000 U/mL leukemia inhibitory factor, 100 U/mL PS, 1 mM sodium pyruvate, 2 mM L-glutamine, 0.1 mM NEAA and 0.1 mM β-mercaptoethanol, at equal densities for each condition to normalize potential effect of differential MEF proliferation on reprogramming efficiency. Several densities were tested (15,000-68,000 cells per cm^2). Every day, medium was either replaced by or supplemented with Dox-containing fresh medium. Once iPS colonies were macroscopically visible, OCT4-GFP+ colonies were counted under an Axiovert 200 M microscope, and alkaline phosphatase (AP) staining was performed using the Leukocyte Alkaline Phosphatase kit (Sigma-Aldrich). Alternatively, MEFs were coinfected with OSKM retroviral vectors 48 h after lentiviral infections and cultured identically thereafter.

T lymphocytes from the spleen of Bcl11b-cKO mice were isolated using the Pan T cell isolation kit (Miltenyi Biotech) according to the manufacter's instructions after removal of red blood cells by NH4Cl treatment. T cells were grown in RPMI medium supplemented with 10% FBS, 100 U/mL penicillin / streptomycin (PS), 1 mM sodium pyruvate, 2 mM L-glutamine, 0.1 mM Non Essential Amino Acids (NEAA), 10 mM Hepes, 0.1 mM β-mercaptoethanol, 10 ng/mL IL-2 and anti-CD3/CD28. T cells were infected with OSKM retroviral vectors in the presence of 8 μg/mL polybrene the day after isolation for two consecutive days. 4 h after infection the medium was replaced by fresh T cell medium. 3 days after the second infection the cells were plated onto irradiated MEFs. The day after the medium was replaced with iPSC medium supplemented with 10 ng/mL IL-2 and Dynabeads Human T-Activator CD3/CD28 (Life Technologies). The medium was changed every other day.

Malignant reprogramming/transformation experiments

For MRT, the LSL-K-ras^{G12D};R26-CRE^{ERT2} MEFs were similarly infected overnight with shRNA-carrying lentiviral stocks in the presence of 8 µg/mL polybrene. 48 h later the cells were co-infected overnight with sh*Trp53*- and *Myc*-carrying viruses concomitantly with 4-hyfroxitamoxifen treatment (1 µM) to induce K-ras^{G12D} expression. Alternatively, the co-infection of sh*Trp53*-, *Myc*- and Hras^{G12V}-carrying viruses was used in WT MEFs to initiate MRT. MEFs were reseeded 48 h post-infection in six-well plates at low density (500, 1,000 or 2,000 cells per well) in focus medium (MEF medium with 5% FBS) for the foci formation assay. Medium was then changed twice a week. After several passages of the cells derived from MRT, soft agar assays were performed. Transformed cells were plated on an agarose-containing MEF medium layer at a density of 25,000-50,000 cells per six-well plate. Foci and soft agar colonies were stained 25-30 days later with a 0.5% cresyl violet solution in 20% methanol.

Immunofluorescence

Cells were fixed with 4% paraformaldehyde for 10 min at room temperature (RT°C), washed 3 times with PBS, permeabilized with 0.1% Triton X-100 for 30 min at RT°C and blocked with 1% bovine serum albumin (BSA) for 1 h. After incubation with primary antibodies against NANOG (Reprocell, RCAB001P), SSEA1 (Santa Cruz Biotechnology, sc-101462) and phospho-Histone H2A.X (Cell Signaling Technology, 2577) overnight at 4°C, cells were washed 3 times with PBS and incubated with fluorophore-labeled appropriate secondary antibodies (Life Technologies).

RNA extraction and RT-qPCR

Total RNAs were extracted using Trizol reagent and 1 µg of RNA was reverse-transcribed with the RevertAid H Minus First Strand cDNA Synthesis kit (Life Technologies). qPCR was performed with the LightCycler 480 SYBR Green I Master mix (Roche) on the LightCycler 96 machine (Roche). *Gapdh* and *Rplp0* were used as housekeeping genes. qPCR primers are listed in Table 1.

Protein extraction and Western blot

Cells were harvested in RIPA buffer (150 mM NaCl, 1% Triton, 0.5% deoxycholate, 0.1% SDS and 50 mM Tris, pH 8.0) supplemented with protease inhibitors and phosphatase inhibitors. After 30 min on ice, lysis by sonication, and centrifugation for 10 min at 15,000*g*, supernatants were collected, proteins were denatured 10 min at 95 °C in Laemmli sample buffer, separated on 4-15% polyacrylamide gel, and transferred onto a nitrocellulose membrane. The membrane was blocked with 5% milk in TBST (Tris-buffered saline, 0.1% Tween 20) for 1 h, incubated with primary antibody at 4°C overnight and secondary antibodies for 1 h at RT°C. Antigens were detected using ECL reagents. The following antibodies were used:

rabbit anti-BCL11A (Novus Biologicals, NB600-261, 1:1,000), rat anti-BCL11B (Abcam, ab18465, 1:500) horse radish peroxidase (HRP)-conjugated anti-ACTIN (Sigma Aldrich, A3854, 1:10,000), HRP-conjugated goat anti-rabbit (Interchim, 111-035-144, 1:5,000) and HRP-conjugated goat anti-rat (Interchim, 112-035-143, 1:5,000).

FACS

The following antibody was used : anti-mouse CD90.2 (Thy-1.2) APC (eBioscience, 17-0902). Analysis was performed on a BD LSRFortessa. Sorting was performed on a BD FACSAria. Apoptosis was measured using the FITC Annexin V/Dead Cell Apoptosis Kit (Invitrogen, V13242). For cell cycle analysis, the cells were fixed in ethanol 70% and stained with 40 µg/mL propidium iodide supplemented with 2 mg/mL RNase.

Xenografts

$3x10^6$ immortalized cells were prepared in 100 µL PBS supplemented with 100 µL matrigel and injected subcutaneously into immunocompromised SCID mice (N = 6 for each group). The volume of the tumor was then measured every 3 days until day 12.

CAM assay

$2.5x10^6$ immortalized cells were inoculated on the chorioallantoic membrane (CAM) in the egg of chick embryos at E11 where they formed a primary tumor. The size of the tumor was evaluated after 7 days. The number of replicates is indicated in the figure legend.

NGS analyses

RNA quality was analysed using a Bioanalyser (Agilent). Libraries were constructed and sequenced on an illumina Hiseq 2000 by the cancer genomics platform on site. ATAC-seq data were generated by the Active Motif company. NGS data were deposited on GEO (record number series GSE137050, secure token for reviewers access yvmpscquvhybzgl).

Statistical analyses

All data are reported as mean ± SEM. Statistical analyses were performed using GraphPad Prism software. Student t tests were used for paired comparisons and one-way ANOVA followed by a Tukey's post hoc test was used for multiple comparisons. P-values are indicated on each graph.

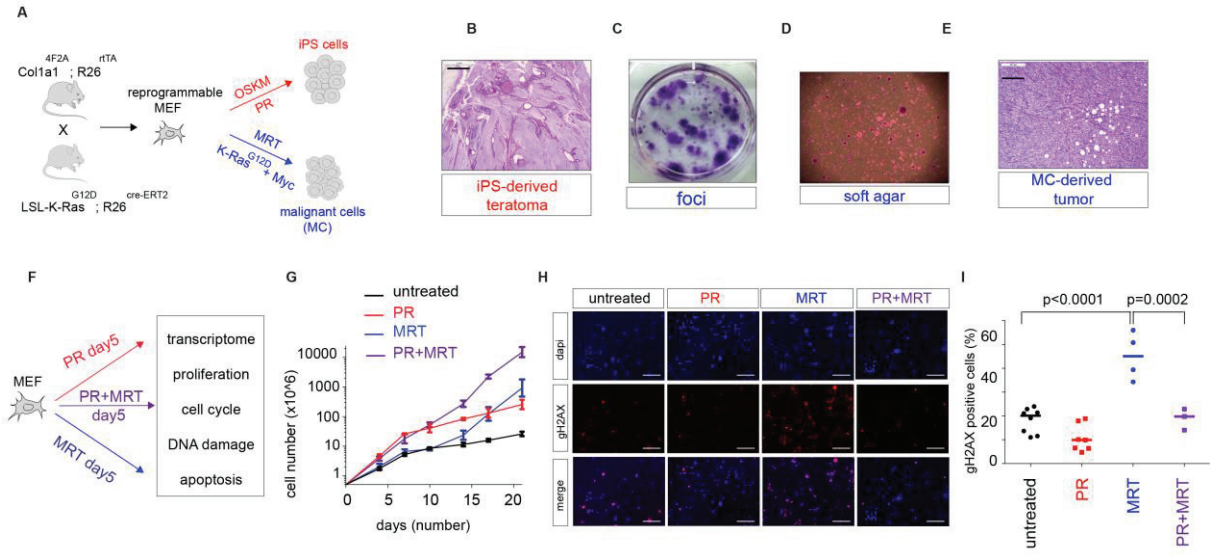

Figure 1. A genetic system to compare iPS cell generation and malignant transformation. (A) A schematic illustration of the genetic construct of R26^{rtTA}; Col1a1^{4F2A}; LSL-K-Ras G12D; R26$^{cre/ERT2}$ mice generated to produce reprogrammable MEFs. PR (doxycycline-induced OSKM expression) or MRT (tamoxifen-induced K-ras^{G12D} expression combined with c-Myc overexpression) are induced to give rise to iPS or malignant cells, respectively. (B) Histological analysis of teratomas derived from PR-induced iPS cells. Scale bar: 1 mm. (C) Foci from MRT-induced malignant cells colored with cresyl-violet. (D) Soft agar colonies derived from MRT-induced malignant cells colored with cresyl-violet. (E) *In vivo* tumor formation in nude mice injected with MRT-induced malignant cells. Scale bar: 0.2 mm. MC: malignant cell. (F) Schematic diagram of the analyses conducted after 5 days of PR, MRT or the combination of both (PR+MRT). (G) Proliferation curves of MEFs upon PR, MRT and PR+MRT treatment for 21 days compared to control MEFs. (H) Immunofluorescent staining of PR-, MRT- and PR+MRT-induced cells for γH2AX after 3 days compared to control MEFs. One representative experiment (from three independent experiments). Scale bar: 100 µm. (I) Counting of γH2AX-positive cells depicted in (H).

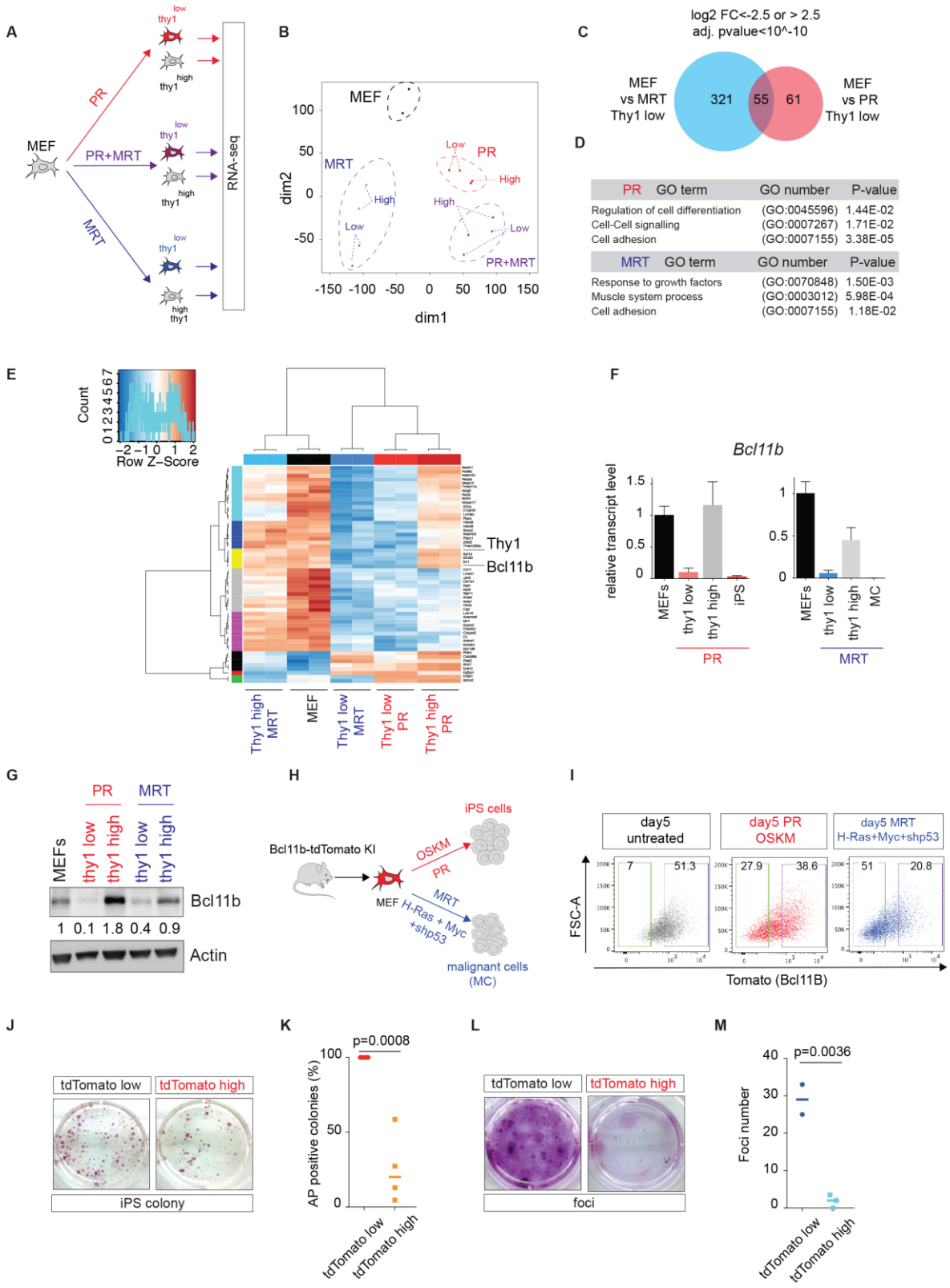

Figure 2. Bcl11b is a MEF marker downregulated in reprogramming cells during both iPS cells generation and malignant transformation. (A) RNA-seq analyses were performed in Thy1^{low}- and Thy1^{high}-FACS sorted cells after 5 days of PR, MRT or the combination of both (PR+MRT) compared to control MEFs. (B) Principal component analysis. (C) Venn diagram showing the number of genes specifically and commonly regulated in Thy1^{low} cells upon PR and MRT. (D) Gene Ontology (GO) enrichment for genes differentially expressed in

Thy1^{low} cells from PR and MRT. (E) Heatmap depicting the expression of the 55 genes commonly regulated in Thy1^{low} cells upon PR and MRT. (F) Relative transcript level of *Bcl11b* determined by RT-qPCR in MEFs, Thy1^{low} and Thy1^{high} cells upon PR and MRT after 5 days and in iPS cells and malignant cells (MCs). (G) Western blot showing Bcl11b expression in MEFs, Thy1^{low} and Thy1^{high} cells upon PR and MRT after 5 days. One representative experiment (from three independent experiments). (H) A schematic illustration of the genetic construct of Bcl11b-tdTomato mice to produce MEFs. PR (retroviral OSKM expression) or MRT (H-ras^{G12V}, c-Myc and shp53 viral inductions) are induced to give rise to iPS or MCs, respectively. (I) FACS analysis of Bc11b-tdTomato upon 5 days of PR or MRT compared to control MEFs. (J) Alkaline Phosphatase (AP) staining of iPS colonies generated from tdTomato^{low} and tdTomato^{high} cells FACS-sorted at day 5 of PR. One representative experiment (from four independent experiments). (K) Counting of AP-positive colonies depicted in (J). (L) Foci staining of malignant cells generated from tdTomato^{low} and tdTomato^{high} cells FACS-sorted at day 5 of MRT. One representative experiment (from three independent experiments). (M) Counting of foci depicted in (L).

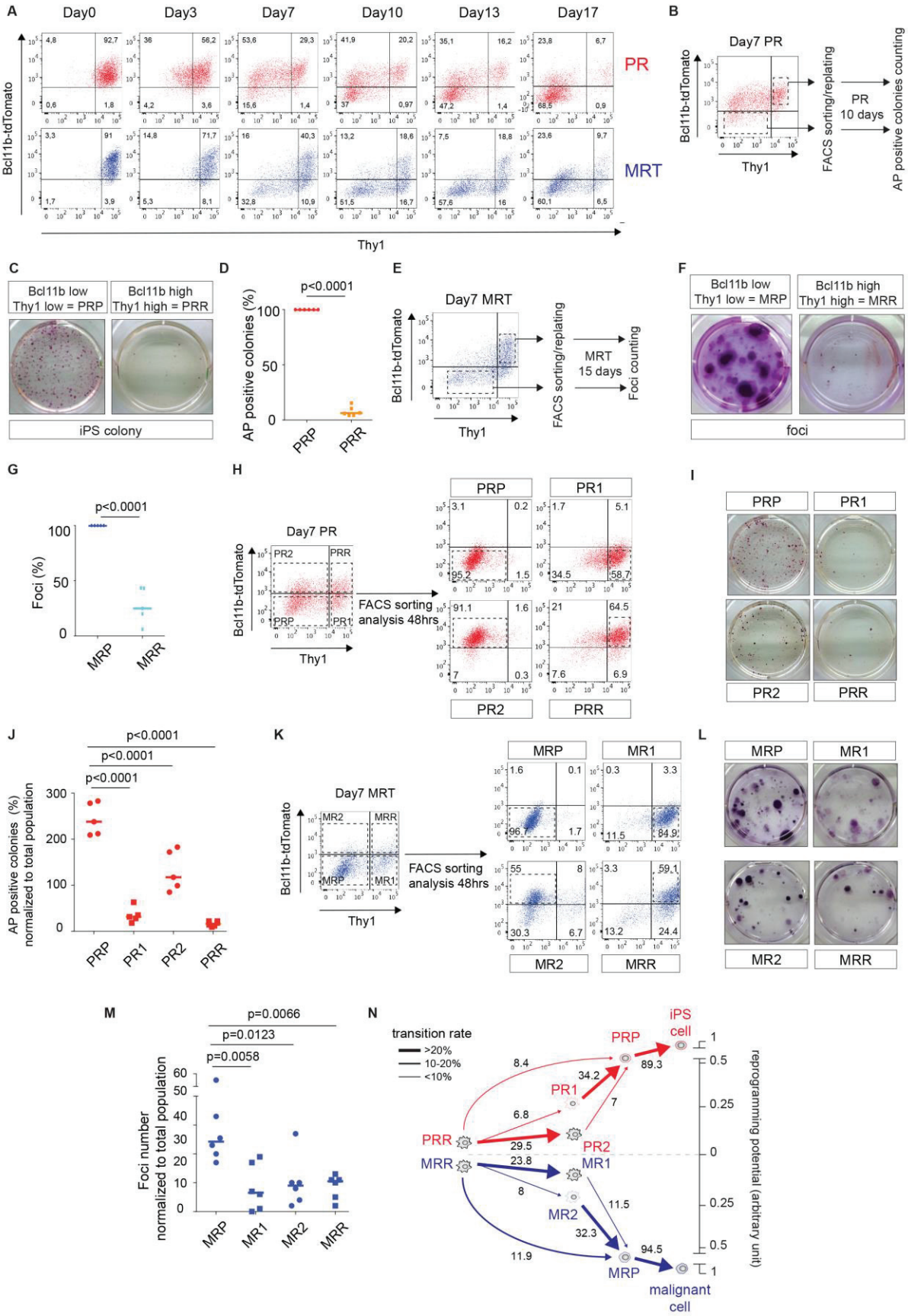

Figure 3. The sequential downregulation of Bcl11b and Thy1 delineates routes toward pluripotency and malignancy. (A) FACS profile of Bcl11b-tdTomato and Thy1 upon PR and MRT from day 0 to day 17. (B)

Bcl11b-tdTomato/Thy1 double negative and double positive cells induced for PR were FACS-sorted at day 7, replated at equal densities in PR conditions and AP staining was performed after 10 days. (C) Alkaline Phosphatase (AP) staining of iPS colonies generated from double negative (PRP: Pluripotent Reprogramming Prone) and double positive (PRR: Pluripotent Reprogramming Refractory) cells FACS-sorted at day 7 of PR. One representative experiment (from six independent experiments). (D) Counting of AP-positive colonies depicted in (C). (E) Bcl11b-tdTomato/Thy1 double negative and double positive cells induced for MRT were FACS-sorted at day 7, replated at equal densities in MRT conditions and foci staining was performed after 15 days. (F) Foci staining of malignant cells generated from double negative (MRP: Malignant Reprogramming Prone) and double positive (MRR: Malignant Reprogramming Refractory) cells FACS-sorted at day 7 of MRT. One representative experiment (from five independent experiments). (G) Counting of foci depicted in (F). (H) Four different subpopulations (Bcl11b-tdTomato^{high}/Thy1^{high}, Bcl11b-tdTomato^{high}/Thy1^{low}, Bcl11b-tdTomato^{low}/Thy1^{high} and Bcl11b-tdTomato^{low}/Thy1^{low}) were FACS-sorted at day 7 of PR and replated. After 2 days, the expression profile of Bcl11b and Thy1 were analyzed for the 4 subpopulations by FACS. (I) AP staining of iPS colonies generated from the different subpopulations described in (H) FACS-sorted at day 7 of PR. One representative experiment (from five independent experiments). (J) Counting of AP-positive colonies depicted in (I). (K) 4 different subpopulations (same as in (H)) were FACS-sorted at day 7 of MRT and replated. After 2 days, the expression profile of Bcl11b and Thy1 were analyzed for the 4 subpopulations by FACS. (L) Foci staining of malignant cells generated from the different subpopulations described in (K) FACS-sorted at day 7 of MRT. One representative experiment (from six independent experiments). (M) Counting of foci depicted in (L). (N) A schematic illustration of the trajectories taken by the different subpopulations of cells during PR and MRT and the reprogramming efficiency associated. PRP: pluripotent reprogramming prone, PR1: pluripotent reprogramming intermediate 1, PR2: pluripotent reprogramming intermediate 2, PRR: pluripotent reprogramming refractory, MRP: malignant reprogramming prone, MR1: malignant reprogramming intermediate 1, MR2: malignant reprogramming intermediate 2, MRR: malignant reprogramming refractory.

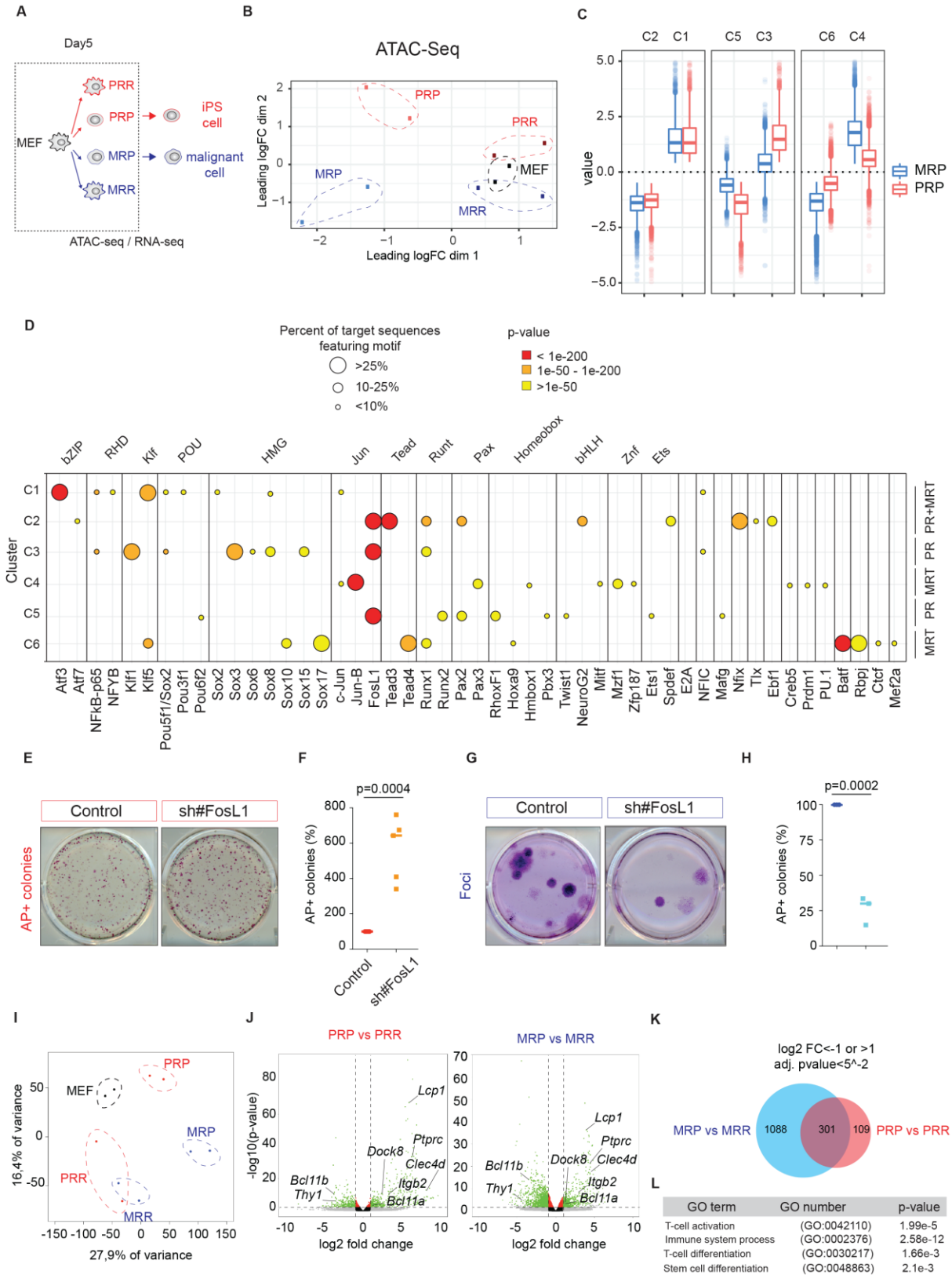

Figure 4. Epigenomic and transcriptomic reconfiguration in pluripotent and malignant reprogramming intermediates. (A) ATAC-seq and RNA-seq analyses were performed at 5 days of PR and MRT in the intermediate cells prone (Bcl11b-tdTomato^{low} /Thy1^{low}: PRP and MRP) and refractory (Bcl11b-tdTomato^{high} /Thy1^{high}: PRR and MRR) to reprogramming and in the final product of each reprogramming process (iPS

and malignant cells). (B) Principal component analysis. (C) Transcription factor motifs enriched in the ATAC-seq peaks of intermediate cells prone to reprogramming at day 5 of PR and MRT. 6 clusters were defined (see main text for description). (D) Enrichment in transcription factors motifs in ATAC-seq clusters. Each point represents a significant enrichment in the motif (x axis) for the cluster (y axis). Point size represents the proportion of sequences in the cluster featuring the motif and color gradient the enrichment significance. (E) Alkaline Phosphatase (AP) staining of iPS colonies generated upon downregulation of FosL1. One representative experiment (from six independent experiments). (F) Counting of AP-positive colonies depicted in (E). (G) Foci staining of malignant cells generated upon downregulation of FosL1. One representative experiment (from three independent experiments). (H) Counting of foci depicted in (G). (I) Principal component analysis of normalized gene expression of the control cells and the reprogramming intermediates. (J) Volcano plot comparing the transcriptomes of PRP *vs* PRR and MRP *vs* MRR cells. Each dot corresponds to a transcript. (K) Venn diagram showing the number of genes specifically and commonly regulated in prone cells (PRP and MRP) upon PR and MRT compared to the refractory cells (PRR and MRR). (L) Gene Ontology (GO) enrichment for genes differentially expressed in PRP and MRP cells.

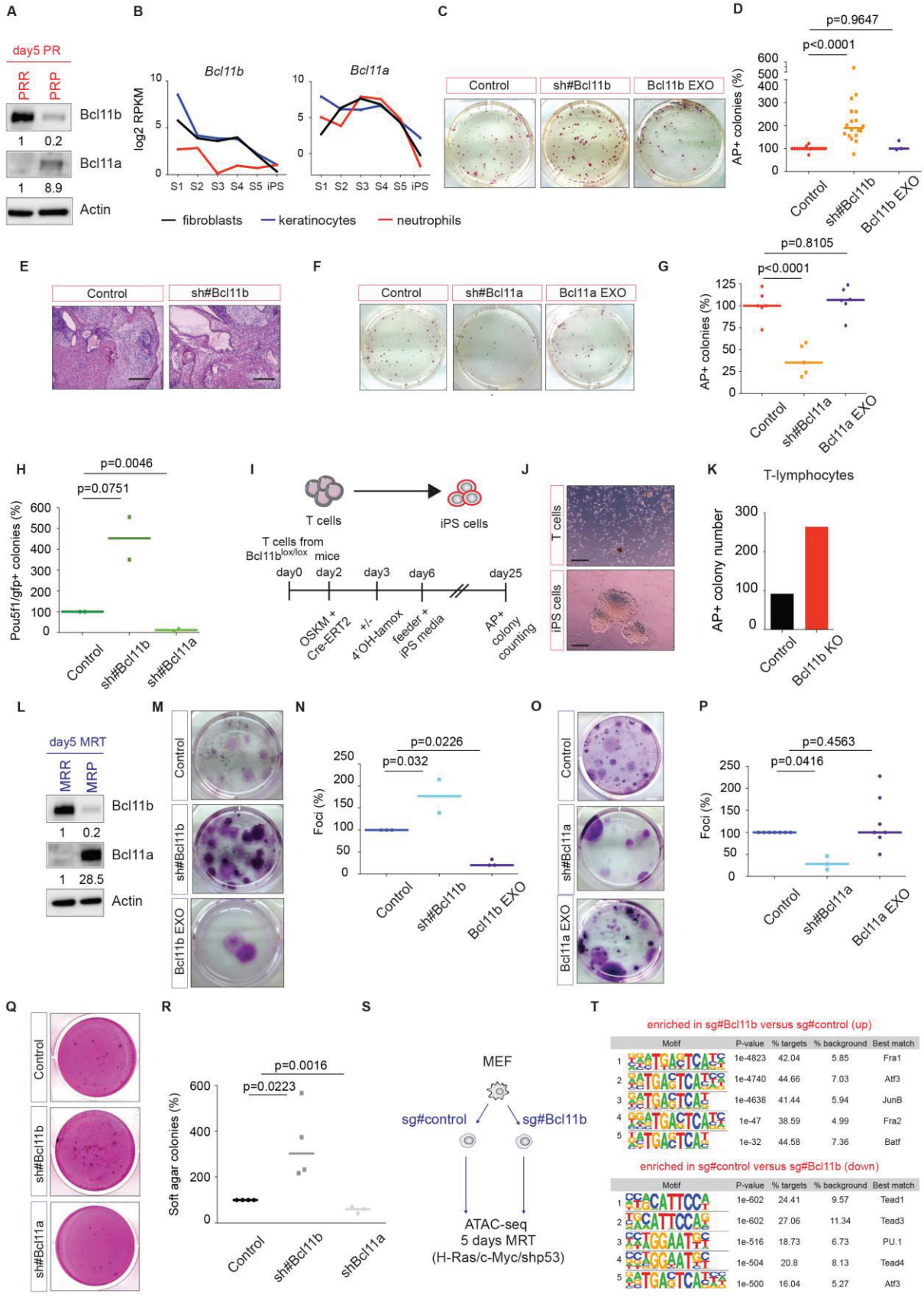

Figure 5. A Bcl11b/Bcl11a switch regulates cellular identity change during iPS cells generation and malignant transformation. (A) Western blot showing the inverse of expression of Bcl11b and Bcl11a in PRR and PRP intermediate cells upon PR after 5 days. (B) RNA-seq data from Nefzger et al., 2017 showing *Bcl11b*

downregulation and *Bcl11a* transient upregulation during defined steps (S1 to S5) of fibroblast, keratinocyte and neutrophil reprogramming into iPS cells. (C) Alkaline Phosphatase (AP) staining of iPS colonies generated upon downregulation (sh#Bcl11b) or exogenous expression (Bcl11b EXO) of Bcl11b. One representative experiment (from at least three independent experiments). (D) Counting of AP-positive colonies depicted in (C). (E) Histological analysis of teratomas derived from PR-induced control iPS cells and derived from cells downregulating Bcl11b. (F) AP staining of iPS colonies generated upon downregulation (sh#Bcl11a) or exogenous expression (Bcl11a EXO) of Bcl11a. One representative experiment (from five independent experiments). (G) Counting of AP-positive colonies depicted in (F). (H) Percentage of Oct4-EGFP positive colonies generated upon downregulation of Bcl11b and Bcl11a. (I) A schematic illustration of the reprogramming of T lymphocytes into iPS cells. (J) Bright-field images of activated T lymphocytes and iPS cells derived from T cells after 18 days. Scale bar: 100 µm. (K) Number of AP+ colonies generated after 25 days of reprogramming of T lymphocytes. (L) Western blot showing the inverse expression of Bcl11b and Bcl11a in MRR and MRP intermediate cells upon MRT after 5 days. (M) Foci staining of malignant cells generated upon downregulation (sh#Bcl11b) or exogenous expression (Bcl11b EXO) of Bcl11b. One representative experiment (from three independent experiments). (N) Counting of foci depicted in (M). (O) Foci staining of malignant cells generated upon downregulation (sh#Bcl11a) or exogenous expression (Bcl11a EXO) of Bcl11a. One representative experiment (from at least three independent experiments). (P) Counting of foci depicted in (O). (Q) Soft agar colonies derived from MRT-induced malignant cells upon downregulation of Bcl11b or Bcl11a. One representative experiment (from at least three independent experiments). (R) Percentage of soft agar colonies depicted in (Q). (S) MEFs were transduced with single guide control or targeting Bcl11b and after 5 days of MRT cells were subjected to ATAC-seq. (T) Top 5 TF motif enrichment.

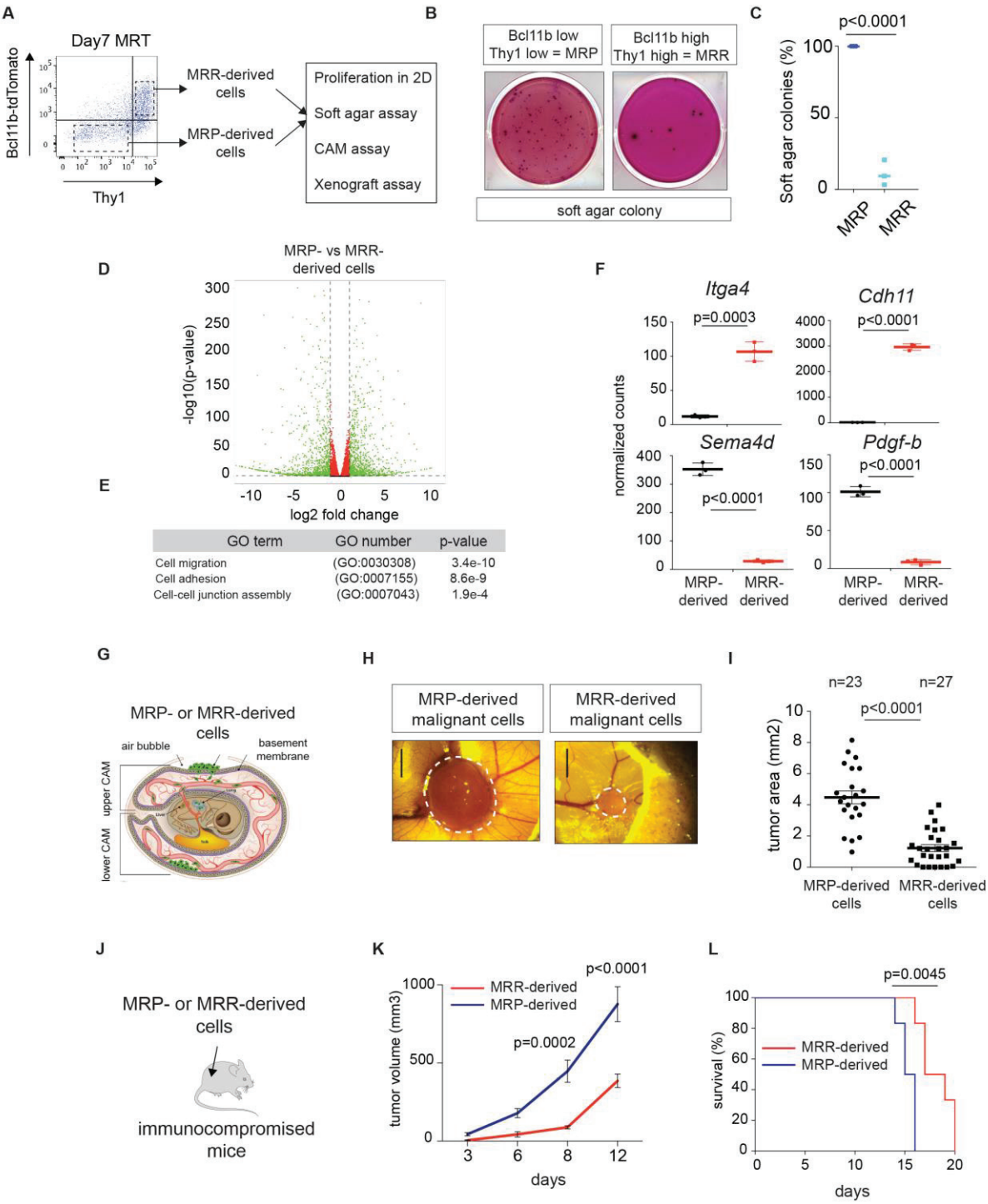

Figure 6. The susceptibility of MEFs to lose their identity impacts the acquisition of malignant properties *in vitro* and *in vivo*. (A) Bcl11b-tdTomato/Thy1 double negative (MRP) and double positive (MRR) cells induced for MRT were FACS-sorted at day 7, replated at equal densities in MRT conditions and expanded for several passages to acquire transformed features. Cells were then subjected to soft agar assay, chorioallantoic membrane (CAM) assay or xenograft assay. (B) Soft agar colonies generated from MRP and MRR cells FACS-sorted at day 7 of MRT. One representative experiment (from three independent experiments). (C) Percentage of soft agar colonies depicted in (B). (D) Volcano plot comparing the transcriptomes of MRR- and MRP-derived malignant cells. Each dot corresponds to a transcript. (E) Gene Ontology (GO) of biological

processes represented in the MRP-derived malignant cells compared to their MRR counterpart. (F) Relative transcript level of *Itgα4*, *Cdh11*, *Sema4d* and *Pdgf-b* determined by RT-qPCR in MRP and MRR-derived malignant cells. (G) MRP or MRR-derived malignant cells were inoculated on the CAM in the egg of chick embryos at E11. (H) The size of the tumor was evaluated after 7 days. (I) Counting of the tumor area depicted in (H). (J) MRP or MRR-derived malignant cells were injected subcutaneously into immunocompromised SCID mice. (K) The volume of the tumors were measured every 3 days until day 12. (L) Survival curve of mice injected with MRP or MRR-derived malignant cells.

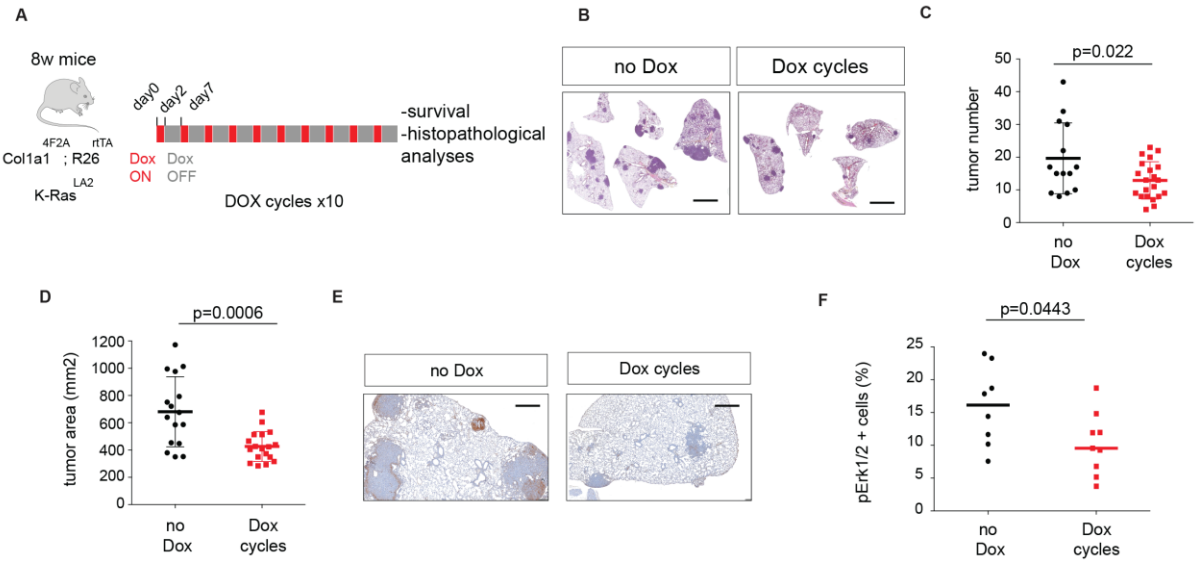

Figure 7. Cyclic OSKM expression constrains Erk1/2 activation and tumor development triggered by K-Ras in the lung. (A) A schematic illustration of the doxycycline cycles given to 8-week old $R26^{rtTA}$; $Col1a1^{4F2A}$; $K\text{-}Ras^{LA2}$ mice. Survival was measured and histopathological analyses were performed after 10 cycles compared to glucose-treated mice. (B) Histopathological analysis of lung sections stained with hematoxylin-eosin in glucose-treated mice (no Dox) and mice treated with cycles of doxycycline (Dox cycles) at 18 weeks of age. (C) Number of tumors counted for each group of mice. (D) Tumor area measured for each group of mice. (E) Immunostaining of lung sections with anti-pErk1/2 in glucose-treated mice (no Dox) and mice treated with cycles of doxycycline (Dox cycles) at 18 weeks of age. (F) Percentage of pErk1/2-positive cells counted for each group of mice.

Supplementary materials

Fig. S1 to S5

Table 1

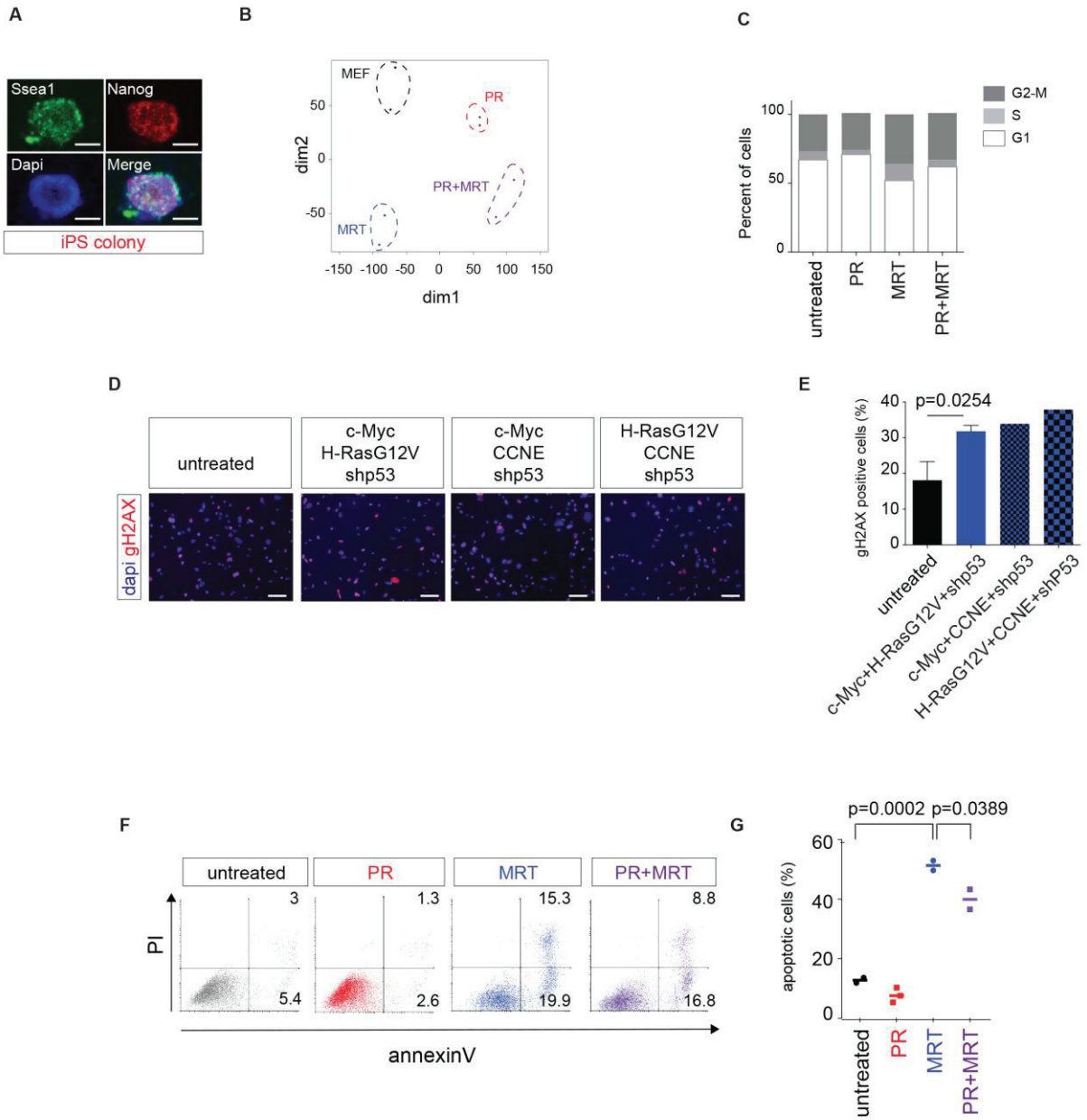

Supplementary figure 1. (A) Immunofluorescent staining of PR-induced iPS cells for Ssea1 and Nanog. Scale bar: 100 µm. (B) Principal component analysis of normalized gene expression of control cells or cells subjected to 5 days of PR, MRT or both programs (PR+MRT). (C) Cell cycle analyzed by FACS in control MEFs and after 5 days of PR, MRT and PR+MRT. (D) Immunofluorescent staining of MRT-induced cells for γH2AX after 3 days with various oncogenic cocktails compared to control MEFs. (E) Counting of γH2AX-positive cells depicted in (D). (F) FACS profile PI/AnnexinV at 3 days of PR, MRT and PR+MRT compared to control MEFs. One representative experiment (from at least two independent experiments). (G) Percentage of total apoptosis depicted in (F).

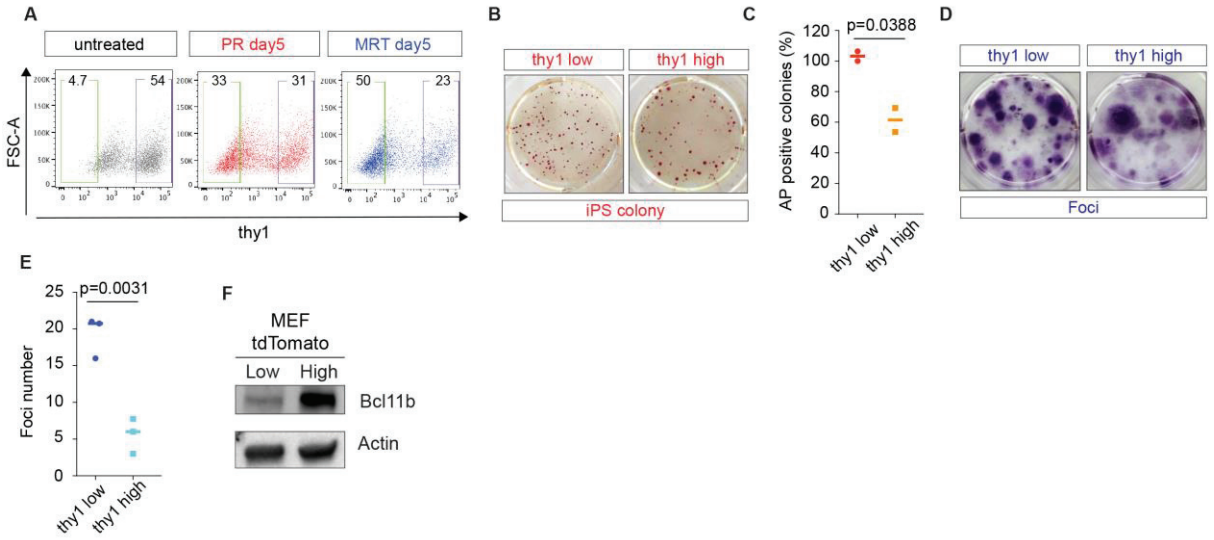

Supplementary figure 2. (A) FACS analysis of the somatic marker Thy1 upon 5 days of PR or MRT compared to control MEFs. (B) Alkaline Phosphatase (AP) staining of iPS colonies generated from Thy1^{low} and Thy1^{high} cells FACS-sorted at day 5 of PR. One representative experiment (from two independent experiments). (C) Counting of AP-positive colonies depicted in (B). (D) Foci staining of malignant cells generated from Thy1^{low} and Thy1^{high} cells FACS-sorted at day 5 of MRT. One representative experiment (from three independent experiments). (E) Counting of foci depicted in (D). (F) Western blot showing the enrichment of Bcl11b in the tdTomato-high fraction after FACS-cell sorting compared to the tdTomato-low fraction.

A

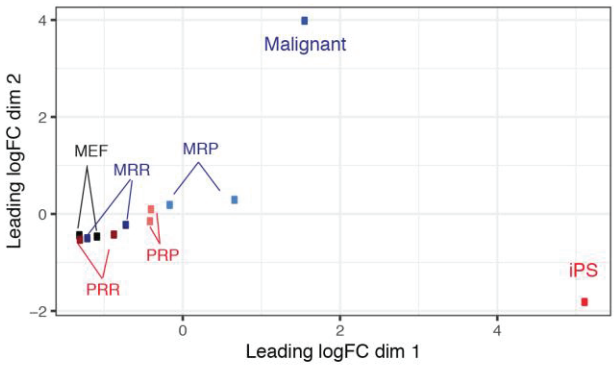

B

Cluster C1: peaks commonly gained in PRP/MRP versus MEFs

	Motif	P-value	% targets	% background	Best match
1		1e-415	25.9	3.5	Atf3
2		1e-94	8.68	1.7	NFkB-p65
3		1e-86	29.9	15.5	Klf5
4		1e-47	5.2	1.2	Pou5f1/Sox2
5		1e-32	9.2	4.1	Sox2
6		1e-26	3.8	1.1	c-Jun
7		1e-22	0.5	0.01	NFYB
8		1e-20	0.7	0.05	Sox8
9		1e-19	0.4	0.01	Pou3f1
10		1e-17	0.4	0.01	E2A

Total target sequences: 2995; Total background sequences: 46808

Cluster C2: peaks commonly lost in PRP/MRP versus MEFs

	Motif	P-value	% targets	% background	Best match
1		1e-833	39.5	7	Fra1
2		1e-213	37.7	17.7	Tead3
3		1e-108	13.4	4.8	Runx1
4		1e-62	20.9	12	Pax2
5		1e-54	26.4	17.1	Nfix
6		1e-53	19.1	11.2	NeuroG2
7		1e-41	17.1	10.4	Tlx
8		1e-37	12.4	7	Atf7
9		1e-36	22.2	15.1	SPDEF
10		1e-35	21.3	14.4	EBF1

Total target sequences: 4522; Total background sequences: 44217

Cluster C3

	Motif	P-value	% targets	% background	Best match
1		1e-411	35.23	5.7	Fra1
2		1e-175	43.27	18.1	Sox3
3		1e-164	33.16	11.77	Klf1
4		1e-85	7.6	1.2	Pou5f1/Sox2
5		1e-58	8.4	2.1	NKkB-p65
6		1e-43	15.07	6.82	Sox8
7		1e-33	10.5	4.5	Runx1
8		1e-29	19.8	11.7	Sox15
9		1e-24	0.6	0.01	Sox6
10		1e-24	7.9	3.43	NFIC

Total target sequences: 2376; Total background sequences: 47091

Cluster C4

	Motif	P-value	% targets	% background	Best match
1		1e-588	33.22	4.9	JunB
2		1e-25	10.4	5.7	Pax3
3		1e-24	5.1	2.2	Creb5
4		1e-24	7.11	3.42	Prdm1
5		1e-20	9.92	5.78	PU.1
6		1e-20	3.05	1.04	Hmbox1
7		1e-19	19.9	14.07	Mzf1
8		1e-18	3.14	1.14	Mitf
9		1e-18	1.27	0.22	Jun
10		1e-18	1.1	0.16	Zfp187

Total target sequences: 3377; Total background sequences: 43758

Cluster C5

	Motif	P-value	% targets	% background	Best match
1		1e-235	59.87	7.49	Fra1
2		1e-20	16.3	5.5	Runx2
3		1e-17	7.7	1.5	Ets1
4		1e-16	15.3	5.7	Pax2
5		1e-15	10.1	2.9	RhoxF1
6		1e-13	5.4	0.9	Twist1
7		1e-13	5	0.8	Mafg
8		1e-12	4.7	0.7	Ets
9		1e-12	3.5	0.4	Pbx3
10		1e-12	1.1	0.01	Pou6f2

Total target sequences: 593; Total background sequences: 47312

Cluster C6

	Motif	P-value	% targets	% background	Best match
1		1e-417	36.5	8.1	Batf
2		1e-104	39	21.6	Tead4
3		1e-62	17	7.8	Klf5
4		1e-43	30.4	19.8	Rbpj
5		1e-42	2.6	0.3	Ctcf
6		1e-41	56.8	44.6	Sox17
7		1e-39	4.8	1.3	Mef2a
8		1e-33	11.2	5.5	Runx1
9		1e-31	10.9	5.4	Sox10
10		1e-24	9.3	4.8	Hoxa9

Total target sequences: 3066; Total background sequences: 46078

Supplementary figure 3. (A) Principal component analysis of ATAC-seq signal of the control cells, the reprogramming intermediates and the final product of each reprogramming process (iPS and malignant

cells). (B) Top 10 motifs enriched in C1/C2 clusters jointly gained/lost in PRP and MRP, in C3/C4 clusters specifically gained in PRP/MRP and in C5/C6 clusters specifically lost in PRP/MRP.

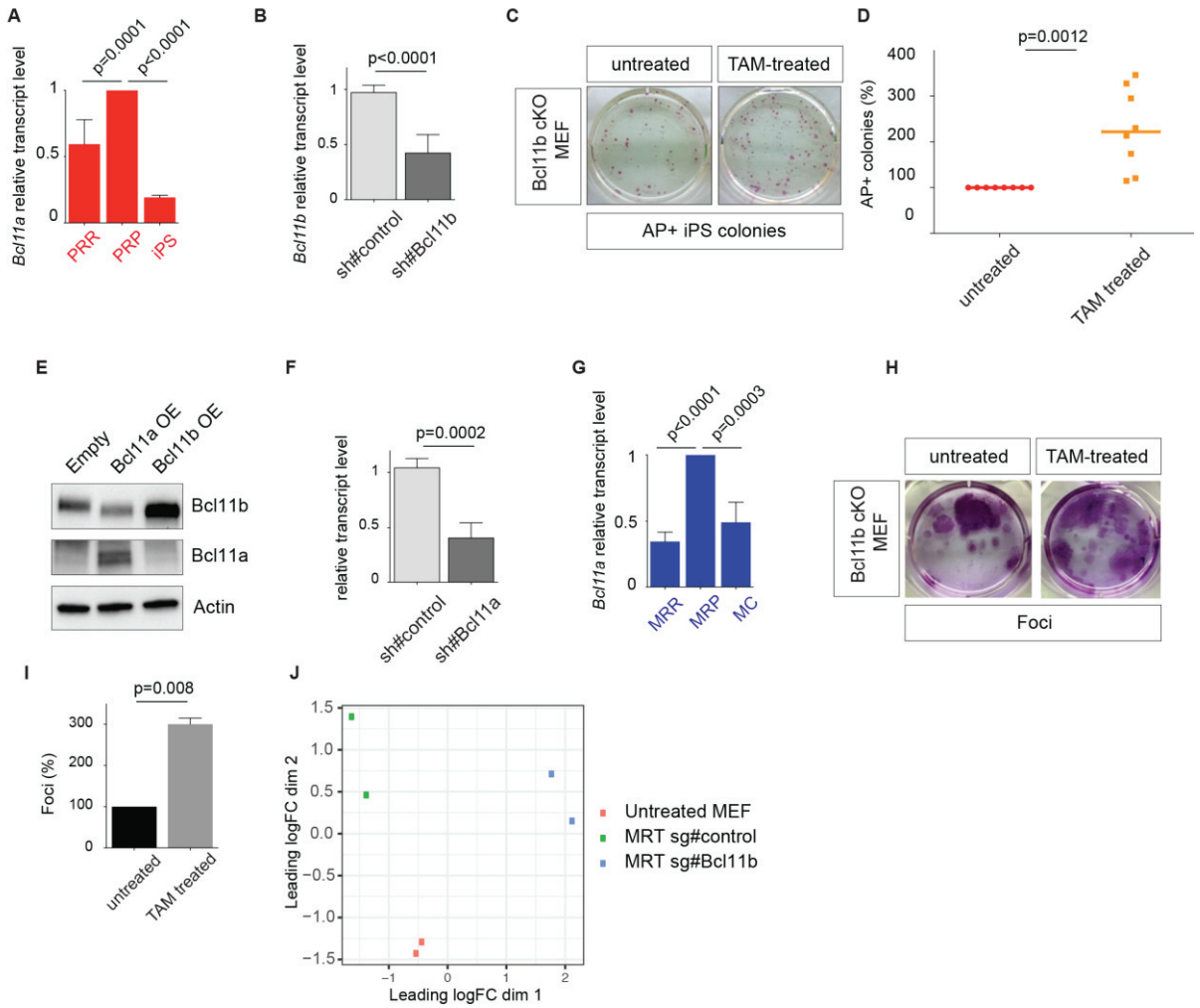

Supplementary figure 4. (A) Relative transcript level of *Bcl11a* determined by RT-qPCR in PRR and PRP intermediate cells upon PR after 5 days and in iPS cells. (B) Relative transcript level of *Bcl11b* determined by RT-qPCR upon shRNA-induced deletion of Bcl11b. (C) Alkaline Phosphatase (AP) staining of iPS colonies generated from Bcl11b-conditional KO MEFs. One representative experiment (from eight independent experiments). (D) Counting of AP-positive colonies depicted in (C). (E) Western blot validating the exogenous overexpression of BCL11B and BCL11A in the reprogramming experiments. OE: overexpression. (F) Relative transcript level of *Bcl11a* determined by RT-qPCR upon shRNA-induced deletion of Bcl11a. (G) Relative transcript level of Bcl11a determined by RT-qPCR in MRR and MRP intermediate cells upon MRT after 5 days and in malignant cells (MCs). (H) Foci staining of MCs generated from Bcl11b-conditional KO MEFs. One representative experiment (from three independent experiments). (I) Counting of foci depicted in (H). (J) Principal component analysis of ATAC-seq signal of the control cells and CRISPR cells control or guide Bcl11b after 5 days of MRT.

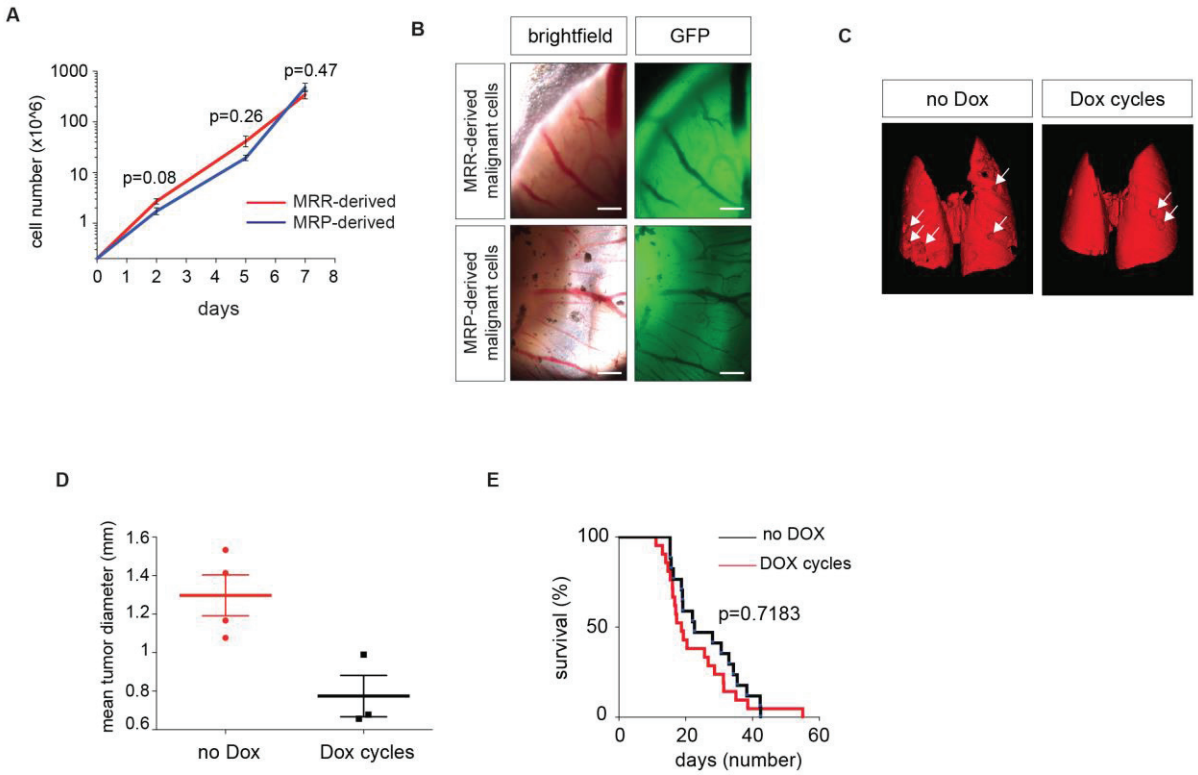

Supplementary Figure 5. (A) Proliferation curves of MRR- and MRP-derived malignant cells (n = 3 independent experiments). (B) Images depicting the injection of GFP-positive MRP and MRR-derived malignant cells onto the CAM of chick embryos. (C) *In vivo* tomography of lung in glucose-treated mice (no Dox) and mice treated with cycles of doxycycline (Dox cycles) at 18 weeks of age. Tumors are depicted by the arrows. (D) Counting of the mean tumor diameter in the *in vivo* tomography images depicted in (C). (E) Survival curves of glucose-treated mice and mice treated with cycles of doxycycline.

Table 1: List of sequences

Transgene	Primer 1 (5'-3')	Primer 2 (5'-3')	Primer 3 (5'-3')
Col1a1^{4F2A}	CCCTCCATGTGTGACCAAGG	TTGCTCAGCGGTGCTGTCCA	GCACAGCATTGCGGACATG
R26^{rtTA}	GCGAAGAGTTTGTCCTCAACC	AAAGTCGCTCTGAGTTGTTAT	GGAGCGGGAGAAATGGATATG
LSL-K-ras^{G12D}	CCTTTACAAGCGCACGCAGACTGTAGA	AGCTAGCCACCATGGCTTGAGTAAGTCTGCA	
R26-CRE^{ERT2}	TGCCACGACCAAGTGACAGC	CCAGGTTACGGATATAGTTCATG	
OCT4-EGFP	CAAGGCAAGGGAGGTAGACA	TGCCAGACAATGGCTATGAG	CCAAAAGACGGCAATATGGT
Bcl11b-tdTomato	GCCGGGTACCGAAGACACCAAACCGCTCTT	GCCCGGATCCTCCCCTTGGCAACTACTGAC	

shRNA sequence

p53	CCCACTACAAGTACATGTGTAA
Bcl11a	GCTCCGTTATCCTGCTAGATT
Bcl11b	CAAGTTCCAGAGCAATCTCAT
FosL1	CCAGTGCCTTGCATCTCCCTT

crispr guide sequence

	Forward sequence	Reverse sequence
Bcl11b	CACC**GCAATGTCCCGCCGCAAACA**	AAAC**TGTTTGCGGCGGGACATTGC**

Q-RTPCR primers

	Forward primer	Reverse primer
Gapdh	CATGGCCTTCCGTGTTCCTA	GCCTGCTTCACCACCTTCTT
Rplp0	GCTGATCATCCAGCAGGTGT	GGACACCCTCCAGAAAGCGA
Bcl11b	GGGAACTCATCACGCCAGAG	TGAGTAGATCAGGGTCGGGG
Bcl11a	CAGGTGGGGAAGGACGTTTA	TCATGTGTTTCTCCAGGGTACTG